



VOL. **631** NOS. **1 + 2** FEBRUARY 12, 1993

COMPLETE IN ONE ISSUE

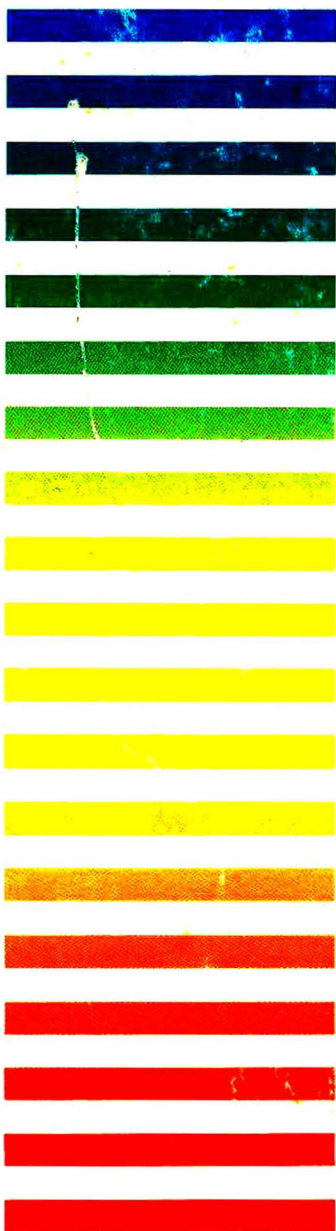
**16th International Symposium  
on Column Liquid Chromatography  
Baltimore, MD, June 14-19, 1992  
Part I**

Period.

JOURNAL OF

# CHROMATOGRAPHY

INCLUDING ELECTROPHORESIS AND OTHER SEPARATION METHODS



## SYMPOSIUM VOLUMES

### EDITORS

E. Heftmann (Orinda, CA)  
Z. Deyl (Prague)

### EDITORIAL BOARD

E. Bayer (Tübingen)  
S. R. Binder (Hercules, CA)  
S. C. Churms (Rondebosch)  
J. C. Fetzer (Richmond, CA)  
E. Gelpi (Barcelona)  
K. M. Gooding (Lafayette, IN)  
S. Hara (Tokyo)  
P. Helboe (Brønshøj)  
W. Lindner (Graz)  
T. M. Phillips (Washington, DC)  
S. Terabe (Hyogo)  
H. F. Walton (Boulder, CO)  
M. Wilchek (Rehovot)

ELSEVIER

# JOURNAL OF CHROMATOGRAPHY

INCLUDING ELECTROPHORESIS AND OTHER SEPARATION METHODS

**Scope.** The *Journal of Chromatography* publishes papers on all aspects of **chromatography, electrophoresis** and related methods. Contributions consist mainly of research papers dealing with chromatographic theory, instrumental developments and their applications. The section *Biomedical Applications*, which is under separate editorship, deals with the following aspects: developments in and applications of chromatographic and electrophoretic techniques related to clinical diagnosis or alterations during medical treatment; screening and profiling of body fluids or tissues related to the analysis of active substances and to metabolic disorders; drug level monitoring and pharmacokinetic studies; clinical toxicology; forensic medicine; veterinary medicine; occupational medicine; results from basic medical research with direct consequences in clinical practice. In *Symposium volumes*, which are under separate editorship, proceedings of symposia on chromatography, electrophoresis and related methods are published.

**Submission of Papers.** The preferred medium of submission is on disk with accompanying manuscript (see *Electronic manuscripts* in the Instructions to Authors, which can be obtained from the publisher, Elsevier Science Publishers B.V., P.O. Box 330, 1000 AH Amsterdam, Netherlands). Manuscripts (in English; *four* copies are required) should be submitted to: Editorial Office of *Journal of Chromatography*, P.O. Box 681, 1000 AR Amsterdam, Netherlands, Telefax (+31-20) 5862 304, or to: The Editor of *Journal of Chromatography, Biomedical Applications*, P.O. Box 681, 1000 AR Amsterdam, Netherlands. Review articles are invited or proposed in writing to the Editors who welcome suggestions for subjects. An outline of the proposed review should first be forwarded to the Editors for preliminary discussion prior to preparation. Submission of an article is understood to imply that the article is original and unpublished and is not being considered for publication elsewhere. For copyright regulations, see below.

**Publication.** The *Journal of Chromatography* (incl. *Biomedical Applications*) has 40 volumes in 1993. The subscription prices for 1993 are:

*J. Chromatogr.* (incl. *Cum. Indexes, Vols. 601-650*) + *Biomed. Appl.* (Vols. 612-651):

Dfl. 8520.00 plus Dfl. 1320.00 (p.p.h.) (total ca. US\$ 5622.75)

*J. Chromatogr.* (incl. *Cum. Indexes, Vols. 601-650*) only (Vols. 623-651):

Dfl. 7047.00 plus Dfl. 957.00 (p.p.h.) (total ca. US\$ 4573.75)

*Biomed. Appl.* only (Vols. 612-622):

Dfl. 2783.00 plus Dfl. 363.00 (p.p.h.) (total ca. US\$ 1797.75).

**Subscription Orders.** The Dutch guilder price is definitive. The US\$ price is subject to exchange-rate fluctuations and is given as a guide. Subscriptions are accepted on a prepaid basis only, unless different terms have been previously agreed upon. Subscriptions orders can be entered only by calendar year (Jan.-Dec.) and should be sent to Elsevier Science Publishers, Journal Department, P.O. Box 211, 1000 AE Amsterdam, Netherlands, Tel. (+31-20) 5803 642, Telefax (+31-20) 5803 598, or to your usual subscription agent. Postage and handling charges include surface delivery except to the following countries where air delivery via SAL (Surface Air Lift) mail is ensured: Argentina, Australia, Brazil, Canada, China, Hong Kong, India, Israel, Japan\*, Malaysia, Mexico, New Zealand, Pakistan, Singapore, South Africa, South Korea, Taiwan, Thailand, USA. \*For Japan air delivery (SAL) requires 25% additional charge of the normal postage and handling charge. For all other countries airmail rates are available upon request. Claims for missing issues must be made within six months of our publication (mailing) date, otherwise such claims cannot be honoured free of charge. Back volumes of the *Journal of Chromatography* (Vols. 1-611) are available at Dfl. 230.00 (plus postage). Customers in the USA and Canada wishing information on this and other Elsevier journals, please contact Journal Information Center, Elsevier Science Publishing Co. Inc., 655 Avenue of the Americas, New York, NY 10010, USA, Tel. (+1-212) 633 3750, Telefax (+1-212) 633 3764.

**Abstracts/Contents Lists** published in Analytical Abstracts, Biochemical Abstracts, Biological Abstracts, Chemical Abstracts, Chemical Titles, Chromatography Abstracts, Clinical Chemistry Lookout, Current Awareness in Biological Sciences (CABS), Current Contents/Life Sciences, Current Contents/Physical, Chemical & Earth Sciences, Deep-Sea Research/Part B: Oceanographic Literature Review, Excerpta Medica, Index Medicus, Mass Spectrometry Bulletin, PASCAL-CNRS, Pharmaceutical Abstracts, Referativnyi Zhurnal, Research Alert, Science Citation Index and Trends in Biotechnology.

**US Mailing Notice.** *Journal of Chromatography* (ISSN 0021-9673) is published weekly (total 58 issues) by Elsevier Science Publishers (Sara Burgerhartstraat 25, P.O. Box 211, 1000 AE Amsterdam, Netherlands). Annual subscription price in the USA US\$ 5622.75 (subject to change), including air speed delivery. Application to mail at second class postage rate is pending at Jamaica, NY 11431. **USA POSTMASTERS:** Send address changes to *Journal of Chromatography*, Publications Expediting, Inc., 200 Meacham Avenue, Elmont, NY 11003. Airfreight and mailing in the USA by Publication Expediting.

**See inside back cover** for Publication Schedule, Information for Authors and information on Advertisements.

© 1993 ELSEVIER SCIENCE PUBLISHERS B.V. All rights reserved.

0021-9673/93/S06.00

No part of this publication may be reproduced, stored in a retrieval system or transmitted in any form or by any means, electronic, mechanical, photocopying, recording or otherwise, without the prior written permission of the publisher. Elsevier Science Publishers B.V., Copyright and Permissions Department, P.O. Box 521, 1000 AM Amsterdam, Netherlands.

Upon acceptance of an article by the journal, the author(s) will be asked to transfer copyright of the article to the publisher. The transfer will ensure the widest possible dissemination of information.

**Special regulations for readers in the USA.** This journal has been registered with the Copyright Clearance Center, Inc. Consent is given for copying of articles for personal or internal use, or for the personal use of specific clients. This consent is given on the condition that the copier pays through the Center the per-copy fee stated in the code on the first page of each article for copying beyond that permitted by Sections 107 or 108 of the US Copyright Law. The appropriate fee should be forwarded with a copy of the first page of the article to the Copyright Clearance Center, Inc., 27 Congress Street, Salem, MA 01970, USA. If no code appears in an article, the author has not given broad consent to copy and permission to copy must be obtained directly from the author. All articles published prior to 1980 may be copied for a per-copy fee of US\$ 2.25, also payable through the Center. This consent does not extend to other kinds of copying, such as for general distribution, resale, advertising and promotion purposes, or for creating new collective works. Special written permission must be obtained from the publisher for such copying.

No responsibility is assumed by the Publisher for any injury and/or damage to persons or property as a matter of products liability, negligence or otherwise, or from any use or operation of any methods, products, instructions or ideas contained in the materials herein. Because of rapid advances in the medical sciences, the Publisher recommends that independent verification of diagnoses and drug dosages should be made.

Although all advertising material is expected to conform to ethical (medical) standards, inclusion in this publication does not constitute a guarantee or endorsement of the quality or value of such product or of the claims made of it by its manufacturer.

This issue is printed on acid-free paper.

Printed in the Netherlands

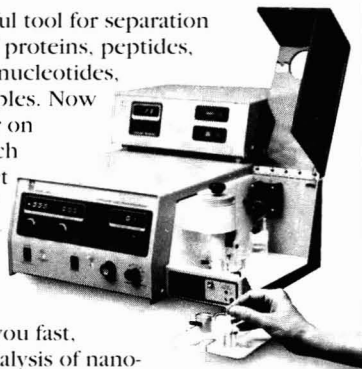
For Contents, see p. VII



# Discover new solutions to your analysis problems

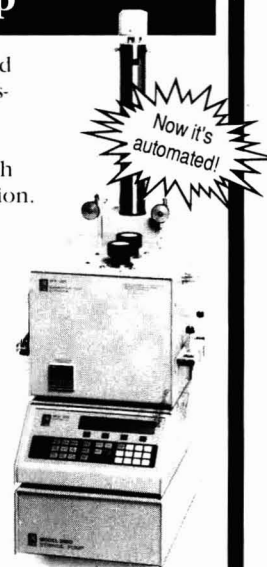
## Capillary Electrophoresis

CE is a powerful tool for separation and analysis of proteins, peptides, organic acids, nucleotides, and other samples. Now put this power on your own bench with a compact "personal CE." For less-than-HPLC prices, a Model 3850 Electropherograph™ gives you fast, quantitative analysis of nanoliter samples. Or if you prefer to build your own modular CE system, our top performing CV<sup>+</sup> detector is the best way to get started.



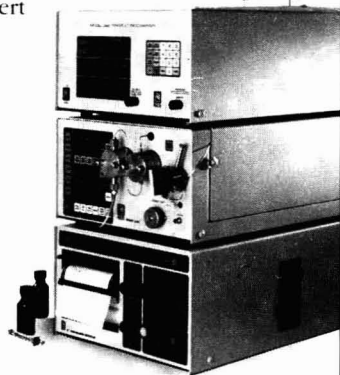
## SFE Sample Prep

High speed supercritical fluid extraction has no solvent disposal problems. These new Isco SFX™ systems give you all the advantages of SFE with automated, hands-off operation. Extract two samples at a time — in minutes — with low-cost, non-toxic CO<sub>2</sub>. Snap-in sample cartridges with finger-tight caps speed up loading and increase throughput. Programmed, precise modifier addition lets you tailor solvating power for the results you want.



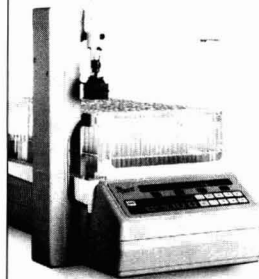
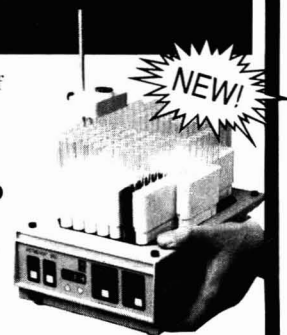
## Bio-inert HPLC

Robust, reliable HPLC systems give you modular flexibility and programmability at a fair price — so you can still get great HPLC value even on a tight budget. And the ProTeam LC™ Inert option assures maximum biocompatibility — including metal-free columns — for biopolymer separations.



## Prep LC

Get no-miss collection of your LC or HPLC peaks with a space-saving Isco fraction collector. **All-new Retriever® 500** is the smallest 100-tube fraction collector — and the most affordable.



**Super-smart Foxy® 200** makes it easy to collect just the peaks you want. Sort and group fractions to get the most out of any separation.

*Call or fax today and find out how  
Isco quality and reliability mean  
more research, less problems.*

Isco, Inc., P.O. Box 5347  
Lincoln NE 68505 U.S.A.  
Tel. (800)228-4250

Isco Europe AG, Brüschstr. 17  
CH18708 Männedorf, Switzerland  
Fax (41-1)920 62 08



Distributors • **Australia:** Australian Chromatography Co. • **Austria:** INULA • **Belgium:** Mettler-Toledo S.A. • **Canada:** Canberra Packard Canada, Ltd. • **Denmark:** Mikrolab Aarhus • **Finland:** ETEK OY • **France:** Ets. Roucaire, S.A. • **Germany:** Colora Messtechnik GmbH • **Italy:** Analytical Control Italia S.p.A. • **Japan:** JSI Co. Ltd. • **Korea:** Sang Chung, Ltd. • **The Netherlands:** Beun-de Ronde B.V. • **Norway:** Dipl. Ing. Houm A.S. • **Portugal:** CAMPOS & Ca., Lda. • **Spain:** VARIAN-CHEMICONTROL, S.L. • **Sweden:** Spectrochrom AB • **Switzerland:** IG Instrumenten-Gesellschaft AG • **UK:** Jones Chromatography Ltd. •

# Liquid Chromatography in Biomedical Analysis

edited by T. Hanai

Journal of Chromatography Library, Volume 50

This book presents a guide for the analysis of biomedically important compounds using modern liquid chromatographic techniques. After a brief summary of basic liquid chromatographic methods and optimization strategies, the main part of the book focuses on the various classes of biomedically important compounds: amino acids, catecholamines, carbohydrates, fatty acids, nucleotides, porphyrins, prostaglandins and steroid hormones.

The different chapters discuss specialized techniques pertaining to each class of compounds, such as sample pretreatment, pre- and post-column derivatization, detection and quantification.

## Contents:

1. Liquid chromatography in biomedical analysis: basic approach (C.K. Lim).
2. Optimization of liquid chromatography for biomedically important compounds (T. Hanai).
3. Amino acids (Y. Ishida).
4. Bile acids (J. Goto and T. Nambara).

5. Carbohydrates (S. Honda).
  6. Catecholamines (K. Mori).
  7. Fatty acids (T. Hirai).
  8. Nucleotides (C.K. Lim).
  9. Porphyrins (C.K. Lim).
  10. Prostaglandins (T. Hirai).
  11. Steroid hormones (T. Hirai).
  12. Miscellaneous (T. Hanai).
- Subject Index.

1991 xii + 296 pages  
Price: US \$ 169.00 / Dfl. 270.00  
ISBN 0-444-87451-8

*"...essential reading for  
biomedical analysts."*

**The Analyst**

*"...highly recommended for  
pharmaceutical-industry  
laboratories that carry out  
pharmacokinetic and  
drug-metabolism studies."*

**LC-GC**



**ELSEVIER**  
SCIENCE PUBLISHERS

*"This book will be valuable for anyone involved in liquid chromatography. It is timely and highlights throughout the techniques that are most successful. This is not so much a book to put on the shelf of the specialist for reference purposes, but instead it is a book which is meant to be read by the general reader to obtain perspective and insights into this general area."*

**Trends in Analytical  
Chemistry**

## ORDER INFORMATION

For USA and Canada  
**ELSEVIER SCIENCE  
PUBLISHERS**  
Judy Weislogel  
P.O. Box 945  
Madison Square Station,  
New York, NY 10160-0757  
Tel: (212) 989 5800  
Fax: (212) 633 3880

In all other countries

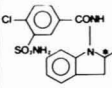
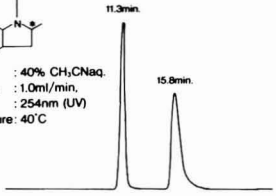
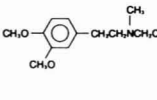
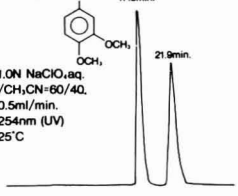
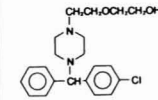
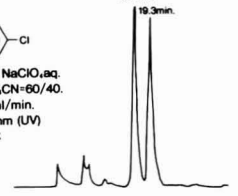
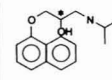
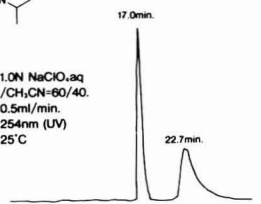
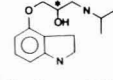
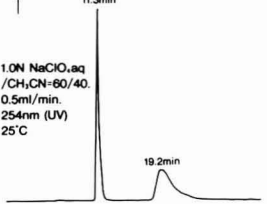
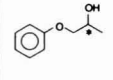
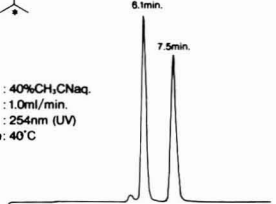
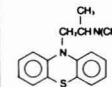
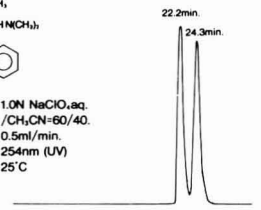
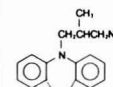
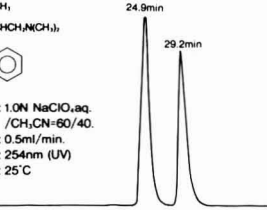
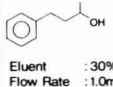
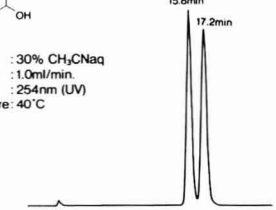
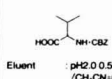
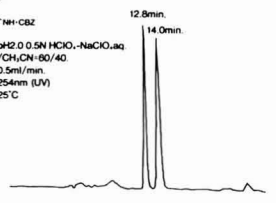
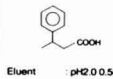
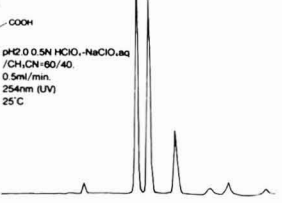
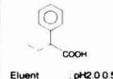
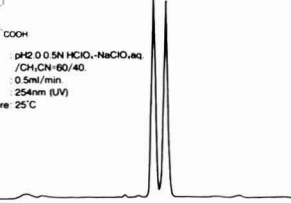
**ELSEVIER SCIENCE  
PUBLISHERS**  
P.O. Box 211  
1000 AE Amsterdam  
The Netherlands  
Tel: (+31-20) 5803 753  
Fax: (+31-20) 5803 705

*US\$ prices are valid only for the USA & Canada and are subject to exchange rate fluctuations; in all other countries the Dutch guilder price (Dfl.) is definitive. Customers in the European Community should add the appropriate VAT rate applicable in their country to the price(s). Books are sent post-free if prepaid.*



# Reversed Phase CHIRAL HPLC Column

## NEW CHIRALCEL<sup>®</sup> OD-R

<p><b>Indapamide</b></p>  <p>Eluent : 40% CH<sub>3</sub>CN,aq. Flow Rate : 1.0ml/min. Detection : 254nm (UV) Temperature : 40°C</p> 	<p><b>Verapamil</b></p>  <p>Eluent : 1.0N NaClO<sub>4</sub>aq. /CH<sub>3</sub>CN-60/40. Flow Rate : 0.5ml/min. Detection : 254nm (UV) Temperature : 25°C</p> 	<p><b>Hydroxyzine</b></p>  <p>Eluent : 1.0N NaClO<sub>4</sub>aq. /CH<sub>3</sub>CN-60/40. Flow Rate : 0.5ml/min. Detection : 254nm (UV) Temperature : 25°C</p> 
<p><b>Propranolol</b></p>  <p>Eluent : 1.0N NaClO<sub>4</sub>aq. /CH<sub>3</sub>CN-60/40. Flow Rate : 0.5ml/min. Detection : 254nm (UV) Temperature : 25°C</p> 	<p><b>Pindolol</b></p>  <p>Eluent : 1.0N NaClO<sub>4</sub>aq. /CH<sub>3</sub>CN-60/40. Flow Rate : 0.5ml/min. Detection : 254nm (UV) Temperature : 25°C</p> 	<p><b>1-Phenoxy-2-Propanol</b></p>  <p>Eluent : 40%CH<sub>3</sub>CN,aq. Flow Rate : 1.0ml/min. Detection : 254nm (UV) Temperature : 40°C</p> 
<p><b>Alimemazine</b></p>  <p>Eluent : 1.0N NaClO<sub>4</sub>aq. /CH<sub>3</sub>CN-60/40. Flow Rate : 0.5ml/min. Detection : 254nm (UV) Temperature : 25°C</p> 	<p><b>Trimepramine</b></p>  <p>Eluent : 1.0N NaClO<sub>4</sub>aq. /CH<sub>3</sub>CN-60/40. Flow Rate : 0.5ml/min. Detection : 254nm (UV) Temperature : 25°C</p> 	<p><b>4-Pheny-2-butanol</b></p>  <p>Eluent : 30% CH<sub>3</sub>CN,aq. Flow Rate : 1.0ml/min. Detection : 254nm (UV) Temperature : 40°C</p> 
<p><b>CBZ-Val.</b></p>  <p>Eluent : pH2.0 0.5N HClO<sub>4</sub>-NaClO<sub>4</sub>aq. /CH<sub>3</sub>CN-60/40. Flow Rate : 0.5ml/min. Detection : 254nm (UV) Temperature : 25°C</p> 	<p><b>3-Phenylbutyric acid</b></p>  <p>Eluent : pH2.0 0.5N HClO<sub>4</sub>-NaClO<sub>4</sub>aq. /CH<sub>3</sub>CN-60/40. Flow Rate : 0.5ml/min. Detection : 254nm (UV) Temperature : 25°C</p> 	<p><b>2-Phenylbutyric acid</b></p>  <p>Eluent : pH2.0 0.5N HClO<sub>4</sub>-NaClO<sub>4</sub>aq. /CH<sub>3</sub>CN-60/40. Flow Rate : 0.5ml/min. Detection : 254nm (UV) Temperature : 25°C</p> 

For more information about CHIRALCEL OD-R column, please give us a call.



**DAICEL CHEMICAL INDUSTRIES, LTD.**

CHIRAL CHEMICALS DIVISION 8-1, Kasumigaseki 3-chome, Chiyoda-ku, Tokyo 100, JAPAN  
Phone: +81-3-3507-3151 Facsimile: +81-3-3507-3193

**AMERICA**  
CHIRAL TECHNOLOGIES, INC.  
730 SPRINGDALE DRIVE  
DRAWER I EXTON, PA 19341  
Phone: 215-594-2100  
Facsimile: 215-594-2325

**EUROPE**  
DAICEL (EUROPA) GmbH  
Ost Street 22  
4000 Düsseldorf 1, Germany  
Phone: +49-211-369848  
Facsimile: +49-211-364429

**ASIA/OCEANIA**  
DAICEL CHEMICAL (ASIA) PTE. LTD.  
65 Chulia Street #40-07  
OCBC Centre, Singapore 0104.  
Phone: +65-5332511  
Facsimile: +65-5326454

# Statistical Treatment of Experimental Data

by J.R. Green and D. Margerison

This book is primarily intended for researchers wishing to analyse experimental data using statistical methods. Statistical concepts and methods which may be employed to treat experimental data are explained, and the ideas and reasoning behind statistical methodology are clarified. Formal results are illustrated by many numerical worked examples mainly taken from the laboratory. Concepts, practical methodology, and worked examples are integrated in the text.

Consideration is given in this work to a large number of practical topics which are often omitted from standard texts. These include; obtaining an approximate confidence interval for a function of some unknown parameters; testing for outliers, stabilization of heterogeneous variances, and significant differences between means; estimation of parameters after performing tests; deciding what numbers of significant figures to quote for sample means and variances; straight-line and polynomial regression, through the origin or not, using weighted points, and testing the homogeneity of a set of such lines or curves.

The numerous examples which are provided throughout the text will serve as models for the various problems encountered by the readers when

employing statistical methods to treat experimental data. Neither a strong mathematical background nor a prior knowledge of probability or statistics is required in order to make use of this work.

In addition to research workers in universities and industry, the book will be of use for first-year students of statistics, and would be especially suitable as the basis of a graduate course in experimental sciences.

**Contents:** 1. Introduction. 2. Probability. 3. Random Variables and Sampling Distributions. 4. Some Important Probability Distributions. 5. Estimation. 6. Confidence Intervals. 7. Hypothesis Testing. 8. Tests on Means. 9. Tests on Variances. 10. Goodness of Fit Tests. 11. Correlation. 12. The Straight Line Through the Origin or Through Some Other Fixed Point. 13. The Polynomial Through the Origin or Through Some Other Fixed Point. 14. The General Straight Line. 15. The General Polynomial. 16. A Brief Look at Multiple Regression. Appendices: 1. Drawing a Random Sample Using a Table of Random Numbers. 2. Orthogonal Polynomials in  $x$ . References. Index.

1977 5th imp. 1988 x + 382 pages  
Price: US \$ 96.00 / Dfl. 168.00  
ISBN 0-444-41725-7



**Elsevier Science Publishers**

P.O. Box 211, 1000 AE Amsterdam, The Netherlands  
P.O. Box 882, Madison Square Station, New York, NY 10159, USA

JOURNAL OF CHROMATOGRAPHY

VOL. 631 (1993)





# JOURNAL of CHROMATOGRAPHY

INCLUDING ELECTROPHORESIS AND OTHER SEPARATION METHODS

## SYMPOSIUM VOLUMES

### EDITORS

E. HEFTMANN (Orinda, CA), Z. DEYL (Prague)

### EDITORIAL BOARD

E. Bayer (Tübingen), S. R. Binder (Hercules, CA), S. C. Churms (Rondebosch), J. C. Fetzer (Richmond, CA), E. Gelpí (Barcelona), K. M. Gooding (Lafayette, IN), S. Hara (Tokyo), P. Helboe (Brønshøj), W. Lindner (Graz), T. M. Phillips (Washington, DC), S. Terabe (Hyogo), H. F. Walton (Boulder, CO), M. Wilchek (Rehovot)



ELSEVIER  
AMSTERDAM — LONDON — NEW YORK — TOKYO

---

*J. Chromatogr.*, Vol. 631 (1993)

© 1993 ELSEVIER SCIENCE PUBLISHERS B.V. All rights reserved.

0021-9673/93/06.00

No part of this publication may be reproduced, stored in a retrieval system or transmitted in any form or by any means, electronic, mechanical, photocopying, recording or otherwise, without the prior written permission of the publisher, Elsevier Science Publishers B.V., Copyright and Permissions Department, P.O. Box 521, 1000 AM Amsterdam, Netherlands.

Upon acceptance of an article by the journal, the author(s) will be asked to transfer copyright of the article to the publisher. The transfer will ensure the widest possible dissemination of information.

**Special regulations for readers in the USA.** This journal has been registered with the Copyright Clearance Center, Inc. Consent is given for copying of articles for personal or internal use, or for the personal use of specific clients. This consent is given on the condition that the copier pays through the Center the per-copy fee stated in the code on the first page of each article for copying beyond that permitted by Sections 107 or 108 of the US Copyright Law. The appropriate fee should be forwarded with a copy of the first page of the article to the Copyright Clearance Center, Inc., 27 Congress Street, Salem, MA 01970, USA. If no code appears in an article, the author has not given broad consent to copy and permission to copy must be obtained directly from the author. All articles published prior to 1980 may be copied for a per-copy fee of US\$ 2.25, also payable through the Center. This consent does not extend to other kinds of copying, such as for general distribution, resale, advertising and promotion purposes, or for creating new collective works. Special written permission must be obtained from the publisher for such copying.

No responsibility is assumed by the Publisher for any injury and/or damage to persons or property as a matter of products liability, negligence or otherwise, or from any use or operation of any methods, products, instructions or ideas contained in the materials herein. Because of rapid advances in the medical sciences, the Publisher recommends that independent verification of diagnoses and drug dosages should be made.

Although all advertising material is expected to conform to ethical (medical) standards, inclusion in this publication does not constitute a guarantee or endorsement of the quality or value of such product or of the claims made of it by its manufacturer.

This issue is printed on acid-free paper.

Printed in the Netherlands



SYMPOSIUM VOLUME



**16TH INTERNATIONAL SYMPOSIUM  
ON  
COLUMN LIQUID CHROMATOGRAPHY**

**PART I**

*Baltimore, MD (USA), June 14–19, 1992*

The proceedings of the *16th International Symposium on Column Liquid Chromatography, Baltimore, MD, June 14–19, 1992*, are published in two consecutive volumes of the *Journal of Chromatography*:

Vols. 631 and 632 (1993). A combined Author Index to both Vols. 631 and 632 only appears in Vol. 632.

## CONTENTS

16TH INTERNATIONAL SYMPOSIUM ON COLUMN LIQUID CHROMATOGRAPHY, BALTIMORE, MD, JUNE 14–19, 1992, PART I

## COLUMN LIQUID CHROMATOGRAPHY

*Theory and general*

- Chromatographic method verification by means of three-dimensional, multivariate visualization  
by F. O. Geiser (Glen Mills, PA, USA), C. Golt and L. Kung, Jr. (Newark, DE, USA), J. D. Justice (Palo Alto, CA, USA)  
and B. L. Brown (Orem, UT, USA) . . . . . 1
- Faster quantitative evaluation of high-performance liquid chromatography–ultraviolet diode-array data by multicomponent  
analysis  
by J.-L. Excoffier, M. Joseph, J.J. Robinson and T. L. Sheehan (Walnut Creek, CA, USA) . . . . . 15
- Deuterium nuclear magnetic resonance spectroscopy as a probe for reversed-phase liquid chromatographic bonded phase solva-  
tion: methanol and acetonitrile mobile phase components  
by D. M. Bliesner and K. B. Sentell (Burlington, VT, USA) . . . . . 23
- Thermodynamics of the adsorption of Tröger's base enantiomers from ethanol on cellulose triacetate  
by A. Seidel-Morgenstern and G. Guiochon (Knoxville and Oak Ridge, TN, USA) . . . . . 37
- New chromatographic hydrophobicity index ( $\phi_0$ ) based on the slope and the intercept of the log  $k'$  versus organic phase concen-  
tration plot  
by K. Valkó and P. Slégel (London, UK) . . . . . 49
- Accurate determination of log  $k'_w$  in reversed-phase liquid chromatography. Implications for quantitative structure–retention  
relationships  
by M.-M. Hsieh and J. G. Dorsey (Cincinnati, OH, USA) . . . . . 63

*Materials and techniques*

- Characterization of a Chiral-AGP capillary column coupled to a micro sample-enrichment system with UV and electrospray mass  
spectrometric detection  
by J. Hermansson and I. Hermansson (Norsborg, Sweden) and J. Nordin (Huddinge, Sweden) . . . . . 79
- Reversed-phase liquid chromatography with microspherical octadecyl-zirconia bonded stationary phases  
by J. Yu and Z. El Rassi (Stillwater, OK, USA) . . . . . 91
- Fimbriated stationary phases for proteins  
by L. Varady (Cambridge, MA, USA), N. Mu (West Lafayette, IN, USA), Y.-B. Yang (Hesperia, CA, USA), S. E. Cook  
(Wilmington, DE, USA), N. Afeyan (Cambridge, MA, USA) and F. E. Regnier (West Lafayette, IN, USA) . . . . . 107
- High-performance liquid chromatography of amino acids, peptides and proteins. CXXIV. Physical characterisation of fluidized-  
bed behaviour of chromatographic packing materials  
by G. Dasari, I. Prince and M. T. W. Hearn (Clayton, Australia) . . . . . 115
- Selectivity of organic solvents in micellar liquid chromatography of amino acids and peptides  
by A. S. Kord and M. G. Khaledi (Raleigh, NC, USA) . . . . . 125
- Axial illumination of fused-silica capillaries. Investigation of fluorescence and refractive index detection  
by A. A. Abbas and D. C. Shelly (Lubbock, TX, USA) . . . . . 133
- Peak tracking with a neural network for spectral recognition  
by P. M. J. Coenegracht, H. J. Metting, E. M. van Loo, G. J. Snoeijer and D. A. Doornbos (Groningen, Netherlands) . . . . . 145
- Primary contribution of the injector to carryover of a trace analyte in high-performance liquid chromatography  
by M. Saha and R. W. Giese (Boston, MA, USA) . . . . . 161

*Applications: chiral separations*

- N-Arylcarbonyl derivatives of amino acids as chiral stationary phases for optical resolution by high-performance liquid chro-  
matography  
by M.-H. Yang and J.-Y. Lin (Taipei, Taiwan) . . . . . 165



Analytical and preparative high-performance liquid chromatographic separation of thienopyran enantiomers by C. J. Shaw, P. J. Sanfilippo, J. J. McNally, S. A. Park and J. B. Press (Raritan, NJ, USA) . . . . .	173
Enantiomer separation by high-performance liquid chromatography with copper(II) complexes of Schiff bases as chiral stationary phases by N. Ôi, H. Kitahara and F. Aoki (Osaka, Japan) . . . . .	177
Retention and enantioselective properties of racemic compounds on modified ovomucoid columns. II. Reaction with glycer-aldehyde, formaldehyde and glutaric anhydride by J. Haginaka, T. Murashima and C. Seyama (Hyogo, Japan) and H. Fujima and H. Wada (Kyoto, Japan) . . . . .	183
Direct chiral separation of almokalant on Chiralcel OD and Chiralpak AD for liquid chromatographic assay of biological samples by K. Balmér, P.-O. Lagerström, S. Larsson and B.-A. Persson (Mölnådal, Sweden) . . . . .	191
Rapid direct resolution of the stereoisomers of all- <i>trans</i> astaxanthin on a Pirkle covalent L-leucine column by S. A. Turujman (Washington, DC, USA) . . . . .	197
<i>Applications: pharmaceuticals</i>	
Determination of ephedrine in urine by high-performance liquid chromatography by C. Imaz, D. Carreras, R. Navajas, C. Rodriguez, A. F. Rodriguez, J. Maynar and R. Cortes (Madrid, Spain) . . . . .	201
Porous graphitized carbon and octadecylsilica columns in the separation of some monoamine oxidase inhibitory drugs by E. Forgács, K. Valkó, T. Cserhádi and K. Magyar (Budapest, Hungary) . . . . .	207
Liquid chromatography–mass spectrometry for the determination of medetomidine and other anaesthetics in plasma by H. Kanazawa, Y. Nagata, Y. Matsushima, N. Takai, H. Uchiyama, R. Nishimura and A. Takeuchi (Tokyo, Japan) . . . . .	215
Reversed-phase high-performance liquid chromatography of the cardiac glycoside LNF-209 with refractive index detection by P. H. Zoutendam, D. L. Berry and D. W. Carkuff (Norwich, NY, USA) . . . . .	221
Determination of oxiracetam in human plasma by reversed-phase high-performance liquid chromatography with fluorimetric detection by R. C. Simpson, V. K. Boppana, B. Y.-H. Hwang and G. R. Rhodes (King of Prussia, PA, USA) . . . . .	227
Column-switching high-performance liquid chromatographic method for the determination of SK&F 106203 in human plasma after fluorescence derivatization with 9-anthryldiazomethane by C. Miller-Stein, B. Y.-H. Kwang, G. R. Rhodes and V. K. Boppana (King of Prussia, PA, USA) . . . . .	233
Determination of baicalin and puerarin in traditional Chinese medicinal preparations by high-performance liquid chromatography by K.-C. Wen, C.-Y. Huang and F.-L. Lu (Taipei, Taiwan) . . . . .	241
Normal-phase high-performance liquid chromatographic determination of epristeride, a prostatic steroid 5 $\alpha$ -reductase enzyme inhibitor, in human plasma by V. K. Boppana, C. Miller-Stein and G. R. Rhodes (King of Prussia, PA, USA) . . . . .	251
Rapid, sensitive high-performance liquid chromatographic method for the quantification of promethazine in human serum with electrochemical detection by A. R. Fox and D. A. McLoughlin (Baltimore, MD, USA) . . . . .	255
<i>Applications: proteins and their constituents</i>	
High-performance liquid chromatography of human glycoprotein hormones by M. A. Chlenov, E. I. Kandyba, L. V. Nagornaya, I. L. Orlova and Y. V. Volgin (Moscow, Russian Federation) . . . . .	261
Immunoaffinity chromatography of recombinant <i>Amb a 1</i> in the presence of a denaturing agent by K. M. Keating, B. L. Rogers, L. Weber, J. P. Morgenstern, D. G. Klapper and M. Kuo (Cambridge, MA and Chapel Hill, NC, USA) . . . . .	269
Separation of interleukins by a preparative chromatofocusing-like method by S. P. Monkarsh, E. A. Russoman and S. K. Roy (Nutley, NJ, USA) . . . . .	277
Kinetic analysis of biotinylation of specific residues of peptides by high-performance liquid chromatography by A. Korosky, B. T. Miller and S. L. Knock (Galveston, TX, USA) . . . . .	281















CHROMSYMP. 2604

# Chromatographic method verification by means of three-dimensional, multivariate visualization

F. O. Geiser

*Geiser Scientific, Inc., 287A Wilson Avenue, Glen Mills, PA 19342 (USA)*

C. Golt and L. Kung, Jr.

*Agriculture Experiment Station, University of Delaware, Newark, DE 19716 (USA)*

J. D. Justice

*Justice Innovations, Inc., 465 El Capitan Place, Palo Alto, CA 94306 (USA)*

B. L. Brown

*Echo Data, Inc., 1010 N. State Street, Orem, UT 84057 (USA)*

---

## ABSTRACT

Using free-fatty-acid model systems, principal-component analysis as automated in Justice Innovations' Chrom Perfect and Echo Data's DataMax software was used to correlate, visualize, and verify the relationships of nine system-suitability parameters. Many-dimensional data were mapped by relaxing the usual 90° axes and by using non-orthogonal vectors. The arccosines of the correlation coefficients were used as the vector angles.

Two types of matrices were non-orthogonally mapped: (1) chromatography system-suitability parameters as the vectors and chromatography components as the objects; (2) chromatography parameters for each component as the vectors and methods as the objects. The first type of matrix was found to be suitable for clustering similar chromatography parameters, for visualizing a single chromatogram, for comparing replicate results, and for verifying expected chromatography correlations.

The second type of matrix had the same results as a chromatographic response function in that a chromatogram was reduced to a single value, or coordinate in the case of a non-orthogonal map. Practical applications include the visualization of multidetector, multiwavelength, multicolumn data. Two examples were demonstrated: (1) chromatography method evaluation by non-orthogonally mapping a 4 × 35 matrix representing resolution, theoretical plates, tailing factor,  $\alpha$ , and capacity factor for a seven-component mixture; (2) identification of optimum concentration, time-course effects, and replicate reproducibility using a 180 × 6 matrix representing 180 multicomponent chromatograms. In each case, Echo Data's DataMax software was found to facilitate more rapid screening than currently possible by the use of computerized statistical analysis alone.

---

## INTRODUCTION

Computerized mathematical approaches which simultaneously account for all chromatography pa-

rameters and which improve on the near inability of the human mind to understand the complex relationships between six chromatography parameters have been described by Guiochon and co-workers [1,2]. Chromatography visualization techniques have typically been limited to orthogonal plotting of one variable for each dimension thus restricting

---

*Correspondence to:* F. O. Geiser, Geiser Scientific, Inc., 287A Wilson Avenue, Glen Mills, PA 19342, USA.

the number of variables that can be simultaneously viewed to three. Brown and co-workers [3,4] have described a visualization technique that maps many-dimensional data in a three-dimensional reduced space by the use of non-orthogonal vectors. The usual 90° axes between vectors are relaxed and instead the arccosines of the correlation coefficients are used as the angles.

The objective of our investigation was to examine whether multivariate, non-orthogonal mapping as described by Brown *et al.* [5] and as automated in Echo Data's DataMax computer software could be useful in visualizing the relationships in multicomponent chromatography data. The suitability of non-orthogonal mapping as applied to chromatography data was evaluated using a seven-component model system. Six free-fatty acids typically found in cow rumen and an internal standard were separated by one temperature-programmed and by four isothermal gas chromatography methods. Isothermal gas chromatography with flame ionization detection was chosen for this initial confirmatory study because of the ease of determining column void volumes. Berridge [6] has noted that computerized capacity factor ( $k'$ ) calculations are limited by the difficulty of precisely determining column void volume and that a technique which could accurately substitute retention time for  $k'$  would be useful. The gas chromatography methods were designed solely to test the visual accuracy of DataMax software using typical system-suitability parameters and were not intended to be rigorous contributions.

The temperature-programmed data were derived from ongoing *in vitro* bovine ruminal studies by Kung and Hession [7] evaluating whether bacterial inoculations in lieu of antibiotic treatment could enhance ruminal fermentations by increasing concentrations of acetic and propionic acids. Ionophore lysocellin, a divalent polyether antibiotic, has been shown to improve daily gain and feed efficiency when fed to growing cattle presumably by increased concentrations of short-chain fatty acids [8]. The heretofore unpublished results presented in this paper included 180 chromatograms consisting of 5 replicated treatments, 2 protocols (5 bacterial concentrations, 12 and 24 h fermentation times, 2 diets, 4 replicates injected twice) and corresponding zero-hour controls (5 bacterial concentrations, 2 diets, 2 injections). A large data set of this type generally

requires time-consuming, computerized statistical analysis [9] for interpretation. A visual technique which could rapidly screen and verify biological activity would be highly useful.

## EXPERIMENTAL

The gas chromatography system consisted of a Hewlett-Packard 5890 Series II gas chromatography (Valley Forge, PA, USA) equipped with a HP 7673A autosampler, flame ionization detector (250°C), and the Justice Innovations' Chrom Perfect data system (Palo Alto, CA, USA). The test mixture consisted of seven short-chain, free-fatty acid standards (Fisher Scientific, Pittsburgh, PA, USA) dissolved in 5% metaphosphoric acid in the following concentrations: 50 mM acetic acid, 30 mM propionic acid, 4 mM isobutyric acid, 8 mM butyric acid, 4 mM isovaleric acid, 4 mM *n*-valeric acid and 4 mM isocaproic acid as the internal standard.

Samples (1  $\mu$ l) were injected on a Hewlett-Packard Carbowax 20M capillary column (10 m  $\times$  0.53 mm I.D., 1.33  $\mu$ m film thickness) using a 7:1 split ratio with an injection temperature of 200°C. Methods 1–4 were identical except for the following variations in isothermal oven temperature and duration time: 100°C (10 min), 90°C (10 min), 80°C (12 min) and 70°C (25 min) for methods 1, 2, 3 and 4, respectively. For the 13.5-min temperature-programmed method, the initial temperature of 70°C was held for 1 min and ramped to 100°C at 5°/min. Helium carrier gas was set at 10.6 ml/min at 90°C.

Chromatographic results in ASCII format were prepared using Justice Innovations' ReportWrite-Plus and RESULTS software, and the multivariate, non-orthogonal maps were prepared using Echo Data's DataMax software (Orem, UT, USA) on an 80486DX microcomputer (PC Science, Morris Plains, NJ, USA), equipped with Microsoft MS-DOS 5.0 and a Hewlett-Packard LaserJet IIP printer. The 180 samples in the temperature-programmed study were prepared using the methodology of Kung *et al.* [8] and consisted of 20 replicated treatment groups (160 chromatograms representing 5 bacterial concentrations, 12 and 24 h fermentation time, 2 diets, 4 replicates injected twice) and of 10 unreplicated controls (20 chromatograms representing 5 bacterial concentrations, 2 diets, zero fermentation time, injected twice).

The following nine system-suitability parameters specified by the US Pharmacopeia [10] and by the Food and Drug Administration [11], were automatically calculated by the Chrom Perfect and Report-WritePlus computer software using the equations described by Justice [12]: resolution (RS),  $\alpha$  (ALPHA), theoretical plates (PLATES), 10 and 5% peak tailing factors (TF5%, TF10%), 10 and 5% peak skew (Skew 10%, Skew 5%), peak half-width (HFWD), and capacity factor,  $k'$  (K'). Normalized values for the nine system-suitability parameters were non-orthogonally mapped by the DataMax software using the principal-component equations described by Brown and Fluckiger [13]. For the

temperature-programmed method, component concentrations for 180 chromatograms were merged into a single ASCII file by the RESULTS software described by Justice [14] and were non-orthogonally mapped by the DataMax software.

## RESULTS

### *System-suitability parameters*

In Fig. 1, nine system-suitability parameters for each of the seven components separated by the 100°C isothermal method were non-orthogonally mapped using the  $7 \times 9$  matrix, correlation calculations, and X-Y-Z object coordinates given in Table

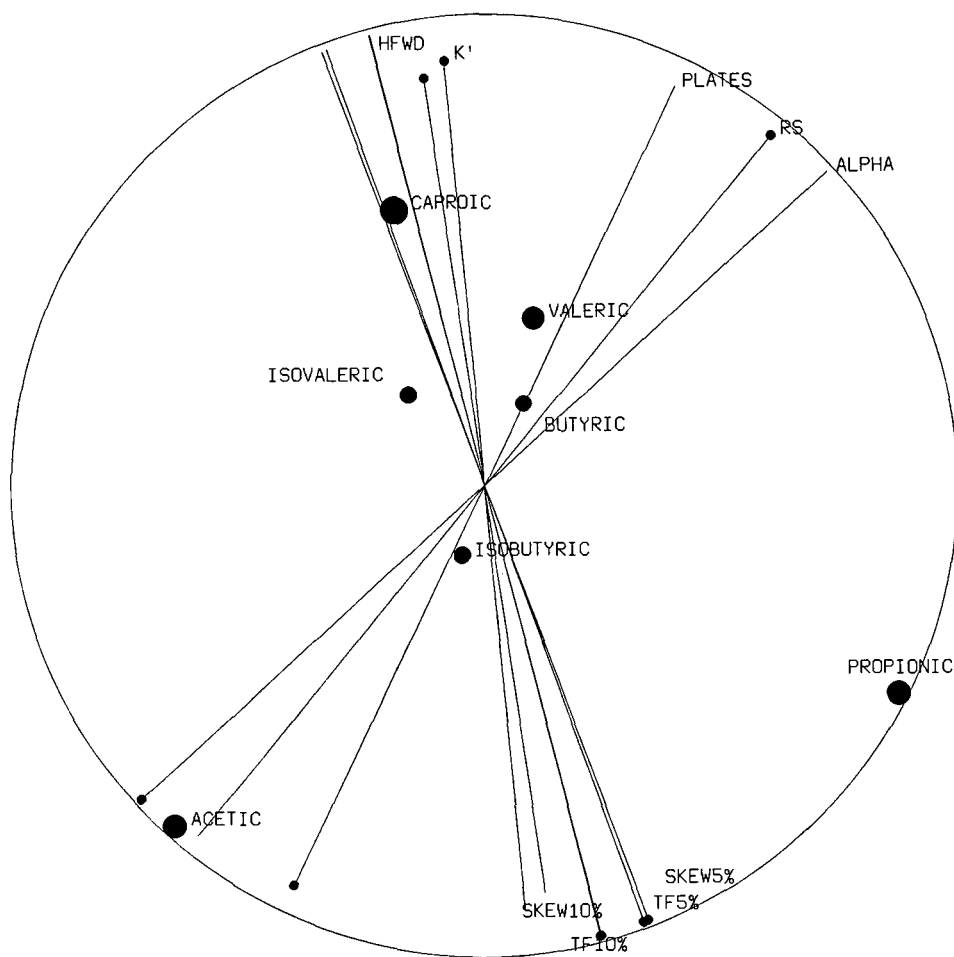


Fig. 1. System-suitability parameters using capacity factor. Non-orthogonal map of 100°C isothermal gas chromatography method as described in Experimental section using  $7 \times 9$  matrix and correlation calculations in Table I. The ninth vector was  $k'$  (capacity factor).

TABLE I  
SYSTEM-SUITABILITY PARAMETERS FOR 100°C METHOD

7 × 10 matrix and correlation calculations for 100°C isothermal gas chromatography method visualized in Figs. 1 and 2. The ninth vector was capacity factor and retention time for Figs. 1 and 2, respectively.

NAME	RS	ALPHA	PLATES	TF10%	TF5%	SKEW10%	SKEW5%	HFWD	K'	RT
ACETIC	0.00	0.00	3834.0	1.41	1.42	1.82	1.84	0.029	4.17	0.77
PROPIONIC	6.02	1.52	6195.0	1.45	1.51	1.90	2.03	0.033	6.28	1.09
ISOBUTYRIC	2.58	1.16	6622.0	1.26	1.27	1.52	1.53	0.036	7.28	1.24
BUTYRIC	5.72	1.36	7328.0	1.14	1.18	1.27	1.37	0.045	9.89	1.63
ISOVALERIC	4.14	1.24	7218.0	1.13	1.16	1.26	1.32	0.055	12.22	1.98
VALERIC	7.00	1.43	7353.0	1.13	1.16	1.27	1.32	0.075	17.39	2.76
CAPROIC	6.88	1.41	7033.0	1.06	1.09	1.11	1.18	0.107	24.50	3.83

Total variance accounted for:

In one dimension: 75.659%

In two dimensions: 91.760%

In three dimensions: 99.256%

Correlations between Attributes:

	RS	ALPHA	PLATES	TF10%	TF5%	SKEW10%	SKEW5%	HFWD	K'
RS	1.0000	0.8944	0.7984	-0.5365	-0.4494	-0.5354	-0.4372	0.6520	0.6945
ALPHA	0.8944	1.0000	0.9031	-0.4698	-0.3880	-0.4689	-0.3800	0.4369	0.4979
PLATES	0.7984	0.9031	1.0000	-0.7570	-0.7012	-0.7547	-0.6954	0.5226	0.5916
TF10%	-0.5365	-0.4698	-0.7570	1.0000	0.9938	0.9998	0.9915	-0.7839	-0.8171
TF5%	-0.4494	-0.3880	-0.7012	0.9938	1.0000	0.9931	0.9998	-0.7653	-0.7945
SKEW10%	-0.5354	-0.4689	-0.7547	0.9998	0.9931	1.0000	0.9907	-0.7838	-0.8164
SKEW5%	-0.4372	-0.3800	-0.6954	0.9915	0.9998	0.9907	1.0000	-0.7631	-0.7919
HFWD	0.6520	0.4369	0.5226	-0.7839	-0.7653	-0.7838	-0.7631	1.0000	0.9964
K'	0.6945	0.4979	0.5916	-0.8171	-0.7945	-0.8164	-0.7919	0.9964	1.0000

Attribute Coordinates:

Attribute Name	Attribute Coordinates:			Comunalities:			
	X	Y	Z	1 D	2 D	3 D	Total
RS	-0.74	0.61	-0.21	0.549	0.373	0.044	0.9657
ALPHA	-0.66	0.73	0.11	0.442	0.532	0.012	0.9864
PLATES	-0.85	0.41	0.33	0.716	0.168	0.112	0.9958
TF10%	0.96	0.24	-0.15	0.915	0.060	0.023	0.9975
TF5%	0.93	0.34	-0.16	0.859	0.113	0.027	0.9996
SKEW10%	0.96	0.25	-0.15	0.914	0.060	0.022	0.9964
SKEW5%	0.92	0.35	-0.17	0.852	0.120	0.028	0.9991
HFWD	-0.87	-0.13	-0.48	0.749	0.016	0.231	0.9959
K'	-0.90	-0.08	-0.42	0.813	0.007	0.177	0.9966

Object Coordinates:

Data Point Name	X	Y	Z
ACETIC	0.720	0.659	-0.194
PROPIONIC	0.446	-0.873	-0.199
ISOBUTYRIC	0.150	0.049	0.311
BUTYRIC	-0.176	-0.084	0.353
ISOVALERIC	-0.195	0.163	0.274
VALERIC	-0.357	-0.106	-0.100
CAPROIC	-0.587	0.193	-0.446

I. Parameter axes were based on interparameter correlations. Since  $k'$  (12 o'clock in Fig. 1) positively correlated with peak width at half height (0.9964), both parameters were plotted on nearly identical axes. Axes scales were based on normalized differences from the mean with high values corresponding to axes labels. For example, the high, midpoint and low values for resolution at 2 o'clock in Fig. 1 were: -1, 0 and +1 corresponding to 9.2, 4.6 and 0, respectively. The data point with the largest deviance from the mean was plotted at either the high or low ends of the axis. Clockwise starting at 1 o'clock, plates, resolution and  $\alpha$  were highly correlated and were plotted on similar axes. The

four asymmetry factors at 5 o'clock were highly correlated to each other and were negatively correlated to HFWD and  $k'$ . The negative correlation was visually represented by plotting asymmetry factors nearly 180° from HFWD as determined by the arccosines of the correlation coefficients. By relaxing the usual 90° orientation, all nine parameters were visualized in three dimensions.

In Fig. 2, normalized numerical values for each component were visualized by the use of orthogonal lines from propionic acid (4 o'clock) to each of the nine vectors. Propionic acid exhibited high asymmetry, low retention time and HFWD, and nearly mean plates, resolution and  $\alpha$ . Although retention

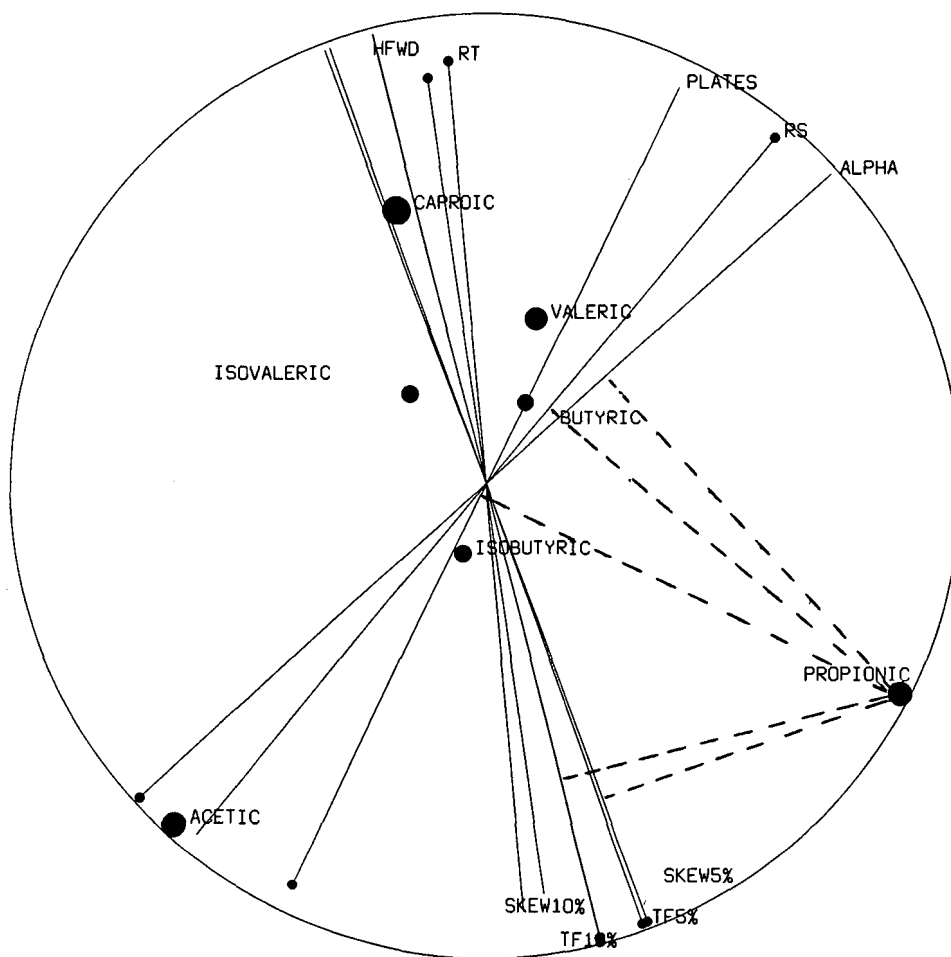


Fig. 2. System-suitability parameters using retention time. Non-orthogonal map of 100°C isothermal gas chromatography method as described in experimental section using 7 × 9 matrix in Table I. The ninth vector was retention time (RT). The perpendicular dotted lines from propionic acid (4 o'clock) to each of the nine vectors aid in visualizing the normalized numerical value for each component.



time was substituted for  $k'$  as the ninth vector, Figs. 1 and 2 were nearly identical because of the use of normalized data.

#### Method optimization

The utility of this visualization approach for method optimization was investigated in Fig. 3 in which resolution and plates for four isothermal temperatures for seven peaks were non-orthogonally mapped using the  $4 \times 14$  matrix in Table II. Resolution values for all four methods were highly correlated and were plotted on the same axes at 1 o'clock. Plates for each peak were not correlated

and were plotted on axes ranging from 2 o'clock to 5 o'clock. M1–100 DEGREES (7 o'clock) exhibited the lowest resolution for all peaks and the lowest plates for acetic and propionic acids. M3–80 DEGREES (2 o'clock) exhibited the highest plates for acetic and propionic acids and nearly mean values for all other parameters. M4–70 DEGREES and M3–80 DEGREES appeared to exhibit optimum resolution for this limited test.

In Fig. 4, a  $4 \times 35$  matrix consisting of five optimization parameters (resolution, plates,  $\alpha$ ,  $k'$  and tailing factor at 10% peak height) for seven components was non-orthogonally mapped.  $k'$ ,  $\alpha$  and res-

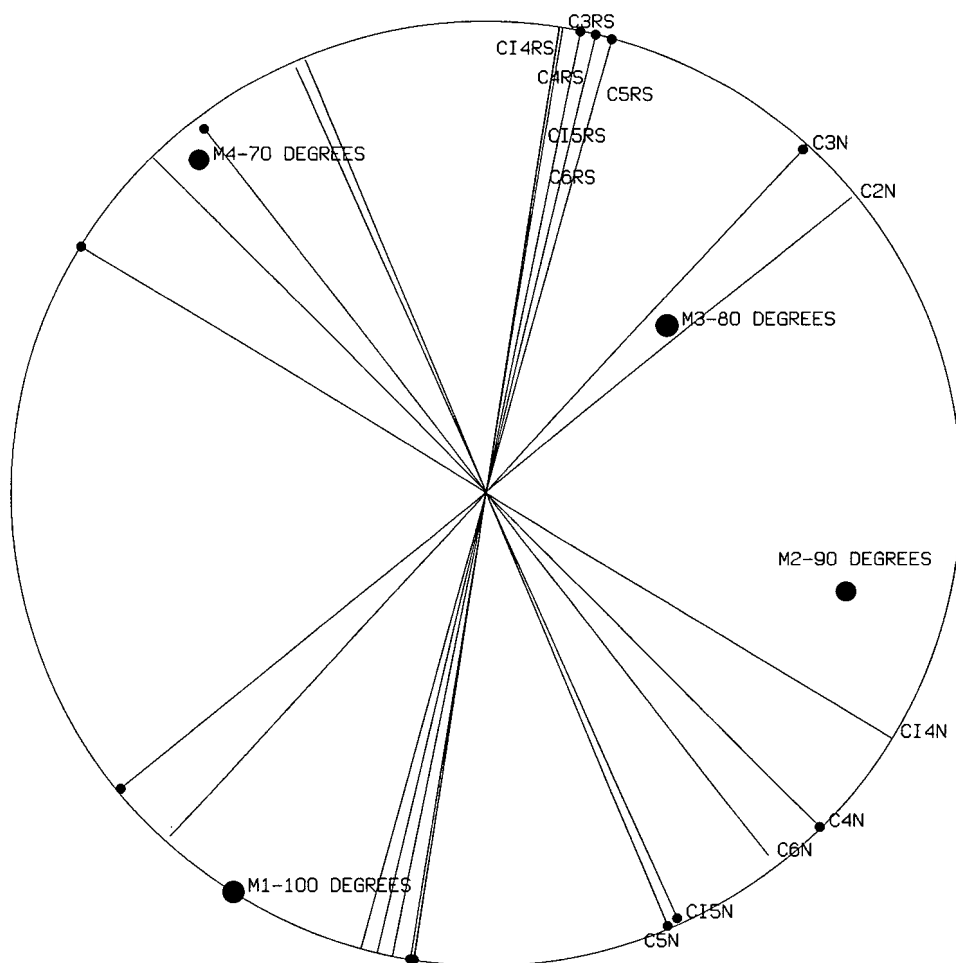


Fig. 3. Method comparison of plates and resolution. Non-orthogonal map comparing four isothermal gas chromatography methods 100°C (M1–100 DEGREES), 90°C (M2–90 DEGREES), 80°C (M3–80 DEGREES), 70°C (M4–70 DEGREES) methods using  $4 \times 14$  matrix and correlations in Table II representing resolution (C2RS, C3RS, C4RS, C5RS, C6RS) and theoretical plates (C2N, C3N, C4N, C5N, C6N) for acetic, propionic, isobutyric, butyric, isovaleric, valeric and isocaproic acids, respectively. Fields with zero values (C2RS) were not plotted.

TABLE II  
METHOD COMPARISON OF PLATES AND RESOLUTION

4 × 14 matrix and correlations representing resolution (C2RS, C3RS, C14RS, C4RS, C15RS, C5RS, C6RS) and theoretical plates (C2N, C3N, C14N, C4N, C15N, C5N, C6N) for acetic, propionic, isobutyric, butyric, isovaleric, valeric and isocaproic acids, respectively, comparing four isothermal gas chromatography methods: 100°C (M1-100 DEGREES), 90°C (M2-90 DEGREES), 80°C (M3-80 DEGREES), 70°C (M4-70 DEGREES). Visualized in Fig. 3.

"VFARSPL.DME",	"C2RS",	"C3RS",	"C14RS",	"C4RS",	"C15RS",	"C5RS",	"C6RS",	"C2N",	"C3N",	"C14N",	"C4N",	"C15N",	"C5N",	"C6N",
"VFA1000",	0.0000,	6.0200,	2.5800,	5.7200,	4.1400,	7.0000,	6.8800,	3834.5000,	6195.3000,	6621.9000,	7328.3000,	7218.0000,	7352.9000,	7032.7000,
"VFA900",	0.0000,	8.3800,	3.2700,	6.5100,	4.6100,	7.6200,	7.2900,	6661.4000,	7206.8000,	7174.7000,	7611.6000,	7041.9000,	7197.4000,	7644.1000,
"VFA800",	0.0000,	9.6300,	3.6500,	6.9400,	4.8900,	7.9500,	7.5600,	6426.1000,	7543.2000,	6709.8000,	7221.2000,	6623.4000,	6739.0000,	6350.6000,
"VFA700",	0.0000,	10.2700,	3.8200,	7.1500,	4.9200,	7.9700,	7.6000,	5699.9000,	7027.6000,	6052.3000,	6502.2000,	5709.1000,	5968.9000,	5618.8000,

Total variance accounted for:  
 In one dimension: - 74.497%  
 In two dimensions: 98.903%  
 In three dimensions: 100.000%

Correlations between Attributes:

	C3RS	C14RS	C4RS	C15RS	C5RS	C6RS	C2N	C3N	C14N	C4N	C15N	C5N	C6N
C3RS	1.0000	0.9999	1.0000	0.9943	0.9915	0.9958	0.7415	0.8171	-0.3784	-0.5905	-0.8310	-0.8480	-0.6586
C14RS	0.9999	1.0000	1.0000	0.9956	0.9928	0.9969	0.7441	0.8225	-0.3736	-0.5851	-0.8261	-0.8438	-0.6575
C4RS	1.0000	1.0000	1.0000	0.9946	0.9917	0.9962	0.7402	0.8175	-0.3797	-0.5911	-0.8308	-0.8481	-0.6608
C15RS	0.9943	0.9956	0.9946	1.0000	0.9993	0.9994	0.7815	0.8683	-0.3086	-0.5209	-0.7746	-0.7965	-0.6177
C5RS	0.9915	0.9928	0.9917	0.9993	1.0000	0.9975	0.8039	0.8839	-0.2740	-0.4909	-0.7541	-0.7761	-0.5883
C6RS	0.9958	0.9969	0.9962	0.9994	0.9975	1.0000	0.7599	0.8527	-0.3402	-0.5481	-0.7928	-0.8146	-0.6440
C2N	0.7415	0.7441	0.7402	0.7815	0.8039	0.7599	1.0000	0.9500	0.3381	0.0914	-0.2712	-0.2895	0.0079
C3N	0.8171	0.8225	0.8175	0.8683	0.8839	0.8527	0.9500	1.0000	0.1853	-0.0330	-0.3594	-0.3917	-0.1952
C14N	-0.3784	-0.3736	-0.3797	-0.3086	-0.2740	-0.3402	0.3381	0.1853	1.0000	0.9647	0.8059	0.8001	0.9198
C4N	-0.5905	-0.5851	-0.5911	-0.5209	-0.4909	-0.5481	0.0914	-0.0330	0.9647	1.0000	0.9325	0.9267	0.9486
C15N	-0.8310	-0.8261	-0.8308	-0.7746	-0.7541	-0.7928	-0.2712	-0.3594	0.8059	0.9325	1.0000	0.9984	0.8981
C5N	-0.8480	-0.8438	-0.8481	-0.7965	-0.7761	-0.8146	-0.2895	-0.3917	0.8001	0.9267	0.9984	1.0000	0.9105
C6N	-0.6586	-0.6575	-0.6608	-0.6177	-0.5883	-0.6440	0.0079	-0.1952	0.9198	0.9486	0.8981	0.9105	1.0000

Attribute Coordinates:

Attribute Name	Attribute Coordinates:			Communalities:			
	X	Y	Z	1 D	2 D	3 D	Total
C3RS	-0.99	0.16	0.03	0.974	0.025	0.001	1.0000
C14RS	-0.99	0.16	0.02	0.973	0.026	0.000	1.0000
C4RS	-0.99	0.16	0.02	0.975	0.024	0.001	1.0000
C15RS	-0.97	0.23	-0.04	0.944	0.054	0.002	1.0000
C5RS	-0.96	0.27	-0.03	0.927	0.072	0.001	1.0000
C6RS	-0.98	0.20	-0.05	0.957	0.040	0.002	1.0000
C2N	-0.62	0.77	0.12	0.390	0.594	0.016	1.0000
C3N	-0.73	0.67	-0.16	0.528	0.448	0.025	1.0000
C14N	0.52	0.85	0.05	0.271	0.727	0.002	1.0000
C4N	0.71	0.70	-0.07	0.501	0.495	0.004	1.0000
C15N	0.90	0.40	-0.16	0.812	0.163	0.025	1.0000
C5N	0.92	0.38	-0.11	0.841	0.148	0.011	1.0000
C6N	0.77	0.60	0.23	0.591	0.356	0.053	1.0000

Object Coordinates:

Data Point Name	Object Coordinates:		
	X	Y	Z
VFA1000	0.844	0.535	-0.026
VFA900	0.212	-0.758	0.092
VFA800	-0.352	-0.384	-0.124
VFA700	-0.704	0.607	0.059

olution values for all four methods were highly correlated and were clustered on axes at 11 o'clock, 12 o'clock, and 1 o'clock, respectively. Tailing factors for each of the seven components were not correlated and were plotted on axes ranging from 11 o'clock (C2T) to 8 o'clock (C5T). For example, M1-100 DEGREES (7 o'clock) exhibited the high-

est tailing factor for *n*-valeric and isobutyric acids. Using this expanded test, five optimization parameters for each of the seven components were simultaneously evaluated. M3-80 DEGREES (2 o'clock) still appeared to be the best compromise separation in that it exhibited nearly mean values for all five optimization parameters.

### Concentration-activity comparisons

Similar types of matrices were used in Figs. 5 and 6 to nonorthogonally visualize a multicomponent data set too large to interpret without the use of computerized statistical analyses. The objective was to visually determine if bacterial inoculation in lieu of antibiotic treatments could enhance ruminal fermentations by increasing concentrations of acetic and propionic acids.

In Fig. 5, mean component amounts for 5 bacterial concentrations, 2 diet protocols (12-h and 24-h

fermentations each) and for ten corresponding 0-h controls were non-orthogonally mapped using the  $30 \times 6$  matrix in Table III. All of the treatments with the highest bacterial concentration (treatment 9 as indicated by 24H9, 24M9, 12H9, and 12M9 labels) exhibited a significant visual deviation and positioned in the quadrant between 1 and 2 o'clock. The corresponding 0-h controls for treatment 9 (OH9 and OM9 at 4 o'clock) were similarly shifted from the other controls which were bunched at 5 o'clock. Although this observation is under investi-

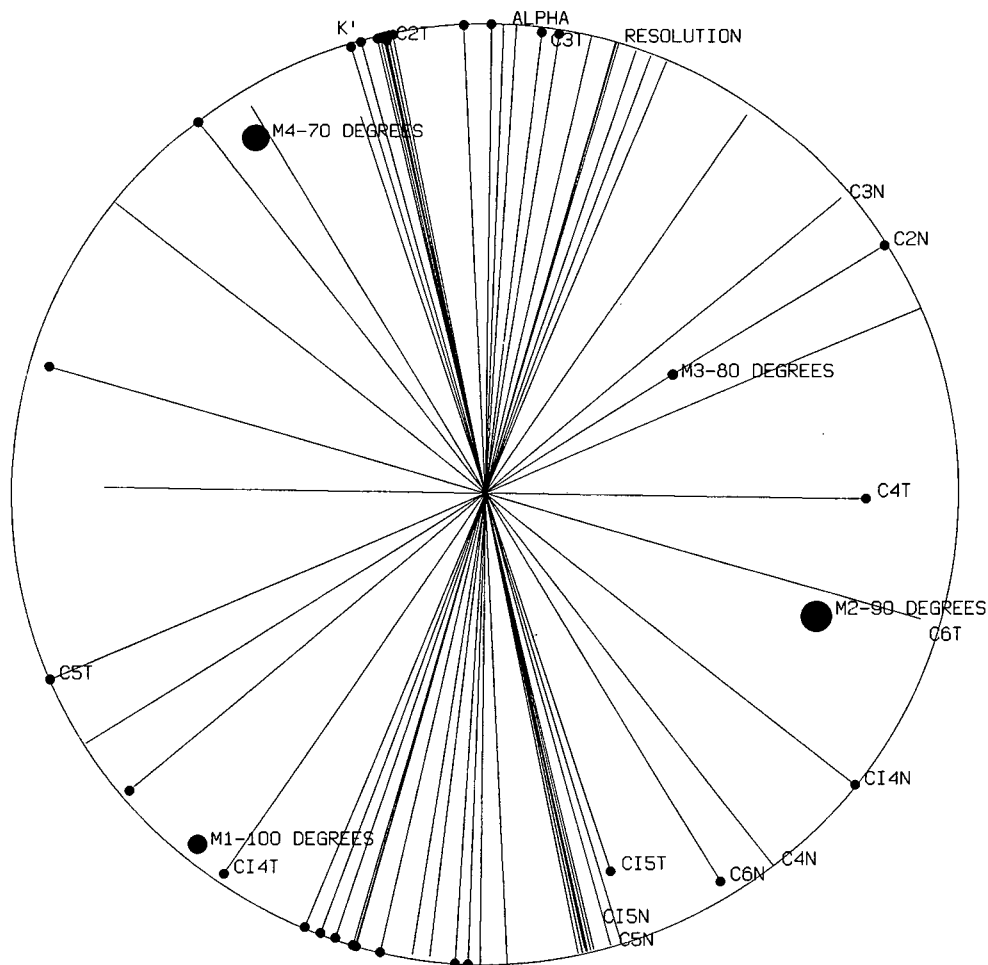


Fig. 4. Method comparison of plates, resolution, tailing factor,  $\alpha$  and  $k'$ . Non-orthogonal map comparing four isothermal gas chromatography methods 100°C (M1-100 DEGREES), 90°C (M2-90 DEGREES), 80°C (M3-80 DEGREES), 70°C (M4-70 DEGREES) methods using  $4 \times 35$  matrix representing resolution (C2RS, C3RS, C4RS, C5RS, C6RS), theoretical plates (C2N, C3N, C4N, C5N, C6N), tailing factor at 10% peak height (C2TF, C3TF, C4TF, C5TF, C6TF),  $\alpha$  (C2A, C3A, C4A, C5A, C6A), capacity factor (C2K, C3K, C4K, C5K, C6K) for acetic, propionic, isobutyric, butyric, isovaleric, valeric and isocaproic acids, respectively. Fields with zero values (C2RS and C2A) were not plotted.

gation, it appears that treatment 9 initially elevated the concentrations of acetic and propionic acids. The concentration-time-diet clustering in Fig. 5 was interesting in that the concentrations of acetic and propionic acid appeared to increase most significantly after 12-h fermentation and were not apparently affected by diet.

In Fig. 6, replicate results for all 20 treatments (5 bacterial concentrations, 2 fermentation times, 2 diets each, 4 replicates injected twice) and the corresponding 0-h controls (5 bacterial concentration, 2 diets, injected twice) were non-orthogonally

mapped using a  $180 \times 6$  matrix representing 180 chromatograms. Replicate reproducibility for treatment 9 can be visualized at 1 and 2 o'clock. The only significant visual outliers occurred at 5 o'clock and corresponded to duplicate injections of a 12-h fermentation sample (vfa. 79A and vfa. 80A, diet 1, no bacterial inoculation). The other 3 replicates for this treatment all exhibited higher concentrations of acetic acid.

Non-orthogonal visualization was found to be a useful tool for screening biologically active treatment protocols as well as for identifying anomalous

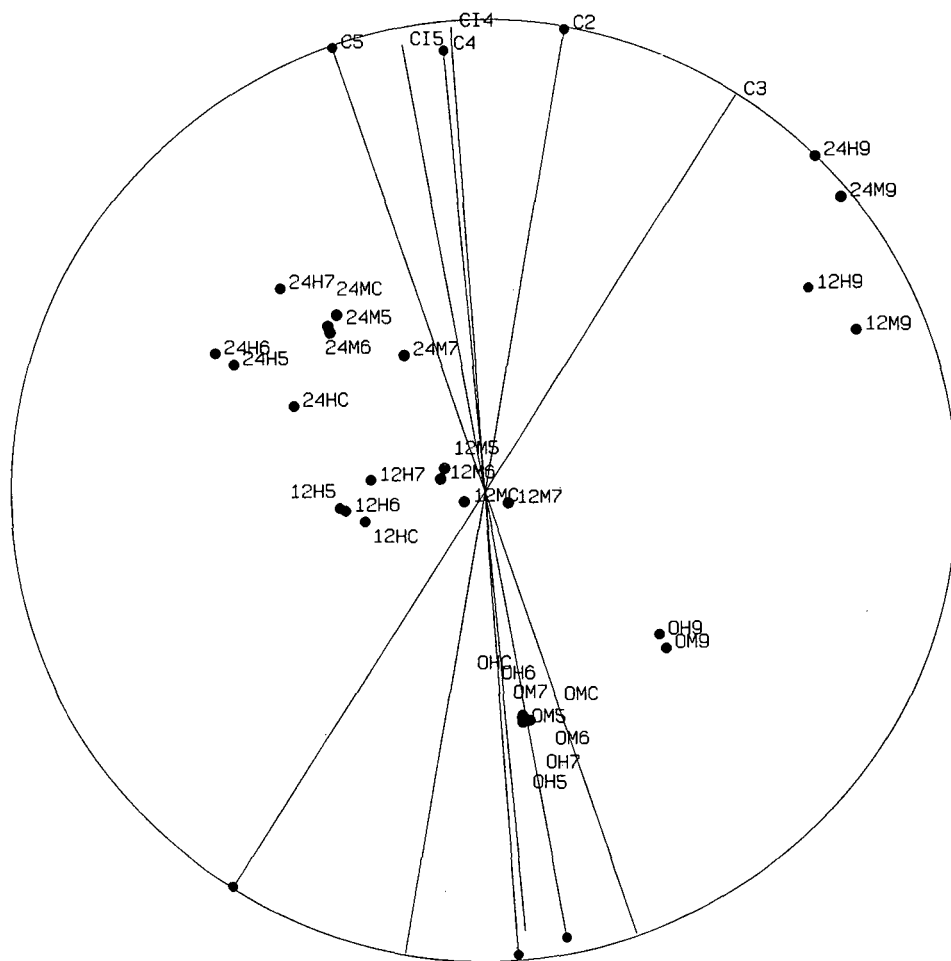


Fig. 5. Comparison of mean bacterial treatments. Non-orthogonal map comparing mean values for 5 bacterial inoculation concentrations: after 0-h fermentation (0HC, 0H5, 0H6, 0H7, 0H9), 12-hr (12HC, 12H5, 12H6, 12H7, 12H9), and 24-h fermentation (24HC, 24H5, 24H6, 24H7, 24H9) for acetic, propionic, isobutyric, butyric, isovaleric and valeric acids (C2, C3, C4, C5, C1, C2, C3, C4, C5, respectively) at 2 diets (M substituted for second diet) using  $30 \times 6$  matrix in Table III.

outliers. Computerized statistical analysis verifying these visual observations will be reported in future publications.

#### CONCLUSIONS

Using free-fatty acid model systems, multivariate visualization as automated in Echo Data's DataMax software was used to correlate, visualize, and verify the relationships of chromatography parameters. Two types of matrices were plotted: (1) chromatography parameters as the vectors and components as the objects (Figs. 1 and 2); (2) chromatog-

raphy parameters for each component as the vectors and methods or chromatograms as the objects (Figs. 3–6). The first type of matrix was shown to be suitable for visualizing the results for a single chromatogram, for clustering similar parameters such as skew and tailing factors, for verifying chromatography relationship such as the correlation between  $\alpha$  and resolution, and for comparing replicate results.

The second type of matrix was shown to have the same result as a mathematically-derived chromatographic response function in that an entire chromatogram was reduced to a single value, or to a coordinate in the case of a non-orthogonal map.

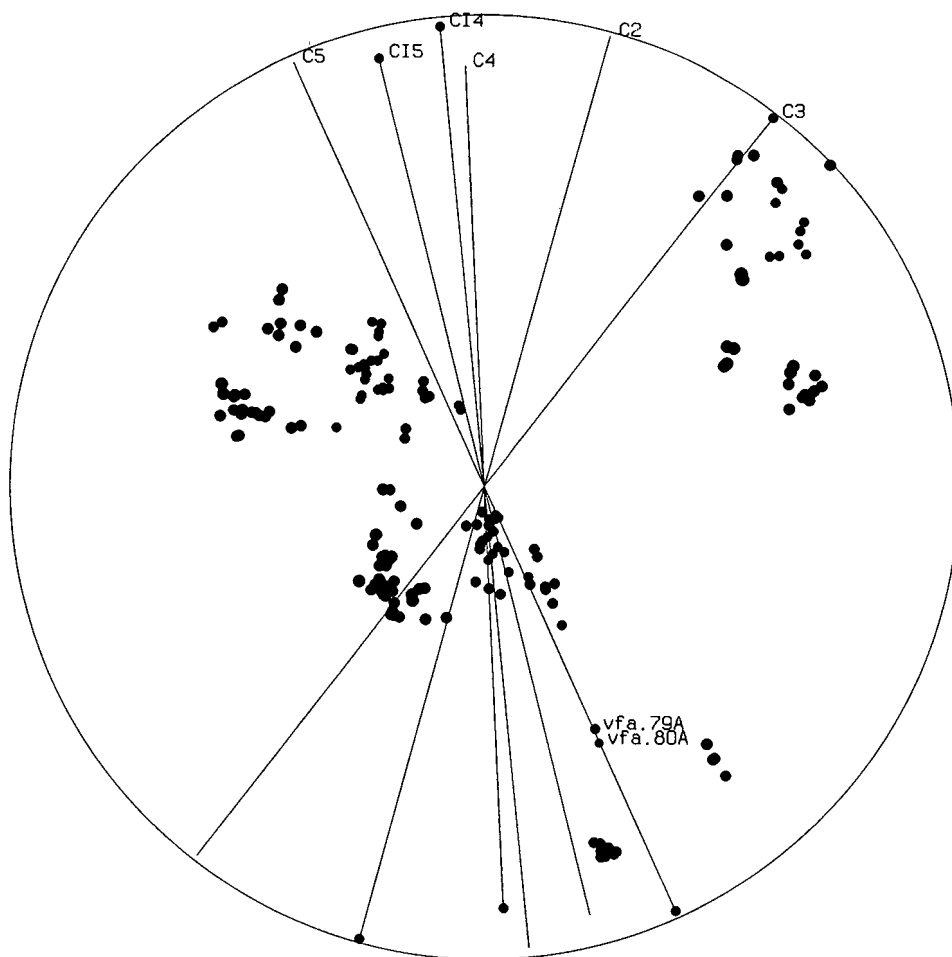


Fig. 6. Replicate comparison for 180 chromatograms. Non-orthogonal pendicular plot comparing replicated data for 5 bacterial inoculation concentrations for 2 diet protocols after 0-h, 12-h, and 24-h fermentation for acetic, propionic, isobutyric, butyric, isovaleric and valeric acids (C2, C3, C4, C5, CI4, CI5, respectively) using  $180 \times 6$  matrix representing 180 chromatograms. 12-h and 24-h treatments were replicated 4 times, 2 injections each. 0-h fermentation were unreplicated, 2 injections each.

TABLE III  
COMPARISON OF MEAN BACTERIAL TREATMENTS

30 × 6 matrix comparing mean values for 5 bacterial inoculation concentrations (C, 5, 6, 7, 9), 2 diet protocols (H and M), after 0-h, 12-h and 24-h fermentations (0, 12, 24) for acetic, propionic, isobutyric, butyric, isovaleric and valeric acids (C2, C3, CI4, C4, CI5, C5, respectively). Visualized in Fig. 5.

"BACTERIAL INOCULATION 12 & 24 HR MEANS",						
"",	"C2",	"C3",	"CI4",	"C4",	"CI5",	"C5",
"0HC",	24.0100,	6.6100,	0.6300,	5.2300,	0.7700,	0.6000,
"0H5",	24.0500,	6.6000,	0.6300,	5.2200,	0.7700,	0.6000,
"0H6",	24.1400,	6.6800,	0.6400,	5.2800,	0.7800,	0.6100,
"0H7",	23.6900,	6.6900,	0.6300,	5.1800,	0.7700,	0.6000,
"0H9",	33.0900,	16.9300,	0.7700,	5.7200,	0.8300,	0.6300,
"0MC",	23.9800,	6.5900,	0.6300,	5.2600,	0.7800,	0.6100,
"0M5",	23.2400,	6.4600,	0.6300,	5.1500,	0.7700,	0.6000,
"0M6",	24.2700,	6.7000,	0.6200,	5.2500,	0.7700,	0.6100,
"0M7",	23.7300,	6.6800,	0.6300,	5.1500,	0.7800,	0.6000,
"0M9",	32.1400,	16.5800,	0.7500,	5.5400,	0.8000,	0.6200,
"12HC",	36.3400,	13.9200,	0.8500,	8.1900,	1.0700,	1.4900,
"12H5",	36.9700,	13.9100,	0.8600,	8.3800,	1.1000,	1.5700,
"12H6",	36.7500,	14.0400,	0.8500,	8.8300,	1.0800,	1.5700,
"12H7",	38.6500,	18.1200,	0.8700,	9.8300,	1.1000,	1.6900,
"12H9",	56.9000,	52.0200,	1.0500,	12.3700,	1.2900,	1.6800,
"12MC",	42.1200,	17.8900,	0.8200,	12.2200,	0.9300,	1.5300,
"12M5",	44.5900,	18.7100,	0.8800,	12.6500,	0.9800,	1.6000,
"12M6",	43.1200,	18.3200,	0.8600,	12.6900,	0.9700,	1.5900,
"12M7",	42.7100,	20.3300,	0.8200,	10.9000,	0.9400,	1.5100,
"12M9",	56.4300,	51.1500,	0.9700,	12.4500,	1.1500,	1.6700,
"24HC",	44.1300,	19.4500,	0.9400,	11.5700,	1.2200,	2.0000,
"24H5",	45.8100,	19.8800,	0.9900,	12.7200,	1.2700,	2.2200,
"24H6",	46.3600,	19.7000,	0.9800,	14.1200,	1.2700,	2.2800,
"24H7",	51.2100,	27.1800,	1.0500,	15.7900,	1.3300,	2.3700,
"24H9",	68.5200,	60.4600,	1.1000,	19.4700,	1.3700,	2.1200,
"24MC",	50.7200,	24.0400,	0.9900,	19.0300,	1.1700,	2.1100,
"24M5",	52.3900,	24.9700,	1.0000,	19.1100,	1.1700,	2.1600,
"24M6",	50.3600,	24.0400,	0.9700,	18.8800,	1.1600,	2.1300,
"24M7",	50.4700,	25.7800,	0.9800,	15.5600,	1.1700,	1.9500,
"24M9",	67.9600,	58.3400,	1.0300,	20.0700,	1.2000,	2.1600,

Total variance accounted for:  
 In one dimension: 88.367%  
 In two dimensions: 96.122%  
 In three dimensions: 99.280%

Correlations between Attributes:

	C2	C3	CI4	C4	CI5	C5
C2	1.0000	0.9108	0.9513	0.9199	0.8786	0.8694
C3	0.9108	1.0000	0.7917	0.7217	0.7211	0.6195
CI4	0.9513	0.7917	1.0000	0.8952	0.9657	0.9448
C4	0.9199	0.7217	0.8952	1.0000	0.8266	0.9045
CI5	0.8786	0.7211	0.9657	0.8266	1.0000	0.9458
C5	0.8694	0.6195	0.9448	0.9045	0.9458	1.0000

Attribute Coordinates:

Attribute Name	Attribute Coordinates:			Comunalities:			
	X	Y	Z	1 D	2 D	3 D	Total
C2	-0.98	0.17	-0.07	0.961	0.030	0.004	0.9949
C3	-0.84	0.54	0.06	0.707	0.288	0.004	0.9979
CI4	-0.99	-0.07	0.10	0.972	0.005	0.009	0.9861
C4	-0.94	-0.09	-0.33	0.876	0.007	0.112	0.9953
CI5	-0.95	-0.17	0.25	0.901	0.030	0.061	0.9921
C5	-0.94	-0.32	-0.00	0.886	0.105	0.000	0.9905

(Continued on p. 12)



TABLE III (continued)

Object Coordinates:			
Data Point Name	X	Y	Z
OHC	0.489	-0.093	-0.016
OH5	0.489	-0.093	-0.016
OH6	0.478	-0.081	-0.010
OH7	0.491	-0.092	-0.014
OH9	0.308	-0.372	0.030
OMC	0.484	-0.081	-0.012
OM5	0.494	-0.081	-0.013
OM6	0.490	-0.098	-0.019
OM7	0.488	-0.086	-0.009
OM9	0.337	-0.387	0.017
12HC	0.066	0.258	0.086
12H5	0.037	0.311	0.097
12H6	0.043	0.298	0.075
12H7	-0.024	0.245	0.066
12H9	-0.430	-0.687	0.148
12MC			0.023
12M5			-0.050
12M6			-0.028
12M7			0.026
12M9			-0.341
24HC			-0.184
24H5			-0.272
24H6			-0.294
24H7			-0.431
24H9			-0.711
24MC			-0.352
24M5			-0.375
24M6			-0.338
24M7			-0.291
24M9			-0.624
			0.045
			0.087
			0.096
			-0.050
			-0.788
			0.407
			0.535
			0.574
			0.435
			-0.703
			0.336
			0.317
			0.332
			0.173
			-0.756
			-0.089
			-0.067
			-0.075
			-0.050
			0.063
			0.086
			0.089
			0.051
			0.055
			0.011
			-0.116
			-0.117
			-0.121
			-0.029
			-0.100

Unlike the chromatographic response functions, data were not simplified and all parameters were simultaneously considered. Practical applications include the visualization of multidetector, multi-wavelength, multicolumn data. Two examples were demonstrated: (1) evaluation of four chromatography methods by non-orthogonally mapping a  $4 \times 35$  matrix representing resolution, theoretical plates, tailing factor,  $\alpha$  and capacity factor for a 7-component mixture; (2) identification of optimum concentration, time-course effects, and replicate reproducibility by non-orthogonally mapping a  $180 \times 6$  matrix representing 180 multicomponent chromatograms. In each case, non-orthogonal visualization was found to facilitate more rapid screening than currently possible by the use of computerized statistical analysis alone.

In summary, non-orthogonal mapping was found to be a useful and accurate technique for visualizing chromatography data because of the high correlations inherent in most chromatography data. This technique is a useful addition to the mathematical approaches described by Guiochon and co-workers [1,2] in which chromatography decisions were based on simultaneous consideration of all measurable variables. Additional chromatographic applications and areas for research include: (1) multiwavelength, multidetector and multicolumn forensic fingerprinting; (2) pattern recognition of complex environmental pollutants such as polychlorinated biphenyls; (3) structure-activity and structure-reactivity screening; (4) identification of significant process parameters; (5) quality control

and replicate comparison of multicomponent samples in the petroleum, perfume, agricultural and food industries. Automated computer processing of separation parameters makes this technique feasible for fast, on-line monitoring of refinery, polymer, medicinal and other chemical processes. The observation that retention time could be substituted for capacity factor resolves the concern expressed by Berridge [6] of computerized determination of column void volumes.

#### ACKNOWLEDGEMENTS

The authors acknowledge the invaluable technical discussions with George Schreiner, Jon Duffy, Professors Georges Guiochon, Linda Betz, Stephen Brown, Barry Lavine and the assistance of Sonya Geiser in manuscript preparation. Published as miscellaneous paper No. 1263 of the Delaware Agricultural Experiment Station.

#### REFERENCES

- 1 J. P. Bounine and G. Guiochon, *Analisis*, 12 (1984) 175-193.
- 2 J. P. Bounine, G. Guiochon and H. Colin, *J. Chromatogr.*, 298 (1984) 1-20.
- 3 S. B. Hendrix and B. L. Brown, *The Surface of Ordered Profiles: A Multivariate Graphical Data Analysis Method*; Proc. 1990 Am. Statistical Assoc., American Statistical Association, Anaheim, CA, 1990.
- 4 N. Hirsh and B. L. Brown, *Visualization in Scientific Computing*, IEEE Computer Society, Los Angeles, CA, 1990, pp. 190-208.
- 5 B. L. Brown, R. N. Williams and C. D. Barlow, *J. PascalAda & Modula-2*, Mar/Apr (1984) 19-24, 48.

- 6 J. C. Berridge, *Techniques for the Automated Optimization of HPLC Separations*, Wiley, New York, 1985.
- 7 L. Kung, Jr. and A. O. Hession, University of Delaware Agriculture Experimental Station, personal communication of unpublished results.
- 8 L. Kung, Jr., R. S. Tung and L. L. Slyter, *J. Animal Sci.*, 70 (1992) 281–288.
- 9 *SAS User's Guide: Statistics*, SAS Inst., Inc., Cary, NC, 1985.
- 10 *US Pharmacopeia, USP XXII*, National Formulary XVII, Rockville, MD, 1990, pp. 1710–1711.
- 11 *Draft Guideline for Submission of Supportive Analytical Data for Methods Validation in New Drug Applications*, US Food and Drugs Administration, Washington, DC, 1984.
- 12 J. D. Justice, *ReportWrite Plus User's Manual; The Custom Report Generator for Chrom Perfect*, Justice Innovations, Palo Alto, CA, 1992.
- 13 B. L. Brown and L. Fluckiger, *Multivariate Graphical Analysis with DataMax*, Echo Data, Orem, UT, 1991.
- 14 J. D. Justice, *RESULTS User's Manual for the Chrom Perfect Chromatography Data System*, Justice Innovations, Palo Alto, CA, 1992.



# Faster quantitative evaluation of high-performance liquid chromatography–ultraviolet diode-array data by multicomponent analysis

Jean-Louis Excoffier, Maureen Joseph, John J. Robinson and Terry L. Sheehan

Varian Chromatography Systems, 2700 Mitchell Drive, Walnut Creek, CA 94598 (USA)

---

## ABSTRACT

Multicomponent analysis is a proven technique to analyze mixes of known UV-absorbing compounds in unknown amounts. While it is routinely used in spectrophotometers, its application to chromatography has so far been limited. This paper discusses an approach to obtain fast and accurate quantitation of unresolved chromatographic data, while providing for the detection of unexpected impurities. The applications of the technique to different conditions of chromatographic resolution are discussed, along with its potential for increasing sample throughput.

---

## INTRODUCTION

Diode arrays are routinely used for qualitative analysis: spectra are used to confirm the identity of a peak, and spectral differences are exploited to assess peak purity. Quantitative analysis, however, still relies on the integration of unidimensional data, and therefore requires baseline resolution of all the compounds to be accurately quantitated.

Overlapping peaks are a fact of the chromatographer's life. Statistical studies [1,2] have shown that overlapping peaks are a likely occurrence in complex mixture, even with high efficiency separations. Even when baseline separation is possible, it may not be desirable, as costs increase with analysis time. Hence, there is an interest in multivariate techniques for the analysis of coelutions.

Different deconvolution techniques based on factor analysis have been proposed in the past to attempt to resolve an overlap of compounds with different UV spectra without knowledge of these spectra [3–5]. These techniques have several limita-

tions: (i) approaching zero resolution, different spectra combine into a single factor; (ii) in the generic case of three or more peaks with low resolution, the problem has an infinity of solutions, all of which satisfy the constraints applied; (iii) not providing reference spectra limits these techniques to qualitative results.

On the other hand, multicomponent analysis (MCA) based on reference spectra works at any degree of resolution and provides accurate quantitative results validated by qualitative results. It also provides an optimum tool for the detection of unexpected impurities.

## THEORETICAL

### *Multicomponent analysis*

The basic hypothesis is that the unknown spectrum **U** results from the combination of known spectra **A**, **B**, **C** in “amounts” *a*, *b*, *c*, ...

$$\mathbf{U} = a \mathbf{A} + b \mathbf{B} + c \mathbf{C} + \dots \quad (1)$$

This system of linear equations can be expressed in matrix notation (**S** is the matrix of the spectra, **X** is the solution vector *a*, *b*, *c*, ...):

$$\mathbf{U} = \mathbf{S} \cdot \mathbf{X} \quad (2)$$

---

Correspondence to: Jean-Louis Excoffier, Varian Chromatography Systems, 2700 Mitchell Drive, Walnut Creek, CA 94598, USA.

In the typical situation there are more wavelengths than compounds analyzed and the system is overdetermined. The matrix  $S$  is not square and cannot be inverted. The system is resolved by a simple "least squares" method. First, both sides of the equation are multiplied on the left by the transpose of the spectra matrix:

$${}^tS \cdot U = {}^tS \cdot S \cdot X \quad (3)$$

then the square matrix  ${}^tS \cdot S$ , which is the correlation matrix of the reference spectra can be inverted, provided the reference spectra are linearly independent. The solution is therefore given by:

$$X = ({}^tS \cdot S)^{-1} \cdot {}^tS \cdot U \quad (4)$$

Because the system is overdetermined, the validity of the decomposition can be assessed by comparing the original data set or target spectrum with the reconstructed spectrum obtained by combining the reference spectra in the calculated amounts. The mathematical aspects of this analysis have been presented in greater detail by Blackburn [6].

#### APPLICATION OF MCA TO CHROMATOGRAPHY

In order to apply this method to HPLC with diode array detection, the concept of *area spectrum* was developed. An area spectrum is the result of the baseline-corrected integration of a region of a chromatogram at each wavelength, and is therefore a spectrum whose coordinates are expressed as peak area instead of peak height. An area spectrum can be thought of as the baseline-corrected spectrum of an elution fraction (Fig. 1a and b). This elution fraction might contain a single peak or a series of closely eluting peaks.

The area spectrum of a pure peak is identical in shape to the spectrum of the compound. Its magnitude represents an amount injected for a given detection system at a given flow-rate.

#### Spectrum analysis

Once area spectra have been collected for injections of known amounts of standards, the area spectrum corresponding to the overlapping peak of an unknown mix can be analyzed by MCA to provide quantitative results (Table I).

By computing the linear combination of the reference spectra with the multiplicative factors

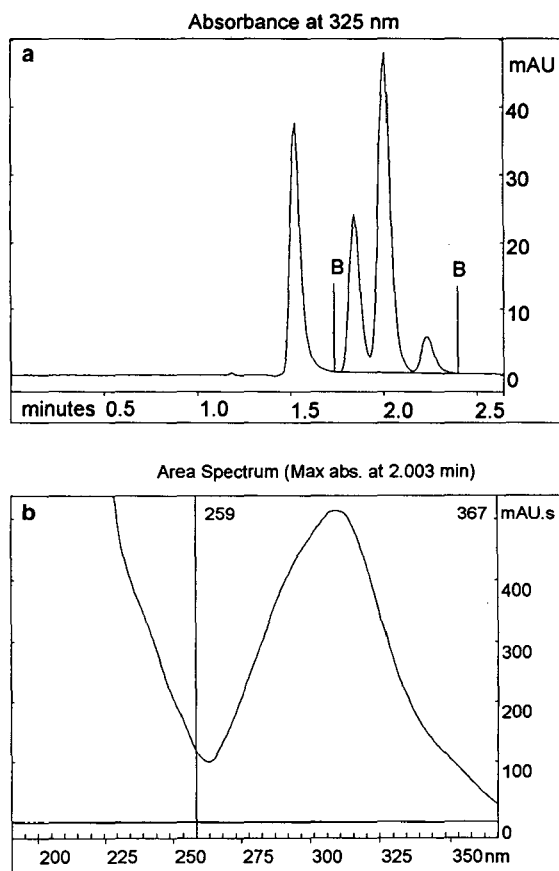


Fig. 1 (a) Integration of a chromatographic region to obtain an area spectrum, showing integration limits (B) and subtracted baseline. (b) Resulting area spectrum.

determined, one obtains a *reconstructed spectrum*, which ideally would be identical to the original or *target spectrum*. To assess the validity of the quantitative results, the reconstructed spectrum is com-

TABLE I  
SPECTRUM ANALYSIS RESULTS OVER 259–367 nm

Name	Amount
MA	0.175 $\mu\text{g}$
OS	0.134 $\mu\text{g}$
OMC	0.119 $\mu\text{g}$
Similarity	1.00000
Dissimilarity	0.00192

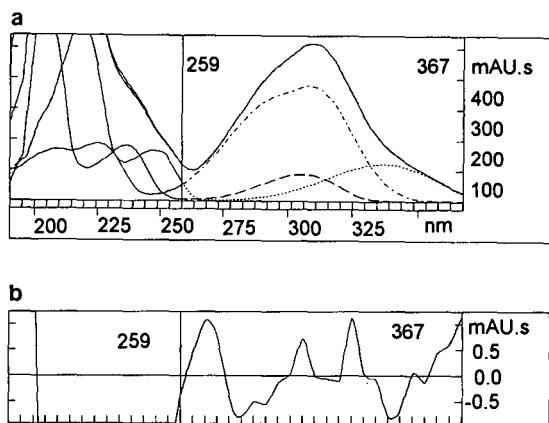


Fig. 2. (a) Spectral overlay. ····· = OMC; ---- = MA; - · - · - = OS; ——— = sum and target. (b) Expanded difference between reconstructed sum and target.

pared to the target spectrum. This comparison can be carried out by graphical and numerical methods.

The graphical evaluation consists of an overlay of the target, the reconstructed sum, and the scaled component spectra (Fig. 2a). Because such a visual evaluation is subjective, small differences are hard to quantify. To make the difference between the target and the reconstructed sum easier to visualize, this difference is plotted separately on an expanded scale (Fig. 2b).

The numerical evaluation of the comparison is provided by two complementary parameters: similarity and dissimilarity. The similarity is also known as the correlation coefficient and is the traditional mathematical approach to comparing two sets of data. However, when the spectra are very similar, the correlation coefficient gets very close to one, is a quadratic measure of the difference between the spectra and is, therefore, not a very human-friendly tool. From the observation that the correlation coefficient is the cosine of the angle between the two vectors stems the idea of using the sine of the angle, which can be called dissimilarity. This parameter has an interesting property: since the sine function is a linear measure of small angles, the dissimilarity provides a linear measurement of the impurity level when comparing to a pure reference.

In a mathematical form,  $A$  and  $B$  being two spectra of coordinates  $A_i$  and  $B_i$ , the parameters can be expressed as:

$$\text{Sim}(A, B) = \frac{\sum A_i B_i}{\sqrt{\sum A_i^2} \sqrt{\sum B_i^2}} \quad (5)$$

$$\text{Dissim}(A, B) = \sqrt{1 - \text{Sim}^2(A, B)} \quad (6)$$

Identical spectra have a similarity of 1 and a dissimilarity of 0. Spectra with a dissimilarity of 0.001 have a similarity of 0.999999. A dissimilarity of 0.002 correspond to a double level of the same impurity, while the corresponding similarity value would be 0.999996.

The dissimilarity parameter can be used to empirically or theoretically establish an acceptable error level based on the noise level. An empirical approach will take into account all experimental errors, instead of basing predictions on a model of the error.

### Chromatogram analysis

At each point of the chromatographic region integrated, the spectrum can be decomposed on the reference spectra. This provides an absorbance value for each component and a residual error. As a result, the individual peak profiles and the sum chromatogram can be reconstructed and overlaid to the original chromatogram (Fig. 3a). Basic parameters such as retention time, peak height, peak width, and resolution can be derived from the peak profiles (Table II).

### Error analysis

The residual error between the reconstructed spectrum and target spectrum in each point of the

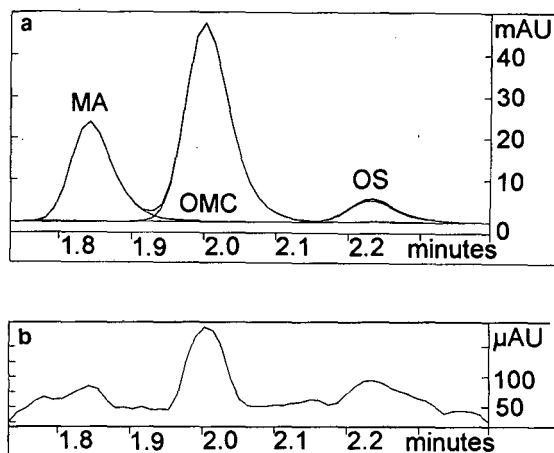


Fig. 3. (a) Reconstructed peak profiles. (b) Error chromatogram.



TABLE II  
PLOT ANALYSIS RESULTS AT 325 nm

Name	$t_R$ (min)	Peak height mAU	Peak width (s)	$R_s$
MA	1.842	23.86	4.1	—
OMC	2.002	47.88	4.2	1.37
OS	2.231	5.08	4.6	1.85

chromatogram can be reduced to a root mean square value:

$$\text{RMS} = \sqrt{\frac{\sum_{i=1}^{i=n} (\mathbf{t}_i - \mathbf{r}_i)^2}{n}} \quad (7)$$

where  $\mathbf{t}_i$  and  $\mathbf{r}_i$  are the coordinates of the target and reconstructed spectra at channel  $i$ . Plotting this residual error for the whole region analyzed will indicate the location of spectral discrepancies caused by unexpected impurities (Fig. 3b). It is equivalent to plotting the modulus of the result of spectral suppression of the component spectra from the original chromatogram [7]. This error plot detects any spectral characteristics that cannot be explained by the component spectra and is therefore an optimum tool for the detection of unexpected impurities.

#### Application to purity analysis

It is worth mentioning that this technique can be used to analyze the spectral homogeneity of a peak independently of any reference. In this case, every spectrum in the peak is compared to the area spectrum, *i.e.*, the average spectrum of the peak. The error plot would reveal the magnitude and location of the spectral discrepancy. An RMS threshold can be derived from the noise level, and used as an objective purity criterion. The threshold can be determined empirically or based on the error analysis theory developed by Malinovski [8–10].

#### Other sources of error

Since MCA is based on linear mathematical techniques, any non-linearity in the spectra results in spectral inhomogeneity. Besides the well-known

scattered light effect, typically observed at absorbances greater than 1.5 AU, non-linearity can also result from scan rate and optical bandwidth effects.

The scanning effect, due to concentration changes during the scanning of the spectrum, can be avoided by a correction in the scanning software as advocated by Keller *et al.* [11] and implemented in the instrumentation used in this study since 1985. As reported by Dose and Guiochon [12], the diode-array hardware typically averages the intensity across the optical bandwidth. This average intensity does not follow the Beer-Lambert law, since the average absorbance is not the logarithm of the average intensity. As a result, regions of fine structure or of high slope/absorbance ratio will show small non-linearities at relatively low absorbances (100 mAU). The effect of these non-linearities may exceed the noise level and create an error pattern. However, since this effect is concentration dependent, the pattern will be centered on the peak. An isolated peak in the error plot, not lined up with one of the component peaks, can only be interpreted as an impurity.

#### EXPERIMENTAL

Mixes of four sunscreen components were analyzed under various resolution conditions: baseline resolution, partial resolution, and no resolution.

#### Instrumentation

All experiments were performed on a Varian LC Star Workstation, composed of a 9010 ternary gradient pump, 9100 AutoSampler, PolyChrom 9065 diode-array detector, equipped with Rev C LC Star Workstation Software, and Rev E PolyView Spectral Processing Software (Varian Chromatography Systems, Walnut Creek, CA, USA). The column used for the separation was a Varian MicroPak SP-C8-IP-5, 5  $\mu\text{m}$ , 15 cm  $\times$  4.0 mm I.D. (Varian, Sunnyvale, CA, USA).

#### Chemicals

The sunscreen agents, menthyl-*o*-aminobenzoate (MA), 2-ethylhexyl *p*-methoxycinnamate (OMC), and 2-ethylhexyl salicylate (OS), were supplied by Haarman & Reimer (Springfield, NJ, USA). The fourth sunscreen agent 2-hydroxy-4-methoxybenzophenone (OXY, oxybenzone) was supplied by Sig-

ma (St. Louis, MO, USA). All reagents were dissolved in methanol. All solvents were supplied by Fisher Scientific (Fair Lawn, NJ, USA). The methanol was optima grade and the water was HPLC grade.

#### Chromatographic procedures

**Baseline resolution.** A complete separation of the four sunscreen components was achieved using a mobile phase gradient of methanol–water (75:25) to methanol–water (95:5) in 8 min at a flow-rate of 1 ml/min. Acetic acid was added to the mobile phase at 0.3%. The 9065 Polychrom diode-array detector was set to display the chromatogram at 306 nm. Data was acquired over the 190–369 nm wavelength range.

A complete separation was also obtained isocratically on the same column with a mobile phase of methanol–water (85:15) at 1 ml/min. A PolyView–MCA library was built to quantitate the sunscreen components based on injections of the individual components using the same mobile phase conditions as the analysis. The library amounts (on column) were: OXY = 406.8 ng, MA = 293.2 ng, OMC = 278.8 ng, and OS = 440.4 ng.

**Partial resolution.** In order to reduce the resolution, the mobile phase was adjusted to 100% methanol and run isocratically at both 1 ml/min and 2 ml/min. A library was built using the same standards as above, but injected individually using the 100% methanol mobile phase.

**Zero resolution.** In this case the sunscreen mixture was reduced to three components (OMC, MA, OS) and a 50 ft. length of coiled stainless-steel tubing was inserted in place of the analytical column. The mobile phase was 100% methanol. Mixtures of the sunscreens were analyzed over the flow-rate range 1–4 ml/min. The mixture injected contained 538.5 ng OMC, 448.5 ng MA, and 349.5 ng OS. To build the library for use with the PolyView–MCA software standard solutions of the sunscreen components were injected individually. These levels were OS = 862 ng, MA = 1.913 ug, and OMC = 6.344 ug. A new library was built since the mobile phase contained no acetic acid, and spectral shifts could occur due to the change in mobile phase.

## RESULTS AND DISCUSSION

#### Baseline resolution

The gradient conditions led to a baseline separation in 10 min (Fig. 4). Results achieved with MCA are presented in Table III. The interpolating baseline correction removes any baseline effects due to the gradient profile. The standard for the first compound (OXY) was found to contain an impurity interfering with the other three and therefore was not used in studies at lower resolutions.

#### Partial resolution

The plot analysis (Fig. 3a) shows the reconstructed peak profiles and a residual error or less

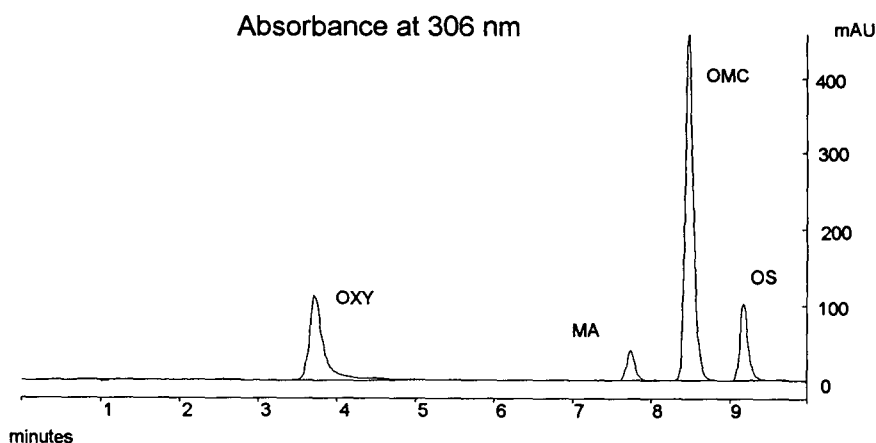


Fig. 4. Baseline separation in 10 min (gradient).

TABLE III  
QUANTITATION RESULTS FOR BASELINE SEPARATION ( $n = 6$ )

Compound	Resolution	Accuracy (%)	Precision (%)	$k'$
2-Hydroxy-4-methoxybenzophenone	9.20	101	1.34	2.36
Menthyl- <i>o</i> -aminobenzoate	16.90	98.1	0.87	5.98
2-Ethylhexyl <i>p</i> -methoxycinnamate	4.13	97.1	0.27	6.66
2-Ethylhexyl salicylate	4.00	99.5	2.7	7.29

TABLE IV  
QUANTITATION RESULTS WITH LIMITED RESOLUTION ( $n = 6$ )

Compound	1 ml/min				2 ml/min			
	Resolution	Accuracy (%)	Precision (%)	$k'$	Resolution	Accuracy (%)	Precision (%)	$k'$
Menthyl- <i>o</i> -aminobenzoate	8.00	102	1.42	0.79	2.83	100	0.21	0.60
2-Ethylhexyl <i>p</i> -methoxycinnamate	1.05	01	0.58	0.92	0.69	101	0.26	0.69
2-Ethylhexyl salicylate	1.99	101	0.84	1.17	1.62	95.4	0.84	0.89

TABLE V  
FIA QUANTITATION WITH ZERO RESOLUTION ( $n = 6$ )

Compound	4 ml/min			3 ml/min		
	Resolution	Accuracy (%)	Precision (%)	Resolution	Accuracy (%)	Precision (%)
Methyl- <i>o</i> -aminobenzoate	0.00	100.6	0.4	0.00	99.6	0.4
2-Ethylhexyl <i>p</i> -methoxycinnamate	0.00	98.0	0.5	0.00	98.0	0.4
2-Ethylhexyl salicylate	0.00	102.3	0.8	0.00	96.0	0.6

Peak Profiles and Error Analysis at 306 nm

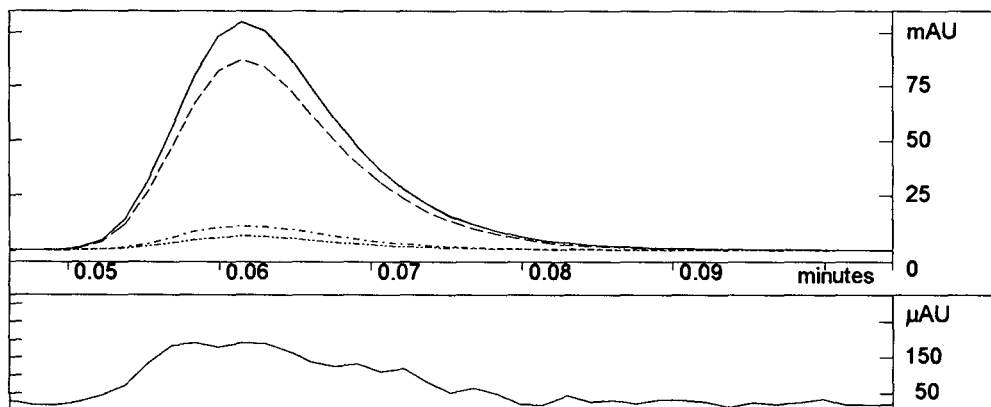


Fig. 5. Reconstructed peak profiles at zero resolution. --- = OMC; - · - · - = OS; · · · · · = MA; ——— = sum and target.

TABLE VI  
SAMPLE THROUGHPUT VS. TYPE OF SEPARATION

Separation	Run time (min)	Equilibration time (min)	Report time (min)	Total analysis time (min)	Samples per hour
Baseline (gradient)	10	10	1.5	21.5	2.8
Baseline (isocratic)	16	0	1.5	17.5	5.2
Incomplete	1.5	0	1.5	3	20
FIA	0.1	0	1.5	1.6	37.5

than 150  $\mu$ AU (Fig. 3b). Table IV summarizes the results for flow-rates of 1 and 2 ml/min. It is worth noting that both sets of results were obtained based on the same reference area spectra acquired at 2 ml/min, which confirms the assumption that area spectra are inversely proportional to the flow-rate.

#### Zero resolution

The flow injection simulation led as expected to zero resolution. The plot analysis reveals the peak profiles of the different compounds. MCA analysis performed as well in these conditions (Fig. 5). Table V summarizes the results as flow-rates of 3 and 4 ml/min. In all cases, accuracy and precision are within the range expected from experimental errors. A quick estimate of the analysis cycle time achieved under different conditions (adding an isocratic baseline separation) shows that MCA can conservatively provide a 5-fold improvement in sample throughput (Table VI).

Poor baseline correction would have an adverse effect on this technique. A practical limitation in trying to speed up a separation is the interference between the void peak and the least retained peaks.

#### CONCLUSIONS

MCA can automate fast quantitation of unresolved chromatographic data, while providing peak identity confirmation and purity evaluation. The validity of the quantitative results is supported by

error analysis features that are used to establish objective fit criteria. A fused group can be analyzed as long as it is baseline-resolved from other groups (or the void peak) and composed of 2 to 6 known components which have different enough spectra. When working with partial separations, a 5-fold increase in sample throughput over complete separations required by common quantitation methods can be achieved. The application to flow injection analysis (FIA) must be limited to mixtures of 2 to 6 compounds. More complex samples need some degree of separation.

#### REFERENCES

- 1 J. M. Davis and J. C. Giddings, *Anal. Chem.*, 55 (1983) 418.
- 2 G. Guiochon, D. P. Herman and M. F. Gonnord, *Anal. Chem.*, 56 (1984) 995-1003.
- 3 W. H. Lawton and E. A. Sylvester, *Technometrics*, 13 (1971) 617-633.
- 4 P. J. Gemperline, *Anal. Chem.*, 58 (1986) 2656-2663.
- 5 D. W. Osten and B. R. Kowalski, *Anal. Chem.*, 56 (1984) 991-995.
- 6 A. J. Blackburn, *Anal. Chem.*, 37 (1965) 1000-1003.
- 7 A. F. Fell, H. P. Scott, R. Gill and A. C. Moffat, *J. Chromatogr.*, 282 (1983) 123-140.
- 8 E. R. Malinowski and D. G. Howery, *Factor Analysis in Chemistry*, Wiley, New York, 1980.
- 9 E. R. Malinowski, *Anal. Chem.*, 49 (1977) 606-612.
- 10 E. R. Malinowski, *Anal. Chem.*, 49 (1977) 612-617.
- 11 H. R. Keller, D. L. Massart, P. Kiechle and F. Erni, *Anal. Chim. Acta*, 256 (1992) 125-131.
- 12 E. V. Dose and G. Guiochon, *Anal. Chem.*, 61 (1989) 2571-2579.



# Deuterium nuclear magnetic resonance spectroscopy as a probe for reversed-phase liquid chromatographic bonded phase solvation: methanol and acetonitrile mobile phase components

David M. Bliesner<sup>☆</sup> and Karen B. Sentell

Department of Chemistry, University of Vermont, Burlington, VT 05405-0125 (USA)

---

## ABSTRACT

Using the inversion-recovery method, deuterium longitudinal relaxation times, ( $T_1$ ), of [ $^2\text{H}_4$ ]methanol and [ $^2\text{H}_3$ ]acetonitrile in enriched methanol–water and acetonitrile–water mobile phases were measured for the neat binary mixtures, and for the mixtures in contact with two different monomeric  $\text{C}_{18}$  reversed-phase stationary phases. Changes in the deuterium relaxation times for the organic modifiers in contact with the stationary phase compared to those observed in neat solution give a qualitative understanding of the degree of association of the organic components with the stationary phase. Both bulk solution microstructure and stationary phase  $\text{C}_{18}$  bonding density play important roles in determining bonded phase solvation.

---

## INTRODUCTION

Reversed-phase liquid chromatography (RPLC) is one of the most widely used methods for separating complex mixtures of compounds with widely varying polarities [1]. However, despite its widespread use, methods development for RPLC separations is often complex and time consuming. This is a manifestation of the overall dearth of understanding about solute retention at the molecular level. Separations in RPLC are thermodynamic processes involving the transfer of solute between the mobile and stationary phases. Originally these transfer processes were modeled in terms of liquid–liquid partitioning processes, such as found in octanol–water systems [2,3]. However, in RPLC this can not be entirely the case, since there is no distinct interfacial boundary between the stationary and

mobile phases. The lack of a well defined boundary between the stationary and mobile phases in RPLC is due to the formation of a solvation layer at the surface of the stationary phase, which results from mobile phase interactions with the grafted alkyl chains as well as the silica support. Preferential sorption of mobile phase components by the stationary phase results in a layer whose thickness and composition varies with the distance from the bonded ends of the alkyl chains. The stationary phase alkyl chains are not isotropic; they exhibit ordering due to their covalent attachment to the rigid silica substrate surface [2–4]. Chain ordering also increases with increasing alkyl chain surface coverage [2–4]. Due to varying degrees of chain interaction, mobile phase components will penetrate into the stationary phase in a non-uniform manner [5]. The resulting structure is not a distinct interface but an *interphase* which exhibits an order gradient that varies along the bonded alkyl chain as a function of distance from the silica surface [2–4].

The overall structure of the RPLC solvation layer is a function of several variables. These include: (i)

---

Correspondence to: K. B. Sentell, Department of Chemistry, University of Vermont, Burlington, VT 05405-0125, USA.

<sup>☆</sup> Present address: ICI Americas, Pharmaceutical Group, NLW2, Wilmington, DE 19897, USA.

the composition of the bulk mobile phase; (ii) the length of the bonded alkyl chain; (iii) the degree of derivatization of the silica surface or bonding density, which is often expressed in units of micromoles of bonded alkyl ligand per square meter of bonded phase surface ( $\mu\text{mol}/\text{m}^2$ ); (iv) the temperature of the system; and (v) the numbers and types of residual silanols remaining on the silica surface following derivatization. In order to obtain a better understanding of the molecular interactions underlying solute retention in RPLC, it is necessary to develop more accurate models of the composition and structure of the solvation layer as a function of all of these variables [5–9].

In the past, researchers have used various methods to probe the composition of the solvation layer. Some of these have included the chromatographic measurement of adsorption isotherms [6,9–13], gas chromatographic (GC) methods [6–8], optical spectroscopy [14–23], and nuclear magnetic resonance spectroscopy (NMR) [24–40]. NMR offers some interesting possibilities in terms of understanding stationary phase–mobile phase interactions in RPLC systems. The technique permits approaching the problem from the perspective of the stationary phase *or* the mobile phase. It also allows study of these systems under chromatographic conditions with minimal perturbation.

The present paper is a discussion of some of our solution state NMR studies of RPLC stationary phase–mobile phase interactions. This approach is not unique in that several researchers have undertaken such experiments in the past and obtained interesting results [24–40]. However, although many of these studies demonstrated the general validity of the technique, they did so using uncommon RPLC solvents [24–28,32,33,38,40] or they encompassed only a small range of mobile phase compositions [26,28–30,32–37,40]. It was our goal to expand on some of these initial studies in order to obtain a more comprehensive understanding of RPLC stationary phase solvation by commonly used organic modifiers using solution state NMR techniques. This was accomplished by measuring deuterium longitudinal relaxation times,  $T_1$ , of deuterated mobile phase components in contact with the stationary phases of interest.

The utility of deuterium longitudinal relaxation time experiments comes about because deuterium is

a quadrupolar nucleus with spin quantum number  $I = 1$ . Therefore its solution state longitudinal relaxation time,  $T_1$ , is described by the following equation:

$$\frac{1}{T_1} = 3\pi^2 \frac{2I + 3}{I^2(2I - 1)} \chi^2 \tau_c \quad (1)$$

Since  $I$  and the quadrupolar coupling constant,  $\chi$ , are constants for a particular nucleus [41], the inverse of the relaxation time (or the rate of relaxation) is directly proportional to  $\tau_c$ . The molecular correlation time,  $\tau_c$ , is given in units of radians per second and is a measure of how long it takes a molecule to rotate through one radian. It is therefore a measure of molecular motion. From eqn. 1 it is evident that as the correlation time increases (*e.g.* molecular motion decreases) the longitudinal relaxation time,  $T_1$ , decreases. Specifically, greater molecular association or restriction causes a decrease in  $T_1$ .

Our current study is based upon work first conducted by Marshall and McKenna [29] in which they measured the solution state longitudinal relaxation times ( $T_1$ ) of deuterium in  $^2\text{H}_2\text{O}$ –acetonitrile mixtures over a composition range of 0% to 50%  $^2\text{H}_2\text{O}$  as a function of their volume-to-volume (v/v) ratios. These measurements of  $T_1$  versus percent  $^2\text{H}_2\text{O}$  in the mobile phase mixtures were made for the neat binary solutions as well as for samples of the mobile phases combined with various chromatographic supports. By comparing the  $T_1$  values in the neat solutions to those for the same solutions in contact with stationary phases, Marshall and McKenna qualitatively gauged the degree of water association with the stationary phase. Their results are interesting in at least two respects. First, they showed that for the samples they studied, the relative amount of water associated with the stationary phase in acetonitrile–water systems is a function of the amount of water in the bulk mobile phase. Secondly, they did not perform measurements at acetonitrile concentrations less than 50%, since uniform wetting of the stationary phase was not possible at the latter solution compositions when the stationary and mobile phase mixtures were combined at atmospheric pressure. In addition to observing  $^2\text{H}_2\text{O}$  relaxation times, they also measured the  $T_1$  for [ $^2\text{H}_3$ ]acetonitrile under a few of their experimen-

tal conditions. Despite these interesting initial results, to our knowledge no further work of the same sort was undertaken, although Ellison and Marshall [30] have made deuterium and nitrogen-14 longitudinal relaxation time measurements to determine the surface fluidity in RPLC systems.

Because of the demonstrated potential of these  $T_1$  experiments we have expanded on Marshall and McKenna's work. For the mobile phases used in our studies we have been able to encompass the entire binary composition range by overcoming the problem of wetting the stationary phase samples with highly aqueous mobile phases. Since our sample preparation method equilibrates the stationary and mobile phases at pressures comparable to those attained under chromatographic operating conditions, it also much more nearly approximates wetting under real chromatographic conditions. We have also performed our  $^2\text{H}$  NMR work using [ $^2\text{H}_4$ ]methanol and [ $^2\text{H}_3$ ]acetonitrile in addition to  $^2\text{H}_2\text{O}$ . The results obtained with [ $^2\text{H}_4$ ]methanol and [ $^2\text{H}_3$ ]acetonitrile are reported in this communication; those for  $^2\text{H}_2\text{O}$  are discussed in a second paper [42]. Finally, we have obtained this information for two well-characterized monomeric  $\text{C}_{18}$  modified stationary phases with greatly different bonding densities in order to investigate the effect of stationary phase alkyl chain interactions upon solvation layer formation.

## EXPERIMENTAL

### *NMR measurements*

$T_1$  values for the methyl deuterons of [ $^2\text{H}_4$ ]methanol–water and [ $^2\text{H}_3$ ]acetonitrile–water mobile phase mixtures, both neat and in contact with stationary phase, were measured on a Brüker WM-250 NMR spectrometer operating at a field strength of 5.875 Tesla and a frequency of 38.4 MHz for  $^2\text{H}$ . The standard inversion recovery pulse sequence was used  $(180^\circ-\tau-90^\circ\text{-Acquire-Delay})_n$  where  $\tau$  ranged from 0.025 to 24 s. The sequence employed no less than ten  $\tau$  values and each acquisition necessitated from 2 to 32 scans. The relaxation delay was in excess of 5  $T_1$  to allow the system to return to equilibrium between measurements. Total acquisition times ranged from 10 to 50 min. Care was taken to minimize reflected power for each sample in order to minimize errors in the  $180^\circ$  and  $90^\circ$  pulse angles.

Spectra were acquired using automatic field frequency lock. Temperature was kept constant at  $30^\circ\text{C}$  (303 K).

$T_1$  values were calculated by manual measurement of peak height for each  $\tau$  value followed by a three-parameter least squares exponential fit of the peak height *versus*  $\tau$  plot. Relative error for replicate measurements was in all cases less than 5%. All  $T_1$  values are stated at confidence level of plus or minus one standard deviation.

### *Chemicals*

[ $^2\text{H}_4$ ]Methanol and [ $^2\text{H}_3$ ]acetonitrile (Isotec, Miamisburg, OH, USA) were used without further purification. HPLC-grade water was obtained in house using a Nanopure (Sybron, Boston, MA, USA) water purification system. Two silica-based stationary phase materials were used in this work. The first was a monomeric, non-endcapped  $\text{C}_{18}$  phase of very high alkyl chain bonding density ( $4.4 \mu\text{mol}/\text{m}^2$ ) which was synthesized in our laboratory under conditions which have been previously described [43]. This  $10\text{-}\mu\text{m}$  particle diameter stationary phase with a pore diameter of  $85 \text{ \AA}$  is designated herein as LT1. The second stationary phase was a partially endcapped Spherisorb S5-ODS-1 (Phase Separations, Norwalk, CT, USA) monomeric  $\text{C}_{18}$  phase with a low bonding density ( $1.5 \mu\text{mol}/\text{m}^2$ ). This  $5\text{-}\mu\text{m}$  particle diameter stationary phase with a pore diameter of  $50 \text{ \AA}$  is designated herein as ODS-1.

### *Sample preparation*

Approximately 3% (by volume) [ $^2\text{H}_4$ ]methanol or [ $^2\text{H}_3$ ]acetonitrile was added to its non-labelled analogue in a chromatographic mobile phase reservoir. These solvents and a separate reservoir of HPLC-grade water were degassed by sonication in an ultrasonic bath under vacuum. The desired mobile phase mixture (v/v % ratio of organic co-solvent–water) was delivered into a 10-mm NMR tube by two Waters (Waters, Milford, MA, USA) Model 510 chromatographic pumps controlled by a Waters Model 680 automated gradient controller. Samples were prepared in 10% or smaller volume increments ranging from 100:0 (v/v) to 10:90 (v/v) for [ $^2\text{H}_4$ ]methanol–water and [ $^2\text{H}_3$ ]acetonitrile–water.  $^2\text{H}$   $T_1$  values for the methyl deuterons of the labeled organic components were then measured for each neat mobile phase sample.



To insure proper wetting of the stationary phase with the labelled mobile phase solutions in the second half of the experiments, mobile–stationary phase mixtures were prepared in the following manner. First, the chromatographic stationary phase was dried under vacuum in excess of 12 h at 110°C to ensure that all physisorbed solvents were removed. The dry stationary phase was hand-packed into an empty 10 cm × 4.6 mm stainless-steel chromatographic column. Mobile phase of the desired volume percent ratio was then pumped through the column at a flow-rate which would generate at least 1500 p.s.i. (10.3 MPa) of backpressure. Approximately 50 ml of solvent was pumped through the column in one direction, at which point the column was reversed and an additional 50 ml was pumped in the opposite direction. Following the wetting procedure, one of the column end fittings was removed from the column, the wetted stationary phase was pumped as a smooth paste into an 8-mm NMR tube and the  $T_1$  experiment was performed as described above for the neat mobile phase samples. It should be noted that at mobile phase compositions containing a very low volume percent of organic solvent, it was necessary to gradually ramp the flow-rate to achieve the desired back pressure and that greater than 100 ml of mobile phase was needed to properly wet the stationary phase. If not properly wetted, the stationary phase would appear either dry or lumpy when pumped from the chromatographic column.

## RESULTS AND DISCUSSION

### Neat mobile phase $^2\text{H}$ $T_1$ measurements

The deuterium longitudinal relaxation times,  $T_1$ , for the methyl deuterons of [ $^2\text{H}_3$ ]acetonitrile–water and [ $^2\text{H}_4$ ]methanol–water solvent mixtures versus percent organic modifier in the mobile phase are shown in Fig. 1. Recall that a decrease in deuterium  $T_1$  implies molecular association or decreased mobility. Over the entire range of [ $^2\text{H}_3$ ]acetonitrile–water mixtures, the  $T_1$  values remained essentially constant, averaging approximately 6 s (Fig. 1a). The binary solvent mixture viscosity has also been determined to be approximately constant throughout the composition range [44]. Katz *et al.* [45] have examined the association of methanol–water, acetonitrile–water and tetrahydrofuran–water mixtures

both theoretically, using equilibrium equations, and experimentally, by measurement of volume changes upon mixing in these solvent systems. They suggest that these mixtures should be considered as ternary rather than binary; the three components of these mixtures would be free organic solvent (*e.g.* that self-associated rather than associated with water), free water and water–solvent mixed complexes. Their predictions and experiments indicate that in mixtures of acetonitrile and water, the proportion of mixed acetonitrile–water complexes is very small, reaching a maximum volume percentage of *ca.* 5% when the nominal solution volume fraction of acetonitrile is 0.5 [45]. Rowlen and Harris [46] have

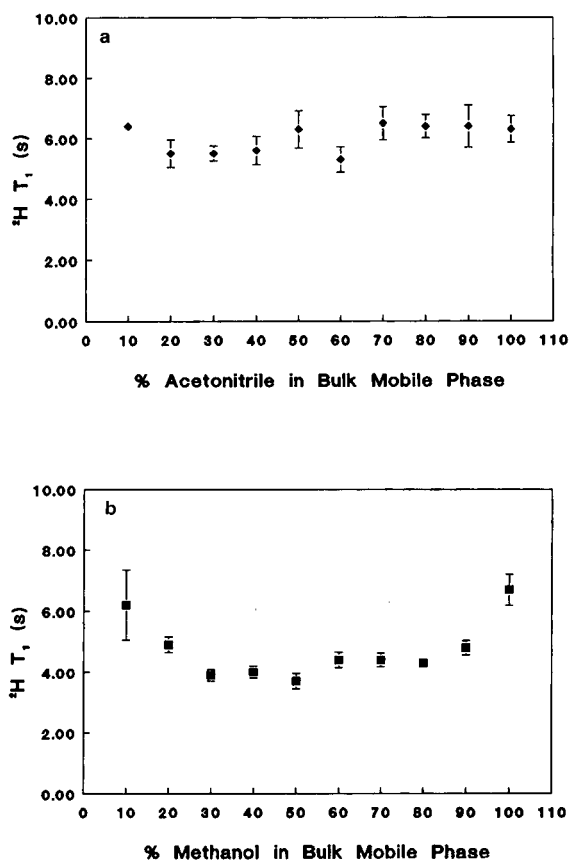


Fig. 1.  $^2\text{H}$  longitudinal relaxation time ( $T_1$ ) for deuterated organic modifier versus volume percent organic modifier in bulk organic modifier–water mixture for (a) [ $^2\text{H}_3$ ]acetonitrile ( $\blacklozenge$ ) and (b) [ $^2\text{H}_4$ ]methanol ( $\blacksquare$ ).

reported Raman spectroscopic studies that provide additional experimental evidence that there is a concentration-dependent equilibrium between forms of acetonitrile in aqueous mixtures. Their measurements on the concentration dependence of the CN stretching band area and bandwidth also indicate that at acetonitrile mole fractions ( $\chi_{\text{ACN}}$ ) greater than 0.3 (*ca.* 0.55 volume fraction), large numbers of self-associated acetonitrile species are present in solution, and that at  $\chi_{\text{ACN}} > 0.55$  (*ca.* 0.78 volume fraction) little to no water–acetonitrile mixed species exist [46]. Alvarez-Zedpeda *et al.* [47] have also described the concentration-dependent microstructure of acetonitrile–water solutions. Upon addition of acetonitrile to pure water, it can initially enter cavities in the water structure. However, once these sites are occupied, acetonitrile becomes increasingly self-associated in aggregates or loosely defined clusters, resulting in bulk *solution* microheterogeneity [47]. The acetonitrile species experience a relatively *homogeneous* solution environment over a large nominal binary composition range, due to their extensive self-association. It is therefore quite reasonable that, as illustrated in Fig. 1a, the  $^{2}\text{H}_3$ acetonitrile  $T_1$  values are approximately constant throughout the composition range.

The plot of  $T_1$  versus percent organic modifier in the mobile phase for the methyl deuterons of  $^{2}\text{H}_4$ methanol–water (Fig. 1b) exhibits different trends than that of the  $^{2}\text{H}_3$ acetonitrile–water system. In this case, the  $^{2}\text{H}_4$ methanol  $T_1$  values are more or less constant from approximately 30% to 80% methanol in the mobile phase. However, at both lower and higher concentrations of methanol, a marked change to higher overall longitudinal relaxation times is noted. The  $T_1$  behavior follows that for viscosity in methanol–water mixtures [44]. There is a much greater degree of hydrogen bonding in methanol–water systems than that exhibited in acetonitrile–water systems, which is primarily due to the presence of an additional pair of unpaired electrons on the methanol oxygen [48]. Katz *et al.* [45,49] have also investigated methanol–water mixtures and have found that they are essentially ternary mixtures with three distinct composition-dependent distributions. Their extensive studies indicate that as the nominal methanol volume fraction increases from zero to *ca.* 0.4, there is a linear increase in water–methanol associated species that

corresponds with a commensurate decrease in free water species; there is little to no free methanol present in solution. As the nominal volume fraction of methanol increases from *ca.* 0.4 to *ca.* 0.8, the amount of free water decreases drastically, that of the water–methanol associated species goes through a maximum at a nominal methanol volume fraction of *ca.* 0.6, and the volume fraction of free methanol increases rapidly. At nominal methanol volume fractions above *ca.* 0.8, the volume fraction of free methanol increases linearly, commensurately with the decrease in water–methanol associated species [45,49]. As seen in Fig. 1b, the measured  $T_1$  values for the  $^{2}\text{H}_4$ methanol maintain a value of approximately 4 s from *ca.* 30 to 80% methanol in the mobile phase, which corresponds to the region in which water–methanol associated species predominate. The greatly decreased  $T_1$  values measured in this composition region (*ca.* 4 s) compared to those measured in the acetonitrile–water solutions (*ca.* 6 s) are indicative of restricted mobility of the methanol species due to the greater extent of hydrogen bonding in water–methanol associated species than in self-associated methanol. At nominal methanol volume percentages less than 30% and greater than 80%, the larger  $^{2}\text{H}_4$ methanol  $T_1$  values indicate that methanol experiences a lesser degree of association than in the intermediate composition region. For the latter region, it is plausible that this is due to the increased number of self-associated methanol species in this composition range [45,49], in which hydrogen bonding is expected to be considerably less strong than in the water–methanol mixed species.

The relaxation time behavior for the composition range from 0–30% methanol is less facile to model. The measured  $T_1$  values for methanol at less than 30% methanol are comparable to those measured for the same nominal volume compositions of the acetonitrile mixtures. One possible explanation for this similarity is that at low nominal concentrations, methanol acts much the way that acetonitrile does, entering cavities in the water structure until these sites are occupied. It is reasonable that methanol in such cavities would have a much larger degree of contact with other methanol molecules in the cavity than with aqueous species in the water structure, resulting in  $T_1$  values comparable to those measured for high methanol content mix-

tures. Once these cavities in the water structure are occupied, methanol will be more actively incorporated into the water structure via the formation of water–methanol associated species.

#### Mobile phase $^2\text{H}$ $T_1$ measurements for contact with the stationary phase

If stationary phase is combined with the neat solutions in the manner described in the experimental section, and the longitudinal relaxation times are re-measured, it becomes useful to compare the change in the methyl deuterium  $T_1$  values in contact with the stationary phase versus those observed in neat solution. Although it may be expected that relaxation time measurements at the bonded phase–mobile phase interface might suffer from interface-induced inhomogeneities in the magnetic field, in practice  $T_1$  measurements are relatively insensitive to magnetic field inhomogeneities, although this is not the case for  $T_2$  [50]. Again, by eqn. 1, which states that a decrease in deuterium  $T_1$  values implies restriction of molecular motion or association, it can be concluded that a decrease in  $T_1$  for the methyl deuterons of  $[\text{}^2\text{H}_4]\text{methanol}$  or  $[\text{}^2\text{H}_3]\text{acetonitrile}$  when combined with the stationary phase compared to that for the neat mobile phase mixture implies a reduction of motional freedom of these species relative to the bulk solution due to association of methanol or acetonitrile with the stationary phase [29].

In Fig. 2a, the relaxation time of  $[\text{}^2\text{H}_4]\text{methanol}$  in the neat mobile phase minus the relaxation time of  $[\text{}^2\text{H}_4]\text{methanol}$  when the same mobile phase is in contact with stationary phase, which will be denoted as  $\Delta T_1$ , is plotted versus percent methanol in the bulk mobile phase for the ODS-1 stationary phase. For this low  $\text{C}_{18}$  bonding density phase ( $1.5 \mu\text{mol}/\text{m}^2$ ) there is relatively little disparity in the deuterium  $\Delta T_1$  values for bulk mobile phase compositions ranging from ca. 30 to 80% methanol. Although there is association of methanol with the stationary phase, which is reflected by a positive value for  $\Delta T_1$ , the degree of association of methanol with the stationary phase is constant throughout this composition range, and is also less than for any other range of bulk methanol–water compositions. This is not surprising in light of the proposed solution structure of methanol–water mixtures in this composition range, as well as our neat mobile phase  $T_1$  mea-

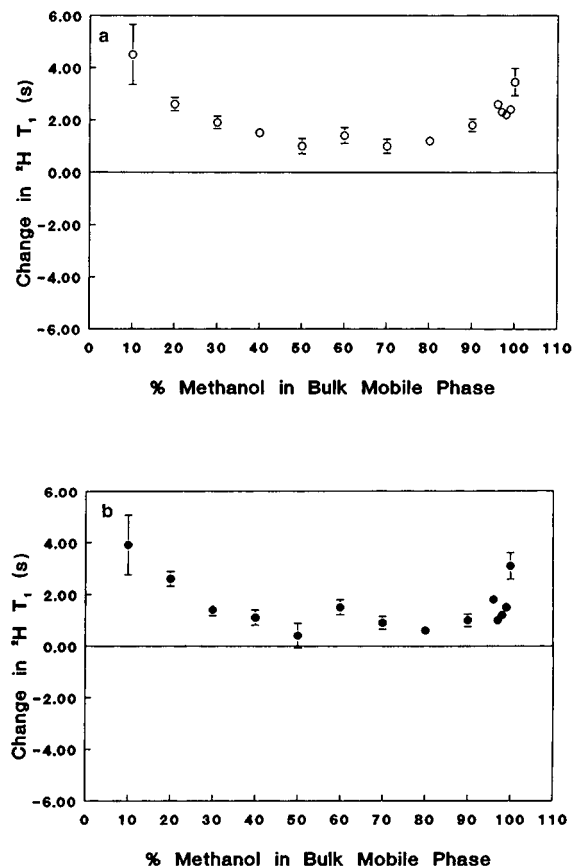


Fig. 2. Change in  $^2\text{H}$  longitudinal relaxation time ( $T_1$ ) for  $[\text{}^2\text{H}_4]\text{methanol}$  in contact with monomeric  $\text{C}_{18}$  stationary phases versus volume percent methanol in bulk methanol–water mobile phase. (a) Low bonding density phase (ODS-1;  $1.5 \mu\text{mol}/\text{m}^2$ ) (○). (b) High bonding density phase (LT1;  $4.4 \mu\text{mol}/\text{m}^2$ ) (●).

surements. Recall that this region corresponds to that in which water–methanol associated species predominate in Katz *et al.*'s model [45,49]. There is a greater degree of hydrogen bonding in water–methanol associated species than in self-associated methanol species. Moreover, the methanol–water hydrogen bonding interactions predominant over this composition range are stronger and more directed than the weaker, predominantly dispersive interactions that take place between methanol and  $\text{C}_{18}$  stationary phases. Doubtless accessible silanol groups on the silica support could also participate in hydrogen bonding with any of the solution species. However, the octadecyl ligands bound to the

silica support are likely to be only partially extended [22] due to limited methanol uptake over this composition range and therefore would provide at least some degree of shielding of mobile phase components from the support surface. Consequently, little if any association of methanol with the stationary phase is expected over this mobile phase composition range, and from the bulk solution behavior, this degree of association would be expected to remain constant. The expected behavior is observed.

At compositions with more than 80% methanol in the mobile phase, the methanol deuterium  $\Delta T_1$  values increase with the volume percent of methanol in the bulk mobile phase. This implies a greater degree of association for methanol with the stationary phase than is exhibited in the intermediate composition region. Recall that at nominal methanol volume fractions above *ca.* 0.8, the volume fraction of self-associated methanol complexes increases linearly, commensurately with the decrease in water–methanol associated species [45,49]. Since the self-associated solution species are not strongly hydrogen bonded with water, they are more likely to experience dispersive interactions with the  $C_{18}$  chains of the stationary phase due to the hydrophobic character of the methyl group [6–8]. Therefore, because of the bulk solution composition of the mobile phase at these higher methanol concentrations, uptake of methanol self-associated species should enable the bonded alkyl chains to assume a more extended configuration [5,15]. Once the stationary phase chains assume a more extended configuration, there is more accessible chain volume for further methanol partitioning and the hydroxyl moiety of the alcohol would also be better able to participate in hydrogen bonding with residual silanol groups on the silica support surface. Although other NMR experiments in our laboratory have indicated that the latter effect is negligible compared to the former [42], the overall effect of methanol uptake is to allow greater penetration and corresponding association of methanol with the stationary phase.

At mobile phase compositions with less than 30% methanol, a marked increase in  $\Delta T_1$  is again observed, implying a larger degree of association of methanol with the stationary phase than observed in the intermediate composition range. It is well known that in highly aqueous mobile phases, the

hydrophobic alkyl stationary phase chains will assume a collapsed or folded configuration in order to minimize their surface contact with the polar mobile phase [3,5,15,51]. This would cause methanol to become entrapped within the collapsed chain structure (most likely within narrow-necked pores in the silica support), and thereby result in a distinct decrease in the  $[^2H_4]$ methanol  $^2H$   $T_1$  values. The analogous  $\Delta T_1$  versus volume percent methanol plot (Fig. 2b) for the high bonding density stationary phase ( $4.4 \mu\text{mol}/\text{m}^2$ ); LT1 illustrates that the same general trends are observed as for the low bonding density phase (ODS-1).

The same types of experiments were also performed using the same stationary phase materials and  $[^2H_3]$ acetonitrile–water mobile phase mixtures. In Fig. 3a and b the changes in  $[^2H_3]$ acetonitrile deuterium  $T_1$  values in contact with ODS-1 and LT1 are shown. Just as exhibited in the bulk solution measurements (Fig. 1a), the  $[^2H_3]$ acetonitrile–water mobile phase system demonstrates distinctly different behavior than the  $[^2H_4]$ methanol–water system. For both the LT1 and ODS-1 stationary phases, the  $\Delta T_1$  values for acetonitrile in contact with stationary phase are essentially constant over the entire concentration range. This reflects the bulk solution properties of  $[^2H_3]$ acetonitrile–water mixtures in the same manner as was seen with  $[^2H_4]$ methanol–water mixtures. Recall that the microstructure of acetonitrile–water solutions is concentration-dependent. In the bulk solution model, acetonitrile enter cavities in the water structure until these sites are occupied. With further increase in the amount of acetonitrile, it becomes increasingly self-associated in aggregates or loosely defined clusters, resulting in bulk solution microheterogeneity [47]. However, the acetonitrile species experience a relatively homogeneous solution environment over a large nominal binary composition range, due to their extensive self-association [45–47]. It is therefore quite reasonable that, as illustrated in Fig. 3,  $[^2H_3]$ acetonitrile exhibits a relatively monotonic degree of association behavior with both stationary phases throughout the composition range. It is interesting to note that the composition at which both the bulk solution (Fig. 1a) and the high chain density stationary phase (Fig. 3b) exhibit their minimum  $T_1$  value is 60% acetonitrile; this is approximately the same composition at which Rowlen and Har-

ris's Raman measurements first indicate large numbers of self-associated acetonitrile species present in solution [45]. The  $\Delta T_1$  values for  $[^2\text{H}_3]\text{acetonitrile}$ -water systems are maximized for the 10% acetonitrile bulk solution, indicating that acetonitrile is most highly associated with the stationary phase at this composition. Just as is the case for comparable methanol compositions, acetonitrile is likely entrapped within silica pores beneath the collapsed chain structure that the hydrophobic alkyl stationary phase chains will assume in order to minimize their surface contact with highly aqueous mobile phases [15].

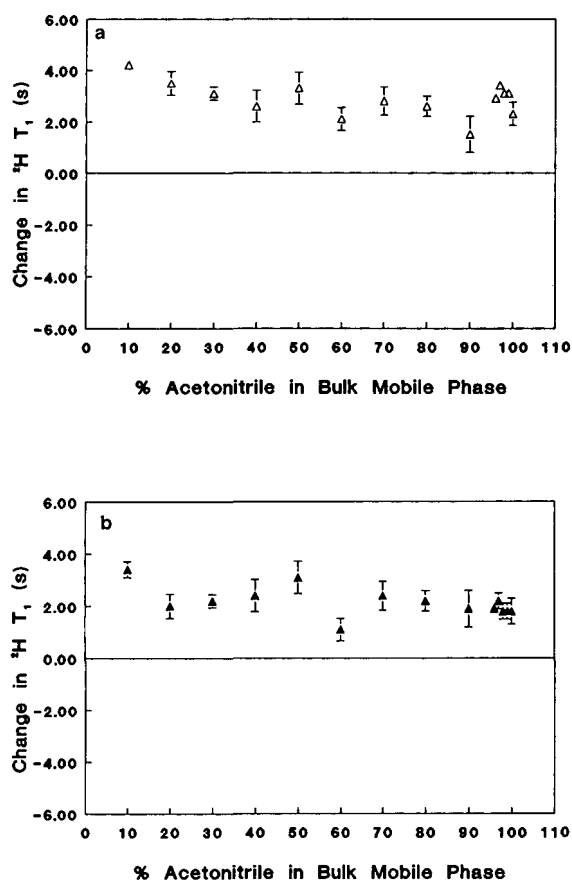


Fig. 3. Change in  $^2\text{H}$  longitudinal relaxation time ( $T_1$ ) for  $[^2\text{H}_3]\text{acetonitrile}$  in contact with monomeric  $\text{C}_{18}$  stationary phases versus volume percent acetonitrile in bulk acetonitrile-water mobile phase. (a) Low bonding density phase (ODS-1;  $1.5 \mu\text{mol}/\text{m}^2$   $\Delta$ ). (b) High bonding density phase (LT1;  $4.4 \mu\text{mol}/\text{m}^2$   $\blacktriangle$ ).

If at this point a comparison of the results for ODS-1 ( $1.5 \mu\text{mol} \text{C}_{18}$  ligand/ $\text{m}^2$  of bonded phase surface) with those obtained for LT1 ( $4.4 \mu\text{mol}/\text{m}^2$ ) is made by superimposing the  $\Delta T_1$  plots (Fig. 4), some subtle but interesting results emerge. Recall that the primary difference between ODS-1 and LT1 is their large difference in the degree of surface derivatization (octadecyl bonding density). Yet as shown in Fig. 4a, the degree of association of methanol with the stationary phase for both chromatographic supports is virtually the same, although upon close inspection, it can be noticed that there is a slightly larger degree of methanol association with the ODS-1 stationary phase than for LT1 at several mobile phase compositions. Although the difference for these compositions is small, it is statistical-

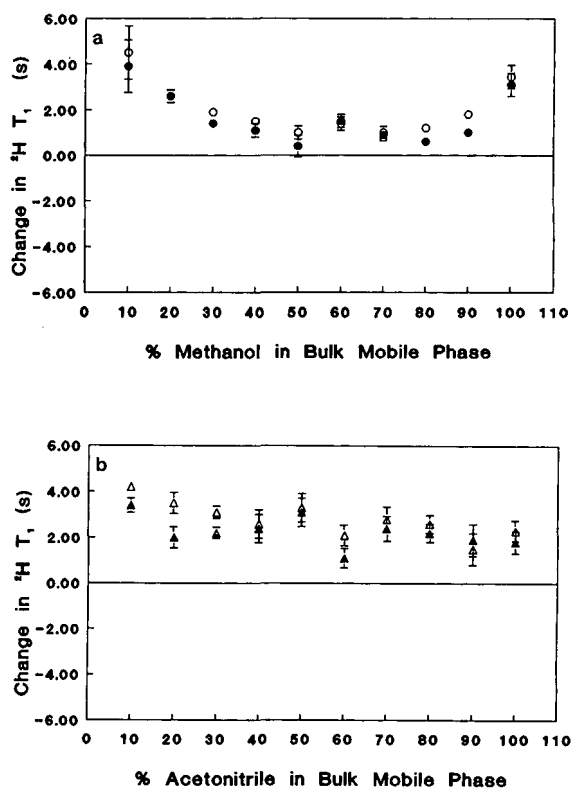


Fig. 4. Comparison of the change in  $^2\text{H}$  longitudinal relaxation time ( $T_1$ ) for the organic modifier methyl deuterons in contact with low versus high density monomeric  $\text{C}_{18}$  stationary phases. (a)  $[^2\text{H}_4]\text{Methanol}$  with ODS-1 ( $\circ$ ) versus LT1 ( $\bullet$ ). (b)  $[^2\text{H}_3]\text{Acetonitrile}$  with ODS-1 ( $\Delta$ ) versus LT1 ( $\blacktriangle$ ).

ly significant. Upon initial considerations, this observation might appear somewhat surprising. Based strictly on the degree of carbon loading, a qualitative prediction might have been made that there would be a *significantly* greater degree of methanol association with the more hydrophobic high bonding density phase (LT1) than with the low bonding density phase (ODS-1). Yet if anything, the reverse is indicated by our experimental measurements. This apparent anomaly is readily explained if a more comprehensive model of reversed-phase stationary phase structure, which takes into account the effect of stationary phase chain organization on solute partitioning, is considered.

As previously discussed, RPLC stationary phases cannot be thought of strictly as bulk phases. The stationary and mobile phase interact significantly, resulting in the formation of the solvation layer. Dill has predicted [2–4] and Sentell and Dorsey have shown experimentally [52] that the degree of bonded phase alkyl chain interaction is a function of bonding density, and that the degree of chain interaction strongly affects the ability of any solute, including mobile phase components, to penetrate the chain structure. At low bonding densities, there are relatively few interactions between neighboring  $C_{18}$  ligands; mobile phase access to the alkyl ligands as well as to residual surface silanols is relatively facile. Methanol species should therefore be able to participate in dispersive interactions with the stationary phase alkyl chains as well as associate with any accessible surface silanols through hydrogen bonding. As alkyl chain surface coverage increases, the latter effect is expected to decrease. Additionally, for monomeric bonded phases there is a critical bonding density at about  $3.0 \mu\text{mol}/\text{m}^2$  wherein the alkyl chains are in close enough proximity for interactions with neighboring chains to become important. Above this value, the degree of chain interaction becomes a significant factor in determining the extent of solute partitioning, since any solute partitioning *into* the stationary phase must overcome these interactions [2–4,52]. As bonding density further increases, the free energy required to overcome these chain interactions becomes increasingly prohibitive, leading to commensurate decreases in solute partitioning [2–4,52]. This should result in a decreasing degree of penetration of mobile phase components into the stationary phase for bonded

phase surface densities of *ca.*  $3 \mu\text{mol}/\text{m}^2$  or greater. Cole and Dorsey [53] have confirmed this experimentally by observing the effects of bonding density on mobile phase re-equilibration volumes following gradient elution.

The comparison between the ODS-1 and LT1 phases in Fig. 4 can be reasonably made using this interphase model for solute partitioning. When the large disparity in bonding densities between LT1 and ODS-1 is considered, the experimental results are logical and it is expected that methanol will be able to participate in a greater degree of association with the ODS-1 stationary phase than with the LT1 phase (Fig. 4a). This is because in the former, there should be much greater accessibility of methanol to both the hydrophobic  $C_{18}$  stationary phase chains and to residual silanols. This provides dual mechanisms for the larger decrease in the  $[^2\text{H}_4]$ methanol  $T_1$  values via association with the ODS-1 phase. In contrast, the very high bonding density of the LT1 phase should lead to at least partial exclusion of methanol from the interphase structure due to the high degree of chain cooperativity as well as decreased access to surface silanols. Therefore it is both expected and observed that  $[^2\text{H}_4]$ methanol undergoes less association with the high density LT1 stationary phase than with the low bonding density ODS-1 phase. The same behavior is observed for  $[^2\text{H}_3]$ acetonitrile (Fig. 4b).

It is more interesting to compare and contrast the  $\Delta T_1$  data between methanol and acetonitrile for both stationary phases. In Fig. 5, the  $\Delta T_1$  plots for each of the stationary phases in contact with the two different mobile phase systems are overlaid. The results show that over the bulk mobile phase composition range from *ca.* 30 to 80% organic modifier, acetonitrile displays a greater degree of association with both stationary phases than methanol does. This is doubtless due to their differences in bulk solution microstructure. Since in this general composition range acetonitrile–water solution chemistry is dominated by the formation of relatively hydrophobic self-associated acetonitrile microphases [45–47] and methanol–water solution behavior is dominated by the formation of much more polar water–methanol associated species [45,49], it is reasonable that acetonitrile would be more highly associated with both stationary phases. At bulk mobile phase compositions with 20% or less organic

modifier, the  $\Delta T_1$  values, and thus the degree of association of the acetonitrile and methanol components of the mobile phase, are comparable. This is doubtless due to the collapsed chain structure assumed by hydrophobic alkyl stationary phase chains in highly aqueous mobile phases. Finally, for purely organic bulk mobile phases, methanol displays a larger  $\Delta T_1$  value than acetonitrile. Since in pure methanol solutions the methanol species are not hydrogen bonded with water, they are much more available to participate in dispersive interactions with the  $C_{18}$  chains of the stationary phase than when water is present. This should bring about a more extended configuration of the bonded alkyl chains, which further increases methanol accessibil-

ity to the bonded phase surface. These two effects allow a greater degree of association of methanol with the stationary phase when water is not present. As discussed previously, acetonitrile exists in bulk solution primarily as self-associated species throughout the binary composition range, enabling its accessibility to interact with the stationary phase to remain more or constant [47].

#### Comparisons to other techniques

Before the results of this study are compared to those obtained by other methods, it must again be stressed that the  $\Delta T_1$  measurements made here are not *quantitative* measurements of the *amount* of sorbed organic modifier in the stationary phase systems, but rather are *qualitative* measurements of how strongly these components of the mobile phase are *associated* with the stationary phase under these conditions. Extremely precise quantitative measurements via integration of these NMR peak areas are very difficult (if not impossible) to make. Additionally,  $T_1$  measurements for solvents in contact with stationary phases will of necessity be a weighted average of the bulk solvent and associated solvent  $T_1$  values, due to exchange between these two sites that is fast relative to the time frame of the NMR experiment [29]. However, because the  $T_1$  values for the bound solvents are typically much shorter than those for the bulk solution solvents and the rate of exchange occurs on a much faster time scale, the  $T_1$  values measured for the paste samples are dominated by the relaxation time of the bound solvent species [29]. Our examination of the *difference* between the bulk solution  $T_1$  values and those measured for the solution in contact with the stationary phase should also help to correct for the contributions from the relaxation of the species of interest in the bulk solution. Finally, it should be noted that any spectroscopic measurement of the interactions of a species of interest with an RPLC bonded phase will be representative of the *average* interaction of that species with the bonded phase surface. For NMR  $T_1$  studies on any solute, it is expected that a distribution of relaxation times would result from the varying degrees of solute association with such a heteroenergetic surface [30].

Despite the above restrictions, our  $^2\text{H}$  NMR  $T_1$  studies provide both comparable and complimentary information to previous studies. Lochmüller

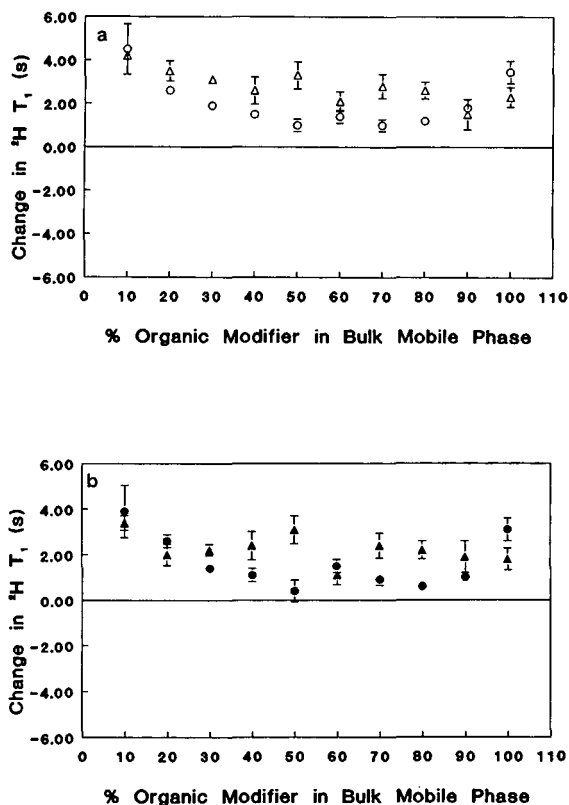


Fig. 5. Comparison of the change in  $^2\text{H}$  longitudinal relaxation time ( $T_1$ ) for  $[\text{H}_3]$ acetonitrile versus  $[\text{H}_4]$ methanol in contact with monomeric  $C_{18}$  stationary phases. (a)  $[\text{H}_4]$ Methanol ( $\circ$ ) versus  $[\text{H}_3]$ acetonitrile ( $\Delta$ ) with ODS-1. (b)  $[\text{H}_4]$ Methanol ( $\bullet$ ) versus  $[\text{H}_3]$ acetonitrile ( $\blacktriangle$ ) with LT1.

and Hunnicutt [15] have stated "...local *n*-alkyl density effects as well as specific solvent–hydrocarbon interactions influence the ultimate conformation of monomeric *n*-octadecyl bonded phases." In acetonitrile mobile phases, our study indicates that the acetonitrile species exhibit a relatively monotonic degree of association behavior with both C<sub>18</sub> stationary phases throughout most of the composition range. Analogous results have been reported from adsorption isotherm studies [6,8,13,54]. A number of spectroscopic studies have also indicated that *changes* in stationary phase polarity as a function of bulk acetonitrile composition in these systems (due to intercalated mobile phase components and/or stationary phase chain extension) are also small [18,21,23]. In contrast, changes in stationary phase polarity have been found to be much more composition dependent for methanol–water mobile phase systems [19,20,23]. Upon inspection, these polarity measurements correspond well with both the bulk solution composition characteristics reported by Katz *et al.* [45,49] and the results of our [<sup>2</sup>H<sub>4</sub>]methanol studies reported here. Accordingly, the cooperative solvation layer formation model for C<sub>18</sub> stationary phases in methanol–water mobile phase systems proposed by Yonker *et al.* [7] is further corroborated by our present studies.

At highly aqueous mobile phase compositions, our present studies indicate that acetonitrile and methanol are highly associated with the stationary phase. These species are likely entrapped in narrow-necked ("ink bottle") pores beneath the collapsed C<sub>18</sub> chain structure that Lochmüller and Hunnicutt [15] have described; the hydrophobic alkyl stationary phase chains will assume this minimum free energy configuration in order to minimize their surface contact with highly aqueous mobile phases. Convincing chromatographic evidence for solvent entrapment under these conditions has been presented by Gilpin and Squires [51] from thermal studies on reversed-phase materials. This description is also consistent with models for alkyl chain conformations at various stages of stationary phase wetting derived from the work of Maciel and Zeigler [31–33], who used CP/MAS solid state <sup>13</sup>C NMR and <sup>2</sup>H solid state quadrupole echo NMR measurements of selectively deuterated C<sub>18</sub> alkyl chain positions to study the mobility of these bonded phases for a variety of contact solvents. From the

results of these studies, they maintain that at high water content the C<sub>18</sub> chains will be associated and collapsed due to hydrophobic interactions. Bayer *et al.* [34–36] and McNally and Rogers [37] have also found significant reductions in <sup>13</sup>C *T*<sub>1</sub> measurements (*i.e.* reduced mobility) for bonded phase carbons in contact with highly aqueous systems.

Our experiments indicate that acetonitrile is for the most part more associated with either stationary phase than methanol. Spin probe studies [55] as well as numerous adsorption isotherm measurements [6,8,10–13] support this conclusion. Furthermore, we have shown that the degree of organic modifier association with the stationary phase is a function of alkyl chain surface density, which correlates well with previous <sup>13</sup>C NMR [25,33], spin probe [55] and chromatographic [53] measurements. In summary, our deuterium NMR studies exhibit very good correlations with studies of mobile and stationary phase interactions carried out via a number of disparate experimental techniques.

## CONCLUSIONS

The work described here confirms the usefulness of using solution state deuterium NMR measurements for studying microenvironments in reversed-phase chromatographic systems. Moreover, it has also been shown that by using the sample preparation method described herein, this technique is applicable to studying a full range of binary mobile phase compositions. The results obtained here give a qualitative picture of the extent of organic mobile phase components' interactions with the stationary phase as a function of bulk mobile phase composition and demonstrate that the degree of this interaction is strongly related to bulk solution structure. They further support a partitioning model for describing solute interactions with the stationary phase in reversed-phase chromatographic systems [2–4] by demonstrating that stationary phase bonding density is an important factor in solvation layer formation. It will be interesting to extend these experiments to include additional stationary phases of intermediate bonding densities, as well as to observe the behavior of other mobile phase systems. Moreover, a complimentary communication forthcoming from our laboratory reports and contrasts the changes we have observed in <sup>2</sup>H<sub>2</sub>O *T*<sub>1</sub> values as a



function of composition for the same mobile and stationary phase systems discussed in this work [42].

#### ACKNOWLEDGEMENTS

The authors thank Antony J. Williams and Anthony J. I. Ward for helpful discussions. The superb technical assistance with the NMR experiments that we have received from Jim Breeyear is greatly appreciated. The authors also thank Charles H. Lochmüller for providing the Partisil silica for the LT1 stationary phase from the Duke Standard Collection established by a grant from Whatman-Chemical Separations. Grateful acknowledgement is made to the University Committee on Research and Scholarship at the University of Vermont, the Society for Analytical Chemists of Pittsburgh and to the donors of the Petroleum Research Fund, administered by the ACS, for partial financial support of this research. Some portions of this work have been presented at the NATO Advanced Study Institute on Theoretical Advances in Chromatography and Related Separation Techniques, held in Ferrara, Italy in August, 1991; at the 1991 Eastern Analytical Symposium and at the 1992 Pittsburgh Conference on Analytical Chemistry and Applied Spectroscopy.

#### REFERENCES

- 1 R. E. Majors, *LC · GC*, 10 (1991) 686.
- 2 J. A. Marqusee and K. A. Dill, *J. Chem. Phys.*, 85 (1986) 434.
- 3 K. A. Dill, *J. Phys. Chem.*, 91 (1987) 1980.
- 4 J. G. Dorsey and K. A. Dill, *Chem. Rev.*, 89 (1989) 331.
- 5 D. E. Martire and R. E. Boehm, *J. Phys. Chem.*, 87 (1983) 1045.
- 6 R. M. McCormick and B. L. Karger, *Anal. Chem.*, 52 (1980) 2249.
- 7 C. R. Yonker, T. A. Zwier and M. F. Burke, *J. Chromatogr.*, 241 (1982) 257.
- 8 C. R. Yonker, T. A. Zwier and M. F. Burke, *J. Chromatogr.*, 241 (1982) 269.
- 9 R. P. W. Scott and C. F. Simpson, *Faraday Symp. Chem. Soc.*, 15 (1980) 69.
- 10 E. H. Slaats, E. Markovski, J. Fekete and J. Poppe, *J. Chromatogr.*, 207 (1981) 299.
- 11 G. Foti, C. Martinez and E. Kovats, *J. Chromatogr.*, 461 (1989) 269.
- 12 G. Foti, C. deReyff and E. Kovats, *Langmuir*, 6 (1990) 759.
- 13 R. K. Gilpin, M. Jaroniec and S. Lin, *Anal. Chem.*, 62 (1990) 2092.
- 14 L. C. Sander, J. B. Callis and L. R. Field, *Anal. Chem.*, 55 (1983) 1068.
- 15 C. H. Lochmüller and M. L. Hunnicutt, *J. Phys. Chem.*, 90 (1986) 4318.
- 16 J. Stahlberg and M. Almgren, *Anal. Chem.*, 57 (1985) 817.
- 17 J. Stahlberg, M. Almgren and J. Alsins, *Anal. Chem.*, 60 (1988) 2487.
- 18 J. W. Carr and J. M. Harris, *Anal. Chem.*, 58 (1986) 626.
- 19 J. W. Carr and J. M. Harris, *Anal. Chem.*, 59 (1987) 2546.
- 20 A. L. Wong, M. L. Hunnicutt and J. M. Harris, *Anal. Chem.*, 63 (1991) 1076.
- 21 J. L. Jones and S. C. Rutan, *Anal. Chem.*, 63 (1991) 1318.
- 22 M. E. Montgomery Jr., M. A. Green and M. J. Wirth, *Anal. Chem.*, 64 (1992) 1170.
- 23 Y.-D. Men and D. B. Marshall, *Anal. Chem.*, 62 (1990) 2606.
- 24 R. K. Gilpin and M. E. Gangoda, *J. Chromatogr. Sci.*, 21 (1983) 352.
- 25 R. K. Gilpin and M. E. Gangoda, *Anal. Chem.*, 56 (1984) 1470.
- 26 R. K. Gilpin and M. E. Gangoda, *J. Magn. Reson.*, 64 (1985) 408.
- 27 M. Gangoda and R. K. Gilpin, *J. Magn. Reson.*, 74 (1987) 134.
- 28 M. E. Gangoda and R. K. Gilpin, *Langmuir*, 6 (1990) 941.
- 29 D. B. Marshall and W. P. McKenna, *Anal. Chem.*, 56 (1984) 2090.
- 30 E. H. Ellison and D. B. Marshall, *J. Phys. Chem.*, 95 (1991) 808.
- 31 G. E. Maciel, R. C. Zeigler and R. K. Taft, in D. E. Leyden (Editor), *Silanes, Surfaces and Interfaces (Chemically Modified Surfaces Series, Vol. 1)*, Gordon and Breach, New York, 1986, p. 413.
- 32 R. C. Zeigler and G. E. Maciel, in D. E. Leyden (Editor), *Chemically Modified Surfaces in Science and Industry (Chemically Modified Surfaces Series, Vol. 2)*, Gordon and Breach, New York, 1988, p. 319.
- 33 R. C. Zeigler and G. E. Maciel, *J. Am. Chem. Soc.*, 113 (1991) 6349.
- 34 K. Albert, B. Evers and E. Bayer, *J. Magn. Res.*, 62 (1985) 428.
- 35 E. Bayer, A. Paulus, B. Peters, G. Laupp, J. Reiners and A. Klaus, *J. Chromatogr.*, 364 (1986) 25.
- 36 K. Albert, B. Pfeleiderer and E. Bayer, in D. E. Leyden (Editor), *Chemically Modified Surfaces in Science and Industry (Chemically Modified Surfaces Series, Vol. 2)*, Gordon and Breach, New York, 1988, p. 287.
- 37 M. E. McNally and L. B. Rogers, *J. Chromatogr.*, 331 (1985) 23.
- 38 P. Shah, L. B. Rogers and J. C. Fetzer, *J. Chromatogr.*, 388 (1987) 411.
- 39 H. A. Claessens, L. van de Ven, J. de Haan, C. A. Cramers and N. Vonk, *J. High Resolut. Chromatogr. Chromatogr. Commun.*, 6 (1983) 433.
- 40 E. C. Kelusky and C. A. Fyfe, *J. Am. Chem. Soc.*, 108 (1986) 1746.
- 41 R. K. Harris, *Nuclear Magnetic Resonance Spectroscopy: A Physicochemical View*, Pitman Books, London, 1983.
- 42 D. M. Bliesner and K. B. Sentell, *Anal. Chem.*, submitted for publication.
- 43 K. B. Sentell, K. W. Barnes and J. G. Dorsey, *J. Chromatogr.*, 455 (1988) 95.

- 44 J. Timmermans, *The Physico-Chemical Constants of Binary Systems in Concentrated Solutions Vol. 4*, Interscience, New York, 1960.
- 45 E. D. Katz, K. Ogan and R. P. W. Scott, *J. Chromatogr.*, 352 (1986) 67.
- 46 K. L. Rowlen and J. M. Harris, *Anal. Chem.*, 63 (1991) 964.
- 47 A. Alvarez-Zepeda, B. N. Barman and D. E. Martire, *Anal. Chem.*, 64 (1992) 1978.
- 48 F. Franks and D. J. G. Ives, *Quart. Rev.*, 20 (1) (1966) 1.
- 49 E. D. Katz, C. H. Lochmüller and R. P. W. Scott, *Anal. Chem.*, 61 (1989) 349.
- 50 J. A. Glasel and K. H. Lee, *J. Am. Chem. Soc.*, 96 (1974) 970.
- 51 R. K. Gilpin and J. A. Squires, *J. Chromatogr. Sci.*, 19 (1981) 195.
- 52 K. B. Sentell and J. G. Dorsey, *Anal. Chem.*, 61 (1989) 2373.
- 53 L. A. Cole and J. G. Dorsey, *Anal. Chem.*, 62 (1990) 16.
- 54 A. Alvarez-Zepeda and D. E. Martire, *J. Chromatogr.*, 550 (1991) 285.
- 55 P. B. Wright, E. Lamb, J. G. Dorsey and R. G. Kooser, *Anal. Chem.*, 64 (1992) 785.



# Thermodynamics of the adsorption of Tröger's base enantiomers from ethanol on cellulose triacetate

Andreas Seidel-Morgenstern<sup>☆</sup> and Georges Guiochon

Department of Chemistry, University of Tennessee, Knoxville, TN 37996-1501 (USA) and Division of Analytical Chemistry, Oak Ridge National Laboratory, Oak Ridge, TN 37831-6120 (USA)

## ABSTRACT

The adsorption isotherms of the (–) and (+)-enantiomers of Tröger's base on microcrystalline cellulose triacetate with ethanol as solvent were measured at 30, 40, 50 and 60°C using frontal analysis. The isotherms of the first eluted (–)-enantiomer can be described satisfactorily with the Langmuir equation at all temperatures. By contrast, the isotherms of the longer retained (+)-enantiomer exhibit a pronounced inflection point in the lower temperature range. This point nearly vanishes at 60°C where the isotherm is almost linear in the concentration range investigated. All these isotherms can be satisfactorily described by a quadratic isotherm equation. The standard thermodynamic functions were derived from these equilibrium data. The enthalpies and the isosteric heats of adsorption are not constant in the temperature region studied. The adsorption enthalpies of both enantiomers increase with increasing temperature. At constant temperature, the isosteric heat of adsorption of the (–)-enantiomer depends only slightly on the stationary phase concentration whereas that of the (+)-enantiomer increases strongly with increasing concentration.

## INTRODUCTION

The direct chromatographic resolution of racemic mixtures is being actively studied for analytical [1,2] and preparative [3] purposes. Several practically useful types of stationary phases have been reported [4], including microcrystalline cellulose triacetate (CTA), one of the first phases used for enantioseparations by preparative chromatography. Several racemates have been successfully separated with this material [5–14]. CTA is produced by the heterogeneous acetylation of microcrystalline cellulose [5]. It has good mechanical properties and is relatively inexpensive compared with other chiral phases.

However, CTA is not stable in all solvents. Its enantioselectivity is achieved only in a swollen state. Methanol, ethanol, 2-propanol and mixtures of

these alcohols with water or with hydrocarbons are the most useful mobile phases. Hesse and Haged [5] concluded that sorption on CTA is not achieved by adhering to one glucose ester moiety, but by insertion between two such moieties. They emphasized the crucial contribution from the crystalline structure and coined the term "inclusion chromatography" to describe the retention mechanism. CTA was extensively studied and characterized by Koller *et al.* [7].

Tröger's base (TB) is a classical racemate. Its enantioseparation was performed on lactose as early as 1944 [9]. In a recent study, the unusual retention behavior of TB on CTA observed by several workers [5,10,14] was explained as the consequence of different isotherm shapes for both TB enantiomers [15]. Whereas the isotherm of the (–)-enantiomer could be described by Langmuir's equation, the isotherm of the longer retained (+)-enantiomer exhibits an inflection point and is accounted for by a quadratic equation. Using the adsorption isotherms measured for both pure enantiomers and the ideal adsorbed solution theory to calculate the competitive iso-

Correspondence to: G. Guiochon, Department of Chemistry, University of Tennessee, Knoxville, TN 37996-1501, USA.

<sup>☆</sup> Present address: Institut für Technische Chemie, Technische Universität Berlin, Berlin, Germany.

therms, the elution bands could be predicted satisfactorily on the basis of the equilibrium dispersive model of chromatography [15].

The main object of this work was an investigation of the influence of temperature on the adsorption equilibrium of both TB enantiomers on CTA and a study of the standard thermodynamic functions describing the interactions between both enantiomers and the stationary and the mobile phases. A comparison of these functions should help to improve our understanding of enantioseparations on CTA. As demonstrated previously for bovine serum albumin as stationary phase [16], such a thermodynamic study can contribute to understanding the mechanism of chromatographic chiral separations.

## THEORY

### Adsorption isotherms

Simple considerations of statistical thermodynamics give the following general adsorption isotherm equation [17,18]:

$$q = q_s \frac{C(b_1 + 2b_2C + 3b_3C^2 + \dots + nb_nC^{n-1})}{1 + b_1C + b_2C^2 + b_3C^3 + \dots + b_nC^n} \quad (1)$$

where the product  $nq_s$  is the saturation capacity of the adsorbent and the temperature-dependent coefficients  $b_i$  are related to the partition functions for an individual molecule adsorbed on the  $i$ th monomolecular layer [17].

The first- ( $b_{2+} = 0$ ) and second-order ( $b_{3+} = 0$ ) equations of the type proposed (eqn. 1) are the Langmuir and the quadratic isotherm equations, respectively [18]. The adsorption of only one molecule on each adsorption site of the saturated monolayer is assumed in the former model and that of two molecules in the latter.

Recently, we demonstrated the applicability of the Langmuir and the quadratic isotherm equations to describe the adsorption behavior of the (–)- and (+)-enantiomers of TB on CTA at 40°C [15].

### Thermodynamics of adsorption

A thermodynamic analysis of adsorption processes can be found in several textbooks (e.g., refs. 18 and 19). The standard thermodynamic functions  $K$ ,  $\Delta G$ ,  $\Delta H$  and  $\Delta S$  at infinite dilution can be determined from the slope of the initial tangent of the isotherm. They can also be derived from the reten-

tion (capacity) factors,  $k'$ . The degree of agreement between these two sets of results is a measure of the validity of the isotherm at low concentrations. Disagreement between them is often caused by few residual, strong adsorption sites on the stationary phase surface.

The thermodynamic equilibrium constant,  $K$ , is the ratio of the activities of a component in the stationary and the mobile phases

$$K = a_s/a_m \quad (2)$$

Assuming a temperature-independent concentration for both phases as the standard state, the equilibrium constant is the initial slope of the adsorption isotherm:

$$K = \lim_{c \rightarrow 0} (q/C) \quad (3)$$

In the case of the isotherm eqn. 1,

$$K = b_1q_s \quad (4)$$

The equilibrium constant is related to the molar Gibbs free energy of adsorption,  $\Delta G$ , by

$$\Delta G = -RT \ln K \quad (5)$$

The following equation, derived from the Gibbs–Helmholtz equation, permits the determination of the molar enthalpy of adsorption,  $\Delta H$ , by plotting  $\ln K$  against  $1/T$ :

$$\frac{\partial(\ln K)}{\partial(1/T)} = -\frac{\Delta H}{R} \quad (6)$$

From  $\Delta G$  and  $\Delta H$  the molar entropy of adsorption,  $\Delta S$ , can be calculated by

$$\Delta S = -\frac{\Delta G - \Delta H}{T} \quad (7)$$

Further, from the adsorption isotherms measured at different temperatures it is possible to derive the isosteric heat of adsorption,  $\Delta H_{st}$ , or heat of adsorption at constant adsorbate concentration, according to the following equation:

$$\left. \frac{\partial(\ln C)}{\partial(1/T)} \right|_q = \frac{\Delta H_{st}}{R} \quad (8)$$

The slope of a plot of  $\ln C$  vs.  $1/T$  at constant  $q$  yields  $\Delta H_{st}$ . The determination of the isosteric heats of adsorption is useful at high concentrations, when the isotherm is no longer linear and  $\Delta H_{st}$  depends on

the surface coverage. In the linear range of the isotherm, the isosteric heat of adsorption is identical with the molar enthalpy of adsorption defined in eqn. 6.

## EXPERIMENTAL

### Equipment

The determination of isotherms by frontal analysis (FA) and the measurement of elution profiles were performed using an HP 1090 liquid chromatograph (Hewlett-Packard, Palo Alto, CA, USA), equipped with a temperature-controlled column chamber, a solvent-delivery system, an automatic sample injector, a rapid-scan UV photodiode array detector and a data station. The column temperature could be controlled with an accuracy of *ca.* 1 K. The detector response was calibrated using the plateaux of the FA runs. For a wavelength of 300 nm the response was fitted with a third-order polynomial for TB concentrations up to 0.006 mol/l.

### Materials

**Stationary phase.** A sample of microcrystalline cellulose triacetate (CTA, 15–25  $\mu\text{m}$ ), Fig. 1, was kindly supplied by Dr. J. N. Kinkel (Merck, Darmstadt, Germany). The application of this material to enantioseparations by preparative chromatography has been described [10,13]. A 10  $\times$  0.46 cm I.D. stainless-steel column was packed using a slurry

technique. Prior to packing, CTA was boiled in ethanol for 30 min to allow its swelling. After cooling and decanting, the suspension was treated in an ultrasonic bath for 5 min at ambient temperature and poured into the packing chamber. An 80-ml volume of ethanol was applied as pushing solvent at a pressure of 275 bar.

Following Koller *et al.* [7], the total column porosity was measured by injecting 1,3,5-tri-*tert.*-butylbenzene (TTB). As its retention time did not change significantly with the temperature, TTB could be considered as non-retained on CTA. The number of theoretical plates of the column for TTB was about 400. The total void volume measured for the column was 1.0 ml, leading to a total porosity  $\varepsilon_T = 0.602$ , corresponding to a phase ratio  $F$  of 0.661, with  $F = (1 - \varepsilon_T)/\varepsilon_T$ .

An additional volume of tubing (0.78 ml) caused a time delay for the step injections performed with the solvent-delivery system compared with injections of small samples made with the automatic sample injector.

**Mobile phase and chemicals.** All experiments were performed under isocratic conditions, using pure ethanol (Midwest Grain Products, 200 proof). A racemic mixture of Tröger's base (TB),  $\text{C}_{17}\text{H}_{18}\text{N}_2$  ( $M = 250.35$  g/mol), Fig. 1, was also supplied by Dr. Kinkel. TB enantiomers with purity >99.5% and 1,3,5-tri-*tert.*-butylbenzene were purchased from Fluka (Buchs, Switzerland). All these compounds were used as received.

### Procedures

Prior to isotherm determinations, some small samples of both TB enantiomers were eluted. The classical parameters of linear chromatography were determined at different temperatures and are reported in Table I. Noteworthy are the high separation factors and the low column efficiency. Because of the considerable band broadening due to slow mass transfer, longer columns would be necessary to deliver the number of theoretical plates required for preparative separations. However, FA is the only chromatographic method allowing accurate isotherm measurements with low-efficiency columns [20]. As the method requires complete saturation of the stationary phase with the sample solution, shorter columns are advantageous to save material and therefore a 10-cm column was used.

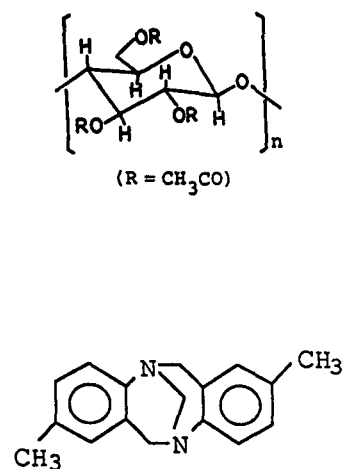


Fig. 1. Structures of microcrystalline cellulose triacetate and Tröger's base.

TABLE I  
PARAMETERS DETERMINED FROM INJECTIONS OF SMALL SAMPLE SIZES (LINEAR CHROMATOGRAPHY)

$T$ (K)	$k' (-)$	$K (-)$	$N_p (-)$	$k' (+)$	$K (+)$	$N_p (+)$	$\alpha$
303	2.50	3.78	29	5.13	7.76	20	2.05
313	1.96	2.96	44	4.24	6.41	31	2.17
323	1.63	2.47	63	3.34	5.05	47	2.04
333	1.19	1.80	105	2.40	3.63	71	2.02

In FA, successive step changes in the eluent composition at the column inlet are made. Solving the integral mass balance equation from each breakthrough curve gives one point of the isotherm. Owing to the self-sharpening of the breakthrough fronts, the concentration steps ought to be positive for isotherms of the Langmuir type, whereas if the isotherm curvature is the opposite, decreasing concentration steps should be used.

In our previous study, we observed an inflection point for the isotherm at 40°C of the (+)-enantiomer in the concentration range 0.0012–0.0024 mol/l [15]. To be sure to determine this feature accurately, the concentration of the solutions used for the FA experiments was chosen to be 0.0048 mol/l for both enantiomers. As the duration of the experiments was several hours, during which the solution is degassed with helium, the concentration of the enantiomer solution increases slightly during the runs, owing to solvent losses. Ten concentration steps were performed to determine ten points for each isotherm. The flow-rate in all the FA experiments was 0.5 ml/min. The column temperature was varied between 30 and 60°C in intervals of 10 K. The primary chromatographic data were transferred to the VAX 8700 computer of the University of Tennessee Computing Center for further processing.

The amount adsorbed during each step of an FA run was calculated from the integral mass balance equation

$$t_R = t_0 \left[ 1 + F \cdot \frac{q(C_E) - q(C_0)}{C_E - C_0} \right] \quad (9)$$

where  $q(C_0)$  is the amount adsorbed at equilibrium before the step change from concentration  $C_0$  to concentration  $C_E$  at column inlet and  $t_0$  is the retention time of a non-retained component. Eqn. 9

allows the determination of the new point of the isotherm,  $q(C_E)$ , from the retention time of the breakthrough front,  $t_R$ . The retention time of each concentration front could be determined with a precision of better than 1.5%.

The FA experiments were carried out using the automatic solvent-delivery system to generate the concentration steps. Only steps of increasing concentration were performed for the (–)-enantiomer of TB. Owing to the observed inflection point of the TB (+)-isotherm at 40°C [15], steps of decreasing concentration were also recorded. The combined analysis of the adsorption and desorption steps permits a more accurate determination of isotherms which have an inflection point. Depending on the concentration range, either the adsorption or the desorption front is sharper and allows a more

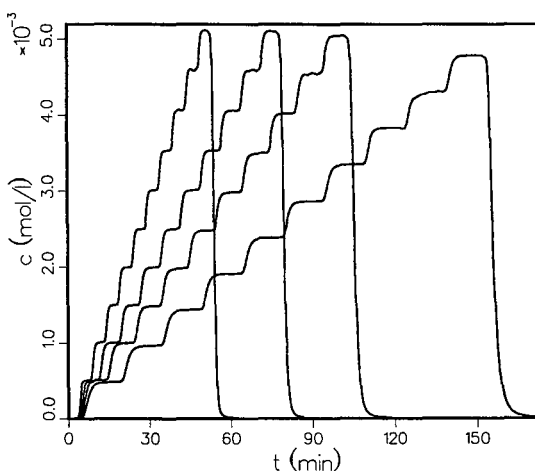


Fig. 2. Frontal analysis to determine the isotherms of the (–)-enantiomer of TB at 30, 40, 50 and 60°C (right to left).

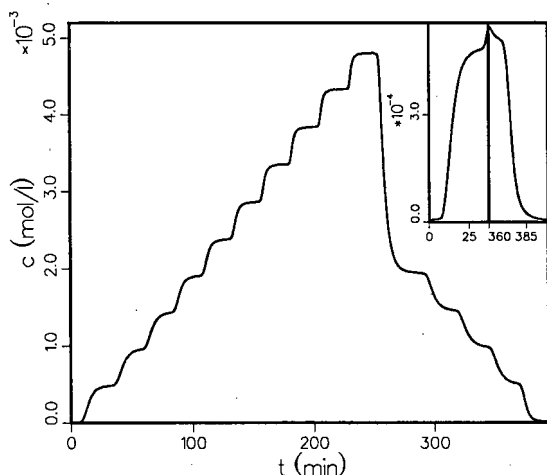


Fig. 3. Frontal analysis to determine the isotherm of the (+)-enantiomer of TB at 30°C. Inset: adsorption and desorption fronts for the lowest concentration range.

accurate determination of the breakthrough retention time and hence of the isotherm point.

Fig. 2 shows the FA chromatograms recorded at the four temperatures investigated for the (-)-isomer. The chromatograms were recorded beginning with 30°C, and in order of increasing temperature. The slight increase in the plateau concentrations mentioned above can be seen. This effect was taken into account in the data analysis. In Fig. 3 the FA analysis at 30°C for the (+)-enantiomer is shown. The inset shows that the adsorption front for the first concentration step is more dispersed than the corresponding desorption front. This indicates an increase in the isotherm slope,  $dq/dc$ , in this concentration region and hence that the isotherm is convex downward.

## RESULTS AND DISCUSSION

### Modeling of the isotherms

The equilibrium isotherms obtained for the adsorption of the enantiomers of TB on CTA at the four temperatures investigated are shown in Fig. 4. The lines were calculated by fitting the data points to the Langmuir isotherm [ $q = q_s b_1 C / (1 + b_1 C)$ ] for the (-)-enantiomer and to the quadratic isotherm [ $q = q_s C (b_1 + 2b_2 C) / (1 + b_1 C + b_2 C^2)$ ] for the (+)-enantiomer. In each instance, the selected model describes the experimental isotherms very well. The

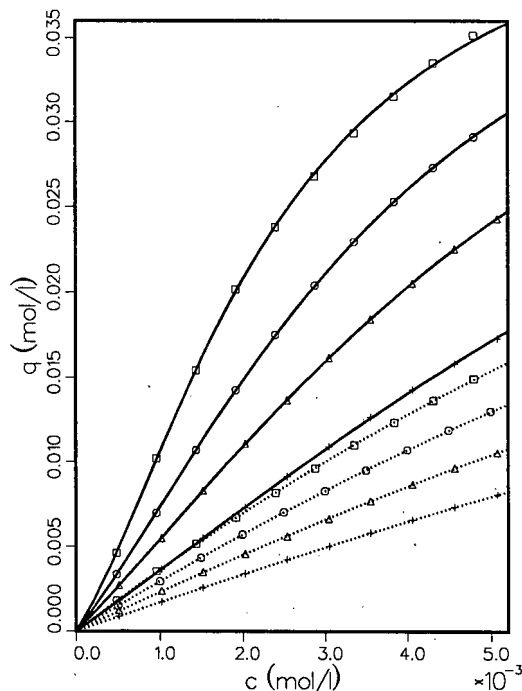


Fig. 4. Isotherms of the (-) and (+)-enantiomers of TB on CTA at 30, 40, 50 and 60°C (top to bottom). The lines are calculated with (dotted lines) the Langmuir isotherm for the (-) and (solid lines) with the quadratic isotherm equation for the (+)-enantiomer; parameters as in Table II. The symbols indicate the experimental data.

Langmuir model was not able to account for the (+)-enantiomer isotherm. The values obtained for the parameters of the equation and the corresponding standard deviations are given in Table II. These values were calculated by minimizing the following objective function, using Marquardt's method [21]:

$$\sigma (\%) = 100 \sqrt{\frac{1}{N_D - P} \sum_{i=1}^{N_D} \left( \frac{q_i^{\text{ex}} - q_i^{\text{th}}}{q_i^{\text{ex}}} \right)^2} \quad (10)$$

where  $N_D$  and  $P$  are the numbers of data points and of model parameters, respectively.

There are two major differences between the isotherms of the two enantiomers as shown in Fig. 4. First, in the concentration range investigated, the adsorption capacity of CTA for the (+)-enantiomer is almost double that for the (-)-enantiomer. Second, the isotherms of the (+)-enantiomer exhibits an inflection point.

The parameters reported in Table II allow an



TABLE II  
PARAMETERS OF THE ISOTHERM EQUATIONS

Enantiomer	$T$ (K)	$q_s$ (mol/l)	$b_1$ (l/mol)	$b_2$ (l <sup>2</sup> /mol <sup>2</sup> )	$\sigma$ (%)
(-)-	303	0.08001	47.59	0	0.50
	313	0.08504	36.00	0	0.28
	323	0.08176	29.17	0	0.79
	333	0.08848	19.73	0	0.38
(+) -	303	0.02386	316.37	173 572	0.65
	313	0.02587	244.29	63 459	0.33
	323	0.02771	183.86	26 430	0.33
	333	0.03116	113.38	8129	0.37

estimation of the saturation capacity of the stationary phase. However, this estimation, which relies on the extrapolation of isotherm data to high concentrations, cannot be very accurate, as the highest concentration investigated in this study is more than an order of magnitude smaller than the solubility concentration of TB in ethanol. The values obtained

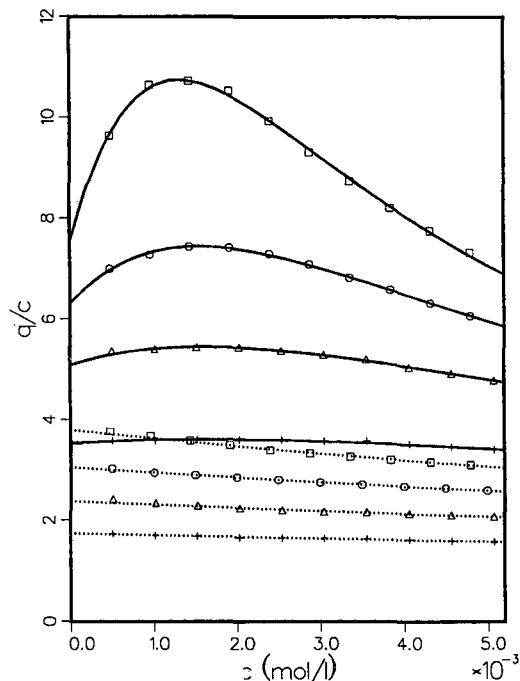


Fig. 5. Plot of the ratio  $q/C$  of the isotherms in Fig. 4 versus the liquid phase concentration  $C$ . Symbols as in Fig. 4.

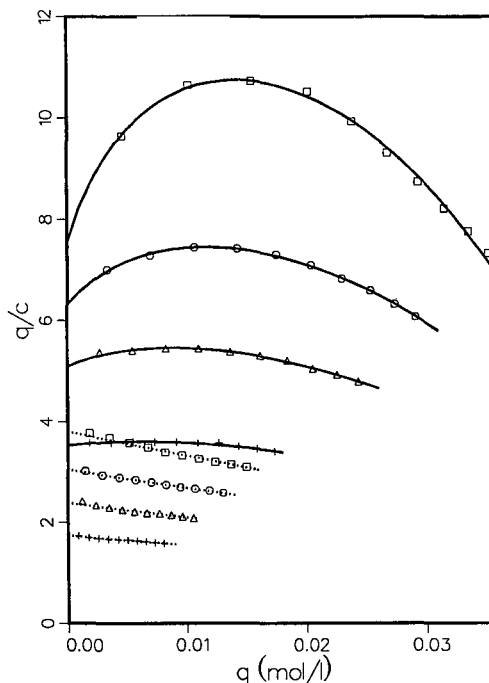


Fig. 6. Plot of the ratio  $q/C$  of the isotherms in Fig. 4 versus the stationary phase concentration. Symbols as in Fig. 4.

for the parameter  $q_s$  of the (-)-enantiomer are almost independent of temperature, suggesting a saturation capacity between 0.08 and 0.09 mol/l. For the (+)-enantiomer the extrapolated values of the saturation capacities are lower. They increase from 0.048 to 0.062 mol/g when the temperature increases from 30 to 60°C. Owing to the complicated course of the (+)-enantiomer isotherm, these values must be considered as uncertain. An accurate determination of the saturation capacity of the stationary phase requires additional measurements in a higher concentration range.

The existence of an inflection point of the TB (+)-isotherms is illustrated in Figs. 5 and 6, where the ratio  $q/C$  for each isotherm is plotted against the mobile and the stationary phase concentration, respectively. For the Langmuir equation, a plot of  $q/C$  vs.  $q$  yields a straight line. The plots corresponding to the data for the (-)-enantiomer obviously fulfil this condition very well. The (+)-enantiomer shows a completely different behavior, giving plots that exhibit a marked maximum. The inflec-

TABLE III

MAXIMA OF THE SLOPES  $dq/dC$  OF THE ISOTHERMS FOR THE (+)-ENANTIOMER AND CORRESPONDING LIQUID PHASE CONCENTRATIONS AND LOADINGS

$T$ (K)	$C$ (mol/l)	$q$ (mol/l)	$dq/dC_{\max}$
303	0.00079	0.0082	11.63
313	0.00095	0.0070	7.77
323	0.00101	0.0055	5.75
333	0.00106	0.0038	3.64

tion point of the isotherm is most pronounced at 30°C. This effect vanishes gradually with increasing temperature. At 60°C, the isotherm is almost linear. The parameter  $b_2$  in eqn. 1 allows for the description of the inflection point. It is about 21 times smaller at 60°C than at 30°C. As can be seen in Figs. 5 and 6, the location of the inflection point shifts between 30 and 60°C in the direction of higher liquid phase concentrations (Fig. 5) and of lower stationary phase concentrations (Fig. 6). To demonstrate this effect more precisely, we report in Table III the mobile and stationary phase concentrations for the maxima of the slope  $dq/dC$  of the TB (+)-isotherm.

TABLE IV

THERMODYNAMIC PARAMETERS

Enantiomer	$T$ (K)	$K$ (-)	$\Delta G$ (kJ/mol)	$\Delta H$ (kJ/mol)	$\Delta S$ (J/mol · K)
(-)-	303	3.807	-3.37		
	308	3.410 <sup>a</sup>	-3.14	-17.27	-45.9
	313	3.061	-2.91		
	318	2.698 <sup>a</sup>	-2.62	-20.96	-57.7
	323	2.385	-2.33		
	328	2.037 <sup>a</sup>	-1.94	-27.88	-79.1
	333	1.746	-1.54		
(+) -	303	7.549	-5.09		
	308	6.901 <sup>a</sup>	-4.94	-14.07	-29.6
	313	6.320	-4.80		
	318	5.669 <sup>a</sup>	-4.59	-18.09	-42.5
	323	5.095	-4.41		
	328	4.234 <sup>a</sup>	-3.94	-32.73	-87.8
	333	3.533	-3.49		

<sup>a</sup>  $K(T) = \exp[\ln K_b - (\Delta H/R)(1/T - 1/T_b)]$ , where  $b$  designates one of the interval borders.

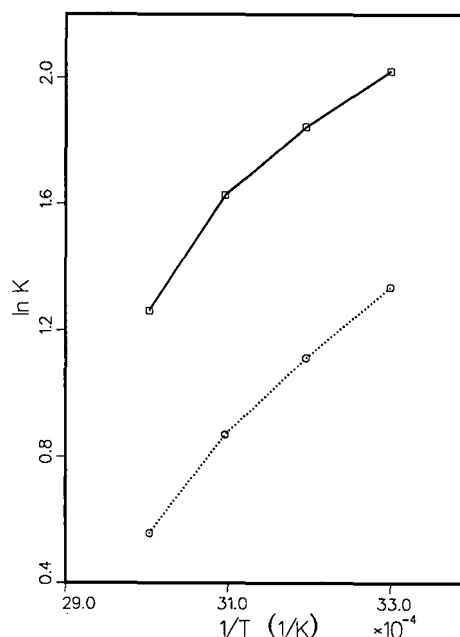


Fig. 7. Temperature dependence of the equilibrium constants of the (dotted line) (-)- and (solid line) (+)-enantiomers.

#### Thermodynamic analysis

The values calculated for  $K$ ,  $\Delta G$ ,  $\Delta H$  and  $\Delta S$  at infinite dilution are summarized in Table IV. The difference between the adsorption equilibrium constants,  $K$ , determined from the retention times of small sample injections in the linear range of the isotherms (Table I) and calculated from the parameters of the experimental isotherms according to eqn. 4 is less than 3.6%, which is satisfactory.

The determination of the adsorption enthalpies at infinite dilution according to eqn. 6 is illustrated in Fig. 7. Obviously the data cannot be represented by a straight line and the adsorption enthalpies depend on the temperature. For this reason, the three temperature intervals were evaluated separately. It was assumed that within each interval the adsorption enthalpy is constant. To calculate the mean Gibbs free energies and adsorption entropies for each temperature interval, an equilibrium constant  $K$  was estimated for the average temperature, using the adsorption enthalpies determined from the interval borders.

The absolute values of  $\Delta H$  obtained (Table IV) in the intervals 30–40 and 40–50°C are smaller for the

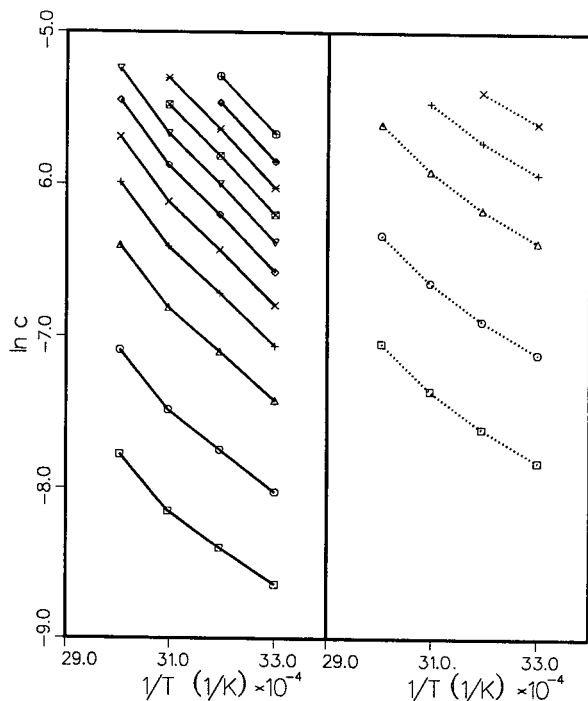


Fig. 8. Plot of  $\ln C$  versus  $1/T$  at constant stationary phase concentration for the (dotted lines) (–)- and (solid lines) (+)-enantiomers. The stationary phase concentrations increase from bottom to top:  $q = 0.0015, 0.003, 0.006, 0.009, 0.012$  (for both enantiomers) and  $0.015, 0.018, 0.021, 0.024, 0.027, 0.030$  mol/l [the (+)-enantiomer].

(+)-enantiomer than for the (–)-enantiomer. The opposite holds true for the interval 50–60°C. For both enantiomers, the adsorption entropies decrease very rapidly with increasing temperature (Table IV). Comparing the values for the (–)- and (+)-enantiomers, the same observations as mentioned above for the adsorption enthalpies can be made in the three temperature intervals.

The plot of  $\ln C$  vs.  $1/T$  at constant  $q$ , given in Fig. 8, demonstrates the determination of the isosteric heat of adsorption for different surface coverages. According to eqn. 8, the slopes of these curves, proportional to the isosteric heat of adsorption, depend on temperature. Again, for each of the three temperature intervals, the isosteric heats of adsorption were estimated separately. The results for both enantiomers are summarized in Fig. 9 as plots of  $-\Delta H_{st}$  versus  $q$ . In these plots, the adsorption enthalpies at infinite dilution (Table IV) are in-

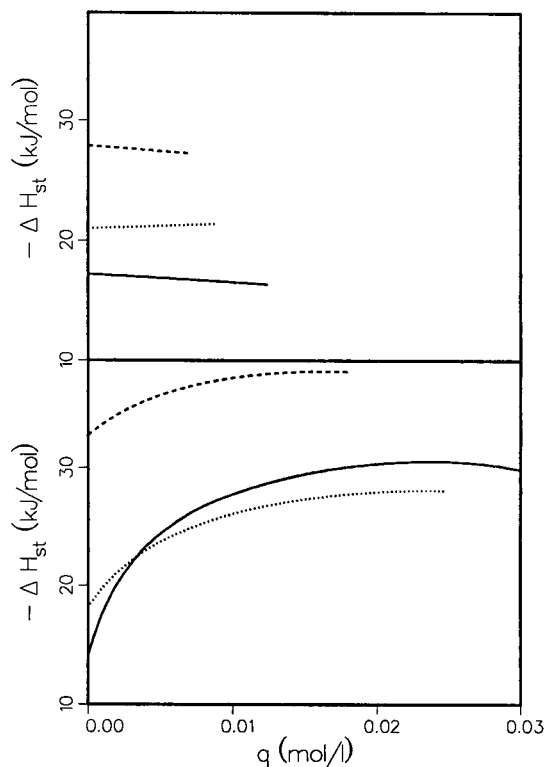


Fig. 9. Plot of the isosteric heat of adsorption versus the stationary phase concentration for the (top) (–)- and (bottom) (+)-enantiomers. The lines belong to different temperature intervals: (solid) 30–40, (dotted) 40–50 and (dashed) 50–60°C.

cluded, as the limit of the isosteric heats of adsorption for zero stationary phase concentrations.

Fig. 9 shows the completely different behavior of the two enantiomers. The loading dependence of the isosteric heat of adsorption is not very pronounced for the (–)-enantiomer; in fact it is barely significant. By contrast, the isosteric heat of adsorption of the (+)-enantiomer increases strongly with increasing mobile phase concentration, up to ca. 0.01 mol/l. This concentration range includes the inflection points of all the TB (+)-isotherms whose shape is strongly effected by it (Table III). The increase in the isosteric heat of adsorption observed is most pronounced between 30 and 40°C and becomes less important at higher temperatures, as does the change in isotherm curvature around its inflection point (Figs. 5 and 6). At high concentrations, the isosteric heat of adsorption of the (+)-enantiomer is less

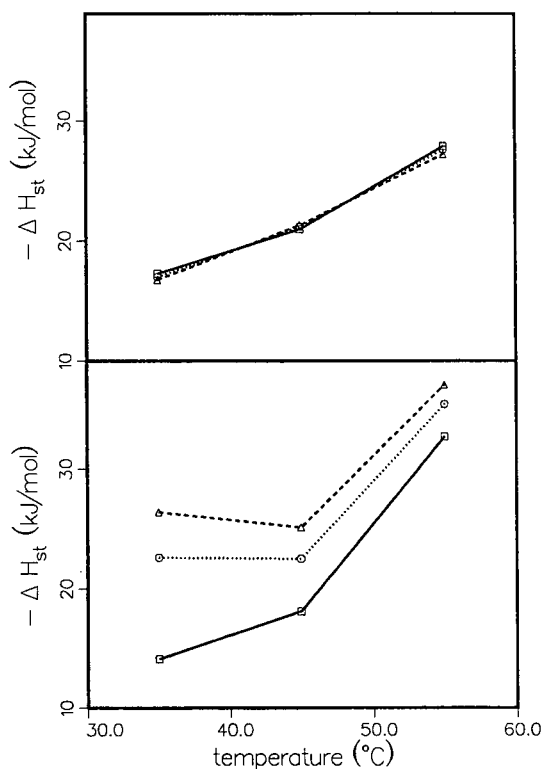


Fig. 10. Plot of the isosteric heat of adsorption versus the average temperatures of the three intervals for the (top) (-) and (bottom) (+)-enantiomers. The lines belong to different loadings: (solid) 0, (dotted) 0.0035 and (dashed) 0.007 mol/l.

dependent on the concentration for all the temperature intervals studied.

Fig. 10 illustrates the dependence of the isosteric heat of adsorption on the temperature at infinite dilution and for two stationary phase concentrations in the region of the inflection point of the (+)-isotherm. For the (-)-enantiomer,  $\Delta H_{st}$  increases nearly linearly with increasing temperature in the considered range and is independent of the stationary phase concentration. The results for the (+)-enantiomer show that at infinite dilution the isosteric heat of adsorption, or adsorption enthalpy, increases with increasing temperature. At the two finite stationary phase concentrations,  $\Delta H_{st}$  is almost constant between 35 and 45°C but increases markedly for the highest temperature. Further, the striking difference between the two enantiomers is the distinct increase in the isosteric heat of adsorp-

tion of the (+)-enantiomer with increasing stationary phase concentration at constant temperature.

All these results demonstrate that the interactions between the TB enantiomers, CTA and ethanol are complex. We have not investigated the interactions between ethanol and CTA or their temperature dependence. The experimental results could also be affected by the possibility of hydrogen bondings between TB and ethanol, which are also temperature dependent. A further interpretation of the observed behavior of the enantiomers of TB on CTA requires, besides adsorption measurements, additional characterization of the changes of the stationary phase at different temperatures and loadings using other methods.

#### Elution profiles

The consequences for the profiles of chromatographic bands of the non-linear behavior of the isotherm are well known [20]. They result from the changes in the slope of the adsorption isotherm with increasing concentration, and in the relationship

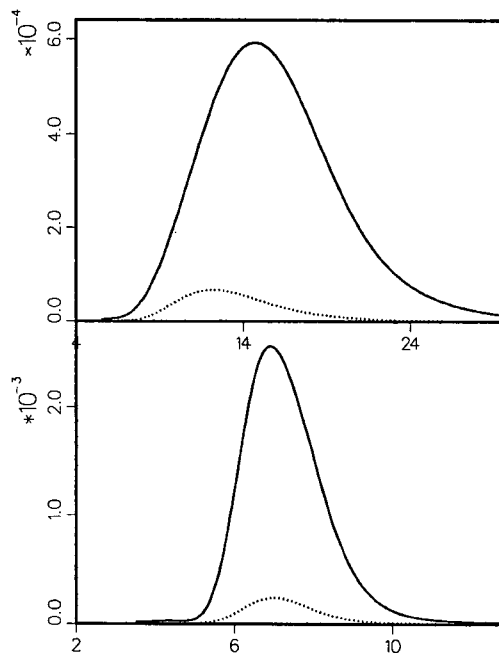


Fig. 11. Elution profile for the (+)-enantiomer at (top) 30 and (bottom) 60°C. Injected sample concentration, 0.06 mol/l; injected volumes, (dotted lines) 5 and (solid lines) 60  $\mu$ l; flow-rate, 0.5 ml/min. The times of the peak maxima are 12.3 and 14.7 min (30°C) and 7.0 and 6.9 min (60°C).

between this slope and the retention time associated with the concentration. When the concentration increases, a decrease in the isotherm slope with increasing concentration leads to a decrease in the retention time, whereas an increase in this slope causes an increase in the retention time.

To demonstrate the influence of an inflection point in the isotherm on the band profile, we compare in Fig. 11 chromatograms recorded for two samples of different sizes of the (+)-enantiomer, at 30 and 60°C. Obviously, there is a significant increase in the retention time with increasing loading at 30°C. This effect can be fully explained with the shape of the adsorption isotherm in the relevant concentration range (compare Figs. 4-6), and results from the fact that  $d^2q/dC^2 > 0$ . At 60°C, the retention times of the two samples are very similar and the peaks are nearly symmetrical, illustrating the consequence of an almost linear adsorption isotherm. The possibility of predicting the elution chromatograms of TB on CTA with the equilibrium-dispersive model using the experimental adsorption isotherms was demonstrated previously [15].

The observed differences in the thermodynamic behavior of the two enantiomers studied are limited to a marked change in elution profiles at high concentrations. Their separation factor remains exceptionally constant, around 2. Nevertheless, these results indicate that the experimental conditions for the separation and purification of two isomers by preparative chromatography should be carefully selected. The knowledge of the adsorption isotherms is the most important prerequisite for the optimization of the temperature and the sample size. In the present instance, the selection of the temperature permits a modulation of the intensity of the displacement effect.

#### SYMBOLS

$a$	Activity
$b_i$	Parameter in isotherm eqn. 1 (l/mol) <sup>i</sup>
$C$	Liquid (mobile) phase concentration (mol/l)
$F$	Phase ratio
$\Delta G$	Molar free energy of adsorption (kJ/mol)
$\Delta H$	Molar enthalpy of adsorption (kJ/mol)
$\Delta H_{st}$	Isosteric heat of adsorption (kJ/mol)
$k'$	Retention factor
$K$	Thermodynamic equilibrium constant

$N_p$	Number of theoretical plates
$N_D$	Number of data
$P$	Number of parameters
$q$	Stationary phase concentration (loading) (mol/l)
$q_s$	Parameter in eqn. 1, related to the saturation loading (mol/l)
$R$	Universal gas constant (kJ/mol · K)
$\Delta S$	Molar entropy of adsorption (J/mol · K)
$t$	Time (s)
$t_R$	Retention time (s)
$t_0$	Retention time of a non-retained component (s)

#### Greek letters

$\alpha$	Separation factor, $\alpha = k'_2/k'_1$
$\epsilon_T$	Total porosity

#### Superscripts

ex	Experimental value
th	Theoretical value

#### Subscripts

E	At column inlet
m	Mobile phase
s	Stationary phase

#### ACKNOWLEDGEMENTS

We acknowledge the gift of microcrystalline cellulose triacetate and Tröger's base samples from Dr. J. N. Kinkel (Merck, Darmstadt, Germany). A.S.-M. is grateful for the support of his stay in Knoxville by the German Academic Exchange Service (DAAD). The HP 1090 liquid chromatograph was a gift from Hewlett-Packard (Palo Alto, CA, USA). This work was supported in part by grant CHE-8901382 from the National Science Foundation and by the cooperative agreement between the University of Tennessee and the Oak Ridge National Laboratory. We acknowledge continuous support of our computational efforts by the University of Tennessee Computing Center.

#### REFERENCES

- 1 D. W. Armstrong and S. M. Han, *CRC Crit. Rev. Anal. Chem.*, 19 (1988) 175.
- 2 W. H. Pirkle and T. C. Pochapsky, *Chem. Rev.*, 89 (1989) 347.

- 3 S. G. Allenmark, *Chromatographic Enantio-separation: Methods and Applications*, Ellis Horwood, Chichester, 1988.
- 4 M. Zief and L. J. Crane, *Chromatographic Chiral Separations*, Marcel Dekker, New York, 1988.
- 5 G. Hesse and R. Hagel, *Chromatographia*, 6 (1973) 277.
- 6 G. Hesse and R. Hagel, *Justus Liebigs Ann. Chem.*, 996 (1976).
- 7 H. Koller, K.-H. Rimbock and A. Mannschreck, *J. Chromatogr.*, 89 (1983) 282.
- 8 Y. Okamoto, M. Kawashima, K. Yamamoto and K. Hatada, *Chem. Lett.*, 739 (1984).
- 9 G. Blaschke, *J. Liq. Chromatogr.*, 9 (1986) 341.
- 10 J. N. Kinkel, K. Reichert and P. Knöll, *GIT-Suppl.*, No. 3 (1989) 104–112.
- 11 C. Roussel, J. L. Beauvais and A. Chemlal, *J. Chromatogr.*, 462 (1989) 95.
- 12 E. Francotte and R. M. Wolf, *Chirality*, 2 (1990) 16.
- 13 A. Werner, *Kontakte (Darmstadt)*, 3 (1989) 50.
- 14 R. Isaakson, P. Erlandsson, L. Hansson, A. Holmber and S. Berner, *J. Chromatogr.*, 498 (1990) 257.
- 15 A. Seidel-Morgenstern and G. Guiochon, *Chem. Eng. Sci.*, in press.
- 16 S. Jacobson, S. Golshan-Shirazi and G. Guiochon, *J. Chromatogr.*, 522 (1990) 23.
- 17 T. L. Hill, *An Introduction to Statistical Thermodynamics*, Addison-Wesley, Reading, MA, 1960.
- 18 D. M. Ruthven, *Principles of Adsorption and Adsorption Processes*, Wiley, New York, 1984.
- 19 J. H. de Boer, *The Dynamical Character of Adsorption*, Clarendon Press, Oxford, 1968.
- 20 A. M. Katti and G. Guiochon, *Adv. Chromatogr.*, 32 (1991) 1.
- 21 D. W. Marquardt, *J. Soc. Appl. Math.*, 11 (1963) 431.



# New chromatographic hydrophobicity index ( $\varphi_0$ ) based on the slope and the intercept of the $\log k'$ versus organic phase concentration plot

Klára Valkó<sup>☆</sup> and Péter Slégel<sup>☆☆</sup>

Department of Pharmaceutical Chemistry, School of Pharmacy, University of London, 29–39 Brunswick Square, London WC1N 1AX (UK)

## ABSTRACT

A new chromatographic hydrophobicity index ( $\varphi_0$ ) is suggested as a measure of the lipophilic character of compounds in reversed-phase high-performance liquid chromatography (RP-HPLC). The parameter  $\varphi_0$  is defined as the organic phase concentration (methanol or acetonitrile) in the mobile phase which is required for  $\log k' = 0$  (retention time is double the dead time), that is, the molar fraction of the compound is identical in the mobile and the stationary phases. The  $\varphi_0$  values therefore range from 0 to 100%, and the higher the value the more hydrophobic is the compound. It is shown that the value of  $\varphi_0$  is characteristic for a compound and depends only on the type of organic modifier, pH and temperature. It is independent of the RP column type and length, flow-rate and the mobile phase compositions where the actual retention measurements are carried out. The other advantages of  $\varphi_0$  are that it can be precisely measured, as it has a concrete physical meaning, namely the organic phase concentration of the mobile phase at which the retention time is exactly double the dead time (not like  $\log k'$  values extrapolated to water as mobile phase), and it is independent of the linear or quadratic function of the  $\log k'$  versus  $\varphi$  relationships. The  $\varphi_0$  values not only reflect the hydrophobic character of compounds but also provide a valuable means for method development in RP-HPLC as they reveal a mobile phase composition with known retention time values. The  $\varphi_0$  values for over 500 compounds were calculated and are presented on the basis of their published retention data. The  $\varphi_0$  values obtained with methanol and acetonitrile showed an excellent correlation with each other. Significant correlations were found between the  $\varphi_0$  values and the logarithm of 1-octanol–water partition coefficients ( $\log P$ ).

## INTRODUCTION

It has been recognized since the work of Overton [1] and Meyer [2] that the hydrophobic properties of drugs play an important role in their pharmacological activity. The hydrophobicity of drugs is most commonly characterized by their 1-octanol–water partition coefficients ( $\log P$ ) was proposed by Hansch and co-workers [3,4]. Consideration of this parameter in structure–activity and structure–toxic-

ity studies might substantially reduce drug development costs [5]. Although the choice of 1-octanol as a solvent reflecting the properties of the lipid components of the cell membrane has occasionally been questioned, the large number of 1-octanol–water partition data collected by Hansch and Leo [6] has made the partition system a common reference standard.

Owing to several difficulties in making  $\log P$  measurements by the traditional shake-flask method, several chromatographic approaches have been published, which were summarized in detail by Braumann [7] and Kaliszan [8]. In reversed-phase high-performance liquid chromatography (RP-HPLC) the chromatographic retention is governed by hydrophobic forces, and therefore various RP-HPLC retention data have been suggested for cal-

Correspondence to: K. Valkó, Department of Pharmaceutical Chemistry, School of Pharmacy, University of London, 29–39 Brunswick Square, London WC1N 1AX, UK.

<sup>☆</sup> On leave from the Central Research Institute for Chemistry, Hungarian Academy of Sciences, Budapest, Hungary.

<sup>☆☆</sup> On leave from EGIS Pharmaceuticals, Budapest, Hungary.



culating the log  $P$  values of compounds. There are three main approaches. The first is the use of RP-HPLC log  $k'$  values obtained on a given column with a given mobile phase composition. The second approach is to use log  $k'$  values extrapolated to 0% organic modifier concentration (log  $k'_w$ ). The log  $k'_w$  values can be directly obtained only for a relatively small number of compounds, and therefore some means of predicting this value must be utilized. Butte *et al.* [9] and Hammers *et al.* [10] used linear extrapolation from the log  $k'$  vs. organic modifier concentration ( $\varphi$ ) plot to predict log  $k'_w$  values. However several results [11,12] showed that the linearity of the plot is not valid for a wide organic modifier concentration, and the log  $k'_w$  values are not the same when they were derived from data obtained by using acetonitrile or methanol as the organic modifier. Schoenmakers *et al.* [13] described quadratic relationships between log  $k'$  and  $\varphi$  values. Wells and Clark [14] suggested the application of the solvophobic theory proposed by Horváth *et al.* [15] for the prediction of log  $k'_w$ . The third approach [16] suggests a backwards extrapolation method for the log  $k'$  values referring to an optimum organic phase concentration in the mobile phase by which the 1-octanol–water partition system can be best modelled. The calculation is based on the slope and the intercept values from the linear portion of the log  $k'$  vs.  $\varphi$  plots.

The aim of this study was to find a chromatographic hydrophobicity index that can be easily and precisely measured, relatively independent of the applied chromatographic conditions (type and dimensions of the column, flow-rate, etc.). A large database was set up from published data and there is a good correlation with 1-octanol–water partition coefficients.

#### THEORETICAL BACKGROUND

The capacity factor,  $k'$ , in chromatography is defined [17] as  $n_s/n_m$ , *i.e.*, the ratio of the total number of moles of X in the stationary phase ( $n_s$ ) to the number of moles of X in the mobile phase ( $n_m$ ). It also can be expressed by the concentrations of X molecules in the mobile and stationary phases according to the equation [18]

$$k' = (X)_s V_s / (X)_m V_m \quad (1)$$

where  $V_s$  and  $V_m$  are the volumes of the stationary and mobile phases, respectively, and (X) is the concentration of X. When  $k' = 1$  (log  $k' = 0$ ), and also the retention time is double the dead time [from  $k' = (t_r - t_0)/t_0$ ], this means that

$$(X)_s V_s = (X)_m V_m \quad (2)$$

The distribution constant,  $K$ , which measures the equilibrium distribution of X between the stationary and the mobile phases, can be expressed by  $(X)_s / (X)_m$ , so by rearranging eqn. 2 we obtain

$$K V_s = V_m \quad (3)$$

$V_s$ , the volume of the stationary phase, can be regarded as constant in a given column, hence  $V_m$  will be proportional to the distribution constant of compound X. If we consider that  $V_m$  can be varied by changing the non-polar volume fraction of the mobile phase, then we can accept that it will be proportional to the distribution constant of X (see Fig. 1).

In order to prove that  $\varphi_0$  values are independent of the column constant ( $V_s/V_m$ ), the following consideration can be made.  $k'$  is proportional to the distribution constant  $K$  according to the equation

$$k' = K(V_s/V_m) \quad (4)$$

Eqn. 4 can be written in logarithmic form:

$$\log k' = \log K + \log (V_s/V_m) \quad (5)$$

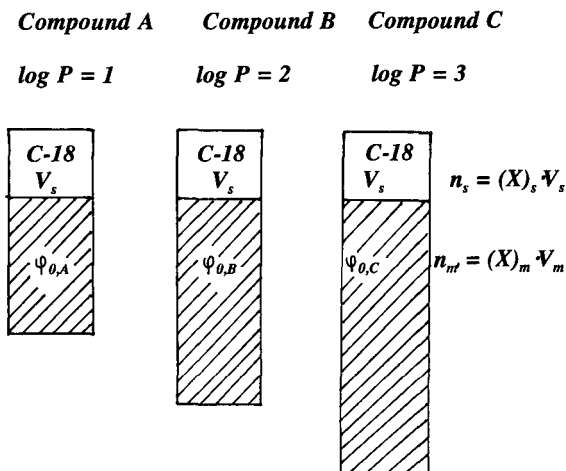
The log  $k'$  values are also dependent on the organic phase concentration and for the sake of simplicity we can consider a linear relationship (a properly small portion of any suggested curve can be regarded as linear, after all), which can be described by the equation

$$\log k' = \log K + \log (V_s/V_m) = S\varphi + \log k'_w \quad (6)$$

where  $S$  and log  $k'_w$  are the slope and the intercept values of the straight line. The intercept value theoretically means the log  $k'$  value extrapolated to pure water as mobile phase and can be expressed by the distribution constant and the phase ratio, as shown by the equation

$$\log k'_w = K_w + \log (V_s/V_m) \quad (7)$$

The slope  $S$  can also be written as the log  $k'$  change caused by changing the organic phase concentration in the mobile phase by 1%, which can be formulated by the equation



if in all cases  $n_s = n_m$  i. e.  $(X)_s V_s = (X)_m V_m$

and  $V_s$  is constant,  $V_m$  is regarded as  $\varphi_0$ ,

then  $\varphi_0$  will be proportional to  $K$

Fig. 1. Illustration of the chromatographic partitioning of compounds A, B and C with increasing hydrophobicity ( $\log P$  values). For achieving a 1:1 molar distribution, the partitioning phase volumes have to be adjusted accordingly.  $V_s$  and  $V_m$  are the stationary and mobile phase volumes,  $n_s$  and  $n_m$  are the molar fractions of the compounds in the stationary and mobile phases, respectively,  $(X)_s$  and  $(X)_m$  are the concentrations of X molecules in the stationary and mobile phases, respectively,  $K = (X)_s/(X)_m$  is the chromatographic partition coefficient and  $\varphi_0$  is the chromatographic hydrophobicity index, i.e., the adjusted organic phase volume to achieve a molar fraction distribution of 1:1 ( $n_s = n_m$ ).

$$S = \log K_{x+1} - \log K_x \quad (8)$$

where  $x$  and  $x+1$  refer to  $x\%$  and  $(x+1)\%$  volume fractions of organic modifier, respectively. The volume fraction of the organic phase in the mobile phase at which  $\log k' = 0$  ( $\varphi_0$ ) can be described on the basis of eqns. 6–9 by

$$\begin{aligned} \log k' = 0 &= \log K_x + \log (V_s/V_m) \\ &= \varphi_0(\log K_{x+1} - \log K_x) + \\ &\quad + \log K_w + \log (V_s/V_m) \end{aligned} \quad (9)$$

$$\varphi_0 = \frac{\log K_x - \log K_w}{\log K_{x+1} - \log K_x} \quad (10)$$

On the basis of eqn. 6, the hydrophobicity index  $\varphi_0$  can also be expressed by the  $S$  and  $\log k'_w$  values:

$$\varphi_0 = -\log k'_w/S \quad (11)$$

With the help of eqn. 11, the  $\varphi_0$  values can be calculated from the experimental data. When the measured  $\log k'$  values are close to zero, the application of the linear fit to the  $\log k'$  vs.  $\varphi$  plot for the calculation of  $\varphi_0$  does not result in large errors. In those cases when basic compounds are investigated, e.g., as published by El Tayar *et al.* [19], two  $\varphi_0$  values can be obtained. The correct  $\varphi_0$  value is that obtained at lower organic phase concentrations, when only hydrophobic interactions govern the retention. The  $\varphi_0$  value belonging to the higher organic phase concentration is caused by a dual retention mechanism (hydrophobic and silanophilic), so it cannot be regarded as the chromatographic hydrophobicity index.

A graphical illustration of the calculation of  $\varphi_0$  values for various compounds is shown in Fig. 2. The hypothetical example shows situations when the  $\log k'$  vs.  $\varphi$  plots are straight lines (compound 1), quadratic (compound 2), cross each other (compounds 2 and 3) and a dual retention mechanism (compound 4). When the mobile phase compositions are such that the measured  $\log k'$  values are close to zero, the error of the linear extrapolation for the calculation of  $\varphi_0$  values is negligible.

As the  $\varphi_0$  values are dependent only on the distribution constants of the compounds in a given aque-

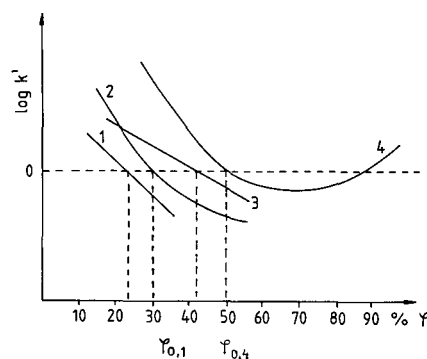


Fig. 2. Graphical illustration of the determination of the chromatographic hydrophobicity index ( $\varphi_0$ ). Numbers refer to hypothetical compounds for which the  $\log k'$  vs.  $\varphi$  plots are straight lines (1), cross each other (2 and 3) or show a dual retention mechanism (4).

ous–organic mixture, the value will depend only on the type of organic phase and the temperature. For ionizable compounds the pH also influences the distribution constant, so  $\varphi_0$  will also depend on the pH. Consequently, the proper way of expressing  $\varphi_0$  values is  $\varphi_{0,op,T,pH}$ , where op represents the type of organic phase and  $T$  represents temperature.

## METHODS

Retention data ( $\log k'$ ) values obtained in various mobile phase compositions were collected from the literature. The retention data for 22 nicotinate esters were published by Reymond *et al.* [20]. The measurements were carried out on LiChrosorb RP-18 (10  $\mu\text{m}$ ) column. The mobile phases were aqueous methanol or acetonitrile in various proportions buffered with 3-morpholinopropanesulphonate (0.02  $M$ , pH 7.4). The retention data for 35 monohydroxyl aromatics were reported by Cooper and Hurtubise [21]. The measurements were carried out on a  $\mu$ Bondapak  $C_{18}$  column with various mixtures of water and methanol. Braumann *et al.* [22] published data for 30 pesticides. The retention data were obtained by varying the methanol concentration in the mobile phase. Schoenmakers *et al.* [23] published retention data for 45 phenoxycarbonic acid derivatives, which were measured using water–acetonitrile mobile phases and a LiChrosorb RP-18 (10  $\mu\text{m}$ ) column. The acidic derivatives were measured with mobile phases that contained 0.5  $M$  acetate buffer (pH 2.9) in order to decrease dissociation. The retention data for 113 aromatic hydrocarbons were measured by Opperhuizen *et al.* [24] on a Hypersil ODS (5  $\mu\text{m}$ ) column with methanol–water mixtures as mobile phases. The data for 143 acidic, basic and neutral drugs were published by Roos and Lau-Cam [25]. Three types of columns were used [ $\mu$ Bondapak  $C_{18}$  (10  $\mu\text{m}$ ), Zorbax ODS (5  $\mu\text{m}$ ) and Ultrasphere ODS (5  $\mu\text{m}$ )]. The mobile phases were variable proportions of methanol, 1.5 parts of acetic acid, 0.5 part of triethylamine and water to yield 100 parts by volume. The pH of the mobile phase was not given. Retention data for 26 drug molecules were published by Valkó [16,26] using both acetonitrile–buffer and methanol–buffer mobile phases. The pH of the mobile phase was adjusted according to the molecules investigated: pH 2 was used for the measurements of acidic com-

pounds to reduce dissociation and pH 8 for the measurements of basic compounds. Retention data referring to acetonitrile–buffer + butanesulphonic acid mobile phases for eleven morphine derivatives were reported by Valkó *et al.* [27]. The same ion-pair chromatographic system was used for the measurements of eleven tricyclic drugs by Kálmán *et al.* [28]. The data for nineteen benzodiazepine derivatives were obtained by Valkó *et al.* [29] by varying the acetonitrile concentration in the mobile phase. Valkó and Slégel [30] published the  $\varphi_0$  values referring to methanol for ten deoxyuridine derivatives. Data for eight aniline and eight phenol derivatives were measured by Gullner *et al.* [31] by changing the methanol concentration in the mobile phase. The  $\varphi_0$  values of 42 adenosine monophosphates, 12 barbiturates and 10 penicillins and cephalosporins were also calculated on the basis of the published retention data of Braumann and Jastorff [32], Yamana *et al.* [33] and Toon *et al.* [34].

The linearity of the  $\log k'$  vs.  $\varphi$  plots was checked over a suitable concentration range. The slope ( $S$ ) and the intercept ( $\log k'_w$ ) values were used for the calculation of  $\varphi_0$  values when the correlation coefficient of the fit was higher than 0.998. The published slope and intercept values were used for the calculation of the chromatographic hydrophobicity index when the authors indicated acceptable high correlation coefficients for the linear fit. The  $\log P$  values of over 500 compounds were calculated using the Pro-LogP Version 4.1 software package (CompuDrug Chemistry, Budapest, Hungary). The correlation analysis was carried out using the Drugidea program system developed for drug design (Chemicro, Budapest, Hungary).

## RESULTS AND DISCUSSION

Table I gives the calculated chromatographic hydrophobicity indices ( $\varphi_{0,ACN}$ ,  $\varphi_{0,MeOH}$ ) and the calculated  $\log P$  values for 22 nicotinate esters. The calculated  $\log P$  and  $\varphi_0$  values referring to methanol for 35 monohydroxyl aromatics are presented in Table II. The  $\log P$  and  $\varphi_0$  values for 30 pesticides and 45 phenoxycarbonic acid derivatives are summarized in Tables III and IV. The calculated  $\log P$  and  $\varphi_{0,MeOH}$  values for the 113 aromatic hydrocarbons are given in Table V. The  $\varphi_0$  and  $\log P$  data for 143 acidic, basic and neutral drugs are presented

TABLE I

CALCULATED LOG  $P$ ,  $\varphi_{0,ACN}$  AND  $\varphi_{0,MeOH}$  VALUES FOR 22 NICOTINATES BASED ON THE RETENTION DATA PUBLISHED BY REYMOND *ET AL.* [20]

No.	Compound	Log $P$	$\varphi_{0,ACN}$	$\varphi_{0,MeOH}$
1	Methyl	0.830	31.75	44.93
2	Ethyl	1.339	42.91	54.93
3	<i>n</i> -Propyl	1.868	50.04	64.92
4	Isopropyl	1.868	49.21	62.86
5	<i>n</i> -Butyl	2.387	59.69	71.67
6	Isobutyl	2.387	58.91	67.50
7	<i>tert.</i> -Butyl	2.387	58.30	67.24
8	<i>n</i> -Hexyl	3.425	77.24	81.73
9	<i>n</i> -Octyl	4.463	84.93	87.64
10	Cyclohexyl	3.061	74.23	78.51
11	TTMCH <sup>a</sup>	4.618	81.66	84.40
12	2-Methoxyethyl	0.833	21.56	43.10
13	2-Butoxyethyl	2.390	54.27	67.91
14	THF <sup>b</sup>	1.507	39.62	52.53
15	2-Chloroethyl	1.784	43.24	57.27
16	3-Hydroxypropyl	0.216	-5.29	33.64
17	Carbamoylmethyl	-0.487	4.35	12.88
18	MCM <sup>c</sup>	0.032	11.47	23.15
19	Benzyl	2.488	54.37	70.90
20	<i>p</i> -Chlorophenyl	2.991	62.18	76.30
21	<i>p</i> -Nitrophenyl	2.014	58.31	67.92
22	2-Phenoxyethyl	2.568	53.23	68.93

<sup>a</sup> *trans*-3,3,5-Trimethylcyclohexyl.

<sup>b</sup> Tetrahydrofurfuryl.

<sup>c</sup> Methylcarbamoylmethyl.

in Table VI. The  $\varphi_{0,ACN}$  and  $\varphi_{0,MeOH}$  data and log  $P$  values for 16 drug molecules are presented in Table VII. Tables VIII and IX contain the calculated data for morphine and tricyclic derivatives obtained from their ion-pair chromatographic retention data. The calculated hydrophobicity index data for benzodiazepine, deoxyuridine and aniline derivatives are shown in Table X, XI and XII, respectively. Tables XIII, XIV and XV give the chromatographic hydrophobicity index values for adenosine monophosphate, barbiturate and  $\beta$ -lactam antibiotic derivatives, respectively.

The exact mechanism governing solute retention in RP-HPLC is of considerable research interest. At present, the most widely accepted mechanism and most extensive treatment of solute retention in RP-HPLC is the solvophobic model developed by Horváth *et al.* [15]. It was assumed that the stationary phase consists of a uniform layer of covalently bound alkyl ligates and the solvophobic theory was

TABLE II

CALCULATED LOG  $P$  AND  $\varphi_{0,MeOH}$  VALUES FOR 35 HYDROXYL AROMATICS BASED ON THE RETENTION DATA PUBLISHED BY COOPER AND HURTUBISE [21]

No.	Compound	Log $P$	$\varphi_{0,MeOH}$
23	1-Acenaphthenol	2.296	65.82
24	5 <i>H</i> -Dibenzo[ <i>a,d</i> ]cyclohepten-5-ol	3.200	71.65
25	7,12-Dimethyl-9-hydroxybenz[ <i>a</i> ]anthracene	6.643	83.65
26	2-Hydroxybenzo[ <i>c</i> ]phenanthrene	5.557	80.16
27	3-Hydroxybenzo[ <i>c</i> ]phenanthrene	5.557	82.04
28	1-(1-Hydroxymethyl)pyrene	5.739	81.29
29	1-(Hydroxymethyl)benzo[ <i>a</i> ]pyrene	5.816	85.77
30	4-Hydroxymethylpyrene	5.739	76.52
31	9-Hydroxyphenanthrene	4.332	76.55
32	13-Hydroxypycene	7.456	90.23
33	1-Hydroxypyrene	5.220	81.32
34	4-Hydroxypyrene	5.220	81.12
35	1-Indanol	1.542	53.89
36	5-Indanol	2.690	64.68
37	1-Naphthol	2.770	64.77
38	2-Naphthol	2.770	62.67
39	3-Phenylphenol	3.444	70.83
40	1,2,3,4-Tetrahydro-4-hydroxy-4-methylphenanthrene	3.853	78.16
41	1,2,3,4-Tetrahydro-1-naphthol	2.061	62.77
42	5,6,7,8-Tetrahydro-1-naphthol	3.209	71.28
43	5,6,7,8-Tetrahydro-2-phenanthrol	3.334	82.35
44	<i>o,o'</i> -Biphenol	2.919	61.13
45	<i>p,p'</i> -Biphenol	2.919	55.40
46	1,2-Dihydroxybenzene	0.972	28.65
47	1,3-Dihydroxybenzene	0.972	20.69
48	1,4-Dihydroxybenzene	0.972	23.72
49	1,3-Dihydroxynaphthalene	2.245	54.79
50	1,6-Dihydroxynaphthalene	2.245	48.39
51	1,7-Dihydroxynaphthalene	2.245	54.03
52	2,3-Dihydroxynaphthalene	2.245	56.33
53	2,6-Dihydroxynaphthalene	2.245	45.09
54	2,7-Dihydroxynaphthalene	2.245	49.69
55	2,5-Dihydroxynaphthalene	2.245	64.69
56	2,6-Dihydroxytoluene	1.491	24.74
57	3,5-Dihydroxytoluene	1.491	35.25

employed to treat quantitatively the role of the eluent in determining retention behaviour on such non-polar stationary phases. As Horváth *et al.* [35] revealed, under many practical conditions in reversed-phase chromatography, particularly when binary aqueous eluents with organic solvents are employed, the retention behaviour and selectivity are governed mainly by solvent effects. Therefore, we believe that the derived  $\varphi_0$  values are independent of the reversed-phase stationary phase applied

TABLE III

CALCULATED LOG  $P$  AND  $\varphi_{0,\text{MeOH}}$  VALUES FOR 30 HERBICIDES BASED ON THE RETENTION DATA PUBLISHED BY BRAUMANN *ET AL.* [22]

No.	Compound	Log $P$	$\varphi_{0,\text{MeOH}}$
58	Fenuron	1.18	50.47
59	Metoxuron	1.98	56.62
60	Monuron	1.91	62.96
61	Monolinuron	1.99	67.21
62	Chlortoluron	2.55	69.24
63	Metobromuron	2.37	69.49
64	Diuron	2.68	72.37
65	Linuron	2.76	75.28
66	Chloroxuron	3.65	77.70
67	Neburon	4.31	80.29
68	Simazine	1.51	66.48
69	Atrazine	2.05	71.81
70	Propazine	2.59	76.05
71	Prometryn	1.91	85.30
72	Desmetryn	2.46	86.16
73	Terbutryn	2.56	87.55
74	2,4-D	2.22	54.24
75	MCPA	2.30	57.25
76	2,4,5-T	2.99	62.00
77	Dichlorprop	2.75	62.23
78	Mecoprop	2.83	64.40
79	Fenoprop	3.52	68.21
80	MCPB	3.53	73.67
81	2,4-D-M	2.64	77.44
82	MCPA-M	2.72	78.51
83	Dichlorprop-M	3.17	81.30
84	Mecoprop-M	3.25	81.76
85	2,4,5-T-M	3.41	82.82
86	MCPB-M	3.95	85.90
87	Fenoprop-M	3.94	85.99

if no dual retention mechanism [36] takes place, and the physico-chemical basis for retention on the investigated stationary phases can be regarded as “homoenergetic”, as was discussed by Melander *et al.* [37].

The correlation between  $\varphi_{0,\text{MeOH}}$  and  $\varphi_{0,\text{ACN}}$  values for the compounds in Tables I, IV and VII was also investigated. These two values refer to isoeutropic eluent mixtures as they both mean the mobile phase composition at which the same retention ( $\log k' = 0$ ) can be obtained. A significant correlation between the two types of chromatographic hydrophobicity index was found for 72 compounds as described by the equation

$$\varphi_{0,\text{MeOH}} = 0.82\varphi_{0,\text{ACN}} + 20.46 \quad (12)$$

$$n = 72, r = 0.96, s = 5.0$$

TABLE IV

CALCULATED LOG  $P$ ,  $\varphi_{0,\text{ACN}}$  AND  $\varphi_{0,\text{MeOH}}$  VALUES FOR 45 SUBSTITUTED AROMATIC COMPOUNDS BASED ON THE RETENTION DATA PUBLISHED BY SCHOENMAKERS *ET AL.* [23]

No.	Compound	Log $P$	$\varphi_{0,\text{ACN}}$	$\varphi_{0,\text{MeOH}}$
88	Acetophenone	1.66	62.28	70.33
89	Aniline	1.10	—	58.74
90	Anisole	2.11	70.99	80.83
91	Benzaldehyde	1.48	61.26	67.92
92	Benzene	2.13	72.37	84.38
93	Benzonitrile	1.56	63.11	67.30
94	Benzophenone	3.18	78.26	84.68
95	Benzyl alcohol	1.10	43.01	58.33
96	Biphenyl	4.02	88.62	91.96
97	<i>n</i> -Butylbenzene	4.26	90.72	95.15
98	Chlorobenzene	2.81	77.41	85.62
99	<i>p</i> -Chlorophenol	2.39	59.86	71.67
100	<i>p</i> -Chlorotoluene	3.33	83.06	89.63
101	<i>o</i> -Cresol	1.96	58.17	68.30
102	<i>o</i> -Dichlorobenzene	3.38	83.28	90.06
103	Diethyl phthalate	3.15	71.43	78.38
104	2,4-Dimethylphenol	2.30	64.60	74.76
105	Dimethyl phthalate	2.11	62.45	68.63
106	<i>m</i> -Dinitrobenzene	1.49	64.81	72.90
107	<i>o</i> -Dinitrobenzene	1.58	64.17	69.66
108	<i>p</i> -Dinitrobenzene	1.46	64.95	69.08
109	2,4-Dinitrotoluene	1.98	68.85	79.00
110	Diphenyl ether	4.20	82.67	90.09
111	Ethylbenzene	3.15	78.34	90.34
112	<i>m</i> -Fluoronitrobenzene	1.99	68.93	78.02
113	<i>p</i> -Fluoronitrobenzene	1.99	67.27	73.63
114	<i>p</i> -Fluorophenol	1.77	51.20	60.00
115	<i>p</i> -Hydroxybenzaldehyde	1.35	37.33	53.28
116	<i>p</i> -Methoxybenzaldehyde	1.68	60.43	70.61
117	<i>p</i> -Methylbenzaldehyde	2.04	68.11	73.63
118	Methyl benzoate	2.12	69.73	79.44
119	Naphthalene	3.37	81.73	89.94
120	<i>p</i> -Nitroacetophenone	1.53	63.40	70.40
121	<i>p</i> -Nitrobenzaldehyde	1.20	60.87	63.94
122	Nitrobenzene	1.85	67.67	75.19
123	<i>m</i> -Nitrophenol	2.00	54.48	66.18
124	<i>o</i> -Nitrophenol	1.79	64.40	74.80
125	<i>p</i> -Nitrophenol	1.91	53.02	63.44
126	Phenol	1.46	48.40	57.02
127	2-Phenylethanol	1.36	50.00	64.06
128	<i>p</i> -Phenylphenol	3.20	68.18	80.65
129	3-Phenylpropanol	1.88	58.02	71.57
130	<i>n</i> -Propylbenzene	3.68	86.02	92.05
131	Toluene	2.69	77.55	86.35
132	2,3,5-Trichlorotoluene	2.92	85.63	91.65

where  $n$  is the number of compounds,  $r$  is the correlation coefficient and  $s$  is the standard error of the estimate. Eqn. 12 suggests a method for the calcula-

TABLE V

CALCULATED LOG *P* AND  $\varphi_{0,\text{MeOH}}$  VALUES FOR 113 AROMATIC HYDROCARBONS BASED ON THE RETENTION DATA PUBLISHED BY OPPERHUIZEN *ET AL.* [24]

No.	Compound	Log <i>P</i>	$\varphi_{0,\text{MeOH}}$	No.	Compound	Log <i>P</i>	$\varphi_{0,\text{MeOH}}$
133	Benzene	2.022	56.10	190	2,2',5-Trichlorobiphenyl	6.189	86.37
134	Toluene	2.541	67.67	191	2,3,4-Trichlorobiphenyl	6.189	90.63
135	Ethylbenzene	3.060	75.83	192	2,3',4'-Trichlorobiphenyl	6.189	90.14
136	Propylbenzene	3.579	81.44	193	2,3',5-Trichlorobiphenyl	6.189	90.59
137	Butylbenzene	4.098	85.88	194	2,3,6-Trichlorobiphenyl	6.189	113.06
138	Pentylbenzene	4.617	89.05	195	2,4,5-Trichlorobiphenyl	6.189	92.82
139	Hexylbenzene	5.136	91.53	196	2,4'-5-Trichlorobiphenyl	6.189	90.27
140	Heptylbenzene	5.655	103.01	197	2,4,6-Trichlorobiphenyl	6.189	90.93
141	Octylbenzene	6.174	95.31	198	2,2',3,3'-Tetrachlorobiphenyl	6.929	87.46
142	Nonylbenzene	6.693	96.80	199	2,2',3,5'-Tetrachlorobiphenyl	6.929	89.02
143	Decylbenzene	7.212	98.08	200	2,2',4,4'-Tetrachlorobiphenyl	6.929	91.62
144	Chlorobenzene	2.762	66.20	201	2,2',4,5'-Tetrachlorobiphenyl	6.929	90.99
145	1,2-Dichlorobenzene	3.502	73.82	202	2,2',4,6-Tetrachlorobiphenyl	6.929	90.06
146	1,3-Dichlorobenzene	3.502	77.50	203	2,2',5,5'-Tetrachlorobiphenyl	6.929	90.28
147	1,4-Dichlorobenzene	3.502	75.02	204	2,2',5,6'-Tetrachlorobiphenyl	6.929	87.03
148	1,2,3-Trichlorobenzene	4.242	81.50	205	2,2',6,6'-Tetrachlorobiphenyl	6.929	82.31
149	1,2,4-Trichlorobenzene	4.242	82.98	206	2,3',4,4'-Tetrachlorobiphenyl	6.929	93.48
150	1,3,5-Trichlorobenzene	4.242	86.96	207	2,3,4,5-Tetrachlorobiphenyl	6.929	95.71
151	1,2,3,4-Tetrachlorobenzene	4.982	87.68	208	2,3',4',5'-Tetrachlorobiphenyl	6.929	93.17
152	1,2,3,5-Tetrachlorobenzene	4.982	90.00	209	2,3',4,6-Tetrachlorobiphenyl	6.929	92.82
153	1,2,4,5-Tetrachlorobenzene	4.982	89.09	210	2,3',5,5'-Tetrachlorobiphenyl	6.929	94.90
154	Pentachlorobenzene	5.722	93.81	211	2,3,5,6-Tetrachlorobiphenyl	6.929	93.07
155	Hexachlorobenzene	6.462	98.10	212	2,4,4',6-Tetrachlorobiphenyl	6.929	92.89
156	2-Chlorotoluene	3.281	76.08	213	3,3',4,4'-Tetrachlorobiphenyl	6.929	93.67
157	3-Chlorotoluene	3.281	75.90	214	2,2',3,4,5'-Pentachlorobiphenyl	7.669	93.84
158	4-Chlorotoluene	3.281	75.22	215	2,2',3',4,5-Pentachlorobiphenyl	7.669	97.85
159	2,4-Dichlorotoluene	4.021	83.93	216	2,2',3,5,6-Pentachlorobiphenyl	7.669	92.09
160	2,5-Dichlorotoluene	4.021	82.54	217	2,2',4,5,5'-Pentachlorobiphenyl	7.669	94.21
161	2,6-Dichlorotoluene	4.021	84.17	218	2,2',4,5,6-Pentachlorobiphenyl	7.669	91.47
162	3,4-Dichlorotoluene	4.021	80.78	219	2,3,4,5,6-Pentachlorobiphenyl	7.669	97.07
163	3,5-Dichlorotoluene	4.021	84.18	220	2,2',3,3',4,4'-Hexachlorobiphenyl	8.409	94.60
164	2,4,5-Trichlorotoluene	4.761	88.43	221	2,2',3,3',5,5'-Hexachlorobiphenyl	8.409	96.35
165	1-Chloronaphthalene	4.035	73.64	222	2,2',3,3',6,6'-Hexachlorobiphenyl	8.409	89.55
166	2-Chloronaphthalene	4.035	82.15	223	2,2',3,4,4',5'-Hexachlorobiphenyl	8.409	95.18
167	1,2-Dichloronaphthalene	4.775	81.12	224	2,2',3,4,5,5'-Hexachlorobiphenyl	8.409	96.53
168	1,3-Dichloronaphthalene	4.775	87.21	225	2,2',3,5,5',6-Hexachlorobiphenyl	8.409	94.00
169	1,4-Dichloronaphthalene	4.775	89.04	226	2,2',4,4',5,5'-Hexachlorobiphenyl	8.409	96.82
170	1,5-Dichloronaphthalene	4.775	89.06	227	2,2',4,5,5',6'-Hexachlorobiphenyl	8.409	95.98
171	1,8-Dichloronaphthalene	4.775	84.59	228	2,2',4,4',6,6'-Hexachlorobiphenyl	8.409	95.49
172	2,3-Dichloronaphthalene	4.775	86.11	229	2,3,3',4,4',5-Hexachlorobiphenyl	8.409	98.84
173	2,7-Dichloronaphthalene	4.775	85.93	230	2,3,3',4,5,6-Hexachlorobiphenyl	8.409	96.72
174	1,3,7-Trichloronaphthalene	5.515	93.43	231	3,3',4,4',5,5'-Hexachlorobiphenyl	8.409	94.26
175	2,3,6-Trichloronaphthalene	5.515	89.53	232	2,2',3,3',4,4',6-Heptachlorobiphenyl	9.149	96.63
176	1,2,3,4-Tetrachloronaphthalene	6.255	98.64	233	2,2',3,4,4',5,6-Heptachlorobiphenyl	9.149	98.00
177	1,2,3,5-Tetrachloronaphthalene	6.255	98.32	234	2,2',3,4,4',5',6-Heptachlorobiphenyl	9.149	97.44
178	1,3,5,7-Tetrachloronaphthalene	6.255	99.87	235	2,2',3,4,5,5',6,6'-Octachlorobiphenyl	9.889	97.26
179	1,3,5,8-Tetrachloronaphthalene	6.255	97.88	236	2,2',3,3',4,4',5,5'-Octachlorobiphenyl	9.889	100.19
180	Octachloronaphthalene	9.215	112.06	237	2,2',3,3',4,4',5,6-Octachlorobiphenyl	9.889	98.97
181	Biphenyl	3.969	74.68	238	2,2',3,3',4,4',6,6'-Octachlorobiphenyl	9.889	99.00
182	2-Chlorobiphenyl	4.709	81.86	239	2,2',3,3',4,5,5',6-Octachlorobiphenyl	9.889	99.15
183	3-Chlorobiphenyl	4.709	85.29	240	2,2',3,3',5,5',6,6'-Octachlorobiphenyl	9.889	97.49
184	4-Chlorobiphenyl	4.709	84.68	241	2,2',3,4,4',5,6,6'-Octachlorobiphenyl	9.889	99.84
185	2,2'-Dichlorobiphenyl	5.449	80.95	242	2,2',3,3',4,4',5,5',6-Nonachlorobiphenyl	10.629	101.38
186	2,4-Dichlorobiphenyl	5.449	88.30	243	2,2',3,3',4,4',5,6,6'-Nonachlorobiphenyl	10.629	100.97
187	2,4'-Dichlorobiphenyl	5.449	89.55	244	2,2',3,3',4,5,5',6,6'-Nonachlorobiphenyl	10.629	100.50
188	2,5-Dichlorobiphenyl	5.449	82.18	245	Decachlorobiphenyl	11.369	103.52
189	2,6-Dichlorobiphenyl	5.449	85.39				

TABLE VI

CALCULATED LOG *P* AND  $\varphi_{0,\text{MeOH}}$  VALUES FOR 143 DRUG MOLECULES BASED ON THE RETENTION DATA PUBLISHED BY ROOS AND LAU-CAM [25]

No.	Compound	Log <i>P</i>	$\varphi_{0,\text{MeOH}}$	No.	Compound	Log <i>P</i>	$\varphi_{0,\text{MeOH}}$
246	Acetanilide	1.131	45.28	300	Ethinylestradiol	5.270	71.68
247	Acetophenazine	2.779	67.38	301	Fluphenazine	4.339	75.07
248	Acetyl sulphisoxazole	-2.192	50.48	302	Homatropine	1.889	28.16
249	Aminopromazine	4.189	68.77	303	Hydrochlorothiazide	-0.070	21.47
250	Amitriptyline	5.993	68.26	304	Hydrocortisone	2.029	62.92
251	Amodiaquin	4.468	60.04	305	Hydroxyamphetamine	1.444	6.79
252	Amphetamine	1.969	27.65	306	Hyoscyamine	2.119	38.54
253	Antazoline	3.233	52.94	307	Imipramine	4.532	68.16
254	Antipyrine	0.551	44.52	308	Isoproterenol	0.647	-5.23
255	Atropine	2.119	37.02	309	Lidocaine	3.134	35.53
256	Atropine methyl	2.679	35.78	310	Meclizine	5.696	84.74
257	Benzatropine	4.064	69.35	311	Medroxyprogesterone acetate	5.027	78.13
258	Bromodiphenhydramine	4.243	65.91	312	Mephentermine	2.792	34.80
259	Bromopheniramine	3.960	60.90	313	Mesoridazine	3.635	60.46
260	Bupivacaine	4.846	54.12	314	Mestranol	5.864	82.59
262	Butacaine	4.287	47.53	315	Metamphetamine	2.273	31.88
263	Butaperazine	4.393	77.70	316	Methapyriline	3.394	49.83
264	Caffeine	0.681	37.59	317	Methotrimeprazine	4.561	66.65
265	Carbinoxamine	2.748	57.47	318	Methoxyamphetamine	1.969	37.21
266	Chlorcyclizine	3.792	66.29	319	Methoxypromazine	4.042	65.61
267	Chlorprocaine	3.010	28.73	320	Methyl Dopate	0.650	26.71
268	Chlorpromazine	4.713	71.90	321	Methylparaben	1.586	55.04
269	Cinchonidine	3.034	52.38	322	Methyltestosterone	5.331	76.64
270	Chinconine	3.034	51.23	323	Naphazoline	2.629	43.56
271	Clenizole	4.709	68.46	324	Norethindrone	4.603	71.36
272	Cyclizine	3.052	49.85	325	Nortriptyline	5.627	69.43
273	Cyclothiazide	1.691	47.74	326	Oxyphenyclimine	3.990	65.95
274	Cycrimine	4.390	49.55	327	Perphenazine	3.930	74.59
275	Desipramine	4.166	56.27	328	Phenacetin	1.719	54.44
276	Dextromethorphan	4.730	48.96	329	Phenindamine	4.532	61.07
277	Dibucaine	3.779	62.95	330	Pheniramine	3.011	46.70
278	Dienestrol	5.883	61.85	331	Phenothiazine	3.764	73.78
279	Diethylstilbestrol	6.247	61.84	332	Phenoxybenzamine	5.401	61.27
280	Dihydrocinchonidine	3.398	55.41	333	Phentermine	2.488	35.32
281	Dihydrocinchonine	3.398	54.34	334	Phentolamine	3.147	49.25
282	Dihydroergocornine	2.339	52.46	335	Phenylpropanolamine	0.874	118.19
283	Dihydroergocristine	2.959	56.82	336	Phenylephrine	0.134	-20.1
284	Dihydroergocryptine	2.858	56.37	337	Phenyltoloxamine	4.425	60.71
285	Dihydroquinidine	3.467	57.68	338	Phthalylsulphathiazole	1.359	43.44
286	Dihydroquinine	3.467	58.85	339	Physostigmine	2.067	34.55
287	Diphenhydramine	3.294	46.99	340	Prednisolone	1.954	62.41
288	Diphenylpyraline	3.390	51.07	341	Prednisone	1.418	58.11
289	Doxylamine	2.527	38.60	342	Procaine	2.270	21.13
290	Dyphylline	-1.049	24.91	343	Prochlorperazine	4.506	82.87
291	Ephedrine	1.178	19.59	344	Progesterone	4.508	79.49
292	Ergonovine	1.750	30.92	345	Promazine	3.973	65.96
293	Ergotamine	1.846	63.40	346	Promethazine	4.551	65.04
294	Estradiol	4.960	73.05	347	Pyrantel	2.790	45.35
295	Estradiol benzoate	6.953	87.66	348	Pyrilamine	2.780	55.27
296	Estradiol cypionate	8.610	91.60	349	Pyrvinium	7.992	78.19
297	Estradiol valerate	7.417	87.51	350	Quinidine	3.103	55.14
298	Estriol	3.865	59.91	351	Quinine	3.103	55.59
299	Estrone	4.424	72.22	352	Salicylamide	0.206	40.64

TABLE VI (continued)

No.	Compound	Log <i>P</i>	$\varphi_{0,\text{MeOH}}$	No.	Compound	Log <i>P</i>	$\varphi_{0,\text{MeOH}}$
353	Salicylic acid	1.225	42.75	370	Sulphapyridine	0.325	28.93
354	Scopolamine	0.752	26.96	371	Sulphathiazole	0.050	27.08
355	Scopolamine aminoxide	0.941	26.07	372	Sulphisomidine	0.255	26.45
356	Spirolactone	5.053	70.03	373	Sulphisoxazole	-0.210	40.52
357	Succinylsulphathiazole	0.156	34.38	374	Testosterone	4.812	74.34
358	Sulphabenzamide	1.896	43.24	375	Testosterone cypionate	8.462	92.31
359	Sulphachlorpyridazine	-0.293	39.06	376	Testosterone enanthate	8.307	91.70
360	Sulphadiazine	-0.783	25.59	377	Testosterone propionate	6.231	84.28
361	Sulphadimethoxine	-0.645	50.36	378	Tetracaine	3.414	57.65
362	Sulphamerazine	-0.264	32.52	379	Theobromine	0.162	22.57
363	Sulphamethazine	0.255	37.52	380	Theophylline	-0.020	26.78
364	Sulphamethizole	0.405	27.11	381	Thioridazine	5.765	74.22
365	Sulphamethoxazole	0.262	39.90	382	Trichlormethiazole	0.872	42.64
366	Sulphamethoxypyridazine	0.400	37.50	383	Trimeprazine	4.492	66.53
367	Sulphanilamide	-0.726	-0.20	384	Tripelennamine	2.711	54.24
368	Sulphanilic acid	-1.690	-18.19	385	Tripolidine	4.707	58.94
369	Sulphaphenazole	1.999	46.52	386	Tropic acid	0.829	39.12

TABLE VII

CALCULATED LOG *P*,  $\varphi_{0,\text{ACN}}$  AND  $\varphi_{0,\text{MeOH}}$  VALUES FOR 26 DRUG MOLECULES BASED ON THE RETENTION DATA PUBLISHED BY VALKÓ [16,26]

No.	Compound	Log <i>P</i>	$\varphi_{0,\text{ACN}}$	$\varphi_{0,\text{MeOH}}$
387	Resorcinol	0.80	17.27	24.39
388	Sulphadimidine	0.32	30.57	40.55
389	Sulphamethoxypyridiazine	0.40	31.30	40.77
390	Barbital	0.65	26.44	39.76
391	Phenobarbital	1.42	42.04	53.14
392	Chloramphenicol	1.14	39.25	51.89
393	Salicylamide	1.28	34.16	46.72
394	Phenacetin	1.58	44.34	58.83
395	Vanillin	1.37	35.49	47.61
396	Benzaldehyde	1.45	51.98	-
397	Acetanilide	1.16	37.78	53.44
398	Nicotinamide	-0.57	6.57	21.77
399	Benzoic acid	1.87	44.08	56.20
400	Salicylic acid	2.25	47.34	59.93
401	Acetylsalicylic acid	1.23	39.60	-
402	Caffeine	-0.07	18.46	43.44
403	Hydrochlorothiazide	-0.07	1.95	25.79
404	Cortexolone	2.46	54.87	-
405	Dexamethasone	1.99	40.98	-
406	Desoxycortone	2.88	76.35	-
407	Sulphaguanidine	-1.22	0.41	-
408	Isoniazide	-1.14	1.59	-
409	Methyl salicylate	2.46	70.63	81.68
410	Hydrocortisone	1.61	33.80	-
412	Progesterone	3.87	95.36	-
413	Testosterone	3.31	75.87	-

tion of the hydrophobicity indices with methanol from those obtained with acetonitrile. The standard error of the estimate shows that in spite of the fact that the data for the 72 compounds were obtained with different columns and buffers or pure water, the hydrophobicity index values obtained with acetonitrile can be used to calculate those with methanol with only a  $\pm 5\%$  error.

The correlation of  $\varphi_{0,\text{ACN}}$  values with the calculat-

TABLE VIII

CALCULATED LOG *P* AND  $\varphi_{0,\text{ACN}}$  VALUES FOR 12 MORPHINE DERIVATIVES BASED ON THE RETENTION DATA PUBLISHED BY VALKÓ *ET AL.* [27]

No.	Compound	Log <i>P</i>	$\varphi_{0,\text{ACN}}$
414	Azidomorphine	1.694	31.35
415	Azidocodeine	2.288	77.97
416	N-Cyclopropylmethylazidomorphine	2.887	63.93
417	Azidoethylmorphine	2.807	97.95
418	N-Phenylmethylazidoethylmorphine	4.465	86.56
419	N-Phenylmethylazidomorphine	3.352	74.93
420	Acetylazidomorphine	1.638	119.25
421	Norazidoethylmorphine	2.441	83.74
422	N-Cyclopropylmethylazidoethylmorphine	4.000	84.74
423	Norazidomorphine	1.328	31.40
424	Normorphine	1.497	12.42
425	Morphine	1.863	15.57



TABLE IX

CALCULATED LOG  $P$  AND  $\varphi_{0,ACN}$  VALUES FOR 11 TRICYCLIC DRUG MOLECULES BASED ON THE RETENTION DATA PUBLISHED BY KÁLMÁN *ET AL.* [28]

No.	Compound	Log $P$	$\varphi_{0,ACN}$
427	EGYT-2347	5.713	86.64
428	EGYT-2509	3.980	88.00
429	EGYT-2474	4.499	84.41
430	EGYT-2541	3.832	90.85
431	RL-205	3.011	74.08
432	RL-215	3.773	93.62
433	RL-218	3.197	74.33
434	Peritol	6.587	88.38
435	Hybernal	4.772	114.49
436	Pipolphen	4.551	89.25
437	Melleril	5.790	111.33

ed log  $P$  values for the data for 140 compounds can be described by the equation

$$\varphi_{0,ACN} = 9.31 \log P + 37.94 \quad (13)$$

$$n = 140, r = 0.88, s = 12.8$$

Eqn. 13 shows a significant correlation between the two parameters, although owing to the relatively

TABLE X

CALCULATED LOG  $P$  AND  $\varphi_{0,ACN}$  VALUES FOR 18 BENZODIAZEPINE DERIVATIVES BASED ON THE RETENTION DATA PUBLISHED BY VALKÓ *ET AL.* [29]

No.	Compound	Log $P$	$\varphi_{0,ACN}$
438	7-Aminonitrazepam	0.950	51.41
439	Bromazepam	1.649	73.32
440	Uxepam	0.981	62.10
441	Oxazepam	1.180	62.48
442	Lorazepam	3.466	64.67
443	Nitrazepam	1.726	71.24
444	Clonazepam	2.466	68.87
445	Chlordiazepoxide	2.443	79.08
446	Alprazolam	3.609	84.53
447	Desmethyldiazepam	2.726	75.75
448	Flunitrazepam	1.814	75.34
449	Chlorazepat	-0.638	77.23
450	Diazepam	2.597	84.01
451	Midazolam	4.345	74.18
452	Medazepam	4.007	91.88
453	Prazepam	3.790	87.55
454	Clobazam	1.994	76.68
455	Tofizopam	3.647	81.37

TABLE XI

CALCULATED LOG  $P$  AND  $\varphi_{0,MeOH}$  VALUES FOR 19 DEOXYURIDINE DERIVATIVES BASED ON THE RETENTION DATA PUBLISHED BY VALKÓ AND SLEGEL [30]

No.	Compound	Log $P$	$\varphi_{0,MeOH}$
456	Deoxyuridine	-0.544	16.00
457	Ethyldeoxyuridine	0.494	24.68
458	Isopropyldeoxyuridine	1.013	30.27
459	<i>sec.</i> -Butyldeoxyuridine	1.532	46.06
460	<i>tert.</i> -Butyldeoxyuridine	1.532	46.46
461	Pentyldeoxyuridine	2.051	57.82
462	Hexyldeoxyuridine	2.570	61.24
463	Vinyldeoxyuridine	0.285	25.14
464	Butenyldeoxyuridine	1.323	48.41
465	Pentenyldeoxyuridine	1.842	58.40
466	Hexenyldeoxyuridine	2.361	67.40
467	Heptenyldeoxyuridine	2.880	72.19
468	Octenyldeoxyuridine	3.399	77.17
469	Propynyldeoxyuridine	0.285	25.97
470	Butynyldeoxyuridine	0.804	32.73
471	Hexynyldeoxyuridine	1.842	56.89
472	Heptynyldeoxyuridine	2.361	48.86
473	Octynyldeoxyuridine	2.880	69.24
474	Methyldeoxyuridine	0.016	21.19

TABLE XII

CALCULATED LOG  $P$  AND  $\varphi_{0,MeOH}$  VALUES FOR 16 ANILINE AND PHENOL DERIVATIVES BASED ON THE RETENTION DATA PUBLISHED BY GULLNER *ET AL.* [31]

No.	Compound	Log $P$	$\varphi_{0,MeOH}$
475	<i>o</i> -Nitroaniline	1.129	60.77
476	<i>m</i> -Nitroaniline	1.447	52.87
477	<i>p</i> -Nitroaniline	0.840	45.79
478	2,4-Dinitroaniline	0.894	64.23
479	2,4,6-Trinitroaniline	0.948	63.48
480	2-Chloro-4-nitroaniline	1.582	67.11
481	4-Chloro-3-nitroaniline	2.189	62.77
482	2,6-Dichloro-4-nitroaniline	2.324	78.05
483	<i>p</i> -Nitrophenol	1.291	57.60
484	2,4-Dinitrophenol	1.345	61.69
485	2,6-Dinitrophenol	1.634	57.72
486	2,4,5-Trinitrophenol	1.399	50.76
487	3,5-Dinitro-4-cyanophenol	0.987	57.41
488	3-Nitro-4-cyano-5-chlorophenol	2.341	71.72
489	3-Nitro-4-cyano-5-bromophenol	2.725	63.30
490	3-Nitro-4-cyano-5-iodophenol	3.367	55.86

TABLE XIII

$\varphi_{0,\text{MeOH}}$  VALUES FOR 42 ADENOSINE MONOPHOSPHATE DERIVATIVES BASED ON THE RETENTION DATA PUBLISHED BY BRAUMANN AND JASTORFF [32]

No.	Compound <sup>a</sup>	$\varphi_{0,\text{MeOH}}$
491	2- <i>n</i> -Hexyl	65.70
492	8-PCTP	60.13
493	6-Benzoyloxy	62.23
494	Dibutyl	55.69
495	2-Phenyl	51.39
496	2- <i>n</i> -Butyl	51.29
497	2'-DNP	54.04
498	2-Thiopropyl	52.20
499	6-( <i>S<sub>p</sub></i> )-DMA-S	46.28
500	2- <i>n</i> -Propyl	42.47
501	6-( <i>R<sub>p</sub></i> )-DMA-S	41.65
502	6-Thiomethyl	41.49
503	6-DMA	40.21
504	2-Ethyl	34.78
505	2-Thiomethyl	34.88
506	Monobutyl	38.07
507	8-Bromo	30.99
508	8-Thioethyl	29.62
509	( <i>S<sub>p</sub></i> )-cAMPS	26.89
510	6-MA	29.65
511	8-Hydroxyisopropyl	27.77
512	1' <i>N</i> <sup>6</sup> -Etheno	26.41
513	8-Methoxy	25.54
514	2-Chloro	31.77
515	( <i>R<sub>p</sub></i> )-cAMPS	23.75
516	6-Methoxy	31.91
517	6-Chloro	31.10
518	8-MA	23.61
519	cAMP	21.96
520	( <i>S<sub>p</sub></i> )-cGMPS	19.28
521	cPuMP	20.91
522	3'-NH-cAMP	21.10
523	5'-NH-cAMP	18.15
524	2-Methyl	16.99
525	8-Thio	13.46
526	8-Amino	14.89
527	8-DMA	14.90
528	cIMP	13.52
529	cGMP	13.13
530	<i>N</i> <sup>1</sup> -Methoxy	12.76
531	<i>N</i> <sup>1</sup> -Oxide	10.42
532	8-Hydroxy	7.04

<sup>a</sup> For abbreviations see ref. 32, Table I.

low correlation coefficient ( $r$ ) and the high standard error of the estimate ( $s$ ) it cannot be used for measurements of  $\log P$  values. The plot of  $\varphi_{0,\text{ACN}}$  values against  $\log P$  is shown in Fig. 3. Similarly a statisti-

TABLE XIV

CALCULATED  $\log P$  AND  $\varphi_{0,\text{MeOH}}$  VALUES FOR 10  $\beta$ -LACTAM ANTIBIOTICS BASED ON THE RETENTION DATA PUBLISHED BY YAMANA *ET AL.* [33]

No.	Compound	$\log P$	$\varphi_{0,\text{MeOH}}$
533	Carbenicillin phenyl	3.14	50.57
534	Dicloxacillin	2.83	47.92
535	Floxacillin	2.58	47.56
536	Cloxacillin	2.48	48.23
537	Phenethicillin	2.19	45.80
538	Penicillin V	1.62	43.78
539	Penicillin G	1.30	34.48
540	Ampicillin	0.94	37.60
541	Amoxicillin	0.48	8.89
542	Sulbenicillin	0.20	3.51

cally significant correlation could be found between the  $\varphi_{0,\text{MeOH}}$  and the  $\log P$  values for the data for 448 compounds:

$$\varphi_{0,\text{MeOH}} = 7.08 \log P + 42 \quad (14)$$

$$n = 448, r = 0.787, s = 13.48$$

On the basis of eqn. 14, exact measurements of  $\log P$  cannot be carried out from measurements of the chromatographic hydrophobicity index, but the good correlation shows that even for a large set of compounds a relationship exists. The high standard error of the estimate ( $\pm 13\%$ ) may be due to the error in the calculation of partition coefficients, to

TABLE XV

CALCULATED  $\log P$  AND  $\varphi_{0,\text{ACN}}$  VALUES FOR 12 BARBITURATE DERIVATIVES BASED ON THE RETENTION DATA PUBLISHED BY TOON *ET AL.* [34]

No.	Compound	$\log P$	$\varphi_{0,\text{ACN}}$
543	5-Ethylbarbituric acid	-1.52	-2.93
544	5-Ethyl-5-methylbarbituric acid	0.02	-0.14
545	Barbital	0.68	3.92
546	5-Ethyl-5- <i>n</i> -propylbarbituric acid	0.87	10.65
547	Butethal	1.70	18.33
548	5-Ethyl-5- <i>n</i> -hexylbarbituric acid	3.08	32.44
549	5-Ethyl-5- <i>n</i> -heptylbarbituric acid	3.64	35.35
550	5-Ethyl-5- <i>n</i> -octylbarbituric acid	3.85	41.98
551	5-Ethyl-5- <i>n</i> -nonylbarbituric acid	4.13	46.26
552	Pentobarbital	2.13	22.35
553	Amobarbital	2.11	23.98
554	Phenobarbital	1.42	14.58

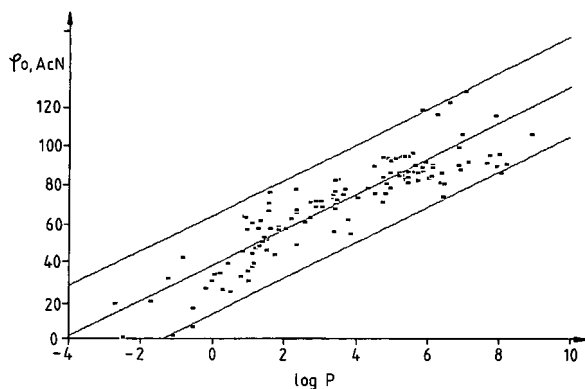


Fig. 3. Plot of  $\log P$  values and  $\varphi_{0,\text{AcN}}$  values for 140 compounds listed in Tables I–XV (eqn. 13).

the error in the measurements of  $\varphi_0$  values and also to the error caused by differences in the chromatographic conditions applied. The main reason for the lack of high correlation coefficients ( $>0.99$ ), however, is that we cannot expect from the reversed-phase chromatographic partition coefficients to be able to model properly another partition system such as 1-octanol–water for structurally unrelated compounds.

The advantage of the proposed chromatographic hydrophobicity index ( $\varphi_0$ ) is that it can also be used for method development in RP-HPLC. When the structures of all the components in a mixture are known, the  $\log P$  values can be calculated. From the  $\log P$  values we can calculate the organic phase concentration at which the components will show  $\log k' = 0$ . The idea of using this kind of relationship was presented by Szepesi and Valkó [38]. On the basis of the relationships obtained and the suggested rule system, CompuDrug Chemistry (Budapest, Hungary) has developed an expert system (ELUEX) for HPLC method development. There is no need for preliminary experiments and it can therefore be regarded as unique at present.

In conclusion, a new chromatographic hydrophobicity index ( $\varphi_0$ ) has been suggested. The value of  $\varphi_0$  reflects the organic phase concentration in the mobile phase (% v/v) at which the molar distribution of the compound between the mobile and the stationary phase is 1:1. This means that the retention time of the compound is exactly double the dead time, *i.e.*  $\log k' = 0$ . The hydrophobicity index relating to methanol showed a very good correla-

tion with that relating to acetonitrile. Significant correlations were found between the  $\log P$  values and the chromatographic hydrophobicity index values for a large number of compounds (140 and 448 compounds relating to acetonitrile and methanol, respectively).

#### ACKNOWLEDGEMENTS

This research was supported by the Hungarian National Research Foundation (OTKA), Grant No. 2670. The contribution of K.V. to the work was supported by a Maplethorpe Fellowship, which is greatly acknowledged.

#### REFERENCES

- 1 E. Overton, *Z. Phys. Chem. (Leipzig)*, 22 (1897) 189.
- 2 H. Meyer, *Arch. Exp. Pathol. Pharmacol.*, 42 (1951) 774.
- 3 C. Hansch and T. Fujita, *J. Am. Chem. Soc.*, 86 (1964) 1616.
- 4 A. J. Leo, C. Hansch and D. Elkins, *Chem. Rev.*, 7 (1971) 525.
- 5 C. Hansch, in B. Chapman and J. Shorter (Editors), *Correlation Analysis in Chemistry and Biology*, Plenum Press, New York, 1978.
- 6 C. Hansch and A. Leo, *Substituent Constants for Correlation Analysis in Chemistry and Biology*, Wiley, New York, 1979.
- 7 T. Braumann, *J. Chromatogr.*, 373 (1986) 191.
- 8 R. Kaliszán, *Quantitative Structure–Activity Chromatographic Retention Relationships*, Wiley, New York, 1987, p. 232.
- 9 W. Butte, C. Fooker, R. Klussmann and D. Schuller, *J. Chromatogr.*, 209 (1981) 7.
- 10 W. E. Hammers, G. J. Meurs and C. L. de Ligny, *J. Chromatogr.*, 247 (1982) 1.
- 11 M. J. M. Wells and C. R. Clark, *J. Chromatogr.*, 235 (1982) 31.
- 12 M. J. M. Wells, C. R. Clark and R. M. Patterson, *J. Chromatogr.*, 235 (1982) 43.
- 13 P. J. Schoenmakers, H. A. H. Billiet and L. de Galan, *J. Chromatogr.*, 185 (1979) 179.
- 14 M. J. M. Wells and C. R. Clark, *J. Chromatogr.*, 284 (1984) 319.
- 15 Cs. Horváth, W. Melander and I. Molnár, *J. Chromatogr.*, 125 (1976) 129.
- 16 K. Valkó, *J. Liq. Chromatogr.*, 7 (1984) 1405.
- 17 L. R. Snyder and J. J. Kirkland, *Introduction to Modern Liquid Chromatography*, Wiley, New York, 1979, p. 23.
- 18 L. R. Snyder and J. J. Kirkland, *Introduction to Modern Liquid Chromatography*, Wiley, New York, 1979, p. 25.
- 19 N. El Tayar, H. van de Waterbeemd and B. Testa, *J. Chromatogr.*, 320 (1985) 305.
- 20 D. Reymond, G. N. Chung, J. M. Mayer and B. Testa, *J. Chromatogr.*, 391 (1987) 97.
- 21 H. A. Cooper and R. J. Hurtubise, *J. Chromatogr.*, 360 (1986) 313.
- 22 T. Braumann, G. Weber and L. H. Grimme, *J. Chromatogr.*, 261 (1983) 329.

- 23 P. J. Schoenmakers, H. A. H. Billiet and L. de Galan, *J. Chromatogr.*, 218 (1981) 261.
- 24 A. Opperhuizen, T. L. Sinnige and J. M. D. van der Steen, *J. Chromatogr.*, 388 (1987) 51.
- 25 R. W. Roos and C. A. Lau-Cam, *J. Chromatogr.*, 370 (1986) 403.
- 26 K. Valkó, *J. Liq. Chromatogr.*, 10 (1987) 1663.
- 27 K. Valkó, T. Friedmann, J. Bati and A. Nagykáldi, *J. Liq. Chromatogr.*, 7 (1984) 2073.
- 28 A. Kálmán, L. Párkányi, K. Valkó, Gy. Mátray, J. Batke and J. Gaál, *Acta Biochim. Biophys. Hung.*, 24 (1989) 143.
- 29 K. Valkó, S. Olajos and T. Cserháti, *J. Chromatogr.*, 499 (1990) 361.
- 30 K. Valkó and P. Slégel, *J. Pharm. Biomed. Anal.*, 9 (1991) 1125.
- 31 G. Gullner, T. Cserháti, B. Bordás and K. Valkó, *J. Liq. Chromatogr.*, 12 (1989) 957.
- 32 T. Braumann and B. Jastorff, *J. Chromatogr.*, 350 (1985) 105.
- 33 T. Yamana, A. Tsuji, E. Miyamoto and O. Kubo, *J. Pharm. Sci.*, 66 (1977) 747.
- 34 S. Toon, J. Mayer and M. Rowland, *J. Pharm. Sci.*, 73 (1984) 625.
- 35 Cs. Horváth, W. Melander and A. Nahum, *J. Chromatogr.*, 186 (1979) 371.
- 36 A. Nahum and Cs. Horváth, *J. Chromatogr.*, 203 (1981) 53.
- 37 W. Melander, J. Stoveken and Cs. Horváth, *J. Chromatogr.*, 199 (1980) 35.
- 38 G. Szepesi and K. Valkó, *J. Chromatogr.*, 550 (1991) 87.



# Accurate determination of $\log k'_w$ in reversed-phase liquid chromatography

## Implications for quantitative structure–retention relationships

Mei-Ming Hsieh and John G. Dorsey

Department of Chemistry, University of Cincinnati, Cincinnati, OH 45221-0172 (USA)

---

### ABSTRACT

With increased understanding of the retention mechanisms of reversed-phase LC has come increased usage of the technique for the measurement of physico-chemical data, especially partitioning information that can be used for quantitative structure–activity relationships. However, the use of chromatographic retention requires that a standard set of mobile phase conditions be chosen. The choice of 100% water has theoretical advantages, as an aqueous phase–membrane phase is the most common system being modeled. However, experimental measurement of  $k'$  values with this mobile phase is difficult or impossible for most real solutes. Various retention extrapolation methods to 100% water have been proposed, but when compared, often yield different values for the same solute. Most of the extrapolation methods are based on the retention as a function of the mobile phase only. However, as the retention is controlled by solute partitioning between the mobile phase and stationary phase, stationary phase effects cannot be ignored. In this paper  $\log k'_w$  values extrapolated from different methods are compared to the measured values. Prediction of  $\log k'_w$  is attempted from the retention as a function of both the mobile phase and stationary phase. Solvatochromic analysis is used to deconvolute stationary and mobile phase effects.  $\log k'_w$  values extrapolated from  $E_T(30)$  plots are recommended as the most meaningful representation of retention for quantitative structure–retention relationships.

---

### INTRODUCTION

Prediction of solute capacity factors in RPLC with pure aqueous mobile phases ( $\log k'_w$ ) has received a lot of attention because of their application in quantitative structure–retention relationship (QSRR) studies [1–5]. The advantages of using  $\log k'_w$  are that it is independent of any organic modifier effects, it reflects polar–non-polar partitioning in a manner similar to shake-flask measurements, and is dependent on the solute's structure and polar functionalities [6–8].

$\log k'_w$  is most often estimated by extrapolating a plot of  $\log k'$  vs. the volume percent organic modifier through the relationships described in eqns. 1 and 2 to the  $y$ -intercept, representing retention in a 100% aqueous phase:

$$\log k' = A\varphi^2 + B\varphi + C \quad (1)$$

$$\log k' = B\varphi + C \quad (2)$$

where  $A$ ,  $B$ ,  $C$  are fitting coefficients, and  $\varphi$  is the volume fraction of organic modifier in the mobile phase. The accuracy of  $k'_w$  extrapolated from eqns. 1 and 2 based on experimental data using mixed methanol–water mobile phases in various composition ranges was studied by Jandera and Kubat [4]

---

Correspondence to: J. G. Dorsey, Department of Chemistry, University of Cincinnati, Cincinnati, OH 45221-0172, USA.

for some pesticides. In their work, the worst  $k'_w$  predicted by extrapolation resulted in a relative mean error of 80% versus measured  $k'_w$ , using the linear function of eqn. 2 to fit the experimental data obtained over a mobile phase composition of 30 to 80% methanol in water. The quadratic function of eqn. 2 was also fitted to a wide range of methanol concentrations from 2 to 90%, yielding a relative error in the extrapolated value of  $k'_w$  of about 30%.

Several shortcomings of lattice models or solubility parameter treatments of solute retention used to derive eqns. 1 and 2 may lead to deviations. For example, it is assumed that solute and solvents have equal molar volumes and no change in volume occurs upon mixing. In addition, the solute and mobile phase components are assumed to be randomly mixed. This neglects any preferential orientation or clustering due to strong intermolecular interactions, such as proton donor–acceptor interactions. Katz and co-workers [9,10] noted that there is a strong association between methanol and water and the binary association constant was found to be  $5.22 \cdot 10^{-3}$  at 23°C. This indicates that methanol–water solvent systems constitute “ternary” mixtures of associated water, associated methanol and water associated with methanol. Distribution of a number of different solutes between *n*-hexadecane and a range of methanol–water mixtures was also studied [10] and it was shown that the distribution coefficient is related to the concentration of methanol unassociated with water, not the concentration of methanol originally added.

Association between acetonitrile molecules was also observed by probing the CN stretching frequency of acetonitrile as a function of concentration in water using Raman spectroscopy [11]. Thus, taking into account both solvent–solvent and solvent–solute species, acetonitrile–water mixtures were more thoroughly described by Rowlen and Harris [11] as having at least six general components: (acetonitrile)<sub>n</sub>, acetonitrile, (acetonitrile)<sub>n</sub>–water, and acetonitrile–water, and (water)<sub>n</sub>. As the concentration is varied, the distribution of interactions must also vary. The unique character of aqueous solvent mixtures employed in LC makes it essential to take into account six components in the mobile phase if retention is to be predicted from solvent composition.

Sadek *et al.* [12] first reported the correlation of

HPLC retention properties with fundamental dipolarity–polarizability and hydrogen bonding properties of solutes and mobile phases. As these physical properties were originally measured by the spectroscopic changes of some indicators in solvent, they are also known as solvatochromic parameters. Sadek *et al.* [12] used solvatochromic parameters and the methodology associated with the linear solvation energy relationships (LSER) [13] to evaluate the multiple interactions that influence HPLC capacity factors. Accordingly, the capacity factor may be determined by three principle types of interactions as shown in eqn. 3

$$\log k' = \log k'_0 + \text{cavity term} + \text{dipolar term} + \text{hydrogen bonding term(s)} \quad (3)$$

Here  $k'_0$  includes the volume phase ratio and dipolar interactions between solute and solvents when  $\pi^*$  is equal to zero. The cavity term measures the endoergic process of separating the solvent molecules to provide a suitably sized enclosure for the solute. This term is usually taken as the product of the solute molar volume ( $\bar{V}$ ) and the square of the Hildebrand solubility parameter ( $\delta_H$ ) of the solvent. The dipolar term may be considered to be the product of the solute and the solvent  $\pi^*$  interactions, where  $\pi^*$  is defined as a measure of the dipolarity–polarizability of the species in question. Finally, the hydrogen bonding terms are written as a cross product of the solute  $\alpha$  [an empirical measure of hydrogen bond donating (HBD) acidity] and the solvent  $\beta$  [a similar scale of hydrogen bond acceptor (HBA) basicity] and the product of the solute  $\beta$  and the solvent  $\alpha$ . Thus, in an expanded format, eqn. 3 becomes:

$$\log k' = \log k'_0 + m(\delta_s^2 - \delta_m^2)\bar{V}_2/100 + s(\pi_s^* - \pi_m^*)\pi_2^* + a(\beta_s - \beta_m)\alpha_s + b(\alpha_s - \alpha_m)\beta_s \quad (4)$$

The subscripts s, m and 2 denote the stationary phase, mobile phase and solute, respectively. Coefficients, *m*, *s*, *a* and *b* are fitting parameters that are independent of solutes and phases considered.

In order to simplify eqn. 4, the solvatochromic properties of the stationary phase may be assumed to be a constant over the entire range of mobile phase compositions and eqn. 4 may be changed as represented by eqn. 5:

$$\log k' = \log k'_0 + m'\delta_m^2 + s'\pi_m^* + a'\beta_m + b'\alpha_m \quad (5)$$

where  $m' = m(\bar{V}_2)/100$ ;  $s' = s(\pi_2^*)$ ,  $a' = a(\alpha_2)$  and  $b' = b(\beta_2)$ . It is difficult to measure the solubility parameter and the solvatochromic properties of solvent mixtures. Even though Cheong and Carr [14] have attempted to measure the physical properties of water and aqueous mixtures of organic solvents, a multiple correlation has not yet been reported.

The  $E_T(30)$  scale, an empirical measure of solvent polarity, may be used to further simplify eqn. 4. The  $E_T(30)$  scale is based on the charge transfer absorption of 2,6-diphenyl-4-(2,4,6-triphenyl-*n*-pyridinio)phenolate (ET-30). This method is also known as a single parameter solvatochromic method. By way of definition,  $E_T(30)$  refers to the value of the polarity measurement and ET-30 is an acronym for the compound's name. The  $E_T(30)$  scale is calculated by eqn. 6:

$$E_T(30) \text{ (kcal/mol)} = 28\,592/\lambda_{\text{max.}} \text{ (nm)} \quad (6)$$

where  $\lambda_{\text{max.}}$  is the maximum absorption wavelength and 28 592 is a product of the speed of light, Planck's constant and Avagadro's number. ET-30 exhibits one of the largest observed solvatochromic dependencies of any known molecule, as the charge transfer absorption maximum shifts from 453 nm in water, a very polar solvent, to 810 nm in diphenyl ether, a very non-polar solvent. ET-30 is thus very sensitive to both solvent dipolarity–polarizability as well as solvent hydrogen bond donor ability. Kamlet *et al.* [13] have further shown that there is a linear relationship between the  $E_T(30)$  value and the  $\pi^*$  and  $\alpha$  scale for a large number of pure polar (both aprotic and protic) and non-polar solvents:

$$E_T(30) = 31.00 + 13.43\pi^* + 15.06\alpha \quad (7)$$

$n = 40, r = 0.984, \text{S.D.} = 1.65$

A linear relationship between  $\pi^*$  and the solubility parameter has also been reported [15]:

$$\delta_H^2 = 44.1 + 95.6\pi^* \quad (8)$$

$n = 17, r = 0.858, \text{S.D.} = 19.7$

Comparing eqns. 7 and 8 to eqn. 5, it may be observed that there is no solvent HBA basicity term,  $\beta$ , in eqns. 7 and 8. Since the contribution of solute HBD acidity and solvent HBA basicity to retention is much smaller than the contributions from other interactions [16,17], the  $a'\beta_m$  term in eqn. 5 can be neglected. Thus eqn. 5 may be simplified to eqn. 9:

$$\log k' = b + m [E_T(30)] \quad (9)$$

The validity of eqn. 9 was empirically proven by Johnson *et al.* [18] Using an extensive base of 332 sets of retention data as a function of mobile phase composition, they compared the  $E_T(30)$  scale with the commonly used volume percent plots and showed that this empirical measure is a better descriptor of mobile phase “strength”.

It was also found that for a solute–column pair, extrapolation of  $\log k'$  vs. volume percentage of organic modifier gives significantly different intercepts for different organic modifiers, while the extrapolation of  $\log k'$  vs.  $E_T(30)$  leads to a common intersection point at approximately the  $E_T(30)$  value of pure water [19]. Using over 200 sets of chromatographic retention data, Michels and Dorsey [20] compared the estimation of  $\log k'_w$  by the volume percentage approach and by the  $E_T(30)$  approach and found that the  $E_T(30)$  approach gave a more reliable estimation of this lipophilicity parameter. This evaluation was based on the relative value of the 95% confidence interval about  $\log k'_w$ , the point of intersection of  $\log k'$  versus solvent strength plots for different modifiers, the scatter of estimations with different modifiers and the goodness of fit of the data to the linear model.

In this paper two short columns which have very little resistance to mobile phase flow to allow very high volume flow-rates were used to measure actual values of  $\log k'_w$  for 15 compounds. Extrapolated values of  $\log k'_w$  from volume percentage and  $E_T(30)$  scales were compared to the measured  $\log k'_w$ . A relatively high bonding density stationary phase ( $3.41 \mu\text{mol/m}^2$ ) was used to reduce the interaction between the solute and residual silanol groups on the stationary phase.

However, either volume percentage or the  $E_T(30)$  scale is a function of the mobile phase only, while chromatographic retention is a function of both the stationary and mobile phases. Numerous studies have shown that structure and composition of the stationary phase change with changing the mobile phase composition, especially for highly aqueous mobile phases, and retention can also be affected [21–31]. Estimation of retention from only the properties of the mobile phase may cause errors. Mobile phase and stationary phase effects on retention can be derived by measuring the retention times for a wide range of solute types with a single mobile phase composition using eqn. 10



$$\log k' = \log k'_0 + m''(\bar{V}_2)/100 + s''\pi_2^* + a''\alpha_2 + b''\beta_2 \quad (10)$$

where  $m'' = m(\delta_s^2 - \delta_m^2)$ ,  $s'' = s(\pi_s^* - \pi_m^*)$ ,  $a'' = a(\beta_s - \beta_m)$  and  $b'' = b(\alpha_s - \alpha_m)$ . Limited ranges of mobile phase compositions (30–90% methanol in water and 40–80% acetonitrile in water) have in fact been studied using eqn. 10 [16,32–34]. In this paper eqn. 10 is solved, for the first time, over the entire range of mobile phase compositions. Predictions of  $\log k'_w$  are attempted from the retention as a function of both the stationary phase and the mobile phase.

## EXPERIMENTAL

### Materials

HPLC-grade methanol and acetonitrile (Fisher Scientific, Fair Lawn, NJ, USA) were used without further purification. Water was obtained from a Barnstead Nanopure II water purification system (Barnstead, Boston, MA, USA) fitted with a 0.45- $\mu\text{m}$  filter. Pure solutes were used as received and stock solutions made in HPLC-grade methanol. Naphthalene, dimethyl phthalate and *p*-chlorophenol were from Eastman Kodak (Rochester, NY, USA). Benzene, toluene, ethylbenzene, *p*-chlorotoluene, acetophenone, pyridine and benzyl alcohol were from Fisher Scientific. Fluorobenzene, 1-nitrobutane, 1-nitrohexane, anisole, methyl paraben and ethyl paraben were from Sigma (St. Louis, MO, USA). ET-30 (Reichardt's Dye) was purchased from Aldrich (Milwaukee, WI, USA).

### Retention measurements

All retention measurements were made using an Applied Biosystems (Ramsey, NJ, USA) Spectroflow 400 pump, with UV detection at 254 nm using a Kratos Spectroflow 757 variable-wavelength absorbance detector. Sample injection was performed using a Valco (Houston, TX, USA) C6W injector fitted with a 10- $\mu\text{l}$  sample loop, and detector output was recorded on a Scientific Products Quantigraph chart recorder (Houston Instruments, Austin, TX, USA). Two "homemade"  $\text{C}_{18}$  columns, 7 cm  $\times$  4.6 mm I.D. and 2 cm  $\times$  4.6 mm I.D., with an alkyl chain bonding density of 3.41  $\mu\text{mol}/\text{m}^2$  were used. The base silica material was from a single lot of 10  $\mu\text{m}$  particle diameter Davisil (W. R. Grace, Balti-

more, MD, USA) with a surface area ( $S_{\text{BET}}$ ) of 300  $\text{m}^2/\text{g}$  and a pore size of 150  $\text{\AA}$ . The synthesis and bonding density determination for this packing material may be found elsewhere [35]. All solutes were dissolved in methanol–water (50:50) or weaker mobile phase. For the short 2-cm columns, a 10- $\mu\text{l}$  injection volume may represent up to 5% of the void volume, and the injection solvent may slightly affect retention time measurements made in very weak mobile phases. The columns were packed by use of a Shandon high-pressure HPLC column packer with a 33-ml slurry reservoir (Shandon Southern Instruments, Sewickey, PA, USA). Each column was thermostatted at 30°C using a water jacket and a Brinkmann Lauda (Westbury, NY, USA) Model MT heater/circulator. The eluent flow-rate was varied from 1.0 to 4.5 ml/min depending on the mobile phase composition. Retention times were determined manually based on the peak maximum position. The breakthrough time ( $t_0$ ) used to calculate capacity factors was determined at each composition by the elution of an injection of  $^2\text{H}_2\text{O}$  (Sigma). Multi-variable regression calculations of eqn. 4 were done by using a self written program run on a personal computer.

## RESULTS AND DISCUSSION

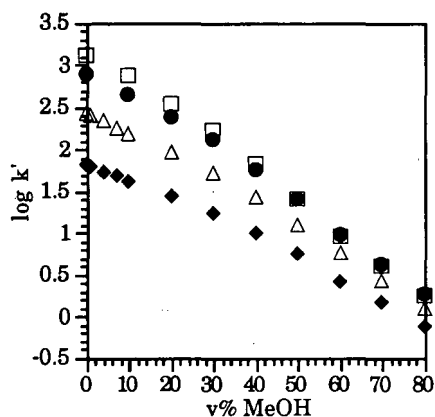
### Comparison of calculated $\log k'_w$ from volume percentage of organic modifier and experimentally measured $\log k'_w$

$\log k'$  values for all compounds are plotted vs. volume percentage of methanol or acetonitrile in Fig. 1a to h. Correlation of determination,  $r^2$ , for these plots is shown in Table I. Obviously, the second polynomial term cannot be neglected for the relationship between  $\log k'$  and volume percentage of acetonitrile. Even though the  $r^2$  values are high for the plots of  $\log k'$  vs. volume percentage of methanol, a distinct curvature can be observed for virtually all the compounds, especially from 0–10% methanol. Because of the curvature, the extrapolated value of  $\log k'_w$  as measured using capacity factors in the range of 10% to 80% methanol in water is different from the experimentally measured  $\log k'_w$ . Measured  $\log k'_w$ , extrapolated  $\log k'_w$  and the percentage errors for various compounds are listed in Table II. It is shown in Table II that the extrapolated value of  $\log k'_w$  from a linear plot of  $\log k'$

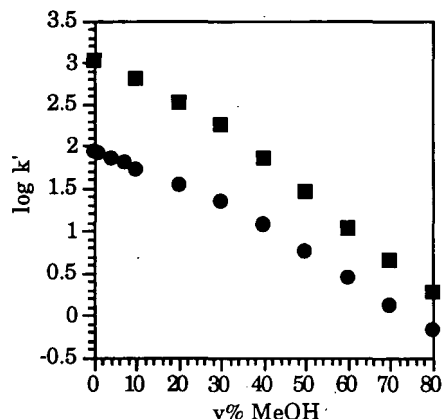
versus volume percentage of methanol can be larger or smaller than the measured  $\log k'_w$  and the sign of the error depends on direction of curvature between 10% and 0% methanol in water. It seems that this direction of curvature for the plot of  $\log k'$  vs. volume percentage of methanol between 10% and 0% methanol in water is related to the inherent polarity nature of a compound. Retention curves for non-polar compounds appear to plateau at volume percentages greater than about 90% water in the mobile phase, and the extrapolated  $\log k'_w$  becomes larger than the actual  $\log k'_w$ . For polar compounds, because of the dramatic increasing  $\log k'$  from 10% to 0% methanol in water, the extrapolated  $\log k'_w$  is smaller than the measured value. To verify the re-

tention behavior in the high percentage water region, retention times for eight compounds were measured using 7%, 4% and 1% methanol in water. A similar trend in sign of the error between the extrapolated and the measured  $\log k'_w$  is also found for polar and non-polar compounds using acetonitrile-water mixtures. Calculation of extrapolated  $\log k'_w$  using the acetonitrile-water mobile phase is based on the quadratic relationship between  $\log k'$  and volume percentage of organic modifier. The different retention behaviors of compounds in the high water content mobile phase (>90%) and lower water content mobile phase (<90%) were also found by Schoenmakers *et al.* [36], Gilpin and Gangoda [37] and Scott and Simpson [27].

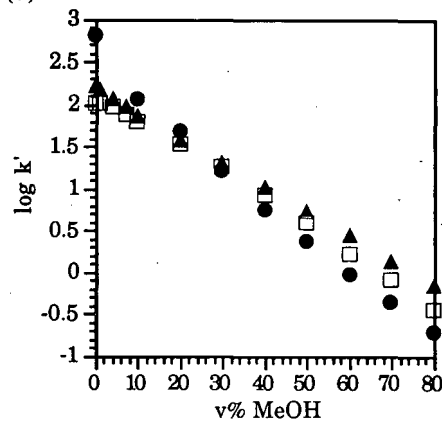
(a)



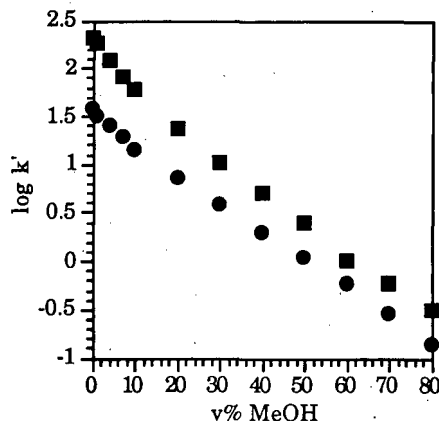
(b)



(c)



(d)



(Continued on p. 68)

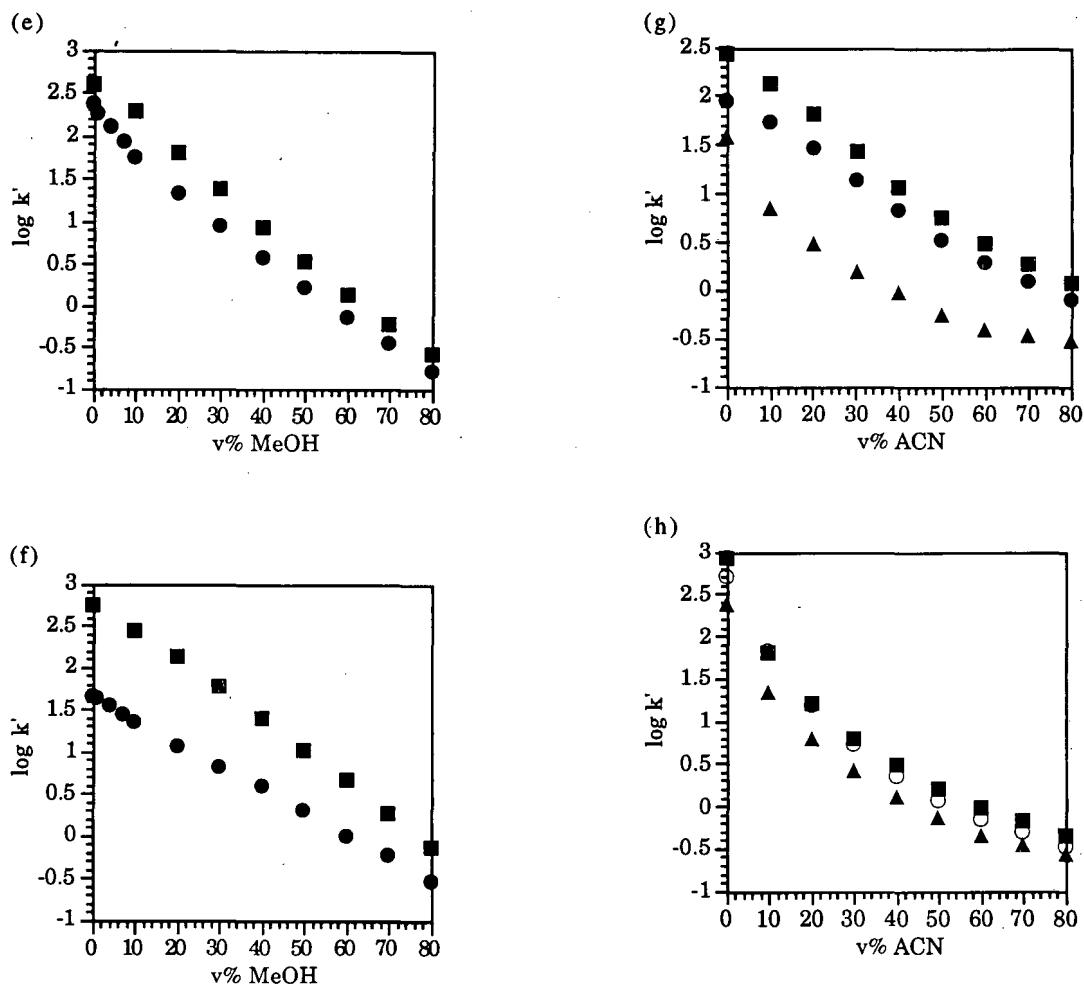


Fig. 1. Log  $k'$  vs. volume percentage (v%) of organic modifier on a column with a bonding density of  $3.41 \mu\text{mol}/\text{m}^2$ . Symbols: (a)  $\square$  = naphthalene,  $\bullet$  = ethylbenzene,  $\triangle$  = toluene,  $\blacklozenge$  = benzene; (b)  $\blacksquare$  = *p*-chlorotoluene,  $\bullet$  = fluorobenzene; (c)  $\square$  = *p*-chlorophenol,  $\bullet$  = dimethyl phthalate,  $\blacktriangle$  = anisole; (d)  $\blacksquare$  = acetophenone,  $\bullet$  = benzyl alcohol; (e)  $\blacksquare$  = ethylparaben,  $\bullet$  = methylparaben; (f)  $\blacksquare$  = nitrohexane,  $\bullet$  = nitrobutane; (g)  $\blacksquare$  = toluene,  $\bullet$  = fluorobenzene,  $\blacktriangle$  = benzyl alcohol; (h)  $\blacksquare$  = dimethyl phthalate,  $\circ$  = ethylparaben,  $\blacktriangle$  = methylparaben.

According to Schoenmakers *et al.* [36] and Gilpin and Gangoda [37], the abnormal retention behaviour observed using  $\leq 10\%$  methanol mobile phase is caused by sorption of organic modifier. Schoenmakers *et al.* [36] believe that eqn. 1 is only valid for mobile phases containing less than 90% water. In order to include the influence of stationary phase modification on retention, one extra term proportional to the square root of  $\phi$  is necessary to

describe the retention over the full range of composition  $0 < \phi < 1$ :

$$\ln k' = A\phi^2 + B\phi + C + E\sqrt{\phi} \quad (11)$$

Based on their study, the curvature of the  $\ln k'$  vs.  $\phi$  plot for the mobile phase composition between 0 and 0.1 changes with  $E$  term and the value of  $E$  is determined by the organic modifier and solute. Ten solutes and three organic modifiers were used to de-

TABLE I

CORRELATION OF DETERMINATION ( $r^2$ ) FOR THE PLOTS BETWEEN  $\log k'$  AND VOLUME PERCENTAGE OF METHANOL OR ACETONITRILE USING MOBILE PHASES FROM (0:100) TO (80:20) ORGANIC–WATER MIXTURES

Compound	$r^2$	
	Methanol	Acetonitrile
Benzene	0.9930	
Toluene	0.9947	0.9907
Ethylbenzene	0.9960	
Fluorobenzene	0.9908	0.9931
Naphthalene	0.9945	
<i>p</i> -Chlorotoluene	0.9944	
Acetophenone	0.9919	
Dimethyl phthalate	0.9846	0.8963
Anisole	0.9996	
Benzyl alcohol	0.9978	0.8918
<i>p</i> -Chlorophenol	0.9962	
Methylparaben	0.9932	0.8859
Ethylparaben	0.9976	0.9204
Nitrobutane	0.9991	
Nitrohexane	0.9939	

TABLE II

MEASURED  $\log k'_w$ , EXTRAPOLATED  $\log k'_w$  FROM VOLUME PERCENTAGE OF ORGANIC MODIFIER AND THE PERCENTAGE ERROR BETWEEN THE EXTRAPOLATED AND MEASURED  $\log k'_w$  USING METHANOL OR ACETONITRILE AS THE ORGANIC MODIFIER

$$\text{Error \%} = \frac{\log k'_w (\text{extrapolated}) - \log k'_w (\text{measured})}{\log k'_w (\text{measured})} \cdot 100$$

Compound	$\log k'_w$ <sup>a</sup> (measured)	$\log k'_w$ <sup>b</sup> methanol	$\log k'_w$ <sup>c</sup> methanol	$\log k'_w$ <sup>d</sup> acetonitrile	Error % <sup>b</sup> methanol	Error % <sup>c</sup> methanol	Error % <sup>d</sup> acetonitrile
Benzene	1.82	1.96	1.82		7.69	0.00	
Toluene	2.43	2.57	2.42	2.59	5.76	-0.41	6.58
Ethylbenzene	2.88	3.08	2.93		6.94	1.74	
Fluorobenzene	1.94	2.10	1.92	2.14	8.25	-1.03	10.31
Naphthalene	3.12	3.31	3.24		6.09	3.85	
<i>p</i> -Chlorotoluene	3.01	3.27	3.13		8.64	3.99	
Acetophenone	2.31	2.02	2.16		-12.55	-6.49	
Dimethyl phthalate	2.81	2.43	2.57	2.31	-13.52	-8.54	-17.79
Anisole	2.22	2.17	2.14		-2.25	-3.60	
Benzyl alcohol	1.58	1.43	1.40	1.24	-9.49	-11.39	-21.52
<i>p</i> -Chlorophenol	2.01	2.18	2.08		8.46	3.48	
Methylparaben	2.37	2.05	2.17	1.84	-13.50	-8.44	-22.36
Ethylparaben	2.58	2.60	2.76	2.41	0.78	6.98	-6.59
Nitrobutane	1.67	1.62	1.58		-2.99	-5.39	
Nitrohexane	2.75	2.86	2.79		4.00	1.45	

<sup>a</sup> Measured  $\log k'_w$ .

<sup>b</sup> Calculation of the extrapolated  $\log k'_w$  is based on the linear function between  $\log k'$  and volume percentage using mobile phases containing 10–80% methanol.

<sup>c</sup> Calculation of the extrapolated  $\log k'_w$  is based on the second polynomial function between  $\log k'$  and volume percentage using mobile phases containing 10–80% methanol.

<sup>d</sup> Calculation of the extrapolated  $\log k'_w$  is based on the second polynomial function between  $\log k'$  and volume percentage using mobile phases containing 10–80% acetonitrile.

termine the validity of eqn. 11 in that paper. Some deviations were observed between the calculated curve (eqn. 11) and the individual data points and no relationship was found between the solute polarity and the value of  $E$ .

Retention for only one solute, ethanol, was studied by Scott and Simpson [27] using methanol–water mixtures with high water content on several different columns. In their study, retention volume of ethanol on a monomeric  $C_{18}$  column was found to reach a maximum at 5% methanol in water and then decreases as the volume percentage of water is increased. The explanation provided for this behavior is that at high water content, the  $C_{18}$  chains tend to interact more strongly with themselves than with the surrounding mobile phase. This dispersive interaction of the hydrocarbon chains results in a reduction in effective chromatographic surface area, and consequently anomalously low retentive characteristics. This explanation is supported by the observation that retention volume on a  $C_2$  column is higher than that on the  $C_{18}$  column using a 100% aqueous mobile phase. In our study, a similar trend is found

for non-polar compounds and *p*-chlorophenol. Different curves under a highly aqueous mobile phase for polar compounds were also observed in our study and cannot be explained by this dispersive interaction between hydrocarbon chains of the stationary phase.

*Comparison of calculated  $\log k'_w$  from  $E_T(30)$  scale and experimentally measured  $\log k'_w$*

$\log k'$  values are plotted against  $E_T(30)$  values in Fig. 2a to h. Correlation of determination,  $r^2$ , for these plots is shown in Table III. Measured  $\log k'_w$ , extrapolated  $\log k'_w$  from the  $E_T(30)$  scale, and the percentage errors for various compounds are listed

in Table IV. Comparison of the correlation of determination of the plots between  $\log k'$  and either  $E_T(30)$  scale or volume percentage of organic modifier in Tables I and III shows that for volume percentage plots,  $r^2$  values are greater than 0.99 using methanol-water mixtures for all compounds and using acetonitrile-water mixtures for non-polar compounds, and  $r^2$  values are between 0.88 and 0.92 for polar compounds using acetonitrile-water mixtures. For  $E_T(30)$  plots using methanol-water or acetonitrile-water mixtures,  $r^2$  values are greater than 0.98 for polar compounds, while  $r^2$  values are between 0.95 and 0.97 for non-polar compounds and *p*-chlorophenol.

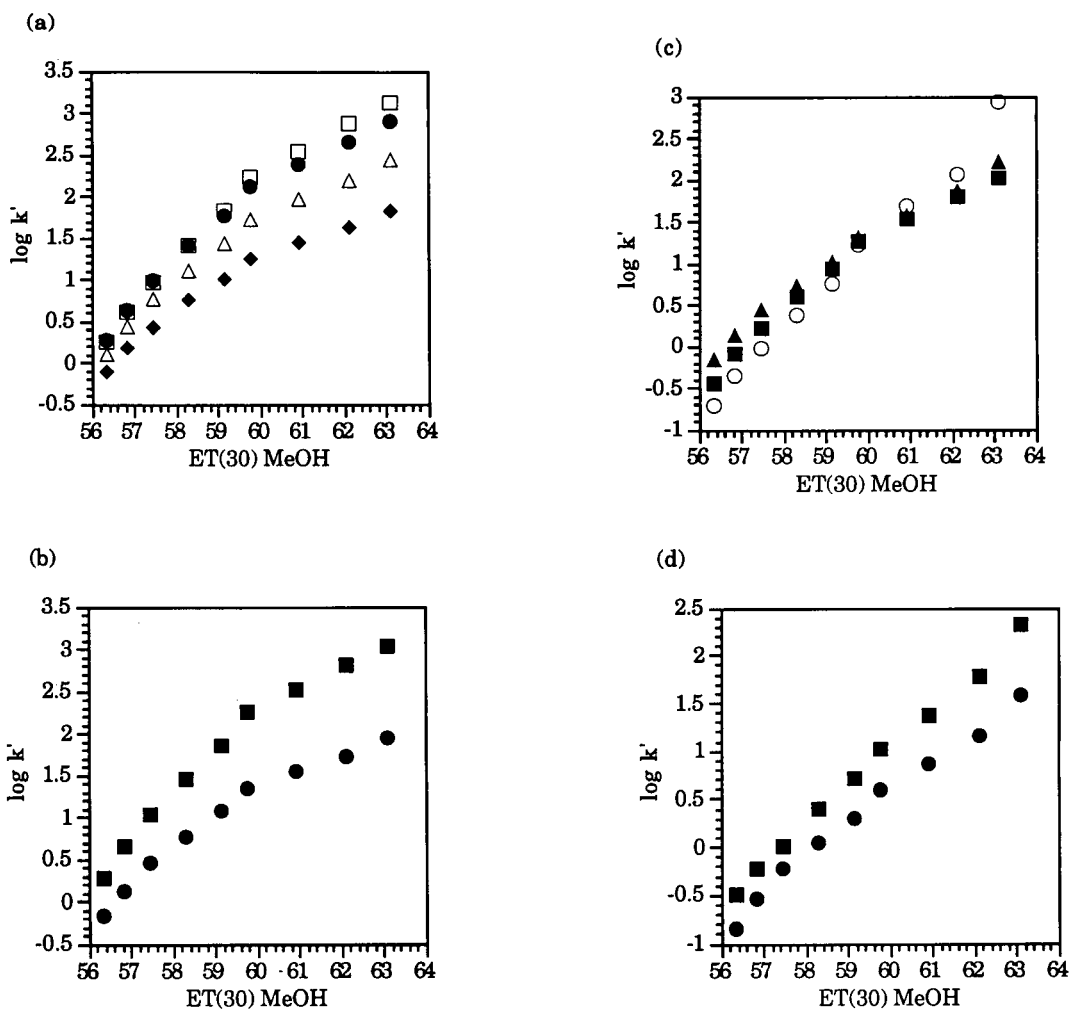


Fig. 2.

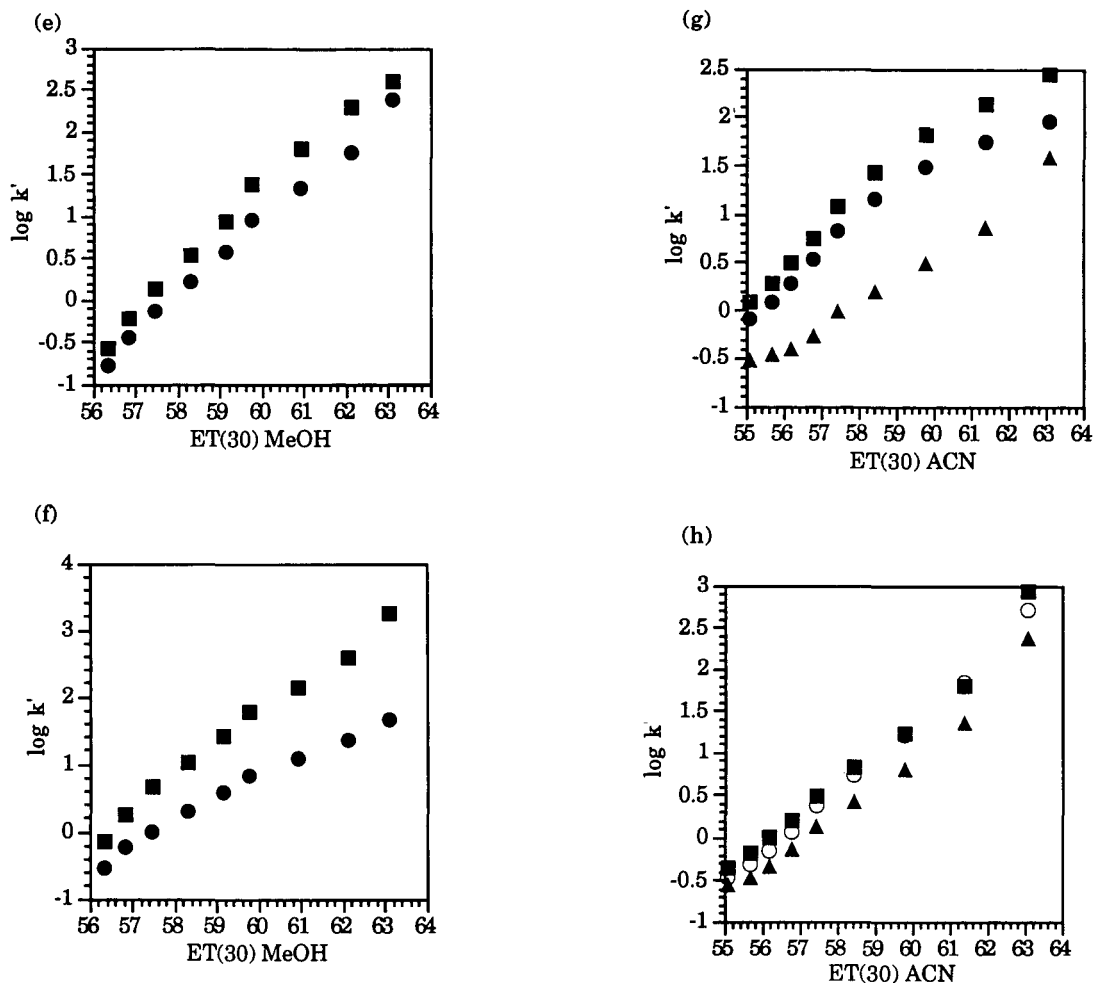


Fig. 2.  $\log k'$  vs.  $E_T(30)$  scale using methanol (or acetonitrile)–water mixtures on a column with a bonding density of  $3.41 \mu\text{mol}/\text{m}^2$ . Symbols as in Fig. 1.

Comparison between the extrapolated  $\log k'_w$  from either  $E_T(30)$  scale or volume percentage of organic modifier and the measured  $\log k'_w$  in Tables II and IV shows that the errors are within a similar range from both extrapolation methods. The errors can be as high as 10% using methanol–water and 20% using acetonitrile–water. Extrapolated  $\log k'_w$  can be obtained from linear plots between  $\log k'$  and  $E_T(30)$  values using both methanol–water and acetonitrile–water mixtures, yet a second polynomial fit between  $\log k'$  and volume percent of organic modifier is needed to predict  $\log k'_w$  when acetonitrile is used as an organic modifier. For non-polar compounds the errors are larger using  $E_T(30)$

plots than using the volume percentage plots. The errors are relatively smaller for polar compounds using  $E_T(30)$  plots than using volume percentage plots. The different curvature in high water (or high polarity) region relative to the low water (or low polarity) region in plots of  $\log k'$  versus  $E_T(30)$  scale shown in Fig. 2 is similar to the volume percentage plots. For non-polar compounds, the retention increases with increasing the polarity of the mobile phase, however, the retention did not increase in high polarity region of mobile phase as expected according to the slope in low polarity region of mobile phase. Thus the retention curve appears to plateau at the polarity of mobile phase above the

TABLE III  
CORRELATION OF DETERMINATION ( $r^2$ ) FOR THE PLOTS BETWEEN  $\log k'$  AND  $E_T(30)$  SCALE USING MOBILE PHASES FROM 0% TO 80% METHANOL (OR ACETONITRILE)-WATER MIXTURES

Compound	$r^2$	
	Methanol	Acetonitrile
Benzene	0.9577	
Toluene	0.9621	0.9697
Ethylbenzene	0.9710	
Fluorobenzene	0.9524	0.9569
Naphthalene	0.9709	
<i>p</i> -Chlorotoluene	0.9672	
Acetophenone	0.9958	
Dimethyl phthalate	0.9907	0.9887
Anisole	0.9843	
Benzyl alcohol	0.9860	0.9818
<i>p</i> -Chlorophenol	0.9663	
Methylparaben	0.9943	0.9803
Ethylparaben	0.9937	0.9980
Nitrobutane	0.9840	
Nitrohexane	0.9896	

$E_T(30)$  value of 60 (ca. 30% organic modifier in water) for non-polar compounds. For polar compounds, there is an abrupt increase in retention from the  $E_T(30)$  value of mobile phase about 62 to 63 (ca. 10% to 0% organic modifier in water). It seems that modification of the stationary phase is very important for solute retention under highly aqueous mobile phase and cannot be neglected in prediction of  $\log k'_w$  values.

*Retention studies by the solvatochromic comparison method*

The solvatochromic parameters ( $\pi^*$ ,  $\beta$ ,  $\alpha$ ,  $\delta$ ) of the solutes listed in Table V were cited from the values reported by Kamlet *et al.* [34]. A polarizability correction factor,  $\delta$ , is defined as zero for aliphatic compounds and 1 for aromatic compounds. These values were chosen to bring the aromatic and aliphatic compounds into line with the select compounds in a wide variety of correlations. There are many ways to determine solute molar volume and it was proved that Leahy's computer-calculated in-

TABLE IV  
MEASURED  $\log k'_w$ , EXTRAPOLATED  $\log k'_w$  FROM THE  $E_T(30)$  SCALE AND PERCENTAGE ERROR BETWEEN THE EXTRAPOLATED AND MEASURED  $\log k'_w$  USING METHANOL OR ACETONITRILE AS THE ORGANIC MODIFIER

Compound	$\log k'_w$ <sup>a</sup> (measured)	$\log k'_w$ <sup>b</sup> methanol	$\log k'_w$ <sup>b</sup> acetonitrile	Error % methanol	Error % acetonitrile
Benzene	1.82	2.10		15.38	
Toluene	2.43	2.73	2.86	12.35	17.70
Ethylbenzene	2.88	3.27		13.54	
Fluorobenzene	1.94	2.25	2.41	15.98	24.23
Naphthalene	3.12	3.52		12.82	
<i>p</i> -Chlorotoluene	3.01	3.47		15.28	
Acetophenone	2.31	2.22		-3.90	
Dimethyl phthalate	2.81	2.65	2.38	-5.69	-15.30
Anisole	2.22	2.34		5.41	
Benzyl alcohol	1.58	1.56	1.23	1.27	-22.15
<i>p</i> -Chlorophenol	2.01	2.36		17.41	
Methylparaben	2.37	2.27	1.84	-4.22	-22.36
Ethylparaben	2.58	2.85	2.43	10.47	-5.81
Nitrobutane	1.67	1.78		6.59	
Nitrohexane	2.75	3.07		11.64	

<sup>a</sup> Measured  $\log k'_w$ .

<sup>b</sup> Calculation of the extrapolated  $\log k'_w$  is based on the linear function between  $\log k'$ , and  $E_T(30)$  scale using mobile phases containing 10-80% methanol or acetonitrile.

TABLE V  
SOLUTE  $V, \pi^*, \beta, \alpha$  AND  $\delta$  VALUES

	$V(1/100)$	$\pi^*$	$\beta$	$\alpha$	$\delta$
<i>Non-polar compounds</i>					
Benzene	0.491	0.59	0.10	0.00	1
Toluene	0.592	0.55	0.11	0.00	1
Ethylbenzene	0.668	0.53	0.12	0.00	1
Fluorobenzene	0.520	0.62	0.07	0.00	1
Naphthalene	0.753	0.70	0.15	0.00	1
<i>p</i> -Chlorotoluene	0.679	0.67	0.08	0.00	1
<i>Compounds with hydrogen bond acceptor groups</i>					
Acetophenone	0.69	0.90	0.49	0.04	1
Dimethyl phthalate	0.98	0.85	0.80	0.00	1
Anisole	0.639	0.73	0.32	0.00	1
Nitrobutane	0.641	0.76	0.25	0.00	0
Nitrohexane	0.837	0.72	0.25	0.00	0
<i>Compounds with hydrogen bond donor groups</i>					
Benzyl alcohol	0.634	0.99	0.52	0.39	1
<i>p</i> -Chlorophenol	0.626	0.72	0.23	0.67	1
<i>Compounds with hydrogen bond acceptor and donor groups</i>					
Methylparaben	0.778	1.34	0.70	0.61	1
Ethylparaben	0.874	1.33	0.69	0.61	1

TABLE VI

MULTIPLE LINEAR REGRESSION BETWEEN  $\log k'$  AND  $V_2/100, \pi_2, \beta_2, \alpha_2$ , AND  $\delta_2$  USING VARIOUS METHANOL-WATER AND ACETONITRILE-WATER COMPOSITIONS

Methanol values were based on a data set of 15 compounds. Acetonitrile values were based on a data set of 6 compounds.  
 $\log k' = \log k'_0 + m''V_2/100 + s''\pi_2 + b''\beta_2 + a''\alpha_2 + d''\delta_2$

Organic modifier (%, v/v)	$m''$	$s''$	$b''$	$a''$	$d''$	$\log k'_0$	$r^2$
<i>Methanol</i>							
80	1.98	0.54	-2.30	-0.44	0.42	-1.63	0.9553
70	2.38	0.52	-2.48	-0.37	0.43	-1.51	0.9578
60	2.85	0.56	-2.72	-0.34	0.47	-1.51	0.9559
50	3.37	0.61	-3.00	-0.33	0.53	-1.52	0.9655
40	3.98	0.69	-3.28	-0.30	0.59	-1.64	0.9688
30	4.66	0.76	-3.47	-0.28	0.68	-1.84	0.9717
20	5.17	0.78	-3.42	-0.29	0.70	-1.94	0.9728
10	5.51	1.08	-3.49	-0.34	0.72	-2.09	0.9400
0	5.35	0.87	-2.59	-0.52	0.72	-1.74	0.9637
<i>Acetonitrile</i>							
80	1.57	-0.65	-1.17	0.41		-0.41	0.9812
70	2.25	-0.46	-1.68	0.29		-0.65	0.9865
60	2.28	-0.20	-2.14	0.09		-0.86	0.9856
50	3.24	0.03	-2.54	-0.05		-0.96	0.9806
40	3.62	-0.07	-2.78	0.08		-0.78	0.9815
30	4.47	0.09	-3.37	0.07		-0.95	0.9810
20	5.43	0.10	-3.87	0.23		-1.10	0.9808
10	6.39	0.23	-4.07	0.35		-1.40	0.9778
0	6.15	0.40	-2.76	0.03		-1.25	0.9482



trinsic volumes ( $V_i$ ) leads to more precise correlations as well as to a “cleaner” dissection of the multiple solute–solvent interactions [32].  $V_i$  can be approximated by using McGowan's characteristic volume ( $V_x$ ) through the relationship between the two sets of volumes [38]:

$$V_i = 0.597 + 0.6823 V_x \quad (12)$$

A comprehensive list of atomic  $V_x$  values can be found in Abraham and McGowan's paper [38]. The unit for solute molar volume is in  $\text{cm}^3 \text{mol}^{-1}$ . Results from this study are shown in Table VI using methanol–water mixtures and acetonitrile–water mixtures. The linear equations in Table VI include aromatic and aliphatic compounds.

From the magnitude of the coefficients in Table VI,  $m''$  and  $b''$  are much larger than  $s''$  and  $a''$  and this result is in accord with other related studies. The most important solute parameters which influence retention are solute size and HBA basicity, but not HBD acidity. The solute dipolarity is a minor but still significant factor. The positive and negative signs of the solute size term and hydrogen bond basicity term show that capacity factor increases with increasing the solute size, and decreases with increasing solute HBA ability at certain mobile phase compositions.

A solvent property complementary to solute intrinsic molar volume is solvent cohesiveness, which is measured by the square of the solubility parameter ( $\delta$ ) difference between the stationary phase and mobile phase. This is the  $m''$  term of eqn. 10. If  $\delta^2$  of the stationary phase does not change with changing the mobile phase composition, the  $m''$  coefficient should be proportional to  $\delta^2$  of the mobile phase. Because water is more cohesive ( $\delta = 23.4 \text{ cal}^{1/2} \text{ cm}^{-3/2}$ ) (1 cal = 4.184 J) than methanol ( $\delta = 14.3 \text{ cal}^{1/2} \text{ cm}^{-3/2}$ ), acetonitrile ( $\delta = 11.75 \text{ cal}^{1/2} \text{ cm}^{-3/2}$ ) and alkanes ( $\delta = 11.75 \text{ cal}^{1/2} \text{ cm}^{-3/2}$ ), the process of forming the cavity in the solvent becomes increasingly endoergic with increasing water content. Accordingly, the  $m''$  increases as the water content is increased from (80:20) to (10:90) organic–water in Fig. 3. However, the  $m''$  coefficient decreases from organic–water (10:90) to pure water. This means that  $\delta^2$  of the stationary phase is not a constant when the composition of mobile phase is changed and it increases significantly from organic–water (10:90) to pure water.

Because stationary phase can be selectively solvated by organic modifier in the mobile phase,  $\delta_s$  may change over the entire range of mobile phase compositions. Abrupt change of  $\delta_s$  from (10:90) to (0:100) methanol–water may be due to the structure change of the stationary phase within this mobile phase region. Numerous studies have shown that alkyl chains of the stationary phase are in a more extended “bristle” state in an organic containing mobile phase, while they are “collapsed” to the surface in a pure water mobile phase [21–27]. This con-

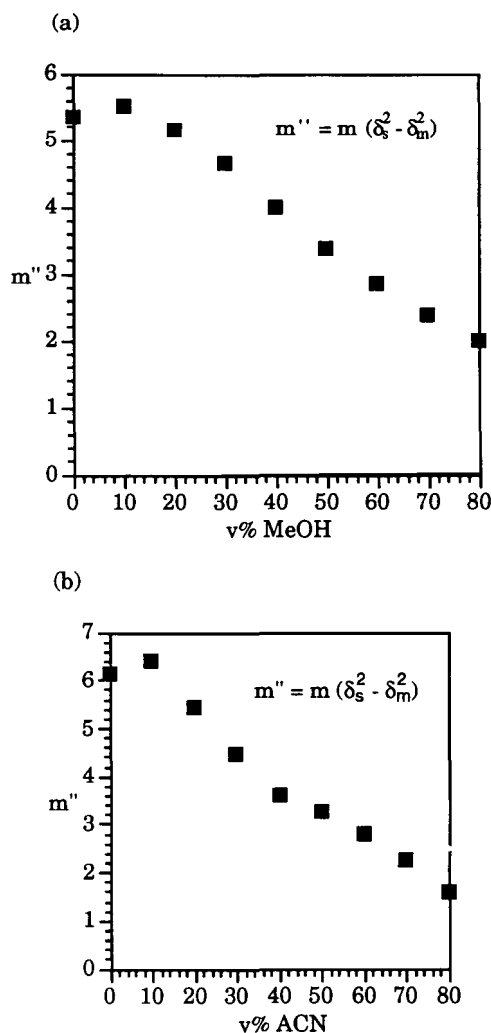


Fig. 3. Plot of the contribution of  $\log k'$  from the cavity formation difference between the stationary phase and mobile phase,  $m''$ , versus volume percentage (v%) of (a) methanol, (b) acetonitrile.

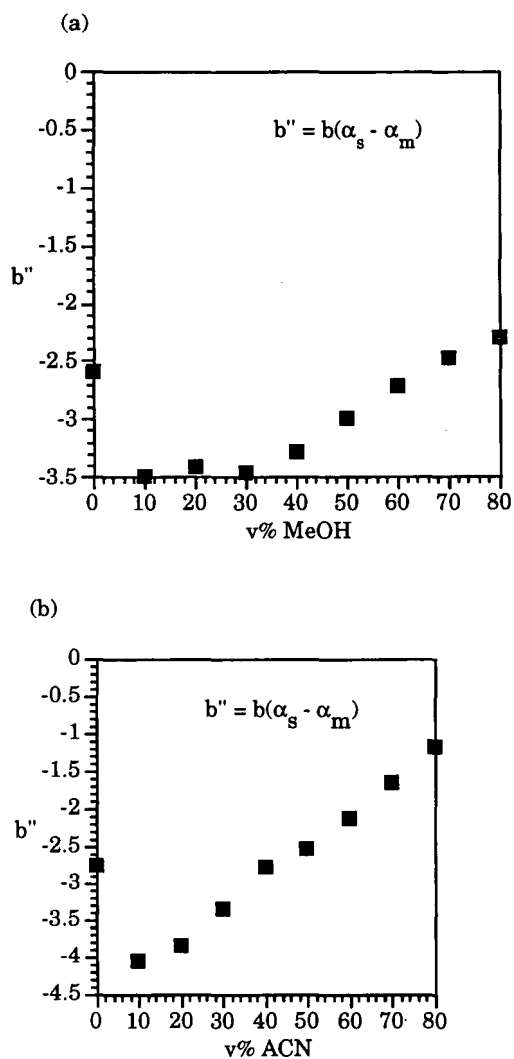


Fig. 4. Plot of the hydrogen bonding term contributed from the hydrogen bond acidity difference between the stationary phase and mobile phase,  $b''$ , versus volume percentage (v%) of (a) methanol, (b) acetonitrile.

formational change reduces the surface area of the stationary phase and the contact interactions between solutes and the stationary phase. Thus,  $m''$  did not increase with increasing the water concentration as expected at highly aqueous region, instead it decreased.

However, the idea of collapsed vs. extended chain configurations was recently rejected by measuring

the orientation and reorientation of a fluorescent probe, 1,4-bis(*o*-methylstyryl)benzene assuming that any changes in the orientational distribution of the chains will cause related changes in the orientational distribution of the probe solute [39]. Montgomery *et al.* [39] found that the  $C_{18}$  chains lie flat on the surface when water is the mobile phase and change little in the presence of small amount of alcohol. Another possible reason for abnormal behavior of  $m''$  is the pore effects. As the mass transfer of solute molecules into and out of the stationary phase zone is controlled mainly by their diffusion within the porous particles, the pore structure of the packing is also important with respect to the retention mechanism. Because of the non-polar alkyl chains on the surface, solute diffusion into the pores is dependent on the organic modifier in the mobile phase. Solutes may diffuse into the pores of silica less effectively in highly polar aqueous mobile phases than in the organic rich mobile phases. As the alkyl chains in the pores are less accessible in a highly aqueous mobile phase compared to the organic rich mobile phase, the effective volume of the stationary phase is reduced, and  $m''$  is reduced also.

The solvent property complementary to solute HBA basicity is the HBD acidity difference between the stationary phase and mobile phase. This is the  $b''$  term of eqn. 4. Since the stationary phase is highly solvated at higher organic content mobile phases, hydrogen bonding interactions are dominated by the interaction between solutes and the mobile phase. As shown in Fig. 4,  $b''$  coefficients become increasingly negative in going from organic–water (80:20) to (10:90) and this is because water is a stronger hydrogen bond donor acid ( $\alpha = 1.17$ ) than methanol ( $\alpha = 0.93$ ) and acetonitrile ( $\alpha = 0.19$ ). However, the  $b''$  coefficient increases significantly from organic–water (10:90) to (0:100). Again, like  $\delta_s$ ,  $\alpha_s$  changes with changing the mobile phase composition and there is a significant increase of  $\alpha_s$  from organic–water (10:90) to (0:100). The possible explanation is that the stationary phase is less solvated at lower organic content mobile phases, so residual silanol groups on the stationary phase might be more exposed to solutes and the hydrogen bonding interactions between solutes and the stationary phase become more significant.

### Correction of predicted $\log k'_w$ by a multivariable equation

Extrapolating  $\log k'_w$  from either volume percentage or  $E_T(30)$  scale from data obtained above organic–water (10:90) assumes that either conformation and composition of the stationary phase do not change with changing the mobile phase composition or solute diffusion within the porous silica particles is independent of mobile phase conditions. It may also assume that solute retention is not affected by the structural change or diffusion process. However, structure of the stationary phase and solute diffusion in pure water may not be the same as in organic–water mixtures. If the extended alkyl chains in organic rich mobile phase collapse to the surface of silica in highly aqueous mobile phase, surface area of the reversed-phase will be reduced. If solute diffusion within the pores of the silica is less efficient in highly aqueous mobile phases than in organic rich mobile phases, accessible volume of the stationary phase will be reduced. For both cases, retention time for non-polar compounds will not increase with increasing the water concentration as expected at highly aqueous region because of the reduction of surface area or volume of the reversed-phase, and the deviation is proportional to

solute size. Because the stationary phase is less solvated at lower organic content mobile phases, hydrogen bonding interactions between polar compounds and hydroxyl groups on the silica surface may increase the retention time.

This suggests that the difference between extrapolated and measured  $\log k'_w$  values is a function of solute properties:

$$\log k'_w (\text{extrapolated}) - \log k'_w (\text{measured}) = a(V/100) + b(\pi_2^*) + c(\beta_2) + d(\alpha_2) + e(\delta_2) + k \quad (13)$$

Deviations as functions of properties of solutes are listed in Table VII. From Table VII, correlation of determination is high for  $\log k'_w$  extrapolated from the  $E_T(30)$  scale using either methanol–water ( $r^2 = 0.9178$ ) or acetonitrile–water ( $r^2 = 0.9844$ ), and it is relatively lower for  $\log k'_w$  extrapolated from the volume percentage of organic modifier using either linear plot ( $r^2 = 0.7065$ ) or second polynomial plot ( $r^2 = 0.7874$ ) in methanol–water. This suggests that  $\log k'_w$  extrapolated from the  $E_T(30)$  plot gives more reproducible, meaningful values for correlation with bioavailability. The actual  $\log k'_w$  can be predicted from the  $E_T(30)$  scale and then corrected by eqn. 13.

TABLE VII

MULTIVARIABLE EQUATION OF DIFFERENCE BETWEEN THE EXTRAPOLATED AND MEASURED  $\log k'_w$  AS FUNCTION OF SOLUTE'S PROPERTIES

$\log k'_w$  values are extrapolated from either the volume percentage or  $E_T(30)$  scale using acetonitrile–water or methanol–water mobile phases.

$$\Delta = \log k'_w (\text{extrapolated}) - \log k'_w (\text{measured}) = a(V/100) + b(\pi_2^*) + c(\beta_2) + d(\alpha_2) + e(\delta_2) + k$$

	<i>a</i>	<i>b</i>	<i>c</i>	<i>d</i>	<i>e</i>	<i>k</i>	$r^2$	$n^a$
<i>Methanol–water</i>								
$\Delta$ (% v/v, lin) <sup>b</sup>	0.41	0.28	-1.03	0.01	0.10	-0.21	0.7065	15
$\Delta$ (% v/v, pol) <sup>c</sup>	0.84	0.32	-0.95	-0.15	0.07	-0.64	0.7874	15
$\Delta$ (ET) <sup>d</sup>	1.07	0.21	-1.37	0.26	0.09	-0.39	0.9178	15
<i>Acetonitrile–water</i>								
$\Delta$ (%, v/v, pol)	1.79	-0.34	-1.91	0.67		-0.44	0.9574	6
$\Delta$ (ET)	2.29	0.05	-2.64	0.27		-0.61	0.9844	6

<sup>a</sup> Number of compounds.

<sup>b</sup> Calculation of the extrapolated  $\log k'_w$  is based on the linear function between  $\log k'$  and volume percentage using mobile phases containing 10–80% organic.

<sup>c</sup> Calculation of the extrapolated  $\log k'_w$  is based on the second polynomial function between  $\log k'$  and volume percentage using mobile phases containing 10–80% organic.

<sup>d</sup> Calculation of the extrapolated  $\log k'_w$  is based on the linear function between  $\log k'$  and  $E_T(30)$  scale using mobile phases containing 10–80% organic.

## CONCLUSIONS

Based on the correlation of determination,  $\log k'$  is linearly in proportion to the  $E_T(30)$  scale using either methanol-water or acetonitrile-water mobile phase and is linearly related to volume percentage of methanol, yet it is a second polynomial function of the volume percentage of acetonitrile. A distinct curvature was observed for all compounds from 0 to 10% organic modifier in water. The direction of curvature was found to correlate with solute polarity. Retention curves for non-polar compounds appear to plateau at volume percentages greater than about 90% water in the mobile phase. An upward curve toward pure water mobile phase was observed for compounds with strong hydrogen-bond acceptor ability. The different retention behaviors of compounds in high water content mobile phases (>90%) and lower water content mobile phases (<90%) causes the errors of prediction of  $\log k'_w$  from extrapolation. Errors of predicted  $\log k'_w$  from either the  $E_T(30)$  scale or volume percentage of organic modifier can be as much as about 10% using methanol-water and 20% using acetonitrile-water. The reason is that either volume percentage or  $E_T(30)$  scale is a function of mobile phase only but chromatographic retention is a function of both the stationary and mobile phases.

Mobile phase and stationary phase effects on retention were partially deconvoluted by the linear solvation energy relationship. Eqn. 10 was solved by retention of 15 compounds over the entire range of mobile phase compositions. It was found that characteristics of the stationary phase in eqn. 10 ( $\delta_s$ ,  $\pi_s$ ,  $\beta_s$ ,  $\alpha_s$ ) are smaller than those of the mobile phase, and changed little using mobile phase from methanol-water (10:90) to (80:20). However, these values changed significantly when 100% water was used as the mobile phase, presumably due to the change of the structure of the stationary phase or the diffusion process of solutes with respect to the mobile phase conditions. Conformational change of the stationary phase from a bristle structure (high organic content mobile phases) to a collapsed structure (high water content mobile phases) reduces the active surface area of the stationary phase. The loss of the efficiency for solute diffusion within the pores of the silica in highly aqueous mobile phases relative to the organic rich mobile phases reduces the volume

of the stationary phase. This provides explanation as to why retention time does not increase in the manner expected with increasing volume percentage of water for non-polar compounds.

As stationary phase is less solvated at highly aqueous mobile phases relative to organic rich mobile phases, the hydrogen bonding interactions between polar compounds and hydroxyl groups on the stationary phase may be stronger at highly aqueous mobile phases. Thus retention of polar compounds at highly aqueous mobile phases is greater than expected from retention at highly organic content mobile phases.

Extrapolating  $\log k'_w$  values from data obtained above methanol-water (10:90) does not represent the actual  $\log k'_w$ . Rather, it represents what the capacity factor would be, if the conformation and composition of stationary phase and solute diffusion process within porous silica particles in pure water were the same as in organic-aqueous mixtures. Thus this extrapolated  $\log k'_w$  value is still valid as an estimator of compound's lipophilicity, which is used heavily in QSRR studies. This is because the extended bristle structure of the RPLC stationary phase using high organic content mobile phase more closely mimics the structure of a biomembrane-water interphase.

Without information on the physical properties of aqueous mixtures of organic solvents, eqn. 5 cannot be solved. However, eqn. 5 can be simplified using the  $E_T(30)$  scale, because  $E_T(30)$  is sensitive to solvent dipolarity-polarizability as well as solvent hydrogen bond donor ability. Thus the  $\log k'_w$  extrapolated from the  $E_T(30)$  plot is more meaningful for correlation with bioavailability. The difference between the calculated and measured  $\log k'_w$  is related to the characteristics of stationary phase and the interaction between solutes and stationary phase, and can be estimated from solute properties according to eqn. 13.

## ACKNOWLEDGEMENTS

The authors are grateful for support of this work by AFOSR 91-0254, by NIH GM-48561, and for continued support of our research by Merck, Sharp & Dohme, West Point, PA, USA.

## REFERENCES

- 1 M. J. M. Wells and C. R. Clark, *J. Chromatogr.*, 235 (1982) 43.
- 2 M. J. M. Wells and C. R. Clark, *J. Chromatogr.*, 284 (1984) 319.
- 3 D. J. Minick, J. H. Frenz, M. A. Patrick and D. A. Brent, *J. Med. Chem.*, 31 (1988) 1923.
- 4 P. Jandera and J. Kubat, *J. Chromatogr.*, 500 (1990) 281–299.
- 5 T. Braumann, *J. Chromatogr.*, 373 (1986) 191–225.
- 6 T. Braumann, M. Weber and L. H. Grimme, *J. Chromatogr.*, 261 (1983) 329.
- 7 M. M. Schantz and D. E. Martire, *J. Chromatogr.*, 391 (1987) 35.
- 8 L. R. Snyder, M. A. Quarry and J. L. Glajch, *Chromatographia*, 24 (1987) 33.
- 9 E. D. Katz, *J. Chromatogr.*, 352 (1986) 67.
- 10 E. D. Katz, C. H. Lochmüller and R. P. W. Scott, *Anal. Chem.*, 61 (1989) 349.
- 11 K. L. Rowlen and J. M. Harris, *Anal. Chem.*, 63 (1991) 964.
- 12 P. C. Sadek, P. W. Carr, R. M. Doherty, M. J. Kamlet, R. W. Taft and M. H. Abraham, *Anal. Chem.*, 57 (1985) 2971.
- 13 M. J. Kamlet, J. L. M. Abboud and R. W. Taft, *Prog. Phys. Org. Chem.*, 13 (1983) 485.
- 14 W. J. Cheong and P. W. Carr, *Anal. Chem.*, 60 (1988) 820.
- 15 M. J. Kamlet, P. W. Carr, R. W. Taft, M. H. Abraham, *J. Am. Chem. Soc.*, 103 (1981) 6062.
- 16 P. W. Carr, R. M. Doherty, R. W. Taft, M. Melander and C. Horváth, *Anal. Chem.*, 58 (1986) 2674.
- 17 M. J. Kamlet, R. M. Doherty, M. H. Abraham, Y. Marcus and R. W. Taft, *J. Phys. Chem.*, 92 (1988) 5244.
- 18 B. P. Johnson, M. G. Khaledi and J. G. Dorsey, *Anal. Chem.*, 58 (1986) 2354.
- 19 J. J. Michels and J. G. Dorsey, *J. Chromatogr.*, 457 (1988) 85.
- 20 J. J. Michels and J. G. Dorsey, *J. Chromatogr.*, 499 (1990) 435.
- 21 R. K. Gilpin, *J. Chromatogr. Sci.*, 22 (1984) 371.
- 22 R. K. Gilpin, *Anal. Chem.*, 57 (1985) 1465A.
- 23 L. C. Sander and S. A. Wise, *CRC Crit. Rev. Anal. Chem.*, 18 (1987) 299.
- 24 J. Nawrocki and B. Buszewski, *J. Chromatogr.*, 449 (1988) 1.
- 25 L. C. Sander, J. B. Callis and L. R. Field, *Anal. Chem.*, 55 (1983) 1068.
- 26 E. Bayer, A. Paulus, B. Peters, G. Laupp, J. Reiners and K. Albert, *J. Chromatogr.*, 364 (1986) 25.
- 27 R. P. W. Scott and C. F. Simpson, *J. Chromatogr.*, 197 (1980) 11.
- 28 C. R. Yonker, T. A. Zwier and M. F. Burke, *J. Chromatogr.*, 241 (1982) 257.
- 29 C. R. Yonker, T. A. Zwier and M. F. Burke, *J. Chromatogr.*, 241 (1982) 269.
- 30 J. W. Carr and J. M. Harris, *Anal. Chem.*, 58 (1986) 626.
- 31 J. Stahlberg and M. Almgren, *Anal. Chem.*, 57 (1985) 817.
- 32 D. E. Leahy, P. W. Carr, R. S. Perlman, R. W. Taft and M. J. Kamlet, *Chromatographia*, 21 (1986) 473.
- 33 J. H. Park, P. W. Carr, M. H. Abraham, R. W. Taft, R. M. Doherty and M. J. Kamlet, *Chromatographia*, 25 (1988) 373.
- 34 M. J. Kamlet, M. H. Abraham, Y. Marcus and R. W. Taft, *J. Chem. Soc. Perkin Trans. II*, (1988) 2087.
- 35 K. B. Sentell, K. W. Barnes and J. G. Dorsey, *J. Chromatogr.*, 455 (1988) 95.
- 36 P. J. Schoenmakers, H. A. H. Billiet and L. de Galan, *J. Chromatogr.*, 282 (1983) 107.
- 37 R. K. Gilpin and M. E. Gangoda, *J. Chromatogr. Sci.*, 21 (1983) 352.
- 38 M. H. Abraham and J. C. McGowan, *Chromatographia*, 23 (1987) 243.
- 39 M. E. Montgomery, Jr., M. A. Green and M. J. Wirth, *Anal. Chem.*, 64 (1992) 1170.

# Characterization of a Chiral-AGP capillary column coupled to a micro sample-enrichment system with UV and electrospray mass spectrometric detection

Jörgen Hermansson and Inger Hermansson

*ChromTech AB, S-145 63 Norsborg (Sweden)*

Jan Nordin

*Department of Clinical Pharmacology, Karolinska Institute, Huddinge University Hospital, S-141 86 Huddinge (Sweden)*

---

## ABSTRACT

A Chiral-AGP capillary column (150 × 0.18 mm I.D.) was used for the separation of enantiomers of racemic drugs at flow-rates of 1–2 µl/min. Small sample volumes (60 nl) were injected directly on to the capillary column, whereas larger sample volumes were injected by enrichment of the sample on a capillary trapping column (45 × 0.25 mm I.D.). The trapping column and the Chiral-AGP capillary column were coupled together by a switching valve. A pH and solvent micro gradient was generated in the trapping system. The micro gradient could be used to compress the migrating bands on the Chiral-AGP capillary column. Thus, large sample volumes could be injected without a significant decrease in detection sensitivity. For some compounds, 45–50% higher detection sensitivity than with direct injection was obtained by injection of large sample volumes on to the trapping column. Sample volumes as high as 20 µl could be injected using the sample-enrichment technique. This sample volume is 330 times higher than the volume injected directly on to the column. The hydrophobicity of the trapping column influences the band broadening. The best detection sensitivity was obtained using the most hydrophilic trapping columns. The low flow-rate used for the Chiral-AGP capillary column allows coupling with a mass spectrometer through an electrospray interface (ESI). The combination of the capillary chiral column, the micro sample-enrichment and the ESI-MS technique permits the analysis of chiral compounds at low concentrations with high detection selectivity and high sensitivity.

---

## INTRODUCTION

The biochemical reactions in living organisms occur on a three-dimensional basis as a result of the asymmetric nature of the macromolecules involved in such reactions. Enantiomers of drugs can be converted by the liver enzymes at different reaction rates or they can be converted into different metabolites [1–4]. As drugs also interfere or participate in the biochemical reactions in the organism, large differences in pharmacodynamic properties can also be obtained for drug enantiomers [5–8].

In order to be able to study the disposition of drug enantiomers in the body, analytical methods are required that permit the analysis of enantiomers present at very low concentrations in a complex matrix such as plasma and urine. It is well known that all chiral columns give lower separation efficiencies than non-chiral columns. Another feature of chiral columns is that they tend to give low selectivity for structural analogues compared with non-chiral columns. Many drugs are tertiary amines and a common metabolic pathway for tertiary amines is N-dealkylation, which means that secondary and primary amines are formed by the liver enzymes. Owing to the lower selectivity for structural analogues obtained by chiral columns compared with non-chi-

---

*Correspondence to:* J. Hermansson, ChromTech AB, S-145 63 Norsborg, Sweden.

ral columns, it can sometimes be problematic to obtain chromatograms with sufficient selectivity between enantiomers of the drug and the metabolites. This type of problem can be solved as reported by Hermansson and co-workers [9,10] for the analysis of the enantiomers of dispyramide and its mono-dealkylated metabolite, by coupling a short non-chiral column in series with the chiral column. The metabolite and disopyramide are resolved on the non-chiral column and are transported to the chiral column for resolution of the enantiomers.

Another approach is to use a column-switching system where the bands of interest are cut out and transported to the chiral column for separation of the enantiomers [11]. A third way to overcome the problem of lower selectivity for structural analogues is to prepare simple enantiomeric derivatives, *e.g.*, by acetylation of secondary and primary amine metabolites by reaction with acetic anhydride or by esterification of acids. The preparation of enantiomeric derivatives affects both the chiral selectivity and the selectivity between the enantiomers and the endogenous compounds. This approach has been utilized for the analysis of the enantiomers of atenolol present in human plasma [12].

A further way to overcome the problems with the relatively low selectivity for structural analogues by chiral columns is to use a detection technique, such as mass spectrometry (MS), which gives very high detection selectivity and high sensitivity. The development of soft ionization techniques coupled with MS has been a very important breakthrough in LC–MS. One of the most promising LC–MS techniques using soft ionization is the electrospray (ES) method [13,14]. This technique has revolutionized MS with its ability to ionize high molecular mass compounds with high efficiency. A few reports have also been published on the use of the electrospray for ionization of low molecular mass compounds [15–18]. However, the electrospray interface (ESI) is not compatible with the high flow-rates used for conventional columns. Flow-rates in the range 1–5  $\mu\text{l}/\text{min}$  are required, which means that capillary columns of I.D. < 350  $\mu\text{m}$  can be used. The drawback with capillary columns is that only very small sample volumes can be injected on to such columns, normally in the range 50–200 nl. This means that low-concentration samples cannot be handled with

this type of system. Therefore, in order to be able to utilize the ESI-MS detection, giving very high detection selectivity for low-concentration samples, the handling of highly dilute samples must be solved.

This paper reports the use of a Chiral-AGP capillary column together with a micro sample-enrichment technique that can be used in a capillary column system, making possible the introduction of large sample volumes on to capillary columns and the use of ESI-MS detection. The AGP column is based on the immobilization of  $\alpha_1$ -acid glycoprotein on silica particles. Since the development of the conventional Chiral-AGP column in 1983 [19], it has been used for the resolution of large numbers of chiral drugs from many different compound classes [20–23, and references cited therein].

## EXPERIMENTAL

### Columns

A Chiral-AGP capillary column (ChromTech, Norsborg, Sweden) with the dimensions 150  $\times$  0.18 mm I.D., packed with 5- $\mu\text{m}$  particles in a fused-silica capillary tube with a polyimide coating, was used.

Five different trapping columns, TrapCap C<sub>1</sub>, C<sub>4</sub>, C<sub>8</sub> and C<sub>18</sub> and TrapCap AGP (ChromTech) were used. The TrapCap columns were packed with 5- $\mu\text{m}$  spherical particles. The dimensions of the columns were 45  $\times$  0.25 mm I.D.

### Apparatus

*UV experiments.* Two HPLC pumps were used, an LKB 2150 (Pharmacia LKB Biotechnology, Uppsala, Sweden) for the capillary column and a Kontron 420 (Tegimenta, Rotkreutz, Switzerland) for the trapping column. To split the flow from the pumps, HPLC columns (100  $\times$  4.0 mm I.D.) packed with 5- $\mu\text{m}$  particles were inserted between the pump and the capillary or the trapping column, using tee connectors. The capillary and the trapping columns were connected through a Valco C6W six-port valve (Vici Valco, Schenkon, Switzerland). In order to keep the dead volume low, polyetheretherketone (PEEK) tubing of 0.13 mm I.D. was used to connect the trapping column to the valve.

In the direct injection experiments, *i.e.*, when the sample was injected directly on to the capillary col-

umn without trapping, the injector was a Valco C14W internal sample injector equipped with a 60-nl internal loop (Vici Valco). When larger sample volumes were injected and trapped on the trapping column, a Rheodyne (Cotati, CA, USA) Model 7125 injector with different external loops between 4 and 20  $\mu\text{l}$  was used.

The Kontron 433 UV detector (Tegimenta) was equipped with a 90 nl capillary cell, with a path length of 20 mm.

All experimental data were collected and analysed on a Kontron (Eching/Munich, Germany) 450 MT2, data system.

*Electrospray MS experiments.* The HPLC system was arranged in the same way as for the UV experiments, except that the following pumps were used: for flow delivery through the capillary column, an LKB 2150, and for flow delivery through the trapping column, a Waters 600-MS (Millipore–Waters, Milford, MA, USA). For automation of the analysis a CMA 240 sample injector (CMA Microdialys, Stockholm, Sweden) was attached to the system.

The MS system consisted of a Finnigan TSQ 700 mass spectrometer equipped with an electrospray interface (Analytica, Branford, CT, USA). The capillary HPLC column was attached to the central needle of the ESI unit with capillary PTFE tubing, drawn to minimize the dead volume. The central needle of the ESI unit was held at ground potential, and was made of stainless steel with I.D. 100  $\mu\text{m}$ . The central needle was adjusted to end at a length of 85 mm from the inside of the flange and to be 0.4 mm longer than the sheath liquid tubing. A stream of pure nitrogen with a flow-rate of 4–4.5 l/min [pressure 30 p.s.i. (1 p.s.i. = 6894.76 Pa)] and with a temperature of 100°C was used for evaporation of the solvent. In some instances, *e.g.*, for disopyramide, methanol was pumped as sheath liquid at a flow-rate between 0.5 and 2  $\mu\text{l}/\text{min}$ , to facilitate ionization. For infusion of the sheath liquid a syringe infusion pump (Model 22, Harvard Apparatus, South Natick, MA, USA) was used.

The potential in the ESI source was adjusted to give a stable signal and was held between 3.2 and 4.3 kV. The current was typically between  $10^{-7}$  and  $10^{-8}$  A.

The mass spectrometer was used as a single quadrupole system with scanning on the first quadrupole. The mass range was *ca.* 200 u with a scan rate

of 2 s per scan, where the ions of interest, *e.g.*,  $\text{MH}^+$  (protonated molecular ion) were focused under 1.8 s and the remainder of the time was spent on the scan. The reason for this was to check the performance of the ionization and the possibility of detecting other compounds.

The electrometer gain was set to  $10^{-8}$  A/V, the electron multiplier to 1200 V and the HV dynode to –15 kV. The pressure in the analyser was typically  $1.2 \cdot 10^{-5}$  Torr (1 Torr = 133.322 Pa). Under automatic overnight operation the Waters 600-MS HPLC pump was controlled by the MS data system and the CMA autoinjector from a PC, with all systems linked together.

### Chemicals

(*E*)-10-Hydroxynortriptyline was obtained as a gift from Dr. Leif Bertilsson (Huddinge University Hospital, Sweden). The other samples were obtained as gifts from the manufacturers. The structures of the compounds used are shown. 2-Propanol, acetonitrile and methanol were of HPLC grade (Lab-Scan, Dublin, Ireland).

### Chromatographic conditions

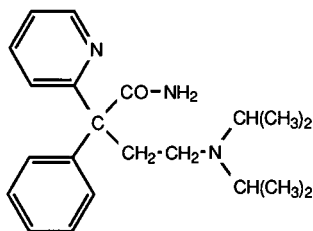
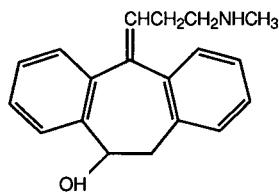
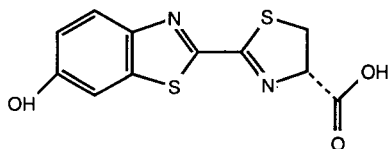
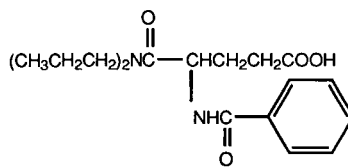
The mobile phases were prepared by adding appropriate concentrations of uncharged organic modifier to an ammonium acetate buffer or to an acetic acid solution. The buffer concentration in the mobile phases for the capillary column was 3 mM and that in the mobile phases used for sample enrichment on the trapping column was between 3 and 18 mM. The flow-rate through the capillary column was normally 1.3  $\mu\text{l}/\text{min}$  and through the trapping column 10  $\mu\text{l}/\text{min}$ . The flow-rate was determined using a microlitre syringe coupled to the outlet of the columns.

### Injection technique

During trapping the sample is introduced into the chromatographic system in the following way.

(1) The six-port valve is in the trapping position, *i.e.*, the trapping and capillary columns are eluted with two different mobile phases (see Fig. 1). The sample is injected via the Rheodyne injector on to the trapping column. The trapping time is dependent on the loop volume and the flow-rate; when using a 4- $\mu\text{l}$  loop, trapping times between 1 and 2 min were used.



**DISOPYRAMIDE****E-10-HYDROXYNORTRIPTYLINE****LUCIFERIN****PROGLUMIDE**

(2) The six-port valve is switched to its elution position, *i.e.*, the trapping column and the capillary column are coupled on-line (see Fig. 1). The trapping column is back-flushed with the capillary column mobile phase and the sample is eluted on to the capillary column. The elution time is dependent on the type of sample and trapping column and on the

elution strength of the mobile phase. Normally elution times between 10 and 13 min were used.

(3) The six-port valve is again switched to its trapping position for re-equilibration of the trapping column with the trapping mobile phase.

#### Calculations

As a solvent and pH gradient is generated by the trapping system (see Results and Discussion), the band width of the peaks was not used for the calculation of the separation efficiency on the Chiral-AGP capillary column. The separation efficiency obtained with the direct injection system was compared with that with the trapping injection system by measuring the detection sensitivity obtained by the two systems. Also, the capacity factors were not calculated when using the trapping system, as this is not an isocratic elution of the compounds. Throughout the study the retention times were used.

However, the apparent plate number,  $N_{app}$ , and the apparent separation efficiency,  $H_{app}$ , were used in one experiment, calculated according to

$$N_{app} = 5.54(t_R/W_{1/2})^2$$

and

$$H_{app} = L/N_{app}$$

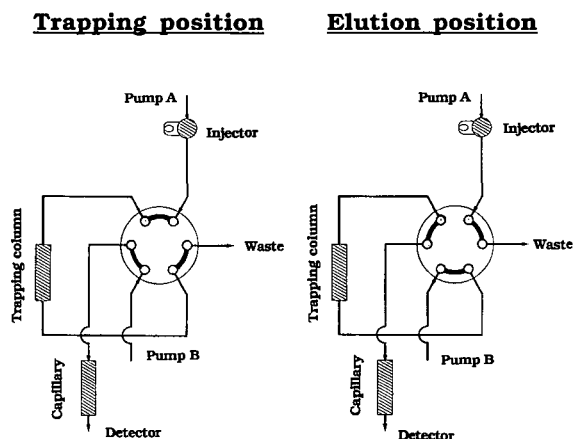


Fig. 1. Schematic illustration of the sample-enrichment system. In the trapping position the sample is loaded on to the trapping column. After switching the valve to the elution position, the trapping column is coupled on-line with the capillary column and back-flushed with the mobile phase from pump B.

where  $L$  = column length (mm), and  $t_R$  = retention time (min), and  $W_{1/2}$  = peak width at the half-height (min).

The resolution,  $R_s$ , is calculated according to

$$R_s = 2(t_{R2} - t_{R1}) / (W_1 + W_2)$$

where  $W_1$  and  $W_2$  = base widths of the peaks (min).

## RESULTS AND DISCUSSION

### *Sample-enrichment system*

The Chiral-AGP column is based on the immobilization of  $\alpha_1$ -acid glycoprotein on silica particles [21]. In this work we studied the Chiral-AGP (Cap-AGP) capillary column (150 × 0.18 mm I.D.) together with a new micro injection system, based on a capillary trapping column (45 × 0.25 mm I.D.), for enrichment of the sample. The capillary trapping system was studied using two types of detectors, a variable-wavelength UV detector equipped with a Z-shaped 90-nl capillary flow-cell, and the ESI-MS detector. The trapping column and the Cap-AGP column are coupled together by a six-port switching valve according to Fig. 1 and, as can be seen from Fig. 1, the sample is introduced by a conventional loop injector. The valve can be switched manually or automatically between the trapping and elution positions. The volume in the trapping column together with the tubes connecting the trapping column with the switching valve is about 5  $\mu$ l, which is almost twice the volume in the Cap-AGP column. The mobile phase used for trapping is a pure buffer, without organic modifier, and with a pH that gives the sample a high affinity to the silica phase, giving a narrow sample band on top of the trapping column. When the valve is switched to the elution position, the mobile phase for the Cap-AGP column is back-flushed through the trapping column. The trapping mobile phase in the trapping column and the connecting tubes is pumped on to the Cap-AGP column. This column is equilibrated with a mobile phase, containing an organic modifier, and it has also a pH that gives a lower binding affinity of the solute to the packing material. Depending on the nature of the modifier, the modifier concentration and the hydrophobicity of the trapping column, the elution of the sample from the trapping column can be regulated.

The initial pH and the buffer concentration on the trapping column can also be used to regulate the elution of the sample from the trapping column. The pH changes slowly to the pH of the analytical mobile phase and the speed depends on the difference in the pH and the concentrations of the two buffers. When the trapping column has reached a certain degree of saturation with organic modifier and when the pH has changed to give the solute a lower affinity, the solute starts to migrate. Before the sample starts to migrate from the trapping column, the organic modifier adsorbed on the protein phase is partly stripped off by the trapping buffer and pushed in front of the mobile phase for the Cap-AGP column, which gives an enrichment of the sample on top of the Cap-AGP column. The pH of the Cap-AGP column has also changed towards the pH of the trapping buffer, also giving the solute a higher affinity.

By using this technique, we generated both a solvent gradient and a pH micro gradient that moves through the column system. The steepness of the gradient can be changed by varying the elution time of the trapping column. By switching the valve before the trapping column has been equilibrated with the Cap-AGP mobile phase, the gradient will be steeper. The pH and the solvent gradients generated by the trapping system can compress the bands on the column, which means that a high detection sensitivity can be obtained despite the fact that very large sample volumes are injected compared with direct injection onto the Cap-AGP column.

Fig. 2 demonstrates the resolution of the enantiomers of luciferin using trapping injection of a 4- $\mu$ l sample. This is a 67 times higher injection volume than the 60-nl sample volume that is normally injected on to the Cap-AGP column by direct injection.

### *Recovery of sample versus elution time*

The recovery of the sample from the trapping column versus the elution time was studied using (*S*)-luciferin. The *S*-form of luciferin was enriched on a TrapCap C<sub>8</sub> column using a mobile phase of 3 mM ammonium acetate with a pH of 4.5. After the introduction of the sample on to the trapping column, the valve was switched to the elution position and the trapping column was eluted with a mobile phase of 4% 2-propanol in 3 mM ammonium acetate (pH

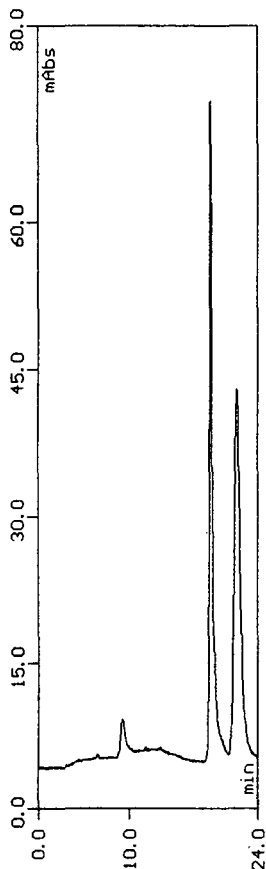


Fig. 2. Resolution of the enantiomers of luciferin. Column, Chiral-AGP capillary (150 × 0.180 mm I.D.); mobile phase, 4% 2-propanol in 3 mM ammonium acetate buffer (pH 6.0); flow-rate, 1.3  $\mu$ l/min; trapping column, TrapCap C<sub>8</sub> (45 × 0.25 mm I.D.); mobile phase, 3 mM ammonium acetate (pH 4.5); flow-rate, 10  $\mu$ l/min; sample concentration, 116 ng/ml of each enantiomer, injection volume, 4  $\mu$ l; detection, UV (327 nm).

6.0). The elution time was varied between 5 and 13 min.

From Fig. 3 it can be seen that after 5 min. elution a recovery of about 40% was obtained. A 100% recovery was obtained after about 9–10 min with the mobile phases and the trapping column used in this study. This means that the sample leaves the trapping column as a broad sample zone. However, when the sample reaches the Cap-AGP column it is enriched on top of this column and the sample zone is compressed by the gradient during the migration on the column. This is demonstrated by measuring the band width of the sample zone

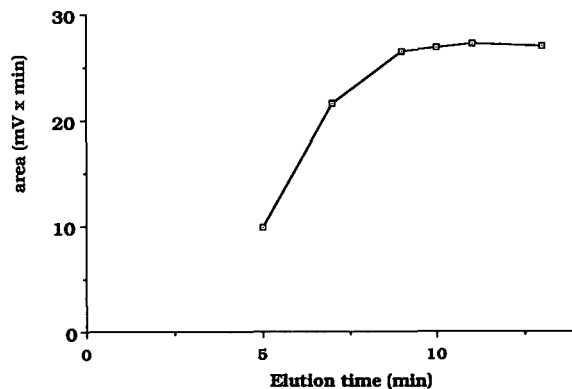


Fig. 3. Recovery of (*S*)-luciferin from the trapping column versus elution time. Column and mobile phases as in Fig. 2.

when it leaves the Cap-AGP column. A band width of 36 s was determined for (*S*)-luciferin presented in Fig. 3 (elution time 10 min) at a retention time of 18.5 min. The sample can be eluted faster from the trapping column by using a higher pH and higher organic modifier concentration, but the chiral selectivity decreases in general for acidic compounds with increasing pH and increasing organic modifier concentration [21,24].

#### Apparent efficiency versus flow-rate

The apparent plate height,  $H_{app}$ , was calculated from  $N_{app}$  as described under Experimental. In order to be able to compare the chromatograms obtained at different flow-rates on the Cap-AGP column, the samples were eluted from the trapping column for a constant time of 10 min using a flow-rate of 1.3  $\mu$ l/min. In the calculation of  $N_{app}$ , this period of 10 min was subtracted from the retention time. After sample introduction, the flow-rate in the Cap-AGP column was varied in the range 0.47–1.8  $\mu$ l/min, corresponding to linear velocities between 0.4 and 1.3 mm/s.

$H_{app}$  versus flow-rate was studied using the same system as described above for luciferin. The results of this experiment are demonstrated in Fig. 4, where it can be seen that  $H_{app}$  increases as expected by increasing the flow-rate in this range. This is most likely caused by mass-transfer effects in the stationary phase [24]. It is interesting to note the large difference in separation efficiency for the two enantiomers. The first-eluted enantiomer gives  $H_{app}$

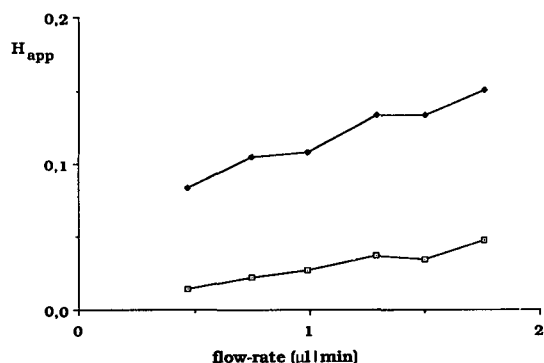


Fig. 4. Apparent separation efficiency of luciferin enantiomers versus mobile phase flow-rate. Columns and mobile phases as in Fig. 2. □ = *S*- and ● = *R*-enantiomers.

values between 0.015 and 0.048 and the corresponding values for the last-eluted enantiomer are 0.084–0.15. Obviously, the first enantiomer is compressed by the micro gradient, formed by the trapping system, to a greater extent than the more retarded enantiomer, which is only slightly affected. By decreasing the flow-rate from 1.8 to 0.47 μl/min the resolution,  $R_s$ , increases from about 2.5 to 3.5. Throughout this study we used very low buffer concentrations in the mobile phases in order to make the chromatographic system compatible with the ES-MS technique. However, the low buffer concentration reduces the separation efficiency.

#### Influence of trapping buffer concentration on sensitivity

The concentration of the trapping buffer can be used to affect the compression effect on the migrat-

ing bands in this chromatographic system. A 40:60 mixture of the enantiomers of luciferin was used as a model compound system. The trapping buffer concentration was varied between 3 and 18 mM and the peak heights and the retention times were measured. The results are summarized in Table I together with the resolution,  $R_s$ . It is interesting to note the strong effect obtained on the first-eluted peak, which is highly compressed at the lowest trapping buffer concentration. A *ca.* four times higher peak was obtained at the lowest concentration of the trapping buffer, 3 mM, compared with that obtained at 18 mM. It can also be noted that the effect on the last-eluted peak was very limited. A reasonable explanation of the influence of the trapping buffer concentration on the peak height is that the gradient generated by the trapping system is not steep enough at the highest buffer concentration, owing to the resistance of this buffer to changes in pH from 4.5 to 6.0 with the weak (only 3 mM) mobile phase buffer. It can also be noted that a slightly higher retention was obtained using higher concentration of the trapping buffer.

#### Influence of large sample volumes on detection sensitivity

The trapping system allows the injection of large sample volumes on to the 180 μm I.D. Cap-AGP column. The detection sensitivity, expressed as the relative peak height obtained by direct injection of 60 nl of proglumide, was compared with the injection of a 4-μl sample by the trapping system. The sample amount injected was constant in both injections, which means that a 67 times lower concentration was injected with the trapping system. A

TABLE I

#### INFLUENCE OF TRAPPING BUFFER CONCENTRATION ON SENSITIVITY AND RESOLUTION

Column, Chiral-AGP capillary (150 × 0.180 mm I.D.); mobile phase, 4% 2-propanol in 3 mM ammonium acetate (pH 6.0), trapping column, TrapCap C<sub>8</sub> (45 × 0.25 mm I.D.); mobile phase, different concentrations of ammonium acetate buffer (pH 4.5); sample, (*R*)- and (*S*)-luciferin (40:60 mixture).

Buffer concentration (mM)	Peak height 1 (mV)	Peak height 2 (mV)	$t_{R1}$ (min)	$t_{R2}$ (min)	$R_s$
18	11.2	17.3	20.4	24.0	2.06
9	33.3	26.8	19.3	21.9	2.25
3	39.6	24.4	19.0	21.7	2.67

TABLE II

## COMPARISON OF SENSITIVITIES USING DIRECT INJECTION AND TRAPPING

Column, Chiral-AGP capillary (150 × 0.180 mm I.D.); mobile phase, 8% acetonitrile in 3 mM ammonium acetate (pH 6.0); flow-rate, 1.4  $\mu\text{l}/\text{min}$ ; trapping column, TrapCap AGP (45 × 0.25 mm I.D.); mobile phase, 3 mM ammonium acetate buffer (pH 4.5); flow-rate, 11.0  $\mu\text{l}/\text{min}$ ; sample, proglumide.

Parameter	Direct injection	Trapping injection
Sample concentration ( $\mu\text{g}/\text{ml}$ )	188.0	2.8
Injection volume (nl)	60	4000
Relative peak height 1	1	0.82
Relative peak height 2	1	0.95
Peak area 1 (mV min)	19.8	20.2
Peak area 2 (mV min)	19.7	19.4

comparison of the peak heights obtained for the enantiomers in the two systems demonstrates that the detection sensitivity decreases to some extent on increasing the injection volume. The results are summarized in Table II. The first peak gives a detection sensitivity that is 82% of the sensitivity obtained by direct injection. However, the sensitivity for the last-eluted enantiomer was only slightly affected and the sensitivity for this peak was 95% compared with direct injection.

It is also possible to obtain a higher sensitivity with the trapping system compared with direct injection. This is demonstrated in Fig. 5, where the enantiomers of disopyramide were resolved after direct injection (60 nl) and by injection of a 4- $\mu\text{l}$  sample by the trapping technique. The sample was enriched on a TrapCap C<sub>4</sub> column using a trapping mobile phase of distilled water. UV detection at 225 nm was used, which means that the disturbances of the equilibria on the Cap-AGP column can easily be detected. As can be seen from the chromatogram, the first-eluted enantiomer of disopyramide is highly compressed and is eluted as a very narrow band. This is due to the fact that the mobile phase in front of this zone retains the solute more strongly than the mobile phase behind the sample zone, therefore the zone is highly compressed. A 54% higher detection sensitivity was obtained for the first-eluted enantiomer using the trapping injection, whereas the peak height for the last-eluted enantiomer was

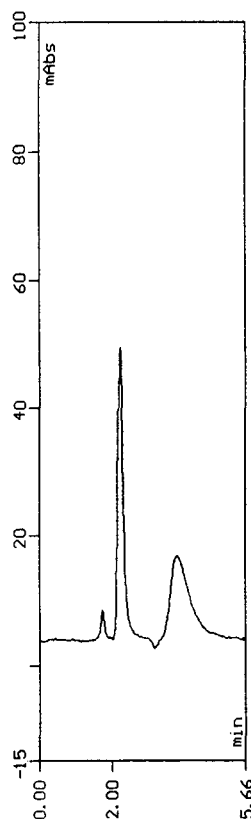
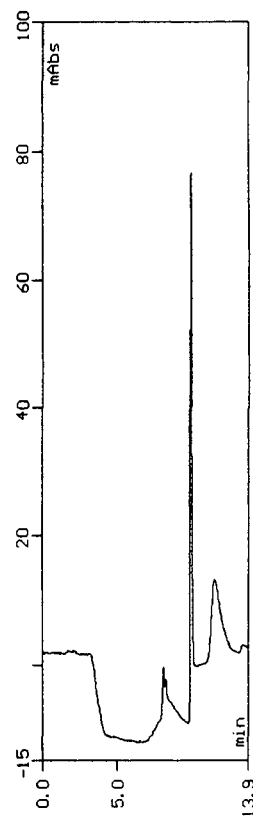
**DIRECT****TRAPPING**

Fig. 5. Separation of disopyramide enantiomers by direct injection and by trapping. Column, Chiral-AGP capillary (150 × 0.180 mm I.D.); mobile phase, 1.2% 2-propanol in 3 mM acetic acid (pH 3.6); trapping column, TrapCap C<sub>4</sub> (45 × 0.25 mm I.D.); mobile phase, distilled water; sample concentration, direct injection 276  $\mu\text{g}/\text{ml}$  (60 nl injected), trapping injection 4.2  $\mu\text{g}/\text{ml}$  (4  $\mu\text{l}$  injected); detection, UV (225 nm).

reduced to 83% of the that obtained by direct injection. The baseline disturbance detected by UV at 225 nm is not obtained using ESI-MS detection (see Fig. 8).

Fig. 6 shows two chromatograms for the resolution of the enantiomers of 10-hydroxynortriptyline where 4- and 12- $\mu\text{l}$  samples were been injected by enrichment of the samples on a TrapCap C<sub>18</sub> column. Comparison of the peak heights demonstrates that the band width is only slightly affected by the increase in injection volume from 4 to 12  $\mu\text{l}$ , as relative peak heights of 0.90 and 1.02 was obtained for

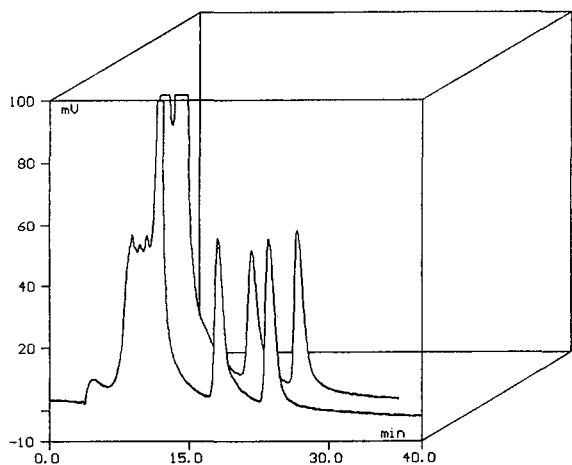


Fig. 6. Injection of large sample volumes using the trapping technique for (*E*)-10-hydroxynortriptyline. Column, Chiral-AGP capillary (150 × 0.180 mm I.D.); mobile phase, 25% 2-propanol in 10 mM phosphate buffer (pH 5.0); trapping column, TrapCap C<sub>18</sub> (45 × 0.25 mm I.D.); mobile phase, 10 mM sodium phosphate buffer (pH 7.0); sample concentration, 4- $\mu$ l injection (front chromatogram) of 2.5  $\mu$ g/ml, 12- $\mu$ l injection (back chromatogram) of 0.83  $\mu$ g/ml; detection, UV (225 nm).

the first- and last-eluted enantiomer, respectively, on injection of 12  $\mu$ l.

As has been reported above, large sample volumes can be injected by the trapping system with a slight decrease in detection sensitivity and in some instances also higher sensitivity could be obtained if the peaks are highly compressed by the micro gradient, generated by the trapping system. The possibility of injecting large sample volumes is demonstrated in Fig. 7, where a 20  $\mu$ l sample of proglumide was injected by the trapping system. This injection volume is about 330 times larger than normally used in direct injection, which means that low-concentration samples could easily be analysed by this technique.

#### Nature of the trapping column versus chromatographic properties

The influence of the nature of the trapping column was studied using 10-hydroxynortriptyline as a model compound. Three different columns were used, TrapCap C<sub>1</sub>, C<sub>4</sub> and AGP and the results were compared by direct injection of the same sample amount in 60 nl. Table III summarizes the rela-

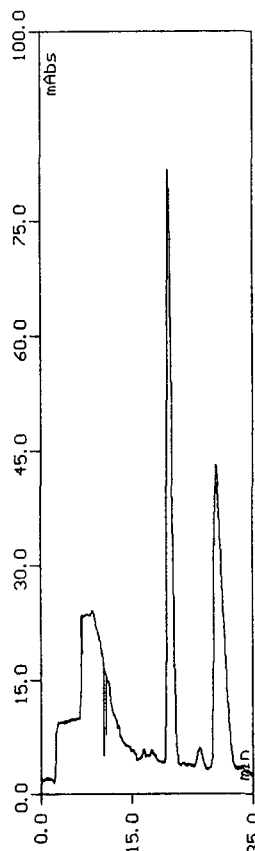


Fig. 7. Injection of large sample volumes using the trapping technique for proglumide. Column, Chiral-AGP capillary (150 × 0.180 mm I.D.); mobile phase, 8% acetonitrile in 3 mM ammonium acetate buffer (pH 6.0); trapping column, TrapCap AGP (45 × 0.25 mm I.D.); mobile phase, 3 mM ammonium acetate buffer (pH 4.5); injection volume, 20  $\mu$ l; detection, UV (225 nm).

tive peak heights, the retention times and the resolutions obtained in the different systems. The results clearly demonstrate that the nature of the trapping column influences the band broadening and the retention to a large extent. Using the most hydrophilic trapping column, TrapCap C<sub>1</sub>, gives the lowest band broadening and thereby the highest detection sensitivity for both enantiomers of 10-hydroxynortriptyline. About a 45% higher detection sensitivity, compared with direct injection, could be obtained for both enantiomers of this compound using the most hydrophilic trapping column. The corresponding value for the C<sub>4</sub> and AGP trapping columns is about 20%. A higher hydrophobicity of the

trapping column gives a higher adsorption capacity of the organic modifier, which means that a less steep gradient will be generated. Hence, using a more hydrophobic trapping column gives less compression and a broader sample band. The higher affinity of the solute to the more hydrophobic column also contributes to this effect.

#### Quantification using the trapping system

The possibility of using the trapping injection system for quantitative work was studied by injection of (*S*)-luciferin at concentrations between 29 and 463 ng/ml. The system described in Fig. 1 was used for this study. The peak area were plotted against the sample concentration and a straight line was obtained. The linear regression equation was.

$$y = 0.2741 + 0.1248x$$

The correlation coefficient,  $r$ , was 0.9999.

#### Electrospray MS detection

The introduction of soft ionization techniques was a very important breakthrough for the LC–MS technique and one of the most promising technique is ESI. This technique has revolutionized mass spectrometry with its ability to ionize high molecular mass compounds with high efficiency, giving femtomole detection limits. The ESI-MS system has been utilized in very few studies for the detection of low-molecular-mass compounds [15–18]. However, previous results and this study demonstrate that this technique can be used for such solutes.

The fact that low flow-rates (1–2  $\mu\text{l}/\text{min}$ ) are used on the Cap-AGP column makes it possible to combine it with the ESI-MS system to give very high detection selectivity and sensitivity. Combination of the novel trapping system with the Cap-AGP column and the ESI-MS system gives the potential to determine low concentrations of enantiomers present in complex matrixes.

Fig. 8 shows a chromatogram of the enantiomers of disopyramide resolved on a  $150 \times 0.18$  mm I.D. Cap-AGP column using ESI-MS detection. The 4- $\mu\text{l}$  sample was enriched on a TrapCap  $C_4$  column and the conditions were identical with those in Fig. 5. A comparison of the chromatograms obtained with UV detection at 225 nm and ESI-MS detection shows that disturbances of the baseline, caused by the disturbances of the equilibria on the Cap-AGP column by the micro gradient, are not observed using ESI-MS detection. Also, the first-eluted enantiomer is not compressed to the same extent as when using a UV detector. This is probably the result of band broadening due to extra-column effects obtained by transport of the sample from the column outlet to the interface. The sample is transported from the column into the ESI by a  $210 \text{ mm} \times 100 \mu\text{m}$  I.D. stainless-steel capillary. This capillary is inserted in another capillary, forming a sheath between the two, where the sheath liquid is pumped. The sheath liquid is an organic solvent such as methanol, 2-propanol or acetonitrile and is pumped into the interface in order to give a better spray and thereby better ionization. For the diso-

TABLE III

#### INFLUENCE OF THE NATURE OF THE TRAPPING COLUMN ON THE CHROMATOGRAPHIC PROPERTIES

Column: Capillary Chiral-AGP ( $150 \times 0.180$  mm I.D.); mobile phase: 16% 2-propanol in 3 mM ammonium acetate buffer pH 6.0. Trapping columns: TrapCap  $C_1$ ,  $C_4$  and -AGP ( $45 \times 0.25$  mm I.D.); mobile phase: distilled water. Sample: *E*-10-hydroxynortriptyline 28  $\mu\text{g}/\text{ml}$  (direct injection 60 nl) and 420 ng/ml (trapping injection 4  $\mu\text{l}$ ).

	Direct injection (60 nl)	Trapping $C_1$ (4 $\mu\text{l}$ )	Trapping $C_4$ (4 $\mu\text{l}$ )	Trapping AGP (4 $\mu\text{l}$ )
Rel. peak height <sub>1</sub>	1	1.44	1.22	1.17
Rel. peak height <sub>2</sub>	1	1.48	1.21	1.19
$t_{R1}$ (min)	12.2	16.9	17.2	19.6
$t_{R2}$ (min)	15.3	20.1	20.7	23.5
$R_s$	1.69	2.43	2.27	2.51

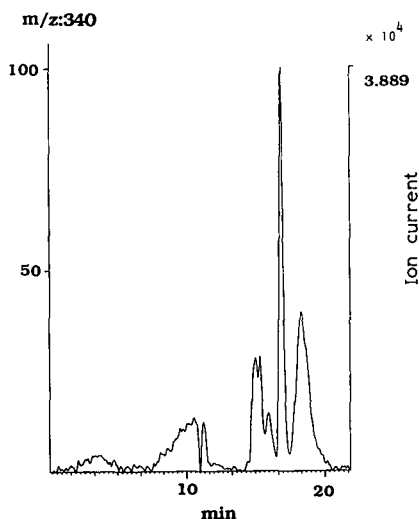


Fig. 8. Separation of disopyramide enantiomers by sample enrichment with ESI-ES detection. Column, Chiral-AGP capillary ( $150 \times 0.180$  mm I.D.); mobile phase, 1.2% 2-propanol in 3 mM acetic acid (pH 3.6); trapping column, TrapCap C<sub>4</sub> ( $45 \times 0.25$  mm I.D.); mobile phase, distilled water; sheath liquid, methanol containing 20% of the above capillary mobile phase; sheath liquid flow-rate, 1.5  $\mu$ l/min; injection volume, 4  $\mu$ l; sample concentration, 182 ng/ml.

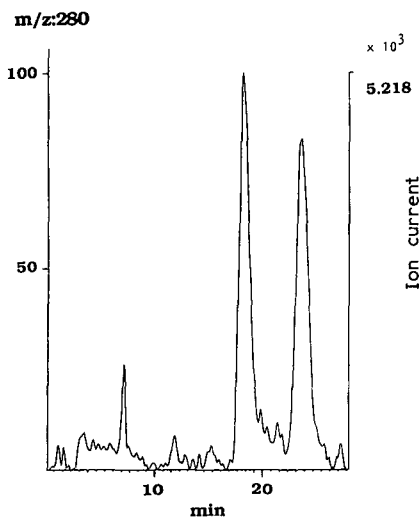


Fig. 9. Separation of (*E*)10-hydroxynortriptyline by sample enrichment with ESI-MS detection. Column, Chiral-AGP capillary ( $150 \times 0.180$  mm I.D.); mobile phase, 16% 2-propanol in 3 mM ammonium acetate buffer (pH 6.0); trapping column, TrapCap C<sub>4</sub> ( $45 \times 0.25$  mm I.D.); mobile phase, distilled water; injection volume, 4  $\mu$ l; sample concentration, 200 ng/ml.

pyramide separation, methanol containing 20% of mobile phase was used as the sheath liquid, and it was pumped at a flow-rate of 1.5  $\mu$ l/min.

Fig. 9 demonstrates the resolution of the enantiomers of 10-hydroxy nortriptyline using the trapping technique and ESI-MS detection. A 4- $\mu$ l sample was injected and trapped on a TrapCap C<sub>4</sub> column. The mobile phase used for this separation contains a relatively high concentration of 2-propanol so it was not necessary to pump a sheath liquid in order to obtain ionization. However, the sensitivity could in many instances be optimized by changing the sheath liquid flow and the nature of the sheath liquid. The sheath liquid can also affect the baseline noise. By using ESI-MS detection low buffer concentrations were used to obtain ionization of the sample. The very low buffer concentration decreases the separation efficiency of the Cap-AGP column for both basic and acidic compounds. Despite this, a high detection sensitivity can be obtained.

## CONCLUSIONS

A capillary sample-enrichment system was developed together with a Chiral-AGP capillary column, permitting the injection and enrichment of the sample from large injection volumes. A pH and solvent micro gradient is generated by the trapping column. The micro gradient can be used to compress the migrating bands on the Cap-AGP column, which means that high sample volumes could be injected and a higher detection sensitivity was obtained for many compounds, compared with direct injection, by injection of large volumes by the trapping system. The low flow-rates (1–2  $\mu$ l/min) used on the Cap-AGP column make it possible to utilize ESI-MS for detection. A combination of the Cap-AGP column, the trapping system and the ESI-MS detector gives the possibility of analysing low-concentration samples with very high detection selectivity.

## REFERENCES

- 1 J. Hermansson and C. von Bahr, *J. Chromatogr.*, 221 (1980) 109.
- 2 C. von Bahr, J. Hermansson and M. Lind, *J. Pharmacol. Exp. Ther.*, 222 (1982) 458.
- 3 J. Hasselström, M. Enquist, J. Hermansson and R. Dahlqvist, *Eur. J. Clin. Pharmacol.* 41 (1991) 481.



- 4 A. K pfer, R. Parwarden, S. Ward, S. Schenker, R. Preisig and R. A. Branch, *J. Pharmacol. Exp. Ther.*, 230 (1984) 28.
- 5 M. Simonyi, *Med. Res. Rev.*, 4 (1984) 359.
- 6 S. Mayson, *New Sci.*, 1393 (1984) 359.
- 7 P. N. Platil, J. B. LaPidus and A. Tye, *J. Pharm. Sci.*, 59 (1970) 1205.
- 8 K. Williams and E. Lee, *Drugs*, 30 (1985) 333.
- 9 J. Hermansson and M. Eriksson, *J. Chromatogr.*, 336 (1984) 321.
- 10 M. Enquist and J. Hermansson, *J. Chromatogr.*, 494 (1989) 191.
- 11 Y. Chu and I. Wainer, *J. Chromatogr.*, 497 (1989) 191.
- 12 M. Enquist and J. Hermansson, *Chirality*, 1 (1989) 209.
- 13 M. Yamashita and J. B. Fenn, *J. Chem. Phys.*, 88 (1984) 4451.
- 14 C. M. Whitehouse, R. N. Dreyer, M. Yamashita and J. B. Fenn, *Anal. Chem.*, 57 (1985) 675.
- 15 K. L. Duffin, R. Wachs and J. D. Henion, *Anal. Chem.*, 64 (1992) 61.
- 16 M. A. Quilliam, B. A. Thompson, G. J. Scott and K. W. Sui, *Rapid Commun. Mass Spectrom.*, 3 (1989) 145.
- 17 T. R. Covey, A. P. Bruins and J. D. Henion, *Org. Mass Spectrom.*, 23 (1988) 178.
- 18 K. L. Duffin, J. D. Henion and J. J. Shieh, *Anal. Chem.*, 63 (1991) 1781.
- 19 J. Hermansson, *J. Chromatogr.*, 269 (1983) 71.
- 20 J. Hermansson and G. Schill, in P. A. Brown and R. A. Hartwick (Editors), *High Performance Liquid Chromatography (Monographs on Analytical Chemistry Series)*, Wiley-Interscience, New York, 1988, pp. 337–374.
- 21 J. Hermansson, *Trends Anal. Chem.*, 8 (1989) 251.
- 22 M. Enquist and J. Hermansson, *J. Chromatogr.*, 519 (1990) 285.
- 23 U. Norinder and J. Hermansson, *Chirality*, 3 (1991) 422.
- 24 J. Hermansson and M. Eriksson, *J. Liq. Chromatogr.*, 9 (1986) 621.

# Reversed-phase liquid chromatography with microspherical octadecyl-zirconia bonded stationary phases

Jim Yu and Ziad El Rassi

*Department of Chemistry, Oklahoma State University, Stillwater, OK 74078-0447 (USA)*

---

## ABSTRACT

Microspherical zirconia particles were synthesized and surface modified with octadecylsilane compounds for reversed-phase high-performance liquid chromatography. Monomeric and "polymeric" octadecyl-zirconia bonded stationary phases were obtained by reacting the support with octadecyldimethylchlorosilane or octadecyltrichlorosilane, respectively. The surface coverage of the zirconia-based stationary phases with octadecyl functions was approximately the same as that of octadecyl-silica sorbents. These phases were evaluated in terms of reversed-phase chromatographic properties with non-polar, slightly polar and ionic species over a wide range of mobile phase composition and pH. Monomeric octadecyl-zirconia with end-capping exhibited some metallic interactions with both basic and acidic solutes, but these interactions were greatly reduced in the presence of competing agents (*e.g.*, tartrate ions) in the mobile phase. The "polymeric" octadecyl-zirconia sorbents exhibited higher retention than the monomeric ones with the various solutes investigated, and their residual adsorptivities toward acidic solutes were much lower. The retention of non-polar and slightly polar aromatic compounds was quasi-homoenergetic on both types of octadecyl-zirconia stationary phases. Stability studies conducted at extreme pH conditions (pH 2.0 and pH 12.0), have shown that "polymeric" octadecyl-zirconia sorbents are more stable than their monomeric counterparts. These stationary phases were quite useful in the separation of polycyclic aromatic hydrocarbons, alkylbenzene and phenyl alkylalcohol homologous series, oligosaccharides, dansyl-amino acids, peptides and proteins.

---

## INTRODUCTION

The enormous expansion of high-performance liquid chromatography (HPLC) has been largely the result of the development of rigid microparticulate stationary phases. Very recently, the various aspects of support materials and their bonded stationary phases have been reviewed in a special issue of *Journal of Chromatography* [1].

Silica-based stationary phases are still the most widely used sorbents in all modalities of HPLC owing to their excellent mechanical strength and availability in a wide range of pore size and particle diameter. These attractive features of silica-based sorbents have apparently overshadowed their limited

chemical stability at extreme pH and undesirable adsorptive properties toward basic species.

The search for rigid microparticulate stationary phases having the mechanical strength of silica gels and yet affording a wider pH range stability for use in HPLC has been a continuing theme of research since the introduction of the technique. Rigid polymer-based stationary phases, *e.g.*, polystyrene-divinylbenzene and other resins based on polyacrylate, hydroxylated polyether copolymers or polyvinyl alcohol, are now available as column packing in various modes of HPLC; for recent review on polymeric packings see ref. 2. Although, polymeric supports afforded the preparation of chemically stable stationary phases over a wide range of pH, they have been less mechanically stable than silica.

Recently, there has been an increasing interest in inorganic sorbents that combine the mechanical

---

*Correspondence to:* Dr. Z. El Rassi, Department of Chemistry, Oklahoma State University, Stillwater, OK 74078-0447, USA.

strength of silica with the chemical stability of polymeric-based stationary phases. In fact, stationary phases based on alumina [3–7], zirconia [8–12] and to a lesser extent titania [4,10] have been evaluated in HPLC. However, an ideal column matrix that is free of all undesirable properties seems to be unrealistic. Thus, it can be anticipated that both organic and inorganic-based sorbents will continue to coexist and complement each other. This would allow the separation of a wide range of species and satisfy the need of many users.

Although alumina-based stationary phases with reversed-phase chromatographic properties such as polymer encapsulated- [5], octadecyl- [7] and polybutadiene alumina [3,6] have showed an excellent chemical stability at high pH, the heterogeneous structure of their pores has limited their applications. Standard alumina has bimodal pore size distribution with most of the surface hidden in small pores [13]. This property has yielded columns with much lower efficiencies than silica columns. In addition, alumina-based stationary phases show residual adsorptivities toward species with phosphate and carboxylate functional groups even if the stationary phase consisted of thick polymer coatings [9].

Octadecyl-titania stationary phases have been very briefly explored [10], and detailed investigations of their chromatographic properties with various types of analytes are lacking. On the other hand, a few reports have recently appeared on hydrocarbonaceous zirconia stationary phases for reversed-phase HPLC. Gahemi and Wall [8] were the first to introduce dynamically modified zirconia with hydrophobic quaternary amine to HPLC. Very recently, Carr and co-workers [9,11,12] and Trüdinger *et al.* [10] introduced and evaluated microparticulate zirconia reversed-phase chromatographic sorbents. These studies have shown the excellent mechanical strength and chemical stability of zirconia based stationary phases. However, polyoxy anions still exhibited strong interactions with the zirconia matrix even when the support was coated with a thick layer of cross-linked polybutadiene [9], and these interactions could be minimized in the presence of phosphate ions in the eluent. The residual adsorptive properties could be further inhibited by coating the zirconia with carbon-clad, and the resulting sorbent did not exhibit peak tailing for

amines or metallic interactions with phosphates and carboxylates [11,12].

Thus far, only porous zirconia packing materials have been evaluated in HPLC. Over the last few years, non-porous silica [15,16] and resin-based [17,18] stationary phases have been developed for the rapid and high-resolution HPLC of large biomolecules. Due to the absence of intraparticle mass transfer resistances, these non-porous sorbents permitted rapid separations of biomacromolecules at relatively high flow-rates without sacrificing column efficiency. This report is concerned with the introduction of “non-porous”, microspherical zirconia particles having a mean particle diameter in the range 1.5–2.8  $\mu\text{m}$  and the evaluation of their bonded octadecyl derivatives in reversed-phase chromatography of small and large molecules. The surface modification of these zirconia microparticles with octadecyl silane reagents yielded sorbents having surface coverage in octadecyl functions similar to that obtained on non-porous silica supports. In addition, the octadecyl-zirconia stationary phases were stable at acidic and alkaline pH for a long period of use, and allowed the rapid separation of proteins, peptides, dansyl-amino acids, oligosaccharides, polycyclic aromatic hydrocarbons and other polar and non-polar aromatic compounds.

## EXPERIMENTAL

### *Instrumentation*

The liquid chromatograph was assembled from an LDC Analytical (Riviera Beach, FL, USA) ConstaMetric 3500 solvent delivery system with a gradient programmer, which was used to control a ConstaMetric Model III solvent delivery pump, a UV interference filter photometric detector Model UV-106 from Linear Instruments (Reno, NV, USA), and a sample injector Model 7125 from Rheodyne (Cotati, CA, USA). Chromatograms were recorded with a computing integrator Model C-R6A from Shimadzu (Columbia, MD, USA).

### *Chemicals*

HPLC-grade acetonitrile, reagent-grade as well as technical-grade isopropanol and methanol, reagent-grade isoamylacetate, benzene, carbon tetrachloride, sodium phosphate monobasic, dibasic and tribasic were from Fisher (Fair Lawn, NJ, USA).

Ethylbenzene, propylbenzene, butylbenzene, benzylamine, hexamethylenetetramine, zirconyl chloride octahydrate and trimethylchlorosilane were purchased from Aldrich (Milwaukee, NJ, USA). Toluene, anhydrous denatured ethanol, butanol, *n*-heptane, light petroleum (b.p. 35–60°C), sodium chloride, and sodium hydroxide were from EM Science (Gibbstown, NJ, USA). *p*-Xylene was from Eastman Kodak (Rochester, NJ, USA). Octadecyldimethylchlorosilane and octadecyltrichlorosilane were obtained from Hüls America (Bristol, PA, USA). Polyoxyethylene 23-lauryl ether (Brij 35), polyoxyethylenesorbitan trioleate (Tween 85), sorbitan monooleate (Span 80), dansyl-L-amino acids, peptides, cytochrome *c*, lactoferrin, lysozyme, ribonuclease A and *p*-nitrophenyl maltooligosaccharides were from Sigma (St. Louis, MO, USA). Polyaromatic hydrocarbons were gifted by Dr. Eisenbraun from our Department.

#### Synthesis of zirconia microparticles and zirconia bonded phases

Microspherical zirconia beads were synthesized according to the procedure of Trüdinger *et al.* [10]. Typically, 160 g of zirconyl chloride were dissolved in 120 ml of water. The zirconium hydroxide sol thus formed was emulsified in 1400 ml of *n*-heptane, which was stabilized by the use of the following emulsifiers: 22.0 g Span 80, 6.70 g Tween 85 and 5.00 g Brij 35. The emulsion was homogenized using a Brinkmann dispersion unit (Westbury, NY, USA) at 8000 rpm for 2 min. Thereafter, 140 g hexamethylenetetramine and 140 g urea were added to the emulsion to initiate the gelation reaction. The reaction mixture was stirred in a 2.0-l round-bottom flask at room temperature for at least 48 h.

After the reaction, the unreacted chemicals and organic solvents were removed in a multi-solvent cleaning process [10], using butanol–light petroleum (1:1), methanol and water. Zirconia microspheres were calcinated at 400°C to clean the organic residues adsorbed or deposited on the surface of the support [10].

To produce “non-porous” zirconia materials, the organic free zirconia microparticles were further calcinated at 800°C for 6 h, a process during which the pore volume has been shown to approach zero [10]. The calcinated materials were then rehydroxylated using an established procedure [19]. The spe-

cific surface area,  $S_{\text{BET}}$ , of the support thus obtained was determined by nitrogen adsorption at Leeds & Northrup (Petersburg, FL, USA) and was found to be 7.3 m<sup>2</sup>/g. Scanning electron micrography (SEM) of the same support taken at the electron microscope facilities of our University revealed that the starting product is polydisperse containing a sizable amount of 0.5–0.8 μm particles, which can explain the relatively moderate specific surface area obtained by nitrogen adsorption. These fine particles did not settle when the starting materials were suspended in isopropanol, and they were washed out by discarding the tops of repetitive suspensions. The classified particles thus obtained were in the size range 1.5–2.8 μm as can be seen in the SEM shown in Fig. 1. It has been shown that non-porous supports in this particle size range would have, on the average, a specific surface area of *ca.* 1.4 m<sup>2</sup>/g [20].

The above zirconia microspheres of narrower

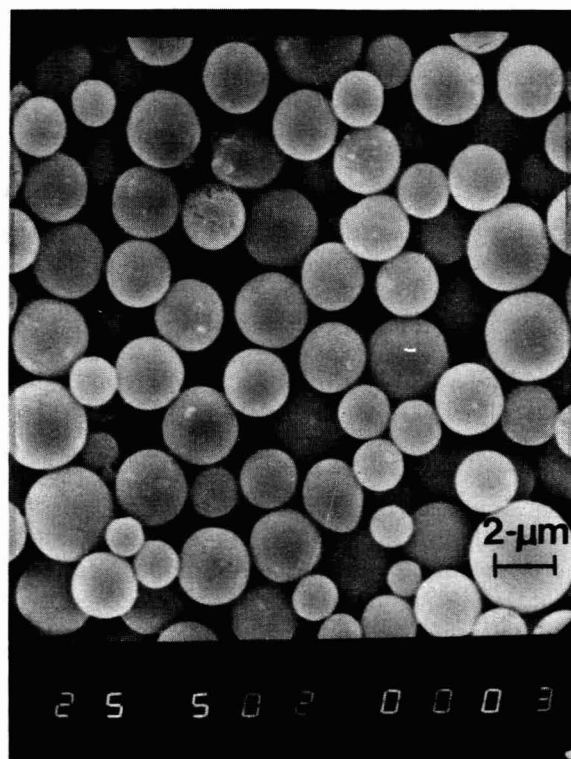


Fig. 1. Scanning electron micrograph of the zirconia microspheres.

particle size range were modified with either monomeric or "polymeric" octadecyl functions according to the following procedures. The monomeric octadecyl-zirconia stationary phase was prepared by first heating a round-bottom flask containing a suspension of 3 g of zirconia microspheres in toluene at 115°C while stirring for at least 30 min. This step was to evaporate the water molecules that might have been adsorbed on the support surface from atmospheric moisture since toluene and water form a positive heteroazeotrope with a b.p. 84.1°C [14]. Thereafter, 1 g of octadecyldimethylchlorosilane was added to the zirconia suspension. The reaction solution was stirred for 12 h at 115°C. After the reaction, the octadecyl-zirconia sorbent was separated from the solution by centrifugation. Technical-grade methanol was used to wash the support thoroughly from unreacted silane and hydrogen chloride formed during the reaction. When the zirconia microsphere suspension was brought to neutral, the support was washed several times with toluene to completely remove methanol solvent. Then the octadecyl-zirconia thus obtained was suspended in toluene and heated to 80°C for at least 30 min to evaporate the residual methanol. Following, the temperature was lowered to 50°C, and 3 ml of trimethylchlorosilane were added to the suspension of modified zirconia in toluene. The reaction was stirred at 50°C for 12 h. The modified zirconia particles were first washed from the unreacted silane compound and hydrogen chloride with methanol, and then dried in the air.

The "polymeric" octadecyl-zirconia stationary phase was prepared by following the same steps as in the above procedure using octadecyltrichlorosilane with the exception that the final product was not end-capped.

#### Column packing

All columns used in this study were precision-bore 316 stainless-steel tubing from Alltech (Deerfield, IL, USA), and having  $3.0 \times 0.46$  cm I.D. as the dimensions. Column end fittings were also 316 stainless steel fitted with 0.5- $\mu$ m stainless-steel frits and distributor disks from Alltech Associated.

The modified zirconia microspheres were then packed from a carbon tetrachloride slurry at 8000 p.s.i. with isopropanol using a Shandon column packer instrument (Keystone Scientific, Bellefonte,

PA, USA). Typically 1.5 g of surface modified zirconia microspheres were needed since zirconia is a relatively dense material (5.8 g/cm<sup>3</sup>) [21]. Carbon tetrachloride, which is characterized by its high density, gave satisfactory results when a relatively high-viscosity solvent such as isopropanol was used as the packing solvent.

## RESULTS AND DISCUSSION

### Surface modification of zirconia

Infrared spectroscopic studies [22,23] have shown that there are at least two types of hydroxyl functional groups at the zirconia surface. The free hydroxyl groups bound to single cations, Zr–OH, similar to those encountered on the silica surface, and bridging hydroxyl groups coordinated to more than a single cation, Zr–(OH)–Zr. The surface concentration of zirconia in hydroxyl groups has been found to be *ca.* 9.8  $\mu$ mol/m<sup>2</sup> [24]. Although the relative chemical reactivity of both types of surface hydroxyl groups has not been yet established, these groups can be used for the covalent attachment of ligands. In addition, zirconia surface contains coordinatively unsaturated zirconium(IV) ions, *i.e.*, hard Lewis acid sites [25]. The Lewis acid sites have been shown to undergo strong interactions with oxyanions such as phosphate containing compounds [24] and their presence can lead to undesirable chromatographic behavior such as peak tailing and irreversible binding of Lewis base solutes. Thus, the major concern in the preparation of zirconia bonded stationary phases is to shield the zirconium sites, and consequently minimize the solute-metal interactions.

Silane derivatives having one or more reactive functional groups can react with surface hydroxyl groups of zirconia to form monomeric or polymeric bonded phases, respectively.

When octadecyldimethylchlorosilane is used a monomeric layer of octadecyl functions covalently bonded to the zirconia surface would result. Because of the steric hindrance caused by the large size of the octadecyl hydrocarbon chains, there still would be some hydroxyl groups on the zirconia surface that remains unreacted. Smaller silane compounds such as trimethylchlorosilane was used as end-capping agent to scavenge the unreacted hydroxyl groups and to minimize their contribution to

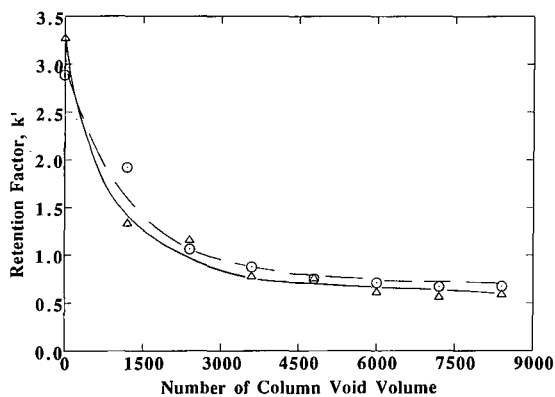


Fig. 2. Plots of retention factor of *p*-xylene versus the number of column void volume of solutions perfused through the column. Solutions used in the stability test, 10 mM  $\text{NaH}_2\text{PO}_4$ , pH 2.0 ( $\circ$ ) and 10 mM  $\text{Na}_3\text{PO}_4$ , pH 12.0 ( $\triangle$ ); flow-rate, 1.0 ml/min. Column, monomeric octadecyl-zirconia with end-capping,  $3.0 \times 0.46$  cm I.D.; mobile phase used in the measurement of solute retention, water at 5% (v/v) acetonitrile; flow-rate, 1.0 ml/min.

solute retention in the ensuing chromatographic separation. This approach is widely practiced with silica bonded stationary phases to minimize silanophilic interactions [26].

The use of octadecyltrichlorosilane would result in a "polymeric" octadecyl stationary phase bonded on the zirconia surface. Besides reacting with the hydroxyl groups of the zirconia surface, multi-func-

tional silane reagents can react with each other to form a cross-linked octadecyl polysiloxane layer. In this process, the zirconia support would have a higher surface coverage with octadecyl functions, which would provide a better sealing of the surface hydroxyl groups and zirconium sites.

#### Stability studies

The chemical stability of the bonded octadecyl functions of the zirconia-based sorbents as well as the support itself was investigated under extreme pH conditions, *i.e.* pH 2.0 and pH 12.0. Monomeric and "polymeric" octadecyl-zirconia columns were perfused with 10 mM phosphate buffer solutions at a flow-rate of 1.0 ml/min. At 5-h intervals, the column was first washed with water, and then equilibrated with the mobile phase. The retention of toluene, *p*-xylene, benzylamine and *trans*-cinnamic acid test solutes was evaluated as a function of the number of column void volume of buffer solutions perfused through the column, and the results are shown in Figs. 2 and 3.

It is interesting to note that throughout the entire stability studies at low and high pH on both monomeric and "polymeric" bonded stationary phases, the column void volume remained unchanged, and no bed compaction was observed. This corroborate earlier findings in that zirconium oxide was very stable in 0.1 M hydrochloric acid, *i.e.*, pH 1.0, and 1.0 M sodium hydroxide, *i.e.*, pH 14.0 [24].

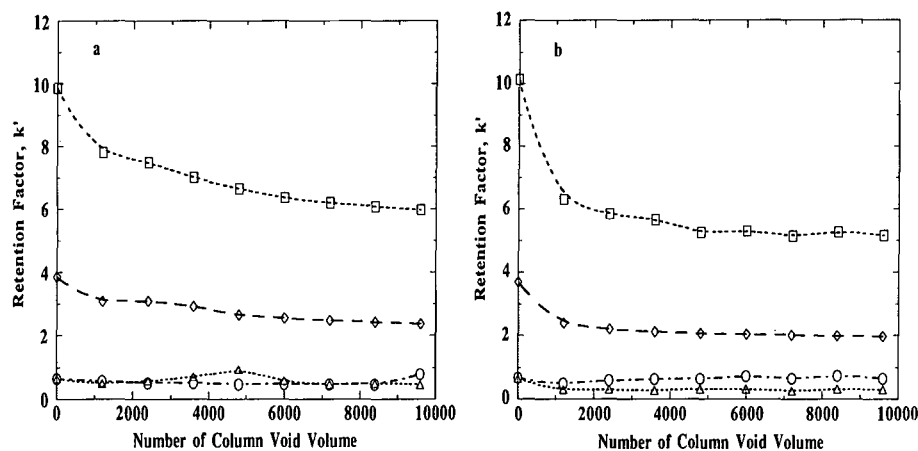


Fig. 3. Plots of retention factor of the test solutes versus the number of column void volume of solutions perfused through the column. Solutions used in the stability test, 10 mM  $\text{NaH}_2\text{PO}_4$ , pH 2.0 in (a) and 10 mM  $\text{Na}_3\text{PO}_4$ , pH 12.0 in (b); flow-rate, 1.0 ml/min. Column, "polymeric" octadecyl-zirconia,  $3.0 \times 0.46$  cm I.D.; mobile phase used in the measurement of solute retention, water at 20% (v/v) acetonitrile; flow-rate, 1.0 ml/min.  $\diamond$  = Toluene;  $\square$  = *p*-xylene;  $\circ$  = benzylamine;  $\triangle$  = *trans*-cinnamic acid.

As shown in Figs. 2 and 3, on both monomeric and polymeric octadecyl-zirconia stationary phases the retention of the test solutes reached a constant value after a certain number of column void volume. On the monomeric octadecyl column, the retention stabilized after 4000 column void volume, whereas on the polymeric column the constancy in retention was attained after 1000–2000 column void volume.

It has to be noted that a preconditioned polymeric octadecyl-zirconia column (*i.e.* after perfusion with acidic or basic solutions) kept his performance in terms of retention and separation efficiencies for a longer period of use than a monomeric octadecyl-zirconia column. The greater stability of “polymeric” octadecyl-zirconia stationary phases may be attributed to the presence of a cross linked alkylpolysiloxane layer, *i.e.*, silicon rubber, that established a greasy layer or strong hydrophobic shield and protects the Zr–O–Si as well as the Si–O–Si bonds from hydrolysis. In fact, the preconditioned polymeric octadecyl-zirconia column yielded the same retention for toluene and *p*-xylene after an additional 12 000 column void volumes with a variety of mobile phases ranging from pH 2.0 to pH 12.0, and the column is still in use. These results are in agreement with those reported by

Trüdinger *et al.* [10] on the stability of octadecyl-zirconia stationary phases. Their results have shown that polymeric octadecyl-zirconia sorbents are stable up to pH 12.0 even after a period of 500 h of use.

#### Chromatography of non-polar and slightly polar solutes

The reversed-phase chromatographic properties of the octadecyl-zirconia stationary phases were evaluated with non-polar and slightly polar aromatic compounds. First, monomeric octadecyl-zirconia microspheres without end-capping packed into a 3.0 × 0.46 cm I.D. column were evaluated with benzene, toluene, *p*-xylene and naphthalene at various acetonitrile concentrations in the mobile phase. Under these circumstances, plots of the logarithmic retention factors of the aromatic solutes *versus* the percent acetonitrile in the mobile phase were not linear. This behavior may indicate the presence of interactions between the  $\pi$ -electrons on the aromatic rings and the exposed zirconium sites on the surface of the support.

Based on the above findings, the monomeric octadecyl-zirconia stationary phases were then reacted with trimethylchlorosilane, *i.e.*, end-capping, to minimize solute–zirconia associations. Fig. 4a and

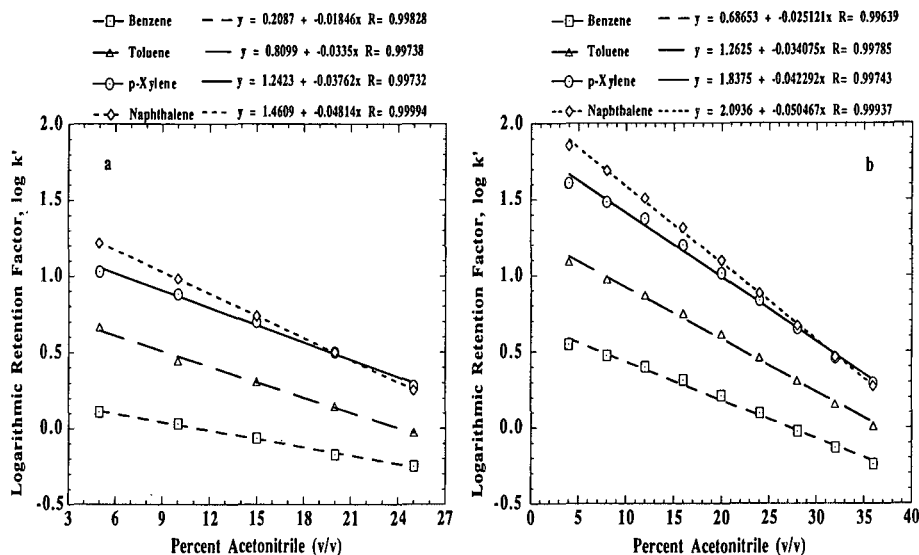


Fig. 4. Plots of logarithmic retention factor *versus* the volume percent acetonitrile in mobile phase for both monomeric (a) and “polymeric” (b) octadecyl-zirconia stationary phase. Columns, 3.0 × 0.46 cm I.D.; mobile phases, water at various volume percent acetonitrile; flow-rate, 2.0 ml/min.

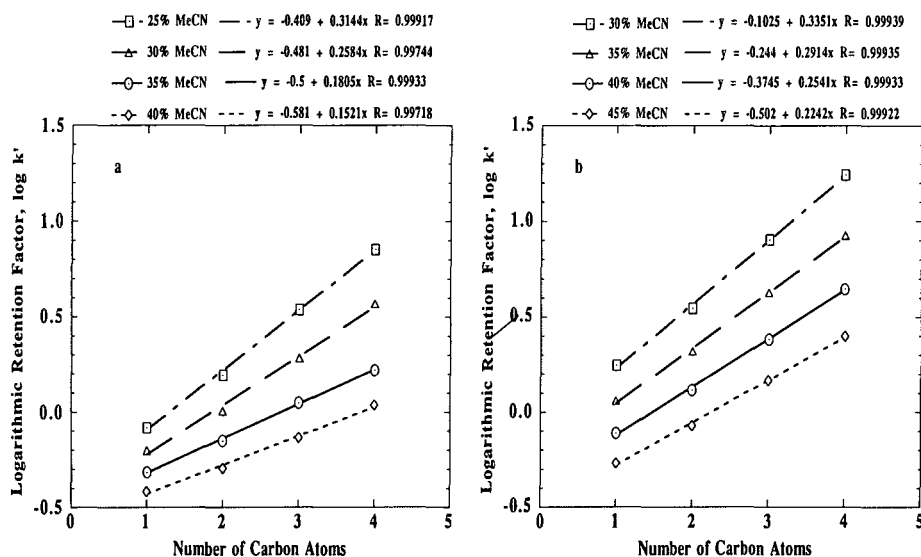


Fig. 5. Plots of logarithmic retention factor *versus* the number of carbon atoms in the alkyl chain of alkylbenzene homologous series for both monomeric (a) and "polymeric" (b) octadecyl-zirconia stationary phases. Columns, 3.0 × 0.46 cm I.D.; mobile phases, water at various volume percent acetonitrile (MeCN); flow-rate 2.0 ml/min. Solutes: toluene, ethylbenzene, propylbenzene and butylbenzene.

b illustrates plots of logarithmic retention factor *versus* the volume percent of acetonitrile in the mobile phase for benzene, toluene, *p*-xylene and naphthalene obtained on monomeric (with end-capping) and "polymeric" octadecyl-zirconia, respectively. These plots are linear with a correlation coefficient varying between 0.996 and 1.000 over a wide range of acetonitrile concentration in the mobile phase. As can be seen in Fig. 4a and b, solute that has larger hydrophobic surface area showed greater response in terms of retention to changes in the organic content of the mobile phase. That is the slope of the line increased in the order of benzene < toluene < *p*-xylene < naphthalene. As expected, the "polymeric" stationary phase having higher surface coverage, *i.e.*, higher phase ratio, exhibited higher retention toward non-polar species.

On both types of bonded stationary phases a switch in the elution order between *p*-xylene and naphthalene was observed, see Fig. 4a and b. This change in the elution order occurred at lower acetonitrile concentration on the monomeric stationary phase.

To further characterize these phases, alkylbenzene homologous series were chromatographed under reversed-phase conditions. The results are

shown in Fig. 5a and b in terms of logarithmic retention factor of the solutes *versus* the number of carbon atoms in their alkyl chains. In all cases,  $\log k'$  increased linearly with increasing number of methylene groups in the homologous series, which confirmed the reversed-phase chromatographic property of the octadecyl-zirconia bonded stationary phases. The slope of the lines, which is the methylene group retention increment, showed that the hydrocarbonaceous phases had higher selectivity toward the homologous series when organic-lean eluents were used, a behavior typical of reversed-phase chromatography.

The selectivity of monomeric and "polymeric" bonded stationary phases toward alkylbenzene homologous series was compared using the methylene group retention increment. The acetonitrile concentration in the mobile phase was adjusted for both types of stationary phases so that the retention of toluene (the smallest solute in the homologous series) on both monomeric and "polymeric" stationary phases would be nearly the same; compare curves obtained at 25% and 40% (v/v) acetonitrile in Fig. 5a and b, respectively. The slope of these two lines shows clearly that both monomeric and "polymeric" stationary phases yield nearly the same se-



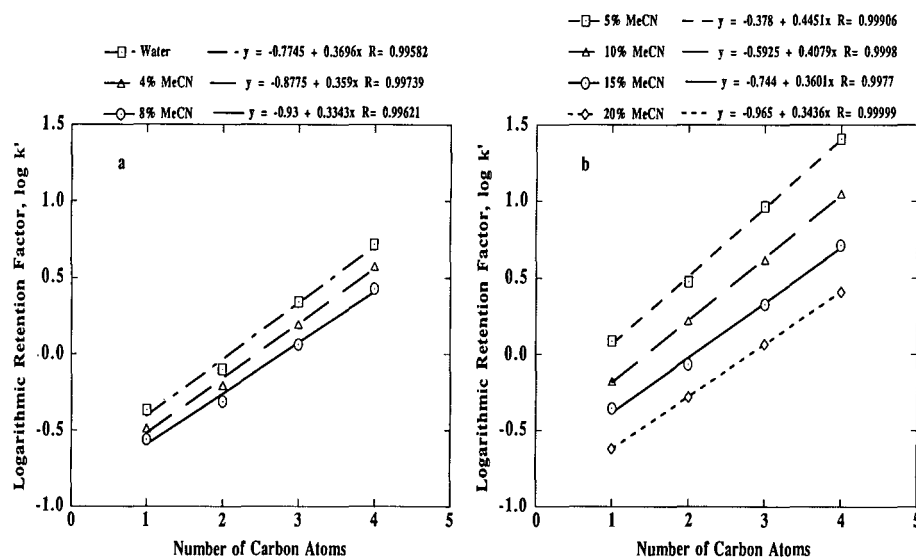


Fig. 6. Plots of logarithmic retention factor *versus* the number of carbon atoms in the alkyl chains of phenylalkylalcohol homologous series for both monomeric (a) and “polymeric” (b) octadecyl-zirconia stationary phases. Columns,  $3.0 \times 0.46$  cm I.D.; mobile phase, water at various volume percent acetonitrile (MeCN); flow-rate, 1.0 ml/min (a) and 2.0 ml/min (b). Solutes: benzyl alcohol, phenethyl alcohol, 3-phenyl-1-propanol and 4-phenyl-1-butanol.

lectivity toward alkylbenzene homologous series, with the difference that it would take lower organic concentration in the mobile phase to bring about the elution and separation of the homologous series with the monomeric bonded phase.

Phenylalkylalcohols homologous series were used to study the retention behavior of slightly polar solutes on the octadecyl-zirconia bonded stationary phases. The results are shown in Fig. 6a and b in terms of logarithmic retention factor *versus* the number of carbon atoms in the homologous series. Straight lines were obtained in pure water as well as in the presence of acetonitrile in the mobile phase. Again, octadecyl-zirconia based stationary phases exhibited reversed-phase properties toward phenylalkylalcohols. As reflected by the slope of the lines, the methylene group retention increments for the phenylalkylalcohols homologous series decreased with increasing acetonitrile concentration in the eluent on both monomeric and “polymeric” bonded octadecyl-zirconia stationary phases.

It has been shown [27,28] that plots of  $\log k'$  obtained on one stationary phase *versus* those obtained on another with the same mobile phase can be utilized to compare the energetic of solute reten-

tion on different columns. If the Gibbs free energies for a given solute are identical in both columns, *i.e.*,

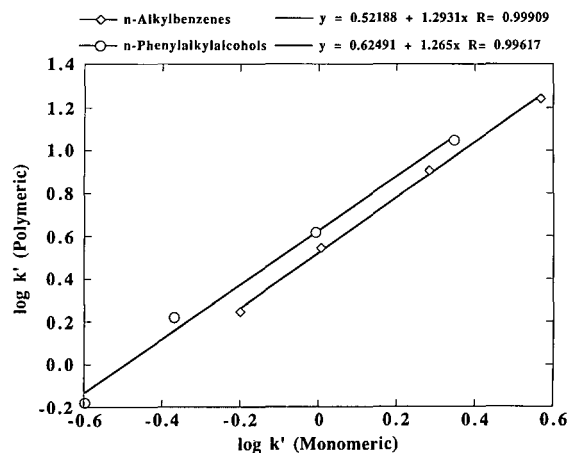


Fig. 7. Plots of logarithmic retention factor of phenylalkylalcohol and alkylbenzene homologous series on the “polymeric” phase *versus* that on the monomeric phase. Columns,  $3.0 \times 0.46$  cm I.D.; mobile phase, water at 30% acetonitrile (v/v) for alkylbenzenes and 10% acetonitrile (v/v) for phenylalkylalcohols; flow-rate 2.0 ml/min. Alkylbenzenes: toluene, ethylbenzene, propylbenzene and butylbenzene; phenylalkylalcohols: benzyl alcohol, phenethyl alcohol, 3-phenyl-1-propanol and 4-phenyl-1-butanol.

the retention is homoenergetic, then plots of  $\log k' - \log k'$  obtained on the two stationary phases yield straight line with unit slope and the intercept is the logarithmic quotient of two columns phase ratios [26]. If the corresponding Gibbs free energies in the two chromatographic systems are not identical but proportional to each other, linear plots are still obtained with a slope different from unity and such retention behavior is termed homoenergetic [27].

The  $\log k' - \log k'$  plot illustrated in Fig. 7 was graphed from retention data obtained with alkylbenzene homologous series on the monomeric and "polymeric" bonded stationary phases. As can be seen in Fig. 7, the  $\log k' - \log k'$  plot is linear with a slope slightly larger than unity indicating that the retention of alkylbenzenes is quasi-homoenergetic on both types of columns, *i.e.*, the retention mechanism is based essentially on hydrophobic interaction between the solute and the hydrocarbonaceous chains of the stationary phase. The antilog of the intercept of the line, which is the quotient of the two columns phase ratios,  $\phi_{\text{poly}}/\phi_{\text{mono}}$ , was equal to 3.33 indicating that the polymeric octadecyl-zirconia column has a phase ratio ( $\phi_{\text{poly}}$ ) of *ca.* 3 times higher than the monomeric one ( $\phi_{\text{mono}}$ ).

Both types of octadecyl-zirconia bonded stationary phases showed quasi-homoenergetic retention with the slightly polar phenylalkylalcohols, as illustrated by Fig. 7. In fact, the slope of  $\log k' - \log k'$  plot is *ca.* 1.27. The quotient of phase ratios  $\phi_{\text{poly}}/\phi_{\text{mono}}$ , defined as the phase ratio of a column relative to that of the reference column, was evaluated as the antilog of the intercept of the  $\log k' - \log k'$  plot and its value was *ca.* 4.22. Based on these results and those obtained with alkylbenzene homologous series the phase ratio of polymeric octadecyl-zirconia is higher than that of monomeric by a factor of *ca.* 3.0–4.0. The retention of these slightly polar species on both monomeric and "polymeric" bonded stationary phases was primarily through hydrophobic interaction between the solutes and the bonded stationary phases.

Furthermore, the retention of non-polar alkylbenzenes was much higher than that of the slightly polar phenylalkylalcohols, suggesting that there was no interaction between the hydroxyl group of the latter homologous series and the zirconia support matrix.

#### Comparison with octadecyl-silica stationary phases

To further evaluate the reversed-phase chromatographic property of the octadecyl-zirconia bonded stationary phases, the retention behavior of *p*-xylene and naphthalene obtained on the zirconia sorbents was compared to that observed on non-porous octadecyl-silica stationary phases. The specific surface areas of both sorbents are low, and the comparison of their energetic of retention for the non-polar solutes would therefore be meaningful. The non-porous microspherical silica support of mean particle diameter of 0.8  $\mu\text{m}$  was synthesized in our laboratory by a seeded growth technique according to well established procedures [29], and was bonded with octadecyl functions by following the same procedure described for the zirconia support, see Experimental.

The values of the logarithmic retention factor obtained at different concentrations of acetonitrile in the mobile phase on zirconia-based stationary phases were plotted against those obtained on octadecyl-silica columns (see Fig. 8). Referring to this figure,  $\log k' - \log k'$  plots were linear, meaning that the retention energetic of the aromatic compounds on the end-capped octadecyl-zirconia stationary phases was the same as that obtained on the octadecyl-silica stationary phases. The antilog of the intercepts of *p*-xylene and naphthalene curves are 1.67 and 1.31, respectively, indicating that the phase ra-

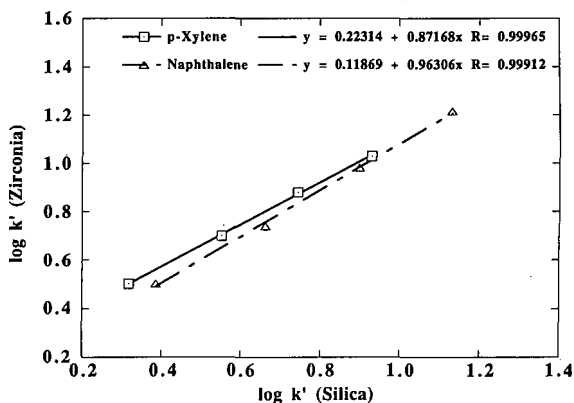


Fig. 8. Plots of logarithmic retention factor of *p*-xylene and naphthalene on octadecyl-zirconia versus that on octadecyl-silica. Columns, monomeric with end-capping, 3.0  $\times$  0.46 cm I.D.; mobile phases, water at various volume percent of acetonitrile, 1, 2, 5, 10, 15 and 20% (v/v).

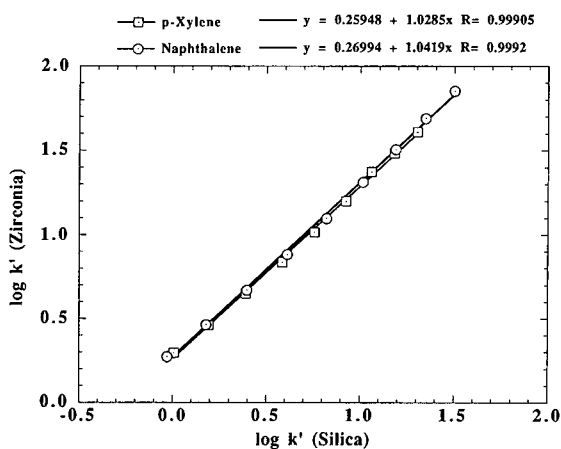


Fig. 9. Plots of logarithmic retention factor of *p*-xylene and naphthalene on octadecyl-zirconia versus that on octadecyl-silica. Columns, “polymeric” octadecyl-zirconia and octadecyl-silica,  $3.0 \times 0.46$  cm I.D.; mobile phase water at various volume percent of acetonitrile, from 4 to 36% (v/v) with an increment of 4%.

tio of octadecyl-zirconia is slightly higher than that of octadecyl-silica. This may be explained by the higher surface area per unit volume for zirconia than for silica. The packing density of non-porous silica has been estimated to be 1.5 g/ml [19]. The packing density of the zirconia particles used in this study was *ca.* 5.6 g/ml. Based on literature data [19], a non-porous silica of 0.8  $\mu\text{m}$  particle diameter similar to that used in this study would have a specific surface area of 3.4  $\text{m}^2/\text{g}$ , whereas the specific surface area of the non-porous zirconia of 1.5–2.8  $\mu\text{m}$  would be on the average 1.4  $\text{m}^2/\text{g}$ . From these data the surface area per unit volume for silica is 5.1  $\text{m}^2/\text{ml}$  versus 7.8  $\text{m}^2/\text{ml}$  for that of zirconia.

As expected, “polymeric” bonded octadecyl-zirconia stationary phases compared favorably with the silica-based stationary phases (Fig. 9). The zirconia surface was well covered with octadecyl functions in this modification process. The antilog of the intercepts of  $\log k' - \log k'$  plots for *p*-xylene and naphthalene were 1.82 and 1.86, respectively. These results and those obtained with monomeric zirconia suggest that the extent of surface modification of silica and zirconia with octadecyl functions are approximately the same.

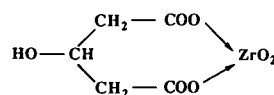
#### Chromatography of charged species

The chromatographic properties of the octade-

cyl-zirconia stationary phases under investigation were further evaluated with ionizable species at different pH. Benzylamine and *trans*-cinnamic acid were chosen as solute probes, and they were chromatographed on both monomeric and “polymeric” octadecyl columns in the presence or absence of 50 mM tartrate in the eluents. Tartrate was added to the mobile phases as a competing agent for the active sites on the zirconia surface, and to minimize solute-support interactions. Other competing agents were very recently investigated in the elution and separation of benzoic acid derivatives and proteins on bare zirconia [30–32].

Bare zirconia has been shown to have both anion- and cation-exchange properties for charged species as well as ligand exchange behavior towards Lewis bases [24,30–32]. The isoelectric point of the ampholytic surface can range from below 3 to above 10 depending on the source and the type of zirconia support [33]. Whereas the ligand exchange property of zirconia is the result of the presence of coordinatively unsaturated zirconium sites, the anion- and cation-exchange behavior is thought to arise from the protonation and deprotonation of surface hydroxyl groups [34], respectively.

When tartrate is added to the mobile phase, this hard Lewis base ligand would form metal chelates with the exposed zirconium sites of the surface of the stationary phase according to the following scheme:



Under these conditions, the empty valence orbitals of the zirconium sites will be filled with the electron pairs donated from the mobile phase additive, and consequently there would be little interaction between the solute and the support matrix. In addition, the doubly charged tartrate ions may reduce the residual ion-exchange of the zirconia matrix.

In the absence of tartrate, benzylamine which was completely ionized at pH below 4.0 ( $\text{p}K_a = 9.33$ ), exhibited very weak hydrophobic interaction with the monomeric and end-capped octadecyl-zirconia stationary phases. When the pH of the eluent was increased to 6.0, the fully ionized benzylamine showed strong interaction with the zirconia matrix

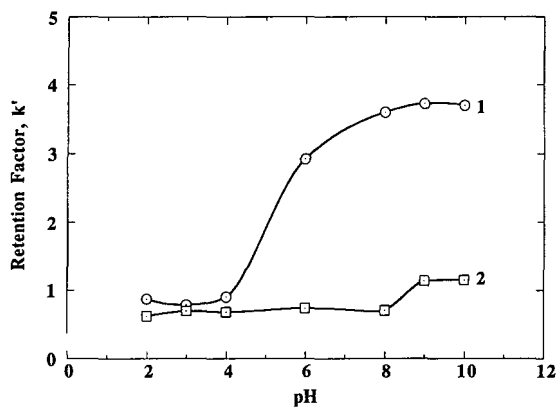


Fig. 10. Plots of the retention factor of benzylamine versus the pH of the mobile phase. Column, monomeric bonded octadecyl-zirconia with end-capping,  $3.0 \times 0.46$  cm I.D.; mobile phases: curve 1, 1% (v/v) acetonitrile in all the buffer solutions; curve 2, same mobile phases as in curve 1 in the presence of 50 mM tartrate. Buffers: (all containing 50 mM NaCl) pH 2.0 and 3.0, 5 mM  $\text{NaH}_2\text{PO}_4$ ; pH 4.0, 5 mM sodium acetate; pH 6.0 and 8.0, 5 mM  $\text{Na}_2\text{HPO}_4$ ; pH 9.0 and 10.0, 5 mM sodium borate; flow-rate, 1.0 ml/min.

of the end-capped monomeric octadecyl-zirconia column (see curve 1 in Fig. 10). As the pH of the mobile phase was increased to above the  $\text{p}K_a$  value of the solute, benzylamine was totally deprotonated and therefore exhibited stronger interaction with both the zirconia matrix and the bonded octadecyl functions of the stationary phase. Thus, solute retention was the highest at  $\text{pH} > 9.0$ .

Since zirconium sites are rather hard Lewis acids, the residual adsorptivity of the monomeric octadecyl-zirconia toward benzylamine, an intermediate soft Lewis base, is may be largely due to the cation-exchange property of the support matrix. In fact, in the pH range 6.0–9.0 whereby benzylamine exhibited strong interaction with the monomeric octadecyl-zirconia, the protonation of the amino group of the analyte would exclude ligand exchange type of retention. However, at pH above 9.0, benzylamine becomes less protonated and ligand-exchange interaction may predominate.

In the presence of tartrate ions in the mobile phase, and at pH below 8.0, the residual interaction of the surface proper of the zirconia support with the fully protonated benzylamine was greatly reduced, and its retention via hydrophobic interaction with the hydrocarbonaceous chains of the sta-

tionary phase was also low (see curve 2 in Fig. 10). At higher pH where benzylamine became deprotonated, its retention increased since its hydrophobic interaction with the bonded stationary phase increased. Thus, upon adding tartrate to the mobile phase, the chromatographic retention was mainly due to hydrophobic interaction.

In the absence of tartrate, benzylamine was eluted as a sharp peak at pH 2.0 and 3.0. At pH 4.0, the solute peak started to show tailing and broadening. This behavior became more pronounced at pH 6.0 and 8.0 due to dual retention mechanism, *i.e.* ion-exchange and reversed phase. Benzylamine has been shown to undergo some interactions with bare zirconia [24]. When the pH reached 9.0 and 10.0, benzylamine peak became less broad indicating that residual adsorptivity from the support matrix was still operating. When tartrate was added to the mobile phase, slight peak tailing appeared only at pH 4.0 and 6.0.

Fig. 11 shows the behavior of benzylamine on polymeric octadecyl-zirconia in the absence and presence of tartrate in the mobile phase at different acetonitrile concentrations. As can be seen in Fig. 11, in the absence of tartrate in the mobile phase the retention factor of benzylamine remained almost unchanged over the entire pH range studied, and decreased with increasing the acetonitrile content of the eluent (see curves 1, 2, 3 and 4 in Fig. 11). The

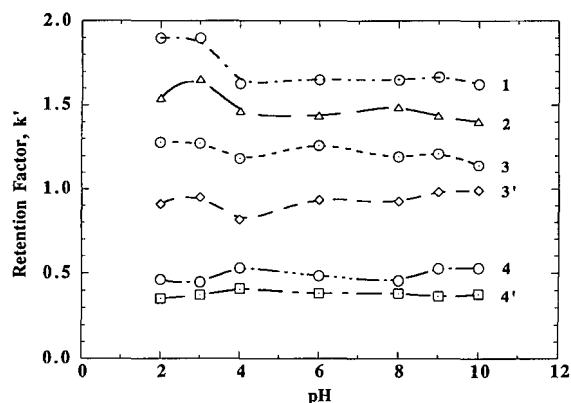


Fig. 11. Plots of the retention factor of benzylamine versus the pH of the mobile phase. Column, "polymeric" bonded octadecyl-zirconia,  $3.0 \times 0.46$  cm I.D.; mobile phases: 1 = aqueous buffer solutions; 2, 3 and 4 = 1, 2 and 14% (v/v) acetonitrile, respectively, in the same buffers as in 1; 3' and 4' = 50 mM tartrate in the same buffers as in 3 and 4. Buffers and flow-rate as in Fig. 10.

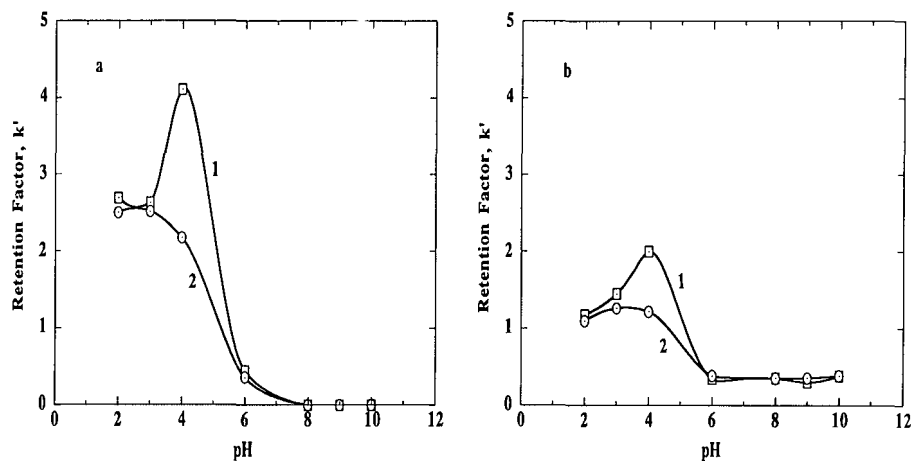


Fig. 12. Plots of retention factor of *trans*-cinnamic acid versus the pH of the mobile phase. Column, monomeric octadecyl-zirconia with end-capping (a) and "polymeric" octadecyl-zirconia (b),  $3.0 \times 0.46$  cm I.D., Mobile phases: (a) 1% acetonitrile and 50 mM NaCl in all the buffer solutions in the absence (1) and presence of 50 mM tartrate (2); (b) 15% (v/v) acetonitrile and 50 mM NaCl in all buffer solutions in the absence (1) and presence of 50 mM tartrate (2). Buffers as in Fig. 10; flow-rate, 1.0 ml/min.

retention factor of benzylamine decreased slightly upon adding tartrate to the eluents, and again showed no dependence on pH (see curves 3' and 4' in Fig. 11). The addition of small amount of tartrate would enhance the ionic atmosphere about the solute molecules, which would cause solute interaction with the hydrophobic phase to decrease [26]. It should be noted that no peak tailing was observed for benzylamine on "polymeric" octadecyl-zirconia column in the presence or absence of tartrate ions in the eluent.

*trans*-Cinnamic acid exhibited the same chromatographic behavior regardless of the bonding chemistry of the stationary phases (see curves 1 in Fig. 12a and b). In the absence of tartrate, *trans*-cinnamic acid had the highest retention at pH 4.0 on both monomeric and "polymeric" octadecyl-zirconia columns, which may be explained by a dual retention mechanism of the solute. *trans*-Cinnamic acid was also reported to undergo solute-support interaction even with zirconia having thick and cross-linked polybutadiene coatings [9].

As can be seen in Fig. 12a and b, the extent of solute interaction with the support proper by ligand exchange and/or ion exchange was higher on the monomeric than on "polymeric" octadecyl zirconia column. This is manifested by the fact that at pH 4.0 the retention modulus of cinnamic acid, which is

defined as the ratio of its retention factor  $k'$  observed in the absence to that obtained in the presence of tartrate, was *ca.* 2.0 on the monomeric versus 1.5 on the "polymeric" octadecyl columns. At pH above its  $pK_a$  value of 4.44, *trans*-cinnamic acid became fully ionized, a fact that explains the decrease in its retention through hydrophobic interaction with the bonded octadecyl stationary phase.

In the presence of tartrate the solute-support interaction was minimized, and *trans*-cinnamic acid was retained primarily by hydrophobic interactions (see curves 2 in Fig. 12a and b). At pH higher than 6.0, *trans*-cinnamic acid was completely ionized and showed no interaction with the support matrix, and very little or no retention in the hydrophobic stationary phase. The surface of zirconia may possess cation-exchange property at high pH and cinnamic acid would undergo coulombic repulsion from the surface. This may explain the fact that at high pH the retention of the solute was almost the same in the presence or absence of tartrate in the mobile phase (see Fig. 12a and b).

On both bonded stationary phases, *trans*-cinnamic acid showed increased band broadening in the pH range 4.0 to 6.0. When tartrate was added to the mobile phase, the solute-support interaction was minimized and *trans*-cinnamic acid eluted as a sharp peak.

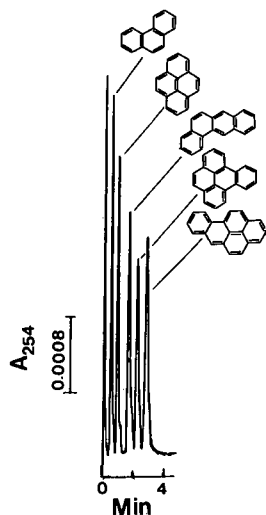


Fig. 13. Separation of polycyclic aromatic hydrocarbons. Column, "polymeric" octadecyl-zirconia,  $3.0 \times 0.46$  cm I.D. Linear gradient in 6 min from 40 to 70% (v/v) acetonitrile in water; flow-rate, 2.0 ml/min. Solutes from left to right: phenanthrene, pyrene, benz[a]anthracene, benzo[e]pyrene and benzo[a]pyrene.

### Selected applications

**Polycyclic aromatic hydrocarbons.** Reversed-phase liquid chromatography with non-polar stationary phases has been the most widely used

HPLC technique for the separation of polycyclic aromatic hydrocarbons (PAHs) (for recent reviews see refs. 35 and 36). It is well documented [35] that octadecyl stationary phases with high carbon loading are required for the high resolution of PAH isomers. Fig. 13 illustrates the separation of a series of PAHs and their isomers on "polymeric" bonded octadecyl-zirconia stationary phase. The retention of the polyaromatic hydrocarbons increased in the order of increasing hydrophobic area of the molecules, or in another word with increasing number of aromatic rings. Within the same groups of isomers, *i.e.*, PAHs having the same number of aromatic rings, the breadth-to-length ratio ( $B/L$ ) determined the relative retention of the isomers. For pyrene and benzo[a]pyrene, their corresponding  $B/L$  are 1.27 and 1.58, whereas for benzo[e]pyrene and benzo[a]pyrene, their respective  $B/L$  are 1.12 and 1.50 [35]. As can be seen in Fig. 13 the isomer of higher  $B/L$  was more retarded. This is identical to that reported [37] on silica-based reversed-phase column. No evidence of solute-support interaction was revealed with this polymeric octadecyl column. On the other hand, with monomeric and end-capped octadecyl-zirconia stationary phase, the PAHs revealed some interaction with the zirconia surface proper and tailing peaks were observed.

**Maltooligosaccharides.** Fig. 14a illustrates the re-

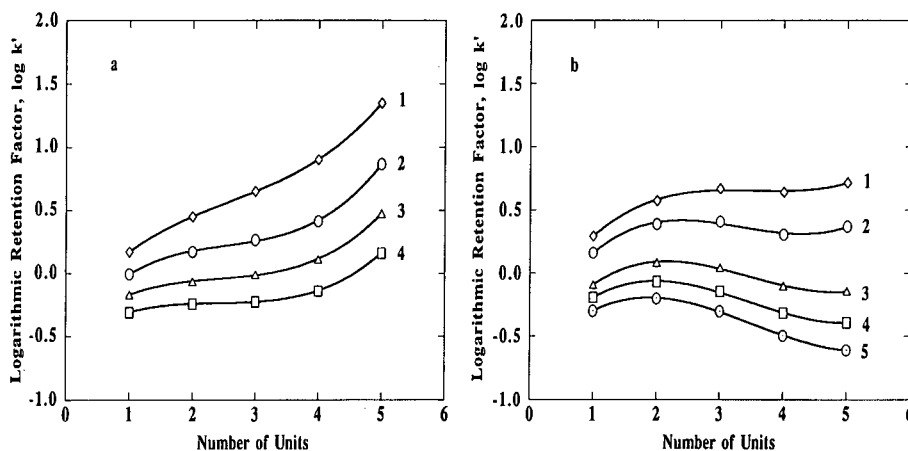


Fig. 14. Plots of logarithmic retention factor of *p*-nitrophenyl derivatives of maltooligosaccharides versus the number of glucose units in the homologous series. Column, "polymeric" octadecyl-zirconia (a) and "polymeric" octadecyl-silica (b),  $3 \times 0.46$  cm I.D. Mobile phases, 0.05% trifluoroacetic acid in water at various volume percent of acetonitrile; (a): 1 = pure water; 2 = 2.0%; 3 = 4.0%; 4 = 6.0%; (b) 1 = pure water; 2 = 1.0%; 3 = 2.0%; 4 = 3.0%; 5 = 4.0%. Flow-rate, 1.0 ml/min. Solutes: *p*-nitrophenyl derivatives of glucopyranoside, maltoside, maltotrioside, maltotetraoside and maltopentaoside.

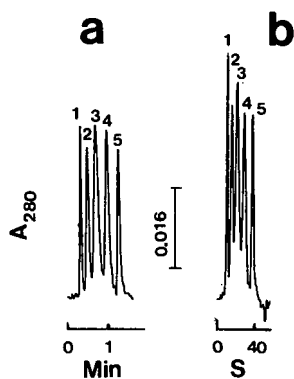


Fig. 15. Chromatograms of *p*-nitrophenyl maltooligosaccharides. Column, "polymeric" octadecyl-zirconia,  $3.0 \times 0.46$  cm I.D., Linear gradient in 1 min (a) and 0.5 min (b) from 0 to 20% (v/v) acetonitrile in water at 0.05% (v/v) trifluoroacetic acid; Flow-rates, 1.0 ml/min (a) and 4.0 ml/min (b). Solutes: *p*-nitrophenyl derivatives of 1 = glucopyranoside; 2 = maltoside; 3 = maltotriose; 4 = maltotetraoside; 5 = maltopentaoside.

tention behavior of *p*-nitrophenyl maltooligosaccharides on polymeric octadecyl-zirconia stationary phases. It can be seen in this figure that the plots of

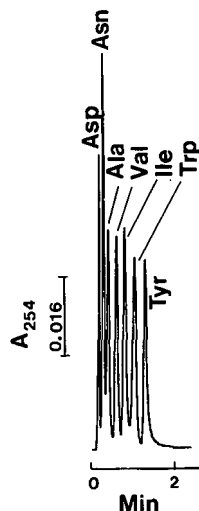


Fig. 16. Chromatogram of dansyl-amino acids. Column, "polymeric" octadecyl-zirconia,  $3.0 \times 0.46$  cm I.D. Consecutive linear gradients, 0.8 min from 0 to 19.5%, and 0.1 min from 19.5 to 30% followed by isocratic elution for 0.2 min with 30% (v/v) acetonitrile in 5 mM  $\text{Na}_3\text{PO}_4$ , pH 11.0; flow-rate, 2.0 ml/min. Solutes: Asp = aspartic acid; Asn = asparagine; Ala = alanine; Val = valine; Ile = isoleucine; Trp = tryptophan; Tyr = tyrosine.

$\log k'$  versus the number of glucose units in the homologous series are not linear, and the deviation from linearity increased as the acetonitrile content of the mobile phase increased.

For comparison, Fig. 14b shows the retention behavior of *p*-nitrophenyl maltooligosaccharides on non-porous polymeric octadecyl-silica stationary phases. With these sorbents, increasing the organic content of the mobile phase resulted in a switch of the elution order of the homologous series, and the five homologues could not be resolved even with plain aqueous mobile phase. This irregular behavior has been previously observed by us with xyloglucan oligosaccharides on porous octadecyl-silica stationary phases [38].

The different elution patterns of the maltooligosaccharides observed on octadecyl-silica and octadecyl-zirconia sorbents may be attributed to the difference in solute-support interactions between the two types of stationary phases.

Fig. 15a and b portrays the rapid separation of *p*-nitrophenyl maltooligosaccharides obtained on a short polymeric octadecyl-zirconia column. These homologues could be separated in less than 40 s when the mobile phase flow-rate was increased to 4.0 ml/min.

*Dansyl-amino acids.* As shown above, polymeric octadecyl-zirconia stationary phases did not exhibit significant interaction with benzylamine and the residual adsorptivity of the sorbent toward *trans*-cinnamic acid was greatly attenuated at high pH and/or in the presence of competing agent such as tartrate. Based on these results, amino acids, which are ampholytic compounds having amino and carboxylic groups in their structure should then be better chromatographed at high pH. Some preliminary studies conducted in our laboratories have already confirmed this prediction. An in-depth study on the chromatographic behavior of dansyl-amino acids on octadecyl-zirconia stationary phases is underway and the results will be published in an upcoming article.

Fig. 16 shows a typical chromatogram for the separation of dansyl-amino acids obtained on polymeric octadecyl-zirconia stationary phases. Seven amino acids can be separated in less than 2 min with a rapid gradient of acetonitrile at pH 11.0. The retention of amino acids followed more or less the reversed-phase mechanism. The species with

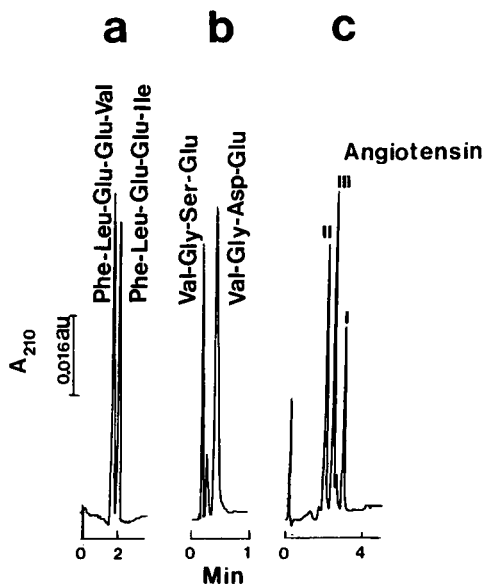


Fig. 17. Chromatograms of peptides. Column, "polymeric" octadecyl-zirconia,  $3.0 \times 0.46$  cm I.D. Linear gradients: (a) 2 min from 0 to 20% (v/v) acetonitrile in 5 mM phosphate, pH 2.0; (b) 2 min from 0 to 20% (v/v) acetonitrile in 5 mM sodium phosphate containing 10 mM decyltrimethylammonium bromide, pH 6.0; (c) 4 min from 0 to 40% (v/v) acetonitrile in 5 mM phosphate, pH 11.0; flow-rates, 2.0 ml/min (a and b) and 1.0 ml/min (c).

charged side chain, *e.g.*, aspartic acid, was the least retained, followed by the amino acid having uncharged polar side chain, *e.g.*, asparagine. The dan-syl-amino acids with non-polar moieties were more retained and eluted in the order of increasing hydrophobicity, *i.e.*, in the order alanine, valine, isoleucine, tryptophan and tyrosine.

**Peptides.** Since "polymeric" octadecyl-zirconia stationary phases exhibited lower metallic interaction than their monomeric counterparts toward charged solutes, these phases were employed in the separation of closely related peptides.

Fig. 17a illustrates the baseline resolution of Phe-Leu-Glu-Ile and Phe-Leu-Glu-Val on the "polymeric" bonded octadecyl-zirconia stationary phase using phosphate buffer, pH 2.0. These two peptides did not separate at pH 6.0, despite the fact that they differ in the amino acid residues at the C-terminal, *i.e.*, isoleucine and valine, with the former being more hydrophobic. On the other hand, at pH 11.5, both peptides did not have much retention.

To further investigate the potential of octadecyl-zirconia, relatively hydrophilic peptides were chromatographed. As expected, Val-Gly-Ser-Glu and Val-Gly-Asp-Glu, having relatively low hydrophobicity, and differing only in one amino acid residue, serine and aspartic acid, showed little retention on the octadecyl stationary phase. To bring about their retention and separation, decyltrimethylammonium bromide ion-pairing agent was used in the mobile phase. Under this condition the peptides were resolved, and, as expected, the peptide with aspartic acid residue was more retained (see Fig. 17b).

Angiotensin I (Arg-Val-Tyr-Ile-His-Pro-Phe-His-Leu), angiotensin II (Ala-Pro-Gly-Asp-Arg-Ile-Tyr-Val-His-Pro-Phe) and angiotensin III (Arg-Val-Tyr-Ile-His-Pro-Phe) were not well resolved on polymeric octadecyl-zirconia bonded stationary phase at low pH. But at pH 11.0, these three peptides were very well separated (see Fig. 17c). As mentioned earlier, at this pH, solute-support interaction was minimized. Although angiotensin II has four more amino acid residues than angiotensin III (*i.e.*, Ala-Pro-Gly-Asp) the presence of an amino acid residue with ionizable side chain (Asp) in this tetrapeptide fragment may have caused angiotensin II to be the least retained, and separated from the other two peptides. Angiotensin I was the most retained of the three peptides on the octadecyl-zirconia bonded stationary phases. The two extra amino

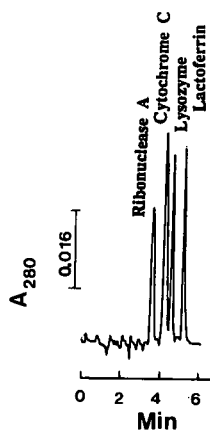


Fig. 18. Chromatogram of proteins. Column, monomeric octadecyl-zirconia,  $3.0 \times 0.46$  cm I.D. Linear gradient in 7.0 min from 0 to 70% (v/v) acetonitrile in water at 0.05% (v/v) trifluoroacetic acid; flow-rate, 1.0 ml/min.



acid residues, histidine and leucine on the C-terminal of angiotensin I may have increased the hydrophobicity of this peptide, and consequently has brought about its higher retention on the reversed-phase column.

**Proteins.** Although monomeric octadecyl-zirconia columns exhibited residual adsorptivities toward small and charged species, high-molecular-mass proteins chromatographed nicely on these phases, and a typical chromatogram is shown in Fig. 18. The four proteins eluted and separated in less than 6 min at a flow-rate of 1.0 ml/min with a linear gradient at moderate acetonitrile concentration in the eluent.

The absence of any significant solute-support interaction is may be due to steric hindrance imposed on the protein analyte by the long octadecyl chains of the stationary phase, thus preventing the large protein molecule from getting into close proximity to the metallic sites as well as the unreacted hydroxyl groups on the surface of the stationary phase.

#### ACKNOWLEDGEMENTS

The financial supports from the College of Arts and Sciences, Dean Incentive Grant Program at Oklahoma State University, from Grant No. HN9-004 of the Oklahoma Center for the Advancement of Science and Technology, Oklahoma Health Research Program and in part from the Oklahoma Water Resources Research Institute are gratefully acknowledged.

#### REFERENCES

- 1 F. E. Regnier, K. K. Unger and R. E. Majors (Guest Editors), *Liquid Chromatography Packings*, *J. Chromatogr.*, 544 (1991).
- 2 O. Mikes and J. Coupek, in K. M. Gooding and F. E. Regnier (Editors), *HPLC of Biological Macromolecules*, Marcel Dekker, New York, 1990, p. 25.
- 3 U. Bien-Vogelsang, A. Deege, H. Figge, J. Köhler and G. Schomburg, *Chromatographia*, 19 (1984) 170.
- 4 R. M. Chicz, Z. Shi and F. E. Regnier, *J. Chromatogr.*, 359 (1986) 21.
- 5 H. Engelhardt, H. Low, W. Beck and W. Gotzinger, in H. A. Mottola and J. R. Steinmetz (Editors), *Chemically Modified Surface*, Elsevier, Amsterdam, 1992, p. 225.
- 6 J. E. Haky, R. Raghani and B. M. Dunn, *J. Chromatogr.*, 541 (1991) 303.
- 7 J. E. Haky, R. Raghani, B. M. Dunn and L. F. Wieserman, *Chromatographia*, 19 (1991) 49.
- 8 Y. Ghaemi and R. A. Wall, *J. Chromatogr.*, 174 (1979) 51.
- 9 M. R. Rigney, J. P. Weber and P. W. Carr, *J. Chromatogr.*, 484 (1989) 273.
- 10 U. Trüdinger, G. Müller and K. K. Unger, *J. Chromatogr.*, 535 (1990) 111.
- 11 T. P. Weber, P. W. Carr and E. F. Funkenbuch, *J. Chromatogr.*, 519 (1990) 30.
- 12 T. P. Weber and P. W. Carr, *Anal. Chem.*, 62 (1990) 2620.
- 13 I. Halasz and K. Martin, *Angew. Chem.*, 90 (1978) 954.
- 14 R. C. Weast, M. J. Astle and W. H. Beyer (Editors), *CRC Handbook of Chemistry and Physics*, CRC Press, Boca Raton, FL, 66th ed., 1986.
- 15 K. K. Unger, G. Gilge, J. N. Kinkel and M. T. W. Hearn, *J. Chromatogr.*, 359 (1986) 61.
- 16 K. Kalghatgi and Cs. Horváth, *J. Chromatogr.*, 398 (1987) 335.
- 17 Y. Kato, T. Kitamura, A. Mitsui and T. Hashimoto, *J. Chromatogr.*, 398 (1987) 327.
- 18 D. J. Burke, J. K. Duncan, L. C. Dunn, L. Cumings, C. J. Siebert and G. S. Ott, *J. Chromatogr.*, 353 (1986) 425.
- 19 H. Engelhardt and P. Orth, *J. Liq. Chromatogr.*, 10 (1987) 1999.
- 20 K. K. Unger, G. Gilge, R. Janzen, J. Giesche and J. N. Kinkel, *Chromatographia*, 22 (1986) 379.
- 21 R. Stevens, *Zirconia and Zirconia Ceramics*, Publication No. 113, Magnesium Electron, Twickenham, 1986.
- 22 W. Hertl, *Langmuir*, 5 (1989) 96.
- 23 R. Agron, E. Fuller and H. Holmes, *J. Colloid Interface Sci.*, 52 (1975) 553.
- 24 M. P. Rigney, E. F. Funkenbusch and P. W. Carr, *J. Chromatogr.*, 499 (1990) 291.
- 25 E. V. Lumina, A. K. Selivanoski, V. B. Golubev, T. Y. Samgina and G. I. Markaryan, *Russ. J. Phys. Chem. (Engl. Transl.)*, 56 (1982) 415.
- 26 W. R. Melander and Cs. Horváth, in Cs. Horváth (Editor), *High Performance Liquid Chromatography—Advances and Perspectives*, Vol. 2, Academic Press, New York, 1980, p. 113.
- 27 W. R. Melander, J. Stoveken and Cs. Horváth, *J. Chromatogr.*, 199 (1980) 35.
- 28 Z. El Rassi and Cs. Horváth, *Chromatographia*, 19 (1984) 9.
- 29 G. H. Bogush, M. A. Tracy, C. F. Zukoski, *J. Non-Cryst. Solids*, 104 (1988) 95.
- 30 J. A. Blackwell and P. W. Carr, *J. Chromatogr.*, 596 (1992) 27.
- 31 J. A. Blackwell and P. W. Carr, *Anal. Chem.*, 64 (1992) 853.
- 32 J. A. Blackwell and P. W. Carr, *Anal. Chem.*, 64 (1992) 863.
- 33 H. Kita, N. Henmi, K. Shimazu, H. Hattori and K. Tanabe, *J. Chem. Soc., Faraday Trans.*, 77 (1981) 2451.
- 34 W. A. Schafer, P. W. Carr, E. F. Funkenbush and K. A. Parson, *J. Chromatogr.*, 587 (1991) 137.
- 35 L. C. Sander and S. A. Wise, *Adv. Chromatogr.*, 25 (1986) 39.
- 36 K. Jinno, *Adv. Chromatogr.*, 30 (1989) 123.
- 37 J. A. Schmit, R. A. Henry, R. C. Williams, and F. Kieckman, *J. Chromatogr. Sci.*, 9 (1971) 645.
- 38 Z. El Rassi, D. Tedford, J. Au and A. Mort, *Carbohydr. Res.*, 215 (1991) 25.

# Fimbriated stationary phases for proteins

L. Varady

*PerSeptive Biosystems, Cambridge, MA 02139 (USA)*

Ning Mu

*Department of Chemistry, Purdue University, West Lafayette, IN 47907 (USA)*

Y.-B. Yang

*Separations Group, Hesperia, CA 92345 (USA)*

S. E. Cook

*International Chemical Industries, Wilmington, DE 19897 (USA)*

N. Afeyan

*PerSeptive Biosystems, Cambridge, MA 02139 (USA)*

F. E. Regnier

*Department of Chemistry, Purdue University, West Lafayette, IN 47907 (USA)*

---

## ABSTRACT

This paper describes synthetic procedures for preparing fimbriated stationary phases on poly(styrene–divinylbenzene) (PS–DVB) packing materials. The synthesis consists of a five-step procedure in which the order in which the steps are carried out may be varied. These steps are (i) polymerization of monomers to form an amphiphilic copolymer or oligomer, (ii) adsorption of either monomers, or polymer onto the PS–DVB surface, (iii) solvent induction of functional group orientation at the PS–DVB–polymer interface and polymer–water interface, (iv) a cross-linking reaction that forms a hydrophilic surface layer, and (v) derivatization of the surface layer with stationary phase.

---

## INTRODUCTION

Polar, filamentous polymer particles such as cellulose, agarose, cross-linked dextrans, and cross-linked acrylates have long been used as supports in the chromatography of proteins [1]. The success of

these filliform matrices is attributed to the fact that they are neutral, hydrophilic, easily derivatized, of high surface area, and chemically stable under use conditions. It is likely that these media were used to purify more than 90% of the proteins currently known. Although of enormous utility, these filamentous, gel-type materials also have serious limitations. One is that they imbibe large quantities of water and are easily deformed under pressure. This

*Correspondence to:* F. E. Regnier, Department of Chemistry, Purdue University, West Lafayette, IN 47907, USA.

precludes their use at elevated mobile phase velocity in high-performance analytical and preparative columns. A second limitation is their resistance to mass transfer. High fillament density, molecular motion of fillament segments, and limited matrix porosity work in concert to restrict intraparticle diffusion and macromolecular mass transfer in gel-type materials.

Efforts to overcome these limitations in the mid-1970s [2–6] focused on the use of microparticulate, high-porosity silica. Through the use of small 10- $\mu\text{m}$  particles to reduce diffusion path length, large 500 Å pores to increase macromolecular diffusivity in the pore matrix, and a thin layer of bonded phase on the support surface to mask silanols, columns were produced that could separate proteins more than an order of magnitude faster than soft gel columns [2]. The negative features of these high-performance silica-based sorbents were their poor stability above pH 8–9, residual silanol effects, and lower capacity.

Several of these problems were addressed with advances in organic surface coatings. Highly cross-linked epoxy surface layers were found to control residual silanol effects and increased the stability of silica-based columns [7]. Sorbents with these organic polymer coatings were used up to pH 10. The loading capacity problem remained, however.

This loading capacity problem was attacked through the use of filamentous or fimbriated polymer layers at the support surface. Incorporating stationary phases into a hair-like border of polymer filaments at the surface of a silica support increased the surface area and loading capacity 3–5 fold in most cases [8–11]. These filliform stationary phases were generally prepared by immobilizing preformed polymers onto silica supports. In other cases, polymerization was initiated at the sorbent surface to create linear “tentacles” [11].

Recent efforts to reduce mass transfer limitations in porous liquid chromatography media have been directed at the preparation of materials that allow mobile phase to flow or perfuse through the support matrix [12]. This perfusion process transports solutes to the interior of a sorbent particle much more rapidly than by diffusion, enabling separations to be achieved in a min or less. Supports used in perfusion chromatography are based on poly(styrene–divinylbenzene) (PS–DVB) with a combination of

large 6000–8000 Å pore diameter, particle transecting pores and smaller 1000–1500 Å interconnecting pores. These very high porosity PS–DVB matrices are generally of lower surface area than either soft gels or high-performance silica supports.

The objective of the work reported in this paper was to develop a surface modification procedure for producing chromatography sorbents for proteins that have good chemical stability and high protein loading capacity. This paper describes the preparation of PS–DVB-based sorbents for ion-exchange and immunoaffinity chromatography of proteins in which a surface layer is established in a multi-step process consisting of polymer adsorption onto PS–DVB, cross-linking, and functionalization of the surface with stationary phase.

## THEORY

Charged polymers may be concentrated from solution at a surface of opposite charge through electrostatic forces [13,14]. When all charges at the sorbent surface are ion paired with complementary groups on the polymer, adsorption ceases. The thickness of this “fuzzy” or fimbriated polymer layer is between 20 and 100 Å, depending on the solvent, polymer concentration, and polymer molecular weight [10]. Subsequent cross-linking of this adsorbed layer provides a surface coating that can only be removed by chemical degradation.

Adsorption is a general phenomenon in which any of a variety of forces could be used to create polymeric surface layers and hold them in place while they are cross-linked into a permanent film. For example, a hydrophobic polymer could be adsorbed from a poor solvent onto the hydrophobic surface of PS–DVB and cross-linked into a continuous layer. The problem is that this would only create a hydrophobic surface with properties similar to those of PS–DVB. This would not create the requisite hydrophilic surface necessary for protein separations.

It is proposed that a hydrophilic surface coating could be created by using a copolymer containing both hydrophobic and hydrophilic monomers units or segments. The copolymer can be a block polymer or an alternating polymer, or even a statistical polymer. If this copolymer were dissolved in a polar solvent and exposed to PS–DVB, hydrophobic seg-

ments of the polymer would adsorb to PS–DVB. The driving force for adsorption would be minimization of the hydrophobic contact area of both the polymer and PS–DVB sorbent with the polar solvent. In contrast, there would be no driving force for adsorption of polar segments of the copolymer. It has been demonstrated that oligomers containing oxyethylene  $-(\text{CH}_2\text{CH}_2\text{O})-$ , glyceryl  $(\text{CH}_2\text{CHOHCH}_2\text{O})-$ , or  $-\text{[CH}_2\text{CH}(\text{CH}_2\text{OH})\text{O}]$ , and vinylalcohol  $-(\text{CH}_2\text{CHOH})-$  are only weakly adsorbed to hydrophobic surfaces [15]. When a hydrophilic segment containing these units is located between two adsorbed hydrophobic segments, the hydrophilic segments would loop outward away from the surface in a filament. In a given copolymer, the ratio and distribution of hydrophobic and hydrophilic units are governed by reaction conditions such as the monomer ratio and the catalyst used. The physical appearance of the polymer at the surface would be that of a loop and train arrangement [16–26] (Fig. 1). It is expected that the hydrophobic character of PS–DVB would be completely masked and that the copolymer-support composite would take on the properties of the polar oligomer filaments.

## MATERIALS AND METHODS

### Reagents

All proteins were obtained from Sigma (St. Louis, MO, USA). Monomers used in the synthesis of surface coatings were purchased from PolyScience (Warrington, PA, USA). The PS–DVB support, POROS R, from PerSeptive Biosystems (Cambridge, MA, USA) was used to prepare all sorbents.

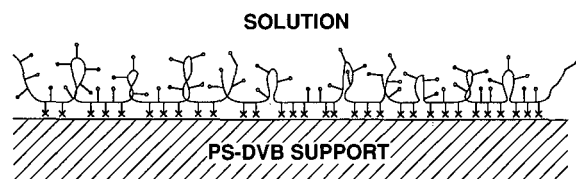


Fig. 1. The proposed physical appearance of the polymer-co-polymer coating at a hydrophobic PS–DVB surface. This is referred to as a “loop and train” arrangement.  $\times$  = hydrophobic functionalities;  $\circ$  = hydrophilic functionalities.

### Instrumentation

Chromatographic separations were carried out on two instruments; a BioCad liquid chromatograph from PerSeptive Biosystems (Cambridge, MA, USA) and a Varian 5500 liquid chromatograph from Varian Instruments (Walnut Creek, CA, USA). Absorbance detectors set at 254 nm were used on both instruments.

### Synthesis of the ether cross-linked polyglycerol coatings (IV)

Epibromohydrin (I) and glycidol (II) (2 ml in a 2:1 ratio) were dissolved in 15 ml of dichloromethane and 50  $\mu\text{l}$  of boron trifluoride etherate added to initiate polymerization. The polymerization reaction was carried out at room temperature for 24 h after which the solvent was evaporated and the remaining viscous polymer (III) dissolved in a mixed solvent comprising 10 ml water, 7 ml polyethylene glycol, and 30 ml of isopropanol. The solution was filtered and 3 g of PS–DVB particles added. After sonication and gentle agitation for 14 h the suspension was filtered, washed with water and dried. The neutral, hydrophilic polyglycerol matrix (PG–OH) was prepared by treating this copolymer-coated PS–DVB matrix for 14 h at 80°C with 3 M KOH. This material was subsequently washed to neutral pH and dried.

The copolymer-coated PS–DVB matrix was also used to prepare a strong anion-exchange sorbent (PG–SAX) (V). These particles (1 g) were suspended in 30 ml of 10% (v/v) dimethylethanolamine in methanol and refluxed for 14 h. The particles were then washed with water, isopropanol, and acetone before drying.

### Synthesis of the polyglycerol–methacrylate coating (IX)

A weak cation-exchange coating was applied to PS–DVB in this coating process. An aliquot of 6 ml of dichloromethane was transferred into a 50-ml round-bottomed flask and 1 ml of glycidyl methacrylate (VI) added with gentle swirling. Boron trifluoride etherate (5  $\mu\text{l}$ ) was added to 2 ml of dichloromethane in a test tube and added to the glycidyl methacrylate solution by drop-wise addition. The round-bottom flask was wrapped in aluminum foil and shaken at room temperature for 24 h after which 6 ml of 50% aqueous propanol was added to

stop the reaction. Solvent was removed by vacuum evaporation and the cloudy solution of polymer (VII) suspended in 16 ml of 50% aqueous polyethylene glycol. PS-DVB particles (1 g) were added to this solution and after a 5-min sonication and degassing, the system was shaken for 24 h.

After filtering and washing three times with 50 ml of water, the polymer-coated PS-DVB (VIII) was transferred into an acrylic acid solution (20 ml, 0.1% v/v) and 0.5 ammonium persulfate added. The reaction was carried out at room temperature under nitrogen for 24 h. Tetramethylene diamine (20  $\mu$ l) was then added and the reaction continued for another 30 min. The reaction was quenched by the addition of 10 mg hydroquinone and the particles washed sequentially with water (3  $\times$  30 ml), methanol (3  $\times$  20 ml), and acetone (50 ml) after which they were dried overnight under vacuum.

#### *Synthesis of the sorbitol (diol) sorbent (XI)*

An amount of 2 g of PS-DVB which had been coated with amphiphilic copolymer (IV) were cross-linked in 10 ml of 2 M KOH for 2 h at room temperature. At the end of this time 2 g of sorbitol (X) was added and the reaction continued for an additional 12 h under the same conditions. The resulting sorbitol containing sorbent was washed to neutrality with water and dried.

#### *Cyanogen bromide activation (XII)*

The sorbitol sorbent (XI) (1 g) was activated with 50 mg of cyanogen bromide at pH 10. As the reaction progressed, the reaction pH was maintained at 10 through the addition of 1 M KOH. After the reaction was completed the sorbent was filtered and washed with 20 ml of 0.05 M sodium carbonate [27,28].

#### *Antibody immobilization on cyanogen bromide sorbent (XIII)*

Cyanogen bromide-activated sorbent (XII) (1 g) was incubated with 100 mg of antibody (IgG) at pH 10 for 12 h [29]. This immunosorbent was then washed with 20 ml of Tris buffer (pH 7) and packed into a column by high-pressure slurry packing.

#### *Preparation of the aldehyde support (XIV)*

The sorbitol (XI) support (1 g) was treated with 100 mg of sodium periodate for 1 h at room temper-

ature. The support was washed with 20 ml of 0.05 M sodium carbonate and used immediately to immobilize antibodies.

#### *Antibody immobilization on the aldehyde sorbent (XVI)*

The aldehyde sorbent (XIV) (1 g) was reacted at pH 10 with 100 mg of antibody (IgG) for 4 h at room temperature. At the end of this reaction the sorbent was washed with 20 column volumes of buffer (pH = 7.0) and treated with 100 mg of NaBH<sub>4</sub> in 10 ml of water for 1 h. The solution was subsequently filtered, washed with 20 ml of buffer (pH = 7.0) and packed into a column by high-pressure slurry packing.

## RESULTS AND DISCUSSION

#### *General features of the coating process*

The coating process used to prepare the packing materials described below can be divided into five steps. The order in which these five steps are presented is not necessarily the order in which they must be carried out to produce a coating. They are: (i) a polymerization reaction that produces a polymer containing segments or units with hydrophobic and hydrophilic functional groups, (ii) adsorption of either polymer or monomers onto the surface of a hydrophobic material, (iii) the triggering of functional groups to orient at the PS-DVB-solvent interface on the basis of polarity, (iv) cross-linking of adjacent oligomers, polymers, or monomers to form a continuous surface layer and (v) derivatization with stationary phase. It will be shown that multiple chromatographic packing materials may be prepared using these five steps and that the sequence of these coating steps may be varied.

The letters A, B, C, D and E will be used to designate different moieties in the surface coating. The general formula for the surface coating derived from the series of steps described above is  $-(A)_1-(B)_m-(C)_n-(D)_o-(E)_p-$ , where (A) designates the hydrophobic moiety that orients inward toward the hydrophobic support surface and is used to adsorb the coating hydrophobically to PS-DVB, (B) designates the hydrophilic functional group (generally hydroxyl) containing moiety or moieties that orient outward away from PS-DVB toward the aqueous medium where they imbibe water and enable PS-

DVB to easily disperse in water, (C) designates the moiety or moieties in the coating that are used to cross-link adjacent chains of oligomer or polymer, (D) designates the monomeric unit that carries the chromatographic stationary phase, and (E) is any other moiety that is incorporated into the coating to convey secondary surface properties. The symbols *l*, *m*, *n*, *o* and *p* are used to designate the quantitative ratio of the various moieties in the adsorbed polymer layer.

### Polyglycerol (PG) coating

The two epoxy monomers, epibromohydrin (or epichlorohydrin) (I) and glycidol (II) were polymerized (Fig. 2) with boron trifluoride in step A of the coating process to give a copolymer (III) that was relatively hydrophobic [30]. By varying the monomer ratio, the *x/y* ratio and concomitantly the hydrophobic character of the polymer could be altered. Hydrophobicity, as judged by hydrophobic interaction chromatography, increased with increasing content of the halide containing moiety. The copolymer (III) was dispersed in water containing polyethylene glycol and then mixed with porous PS–DVB. Step B of the coating process in Fig. 2 indicates that the copolymer (III) is adsorbed onto the hydrophobic surface of PS–DVB with specific functional group orientation. This concept is based on the fact that neither the copolymer (III) nor PS–DVB could be dispersed in water until the two were combined, after which PS–DVB particles were easily dispersed. The most likely explanation for this behavior is that the non-polar halide containing functional groups orient inward toward the PS–DVB surface and hydroxyl containing functional groups orient outward where they are solvated with water. Step C of this coating process involves cross-linking by ether bond formation in strong base according to Fig. 2. Reaction time and temperature determine the amount of residual halide. When it was the intention to prepare a hydrophilic, underivatized surface layer, reaction was continued until all halide was displaced from the matrix. This material (IV) will be referred to henceforth as PG–OH. One route for functionalization of the surface was to interrupt the reaction before complete halide displacement. Step D indicates how a strong anion-exchange sorbent (PS–SAX) was prepared by nucleophilic displacement of residual halide in the surface layer.

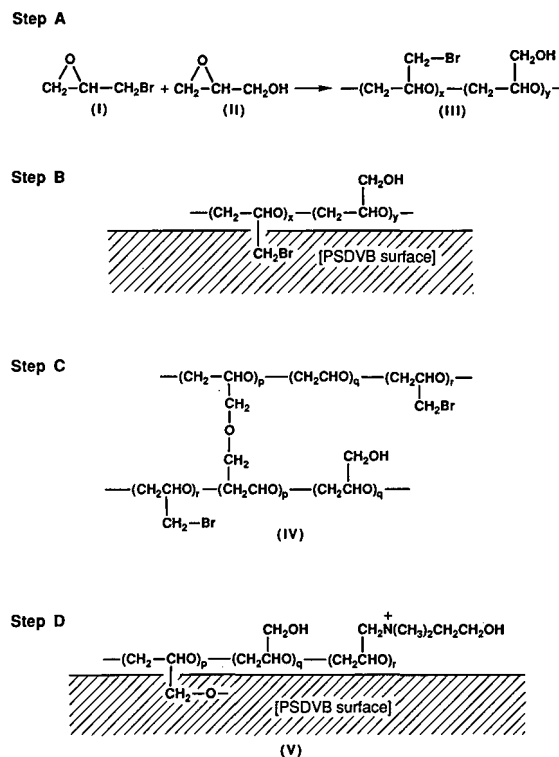


Fig. 2. Preparation of a strong anion-exchange sorbent based on the polyglycerol (PG) coating.

Because the support matrix is PS–DVB and there are no hydrolyzable functional groups in the coating, this sorbent may be operated in either strong base or acid. The PG–SAX sorbent (V in Fig. 2) was subjected to 300 wash cycles with 1 *M* KOH and 60% formic acid. No loss of the coating was observed either after this treatment nor 3000 chromatographic cycles of operation as determined by the chromatographic retention of anionic analytes.

A protein separation on the strong anion-exchange sorbent (V) is seen in Fig. 3. The wide separation of  $\beta$ -lactoglobulin A and B ( $M_r = 35\,000$ ) which vary by four amino acids indicates good selectivity and resolution with this strong anion-exchange matrix. Derivatization of the PG–OH matrix (IV) with either ethane sulfonic acid or the carboxymethyl group provide cation exchangers that were used in the resolution of a series of cationic proteins such as chymotrypsinogen, ribonuclease A, cytochrome *c*, and lysozyme (data not shown). The base stability and surface abundance of hy-

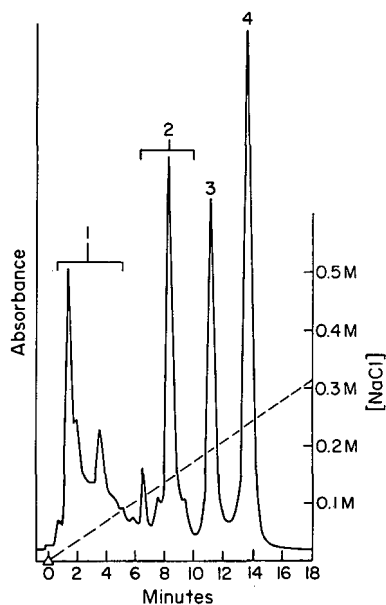


Fig. 3. Separation of proteins on the strong anion-exchange sorbent based on PG coating. Column:  $5 \times 0.46$  cm I.D. (Poros R/H,  $10 \mu\text{m}$ ); mobile phase: A =  $10 \text{ mM}$  Tris-HCl buffer (pH 8.0), B =  $0.32 \text{ M}$  NaCl in A; flow-rate:  $1 \text{ ml/min}$ ; gradient: 0–100% B in 20 min. Detection: UV 254 nm. Peaks: 1 = conalbumin; 2 = ovalbumin; 3 =  $\beta$ -lactoglobulin B; 4 =  $\beta$ -lactoglobulin A.

droxyl groups allow the PG-OH matrix (IV) to be derivatized in Williamson ether syntheses similar to the manner in which cellulose is functionalized with stationary phases [31].

Based on Bradford [32] assays, recovery from these ion-exchange columns was greater than 94% for the proteins examined in Fig. 3. The dynamic loading capacity of the SAX sorbent was determined to be  $30 \text{ mg/ml}$  by frontal analysis [33]. The capacity is within the range of several commercial strong cation-exchange (SCX) and SAX packing materials such as the Monobead and Neobar resins.

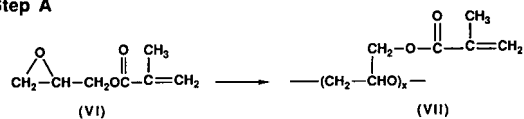
#### Polyglycerol-methacrylate (PGM) coating

Methacrylate-containing polyglycerol oligomers were used to further test the concept of using a hydrophobic support to sterically organize amphiphilic oligomers at a surface in the generation of chromatographic stationary phases. Hydrophobic adsorption of the copolymer and cross-linking in this case is due to the presence of methacryl groups instead of  $-\text{CH}_2\text{Br}$  groups in the oligomer (III). The

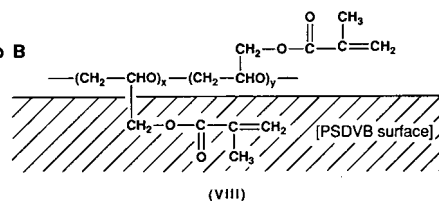
first step in the synthesis (Fig. 4) is the boron trifluoride-catalyzed polymerization of glycidyl methacrylate (VI) to form the glyceryl methacrylate polymer (VII). Mass Spectroscopy indicated that the chain length of the polymer varied from 5 to 15 residues. Following deposition of the oligomer (VII) onto PS-DVB, the coated PS-DVB support was suspended in an aqueous solution of methacrylic acid containing ammonium persulfate. The  $x/y$  ratio in VIII, *i.e.*, the ratio of methacryl groups oriented inward toward the surface as opposed to those oriented outward toward the solution, is not known. Cross-linking of methacrylate groups in the coating and polymerization of methacrylic acid in the solution was initiated simultaneously upon addition of the catalyst. During the course of polymerization, methacrylate oligomers in the solution were grafted to the surface of the sorbent through reaction with methacryl groups in the coating. The coating on this cation-exchange sorbent (IX) was stable to both organic and aqueous mobile phases from pH 2–10.

The chromatographic properties of this weak cation-exchange sorbent are seen in Fig. 5. Elution or-

#### Step A



#### Step B



#### Step C

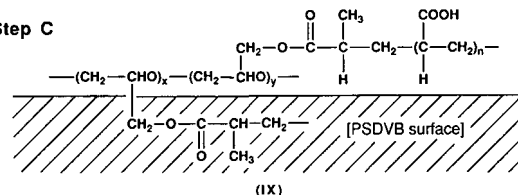


Fig. 4. Preparation of a weak cation-exchange sorbent based on the methacrylate cross-linked polyglycerol coating.

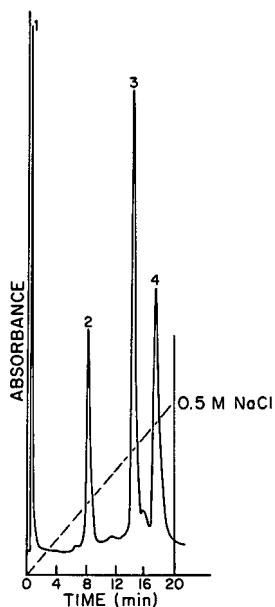


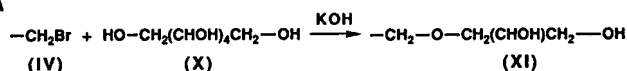
Fig. 5. Separation of proteins on the weak cation-exchange column based on polymeric glycidyl methacrylate. Column:  $5 \times 0.41$  cm I.D. (Poros,  $10 \mu\text{m}$ ); mobile phase: A =  $50 \text{ mM}$  phosphate buffer (pH = 7.0), B =  $0.5 \text{ M}$  NaCl in A; flow-rate:  $1.0 \text{ ml/min}$ ; gradient: 0–100% B in 20 min; detection: UV 254 nm. Peaks: 1 = myoglobin; 2 = ribonuclease A; 3 = cytochrome c; 4 = lysozyme.

der of cationic proteins is similar to that of other high-performance ion-exchange materials. The dynamic loading capacity of this material (IX) for lysozyme was  $90 \text{ mg/ml}$  as measured by frontal chromatography [33]. By changing acrylic acid to other monomers in the coating process, a series of stationary phases can be produced. Detailed properties of these materials will be described in a future publication.

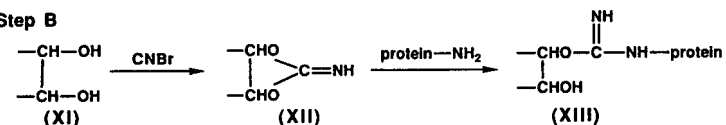
#### Diol phase

Carbohydrate matrices with vicinal hydroxyl groups are widely used in the preparation of affinity chromatography matrices, particularly in the case of cyanogen bromide-activated materials. A “diol” type sorbent was prepared in these studies by coupling sorbitol to a PS–DVB support that had been coated with the epibromohydrin–glycidol copolymer (III) and incompletely cross-linked. It was noted above that when cross-linking of copolymer (III) was interrupted, residual halide ( $-\text{CHBr}$ ) remains in the coating. Sorbitol was coupled to the PG-OH (IV) phase through an ether linkage as shown in Fig. 6. Two types of affinity matrices were prepared by the sorbitol sorbent (XI)

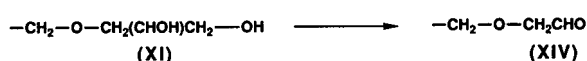
#### Step A



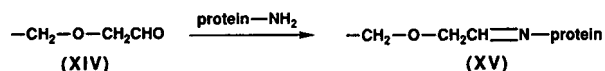
#### Step B



#### Step C



#### Step D



#### Step E

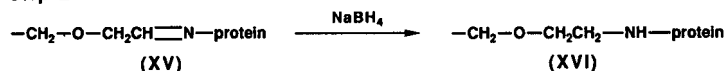


Fig. 6. Preparation of matrices for protein immobilization. Although it is indicated that sorbitol is coupled exclusively through primary hydroxyl groups, it is probable that immobilization also occurred through secondary hydroxyl groups.



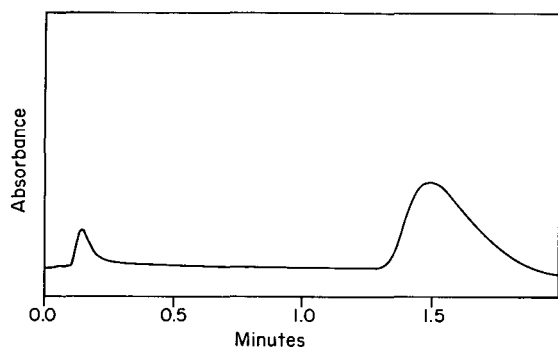


Fig. 7. Elution of Human Serum Albumin (HSA) from an anti-HSA IgG immobilized on PG-coated Poros R/H (10  $\mu$ m). Column: 5  $\times$  0.46 cm I.D.; mobile phase: binding buffer: 150 mM NaCl in 20 mM phosphate buffer (pH = 7.5), elution buffer: 0.3 M MgCl in 20% AcOH; flow-rate: 1.0 ml/min; detector: UV 280 nm.

(Fig. 6). Cyanogen bromide activation produced a material (XII) that immobilized proteins through an isourea linkage to amino groups on the surface of the protein [28]. Periodate oxidation produced an aldehyde material (XIV) [7] capable of immobilizing proteins by Schiff base formation. Subsequent reduction of the Schiff base with borohydride produced a stable coupling of the protein to the sorbent through a secondary amine linkage. Both of these forms of activation produced sorbents which were capable of immobilizing approximately 10 mg/ml of IgG. Application of an immunosorbent prepared from the aldehyde material (XIV) in an immunoaffinity chromatographic separations is seen in Fig. 7.

#### CONCLUSIONS

It may be concluded that adsorption and subsequent cross-linking of amphiphilic copolymers onto the surface of PS-DVB can produce chromatographic matrices that are both hydrophilic and stable. When these coated materials are derivatized with either ion-exchanging stationary phases or antibodies they may be used in high-performance separations of proteins.

#### ACKNOWLEDGEMENT

The authors gratefully acknowledge support from the National Institute of Health (NIH grant number 25431).

#### REFERENCES

- 1 T. Kremmer and L. Boross, *Gel Chromatography*, Wiley, New York, 1979.
- 2 K. K. Unger, R. Kern, M. C. Ninov and K.-F. Krebs, *J. Chromatogr.*, 99 (1974) 435.
- 3 S.-H. Chang, K. M. Gooding and F. E. Regnier, *J. Chromatogr.*, 125 (1976) 103.
- 4 F. E. Regnier and K. M. Gooding, *Anal. Biochem.*, 103 (1980) 1.
- 5 K. Tsiji and J. H. Robinson, *J. Chromatogr.*, 112 (1975) 663.
- 6 S. Ohlson, L. Hansson, P. O. Larsson and K. Mosbach, *FEBS Lett.*, 93 (1978) 5.
- 7 S.-H. Chang, R. Noel and F. E. Regnier, *Anal. Chem.*, 48 (1976) 1836.
- 8 G. Vanecek and F. E. Regnier, *Anal. Biochem.*, 121 (1982) 217.
- 9 D. J. Burke, J. K. Duncan, L. C. Dunn, L. Cummings, C. J. Siebert and G. S. Ott, *J. Chromatogr.*, 353 (1986) 425.
- 10 W. Kopaciewicz, M. A. Rouhds and F. E. Regnier, *J. Chromatogr.*, 358 (1986) 107.
- 11 W. Muller, *J. Chromatogr.*, 510 (1990) 133.
- 12 N. B. Afeyan, N. F. Gordon, I. Mazsaroff, L. Varady, S. P. Fulton, Y.-B. Yang and F. E. Regnier, *J. Chromatogr.*, 519 (1990) 1.
- 13 A. T. Alpert and F. E. Regnier, *J. Chromatogr.*, 185 (1979) 375.
- 14 M. A. Rounds, W. D. Rounds and F. E. Regnier, *J. Chromatogr.*, 397 (1987) 25.
- 15 C. P. Desilets, M. A. Rounds and F. E. Regnier, *J. Chromatogr.*, 544 (1991) 25.
- 16 F. Hesselink, *J. Phys. Chem.*, 73 (1969) 3488.
- 17 J. M. Scheutjens and G. J. Fleer, *J. Phys. Chem.*, 83 (1979) 1619.
- 18 P. G. de Gennes, *Macromolecules*, 14 (1981) 1637.
- 19 J. M. Scheutjens and G. J. Fleer, *Macromolecules*, 18 (1985) 1882.
- 20 I. D. Robb and R. Smith, *Eur. Polym. J.*, 10 (1974) 1005.
- 21 I. D. Robb and R. Smith, *Polymer*, 18 (1977) 500.
- 22 M. Kawaguchi, M. Hagakawa and A. Takahishi, *Polym. J.*, 12 (1980) 265.
- 23 K. Furusawa and K. Yamamoto, *Bull. Chem. Soc. Jap.*, 56 (1983) 1958.
- 24 H. Sakai and Y. Imamura, *Bull. Chem. Soc. Jap.*, 60 (1987) 1261.
- 25 G. J. Fleer and J. Lyklema, *Biol. Chem. Hoppe-Seyler*, 368 (1987) 741.
- 26 A. E. Ivanov, V. V. Saburov and V. P. Zubov, *Adv. in Polym. Sci.*, in press.
- 27 R. Axen, J. Porath and S. Ernback, *Nature (London)*, 214 (1967) 1303.
- 28 J. Porath, R. Axen and S. Ernback, *Nature (London)*, 215 (1967) 1491.
- 29 H. H. Weetall and C. C. Detar, *Biotechnol. Bioeng.*, 17 (1974) 295.
- 30 K. J. Ivin and T. Sacqusa, *Ring-Opening Polymerization*, Elsevier Applied Sci. Publ., London, New York, 1984.
- 31 L. Varady, Y.-B. Yang, S. E. Cook and F. E. Regnier, *US Pat.*, 5 030 352 (1991).
- 32 M. M. Bradford, *Anal. Biochem.*, 72 (1982) 248.
- 33 W. Kopaciewicz, S. Fulton and S.-Y. Lee, presented at the 6th International Symposium on HPLC of Proteins, Peptides and Polynucleotides, Baden-Baden, Oct. 20–22, 1986, abstract No. 807.

# High-performance liquid chromatography of amino acids, peptides and proteins

## CXXIV<sup>☆</sup>. Physical characterisation of fluidized-bed behaviour of chromatographic packing materials

Gopal Dasari, Ian Prince and Milton T. W. Hearn

*Centre for Bioprocess Technology, Monash University, Clayton, Victoria - 3168 (Australia)*

---

### ABSTRACT

Bed expansion characteristics of several different chromatographic sorbent materials have been studied in liquid–solid fluidized bed systems with different column diameters. The sorbents used were sized below particle diameters ( $d_p$ ) of 100  $\mu\text{m}$ , and most were non-spherical in shape. The effect of particle shape and size distribution on the bed expansion behaviour and the values of bed expansion index were evaluated in relation to existing empirical correlations of bed voidage and fluid velocity under laminar flow conditions. The effect of fluid properties on the bed behaviour was studied using viscous bovine amniotic fluid as the feed stock. An axial dispersion model was used to compare the liquid mixing behaviour of the fluidized bed system with two different particle sizes of porous silica in 2.24 cm I.D. and 5.0 cm I.D. columns. The results on the bed expansion characteristics with these systems are discussed in terms of the dispersion coefficient,  $D_x$  and the Peclet number  $N_{pe}$  for these sorbents fluidised under laminar flow conditions.

---

### INTRODUCTION

Since the late 1940s, liquid–solid fluidized beds have been widely used in many areas of the chemical industry, for example, in ion-exchange adsorption in wastewater management and hydrometallurgical operations. Extension of these techniques to biotechnological applications in the 1960s and 1970s met with limited success, partly due to the limitations with physical parameters, such as the small density differences between the liquid feedstock and the solid particle, but also due to the complexity of the feed stock composition. In recent years, however, there has been renewed interest in the applica-

tions of fluidized bed systems in biotechnological applications with the emergence of improved sorbents capable of exhibiting the desired physical and adsorptive characteristics.

Packed bed systems are the most commonly used configuration for the chromatographic separation of proteins. On a large scale, packed bed systems often pose considerable operational difficulties when large volumes of viscous fluids are involved. In addition, most feedstocks require clarification and removal of particulate matter (cell debris, etc.) to avoid clogging of the packed bed. Moreover, with industrial process bed systems, packed with the more widely used type of soft, deformable, adsorbent particles, flow-rates must be tightly constrained to avoid high operating pressures and concomitant bed compression. The application of fluidized bed systems conceptually thus offers a number of advantages over packed bed chromatographic columns for large-scale operation, particularly when large vol-

---

*Correspondence to:* Milton T. W. Hearn, Centre for Bioprocess Technology, Monash University, Clayton, Victoria 3168, Australia.

\* For Part CXXIII see ref. 38.

umes of fluid must be treated to isolate and purify a bioproduct which may be present in only very low concentrations.

Included in these potential advantages are: (i) High flow-rates are possible at comparatively low operational pressures. Low pressure drop operations allow much easier process scale-up and eliminate the need for high pressure pumping equipment. (ii) Pretreatment or removal of particulate/cellular matter from fermentation broths or biological fluids may not be necessary prior to adsorption. Since the adsorbent particles in the fluidized bed are separated from each other by upward (or downward) flow of the liquid, the broth solids may be able to pass through the bed without clogging. When used in this way, fluidized beds potentially eliminate the costly removal of solids by centrifugation or filtration (see for example refs. 1–8). (iii) Greater flexibility exists for continuous modes of operation under automated and semi-automated conditions. It is conceivable that after the initial adsorption stage is completed, the adsorbent material from the fluidized bed could be pumped out by increasing the fluid velocity, to a second fluidized column, where the washing of adsorbent can be carried out, and then pumped to a third column where the desorption of protein can be carried out.

Counter-balancing these advantages are potential problems whose magnitude remains unknown [1,4] but include the potential for reduced bed capacity, unfavourable mixing at some liquid flow-rates, particle size segregation and adventitious particulate loading.

Preliminary studies on fluidized beds in this and other laboratories [2,3,5,7–9] have demonstrated the feasibility of the technique for the fractionation of proteins and other biotechnological products. Except for one study where a magnetically stabilized fluidized bed was used [2], systems previously studied have typically employed low density, soft gels (*i.e.*, densities not dissimilar to those of the fluidizing liquid), and relatively large particles ( $>100 \mu\text{m}$ ) with wide size distribution. Nevertheless, the substantial economic advantage that may accrue in large-scale operation has been demonstrated recently with therapeutic proteins [10] as well as with the whole broth extraction of the antibiotic immunomycin [6]. With the advent of high density adsorbent particles, specifically developed in narrow size ranges

for fluidized applications, and their further refinement and surface modification in these laboratories [11] and elsewhere (see for example ref. 12), the performance characteristics of fluidization systems in biotechnological application are likely to be further enhanced in the near future.

The bed expansion characteristics of liquid–solid fluidized bed systems in various traditional chemical applications have been studied by many investigators [13–21]. Almost invariably large particles ( $d_p > 100 \mu\text{m}$ ) have been used. Various applications of these large particle systems have been reviewed by Joshi [22]. Many correlations have been proposed from these investigations to establish a velocity–voidage relationship for fluidization and sedimentation with these liquid–solid systems. The majority of these correlations are applicable over a restricted range of Reynolds numbers. Among all, the correlation of Richardson and Zaki [16] has received particularly widespread recognition and use. For fluidized beds of homogeneous rigid spherical particles, these authors have proposed that the relationship between the liquid superficial velocity  $U$ , and the terminal settling velocity in infinite medium,  $U_i$ , can be given by

$$\frac{U}{U_i} = \varepsilon^n \quad (1)$$

where

$$\log U_i = \log U_t - \frac{d_p}{D} \quad (2)$$

and  $U_t$  is the particle terminal settling velocity,  $\varepsilon$  is the bed voidage,  $d_p$  is the particle diameter, and  $D$  is the column diameter.

The bed expansion index,  $n$ , is a function of the terminal settling Reynolds number ( $N_{\text{Ret}}$ ) and the particle to bed diameter ratio, ( $d_p/D$ ), such that over the range  $0.2 < N_{\text{Ret}} < 500$  the value of  $n$  can be approximated by:

$$\begin{aligned} n &= 4.65 + 20 (d_p/D) && (N_{\text{Ret}} < 0.2) \\ n &= 4.4 + 18 (d_p/D) N_{\text{Ret}}^{-0.03} && (0.2 < N_{\text{Ret}} < 1) \\ n &= 4.4 + 18 (d_p/D) N_{\text{Ret}}^{-0.1} && (1 < N_{\text{Ret}} < 200) \\ n &= 4.4 N_{\text{Ret}}^{-0.1} && (200 < N_{\text{Ret}} < 500) \\ n &= 2.4 && (N_{\text{Ret}} > 500) \end{aligned}$$

For spherical particles greater than  $100 \mu\text{m}$  in average diameter, fluidized in large diameter tubes,

the values of  $n$  range between 2.39 for large  $N_{Ret}$  values and 4.65 for  $N_{Ret} < 0.2$ . Recently, Rowe [23] developed a logistic curve for the above correlation and related  $n$  and  $N_{Ret}$ , for cases where the particle size is small compared to column diameter, as a continuous function encompassing laminar through to turbulent flow regimes. However, with small ( $d_p < 100 \mu\text{m}$ ) spherical [24] and non-spherical particles [18], larger values of  $n$  have been obtained compared to the values predicted by eqn. 2. In particular, the study of Jottrand [18] has shown that for finely crushed sands, with particle sizes ranging from 20 to 113  $\mu\text{m}$ , fluidized in water, a constant value of  $n = 5.6$  was observed in the laminar flow range,  $0.004 < N_{Ret} < 0.7$ , which is substantially lower than the range investigated by Richardson and Zaki [16].

Fouda and Capes [21] have proposed a modified form of the Richardson and Zaki [16] correlation, namely

$$\frac{U}{U_t} = [1 - k(1 - \epsilon)]^n \quad (3)$$

to account for non-spherical shapes of the particles, with similar relations between  $n$  and  $N_{Ret}$  applying for spherical particles. The parameter  $k$  was introduced to account for the effective hydrodynamic volume of the particles during fluidization.

Data on axial dispersion effects in fluidized beds are scarce, with only a limited number of studies [25–31] having been performed with spherical particles above 100  $\mu\text{m}$  in average particle diameter. No general correlation for axial dispersion coefficients in liquid–solid fluidized beds, which incorporates the effects of liquid velocity, particle size and column diameter, is currently available. However, Gunn [28] has discussed the results of Kramers *et al.* [25], Bruinzeel *et al.* [26], and Cairns and Prausnitz [27] in terms of the Peclet number ( $N_{Pe} = UL/D_x$ ) and the Reynolds number ( $N_{Re} = d_p U \rho / \mu$ ) for the purpose of comparison (where  $L$  = axial distance of fluidized bed,  $\rho$  = fluid density and  $\mu$  = fluid viscosity). The effect of the ratio of the column to particle diameter encompassing the range  $17 < (D/d_p) < 50$  on liquid mixing has been documented in the results of two studies [25,27] whilst the results of Bruinzeel *et al.* [26] indicate that there was no effect of the  $D/d_p$  ratio on liquid mixing over the range,  $500 < (D/d_p) < 5000$ . No general correlation between Peclet number and the Reynolds number has emerged from these three

studies. Chung and Wen [29] studied the axial liquid mixing in fluidized and fixed beds using sinusoidal and pulse response techniques with a fluorescein dye as a tracer. A systematic study of fluidization of glass, aluminium and steel particles ( $d_p$  in the range 0.20–0.64 cm) in water in a 5.08-cm I.D. column was carried out by these investigators. For the Reynolds number ranging from 51 to 1286, they obtained values of Peclet numbers in the range of 0.1 to 0.91. Moreover, these investigators found that the dispersion coefficient increased with increases in liquid velocity for constant particle density. From these experimental data and other data from the literature, a correlation of liquid axial dispersion coefficients of fixed and fluidized beds in terms of Peclet number and Reynolds number was developed by Chung and Wen [29]. Recently, Webster and Perona [30,31] have studied the liquid mixing characteristics in cylindrical and tapered liquid–solid fluidized beds with three particle sizes of glass (average  $d_p$  114, 440 and 1210  $\mu\text{m}$ ) and 320  $\mu\text{m}$  size coal particles. Their results show that the dispersion coefficient decreased for 114  $\mu\text{m}$  size glass and for 320  $\mu\text{m}$  size coal particles but increased for bigger size particles of glass with increasing void fraction or liquid velocity in a cylindrical column. However, they found that the Peclet number also increased Reynolds numbers.

The rheological characteristics of biological fluids can be anticipated to have considerable bearing on the design and the operation of a fluidized bed system for protein recovery and purification processes. An increase in fluid viscosity would decrease the range of liquid velocities achievable in the fluidized bed, since the terminal settling velocity of particles is inversely related to the viscosity of the fluid. In addition, the fluid characteristics play an important role in the mixing behaviour, and mass transfer. These effects will impact on the detector or biosensor responses required for the on-line control monitoring of the bioprocessing of crude feedstocks during scale-up procedures [32].

In order for the full potential of fluidized systems to be evaluated for biorecovery and biopurification tasks, fundamental characterisation of these systems must be achieved. This study examines the fluidized bed characteristics, in terms of bed expansion and liquid mixing as a function of liquid superficial velocity, with various sizes of chromatographic sor-

bent materials of spherical and non-spherical particles suspended in columns of different internal diameters. The effect of liquid properties on bed expansion behaviour was also studied using bovine amniotic fluid.

## EXPERIMENTAL

### Materials

Lichroprep Si 60 (average pore size 6 nm) silica in two types of particle size range, 25–40  $\mu\text{m}$  and 40–63  $\mu\text{m}$ ; Lichroprep-diol (average pore size 6 nm), derivatised silica 40–63  $\mu\text{m}$ ; Fractosil 1000 (average pore size 100 nm) silica 63–100  $\mu\text{m}$  and Fractogel TSK HW55(F) (pores could accommodate up to 90 000 molecular mass proteins), 32–63  $\mu\text{m}$  were obtained from E. Merck (Darmstadt, Germany). Fluorescein (water soluble) tracer was obtained from Selbys (Melbourne, Australia). Bovine amniotic fluid was supplied by Filtron (Melbourne, Australia).

### Methods

Particle size analysis for all the sorbent samples was performed using a Malvern 2600 particle sizer. The Sauter mean diameter (S.M.D.) was computed based on the size distribution by weight percent in each size range.

Viscosity measurements were performed using a Contraves Low Shear 30 sinus rheometer with temperature control arrangement. This rheometer is capable of measuring the rheological properties of low viscosity fluids in both the steady and oscillatory modes yielding data such as shear stress, storage modulus and loss modulus. The shear rate ranges from 0.02 to 118.2  $\text{s}^{-1}$ , with different bob and cup geometry, with 1–3 ml sample holding capacity. The viscosity of bovine amniotic fluid was measured at 20°C.

Particle density of porous silica gels and Fractogel in water were measured by the displacement method. A known amount of gel was soaked in water and degassed, then the gel was filtered using vacuum suction pump at 3333 Pa to remove the interstitial water. A known amount (25 g) of this gel was placed in a measuring cylinder and the total volume was measured by adding 20 ml of water to the gel. The displaced volume is equivalent to the volume of the gel. The particle density calculation

was based on the known weight and the volume of the gel. The density of amniotic fluid was measured using a specific gravity bottle at 20°C.

### Fluidized bed studies

Fig. 1 is a schematic diagram showing the experimental set-up used in the bed expansion characteristics and residence time distribution (RTD) studies. Two columns of 100  $\text{cm}^3$  (2.24 cm I.D.  $\times$  26 cm) and 200  $\text{cm}^3$  (2.34 cm I.D.  $\times$  54 cm) volume, made of polycarbonate material, and one column of 1000  $\text{cm}^3$  (5 cm I.D.  $\times$  60 cm) volume, made of glass using an adapted Pharmacia K 50 column (Pharmacia Aust., Sydney, Australia), were used in these studies. All these columns had a bottom distributor section, filled with glass beads ( $d_p$  250  $\mu\text{m}$ ), to permit uniform distribution of the liquid into the column. The adjustable adaptors at the top on the columns were fitted with 10  $\mu\text{m}$  nylon filters to prevent the loss of sorbent particles. Except where bovine amniotic fluid was used, all other studies were performed with distilled water as a liquid medium at 22°C.

### Measurement of degree of mixing or dispersion

The degree of mixing or dispersion in a fluidized bed was determined using residence time distribu-

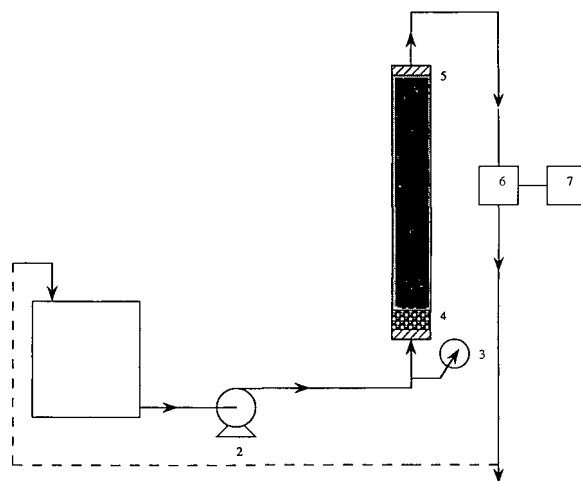


Fig. 1. Schematic diagram of a fluidized bed set up: 1 = feed tank, 2 = pump, 3 = pressure gauge, 4 = distributor, 5 = adjustable adaptor with retention filter, 6 = spectrophotometer with flow cell arrangement, 7 = chart recorder.

tion (RTD) studies. The pulse injection technique has been used, employing fluorescein as a tracer. To achieve a good tracer pulse injection, a micro-syringe was used to inject 100  $\mu\text{l}$  of fluorescein (5 mg/ml) under stable bed conditions. The adaptors at the top of fluidized columns were adjusted close to the expanded bed upper surface to avoid dead space effects in the columns. The effluent was recorded continuously at a wavelength of 490 nm using a spectrophotometer (LKB, Ultrospec-II) with flow cell arrangement. These studies were performed in two different column diameters with various amounts of porous silica gel (Lichroprep Si 60) with two particle size ranges.

The axial dispersion model [33] was used to estimate the degree of liquid dispersion in the fluidized bed system. The extent of mixing was measured by calculating the dispersion number ( $D_x/UL$ ) from the data of the tracer response curves. The axial dis-

person number estimation was based on the closed vessel situation since the techniques used for injection and dispersion sampling represent the closed vessel boundary conditions.

## RESULTS AND DISCUSSION

### Bed expansion characteristics

The ratio of height of the expanded bed to the settled bed ( $H_L/H_0$ ) with increasing liquid velocities ( $U$ ) for all the studied sorbent materials and the columns of different diameters is plotted in Fig. 2. The results evident from these ( $H_L/H_0$ ) versus  $U$  plots clearly indicate that the operating range of liquid velocities for the Fractogel TSK HW55F is very narrow due to its low particle density. On the other hand, the velocity range for Fractosil 1000 material is rather broad, due to its higher particle density and larger particle size range compared to Fractogel TSK HW55F or other sorbents. The bed expansion results for Lichroprep Si 60 in two particle size distributions show the effect of particle size on the operating range of liquid velocities that can

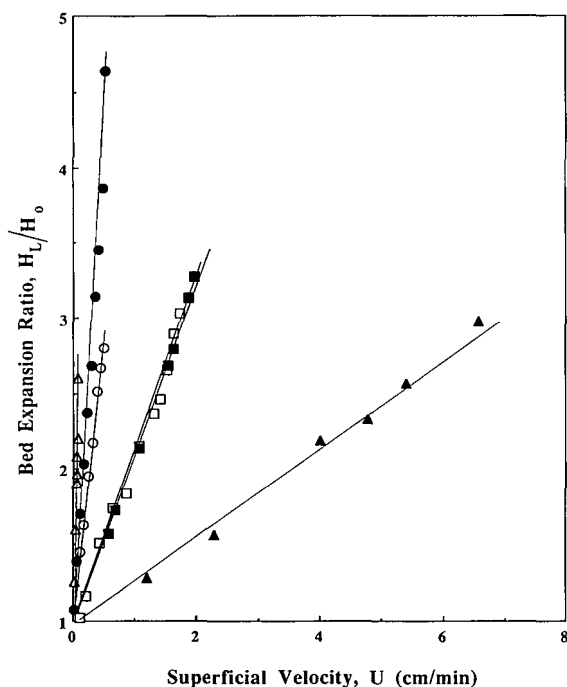


Fig. 2. Fluidized bed expansion characteristics in columns with varying diameters using different chromatographic materials. (○) 25–40  $\mu\text{m}$ , Lichroprep Si 60, 2.24 cm I.D.; (□) 40–63  $\mu\text{m}$  Lichroprep Si 60, 2.24 cm I.D.; (●) 25–40  $\mu\text{m}$ , Lichroprep Si 60, 5.00 cm I.D.; (■) 40–63  $\mu\text{m}$ , Lichroprep Si 60, 5.00 cm I.D.; (△) 32–63  $\mu\text{m}$ , Fractogel TSK HW 55F, 2.34 cm I.D.; (▲) 63–100  $\mu\text{m}$ , Fractosil 1000, 2.34 cm I.D.

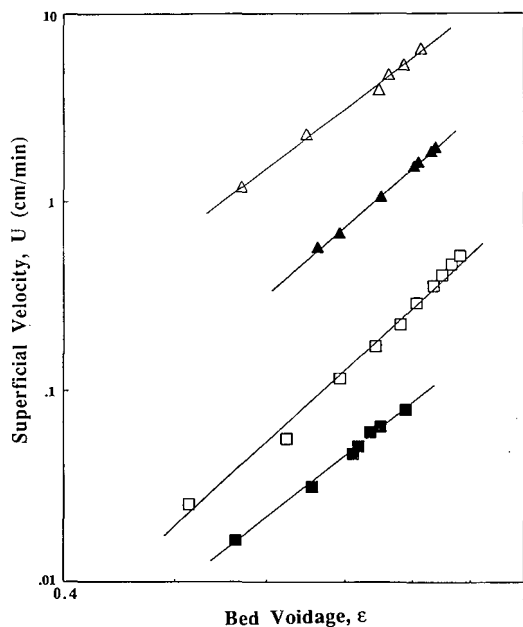


Fig. 3. Liquid superficial velocity versus bed voidage for different chromatographic materials. (□) Lichroprep Si 60, 25–40  $\mu\text{m}$ ; (▲) Lichroprep Si, 40–63  $\mu\text{m}$ ; (■) Fractogel TSK HW 55F, 32–63  $\mu\text{m}$ ; (△) Fractosil 1000, 63–100  $\mu\text{m}$ .

TABLE I  
PHYSICAL PROPERTIES AND BED EXPANSION CHARACTERISTICS OF PARTICLES

	Particle size range ( $\mu\text{m}$ )	Mean diameter ( $\mu\text{m}$ )	Shape	Shape factor ( $\phi$ )	Particle density ( $\text{g}/\text{cm}^3$ )	$N_{\text{Ret}}$	Bed expansion index ( $n$ )
Richardson and Zaki [16] Jottrand [18]	<sup>a</sup>	> 100	Spherical	1.00	<sup>a</sup>	< 0.2	4.65
	<sup>a</sup>	20.2	Angular (crushed sand)	0.73	2.685	0.004 <sup>b</sup>	5.60
		28.7	Angular (crushed sand)	0.73	2.685	0.012	5.60
		43.1	Angular (crushed sand)	0.73	2.685	0.039	5.60
		63.0	Angular (crushed sand)	0.73	2.685	0.111	5.60
		86.2	Angular (crushed sand)	0.73	2.685	0.312	5.60
		113.0	Angular (crushed sand)	0.73	2.685	0.706	5.60
		24.9	Angular	0.73	1.345	0.001	5.77 $\pm$ 0.56 <sup>c</sup>
		62.9	Angular	0.73	1.361	0.019	5.27 $\pm$ 0.28 <sup>c</sup>
		61.9	Angular	0.73	1.311	0.016	5.02
LiChroprep Si 60	24-50		Angular	0.73	1.389	0.044	4.68
LiChroprep-diol	40-63		Angular	0.73	1.087	0.005	4.74
Fractosil 1000	63-100		Angular	0.73			
Fractogel	32-63		Spherical	1.00			
TSK HW55(F)							

<sup>a</sup> Not reported by these investigators.

<sup>b</sup>  $N_{\text{Ret}}$  values were calculated based on Jottrand's data assuming  $\phi_s = 0.73$ , for the purpose of comparison.

<sup>c</sup> Standard deviation.

be obtained in two columns of different diameters. The results also indicate that the effect of column diameter on the bed expansion behaviour is negligible.

The bed voidage *versus* liquid velocity data for all the sorbent materials exhibited linear relationships in their log–log plots (Fig. 3). The slope of these plots yields the bed expansion index ( $n$ ), whilst extrapolation of the data to  $\varepsilon = 1$  yields  $U_t$ , the terminal settling velocity of the particle. The values of  $n$  are presented in Table I along with other values of  $n$  available in the literature and the physical properties of the materials used. The mean diameters of the particles used for the calculations of the present study were based on Sauter mean diameter of the particles, measured using the Malvern 2600 laser based particle sizer. The values of  $n$  varied from 5.77 to 4.68 for the angular silica gels and was 4.74 for spherical shaped Fractogel beads.

Except for Jottrand's work [18], there appear to be no other data in the literature on bed voidage–velocity relationships for small particles ( $d_p < 113 \mu\text{m}$ ) of non-spherical shape (Table I). In this earlier study a single value of  $n = 5.6$  was obtained for all the particle sizes of crushed sand used in liquid–solid fluidization experiments. Our results indicate that the value of  $n$  increases with the decrease in size of particles of similar shape characteristics, *e.g.*  $n = 4.68$  to 5.77 for particles with average  $d_p$  ranging from 25 to 81  $\mu\text{m}$  respectively. These  $n$  values correspond closely to the literature  $n$  values for larger particles. For example, the value of  $n$  reported by Richardson and Zaki [16] for spherical particles ( $d_p > 100 \mu\text{m}$ ) at  $N_{\text{Ret}} < 0.2$ , was 4.65 based on the experimental data from sedimentation and fluidization studies with a large number of particle sizes of different densities and with liquids of various viscosities. Richardson and Meikle [24] found with sedimentation experiments involving the suspension of spheres ( $d_p < 100 \mu\text{m}$ ) that  $N_{\text{Ret}}$  was less than 0.2, and the mean value of  $n$  was 4.79. These investigators also reported that for fine alumina particles ( $d_p 5.5 \mu\text{m}$ ), the value of  $n$  was 10.5. However, Fouda and Capes [21], in studies on the effect of the particle shape factor on bed expansion characteristics, used various materials of different densities and particles sizes more than 137  $\mu\text{m}$  in diameter except for one crushed silica with particle size of  $d_p 52 \mu\text{m}$  and obtained lower  $n$  values.

Based on their correlation and values of  $k$  calculated for the crushed silica of  $d_p 52 \mu\text{m}$ , the maximum value of  $n$  was found to be only 4.49.

The larger values of  $n$  obtained in the present investigation for small particles with irregular shapes may be due to the higher levels of immobile fluid trapped with the solids due to particle agglomeration, occlusion in surface irregularities or simply due to the increased volume of the boundary layer relative to the particle volume. This concept has been early proposed by Steinour [34–36] to account for the involvement of similar effects in the sedimentation of fine spherical, irregular and flocculated particles. This explanation may not however be valid for larger particles, as evident from our result with Fractosil 1000, where  $n = 4.68$  is close to the value reported by Richardson and Zaki [16]. Their  $n$  value also fits reasonably well with our data for spherical shaped Fractogel beads (Table I).

The effect of fluid viscosity on bed expansion behaviour was studied using bovine amniotic fluid,  $\mu = 1.454$  centipoise, using Lichroprep-diol porous silica ( $d_p 40\text{--}63 \mu\text{m}$ ). The rationale behind the selection of bovine amniotic fluid for this study arose from our interest in separation and purification of pharmaceutically important growth factors from this feed-stock source [11]. Amniotic fluid comprises a complex mixture of proteins and polysaccharides. The rheological and compositional characteristics of this fluid have been determined and the results are presented in another manuscript [37]. The bed expansion results indicate a pseudoplastic behaviour. The data of shear stress and shear rate was best represented by a power law fluid. The results on these investigations are presented in Fig. 4A and B. The value of  $n$  for Lichroprep-diol silica with amniotic fluid was found to be 7.75 whilst the value with water was 5.02. The liquid properties, the values of Reynolds number based on particle terminal settling velocity and  $n$  are presented in Table II. The values of  $n$  obtained for angular silica gels indicate that there is a linear dependency on the particle size for the range of particles tested under the same fluidization conditions (Fig. 5). There also appears to be a linear relation between  $n$  and  $N_{\text{Ret}}$  for the range of Reynolds numbers studied.

#### Liquid mixing studies

These studies were conducted with two particle



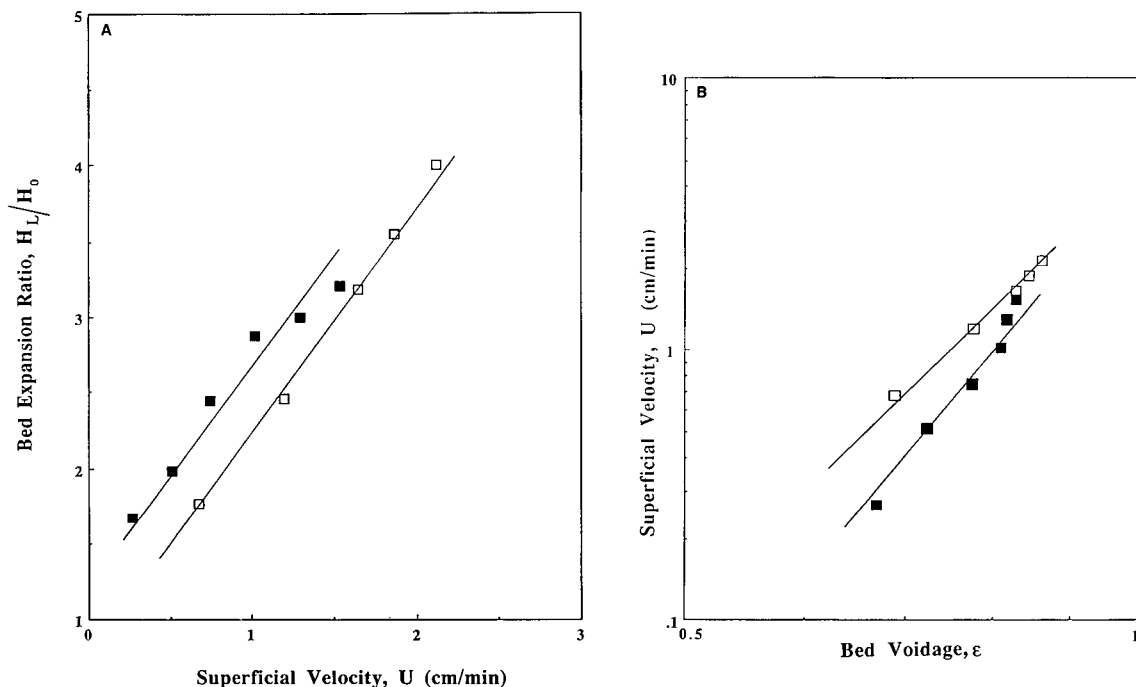


Fig. 4. (A) Effect of fluid viscosity on bed expansion characteristics: Lichroprep-diol ( $d_p$  40–63  $\mu\text{m}$ ) with water and bovine amniotic fluid. (B) Effect of fluid viscosity on bed voidage: Lichroprep-diol ( $d_p$  40–63  $\nu$ ) with water and bovine amniotic fluid. ( $\square$ ) Water, ( $\blacksquare$ ) bovine amniotic fluid.

sizes of the Lichroprep Si 60 porous silica in two fluidized columns of different diameter. The data on dispersion coefficient *versus* superficial velocity are presented in Fig. 6. These plots reveal that the dispersion coefficient increases with the increasing superficial velocity. Similar observations for large spherical particles in liquid–solid fluidization systems have been reported by Cairns and Prausnitz [27], Kramers *et al.* [25] and Chung and Wen [29]. However, Webster and Perona [30] observed that the dispersion coefficient for 114  $\mu\text{m}$  size glass and

320  $\mu\text{m}$  size coal particles decreased with increasing bed voidage or superficial velocity but increased for bigger size glass particles. It has also been observed in the present study with small size particles ( $d_p$  25–40  $\mu\text{m}$ ) that the dispersion coefficients are higher than obtained with bigger particles in the same column system. Chung and Wen [29] noted that the effect of very large particle size (average  $d_p$  2032–6350  $\mu\text{m}$ ) on dispersion coefficients with increasing velocity was not significant. As evident from our results with silica based sorbents, there is a notice-

TABLE II

EFFECT OF LIQUID PROPERTIES ON BED EXPANSION INDEX WITH LICHROPREP-DIOL SILICA GEL (40–63  $\mu\text{m}$ )

Liquid	Viscosity (centipoise)	Density ( $\text{g}/\text{cm}^3$ )	$N_{\text{Ret}}$	Bed expansion ( $n$ )
Water	1.000	1.000	0.016	5.02
Bovine amniotic fluid	1.454	1.013	0.020	7.75

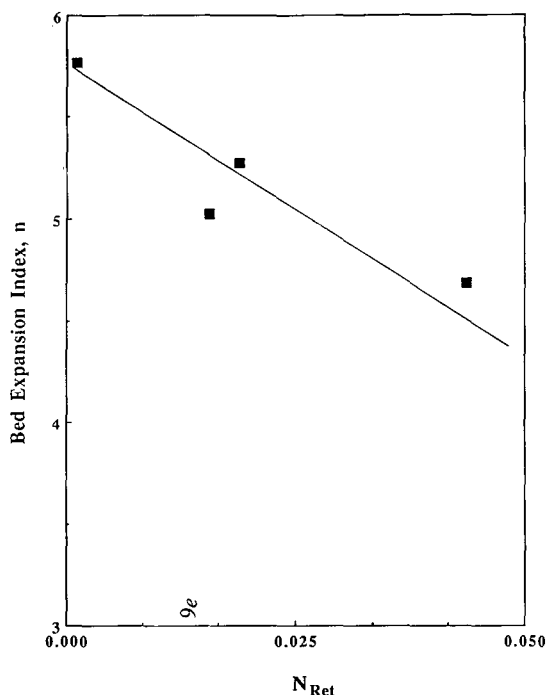


Fig. 5. Bed expansion index,  $n$  versus particle Reynolds number for angular silicas.

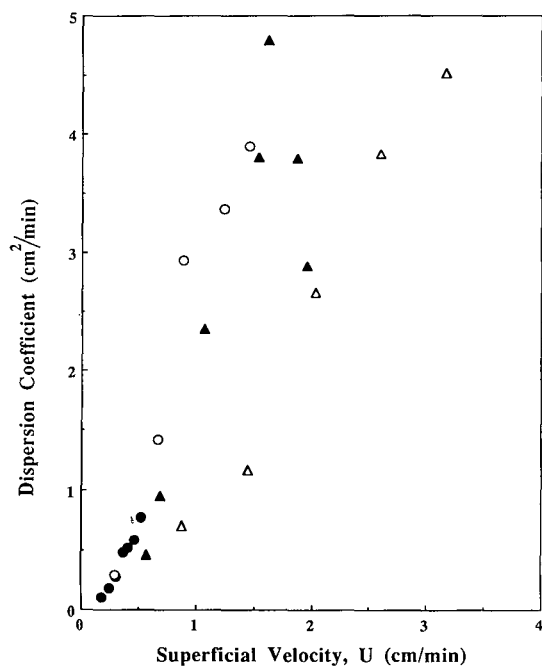


Fig. 6. Dispersion versus liquid velocity in fluidized beds with varying column diameter using Lichroprep Si 60 silica. (○) 25–40  $\mu\text{m}$ , 5.00 cm I.D.; (●) 25–40  $\mu\text{m}$ , 2.24 cm I.D.; (△) 40–63  $\mu\text{m}$ , 5.00 cm I.D.; (▲) 40–63  $\mu\text{m}$ , 2.24 cm I.D.

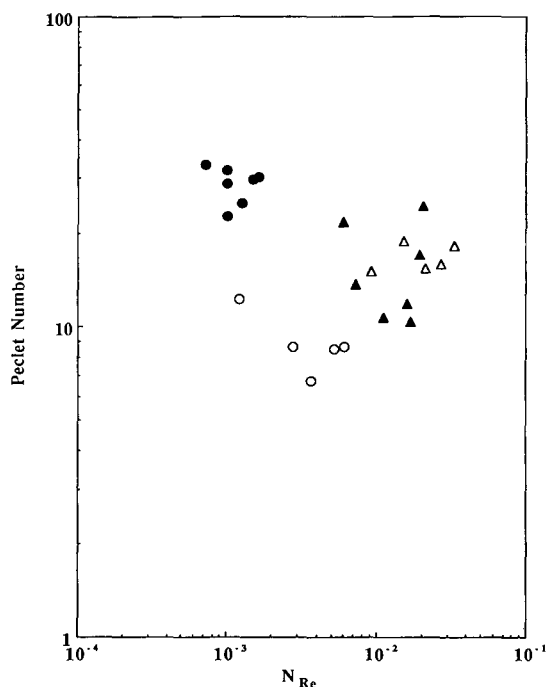


Fig. 7. Peclet number versus Reynolds number in fluidized beds with varying column diameter using Lichroprep Si 60 silica. (○) 25–40, 2.24 cm I.D.; (●) 40–63  $\mu\text{m}$ , 2.24 cm I.D.; (△) 25–40  $\mu\text{m}$ , 5.00 cm I.D.; (▲) 40–63  $\mu\text{m}$ , 5.00 cm I.D.

able effect of the  $(D/d_p)$  ratio on dispersion coefficient with increasing velocities or bed voidage. The mixing data has also been evaluated in terms of Peclet number and Reynolds number based on the fluid velocity for both particle sizes. These results indicate that for the range of Reynolds numbers tested in the present study the mixing behaviour is in the regime of dispersed-plug flow. Although liquid mixing appears to be higher for small particles compared to larger particles in the 2.24 cm I.D. column, the difference in the 5 cm I.D. column is not significant (Fig. 7).

#### CONCLUSIONS

The bed expansion characteristics have been studied for several microparticulate angular silicas, and spherical particles of Fractogel, in terms of bed expansion and bed voidage as a function liquid superficial velocity. The higher values of bed expansion index ( $n$ ) obtained for the smaller silicas could

be due to the irregular shape of the particles. The bed expansion index was found to be linearly related to the particle Reynolds number over the range tested. The liquid mixing studies performed in 2.24 and 5 cm I.D. columns with two particle sizes ( $d_p$  25–40 and 40–63  $\mu\text{m}$ ) of silica exhibited dispersed-plug flow characteristics under laminar flow conditions. In associated publications, the use of these parameters in the design and application of expanded bed systems with silica-based affinity sorbents for the large scale fractionation of proteins from natural and recombinant DNA feedstock sources will be described.

#### ACKNOWLEDGEMENTS

These investigations were supported by the Industrial Research and Development Board, Australian Department of Industry, Trade and Commerce, and Monash University Research Fund.

#### REFERENCES

- 1 A. Buijs and J. A. Wesselingh, *J. Chromatogr.*, 201 (1980) 319.
- 2 M. A. Burns and D. J. Graves, *Biotechnol. Prog.*, 1 (1985) 95.
- 3 C. M. Wells, A. Lyddiatt and K. Patel, in M. S. Verral and M. J. Hudson (Editors), *Separation for Biotechnology*, Ellis Horwood, Chichester, 1987, pp. 217–224.
- 4 C. H. Lochmuller, C. S. Ronsick and L. S. Wigman, *Prep. Chromatogr.*, 1 (1988) 93.
- 5 W. Somers, K. van 't Reit, H. Rozie, F. M. Rombouts and J. Visser, *Chem. Eng. J.*, 40 (1989) B47.
- 6 F. P. Gailliot, C. Gleason, J. J. Wilson and J. Zwarick, *Biotechnol. Prog.*, 6 (1990) 370.
- 7 N. Drager and H. Chase, *Inst. Chem. Eng. Symp. Ser.*, 118 (1990) 161.
- 8 H. Chase and N. Drager, *J. Chromatogr.*, 597 (1992) 129.
- 9 G. Dasari, G. Finette, I. Prince and M. T. W. Hearn, *Aust. J. Biotechnol.*, 10 (1992) 312.
- 10 M. T. W. Hearn, G. Dasari, I. Prince, M. Bjorklund and G. Finette, *Patents Pending* (1991).
- 11 M. T. W. Hearn, M. Gani, P. Chen and P. Rossiter, *Patents Pending* (1992).
- 12 K. K. Unger, in K. K. Unger (Editor), *Packings and Stationary Phases in Chromatographic Techniques*, Marcel Dekker, New York, 1990.
- 13 R. H. Wilhelm and M. Kwauk, *Chem. Eng. Prog.*, 44 (1948) 201.
- 14 W. K. Lewis, E. R. Gilliland and W. Bauer, *Ind. Eng. Chem.*, 41 (1949) 1104.
- 15 W. K. Lewis and E. W. Bowerman, *Chem. Eng. Prog.*, 48 (1952) 603.
- 16 J. F. Richardson and W. N. Zaki, *Trans. Inst. Chem. Eng.*, 32 (1954) 35.
- 17 A. L. Loeffler and B. F. Ruth, *AIChE J.*, 5 (1959) 310.
- 18 R. Jottrand, *J. Appl. Chem. (London)*, 2 Suppl. Issue I, (1952) S17-S26.
- 19 C. Y. Wen and Y. H. Yu, *Chem. Eng. Prog. Symp. Ser.*, 62 (1966) 100.
- 20 J. Garside and M. R. Al-Dibouni, *Ind. Eng. Chem. Process Des. Dev.*, 16 (1977) 206.
- 21 A. E. Fouda and C. E. Capes, *Can. J. Chem. Eng.*, 55 (1977) 386.
- 22 J. B. Joshi, *Chem. Eng. Res. Des.*, 61 (1983) 143.
- 23 P. N. Rowe, *Chem. Eng. Sci.*, 42 (1987) 2795.
- 24 J. F. Richardson and R. A. Meikle, *Trans. Inst. Chem. Eng.*, 39 (1961) 348.
- 25 H. Kramers, M. D. Westermann, J. H. de Groot and F. A. Dupont, *3rd Cong. Eur. Fed. Chem. Eng.*, Olympia, London, 1962, pp. 114–119.
- 26 C. Bruinzeel, G. H. Reman and E. Th. van der Laan, *3rd Cong. Eur. Fed. Chem. Eng.*, Olympia, London, 1962, pp. 120–126.
- 27 E. J. Cairns and J. M. Prausnitz, *AIChE J.*, 6 (1960) 400.
- 28 D. J. Gunn, *The Chemical Engineer*, London, CE153, 1968, p. 219.
- 29 S. F. Chung and C. Y. Wen, *AIChE J.*, 14 (1968) 857.
- 30 G. H. Webster and J. J. Perona, *AIChE Symp. Ser.*, 86 (276) (1987) 104.
- 31 G. H. Webster and J. J. Perona, *AIChE J.*, 34 (1988) 1398.
- 32 M. Charles, *Adv. Biochem. Eng.*, 8 (1978) 1.
- 33 O. Levenspiel, *Chemical Reaction Engineering*, Wiley, New York, 2nd ed., 1972.
- 34 H. H. Steinour, *Ind. Eng. Chem.*, 36 (1944) 901.
- 35 H. H. Steinour, *Ind. Eng. Chem.*, 36 (1944) 840.
- 36 H. H. Steinour, *Ind. Eng. Chem.*, 36 (1944) 618.
- 37 G. Dasari, I. Prince and M. T. W. Hearn, in preparation.
- 38 A. W. Purcell, M. I. Aguilar and M. T. W. Hearn, *Anal. Chem.*, (1992) in press.

# Selectivity of organic solvents in micellar liquid chromatography of amino acids and peptides

Alireza S. Kord<sup>\*</sup> and Morteza G. Khaledi

*Department of Chemistry, North Carolina State University, Raleigh, NC 27695-8204 (USA)*

---

## ABSTRACT

The influence of the type of organic modifiers on retention behavior in micellar liquid chromatography is studied. A group of amino acids and small peptides was used as the test mixture. It is shown that the chromatographic selectivities of 2-propanol, acetonitrile and tetrahydrofuran which belong to three different groups in Snyder's classification, are considerably similar in the presence of micelles for the test mixture. On the other hand, the selectivities of 2-propanol and butanol which belong to the same solvent selectivity group are different for these solutes in the micellar mobile phases.

---

## INTRODUCTION

At the present time reversed-phase liquid chromatography (RPLC) using *n*-alkyl bonded phases is the most frequently used technique for separation of non-volatile compounds [1]. One of the advantages of this technique is the feasibility of manipulating retention by a careful selection of mobile phase parameters [2,3]. The most important among these parameters are type and concentration of organic solvents, pH, and addition of surfactant. Organic modifiers are used in the RPLC mobile phases to control the solvent strength as well as to improve selectivity [4].

A widely accepted technique for characterizing of LC solvents is the Snyder's selectivity triangle [3,5]. This technique classifies various organic solvents on the basis of their relative ability to engage in proton accepting, proton donating and strong dipolar interactions. When the resulting values are plotted on three axes in the form of a triangle, solvents having

similar functionalities tend to fall within the same area of the triangular plot. In principle, the solvents grouped in the same area of the triangle should have similar chromatographic selectivity, while solvents from other groups should exhibit different selectivity for a given separation [5]. This theory has been widely accepted and has often formed the rationale for solvent selection for optimizing a given HPLC separation [6–10].

The use of secondary chemical equilibria in RPLC has greatly extended its separation capability [11]. A good example of these secondary equilibria is micellar liquid chromatography (MLC). The retention of a solute in MLC is determined by three competing equilibria among micelle, bulk aqueous solvent and stationary phase. It has been demonstrated that the use of organic modifiers in MLC has a great influence on chromatographic behavior [12–18]. In previous papers, we reported a rather unique phenomenon of simultaneous enhancement of solvent strength and selectivity in MLC through optimizing the concentrations of an organic modifier and micelles [13–18]. However, adequate attention has not been paid to the chromatographic selectivity of different organic solvents in the presence of micelles. In this paper, the results of an explor-

---

*Correspondence to:* M. G. Khaledi, Department of Chemistry, North Carolina State University, Raleigh, NC 27695-8204, USA.

<sup>\*</sup> Present address: Mallinckrodt Medical Inc., 675 McDonnell Boulevard, P.O. Box 5840, St. Louis, MO 63134, USA.

tory study on the chromatographic selectivity of organic solvents in micellar media are described.

## EXPERIMENTAL

### Apparatus

The HPLC system consisted of a pump (Model 400; Applied Biosystems, Foster City, CA, USA) and a variable-wavelength absorbance detector (Model 783 A, Applied Biosystems) set at 210 nm, controlled by Chemresearch chromatographic data management system controller software (ISCO, Lincoln, NE, USA) running on a PC-88 Turbo personal computer (IDS, Paramount).

The retention behavior of individual solutes was studied using a 5- $\mu$ m particle size Ultremex C<sub>18</sub> column (Phenomenex, Torrance, CA, USA), 100  $\times$  4.6 mm I.D. The column dead volume (0.6 ml) was measured by making multiple injections of water samples. The test mixture was separated using a longer (250  $\times$  4.6 mm I.D.) Ultremex column (dead volume: 2.1 ml) in order to generate larger number of theoretical plates. The columns were thermostated at 40°C by a water circulator bath (Lauda Model MT-6; Brinkmann Instruments, Westbury, NY, USA). A silica precolumn was used to saturate the mobile phase with silicates and to protect the analytical column.

The software used to evaluate the separation at different mobile phase compositions was based on an extended version of the iterative regression optimization strategy [17–20]. The simulated chromatograms are based on a Gaussian peak shape, using the plate-count and dead volume observed in chromatographic experiments.

### Reagents

The stock solution of sodium dodecyl sulfate (SDS) was prepared by dissolving the required amount of surfactant in doubly distilled deionized water and filtering through a 0.45- $\mu$ m nylon membrane filter (Gelman, Ann Arbor, MI, USA). The test solutes were: (1) tyrosine (Y), (2) methionine (M), (3) alanyl-tyrosine (AY), (4) tryptophan (W), (5) aspartyl-phenylalanine (DF), (6) leucyl-tyrosine (LY), (7) glycyl-leucyl-tyrosine (GLY), (8) leucyl-tryptophan (LW) and (9) phenylalanyl-phenylalanine (FF). The sample solutions were prepared by diluting stock solutions (10 mg/ml in water or tetra-

hydrofuran) in the mobile phase. The ionic strength was adjusted by adding phosphate buffer such that the total buffer concentration in the final concentration was 0.02 M. After adding the required amount of 2-propanol the pH was adjusted to 2.5.

## RESULTS AND DISCUSSION

In the following sections, the influence of four organic modifiers on the chromatographic behavior of a group of amino acids and small peptides in MLC will be discussed. The organic solvents are 2-propanol (PROH) and butanol (BUOH) (which both belong to group II of Snyder's triangle), acetonitrile (ACN) (group VIb) and tetrahydrofuran (THF) (group III).

### 2-Propanol, acetonitrile and tetrahydrofuran

In RPLC using hydro-organic mobile phases the relationship between retention factor and volume fraction of organic modifier ( $\varphi$ ) is often a quadratic equation as eqn. 1 [4].

$$\ln k' = -A\varphi^2 + B\varphi + \ln k'_w \quad (1)$$

where a coefficient  $A$  is expected to be positive,  $B$  is a negative, and  $\ln k'_w$  is the natural logarithm of the retention factor in pure water.

Over a limited range of  $\varphi$  the relationship between retention factor and  $\varphi$  can be written as eqn. 2:

$$\ln k' = -S\varphi + \ln k'_w \quad (2)$$

where  $S$  is solvent strength parameter. The linearity of eqn. 2 deteriorates in the low (less than 10%) and high (more than 90%) concentration ranges of organic solvents. In conventional RPLC with water-rich eluents ( $\varphi < 10\%$ ), even a quadratic fit of  $\ln k'$  vs.  $\varphi$  would be inadequate.

Likewise, in MLC with hybrid eluents of micelles-organic modifier, the relationship between retention and volume fraction of organic modifiers is also linear:

$$\ln k' = -S_{\text{hyb}}\varphi + \ln k'_0 \quad (3)$$

where  $S_{\text{hyb}}$  is solvent strength parameter in hybrid system and  $\ln k'_0$  is the retention in purely aqueous micellar eluent [13–16].

Eqn. 3 adequately described ( $r^2 > 0.986$ ) the retention behavior of the test mixture of amino acids

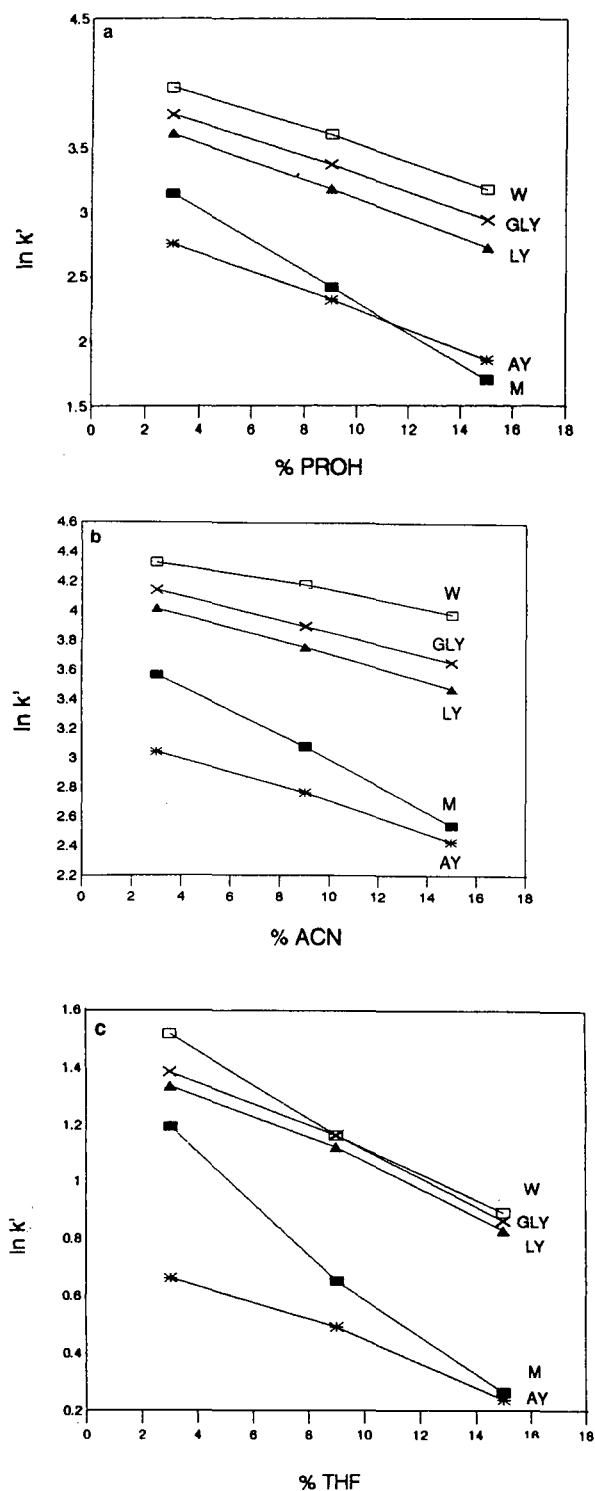


Fig. 1. Plots of  $\ln k'$  vs.  $\phi$  for (a) PROH, (b) ACN and (c) THF.

and small peptides in MLC with hybrid mobile phases as a function of volume fraction of three organic modifiers, 2-propanol acetonitrile, and tetrahydrofuran, over a range of 3–15% (Fig. 1).

The solvent strength parameters (*i.e.*  $S$  and  $S_{\text{hyb}}$ , the slopes of eqns. 2 and 3), represent the sensitivity of solutes retention with volume fraction of organic modifiers in hydroorganic and hybrid systems respectively. The relation between the slope and the intercept of these equations has a significant effect on chromatographic selectivity. The selectivity between those solutes whose slopes and intercepts are directly related to one another, would decrease with an increase in organic solvent concentration [13,14]. In contrast, for cases where there is no direct relationship between the slope and the intercept, the selectivity would increase with volume fraction of organic modifiers [14]. In RPLC with methanol–water mobile phases, linear correlations have been reported for the slope vs. intercept of eqn. 2 for a large group of compounds [4]. For hybrid eluents in MLC, the results of slope vs. intercept of eqn. 3 are illustrated in Fig. 2. As shown, unlike conventional hydro–organic eluents in the presence of micelles no correlation was observed between  $S_{\text{hyb}}$  and  $\ln k'_0$  for PROH-, ACN- and THF-modified micellar eluents. One can then anticipate a different selectivity behavior for PROH, ACN and THF in the presence of micelles.

Fig. 3 illustrates the chromatographic selectivities of PROH, ACN and THF in the presence of a fixed concentration of micelle (0.02 M SDS) for a sample mixture of seven amino acids and peptides. The volume fraction of the organic solvents are adjusted so that the solvent strength (analysis time) of all three mobile phases remain approximately the same. Interestingly, the elution order and selectivity of all solutes are similar for THF, PROH and ACN except for the different elution order of peaks 1 and 3 for PROH as compared to those for THF and ACN, and poor resolution of peaks 5 and 6 for PROH and ACN (Fig. 3).

As was discussed previously, both micelle concentration and volume fraction of an organic modifier influence the elution strength and selectivity [13–18]. Likewise, in order to achieve an understanding of the influence of the type of organic modifier, one should also simultaneously consider the role of micelles. In other words, one should

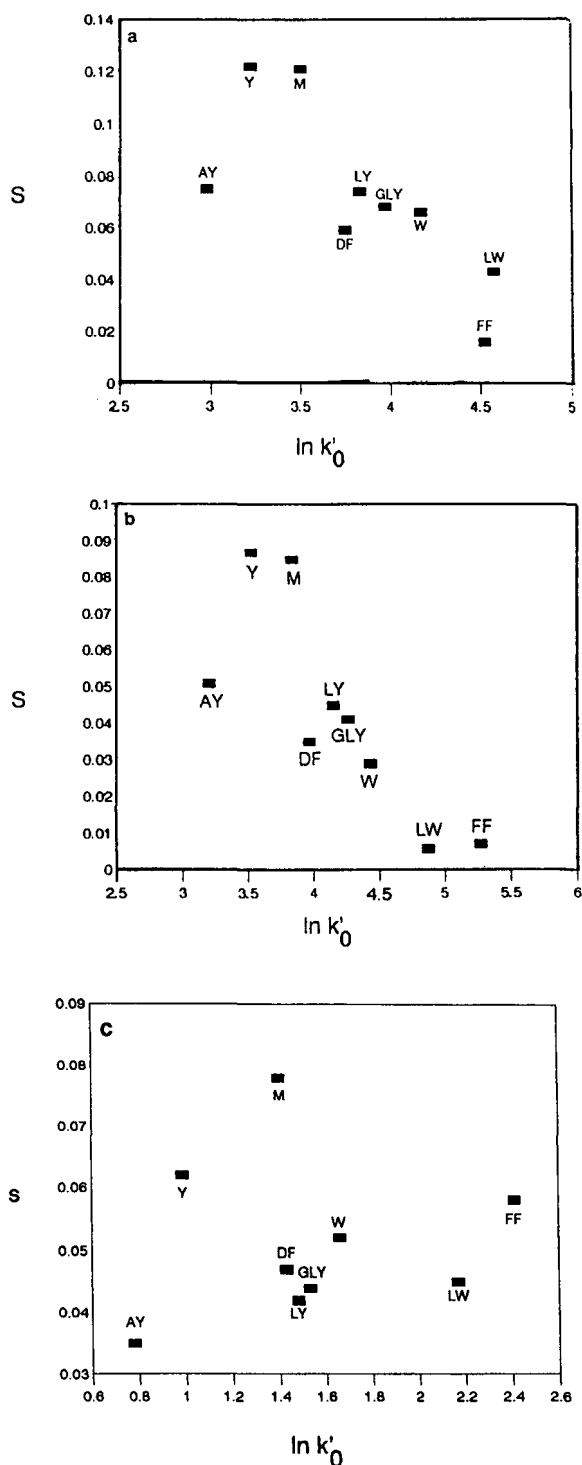


Fig. 2. The relation between  $S$  value and  $\ln k'_0$  for (a) PROH, (b) ACN and (c) THF.

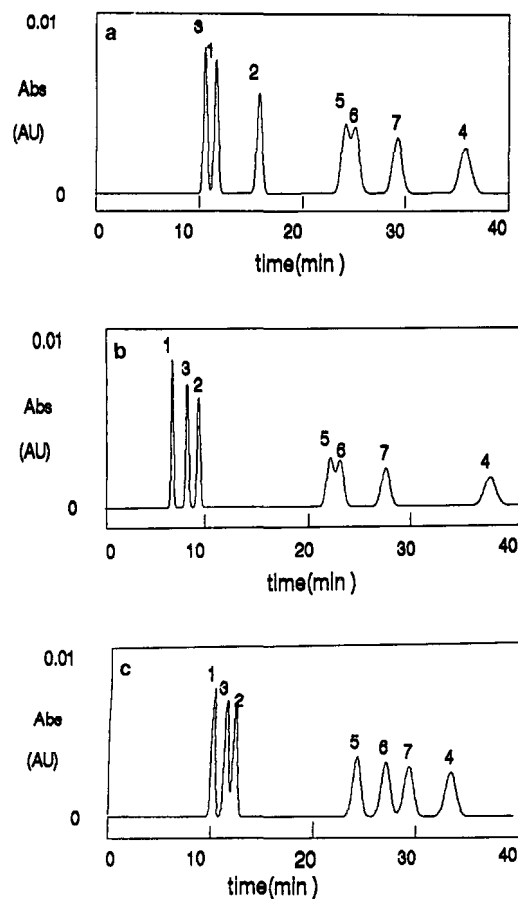


Fig. 3. The reconstructed chromatograms of a mixture of amino acids and peptides based on experimental retention data at (a) 0.02 M SDS and 3% PROH, (b) 0.02 M SDS and 12.5% ACN and (c) 0.02 M SDS and 3% THF. The solutes are identified in the Experimental section.

compare the three organic modifiers under optimized elution strength and selectivity.

For this purpose, we used iterative regression (IR) procedure to predict the optimum mobile phase compositions (*i.e.* micelle concentration and organic modifier volume fraction). This procedure was originally described by Drouen *et al.* [19] and extended by Van Renesse *et al.* [20]. We have recently reported the successful application of this technique for the two- and three-parameter optimization of micelle concentration, PROH% and pH [17,18].

A two-dimensional parameter space (surfactant and organic solvent concentration) was used as is

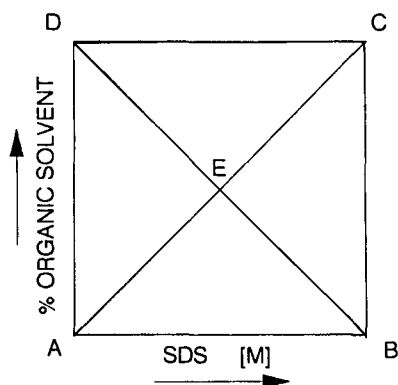


Fig. 4. The parameter space for iterative regression procedure. The five initial measurements were performed using the following mobile phases: (A) 0.02 M SDS + 3% organic solvent, (B) 0.20 M SDS + 3% organic solvent, (C) 0.20 M SDS + 15% organic solvent, (D) 0.02 M SDS + 15% organic solvent and (E) 0.11 M SDS + 9% organic solvent. This parameter space was used for the three organic solvents: PROH, ACN and THF.

shown in Fig. 4. This optimization procedure is based on linear modelling of the solutes retention ( $\ln k'$ ) in the mixture as a function of mobile phase parameters using a limited number of initial experiments [16-10]. The retention of the solutes in a mixture will then be predicted within the parameter space through interpolation of the assumed linear

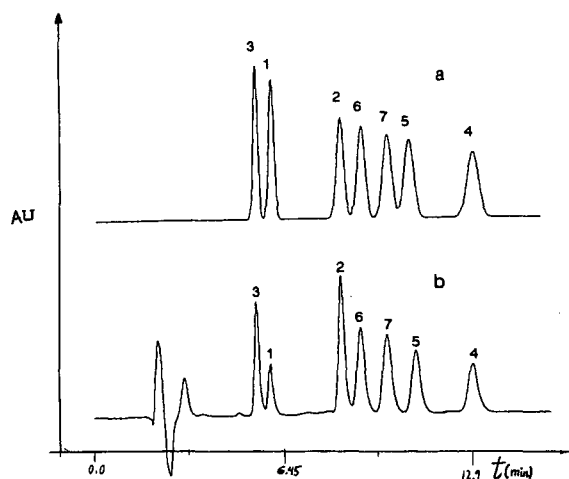


Fig. 5. The predicted (a) and measured (b) chromatograms for amino acids and peptides at 0.17 M SDS + 12.6% PROH. The identities of solutes are listed in the Experimental section of the text.

model of  $\ln k'$  vs. parameters. Based on the predicted retention behavior of all compounds in a mixture, the quality of separation (e.g. minimum resolution) at all mobile phase compositions within the parameter space will be calculated and an optimum is predicted. If the observed quality of separation at the predicted optimum mobile phase compositions is not satisfactory, more experiments will have to be performed (i.e. through an iterative process) in order to locate the global optimum in the parameter space. The success or failure of finding the optimum parameter mobile phase composition would largely depend on the correctness of the linearity assumption of the model [16-20].

The retention of seven amino acids and peptides were measured at five mobile phase compositions. Four measurements at the corners of the selected two dimensional parameter space, and one measurement at the center. The parameter space consists of four triangle subspaces defined by three of the five measurements, i.e. two corner points and the central point. The boundaries of the parameter space are determined by practical limitations of the chromatographic system. The lower surfactant con-

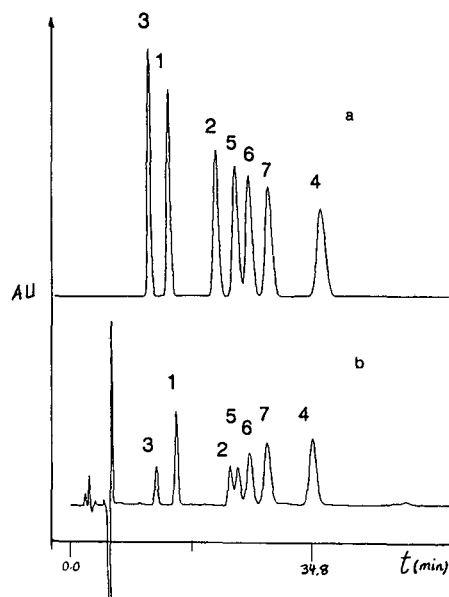


Fig. 6. The predicted (a) and measured (b) chromatograms for amino acids and peptides at 0.12 M SDS + 7.5% ACN. The identities of solutes are listed in the Experimental section of the text.



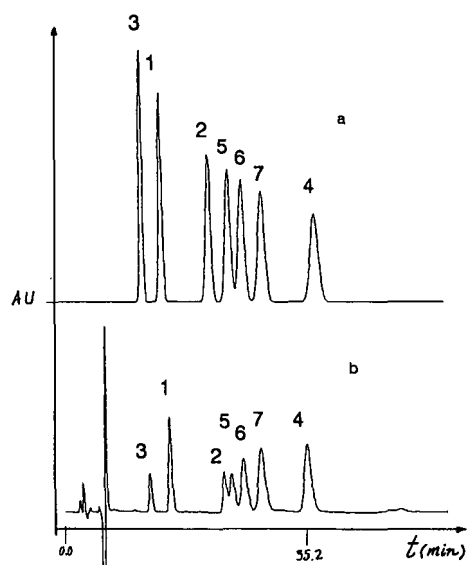


Fig. 7. The predicted (a) and measured (b) chromatograms for amino acids and peptides at 0.07 M SDS + 4.2% THF. The identities of solutes are listed in the Experimental section of the text.

centration must be well above the critical micelle concentration (8 mM at room temperature and in pure water) and must be strong enough to cause elution of solutes. The upper surfactant concentration is determined by a combination of solubility of the surfactant, the viscosity of the resulting mobile phase, and degradation of efficiency at higher concentration [17]. The volume fraction of organic solvent was limited to a maximum of 15% to protect the integrity of micelles.

The applicability of the IR procedure for these three solvents was examined. The agreements between predicted and measured chromatograms for PROH-SDS-, ACN-SDS- and THF-SDS-modified eluents are excellent, good and fair, respectively, as shown in Figs. 5–7. It is shown that there is a considerable similarity between the chromatograms for THF, ACN and PROH.

#### 2-Propanol vs. butanol

According to Snyder's solvent classification the chromatographic selectivity for 2-propanol and butanol should be the same at equal solvent strengths in hydro-organic mobile phases because they belong to the same selectivity group.

	PROH	BUOH
DF	14.1	35.5
W	16.3	36.3
LY	17.5	37.1
GLY	18.4	44.6
LW	18.7	50.2
FF	20.4	53.2

Fig. 8. The  $S$  values of some amino acids and peptides for PROH-water and BUOH-water mobile phases.

The  $S$  values of most of solutes used in this study for hydro-organic eluents (*i.e.* PROH-water and BUOH-water) are ranked in Fig. 8. An attempt for measuring the  $S$  value of the rest of solutes for these mobile phases (*i.e.* AY, Y and M) was unsuccessful due to the lack of adequate retention. As expected, the  $S$  values of solutes in BUOH containing eluents are larger than those for PROH, however, the ranks of  $S$  values of different solutes for both BUOH and PROH are the same. In other words, selectivity in retention of solutes in BUOH-water and PROH-water mobile phases should be similar at equal solvent strength. Since in MLC organic modifiers associate with micelles and on the other hand compete with micelles to interact with solute, the chromatographic selectivity of organic solvents may no longer be the same. The  $S_{\text{hyb}}$  values for the test solutes in the hybrid systems of PROH-SDS and BUOH-SDS at a micelle concentration are shown in Fig. 9.

	PROH	BUOH
LW	7.07	21.1
FF	7.32	22.1
GLY	7.49	23.3
LY, DF	8.77	25.7
		28.3
W	11.80	34.0

Fig. 9. The  $S$  values of some amino acids and peptides for PROH and BUOH at 0.02 M SDS.

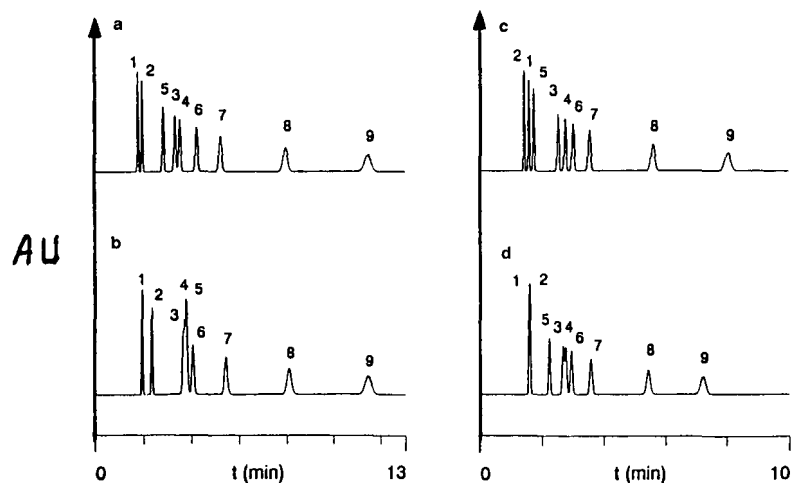


Fig. 10. The reconstructed chromatograms on the basis of measured retentions for nine amino acids and peptides at 0.08 *M* SDS and (a) 8% PROH, (b) 1.9% BUOH, (c) 14% PROH, and (d) 3.6% BUOH.

The rank of  $S_{\text{hyb}}$  values of some solutes for BUOH is different from that for PROH. For example, at 0.02 *M* SDS the  $S_{\text{hyb}}$  value of FF for PROH is the second highest and for BUOH is the second lowest, or the  $S_{\text{hyb}}$  value of LY for PROH is the second lowest while for BUOH is the second highest (Fig. 9). A comparison of the Figs. 8 and 9 shows that the  $S$  values of all solutes in both PROH and BUOH decrease due to the inclusion of micelles in the aqueous–organic media [*i.e.*  $S_{(\text{hyb})} < S_{(\text{hydro-organic})}$ ] [13,14]. The magnitude of the reduction in  $S$  values depend upon the degree of interactions of solutes and organic solvents with micelle [13–15]. Micelles control the solvation ability of organic solvent and as a result their chromatographic selectivity. The ranks and the magnitudes of the  $S_{\text{hyb}}$  values for PROH and BUOH changed with the micelle concentration. Consequently, one can expect that the organic solvent selectivity in MLC be a function of micelle concentration. The reasons behind these observations have been reported elsewhere [14,15].

The chromatograms of amino acids and peptides for different concentrations of BUOH and PROH at a fixed micelle concentration (0.08 *M* SDS) in the hybrid systems are illustrated in Fig. 10. In this figure the strengths of the PROH and BUOH hybrid mobile phases are adjusted so that the retention of the last peak remains the same. One can observe that although all peaks are well separated for

PROH, there exist strong overlaps and coelution of peaks 3, 4 and 5 in BUOH. The elution strength for chromatograms c (PROH) and d (BUOH) are also the same. A close look at chromatograms c and d shows that, again all peaks for PROH are well resolved, while for BUOH peaks 1 and 2 are coeluted and peaks 3 and 4 have very poor resolution. As a result of these observations one can conclude that the chromatographic selectivity of BUOH is different as compared to that of PROH.

## CONCLUSIONS

The presence of micelles in the mobile phases of RPLC has a great influence on the chromatographic selectivity of organic solvents. As a result the classification of organic solvents established by Snyder may not be fully valid in MLC. Further investigations should be made on the effect of micelles on chromatographic selectivity of organic solvents.

## ACKNOWLEDGEMENTS

The authors thank J. K. Strasters for modifying the IR program. The support of this work by a research grant from the National Institutes of Health (FIRST Award, GM38738) is gratefully acknowledged.

## REFERENCES

- 1 N. Tanaka, H. Goodel and B. L. Karger, *J. Chromatogr.*, 158 (1978) 233.
- 2 L. R. Snyder, *J. Chromatogr. Sci.*, 16 (1978) 223.
- 3 L. R. Snyder and J. J. Kirkland, *Introduction to Modern Liquid Chromatography*, Wiley, New York, 2nd ed., 1979, p. 260.
- 4 P. J. Schoenmakers, *Optimization of Chromatographic Selectivity (Journal of Chromatography Library, Vol. 35)*, Elsevier, Amsterdam, 1986, ch. 2.
- 5 L. R. Snyder, *J. Chromatogr.*, 92 (1974) 223.
- 6 J. L. Glajch, J. J. Kirkland, K. M. Squire and J. M. Minor, *J. Chromatogr.*, 199 (1980) 57.
- 7 P. L. Smith and W. T. Cooper, *J. Chromatogr.*, 410 (1987) 249.
- 8 W. T. Cooper and L.-Y. Lin, *Chromatographia*, 21 (1988) 335.
- 9 R. M. Smith, *Anal. Chem.*, 56 (1984) 256.
- 10 R. M. Smith, *J. Chromatogr.*, 324 (1985) 243.
- 11 J. P. Foley and W. E. May, *Anal. Chem.*, 59 (1987) 102.
- 12 F. P. Tomasella, J. Fett and J. Cline Love, *Anal. Chem.*, 63 (1991) 474.
- 13 M. G. Khaledi, E. Pueler and J. Ngeh-Ngwani, *Anal. Chem.*, 59 (1987) 2738.
- 14 M. G. Khaledi, J. K. Strasters, A. H. Rodgers and E. D. Breyer, *Anal. Chem.*, 62 (1990) 130.
- 15 A. S. Kord and M. G. Khaledi, *Anal. Chem.*, 64 (1992) 1894.
- 16 A. S. Kord and M. G. Khaledi, *Anal. Chem.*, 64 (1992) 1901.
- 17 J. K. Strasters, E. D. Breyer, A. A. Rodgers and M. G. Khaledi, *J. Chromatogr.*, 511 (1990) 17.
- 18 J. K. Strasters, S.-T. Kim and M. G. Khaledi, *J. Chromatogr.*, 586 (1991) 221.
- 19 A. C. J. H. Drouen, H. A. H. Billiet, P. J. Schoenmakers and L. de Galan, *Chromatographia*, 16 (1982) 48.
- 20 A. van Renesse, J. K. Strasters, H. A. H. Billiet and L. de Galan, presented at the *13th Symposium on Column Liquid Chromatography, Stockholm, June 1989*, paper M/TU-P-164.

## Axial illumination of fused-silica capillaries

# Investigation of fluorescence and refractive index detection

Ahmad A. Abbas and Dennis C. Shelly

*Department of Chemistry and Biochemistry, Texas Tech University, Lubbock, TX 79409 (USA)*

---

### ABSTRACT

The optical waveguide properties of fused-silica capillaries enable greater illuminated sample volume by axial illumination, as compared to cross capillary illumination. Several modes of light propagation inside these unique optical waveguides are described. A micro-LC flow cell featuring axial illumination with mobile phase elimination by nebulization has been developed and evaluated. This device was used in the construction and evaluation of laser-induced fluorescence and laser-based refractive index detectors. A summary of results from our studies and a survey of the various detection possibilities, theoretically compatible with axial illumination of capillary waveguides, are presented.

---

### INTRODUCTION

While small-dimensional capillaries (10–250  $\mu\text{m}$  inner diameter) provide high-efficiency separations, these capillaries generate extremely small path lengths when cross-capillary illumination is employed. This results in very small probed volumes, hence very small analytical signals, complicating detection by photometric means. This problem can be largely overcome by axial illumination. Here, the entire sample band can be illuminated generating significantly higher detection efficiency.

Axial illumination of fused-silica capillaries has recently been utilized as a technique for increasing detection capabilities in capillary separations. Significant increases in concentration sensitivities of absorption and fluorescence detection, due to the increased optical path length achievable with axial

illumination, have been shown. Grant and Steuer [1] first reported on an “extended path length” UV absorbance detector for capillary electrophoresis in 1990. The measurement was based on indirect fluorescence which was spatially modulated by fluorophore displacement. Xi and Yeung [2] demonstrated enhanced performance for absorption detection in open tubular capillary liquid chromatography. A 1000-fold increase in pathlength was observed. Further, it was noted that the entire sample band could be illuminated, thus confining the detection region to the chromatographic band. Even with the very low flow-rates of open tubular capillary liquid chromatography, optical distortions were observed as light was coupled into the capillary flow cell. Taylor and Yeung [3] described an axial-beam absorbance detector for capillary electrophoresis that was used to monitor the separation of bromothymol blue and bromocresol green. A red helium–neon laser was used for excitation. A conventional light source (actually a commercially available UV–Vis absorption detector) and axial illumination has also been used

---

*Correspondence to:* D. C. Shelly, Department of Chemistry and Biochemistry, Texas Tech University, Lubbock, TX 79409, USA.

for absorbance detection in capillary electrophoresis [4]. Fluorescence detection in capillary zone electrophoresis, via axial illumination, has been reported by Sweedler *et al.* [5]. Axial illumination combined with the unique scanning capabilities of a charge coupled device detector resulted in concentration detection limits between  $2 \cdot 10^{-20}$  and  $8 \cdot 10^{-20}$  mol for fluorescein isothiocyanate–amino acids conjugates.

Despite these recent reports of axial illumination detection in open tubular capillary liquid chromatography and capillary electrophoresis, to date, no effort has been documented for the coupling of axial illumination with slurry packed capillary LC (micro-LC) [6]. The major impediment to this instrumental achievement is solvent elimination with minimal optical distortion in this higher mobile phase flow-rate separation technique [7]. Flow-rates of 1 to 3  $\mu\text{l}/\text{min}$  result in significant difficulty in effectively coupling light into the exit capillary (waveguide). The liquid droplet acts as a lens, defocusing the beam and modulating the light energy distribution in the capillary. The mobile phase must be eliminated from the waveguide orifice to prevent distortions of optical coupling.

This paper described our attempts in coupling axial illumination with micro-LC. A unique, nebulizing flow cell was designed and fabricated. The operating characteristics of this flow cell and the detection performance of a laser-induced fluorescence instrument and a laser-based refractive index detector are presented.

## THEORY

Axial illumination of long capillary cells has been fairly extensively studied. Lei *et al.* [8] used 50-m capillary cell for colorimetry. Improvement in absorbance of between 130 and 300 was reported for carbon disulfide solutions of phosphomolybdenum heteropoly blue. Dasgupta [9] reported wide dynamic range and high sensitivity using a reflective helical cell. A decreasing non-linear dependence of effective pathlength with increasing solution absorbance was noted. Tsunoda *et al.* [10] have analyzed the optical transmission characteristics of long capillary cells where total internal reflection occurred at the outer wall surface. A borosilicate glass capillary showed better transmission than one with mirrored

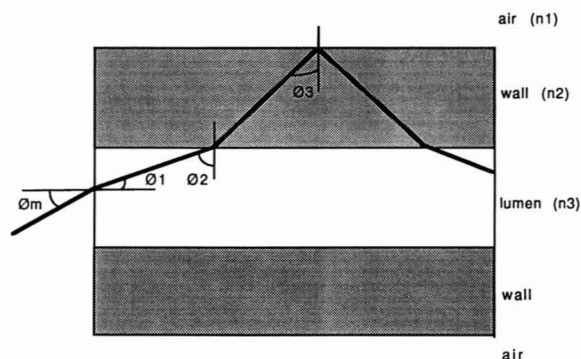


Fig. 1. Ray diagram for light propagation in a capillary waveguide.  $n_1$ ,  $n_2$  and  $n_3$  are the refractive indices of air, wall and lumen, respectively.  $\theta_2$  and  $\theta_3$  are the angles subtended by light at the lumen-wall and wall-air interfaces, respectively.  $\theta_m$  is half the acceptance angle.

walls. The importance of wall refractive index was noted which contributed to a subsequent paper describing the use of poly(tetrafluoroethylene cohexafluoropropylene) tubing (refractive index was almost identical to water) for such cells [11]. Since a detailed analysis of light transmission in fused-silica capillaries is somewhat redundant and beyond the scope of this paper, we present a brief treatment of this topic, showing the relationship of mobile phase refractive index and effective optical pathlength in an axially illuminated capillary column/flow cell.

When light is launched axially in the lumen of a circular fused-silica capillary, all light energy can be trapped inside the capillary if total internal reflection at the wall/air interface occurs as shown in Fig. 1. This is possible only if inequality 1, based on Snell's law, is satisfied.

$$\sin \theta_2 > n_1/n_3 \quad (1)$$

The light energy distribution inside these capillary optical waveguides can be classified into three pathways: (a) light energy distributed only in the wall of the capillary; (b) light energy distributed only in the lumen; and (c) light energy distributed in the wall and the lumen of the fused-silica capillary. These three pathways are illustrated in Fig. 2, using a classical ray diagram approach. Pathways b and c, where light energy transmits across the medium inside the lumen, is of prime importance when mak-

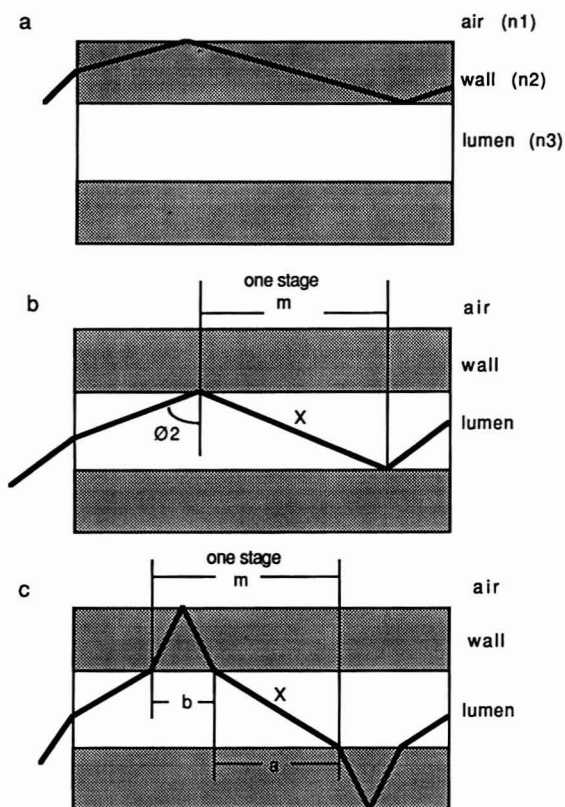


Fig. 2. Light propagation pathways in capillary waveguides. (a) Wall propagation; (b) lumen propagation; (c) combination propagation.  $\theta_2$  is any angle from the critical angle to  $90^\circ$ .  $m$ ,  $X$ ,  $a$  and  $b$  are distances, as shown.

ing absorbance, fluorescence or refractive index measurements.

Most of light energy will be distributed in pathway b if

$$n_2 < n_3 \sin \theta_2 \tag{2}$$

where  $\theta_2$  is the range of angles from the critical angle to  $90^\circ$ . Here,  $n_2 < n_3$ , the refractive index of fused silica ( $n_2 = 1.458$ ) is less than that of the mobile phase. If  $n_2 > n_3$  then light will traverse according to pathway c. It should be clear that most hydroorganic mobile phases will result in either pathways b or c. Pathway a explicitly occurs only when light is launched into the capillary wall.

Only radiation which traverses the lumen will significantly interact with chromatographic analytes. The effective pathlength ( $l_e$ ), defined as the total dis-

tance travelled by light in the lumen, is an indication of the light energy distribution inside a capillary optical waveguide.  $l_e$  is the product of the distance that light travels in the lumen for one “stage” (see ref. 11) and the number of “stages”. We have chosen an optical window of 0.9 cm, which is the diameter of our photomultiplier tube. For pathway b,  $l_e$  is calculated using eqn. 3.

$$l_e = nX = l_p / \sin \theta_2 \tag{3}$$

where  $X$  is the distance that light travels in the lumen in one stage (see Fig. 2).  $l_p$  is the physical cell length, which depends on the imaged detector diameter. For pathway c,  $l_e$  is calculated using eqn. 4.

$$l_e = l_p X / (A + B) \tag{4}$$

where  $A$  is the ratio of  $(d_w n_1)$  to  $(\cos \theta_2 n_3)$  and  $B$  is the ratio of  $(2d_w n_1)$  to  $(\cos \theta_3 n_2)$ .  $\theta_3$  is shown in Fig. 1.  $d_e$  and  $d_w$  are the lumen and wall thicknesses, respectively. The derivation of eqns. 3 and 4 and the detailed interpretation of them are the subject of a future paper.

The dependence of  $l_e$  on mobile phase refractive index is illustrated in Fig. 3. Since  $n_1$  and  $n_2$  are fixed,  $l_e$  varies with  $n_3$  for each pathway, as shown. For pathway b, effective pathlength varies linearly with lumen refractive index ( $n_2 < n_3$ ), while for pathway c, effective pathlength varies non-linearly with lumen refractive index ( $n_2 > n_3$ ). Note the dis-

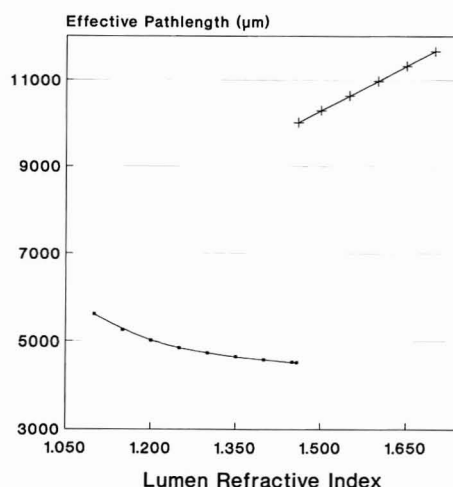


Fig. 3. Variation of effective pathlength with lumen refractive index. (□)  $n_2 > n_3$ ; (+)  $n_2 < n_3$ .

continuity in the plot. This occurs at the refractive index of fused silica, 1.458, where propagation pathway c sharply changes to pathway b. The relative magnitudes of  $l_e$  approximate those of a solute band. These effective pathlengths correspond to illuminated volumes of 100 to 500 nl, typically found in micro-LC.

The variation of light energy distribution with lumen refractive index is, in fact, more complicated than that described above. For both pathways the acceptance angle (the solid angle through which light is gathered into propagating modes in the waveguide) changes with  $n_3$ , the lumen refractive index. For pathway b, the acceptance angle increases from 9 to 25° when  $n_3$  goes from 1.468 to 1.510. For pathway c, the acceptance angle increases from 27 to more than 90° when  $n_3$  extends from 1.359 to 1.432. Thus, in pathway c much more light is coupled into the capillary than for pathway b. Remembering that typical mobile phase refractive indices are less than that of fused silica, pathway c represents the situation for axial illumination detection in most chromatographic applications. Even though  $l_e$  decreases as the mobile phase refractive index approaches that for fused silica, for pathway c, the light gathering power increases tremendously, allowing more light to couple into the cell, resulting in greater light energy distribution in the lumen. This issue will also be treated in a separate, more detailed publication.

By examining the above ray diagrams and plots it should be clear that axial illumination affords several types of detection modes. If incident light is not absorbed by analyte, propagating light may be coupled out of the capillary for a measurement of lumen refractive index. If exciting light is absorbed, is not reemitted as fluorescence, and is coupled out of the capillary a measurement of absorbance is accomplished. Fluorescence is also measurable if this emitted light can be detected. The unique feature of these possibilities is the manner in which the analytical signal is detected, *i.e.* how the light is coupled out of the capillary. We show, in this paper, the measurement of refractive index and fluorescence. Absorbance measurements have already been reported by Xi and Yeung [2].

## EXPERIMENTAL

### *Axial illumination micro-LC flow cell*

The key component of our detection systems is a flow cell that permits axial illumination with simultaneous mobile phase elimination by nebulization. Fig. 4 shows a drawing of the key features of this cell. Nebulization is based on the Babington principle (see ref. 12). The capillary orifice is carefully positioned over the gas outlet as shown. The gas jet is formed by the conical-shaped polyurethane film that is compressed between the plastic manifold and the metal plate. The capillary (Polymicro Technologies, Phoenix, AZ, USA), which has been stripped of its polyimide, is held against the plastic gas manifold with a glass plate. This assembly is positioned against a modified mirror mount (Newport Corp., Fountain Valley, CA, USA) with an aluminum clamp, as shown in Fig. 5. A spray barrier prevents contamination of optics. Using 100 p.s.i. (1 p.s.i. = 6894.76 Pa) air, mobile phase flow-rates approaching 10  $\mu$ l/min can be nebulized with this cell. Neither the flow cell nor the nebulizing gas are heated.

### *Laser-induced fluorescence apparatus*

The laser-induced fluorescence apparatus was similar to that described previously [13]. The instrument consisted of a Model 4220N (442 nm) helium–cadmium laser and a Model 3315I (325 nm) helium–cadmium laser (Liconix, Santa Clara, CA, USA), a miniature photon-counting detector [14] and suitable optics, as illustrated in Fig. 6. A quartz, f/1.5 plano convex lens (Oriel, Stratford, CT, USA) was used to focus the 325-nm laser beam onto the capillary orifice. A 10  $\times$  microscope objective performed this function for the 442-nm laser. Fluorescent light was collected through the large opening, orthogonal to the capillary flow/excitation optical axis using an integrally-mounted cylindrical lens (f/1.5, Melles Griot, Irvine, CA, USA). The sampling rate for the data system was based on a counting gate time of 64 ms.

### *Refractive index apparatus*

The refractive index detection apparatus consisted of the Micro LC flow cell, in somewhat modified form, and a helium–neon laser (Melles Griot, Irvine, CA, USA). The refractive index flow cell is shown in Fig. 7. Here, an optical fiber (200  $\mu$ m core

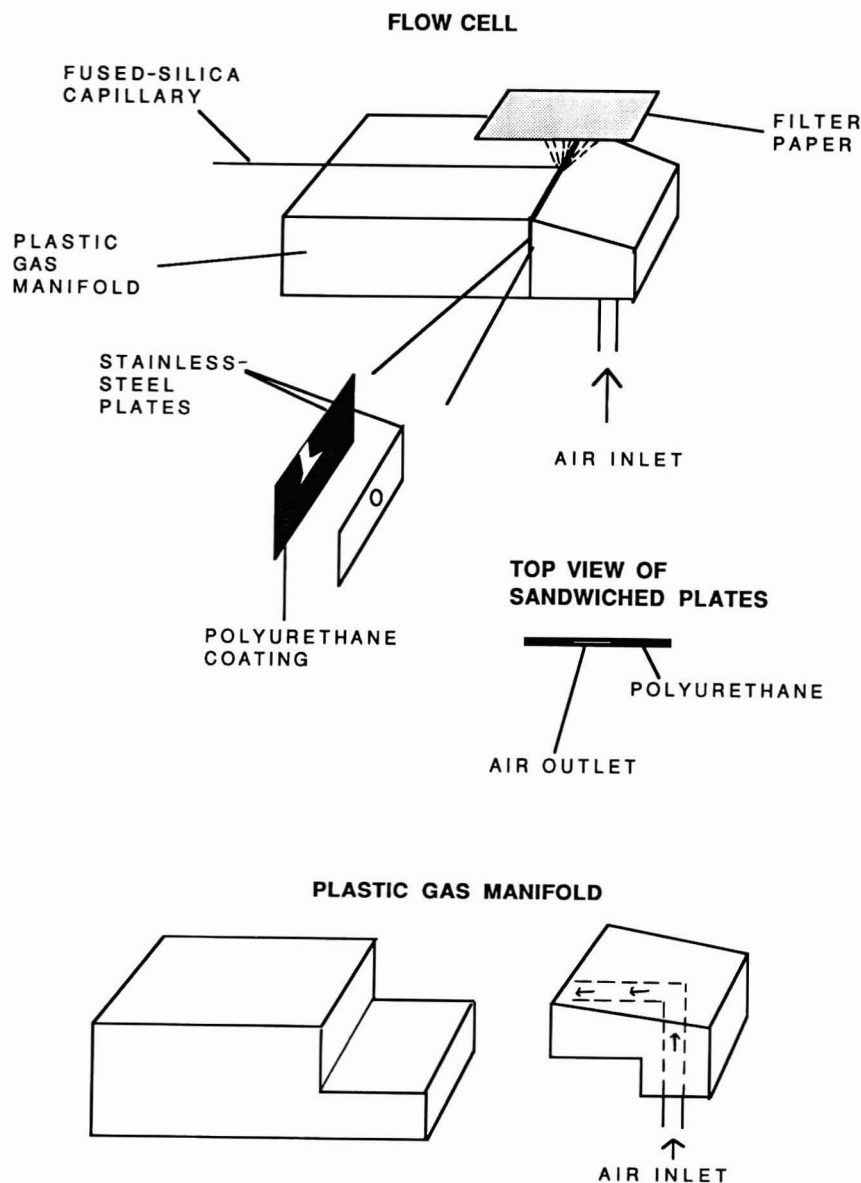


Fig. 4. Functional drawing of nebulizing micro-LC flow cell.

diameter, Polymicro Technologies) was optically coupled to the flow cell capillary using an optical coupling gel (General Fiber, Cedar Grove, NJ, USA). The distance between the contact/coupling point and the capillary orifice was about 2 cm. As shown in Fig. 8, a beam splitter (microscope slide) directed a portion of the helium neon laser beam to

a reference fiber. A  $10\times$  microscope objective focused the laser beam onto the capillary orifice. The sample and reference fibers were optically coupled with miniature photocell detectors (S2007; Electronic Goldmine, Scottsdale, AZ, USA). The output from each photocell was electronically connected to a log ratio amplifier (AD757N; Analog De-



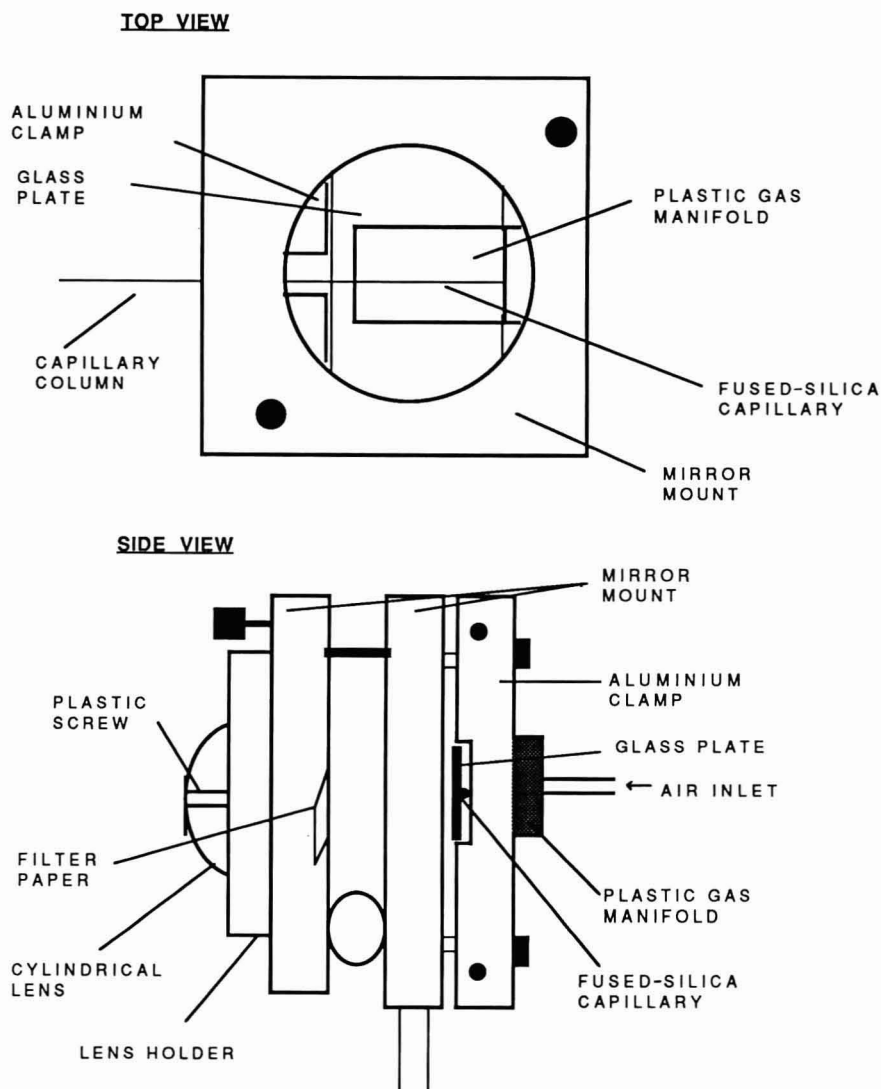


Fig. 5. Schematic diagram of fluorescence flow cell.

vices, Norwood, MA, USA). Analog output was recorded on a standard, laboratory strip chart recorder.

#### *Micro liquid chromatography*

Our micro-LC system consisted of a Model 8500 syringe pump (Varian, Walnut Creek, CA, USA) and a C14W microinjector (Valco, Houston, TX, USA) that was equipped with a 100-nl internal loop. All injections were of the moving loop type

[15]. 250  $\mu\text{m}$  inner diameter fused-silica capillaries (Polymicro Technologies) were packed with a computer-controlled pump [16]. Dynamic measurements of perylene were based on a reversed-phase separation, for which Spherisorb ODS2 (5  $\mu\text{m}$ ) packing was used. For aflatoxin chromatography LiChrosorb SiOH (10  $\mu\text{m}$  diameter) particles were used to pack the column. All packings were obtained from Alltech (Deerfield, IL, USA) and both micro-LC columns were 70 cm long.

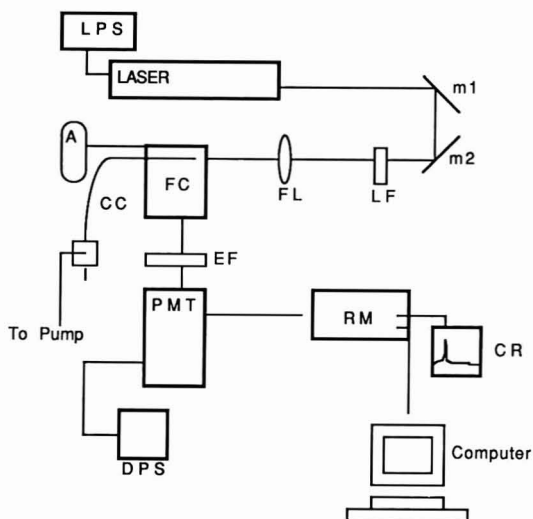


Fig. 6. Schematic of fluorescence apparatus. LPS = Laser power supply; m1, m2 = first surface mirrors; LF = liquid filter; FL = focusing lens; FC = flow cell; CC = chromatographic column; A = air supply; I = microinjector; EF = emission filter; PMT = photomultiplier tube; DPS = detector power supply; RM = ratemeter; CR = chart recorder.

### Chromatogram and data analysis

All fluorescence chromatograms were analyzed with DADiSP (DSP Development Corp., Cambridge, MA, USA), digital signal processing software. Various operations, such as signal acquisition of baseline and peaks, peak integration, width at half height, etc., were easily performed with this system.

### Chemicals and reagents

All mobile phase reagents were "HPLC" grade or "reagent" grade and were used without further purification. Purified water was obtained from a Nanopure treatment system (Sybron/Barnstead, Boston, MA, USA). All chromatographic solutes were "reagent" grade and were not further purified prior to use. The aflatoxins were purchased as a kit, AF-1, from Sigma (St. Louis, MO, USA).

## RESULTS AND DISCUSSION

### Flow cell set-up and operation

The successful operation of our flow cell depended entirely on how well the liquid droplet was elim-

inated at the outlet orifice of the capillary. For efficient nebulization it was important to have the dimensions of the nebulizer as small as possible. The jet orifice dimensions were  $50\ \mu\text{m}$  width and  $500\ \mu\text{m}$  length. Optimum placement of the capillary relative to the jet orifice was necessary for continuous and stable nebulization. It has been reported that vibrations of the capillary produced tremendous optical distortions [2] with axial illumination. In our design a glass plate was placed over the capillary cell and clamped into position, thus eliminating vibrations and microbending losses. Tremendous baseline fluctuations (optical distortions) resulted when either inefficient nebulization or an incompletely fixed capillary occurred. The design of our flow cell made it convenient to work with stripped fused-silica capillaries, even though removal of the polyimide coating gave a fragile capillary flow cell. Another important factor was that extreme cleanliness of the excitation and emission optics was necessary to maintain the highest possible sign-to-noise ratio. Our nebulizing flow cell was effective in nebulizing all mobile phases tested, which included 100% methanol, 100% ethanol, benzyl alcohol-ethanol, acetonitrile-water and toluene-ethylacetate-methanol-formic acid mixtures.

### Laser-induced fluorescence measurements

To evaluate our flow cell design we performed a series of experiments using perylene solutions of different concentrations. Static and dynamic measurements of perylene were made, using solutions ranging from  $1.34 \cdot 10^{-9}$  to  $1.34 \cdot 10^{-6}$  M and  $1.31 \cdot 10^{-8}$  to  $1.31 \cdot 10^{-5}$  M, respectively. Normal-phase micro-LC of aflatoxins was performed in order to determine the practical limits of detection.

### Static evaluation

Using a syringe pump (Harvard Apparatus, Dover, MA, USA), perylene solutions of different concentrations were pumped, at a flow-rate of  $5\ \mu\text{l}/\text{min}$ , through the optical window (stripped fused-silica capillary flow cell), whose dimensions were: inner diameter  $99\ \mu\text{m}$ , length 0.9 cm, volume 69.2 nl. Fluorescence was recorded over a 20–30-min period for each solution. Laser power (442 nm) at the flow cell entrance was approximately 1.5 mW.

As shown in Table I, four different concentrations of perylene were prepared in each of four sol-

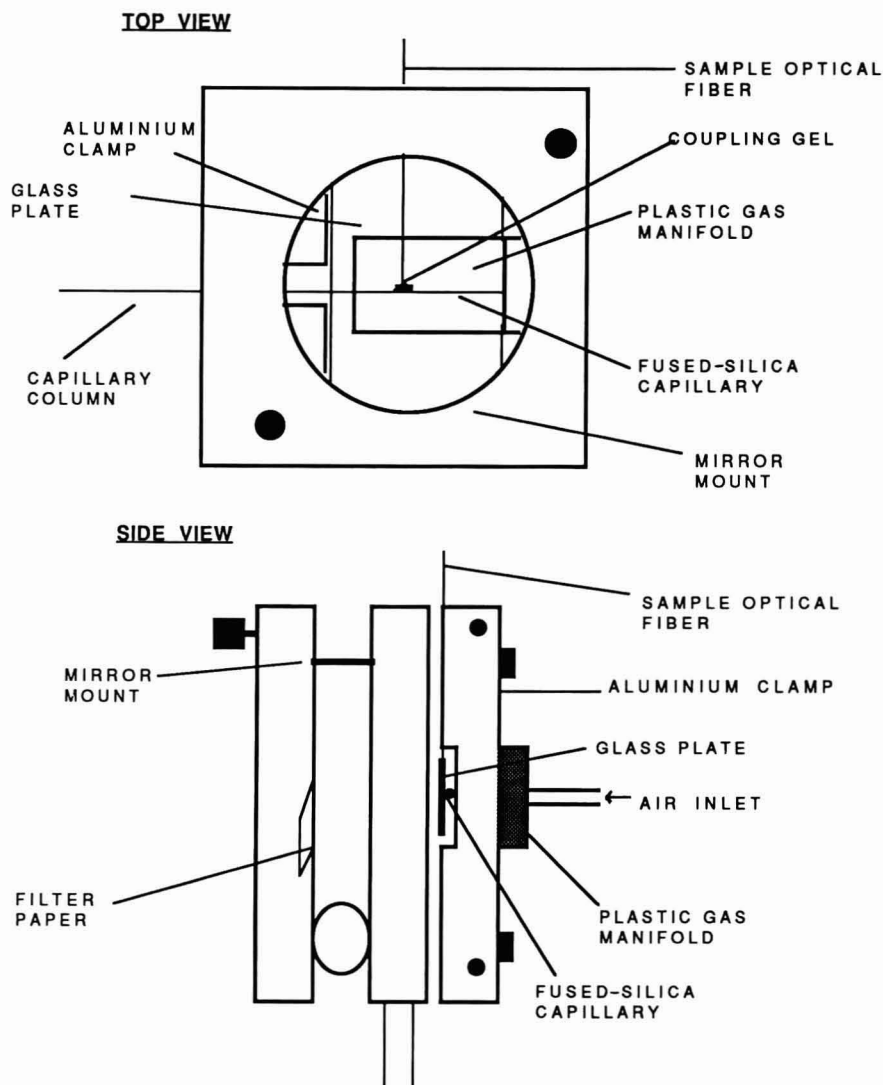


Fig. 7. Drawing of refractive index flow cell.

vents, containing various proportions of ethanol ( $n = 1.359$ ) and benzyl alcohol ( $n = 1.54$ ) in order to achieve different refractive index values. Two solutions had refractive indices lower than fused silica and two solutions had higher refractive indices than fused silica. Table I shows the mean photon counts, after subtracting the blank (photon counts for solution without perylene), obtained for the sixteen solutions. The blank spaces for  $10^{-6} M$  and  $10^{-9} M$  solutions are explained by the fact that  $10^{-9} M$  so-

lutions (refractive index lower than that of fused silica) were too weak to be detected and the signal for  $10^{-6} M$  solutions (refractive index greater than that of fused silica) was so high that it saturated the PMT photocathode!

Fig. 9 shows a series of signal *versus* concentrations plots of the 4 datasets listed in Table I. The slopes (sensitivities) are given in the caption. Notice that sensitivities increase with lumen refractive index. The large difference in the slope values for so-

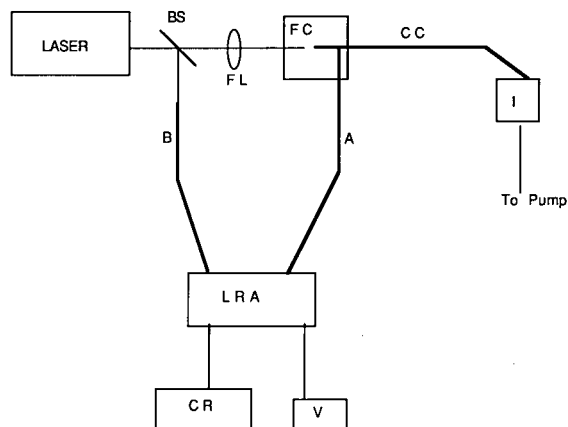


Fig. 8. Schematic of refractive index apparatus. BS = Beam splitter; FL = focusing lens; FC = flow cell; A = sample optical fiber; B = reference optical fiber; LRA = log ratio amplifier; CR = chart recorder; V = voltmeter; CC = chromatographic column; I = microinjector.

lutions which have refractive indices less than 1.458 compared to those solutions with refractive indices greater than 1.458 can be attributed to the fact that when the lumen refractive index is less than the refractive index of the fused-silica wall, pathway c (refer to Fig. 2) is the dominant mode of light propagation inside the flow cell. Therefore, light energy is distributed in *both* the wall and the lumen of the fused-silica capillary flow cell. When the refractive index of the lumen is higher than that of fused silica, pathway b (see Fig. 2) is the preferred mode of propagation. In this case, almost all light energy is trapped inside the lumen, resulting in higher slopes, hence greater detection sensitivities. More light-

TABLE I  
STATIC MEASUREMENTS OF PERYLENE

S1, S2, S3 and S4 are signal intensities for solutions of refractive index = 1.359, 1.432, 1.468 and 1.510, respectively.

Concentration ( $M$ )	S1	S2	S3	S4
$1.34 \cdot 10^{-9}$			10.4	15.4
$1.34 \cdot 10^{-8}$	11.6	15.4	54.2	78.8
$1.34 \cdot 10^{-7}$	46.1	103.3	590.6	851.8
$1.34 \cdot 10^{-6}$	286	1047.3		

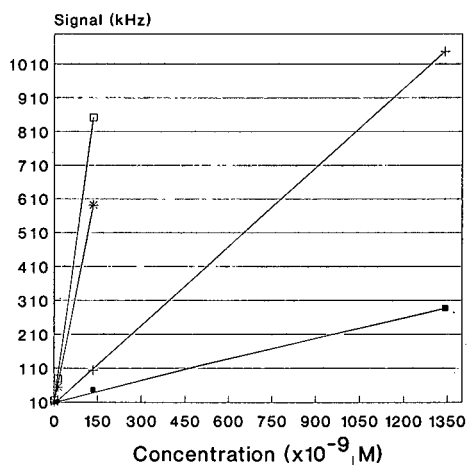


Fig. 9. Response plots, static perylene measurements. ■ = Ethanol,  $n_3 = 1.359$  (slope 0.204); + = ethanol-benzyl alcohol (3:2, v/v),  $n_3 = 1.432$  (slope 0.779); \* = ethanol-benzyl alcohol (2:3, v/v),  $n_3 = 1.468$  (slope 4.40); □ = ethanol-benzyl alcohol (1:4, v/v),  $n_3 = 1.510$  (slope 6.34).

sample interaction occurs when lumen refractive index is close to and higher than that of the wall.

#### Dynamic evaluation

In order to make dynamic measurements of perylene we connected the flow cell to a 70-cm long slurry-packed capillary column. An acetonitrile-water (96:4) mobile phase, with a refractive index of 1.344, was passed through the column at constant pressure (3000 p.s.i.), which corresponded to a flow-rate of about  $5 \mu\text{l}/\text{min}$ . Perylene solutions, varying in concentration from  $1.31 \cdot 10^{-8}$  to  $1.31 \cdot 10^{-5} M$ , were injected onto the column using a 10-s moving loop technique. The volume injected was approximately 80 nl.

Perylene detection in the dynamic mode showed reasonable analytical figures of merit. The minimum detectable concentration and quantity (with signal-to-noise ratio 3) are calculated as  $3.46 \cdot 10^{-10} M$  and  $1.38 \cdot 10^{-14} g$ , respectively, using the procedure described by Scott [17]. The response index (linearity) was calculated as 0.486 over the range cited above, therefore the linear range was less than 4 orders of magnitude. These are not quite as good as we have achieved in the past [13] due, mostly, to very low laser power (1.5 mW) delivered

to the cell with the microscope objective. Other factors include low mobile phase refractive index and the small PMT photocathode area. Rationale, for the former is explained above. The influence of detector area is obvious when considering that less light, hence less illuminated volume, is detected with a small area photodetector.

#### Aflatoxin micro-LC

Aflatoxins are among the most potent carcinogens known [18]. Aflatoxins B1, B2, G1 and G2 are the commonly occurring aflatoxins in food products. Subpicogram levels of these aflatoxins have been quantitatively detected using high-pressure liquid chromatography in conjunction with laser-induced fluorescence [19]. The most potent of these aflatoxins, B1, is the least fluorescent and its detection at very low levels has been a challenge. It has been shown that the mobile phase plays an important role in fluorescence properties of these species. With mobile phases such as chloroform and dichloromethane G1 and G2 showed excellent fluorescence but emission from B1 and B2 was markedly quenched [20]. One paper reported that the use of a mobile phase mixture consisting of toluene–ethyl acetate–methanol–formic acid (89:7.5:1.5:2), gave the largest magnitude signals with the shortest overall separation time [21]. Any changes in this “optimum” ratio changed both the chromatographic and fluorescence properties of the analytes.

Since the refractive index of this unique mobile

phase is very close to the refractive index of toluene (1.49), we found that it would be the most suitable for exploring the capabilities of fluorescence detection with axial illumination. A 150- $\mu\text{m}$  capillary yielded a flow cell volume of 159 nL, length = 0.9 cm, and was used in the nebulizing flow cell for isocratic, normal-phase chromatography of aflatoxins B1, G1 and G2. Fig. 10 shows a typical chromatogram of the mixture, at injected concentrations  $6.4 \cdot 10^{-6}$ ,  $7.8 \cdot 10^{-6}$  and  $6.4 \cdot 10^{-6}$  M, respectively. The inset shows the three components near their detection limits.

Prior to obtaining analytical figures of merit, we studied the effect of formic acid concentration on retention and detectability. When added in the proportions 0.3, 1 and 2% (v/v), we found that larger amounts of formic acid dramatically increased detection and decreased retention, especially at the 2% level (data not shown). Levels higher than 2% were not attempted due to incompatibilities with the syringe pump.

Analytical figures of merit for the chromatogram of Fig. 10 are listed in Table II. These data show better concentration and mass detectability, compared to perylene. We attribute this to better laser focussing since the laser power at the entrance of the capillary flow cell was 6.5 mW, approximately 4 times greater than the laser power attained in the perylene measurements. Also, the aflatoxin mobile phase refractive index was higher than the perylene mobile phase, allowing more light to interact with the analytes in the aflatoxin detection.

#### Refractive index measurements

Any light energy that propagates in the capillary wall can be coupled out of the tubular lightguide

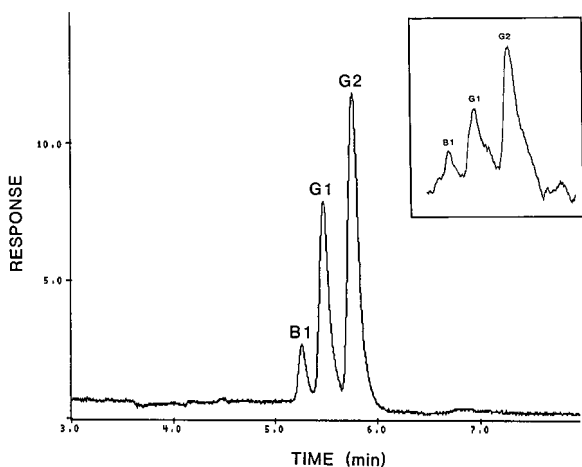


Fig. 10. Aflatoxin chromatogram. See text for details.

TABLE II

#### ANALYTICAL FIGURES OF MERIT FOR AFLATOXINS

MDC = Minimum detectable concentration; MDQ = minimum detectable quantity.

	Aflatoxin		
	B1	G1	G2
MDC	$1.02 \cdot 10^{-9}$ M	$1.45 \cdot 10^{-10}$ M	$3.7 \cdot 10^{-11}$ M
MDQ	$5.05 \cdot 10^{-14}$ g	$7.56 \cdot 10^{-15}$ g	$1.94 \cdot 10^{-15}$ g

and detected. The amount of light that propagates in the wall will be strongly influenced by lumen refractive index, as seen in the Theory section. In this way, the axial illumination flow cell may be used for refractive index measurements, provided that the analyte does not absorb at the analytical wavelength. Several techniques have been used for coupling light from optical lightguides [22]. The simplest approach is to provide a high index of refraction pathway between capillary and optical fiber using coupling gel. A straightforward ratio measurement, using a portion of the incident light as a reference, should suffice as a quantitative indication of refractive index. This is the first report of such a measurement. Our preliminary results include evaluation of both static and dynamic operating modes.

**Static evaluation.** Axial illumination refractive index measurements were made for air, methanol and ethanol, with the liquids being delivered to the flow cell with flow-rates of 10  $\mu\text{l}/\text{min}$ . The measured signals for air, methanol and ethanol were 0.0, 0.71 and 0.90 V, respectively. Using the reference refractive index values of 1.000, 1.326 and 1.359 for these materials, we obtained a response sensitivity of 0.38 RIU/V, where RIU = refractive index unit. Unfortunately, there was significant baseline noise, about  $\pm 0.015$  RIU, in the methanol and ethanol cases. The noise for methanol was slightly larger than for ethanol, an observation that we attribute to fluctuations in the degree of evaporative cooling at the capillary orifice. There were also long term variations, presumably due to mobile phase flow instabilities. Flow and temperature effects have been observed to influence the stability of “on column” refractive index detectors [23].

**Dynamic evaluation.** With a methanol mobile phase and reversed-phase column, injections of a

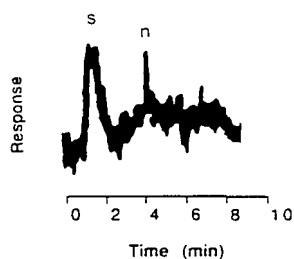


Fig. 11. Refractive index chromatogram. s = 80-nl injection of toluene–methanol with refractive index 1.408; n = electronic noise spike.

methanol–toluene mixture, with a refractive index of 1.408, were made and the signal was recorded. A typical chart recording is shown in Fig. 11. The peak height was 0.06 RIU, which when added to 1.326 (methanol mobile phase) gives a measured value of 1.386. This is very reasonable, considering dilution on the column. The methanol–toluene peak represents detection close to the detection limit, due to significant baseline noise. Obviously, we are less confident in these results, relative to the fluorescence measurements. We observed degraded column performance and unstable electronics, both in the laser and the log ratio amplifier. The basic premise of a dynamic measurement, however, was supported, namely that a transient signal could be recorded accurately and reproducibly.

## CONCLUSIONS

We have demonstrated the successful coupling of micro-LC with axial illumination fluorescence and refractive index detection. The promise of significantly enhanced concentration detectability was not realized in our studies, probably due to low mobile phase refractive index, low laser power (perylene fluorescence measurements), small area detector and, to a certain extent, nebulization noise. Higher mobile phase refractive index would have given more light interaction with the lumen and larger signals. Since the detector area determines the detected volume, a larger detector area (*e.g.* that for a 25-mm diameter photomultiplier) would have resulted in larger detected volume and higher signal levels. Less nebulization noise would have yielded higher signal to noise values, throughout. Effective nebulization of mobile phase at the 5 and 10  $\mu\text{l}/\text{min}$  flow-rate levels was achieved with our flow cell. Despite these limitations, we have obtained reasonable results for *both* detection schemes.

The most significant noise sources appeared to be related to nebulization and electronics. Two possible contributions include refractive index perturbations at the liquid orifice of the capillary during nebulization and microbending losses from a “vibrating” capillary. The Babington nebulization technique was very effective, especially in being easily miniaturized and immune from problems such as residue formation and significant cooling. Alternatives to this approach would not likely be as effective.

tive. Immobilizing the capillary in our flow cell was easily done, however some vibrations remained especially in the refractive index flow cell. Operating the device at elevated, constant temperature would have been helpful in minimizing drift and some spurious low frequency noise. Refinements in both optics and electronics are needed to realize optimum performance.

Axial illumination is a versatile technique for detection in miniaturized liquid chromatographic methods. The technique has been demonstrated for absorbance detection [2], fluorescence and refractive index measurements. Improvements in materials and fabrication techniques may result in more effective designs and higher performance. Technological advances in the area of integrated optical devices may serve as a model. An exciting possibility, whole column detection, using the axial illumination technique may be demonstrated in the near future.

#### ACKNOWLEDGEMENTS

We are grateful to Dr. Mack Harvey of Valco Instruments for the loan of the electric actuator for the microinjector. We also thank Mr. Kavin Morris of the TTU Chemistry machine shop for fabrication of the flow cell.

#### REFERENCES

- 1 I. H. Grant and W. Steuer, *J. Microcol. Sep.*, 2 (1990) 74–79.
- 2 X. Xi and E. S. Yeung, *Anal. Chem.*, 62 (1990) 1580–1585.
- 3 J. A. Taylor and E. S. Yeung, *J. Chromatogr.*, 550 (1991) 831–837.
- 4 X. Xi and E. S. Yeung, *Appl. Spectrosc.*, 45 (1991) 1199–1203.
- 5 J. V. Sweedler, J. B. Shear, H. A. Fishman, R. N. Zare and R. H. Scheller, *Anal. Chem.*, 63 (1991) 496–502.
- 6 K. Jinno and C. Fujimoto, *LC · GC*, 7 (1989) 328–338.
- 7 A. Abbas and D. C. Shelly, *47th Southwest Regional American Chemical Society Meeting, San Antonio, TX, Oct. 1991*, paper No. 38.
- 8 W. Lei, K. Fujiwara and K. Fuwa, *Anal. Chem.*, 55 (1983) 951–955.
- 9 P. Dasgupta, *Anal. Chem.*, 56 (1984) 1401–1403.
- 10 K. Tsunoda, A. Nomura, J. Yamada and S. Nishi, *Appl. Spectrosc.*, 43 (1989) 49–55.
- 11 K. Tsunoda, A. Nomura, J. Yamada and S. Nishi, *Appl. Spectrosc.*, 44 (1990) 163–165.
- 12 R. F. Browner and A. W. Boorn, *Anal. Chem.*, 56 (1984) 875A–888A.
- 13 T. J. Edkins and D. C. Shelly, *J. Chromatogr.*, 459 (1988) 109–118.
- 14 T. J. Edkins and D. C. Shelly, *Anal. Chim. Acta*, 246 (1991) 151–159.
- 15 M. C. Harvey and S. D. Stearns, *J. Chromatogr. Sci.*, 21 (1983) 473–477.
- 16 D. C. Shelly, V. L. Antonucci, T. J. Edkins and T. J. Dalton, *J. Chromatogr.*, 458 (1989) 267–279.
- 17 R. P. W. Scott, *Liquid Chromatography Detector (Journal of Chromatography Library, Vol. 33)*, Elsevier, Amsterdam, 2nd ed., 1986, pp. 18 and 22.
- 18 L. S. Lee, *J. Am. Oil. Chem. Soc.*, 66 (1989) 1398–1409.
- 19 G. J. Diebold and R. N. Zare, *Science, (Washington, D.C.)*, 196 (1977) 1439–1441.
- 20 T. Panalaks and P. M. Scott, *J. Assoc. Off. Anal. Chem.*, 60 (1977) 583–589.
- 21 M. Manabe, T. Goto and S. Matsuura, *Agric. Biol. Chem.*, 42 (1978) 2003–2007.
- 22 S. B. Miller, in D. Marcuse (Editor), *Integrated Optics*, IEEE Press, New York, 1973, pp. 18–22.
- 23 A. E. Bruno, B. Krattiger, F. Maystre and H. M. Widmer, *Anal. Chem.*, 63 (1991) 2689–2697.

# Peak tracking with a neural network for spectral recognition

P. M. J. Coenegracht, H. J. Metting, E. M. van Loo, G. J. Snoeijer and  
D. A. Doornbos

*Chemometrics Research Group, University Centre for Pharmacy, NL-9713 AW Groningen (Netherlands)*

---

## ABSTRACT

A peak tracking method based on a simulated feed-forward neural network with back-propagation is presented. The network uses the normalized UV spectra and peak areas measured in one chromatogram for peak recognition. It suffices to train the network with only one set of spectra recorded in one chromatogram of a sample to recognize the sample peaks in other chromatograms recorded in different mobile phases. The peak recognition method was used in a mixture design-based optimization of the separation of eight sulphonamides, some of which have very similar spectra. Even peaks in a cluster of four to five overlapping peaks could be recognized.

---

## INTRODUCTION

### *Peak tracking*

For the optimization of ternary and quaternary mobile phases in HPLC by simultaneous methods, mixture designs are often used [1–3]. Peak tracking is essential for the application of these methods because the capacity factor of each analyte in the sample has to be determined in every design point. Peak recognition has to be discerned from solute identification. In solute identification the chemical identity of a peak is determined by comparison with the retention time or spectrum of a reference standard. If the number of analytes is not known then the issue of the peak homogeneity has to be addressed, otherwise peak recognition is sufficient. If the number of solutes is known it suffices to keep track of the band identity when the chromatographic conditions are changed.

Even if two peaks overlap completely, identification by exclusion is possible if the other peaks are recognized, and both can be given the same value of

the capacity factor. Severely overlapping peaks pose a different problem as their identity has to be established unequivocally. This may be done by separate injection of the reference substances and comparison of retention times. This is time consuming and reference substances have to be available. If reference substances are not available, comparison of peak areas is another possibility. At least a 20% difference in peak areas is needed for the correct assignment of each peak and the number of peaks has to be equal to the number of solutes in all chromatograms [4]. Moreover, peak areas may change considerably when the changing chromatographic conditions shift the UV spectra of the solutes.

Multiple-wavelength detection considerably increases the information content of the chromatograms and spectral matching can be used to recognize peaks in different runs. Deconvolution techniques can also be used to extract peak profiles and even component spectra for overlapping peaks [5]. By factor analysis methods and a set of reference spectra the presence of a solute in peak cluster can be revealed [target transformation factor analysis (TTFA)]. Both the individual profiles and component UV spectra can be derived by an iterative

---

*Correspondence to:* P. M. J. Coenegracht, Chemometrics Research Group, University Centre for Pharmacy, Ant. Deusinglaan 2, NL-9713 AW Groningen, Netherlands.



procedure (ITTFA) [5]. These methods are very powerful, have complementary characteristics and require expert knowledge for their correct implementation.

Peak size plus relative retention have been combined in a peak tracking procedure [6], but the combination of peak size and spectral information has also been used [6,7]. Reviews of different peak tracking methods have been published recently [4,8,9].

Wright *et al.* [10] used a peak recognition strategy based on comparison of peak integrals determined at different wavelengths in an automated optimization procedure. They stated that the procedure requires only complete resolution of each solute in one of the seven chromatograms resulting from the mixture design and complete resolution of all components in a single chromatogram is not required. The tracking procedure was shown to deal with situations where moderate two component overlap occurs.

The tracking procedure proposed in this paper uses UV spectra collected by a multi-channel diode-array spectrophotometer and peak areas measured at one wavelength. The spectra of all components are measured in one chromatogram, normalized and multiplied by the corresponding peak areas and used for training a neural network. To obtain the training set of the pure spectra, the front or tail of a two-component chromatographic peak has to contain the single pure component and complete resolution is not necessary. The trained network is used for peak recognition and again complete resolution is not necessary. In principle, none of the chromatograms resulting from the mixture design has to be separated completely, the spectral similarity of the different solutes can be high and shifts of the UV spectra on changing the mobile phase composition are permitted.

### Neural network

Neural networks are mathematical systems designed for parallel processing of information consisting of processing elements, neurons or nodes. The following description applies to a typical feedforward neural network with back-propagation and is restricted to the information necessary to understand its functioning. Books on different types of network [11], the back-propagation network [12]

and papers reviewing [13] or describing the theory and application of the back-propagation network [14–17] have appeared recently.

The typical feedforward neural network with back-propagation has three layers of nodes: the input, the hidden and the output layer. The nodes of the input layer accept the input vector  $\mathbf{X}_k$  (absorbance values measured at different wavelengths of the UV spectrum in this instance) and each node is connected to every node of the hidden layer. Each node of the hidden layer is connected to every node of the output layer that produces the output vector,  $\mathbf{Y}_k$ . These connections are weights which are applied to signals passed from one neuron to the next. The nodes in one layer are not interconnected.

There is one input node per variable in a spectrum. The input nodes pass the weighted input signals to the nodes in the hidden layer. The hidden layer nodes transform the sum of the weighted inputs by a non-linear, sigmoidal transfer function and pass weighted signals to the nodes of the output layer. The output nodes produce output signals that are obtained by applying again a sigmoidal transfer function (eqn. 1) upon the sum of the weighted values passed to them.

$$f(x) = \frac{1}{1 + e^{-(x+\theta)}} \quad (1)$$

The bias parameter,  $\theta$ , can be treated as an additional weight that is always added to the weight vector of every node, but is multiplied by a value of 1 instead of  $y_j$  or  $y_i$  (see eqns. 2 and 4). It can be regarded as a threshold value at which the output of a neuron is released.

The number of output nodes is equal to the number of components of the sample; the number of hidden nodes is an adjustable parameter and was chosen to be equal to the number of input nodes.

The weights or connection strengths between the nodes in the consecutive layers of the network form two matrices, which contain random numbers in the untrained network. In the trained network the matrices contain the modified weights and represent the knowledge of the network. The weights are modified by supervised learning. During the training pairs of input and output vectors,  $\mathbf{X}_k$  and  $\mathbf{T}_k$ , are presented to the network. The training set consists of spectra of the solutes and the corresponding target vectors. During the training the produced output

vector,  $Y_k$ , is repeatedly compared with the target vector,  $T_k$ . Each time the weights are adjusted in the direction of the correct answer. The change of a weight,  $\Delta w_{jk}$ , between a node  $j$  of the hidden layer and a node  $k$  of the output layer is proportional to the difference,  $\delta_k$ , between an element of the target vector and the corresponding element of the output vector and to the value  $y_j$  of the signal passed on by the node of the hidden layer to the output node (delta rule):

$$\Delta w_{jk} = \eta \delta_k y_j \quad (2)$$

where  $\eta$  is the learning rate and

$$\delta_k = (t_k - y_k) y_k(1 - y_k) \quad (3)$$

For the calculation of the error term,  $\delta_j$ , of node  $j$  of the hidden layer, comparison with a target value is not possible, but the error has to be calculated from the output layer:

$$\Delta w_{ij} = \eta \delta_j y_i \quad (4)$$

$$\delta_j = \sum_k (\delta_k w_{jk}) y_j(1 - y_j) \quad (5)$$

where  $\Delta w_{ij}$  is the weight between node  $i$  of the input layer and node  $j$  of the hidden layer and  $y_i$  is the output of input node  $i$ .

To summarize the back-propagation algorithm:  $X_k$  is propagated through the network to the output layer. The output  $Y_k$  is compared with the target,  $T_k$ , node by node and used to correct the weights. Corrections for the hidden layer are calculated from the errors of the output layer.

To complete the description of the back-propagation network, the momentum term has to be discussed. The momentum factor,  $\alpha$ , relates the present value of  $\Delta w(t)$  to its value in the previous learning cycle,  $\Delta w(t-1)$ , and furthers faster convergence with fewer oscillations and avoids entrapment in local minima.

$$\Delta w_{ij}(t) = \eta [(1 - \alpha) \delta_j y_i + \alpha \Delta w_{ij}(t-1)] \quad (6)$$

The neural network programme used in this investigation uses eqn. 6 and a value of 0.9 for  $\alpha$ . When a neural network is used for spectral recognition one attempts to obtain a model that produces the correct set of outputs for a set of spectra. Such a model is obtained by training the network. The trained neural network should be able to generalize from the examples presented during the training,

*i.e.*, spectra of several analytes recorded in a given mobile phase composition, to other inputs that it has not yet seen, *i.e.*, spectra of the same analytes recorded in different mobile phase compositions.

An important issue in the application of a neural network is the choice of the training set: how many examples are necessary and how well has the variable space to be covered by the selected examples to obtain a trained network that produces correct outputs?

In this work we obtained two collections of spectra, one of twelve sulphonamide derivatives and another of fifteen mainly benzene derivatives, recorded in six different mobile phase mixtures composed of water, methanol (MeOH) and acetonitrile (MeCN) (Tables I and VI) to train two networks. Each collection of spectra consists of six sets of twelve and fifteen spectra, respectively. First we investigated how many of the six sets were needed to obtain a trained network that could recognize the spectra in the remaining sets correctly. We also investigated whether the number of training sets could be reduced by multiplying the normalized spectra with a number corresponding to the peak area. Second, a subset of eight sulphonamide derivatives was optimized by a mixture design procedure [3] using the same variable space to test the procedure. To make the test more severe, an old column with a low plate number was used.

## EXPERIMENTAL

### *Apparatus and materials*

The spectra were recorded with a Philips PU4120 diode-array detector. This detector was combined with a Waters Assoc. Model 6000 A pump and a Rheodyne Model 7010 injection valve fitted with a 20- $\mu$ l loop. Separations were performed at room temperature (*ca.* 20°C) on a 200  $\times$  4 mm I.D. stainless-steel column packed with Nucleosil RP-8, particle size 5  $\mu$ m,  $N = 2000$ . The flow-rate was 1.0 ml/min. The dead time was measured at all design points by injection of uracil and was 2.0 min.

All calculations, *i.e.*, data handling of the diode-array spectra, peak integration, principal component analysis (PCA) and simulation and training of the neural network were performed on an IBM-compatible AT 286 personal computer with mathematical coprocessor.

Mobile phases were prepared from HPLC-grade methanol and acetonitrile (Labscan) and purified deionized water (Milli-Ro/Milli-Q system; Millipore). In the sulphonamide experiments water was acidified with 1% acetic acid. The test solutes were used as purchased. The sulphonamides, diazepam, nicotinic acid and theophylline were of pharmacopoeial grade and the benzene derivatives of "zur Synthese" grade (Merck, Darmstadt, Germany). The test solutions for recording of the spectra were prepared freshly at concentrations varying from 5  $\mu\text{g/ml}$  for the sulphonamides to between 1 and 150  $\mu\text{g/ml}$  for the other solutes, depending on their molar absorptivities. The sulphonamide solutions were acidified with 1% acetic acid. The concentration of the sulphonamides in the test sample for the optimization varied from about 30 to 160  $\mu\text{g/ml}$ .

The spectra of the sulphonamides, A–L (Fig. 1), constituted the first data set. The second data set was formed by the spectra of aniline (A, 0.27), N-butyl *p*-aminobenzoate (B, 0.57), *p*-cresol (C, 0.63), dimethyl phthalate (D, 0.39), ethylbenzene (E, 0.33), *p*-nitrobenzaldehyde (F, 0.69), nitrobenzene (G, 0.45), 2-phenylethanol (H, 0.21), *n*-propyl *p*-hydroxybenzoate (I, 0.15), *p*-toluidine (J, 0.87), toluene (K, 0.93), diazepam (L, 0.51), nicotinic acid (M, 0.75), theophylline (N, 0.81) and uracil (O, 0.99), where the numbers in parentheses refer to peak area-factors mentioned below.

### Software

The following programmes were used: neural network simulation, Brainmaker vs. 2 (California Scientific Software, Sierra Madre, CA, USA); diode-array data handling, Philips PU 6003 vs. 3.0 software (Analytical Chromatography); data system, vs. 6.0, Philips PU 6000 integration software; principal components analysis, Unscrambler II, vs. 3.5 (Camo, Trondheim, Norway); and optimization software, POEM (predicting optimum eluent mixtures), vs. 3.1 (University Centre of Pharmacy, Groningen, Netherlands [3]).

## RESULTS

### Neural network training

**Sulphonamides.** The spectra of the twelve sulphonamides (Fig. 1A–L) were recorded from 237 to 390 nm in the six eluent mixtures indicated in

Table I. One spectrum consisted of 98 absorbance values, which were scaled to the same area under the curve to remove the concentration effect from the spectra. The normalized area is equal to the number of data points in the spectrum. To obtain an impression of the spectral similarity, the correlation coefficients between the twelve spectra recorded in design point 4 of Table I were calculated and all 72 spectra were subjected to a PCA. The results are shown in Table II and Fig. 2. The first two PCs explained 87% of the variation in the data. From the score plot a strong overall similarity is indicated between the spectra of analytes G, J and D, D and E and K and A. This result is corroborated by high values of the corresponding correlation coefficient of the corresponding analytes in one eluent composition (Table II). From the score plot one can conclude that two PCs are not sufficient to identify the analytes.

The neural network was designed to have 98 input nodes, 98 nodes in the hidden layer and 12 output nodes, the learning rate  $\eta = 1$  and the momentum factor  $\alpha = 0.9$ . The value of the output nodes can vary between 0 and 1. The network was trained by presenting repeatedly a number of training sets to the network. One set can consist of twelve spectra recorded in one eluent plus twelve output vectors. For example, the spectrum of sulphonamide A is presented together with an output vector consisting of twelve elements, where 1 is the first element and the remaining eleven elements are zeros; the spectrum of sulphonamide B is combined with a vector of which the second element is 1 plus eleven zeros, etc. The training stops if the difference between the output value of each node and the desired value is 0.1. The trained network is presented with a test set of twelve spectra recorded in an eluent that has not been used in the training set and the network is expected to produce the correct output vector. The output vector was assumed to be correct if the value of the correct output node was greater than 0.7 while the remaining output values were smaller than 0.3. These limit values were chosen arbitrarily but are considered to be a severe criterion for making a decision.

It is to be expected that if a network is trained with a training set of 48 spectra recorded in eluents 1, 2, 3 and 4 of Table I, the network should produce the correct output vectors, because these design points

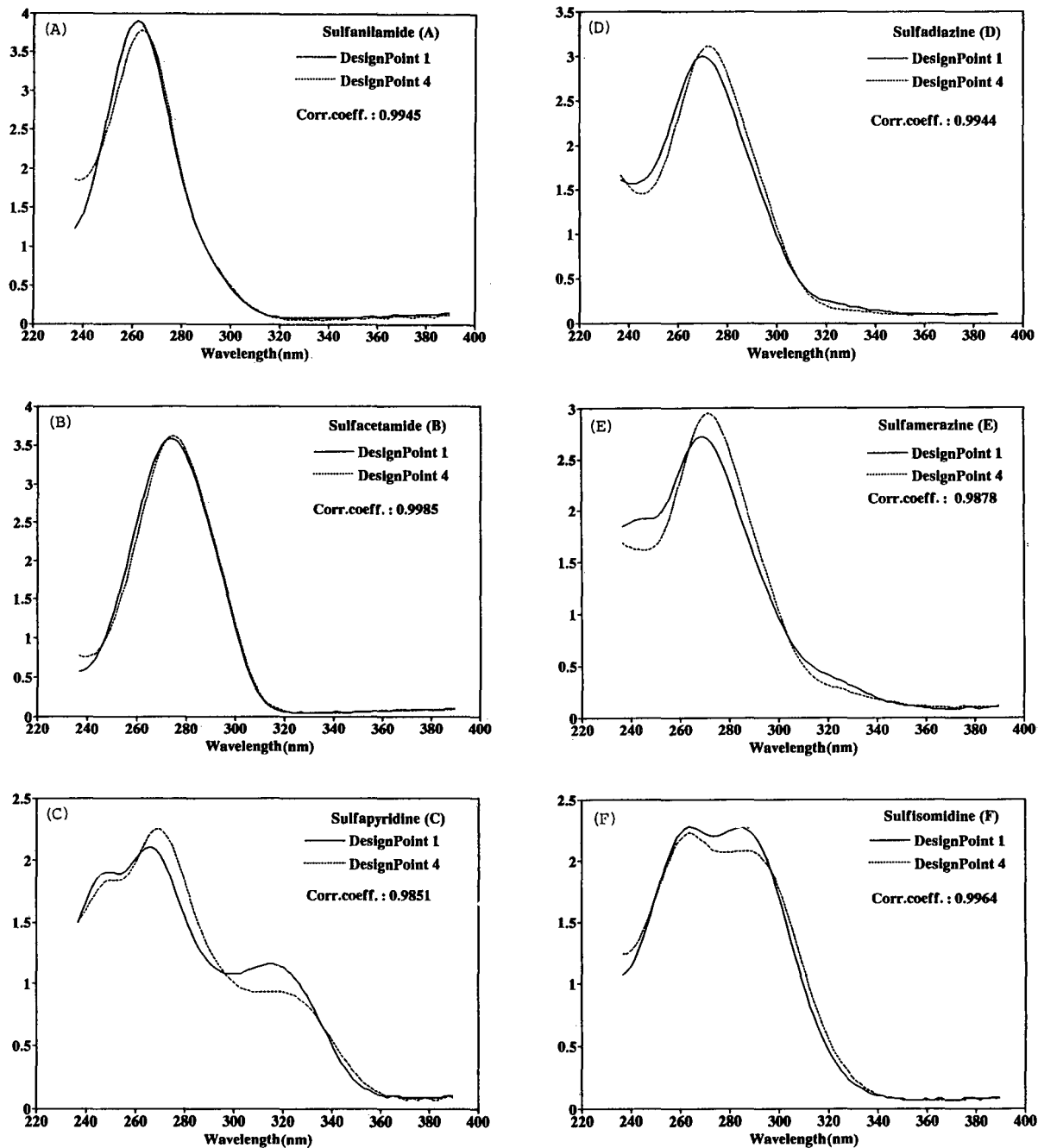


Fig. 1.

(Continued on p. 150)

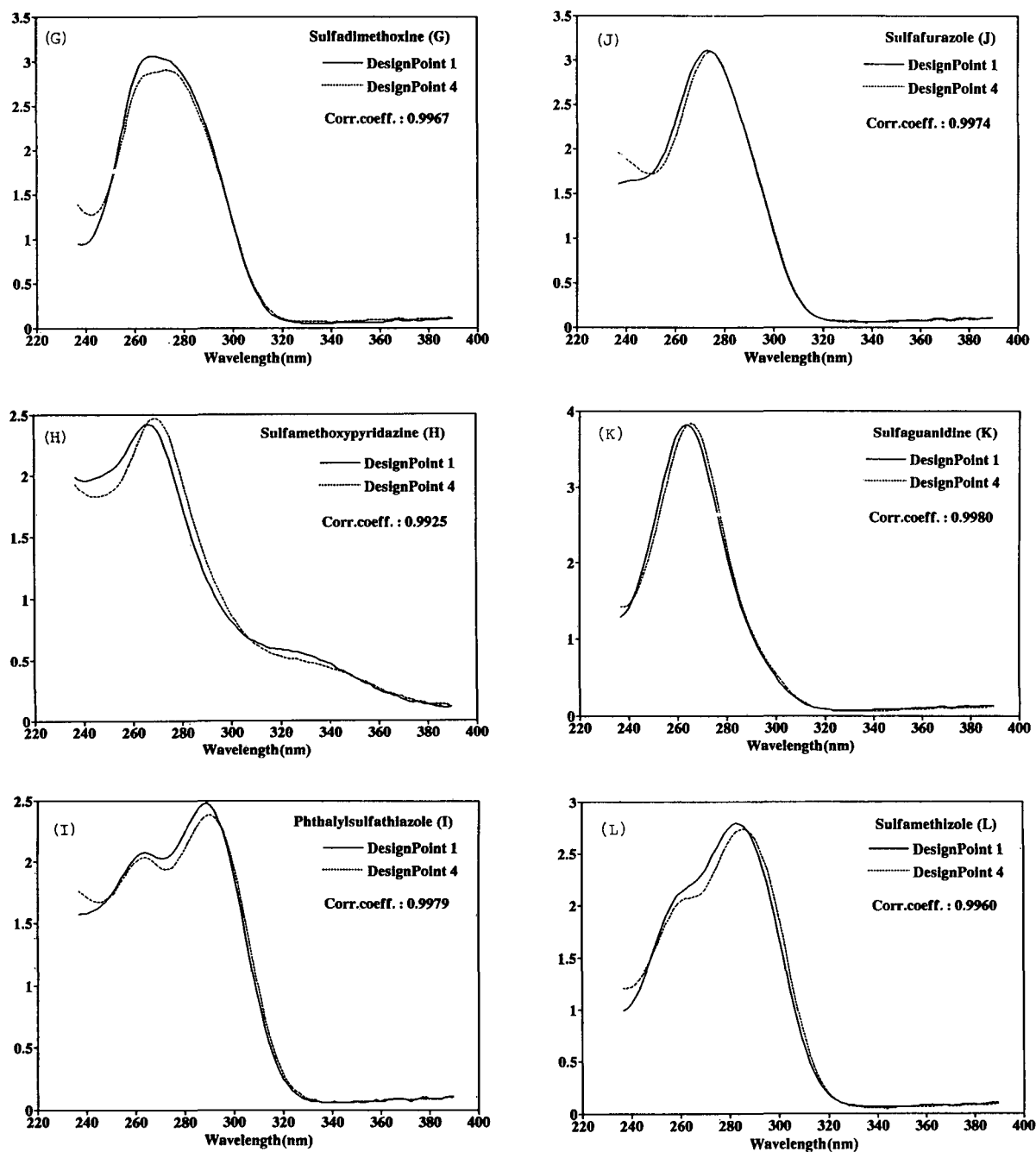


Fig. 1. Spectra of twelve sulphonamides normalized to the same area under the curve. The spectra were recorded in eluent compositions (solid lines) 1 and (dotted lines) 4 in Table I. The correlation coefficient between the two spectra is shown.





TABLE IV  
PEAK AREA VALUES FOR SULPHONAMIDES A–L

Sulphonamide	Peak area	Sulphonamide	Peak area
A	0.69	G	0.55
B	0.83	H	0.48
C	0.76	I	0.34
D	0.41	J	0.20
E	0.90	K	0.27
F	0.62	L	0.97

between the different analytes is smaller, but the spectral shifts of the individual analytes in different eluents are larger (Fig. 3). The clusters in Figs. 3 and 2 seem to be similar, but the first two PCs explain 80% of the variance in the spectra of the benzene derivatives against 87% in Fig. 2.

Spectra were recorded from 190 to 346 nm. Per spectrum 100 absorbance values were collected and after normalization the spectra were presented to a network consisting of 100 input nodes, 15 output nodes and a variable number of nodes in the hidden layer. In one experiment the normalized spectra were multiplied by area factors ranging from 0.15 to 0.99 (see Experimental). From the results presented in Table VII one can conclude that the performance of the network decreases as indicated by the NER and that the training time increases as indicated by

TABLE V  
NER AFTER TRAINING WITH ONE SET OF AREA MULTIPLIED SULPHONAMIDE SPECTRA

Number of eluent in Table I used						
Training	Testing					
	1	2	3	4	5	6
1	—	0.83	1.00	0.83	0.83	0.92
2	1.00	—	1.00	1.00	1.00	1.00
3	1.00	1.00	—	1.00	1.00	1.00
4	0.83	0.83	0.92	—	0.92	0.92
5	1.00	1.00	0.92	1.00	—	0.92
6	0.92	0.83	1.00	1.00	0.92	—

TABLE VI  
ELUENT COMPOSITIONS AT DESIGN POINTS 1–6 (BENZENE DERIVATIVES)

Design point No.	Fraction		
	Water	MeOH	ACN
1	0.60	0.40	0.00
2	0.40	0.60	0.00
3	0.65	0.00	0.35
4	0.45	0.00	0.55
5	0.55	0.25	0.20
6	0.45	0.25	0.30

the number of cycles when the number of hidden nodes is decreased from 120 to 10. The decrease in performance is not linearly related to the number of nodes. There seems to be an optimum number of nodes for the hidden layer at about 120 nodes; with 130 nodes in the hidden layer the performance seems to decrease also. For the existence of an optimum number of nodes in the hidden layer more indications were found from experiments with a network that had two hidden layers.

The number of cycles is an indication of the time necessary to train the network, but the training time also depends on the amount of data in the training set and on the performance of the computer. On a training set of twelve spectra the network is trained in a few minutes on a fast PC. The last two experiments of Table VII show clearly that it is essential to multiply the normalized spectra by an area factor to train a neural network successfully on only one training set.

#### Peak tracking and optimization

It is the aim of this paper to demonstrate the feasibility and some limitations of peak tracking with a neural network in an optimization procedure based on a simplex lattice mixture design. A subsample of eight of the sulphonamides was selected, because the spectra of the sulphonamides are very similar. It was decided to use a ternary mobile phase consisting of water, methanol and acetonitrile, because we prefer this approach to the use of a quaternary eluent consisting of three isoelutotropic binary eluents of water with methanol, acetonitrile and tetrahydrofuran. With the preferred approach it



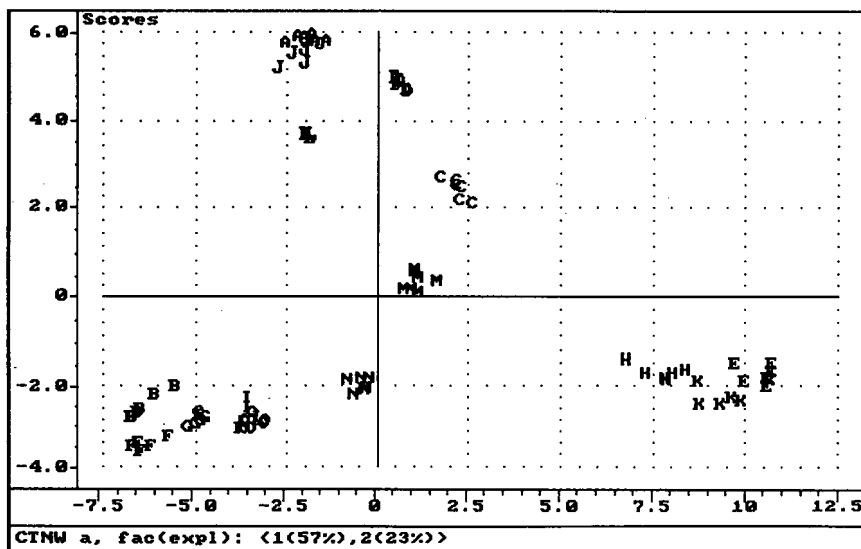


Fig. 3. Score plot of fifteen benzene derivative spectra recorded in the six eluent compositions in Table VI.

is possible to optimize simultaneously the solvent strength and solvent selectivity and no experiments have to be performed to select the appropriate isoelutotropic eluents if one has an approximate knowledge of the required solvent strength [18]. The factor space and the design points are shown in Fig. 4; the corresponding mobile phase compositions and measured peak areas in Table VIII.

Chromatograms were recorded for the nine mo-

bile phases required by the design and peak areas were determined with the integration software at 270 nm (Table VIII). Every 2 s a spectrum was recorded and for each peak of every chromatogram one spectrum was selected at the peak maximum. The selected spectra were normalized and multiplied by the peak areas. In this way a set of eight spectra per chromatogram were obtained to be used for peak recognition by the trained network. The net-

TABLE VII

RESULTS OF TRAINING DIFFERENT NETWORKS WITH DIFFERENT SETS OF NORMALIZED BENZENE DERIVATIVE SPECTRA

Number of eluent in Table VI used		Number of hidden nodes	NER	Cycles
For training	For testing			
1+2+3+4	5+6	130	0.93	96
1+2+3+4	5+6	120	1.00	93
1+2+3+4	5+6	115	0.97	104
1+2+3+4	5+6	100	0.93	106
1+2+3+4	5+6	58	0.90	216
1+2+3+4	5+6	10	0.87	235
5	1+2+3+4	100	0.60	—
5 <sup>a</sup>	1+2+3+4	100	1.00	75

<sup>a</sup> Spectra multiplied by area factor.

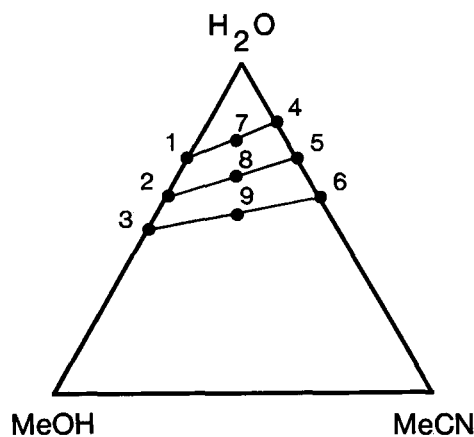


Fig. 4. Mixture triangle which shows the location of the design points in the factor space used for the optimization of the separation of sulphonamides.

work was trained with the spectra obtained from the chromatogram recorded with mobile phase 7 (Fig. 4), which then was taken as the reference chromatogram (Fig. 5G). The reference substances were injected separately in the mobile phase of design point 8 (Fig. 4) to establish the chemical identity of the peaks. The peak areas of the same peak measured in the different chromatograms are not constant (Table VIII) as they are determined for fused peaks by the perpendicular drop method. In a

few instances only one integration value was produced by the software for a pair of fused peaks and the individual peak areas were estimated (see Table VIII, values marked <sup>a</sup>) from the produced value using the ratio of the reference chromatogram. The inaccuracy of the area factor probably sometimes affected peak recognition.

In the chromatogram in Fig. 5E (design point 5) peak A was attributed by the network to sulphanilamide and sulphadimetoxine with almost the same output value. In this chromatogram, however, peak G was correctly recognized as sulphadimethoxine and therefore it was safe to assume that peak A belonged to sulphanilamide. The same problem occurred in the chromatogram in Fig. 5H (design point 8) with peaks E and J: two solutes were attributed to each peak. As the remaining peaks of the chromatogram were recognized unequivocally, it was nevertheless possible to attribute the correct solutes to the peaks in question by selecting the two solutes that had not been attributed unequivocally to the other peaks and choosing between them on the basis of the retention time. The recognition of the remaining peaks in chromatograms of design points 1, 2, 4, 5 and 8 (Fig. 5A, B, D, E and H) on the basis of the highest output value of the network was correctly performed without problems.

The chromatograms in Fig. 5C, F and I posed a serious problem owing to very strong overlap of several peaks. In the chromatogram in Fig. 5C the

TABLE VIII

ELUENT COMPOSITIONS AT THE DESIGN POINTS 1–9 OF FIG. 4 AND PEAK AREAS OF THE SULPHONAMIDES

Design point No.	Fraction			Sulphonamide							
	Water	MeOH	MeCN	A	F	C	E	H	J	I	G
1	0.70	0.30	0.00	2.8	7.2	4.2	7.3	2.7	1.6	0.8	5.8
2	0.60	0.40	0.00	3.4	6.2 <sup>a</sup>	6.2 <sup>a</sup>	7.5	2.8	1.8	0.9	6.0
3	0.50	0.50	0.00	3.0	6.4	5.0	7.5	3.0 <sup>a</sup>	1.8 <sup>a</sup>	0.9	5.7
4	0.80	0.00	0.20	3.2 <sup>a</sup>	8.2	5.5	8.7	4.0	2.0	0.9	6.5
5	0.70	0.00	0.30	2.4	7.4	5.5	7.8 <sup>a</sup>	3.7 <sup>a</sup>	2.1	1.0	6.4
6	0.60	0.00	0.40	3.3 <sup>a</sup>	6.8	5.5 <sup>a</sup>	7.1	3.6 <sup>a</sup>	2.0	1.0	6.0
7 <sup>b</sup>	0.76 <sup>b</sup>	0.12 <sup>b</sup>	0.12 <sup>b</sup>	2.1 <sup>b</sup>	6.7 <sup>b</sup>	4.5 <sup>b</sup>	7.3 <sup>b</sup>	2.8 <sup>b</sup>	1.9 <sup>b</sup>	0.9 <sup>b</sup>	5.8 <sup>b</sup>
8	0.66	0.17	0.17	3.2	6.6	4.6	7.4	2.6	1.5	1.0	5.6
9	0.56	0.22	0.22	5.3	6.2	4.8	8.5	3.0	1.8	1.3	5.6

<sup>a</sup> Estimated values.

<sup>b</sup> Values of reference chromatogram.

merged second and third peaks contain six solutes and peak recognition fails. Normally we would have reduced the design space by moving the lower

boundary in the direction of the apex of the triangle after the registration of the chromatogram in point 3 (Fig. 5C), because the resolution is too low. It was

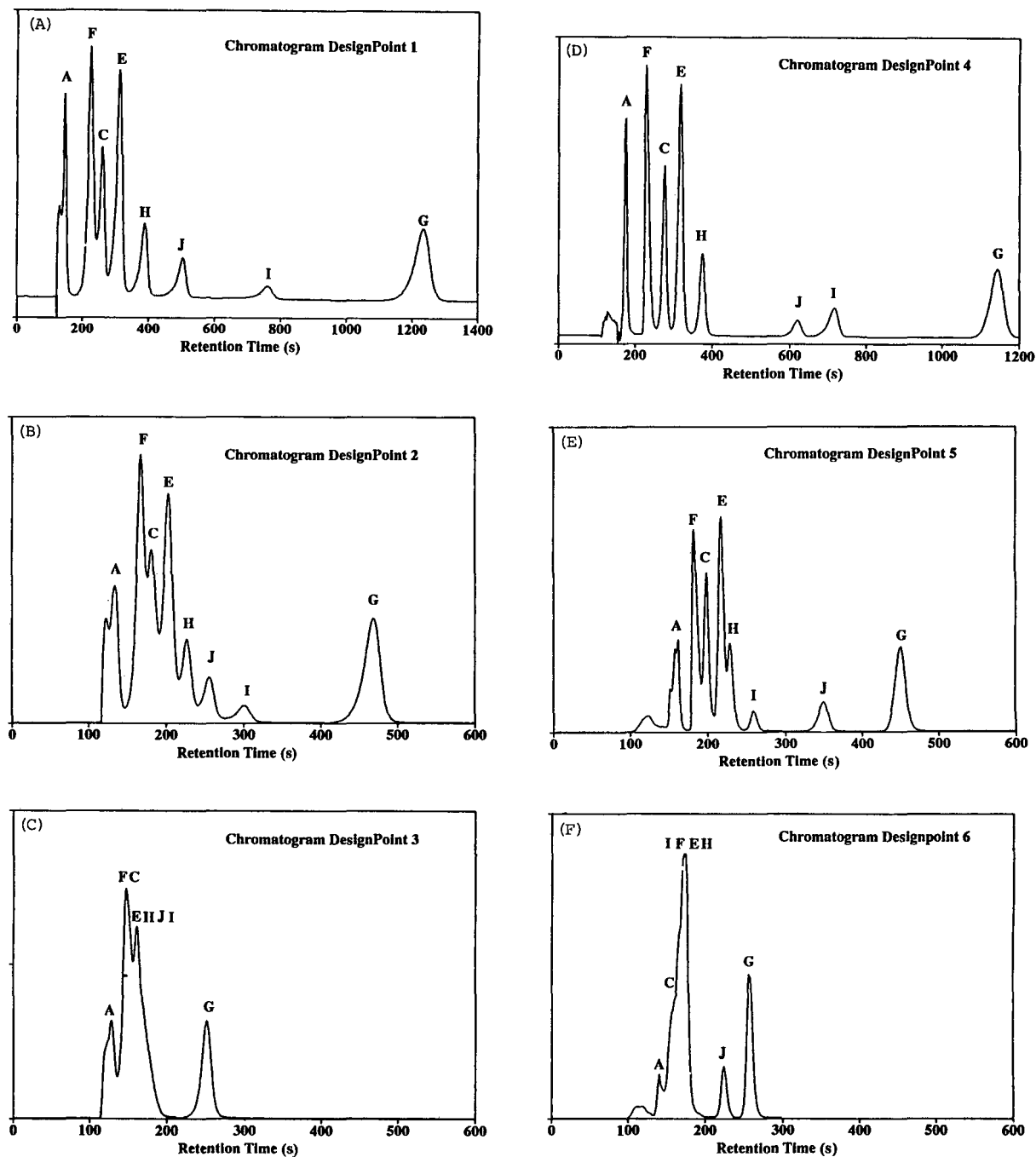


Fig. 5.

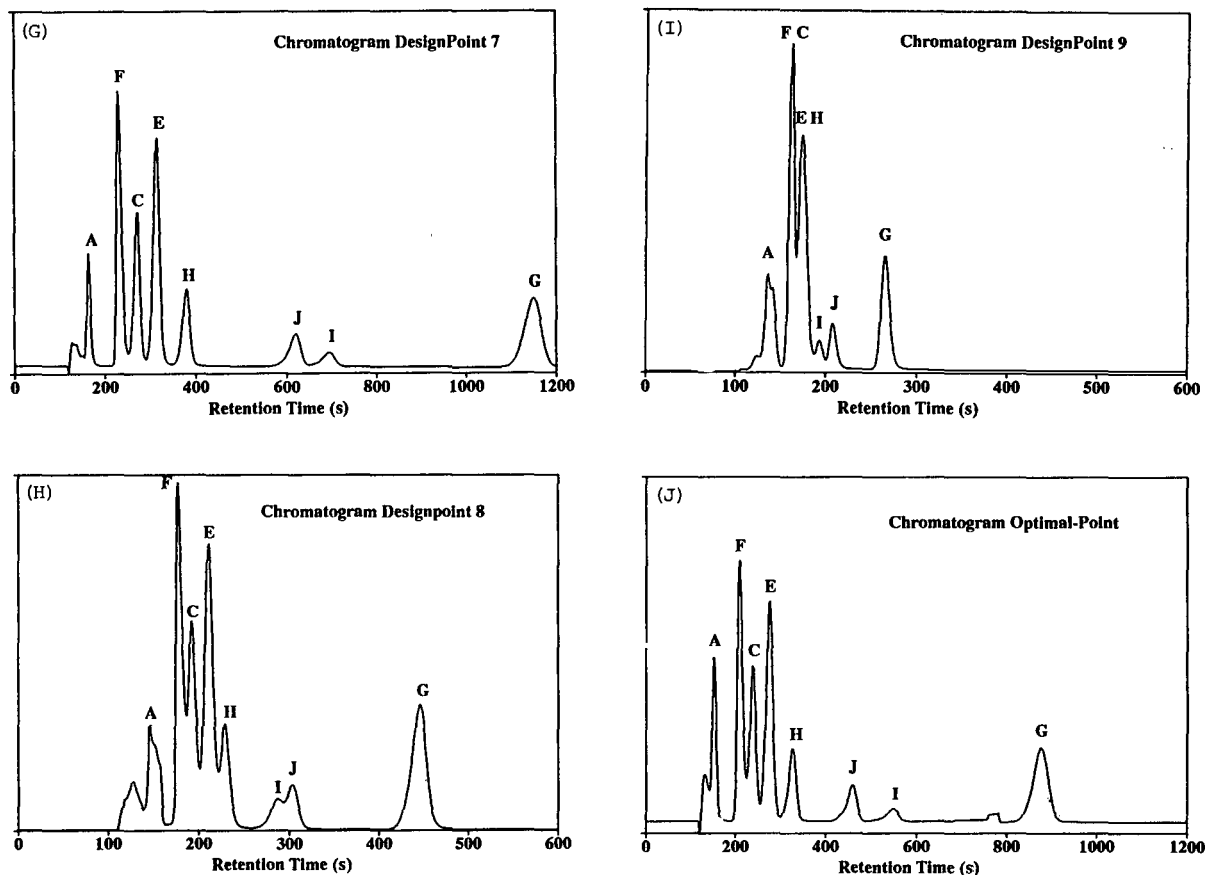


Fig. 5. Chromatograms recorded at the nine design points in Fig. 4 plus one PO chromatogram which offers a good compromise between resolution and analysis time. The first peak in every chromatogram is uracil, which was used to determine the dead time.

decided, however, to continue and divide the original sample of eight solutes into two subsamples. The two subsamples were injected separately. One subsample contained the solutes E, F and J and the other the remaining solutes. Peak recognition was possible in the subsample chromatograms, except in design point 6, where the first subsample still showed strong overlap. Additional single injections of solutes E and F were necessary for the determination of the capacity factor and a total of fourteen injections was needed to complete the determination of the capacity factors of eight solutes in nine mobile phase compositions.

The capacity factors of the eight solutes were used to model the logarithm of the capacity factor of every solute as a function of  $x_1$ ,  $x_2$  and  $x_3$ , which are

the fractions of the components of the water–MeOH–MeCN mobile phase. Polynomial models were estimated by multiple linear regression. A grid search of the response surfaces predicted the capacity factor of every solute at all eluent compositions of the design space necessary to construct a grid with a 1% interval in the eluent composition. In every grid point two optimization criteria were calculated: the resolution of the worst separated pair of adjacent peaks, *i.e.*, the minimum resolution or  $R_{s\ min}$ , and the capacity factor of the last-eluted peak,  $k_{\max}$ , which is a measure of the analysis time. A contour map of the  $R_{s\ min}$  (Fig. 6) shows two local maxima between which one may choose. The choice is guided by the second criterion,  $k_{\max}$ , because it advantageous to obtain a sufficient value of  $R_{s\ min}$  in the shortest

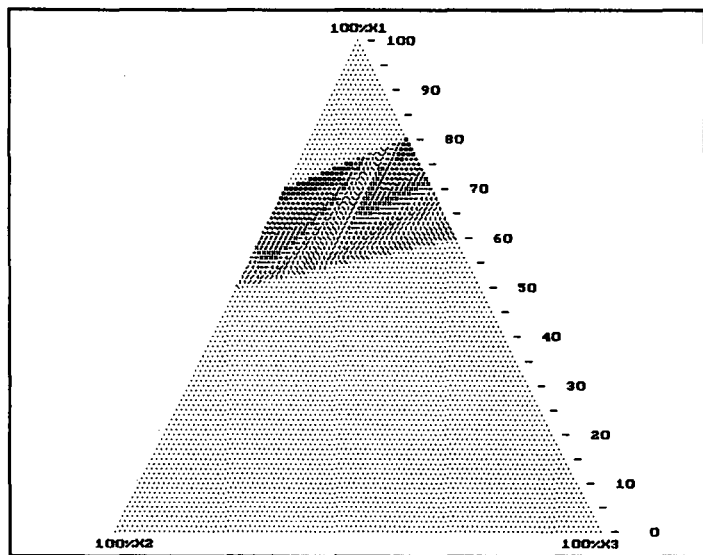


Fig. 6. Response surface of the minimum resolution,  $R_{s\ min}$ , of the non-isoelectrotropic ternary system water ( $x_1$ )–MeOH ( $x_2$ )–MeCN ( $x_3$ ). Different symbols correspond to ten different ranges of values of  $R_{s\ min}$ . The lowest range is indicated by backslashes (0.00–0.16) in the middle and lower right part of the design space and the highest range by black squares (1.44–1.60) at the left and extreme right of the upper boundary of the design space.

analysis time possible, *i.e.*, at the lowest value of  $k_{\max}$ .

The multi-criteria decision making (MCDM) procedure [19,20] is well suited to achieve a quantitative weighting of both criteria against each other. Therefore, an MCDM diagram is constructed, consisting of two perpendicular coordinate axes. On the hori-

zontal or time axis a scale for  $k_{\max}$  is indicated and on the vertical axis a scale for  $R_{s\ min}$  is shown. Every eluent composition of the design space generates one value of  $R_{s\ min}$  and one value for  $k_{\max}$ . Hence every eluent composition can be represented by one point in the MCDM diagram. From the resulting cloud of points only the “pareto optimum” (PO) points are

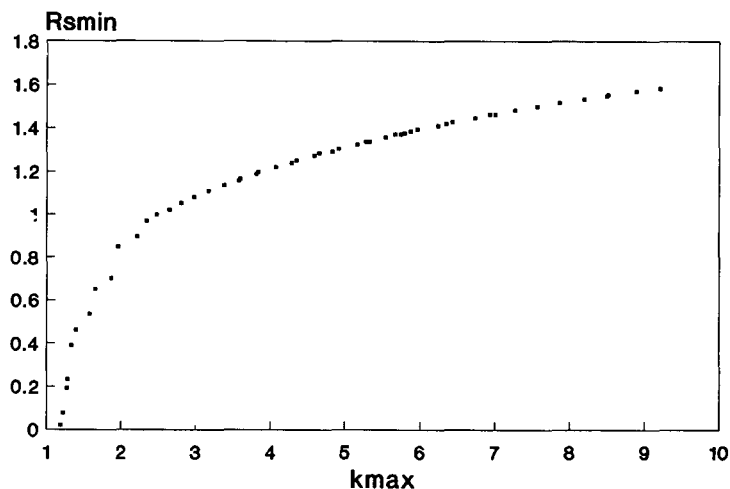


Fig. 7. MCDM diagram. Points represent PO eluent compositions which give the best combinations of  $R_{s\ min}$  and  $k_{\max}$ .

TABLE IX  
MEASURED PEAK AREAS AND PREDICTED AND MEASURED RETENTION TIMES FOR CHROMATOGRAM IN FIG. 5J

Peak	Area	Retention time (s)	
		Measured	Predicted
A	2.9	148	140
F	6.8	202	198
C	4.7	232	234
E	7.4	268	268
H	2.9	316	317
J	1.9	448	448
I	0.8	544	534
G	5.7	868	875

shown in the diagram (Fig. 7). A point is called a PO point if no other point in the diagram exists that yields an improvement in one criterion without causing a deterioration of the other criterion. The PO points give the eluent compositions that provide the best possible combinations of the two criteria and show the pay-off between the two criteria. If a value of 1.4 for the  $R_{s\min}$  is acceptable, then the value of  $k_{\max}$  is 6.2 for an eluent consisting of water–MeOH–MeCN (70:22:8). The corresponding, measured chromatogram is shown in Fig. 5J. Owing to peak asymmetry, the measured  $R_{s\min}$  is lower than the predicted value. The predicted retention times, however, correspond well with the measured retention times (see Table IX, which also shows the measured peak areas). The mean, relative difference between the measured and predicted values is 1.4%. All peaks were correctly recognized by the trained neural network.

## CONCLUSIONS

It has been shown that a simulated feed-forward neural network with back-propagation consisting of an input, hidden and output layer can be used for peak recognition in mixture design-based optimization procedures.

For peak recognition the normalized UV spectrum of the components and the peak areas were used to train the network. Both were required to be

able to train the network with only one set of training data, *i.e.*, the spectra and areas measured in only one mobile phase composition. This means that the data of only one reference chromatogram were needed for tracking the peaks in other chromatograms, which were obtained with different mobile phase compositions. If only spectra were used to train the network then the spectra recorded in at least two different mobile phases are necessary to train the network. In that event one reference chromatogram is not sufficient and at least two are needed, which makes the procedure much less attractive.

The spectra and peak areas of eight sulphonamides were used in an illustrative example. Peak recognition of single peaks and of peaks in fused clusters of 2–6 components was possible, although the spectra of some components were very similar and the mean relative standard deviation in the measured peak areas was 13%.

Spectra were recorded at the peak maxima and the peaks in the reference chromatogram were almost completely separated. The results of this investigation, however, suggest that complete separation of the peaks in one reference chromatogram is not a necessary condition for the success of the procedure. It suffices that one can measure for each component one spectrum and one peak area. This may be done in one or more chromatograms, and single but also overlapping peaks can be used, if the spectra can be measured at the peak flanks and the peak areas can be measured with moderate precision. Almost the whole peak tracking procedure was performed with commercially available software, *i.e.*, the measurement of spectra and peak areas and the configuration and running of the network. Only for the spectrum normalization and the multiplication by the peak area did software have to be developed. In our opinion, expert knowledge is not required for the application of this technique. Once the necessary software is available the technique is straightforward and fast: network configuration and training take a few minutes and peak recognition is instantaneous after presentation of the test data to the network. The technique can speed up computer-assisted method development and contribute to the development of automated optimization procedures based on simplex lattice mixture designs.

## REFERENCES

- 1 H. J. G. Debets, *J. Liq. Chromatogr.*, 8 (1985) 2725.
- 2 J. L. Glajch, J. J. Kirkland and J. M. Minor, *J. Liq. Chromatogr.*, 10 (1987) 1727.
- 3 P. M. J. Coenegracht, A. K. Smilde, H. J. Metting and D. A. Doornbos, *J. Chromatogr.*, 485 (1989) 195.
- 4 G. Szepesi, *HPLC in Pharmaceutical Analysis*, Vol. I, CRC Press, Boca Raton, FL, 1990, pp. 151–179.
- 5 J. K. Strasters, *Thesis*, Technical University of Delft, Delft, 1989.
- 6 J. L. Glajch, M. A. Quarry, J. F. Vasta and L. R. Snyder, *Anal. Chem.*, 58 (1986) 280.
- 7 P. J. Schoenmakers, *Optimization of Chromatographic Selectivity*, Elsevier, Amsterdam, 1986.
- 8 J. W. Dolan, *LC · GC Int.*, 3 (1990) 17.
- 9 A. F. Fell and B. J. Clark, in R. W. Frei and K. Zech (Editors), *Selective Sample Handling and Detection in HPLC (Journal of Chromatography Library*, Vol. 39A), Elsevier, Amsterdam, 1988, pp. 289–309.
- 10 A. G. Wright, A. F. Fell and J. C. Berridge, *J. Chromatogr.*, 458 (1988) 335.
- 11 M. Caudill and C. Butler, *Naturally Intelligent Systems*, MIT Press, London, 1990.
- 12 J. Stanley and S. Luedeking, *Introduction to Neural Networks*, California Scientific Software, Sierra Madre, CA, 2nd ed., 1989.
- 13 J. Zupan and J. Gasteiger, *Anal. Chim. Acta*, 248 (1991) 1.
- 14 T. Wolf, *MC, Magazin für Computerpraxis*, (1990) 92.
- 15 J. R. Long, V. G. Gregoriou and P. J. Gemperline, *Anal. Chem.*, 62 (1990) 1791.
- 16 M. Bos, A. Bos and W. E. van der Linden, *Anal. Chim. Acta*, 233 (1990) 31.
- 17 A. Bos, M. Bos and W. E. van der Linden, *Anal. Chim. Acta*, 256 (1992) 133.
- 18 J. W. Weyland, C. H. P. Bruins and D. A. Doornbos, *J. Chromatogr. Sci.*, 22 (1984) 31.
- 19 A. K. Smilde, A. Knevelman and P. M. J. Coenegracht, *J. Chromatogr.*, 369 (1986) 1.
- 20 P. M. J. Coenegracht, A. Knevelman and A. K. Smilde, *J. Liq. Chromatogr.*, 12 (1989) 77.

# Primary contribution of the injector to carryover of a trace analyte in high-performance liquid chromatography

Manasi Saha and Roger W. Giese

*Department of Pharmaceutical Sciences in the College of Pharmacy and Allied Health Professions, and Barnett Institute of Chemical Analysis and Materials Science, Northeastern University, Boston, MA 02115 (USA)*

---

## ABSTRACT

When a low-nanogram amount of N1,N3-bis-(pentafluorobenzyl)-N7-(2-[pentafluorobenzyloxy]ethyl)xanthine was subjected to HPLC, low-picogram amounts of the compound could be detected subsequently (off-line by gas chromatography–electron-capture negative-ion mass spectrometry) after injection of pure mobile phase. This was in spite of significant, intermediate washing of the injector and column. It was determined that essentially 99.9% of this analyte contamination came from the injector. Use of two injectors is a practical remedy for this problem.

---

## INTRODUCTION

It is well known that sample carryover can be a problem in the analysis of trace analytes by HPLC. For example, Lin and Desiderio [1] encountered this difficulty in the separation of neuropeptides by reversed-phase HPLC. Generally the HPLC system is simply washed thoroughly to overcome carryover of analyte, without an effort to determine the mechanism. An exception to this is work which showed that the carryover was due to sample adsorption in the injection loop [2]. In this case, a fixed-volume loop was used in the overflow mode with a weak injection solvent. Similar observations have been made by Simonson and Nelson [3].

We are pursuing the detection of N7-(2-hydroxyethyl)guanine, an ethylene oxide DNA adduct, by gas chromatography–electron-capture negative-ion mass spectrometry (GC–ECNI-MS) [4]. Towards this goal, we are purifying N1,N3-bis-(pentafluorobenzyl)-N7-(2-[pentafluorobenzyloxy]ethyl)-xan-

thine, a derivative of this analyte, by reversed-phase HPLC prior to its detection by GC–ECNI-MS. As we reported before [4], we encountered analyte carryover of the latter compound in the HPLC system. We circumvented the problem, at least at the 100-pg level of analyte, by purifying the compound instead by solid-phase extraction on silica. However, the overall GC–ECNI-MS chromatograms were cleaner when the samples were first purified by HPLC. This result, plus the fact that we intend to extend the method to lower-analyte levels, has maintained our interest in using HPLC for sample cleanup of this compound prior to its detection by GC–ECNI-MS.

In this paper, we examine the contribution of the injector to this problem of analyte carryover.

## EXPERIMENTAL

All the equipment and reagents were the same as reported before [4], except that here we substituted methanol for acetonitrile in the HPLC system since methanol is a lower cost, less toxic solvent.

### *Experiment I*

A 15-ng amount of analyte was injected twice in-

---

*Correspondence to:* R. W. Giese, Department of Pharmaceutical Sciences in the College of Pharmacy and Allied Health Professions and Barnett Institute of Chemical Analysis and Materials Science, Northeastern University, Boston, MA 02115, USA.



to the HPLC system with UV detection, to establish the retention time. [Mobile phase, methanol–water, 80:20 (v/v) at 1.0 ml/min; column, Microsorb silica reversed-phase, 150 × 4.6 mm I.D., 10 μm, Rainin, Woburn, MA, USA; injector, Model 7125, Rheodyne, Cotati, CA, USA; retention time, 9.0 min. In all cases, the sample or mobile phase blank was loaded and injected immediately after washing the injector.] A clean injector (previously unused) of the same type was substituted and flow of the mobile phase was continued for 30 min. An aliquot of 50 μl of mobile phase was injected and the appropriate 2-ml fraction was evaporated, redissolved in 10 μl of toluene, and 1 μl was injected into the GC–EC–NI–MS system: observe 16 fg, corresponding to a carryover of 160 fg in the 2 ml fraction (0.00005% of the 30 ng injected originally). After the mobile phase was flowed for 30 min, mobile phase was injected. Carryover: 20 fg/2 ml, which is 8-fold lower than in step 3. A gradient was conducted [methanol–water, 80/20 (v/v) up to 100% methanol in 10 min, hold for 4 min, then return to the original composition in 10 min] and mobile phase was injected. Carryover: none observed (<1 fg). The prior (ng-exposed) injector was installed and mobile phase was injected. Carryover: 24 pg (0.08% of 30 ng). After the mobile phase was flowed for 30 min, the injector was washed (using a needle port cleaner, part No. 7125-054 from Rheodyne; the injector was flushed in the load position with 3 × 0.5 ml of warm methanol, and similarly in the inject position, and this entire washing procedure was repeated twice), and mobile phase was injected. Carryover: 10.8 pg.

#### Experiment II

The above step 1 was repeated, using the ng-exposed injector (but which had been cleaned prior to this second experiment by repetition of the above washing procedure until carryover was absent). After the clean injector was re-installed, a mobile phase gradient was conducted as above, and mobile phase was injected. Carryover: 60 fg. The gradient and injection of mobile phase was repeated. Carryover: none detected (<1 fg). The prior (ng-exposed) injector was re-installed and washed with 2.5 ml of warm methanol in the load position, the same in the inject position, and mobile phase was injected immediately. Carryover: 7.7 pg.

## RESULTS AND DISCUSSION

In order to determine the contribution of the HPLC injector to the analyte carryover that we observed, we employed two injectors, one for injection a nanogram amount of analyte to establish its retention time (and for intentional contamination of the HPLC system), and a second, clean injector for performing subsequent injections of pure mobile phase as blanks. Thus any carryover of analyte observed after the second injector was installed would have to arise subsequent to this injector in the HPLC system, presumably in the column.

The two experiments that we conducted, and our results, are presented in detail in Experimental. As indicated, Experiment I establishes that it is the injector which contributes essentially 99.9% of the picogram level carryover arising from the prior nanogram level injections. The mechanism(s) for holdup of this tiny fraction of analyte in the injector were not studied, but must be due to active sites, solvent dead volumes (e.g. from crevices and cracks), or both in the injector. In regard to the possible role of active sites, the sample contacts polytetrafluoroethylene, Vespel, alumina ceramic and stainless steel surfaces in this injector according to the manufacturer [5].

In Experiment I, the remaining carryover of analyte, apparently from the HPLC column, disappeared only after a mobile phase gradient was conducted. We wondered whether the gradient *per se* was important, or whether it was just the additional flow of mobile phase with time that cleaned the system. After all, the residual carryover of analyte had already decreased significantly (from 160 to 20 fg) during the prior interval of isocratic elution, and the composition of the mobile phase only underwent a small change (80 to 100% methanol) during the gradient.

We answered this second question in Experiment II, which is also summarized in detail in Experimental. As indicated, conducting a gradient immediately after the installation of the clean injector still gave comparable carryover of analyte (60 fg) relative to that observed in Experiment I. Thus, washing isocratically appeared to be just as effective for cleaning as conducting a gradient.

The total carryover of analyte that we have observed is far below 1% of the originally injected

sample. Most applications of HPLC would not be bothered by this tiny amount of carryover. However, as HPLC increasingly is coupled directly or indirectly to sensitive detectors like GC–ECNI–MS, more workers will need to deal with this event.

The work also suggests a practical remedy for the problem: use two injectors, each dedicated to a different level of analyte. At least for the application presented here, we find this strategy more attractive than the practice of injecting a trace amount of a radiolabeled analyte standard to establish the retention time.

#### ACKNOWLEDGEMENT

This work was supported by Grant OH02792 from the National Institute for Occupational Safety and Health, Centers for Disease Control. Contribution No. 555 from the Barnett Institute of Chemical Analysis.

#### REFERENCES

- 1 D. Lin and D. M. Desiderio, *J. Chromatogr.*, 422 (1987) 61.
- 2 J. W. Dolan, *LC · GC*, 9 (1991) 22.
- 3 L. Simonson and K. Nelson, *LC · GC*, 10 (1992) 533.
- 4 M. Saha and R. W. Giese, *J. Chromatogr.*, 629 (1993) 35.
- 5 S. Bakalyar, Rheodyne, personal communication.



# N-Arylcarbamoyl derivatives of amino acids as chiral stationary phases for optical resolution by high-performance liquid chromatography

Mei-Hui Yang and Jer-Yann Lin

Department of Chemistry, National Taiwan University, Taipei 10764 (Taiwan)

---

## ABSTRACT

A series of twelve chiral stationary phases (CSPs) with arylcarbamoyl derivatives of amino acids bonded either ionically or covalently to 3-aminopropyltriethoxysilane-modified silica gel were prepared. These CSPs, except covalent CSP containing phenylcarbamoyl-(*S*)-phenylglycine, provide recognition ability for the separation of enantiomeric amide derivatives of amino acids, amino alcohols, amines and acids by high-performance liquid chromatography. Generally, the ionic type of CSPs were observed to be more effective than the corresponding covalent type. Among the twelve CSPs, the ionic type of CSPs bearing (*S*)-phenylcarbamoyl-(*S*)- or -(*R*)-phenylglycine show the best chiral resolution performance for the four types of enantiomeric solutes. Especially for enantiomeric ibuprofen, the separation factor is the best among all reported values. Based on the chromatographic behaviour in this study, it is concluded that the stereoselectivity is due to the stereochemical elements of the CSPs, the hydrogen-bonding interaction on the urea linkage, and the  $\pi$ - $\pi$  interactions of the aromatic rings. A chiral recognition model of these CSPs for enantiomer separations is proposed.

---

## INTRODUCTION

The development of chiral stationary phases (CSPs) has grown considerably in recent years. Chemically bonded N-(3,5-dinitrobenzoyl)phenylglycine prepared by Pirkle *et al.* [1] is a typical CSP. Although the separation mechanism for this CSP is not clearly understood in all instances, interaction forces such as charge-transfer interactions, hydrogen-bonding interactions, dipole-dipole interactions and steric effects may be involved [2]. As the dinitrobenzoyl (DNB) group is a  $\pi$ -acceptor, possible  $\pi$ - $\pi$  charge-transfer interactions may occur between this group and the aromatic ring of the solute in the envisioned chiral recognition models for the resolution of enantiomeric aryl-containing amides [3,4].

Several CSPs with naphthyl or phenyl groups linked to the asymmetric carbon atom of the chiral

group have also been prepared and showed chiral recognition ability for the separation of aryl-containing enantiomers [5–8]. However, the role of a benzyl group linked to the asymmetric carbon atom of the CSP for chiral resolution is still not clear.

Chromatographic resolution on CSPs containing two asymmetric centres has also been studied [8–11]. Unfortunately, chiral resolution on a CSP containing two phenyl groups located on two chiral carbons separately has not been reported elsewhere. In addition, the comparison of chromatographic behaviours on ionic- and covalent-type CSPs containing two chiral moieties has seldom been discussed.

Owing to the conformational rigidity and polar nature of the urea linkage, the urea linkage was found to be a reasonable means of connecting a chiral moiety to the silica support [12–14]. However, the chromatographic behaviour of the ionic type of CSPs containing a urea linkage has not been reported. Moreover, the role of the phenyl group of the phenylcarbamoyl moiety in the chiral recogni-

---

Correspondence to: M. H. Yang, Department of Chemistry, National Taiwan University, Taipei 10764, Taiwan.

tion process has not yet been characterized as an active site for the charge-transfer interaction.

In this study, eleven of twelve CSPs (Fig. 1) were prepared by bonding N-arylcarbamoyl (CSP-7 was prepared by bonding N-phenylthiocarbamoyl) derivatives of optical active amino acids either covalently or ionically to 3-aminopropyltriethoxysilane (APS)-modified silica gel. We examined their chiral recognition ability and the contribution of the charge-transfer interaction provided by the phenyl groups of CSPs in chiral recognition. Various binding sites capable of  $\pi$ - $\pi$  interactions were investigated on these CSPs.

CSPs containing two chiral moieties in which two phenyl groups attached separately to two different asymmetric centres were also studied. A comparative study was also made between these CSPs and the CSPs containing either one of these chiral moieties in order to shed more light on the chiral recognition process of enantiomers on these CSPs.

	R <sup>2</sup>	X	R <sup>1</sup>	Z	Configuration for	
					C <sup>*</sup>	C <sup>*</sup>
CSP-1		O	iPr	-COO <sup>-</sup> +NH <sub>3</sub> <sup>+</sup> -	S	
CSP-2		O	iPr	-CONH-	S	
CSP-3		O		-COO <sup>-</sup> +NH <sub>3</sub> <sup>+</sup> -	S	
CSP-4		O		-CONH-	S	
CSP-5		O		-COO <sup>-</sup> +NH <sub>3</sub> <sup>+</sup> -	S	
CSP-6		O		-CONH-	S	
CSP-7		S		-COO <sup>-</sup> +NH <sub>3</sub> <sup>+</sup> -	S	
CSP-8		O		-COO <sup>-</sup> +NH <sub>3</sub> <sup>+</sup> -	S	
CSP-9		O		-COO <sup>-</sup> +NH <sub>3</sub> <sup>+</sup> -	S	
CSP-10		O		-COO <sup>-</sup> +NH <sub>3</sub> <sup>+</sup> -	S	S
CSP-11		O		-CONH-	S	S
CSP-12		O		-COO <sup>-</sup> +NH <sub>3</sub> <sup>+</sup> -	S	R

Fig. 1. Structures of CSPs.

These CSPs, except covalent CSP containing phenylcarbamoyl-(*S*)-phenylglycine (CSP-6), provide a recognition ability for the separation of enantiomeric amide derivatives of amino acids, amino alcohols, amines and acids by high-performance liquid chromatography (HPLC). However, the magnitude of the recognition ability varies with the detailed structures of these CSPs. A CSP containing a urea functional group has a better recognition ability than the corresponding CSP containing a thiourea functional group for the resolution of the same enantiomers. Generally, the ionic-type CSPs were observed to be more effective than the corresponding covalent-type CSPs for the chiral resolution of enantiomeric solutes. Among the nine CSPs containing one chiral moiety, the ionic-type CSP containing benzylcarbamoyl-(*S*)-phenylglycine (CSP-9) showed the best recognition ability for all types of test solutes. Moreover, the CSPs containing two chiral moieties were found to provide a better ability than the corresponding CSPs containing only one chiral moiety for the effective resolution of the four types of enantiomeric solutes.

Our results indicate that the chiral recognition model of these CSPs for enantiomer separation is based on steric interactions close to the chiral centres, the hydrogen-bonding interaction of the urea linkage and the  $\pi$ - $\pi$  interaction of the aromatic moiety. Moreover, the chiral recognition ability of CSPs is apparently enhanced by an additional chiral centre attached to the other nitrogen atom of the carbamoyl group.

## EXPERIMENTAL

### Chemicals

All optically active amino acids, aryl isocyanates and (*S*)-phenylethyl isocyanate were obtained from Aldrich. The silica gel used was Nucleosil (pore size 100 Å; particle size 10  $\mu$ m; surface area 350 m<sup>2</sup>/g), obtained from Macherey-Nagel. APS was purchased from Chisso. The solutes used in the chromatographic experiments were of synthetic reagent grade (Merck).

### Preparation of N-arylcarbamoyl derivatives of optically active amino acids

The amino acids used were L-phenylglycine, D-phenylglycine, L-valine and L-phenylalanine. To a

stirred solution of 0.02 mol of amino acid in 10 ml 2 M NaOH, a solution of 0.02 mol of aryl isocyanate in 4 ml of acetone was added. The mixed solution was reacted at room temperature for 30 min. The product was precipitated by acidifying with 2.5 ml of 1 M HCl, filtered, washed with distilled water and dried at 100°C for 2 h.

#### Preparation of 3-aminopropylsilanized silica gel

Silica gel (3 g) dried at 180°C for 10 h, was suspended in 100 ml of dry toluene. After 1.5 ml of APS had been added, the reaction mixture was refluxed under nitrogen for 10 h with stirring. The silane-modified silica gel thus obtained was filtered, washed with methanol, water and acetone and then dried under vacuum overnight. Results of elemental analysis are given in Table I.

#### Preparation of ionic-type CSPs

To a solution of 0.01 mol of arylcarbamoyl derivative of optically active amino acid in 100 ml of tetrahydrofuran (THF), 2.5 g of silanized silica gel were added. The mixture was subjected to ultrasonic vibration for 10 min, followed by further stirring for 4 h. The product was filtered, washed with THF and dried under vacuum overnight.

#### Preparation of covalent-type CSPs

A solution of 0.01 mol of arylcarbamoyl derivative of L-amino acid in 100 ml of dimethylformamide was cooled in an ice-bath, 10 mmol of N-hydroxysuccinimide and 0.01 mol of dicyclohexylcarbodiimide (DCC) were added to the above solution at 0°C and the mixture was stirred at room temperature for 24 h. After removal of the suspended solid dicyclohexylurea, 2.5 g of 3-aminopropylsilanized silica were added and stirred for 48 h. After filtration, the product was suspended in 100 ml of toluene and end-capped by reaction with trimethylchlorosilane at 40°C for 4 h. The final product was filtered and washed with methanol, water and acetone and then dried under vacuum overnight.

The results of elemental analyses of all the prepared CSPs are given in Table I.

#### Chromatographic studies

The chromatographic studies were carried out with a Kratos liquid chromatographic system which

TABLE I

CHARACTERISTICS OF 3-AMINOPROPYLSILICA AND THE CSPs

Sample	Elemental analysis (%)			Loading capacity <sup>a</sup> (mmol/g)
	C	H	N	
3-Aminopropylsilica	3.74	1.00	1.31	0.93
CSP-1	11.12	1.80	2.58	0.47
CSP-2	11.52	1.82	2.33	0.38
CSP-3	13.66	1.98	2.35	0.39
CSP-4	13.60	1.90	2.32	0.37
CSP-5	10.00	1.48	2.20	0.34
CSP-6	9.97	1.50	1.91	0.33
CSP-7	11.91	1.95	2.15	0.32
CSP-8	19.93	3.24	2.33	0.38
CSP-9	11.29	1.82	2.35	0.39
CSP-10	13.85	1.57	2.63	0.48
CSP-11	11.21	1.54	2.24	0.35
CSP-12	13.76	1.98	2.54	0.46

<sup>a</sup> Based on the percentage of nitrogen.

consisted of a Spectroflow 400 solvent-delivery system, a Spectroflow 480 injector and a Spectroflow 757 variable-wavelength UV detector. The recorder used was a Model 12 SIC Chromatocorder. Stainless-steel columns (300 mm × 4 mm I.D.) were packed by the balanced-density slurry method, using an Econo-packing pump (Inpac International) at 400 kg/cm<sup>2</sup>. Mixtures of *n*-hexane and 2-propanol (90:10–99:1, v/v) were used as the mobile phase, which was filtered through a 0.45- $\mu$ m membrane filter and degassed by ultrasonic vibration prior to use. The flow-rate was 1.0 ml/min. The detector was operated at 254 nm. Experiments were carried out at room temperature. Sample solutes, which were derivatized by a routine method, were dissolved in methanol and suitable amounts of the solutions were injected. Chromatographic peaks were assigned by injecting the corresponding derivative of enantiomeric enriched solute.

#### RESULTS AND DISCUSSION

Twelve chiral stationary phases were successfully prepared by bonding N-arylcarbamoyl and N-phenylthiocarbamoyl derivatives of optically active amino acids either covalently or ionically, to APS-modified silica gel as shown in Fig. 2. Fig. 1 shows the structures of these CSPs. The presence of the

TABLE II  
RESOLUTION OF DERIVATIZED ENANTIOMERS ON CSPs

Solute	$\alpha^c$ (configuration <sup>b</sup> )											
	Ionic-type CSPs					Covalent-type CSPs						
	1	3	8	7	5	9	10	12	2	4	6	11
<i>Amino acids<sup>d</sup></i>												
Valine	1.18 (R)	1.20 (R)	1	1.12 (S)	1.18 (S)	1.67 (S)	1.27 S	2.64 (R)	1.27 (R)	1.13 (R)	1	1.37 (S)
Leucine	1.26 (R)	1.28 (R)	1	1.24 (S)	1.26 (S)	1.58 (S)	1.41 S	1.82 (R)	1.32 (R)	1.14 (R)	1	1.18 (S)
Phenylalanine	1.18 (R)	1.18 (R)	1	1.07 (S)	1.06 (S)	1.39 (S)	1.22 S	1.71 (R)	1.26 (R)	1.02 (R)	1	1.17 (S)
Alanine	1.26 (R)	1.32 (R)	1	1	1.06 (S)	1.18 (S)	1	1.56 (R)	1.18 (R)	1.01 (R)	1	1.19 (S)
Methionine	1.31 (R)	1.31 (R)	1.47 (S)	1.08 (S)	1.06 (S)	1.30 (S)	1.18 S	1.91 (R)	1.36 (R)	1.11 (R)	1	1.21 (S)
<i>Amino alcohols<sup>d</sup></i>												
2-Aminobutanol	1.17 (R)	1.12 (R)	1	1.08 (S)	1.13 (S)	1.41 (S)	1.57 S	1.74 (R)	1.08 (R)	1	1	1
2-Aminopropanol	1.11 (R)	1.13 (R)	1	1	1	1.24 (S)	1.32 S	1.41 (R)	1	1	1	1
Norephedrine	1.12	1.11	1	1	1.06	1.02	1.14	1.09	1	1	1	1
<i>Amines<sup>d</sup></i>												
1,2-Diaminopropane	1.19	1.15	1	1	1.15	1.09	1.04	1.16	1	1	1	1.07
Phenylethylamine	1	1	1	1	1.04 (R)	1.09 (R)	1.37 R	1.18 (R)	1	1	1	1.18 (R)
1-Methylbutylamine	1	1	1	1.07	1.13	1.18	1.25	1.23	1	1	1	1
<i>Acids<sup>e</sup></i>												
Ibuprofen	1	1	1.12 (R) <sup>f</sup>	1	1.14 (R) <sup>f</sup>	1.16 (S)	1.93 S	1.20 (S)	1	1	1	1.32 (S)
						1.18 (S) <sup>f</sup>						

<sup>a</sup> The separation factor of the enantiomers is the ratio of their capacity factors. Mobile phase: 2-propanol-hexane (10:90).

<sup>b</sup> Configuration of the first-eluted enantiomer.

<sup>c</sup> As N-dinitrobenzamide-O-methyl ester derivatives.

<sup>d</sup> As N-dinitrobenzamide derivatives.

<sup>e</sup> As dinitroanilide derivatives, except where indicated.

<sup>f</sup> As N-naphthylamide derivatives.

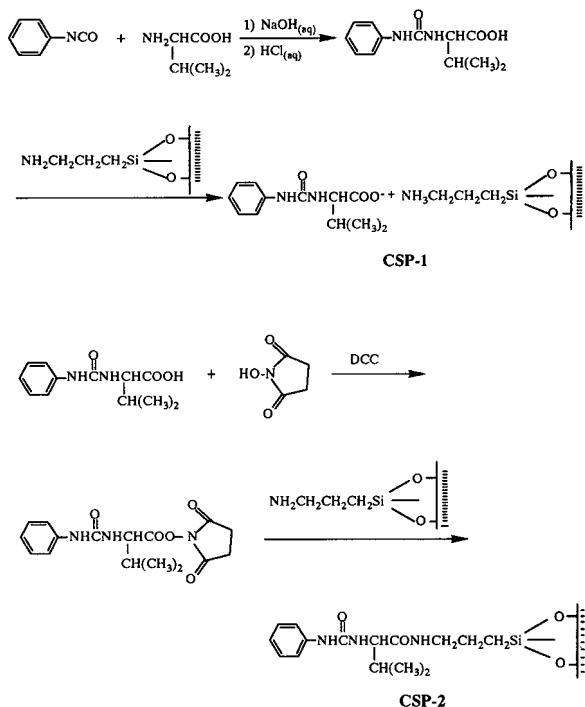


Fig. 2. Examples of the preparation of CSPs.

chiral ligands on the silica surface of the prepared CSPs was characterized by FT-IR spectrometry and combustion elemental analysis (Table I).

#### Chromatographic behaviours of CSPs

The chromatographic resolution ability of the amide derivatives of some representative racemic amino acids, amino alcohols, amines and carboxylic acids on these CSPs were examined and the results are summarized in Table II. Typical chromatograms are presented in Fig. 3. According to the separation factors ( $\alpha$ ), nearly all of the arylcarbamoyl-derived CSPs provide sufficient resolution for N,N-dinitrobenzamide (DNB) or N,N-dinitroanilide (DNA) derivatives. In general, the ionic-type CSPs were found to be more effective than the corresponding covalent-type CSPs for the resolution of enantiomeric amide derivatives. It is interesting that there were no significant resolutions on the covalent type of phenylcarbamoyl-(S)-phenylglycine (CSP-6) for any of the chosen solutes, whereas excellent resolutions for amino acids were obtained on the covalent type of phenylcarbamoyl-(S)-valine (CSP-2).

#### Contribution of the carbamoyl moiety

Compared with the ionic-type phenylcarbamoyl-(S)-phenylglycine-derived CSP-5, the corresponding thiourea linkage-containing CSP-7 showed a worse resolution ability and shorter solute retention. This indicates not only that did the thiourea linkage form weaker intermolecular complexes than the urea linkage with solutes, but also that the hydrogen bonding interaction contributed by the urea functional group is stereoselective in chiral recognition. Other than hydrogen bonding sites in CSPs, the hydrogen bonding interaction site of the solute also supported this assumption. Although the DNB derivative of 2-methylbutylamine with an amide group attached to an achiral carbon could not be resolved on all CSPs, the DNB derivative of 1-methylbutylamine could be effectively resolved on phenylglycine-derived CSPs (Table II).

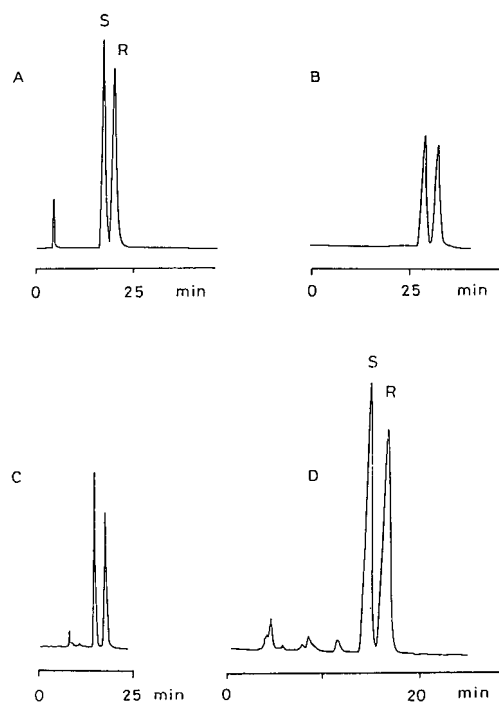


Fig. 3. Chromatographic separation of the enantiomers on CSPs. (A) Alanine and DNB-O-methyl ester derivative on CSP-11; (B) norephedrine as DNB derivative on CSP-10; (C) 1-methylbutylamine as DNB derivative on CSP-10; (D) ibuprofen as N-naphthylamide derivative on CSP-9. Mobile phase: (A–C) 2-propanol-*n*-hexane (10:90); (D) 2-propanol-*n*-hexane (1:99).



### *Steric effect of the carbamoyl moiety*

Naphthylcarbamoyl-(*S*)-phenylglycine-derived CSP-8, with a bulky R<sup>2</sup> group, showed significant resolution only for methionine DNB derivatives and ibuprofen DNA derivatives. However, benzylcarbamoyl-(*S*)-phenylglycine-derived CSP-9, with a less hinder R<sup>2</sup> group than the phenyl group on the carbamoyl moiety, showed the best chiral resolution performance for all test solutes among the nine CSPs that contained one chiral moiety. Hence the steric effect of the arylcarbamoyl moiety on the phenylglycine-derived CSPs was quite important.

### *Contribution of phenyl groups on the CSPs*

According to the  $\alpha$  values, the effects of the position of the phenyl group on the CSPs were different for the various solutes. For DNB derivatives of amino acids, amino alcohols and diamines, a phenyl group either attached to any of the chiral centres or as a substituent of the carbamoyl moiety of the CSPs will contribute an active  $\pi$ - $\pi$  interaction site for chiral recognition. For the amide derivatives of amines and acids, the stereoselective  $\pi$ - $\pi$  interaction site must be directly attached to the chiral centre on either side of the urea linkage. If the phenyl group is removed from this centre by even a urea linkage or a single methylene group, as in CSP-1 and CSP-3, there was no chiral resolution at all. As shown in Table II, an additional phenyl-substituted chiral moiety (as in CSP-10 vs. CSP-9) could provide a great improvement in the resolution of the amide derivatives of amines and acids.

The good resolution for the DNB derivatives of amino acids, amino alcohols and diamines on CSP-1 suggested that the phenyl group removed from the chiral centre by a urea linkage presumably contributed a stereoselective  $\pi$ - $\pi$  interaction site for racemates. The enantiomeric elution order was determined by the amide synthesis either from L-amino acids or amino alcohols. The *R*-form enantiomer was first eluted on phenylcarbamoyl-(*S*)-valine-derived CSPs, whereas the *S*-form enantiomer was eluted first on arylcarbamoyl-(*S*)-phenylglycine-derived CSPs. Unlike CSP-1, both CSP-5 and CSP-3 provide an additional  $\pi$ - $\pi$  interaction owing to the presence of phenyl and benzyl groups attached to the chiral centre of the L-amino acid moiety, respectively. However, the opposite elution order observed on CSP-5 suggests that the additional  $\pi$ - $\pi$

interaction provided by a phenyl group attached to the chiral centre presumably results in an alternative chiral recognition model other than that on CSP-1, whereas the additional  $\pi$ - $\pi$  interaction provided by a benzyl group attached to the chiral centre (CSP-3) does not. Further, it was also found that in CSP-10 and CSP-12, the change in the configuration on the chiral centre of the amino acid moiety on the CSP resulted in a change in the enantiomeric elution orders for the DNB derivatives of amino acids and amino alcohols. These facts reveal that, in the prepared CSPs, the  $\pi$ - $\pi$  interaction provided by the phenyl group, but not the benzyl group, which is attached to the chiral centre of the amino acid moiety on the CSP acts as a stereoselective site and is important for the chiral discrimination of all the enantiomers in this work.

### *Advantage of two chiral moieties in the same CSP*

Baseline separation was achieved for almost all of the enantiomeric solutes on the CSPs containing two chiral moieties. Especially the selectivity for enantiomeric ibuprofen, which is a non-steroidal anti-inflammatory antipyretic analgesic, is the best among all values reported. In order to shed more light on the chiral recognition process of enantiomers on these CSPs, a comparative study between these CSPs and CSPs containing either one of these chiral moieties was made. The separation factors of amino acids, amino alcohols and amines on ionic- and covalent-type CSPs with two chiral centres (CSP-10 and CSP-11) were greater than those on the corresponding types with one chiral centre (CSP-5, -6 and -9). In addition, the chiral resolution on CSP-11 was also found to be more effective than that on Supelcosil LC-(*R*)-urea [13], in which the phenylethylamino chiral moiety was bonded to 3-aminopropylsilica through a urea functional group, for the enantiomeric separation of amino acids [4]. These results indicate that the chiral recognition ability can be improved by introducing an additional chiral moiety to the CSP backbones.

## CONCLUSIONS

In the series CSPs derived from N-arylcarbamoyl derivatives of optically active amino acids, it is clear that in an arylcarbamoyl-derived CSP, owing to the

conformational rigidity and the hydrogen bonding available from the urea linkage, both the aryl group and the carbamoyl group of the carbamoyl moiety may interact with the racemates stereoselectively in the chiral recognition process. Ionic-type CSPs with the urea linkage always show better chiral recognition ability than the corresponding covalent-type CSPs. The elution orders of the analytes makes it clear that a phenyl group which is directly attached to the chiral centre of the CSPs provides stereoselective interaction, whereas a benzyl group does not. A phenyl group removed from the chiral centre by a urea linkage or a single methylene group shows no resolution ability for amide derivatives of amines and acids. Both chiral centres on either N atom of the urea linkage are stereoselective in the chiral recognition process. Therefore, CSPs containing two such chiral moieties provide the best chiral recognition ability and result in baseline separations for nearly all the chosen solutes.

#### ACKNOWLEDGEMENT

The authors thank the National Science Council, Taiwan, for financial support.

#### REFERENCES

- 1 W. H. Pirkle, J. M. Finn, J. L. Schreiner and B. C. Hamper, *J. Am. Chem. Soc.*, 103 (1981) 3964.
- 2 W. H. Pirkle, C. J. Welch and M. H. Hyun, *J. Org. Chem.*, 48 (1983) 5022.
- 3 W. H. Pirkle, T. C. Pochapsky, G. S. Mahler and R. E. Field, *J. Chromatogr.*, 348 (1985) 89.
- 4 I. W. Wainer and T. D. Doyle, *J. Chromatogr.*, 284 (1984) 117.
- 5 N. Oi, M. Nagase and T. Doi, *J. Chromatogr.*, 257 (1983) 111.
- 6 W. H. Pirkle and M. H. Hyun, *J. Org. Chem.*, 49 (1984) 3043.
- 7 D. J. Gisch, presented at *9th International Symposium on Column Liquid Chromatography, Edinburgh, 1985*.
- 8 N. Oi and H. Kitahara, *J. Liq. Chromatogr.* 9 (1986) 511.
- 9 J. Yamashita, H. Satoh, S. Oi, T. Suzuki, S. Miyano and N. Takai, *J. Chromatogr.*, 464 (1989) 411.
- 10 W. H. Pirkle and J. E. McCue, *J. Chromatogr.*, 471 (1989) 271.
- 11 W. H. Pirkle and J. E. McCue, *J. Chromatogr.*, 11 (1988) 2165.
- 12 W. H. Pirkle and M. H. Hyun, *J. Chromatogr.*, 322 (1985) 295.
- 13 N. Oi and H. Kitahara, *J. Chromatogr.*, 285 (1984) 198.
- 14 N. Oi and H. Kitahara, *Bunseki Kagaku*, 33 (1984) 386.



CHROMSYM. 2580

# Analytical and preparative high-performance liquid chromatographic separation of thienopyran enantiomers

Charles J. Shaw, Pauline J. Sanfilippo, James J. McNally, Sung Ae Park and Jeffery B. Press

The R. W. Johnson Pharmaceutical Research Institute, 1000 Route 202, Raritan, NJ 08869-0602 (USA)

---

## ABSTRACT

The analytical and preparative enantiomeric resolution of a racemic substituted thienopyran was obtained with a  $\beta$ -cyclodextrin bonded-phase column using isocratic conditions. Baseline separations were obtained with short run times. The analytical method is accurate, reliable and reproducible for measuring enantiomeric excess. A semi-preparative high-performance liquid chromatographic method was used to obtain the enantiomers for pharmacological testing prior to developing an asymmetric synthesis of RWJ 26629.

---

## INTRODUCTION

RWJ 26629 [1,2] is a racemic substituted thienopyran currently under investigation as a potassium channel opener for the treatment of hypertension and other vascular disorders. In the early development phase of this medicinal compound, it was essential to know the primary pharmacological profile of each enantiomer. Enantiomers not only have quantitative differences in comparable activity with the opposite isomer but they can also have pharmacological, therapeutic and pharmacokinetic differences [3–5]. Thus, it is desirable to have each enantiomer available for testing whether they are obtained by (1) asymmetric synthesis, (2) classical resolution or (3) separation by preparative chromatography using an enantiomeric stationary phase. In all cases, a quantitative method is needed to determine enantiomeric excess. The application of cyclodextrin stationary phases for the high-performance liquid chromatographic (HPLC) separation of

drug stereoisomers has been demonstrated [6–8]. The enantiomeric excess of RWJ 26629 was determined by HPLC using a  $\beta$ -cyclodextrin column. The analytical method was modified to provide a convenient semi-preparative method for the isolation of the enantiomers prior to the development of an asymmetric synthesis.

## EXPERIMENTAL

### Chemicals

( $\pm$ )-5,6-Dihydro-6-hydroxy-5,5-dimethyl-2-nitro-7-(2-oxopiperidin-1-yl)-5H-thieno[3,2-*b*]pyran, (–)-(6*S*,7*S*)-*trans*-5,6-dihydro-6-hydroxy-5,5-dimethyl-2-nitro-7-(2-oxopiperidin-1-yl)-7H-thieno[3,2-*b*]pyran and (+)-(5*R*,6*S*)-5,6-dihydro-6-hydroxy-5,5-dimethyl-2-nitro-7-(2-oxopiperidinyl-1-yl)-7H-thieno[3,2-*b*]pyran were synthesized at The R.W. Johnson Pharmaceutical Research Institute. Specific rotations were obtained in chloroform at 25°C at 589 nm. The specific rotations observed for the (–) and (+) enantiomers are 80.1 and 81.6°, respectively. HPLC-grade ammonium acetate, chloroform, methanol and acetonitrile were obtained from Fisher Scientific (Springfield, NJ, USA).

---

Correspondence to: Dr. C. J. Shaw, The R. W. Johnson Pharmaceutical Research Institute, 1000 Route 202, Raritan, NJ 08869-0602, USA.

### Chromatography

A Perkin-Elmer (Norwalk, CT, USA) Model 410 solvent delivery system and Hewlett-Packard (Avondale, PA, USA) Series 1050 diode-array detection system were used for the analytical separations. The solvent delivery system for the preparative separations consisted of two Rainin (Woburn, MA, USA) HPX pumps with 25 ml/min heads and an Apple Macintosh Plus (Cupertino, CA, USA) controller. A Rainin HPX dispensing pump was used to inject a 2-ml sample. A Gilson Model 116 UV detector and Kipp & Zonen BD 41 strip-chart recorder was used to monitor the preparative separations. Resolution of the enantiomers were obtained on an Advanced Separation Technologies (Whippany, NJ, USA) Cyclobond I prepacked HPLC column. Quantitative measurements were made using the Hewlett-Packard 3350 laboratory automation system.

A 10- $\mu$ l volume of a 1 mg/ml solution of the racemate was injected onto a 250  $\times$  4.6 mm I.D. column, and a mobile phase of methanol–acetonitrile–ammonium acetate (5:23:72) at a flow-rate of 0.7 ml/min was used for the analytical resolution of the enantiomers, which is shown in Fig. 1. Preparative resolution of the enantiomers was obtained with a 250  $\times$  10 mm I.D. column using a 2-ml injection of 15 mg/ml. A mobile phase of acetonitrile–ammonium acetate (13:87) at a flow-rate of 7 ml/min was used with a total elution time of 25 min.

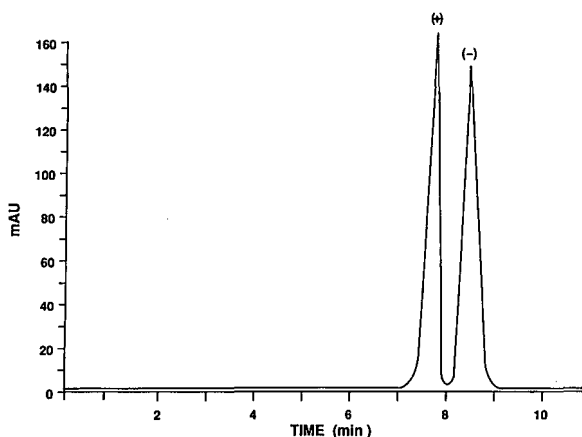


Fig. 1. HPLC of the analytical resolution of racemic RWJ 26629.

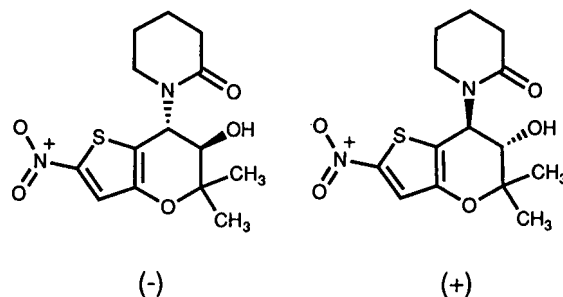


Fig. 2. Structures of the thienopyran enantiomers.

### RESULTS AND DISCUSSION

The thienopyran enantiomers were resolved on a single enantiomeric column using isocratic conditions. Samples of the individual enantiomers, which are shown in Fig. 2, were used to determine the elution order. A separation factor ( $\alpha$ ) of 1.09 and peak resolution factor ( $R$ ) of 1.35 were obtained [9]. The (+) enantiomer eluted prior to the (-) enantiomer. A correlation coefficient of 0.998 was obtained for the calibration curve which had a concentration range of 0.2–25.0% (w/w). The detection limit was 0.1%, where the limit detection is equal to  $1.5 + R_n$  (maximum amount of peak to peak noise level). Enantiomeric composition of the fractions examined are presented in Table I. The excess of one enantiomer decreasing between experiments I,

TABLE I

ENANTIOMERIC COMPOSITION OF FRACTIONS OBTAINED FROM PREPARATIVE HPLC

Experiment	Fraction	Percent (-) enantiomer
I	1	100
	2	81.8
	3	16.5
	4	4.1
II	1	99.6
	2	97.4
	3	12.0
	4	3.6
III	1	93.2
	2	85.2
	3	12.3
	4	1.7

II and III may be attributed to human error in the collection of the appropriate fractions. Preparative HPLC isolation of the enantiomers using a 10 mm I.D. column offers a simple and direct approach to provide sufficient material for pharmacological testing. It provides the best compromise between resolution, separation time and solvent consumption. A loading study showed that the maximum amount of racemate the 10 mm I.D. column could tolerate without compromise to resolution was 30 mg. A single pass was made for each injection and two fractions were collected for each peak. This method provided 100 mg of the (–) enantiomer in 99.8% enantiomeric excess and 100 mg of the (+) enantiomer in 99.4% enantiomeric excess.

## REFERENCES

- 1 J. B. Press, P. J. Sanfilippo, J. J. McNally and R. Falotico, *U.S. Pat.*, 4 992 435 (1991).
- 2 P. J. Sanfilippo, J. J. McNally, J. B. Press, L. Fitzpatrick, M. J. Urbanski, L. B. Katz, E. Giardino, R. Falotico, J. Salata, J. B. Moore and W. Miller, *J. Med. Chem.*, in press.
- 3 D. E. Drayer, *Clin. Pharmacol. Ther.*, 40 (1986) 125–133.
- 4 F. Y. W. Lam, *Pharmacotherapy*, 8 (1988) 147–157.
- 5 F. Jamali, R. Mehvar and F. M. Pasutto, *J. Pharm. Sci.*, 78 (1989) 695–715.
- 6 W. L. Hinze, in C. J. Vaoss (Editor), *Application of Cyclodextrin in Chromatographic Separation and Purification Methods*, Vol. 10, Marcel Dekker, New York, 1981.
- 7 S. Allenmark, *Chromatographic Enantioseparation Methods and Applications*, Ellis Horwood, Chichester, 1988.
- 8 A. Berthod, H. L. Jin, T. E. Beasley, J. D. Duncan and D. W. Armstrong, *J. Pharm. Biomed. Anal.*, 8 (1990) 123.
- 9 L. R. Snyder and J. J. Kirkland, *Introduction to Modern Liquid Chromatography*, Wiley, New York, 2nd ed., 1979, pp. 34–35.



# Enantiomer separation by high-performance liquid chromatography with copper(II) complexes of Schiff bases as chiral stationary phases

Naobumi Ôi, Hajimu Kitahara and Fumiko Aoki

Sumika Chemical Analysis Service, Ltd., 3-1-135, Kasugade-naka, Konohana-ku, Osaka 554 (Japan)

---

## ABSTRACT

Copper(II) complexes of Schiff bases of chiral amino alcohols were examined as chiral ligand-exchange phases for high-performance liquid chromatography. The direct separation of a large number of amino alcohol, amine, amino acid and hydroxy acid enantiomers was accomplished using octadecylsilanized silica coated with the binuclear copper(II) complex of N-salicylidene-(*R*)-2-amino-1,1-bis(2-butoxy-5-*tert*-butylphenyl)-3-phenyl-1-propanol (**1**) and water or water-organic eluents containing copper(II) ion as mobile phases. The interaction of various enantiomers with the copper(II) complex **1** for chiral discrimination was discussed.

---

## INTRODUCTION

Chiral ligand-exchange high-performance liquid chromatography (HPLC), as shown by Davankov and co-workers [1–3], is a very powerful tool for enantiomer separations. In this technique various amino acids and their derivatives have mainly been used as ligands in either chiral stationary phases or as chiral additives to the mobile phases [4–12]. It has also been shown that non-amino acid-type chiral ligands, such as L-2-isopropyl-4-octyldiethylenetriamine, (–)-*trans*-1,2-cyclohexyldiamine, (1*R*,2*S*)- or (1*S*,2*S*)-2-carboxymethylamino-1,2-diphenylethanol, (*R,R*)-tartaric acid and (*S*)-mandelic acid, can be used [13–19].

Schiff bases are well known to form stable metal complexes, but they have never been utilized as ligands for chiral ligand-exchange HPLC. Gelber and co-workers [20,21] reported a method for the enantiomeric resolution of primary amino alcohols

involving derivatization to the salicylaldehyde Schiff base followed by ligand-exchange HPLC with an L-proline-bonded stationary phase. This result suggested that Schiff bases of chiral amino alcohols may be valuable as chiral ligands for enantiomer separations, and we have achieved [22] efficient separations of amino alcohol, amino acid and amine enantiomers by HPLC on reversed-phase silica gel coated with the copper(II) complex of N-salicylidene-(*R*)-2-amino-1,1-bis(2-butoxy-5-*tert*-butylphenyl)-3-phenyl-1-propanol (**1**).

In this paper we report enantiomer separations by HPCL with the copper(II) complexes of Schiff bases **1** and **2** [23,24] as chiral stationary phases. These copper(II) complexes are known to be effective catalysts for practical asymmetric syntheses.

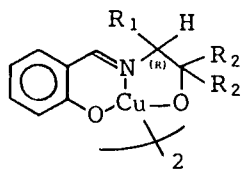
## EXPERIMENTAL

Two binuclear copper(II) complexes of N-salicylidene-(*R*)-2-amino-1,1-bis(2-butoxy-5-*tert*-butylphenyl)-3-phenyl-1-propanol (**1**) and N-salicylidene-(*R*)-2-amino-1,1-bis(5-*tert*-butyl-2-octyloxyphenyl)-1-propanol (**2**) were kindly provided by Dr. T. Aratani (Sumitomo Chemical). The

---

Correspondence to: Dr. N. Ôi, Sumika Chemical Analysis Service, Ltd., 3-1-135, Kasugade-naka, Konohana-ku, Osaka 554, Japan.





- 1** R<sub>1</sub> = benzyl  
R<sub>2</sub> = 2-butoxy-5-*tert.*-butylphenyl
- 2** R<sub>1</sub> = methyl  
R<sub>2</sub> = 5-*tert.*-butyl-2-octyloxyphenyl

coating of phases **1** and **2** on Sumipax ODS columns (150 mm × 4.6 mm I.D.) packed with octadecylsilanized silica (5 μm) was accomplished by passing a 0.05% tetrahydrofuran–water (50:50) solution of **1** and **2** through the column followed by a 1 mM aqueous solution of copper(II) acetate. The column coated with phase **1** is available from Sumika Chemical Analysis Service (Osaka, Japan) as Sumichiral OA-5500. All chemicals and solvents were of analytical-reagent grade from Wako (Osaka, Japan). Some samples were provided by Sumitomo Chemical. The experiments were carried out using a Waters Model 510 high-performance liquid chromatograph equipped with a variable-wavelength UV detector.

## RESULTS AND DISCUSSION

The HPLC separation of six racemic compounds was tested with the two copper(II) complexes **1** and **2** under the same chromatographic conditions in order to compare their enantioselectivities. As shown in Table I, approximate separation factors ( $\alpha$ ) were obtained, and further experiments were performed with the complex **1**, which is more convenient to prepare. The results of enantiomer separations of various racemic compounds with **1** are summarized in Table II; the structures of the racemic amino alcohols and amines are shown in Fig. 1. Typical chromatograms are shown in Figs. 2–5.

Racemic amino alcohols such as phenylalaninol and 2-amino-1-phenylethanol, which contain either an amino group or a hydroxyl group directly attached to the asymmetric carbon atom, were efficiently resolved, and no enantiomeric separation was obtained for racemic 1-phenylethylamine and 1-phenylethanol in a complementary experiment. These results show that both amino and hydroxyl groups in amino alcohols may play an important cooperative role in the interaction with phase **1** for chiral discrimination. The fact that the efficient enantiomer separation of racemic amines such as 1,2-diphenylethylamine and ketamine, which contain several aromatic or polar groups, was accomplished suggests similar complexation with **1** in

TABLE I  
ENANTIOMER SEPARATIONS BY HPLC WITH PHASES **1** AND **2**

Mobile phase: (A) 1 mM copper(II) sulphate in water; (B) 2 mM copper(II) sulphate in water–acetonitrile (85:15). A flow-rate of 1 ml/min was typically used for the 150 × 4.6 mm I.D. columns at room temperature. An injection volume of 5 μl (2 mg/ml) was typically used.  $k'_1$ ,  $k'_2$  = Capacity factors of first- and second-eluted isomers, respectively;  $\alpha$  = separation factor ( $k'_2/k'_1$ ).

Compound	Phase 1			Mobile phase	Phase 2			Mobile phase
	$k'_1$	$k'_2$	$\alpha$		$k'_1$	$k'_2$	$\alpha$	
2-Amino-1-phenylethanol	4.50	5.36	1.19	A	2.64	3.14	1.19	A
Octopamine	1.46	1.90	1.30	A	0.59	0.76	1.29	A
Phenylglycinol	2.78	3.75	1.35	A	1.63	1.84	1.13	A
1,2-Diphenylethylamine	7.42	12.17	1.64	B	4.62	7.54	1.63	A
Phenylglycine	6.54 (D)	8.10 (L)	1.24	A	11.85 (D)	16.68 (L)	1.45	A
Tyrosine	6.18 (D)	12.73 (L)	2.06	A	6.69 (D)	32.76 (L)	4.90	A

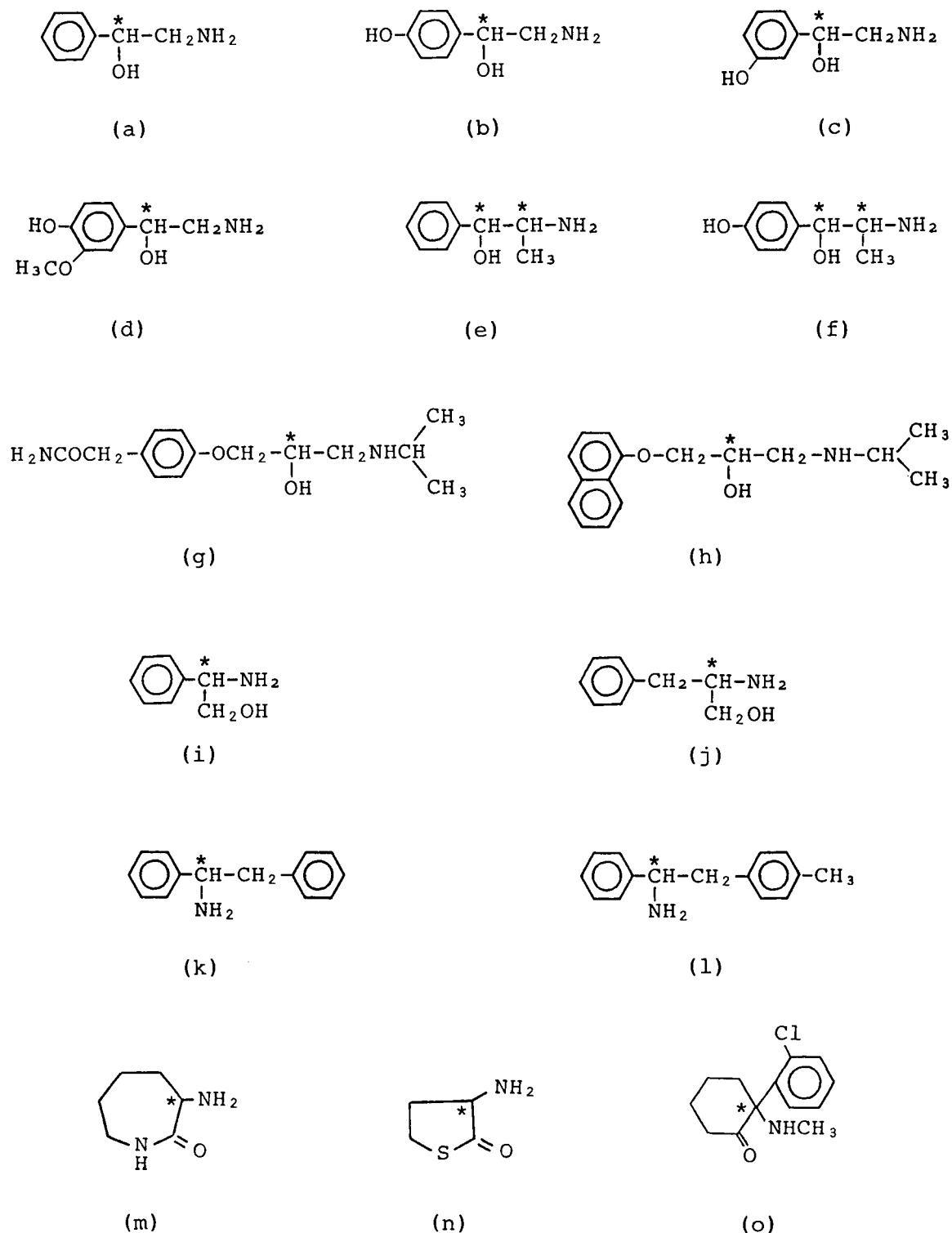


Fig. 1. Structures of amino alcohols and amines: (a) 2-amino-1-phenylethanol; (b) octopamine; (c) norphenylephrine; (d) normethan-ephrine; (e) norephedrine; (f) *p*-hydroxynorephedrine; (g) atenolol; (h) propranolol; (i) phenylglycinol; (j) phenylalaninol; (k) 1,2-diphenylethylamine; (l) 1-phenyl-2-(*p*-tolyl)ethylamine; (m)  $\alpha$ -amino- $\epsilon$ -caprolactam; (n) homocysteine thiolactone; (o) ketamine.

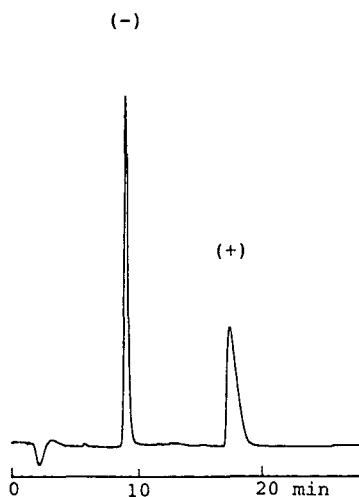


Fig. 2. HPLC separation of racemic phenylalaninol with phase I. Chromatographic conditions as in Table II.



Fig. 3. HPLC separation of racemic 1-phenyl-2-(*p*-tolyl)ethylamine with phase I. Chromatographic conditions as in Table II.

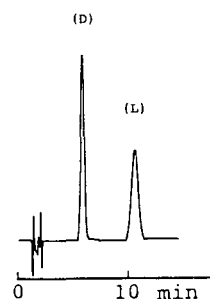


Fig. 4. HPLC separation of racemic tryptophan with phase I. Chromatographic conditions as in Table II.

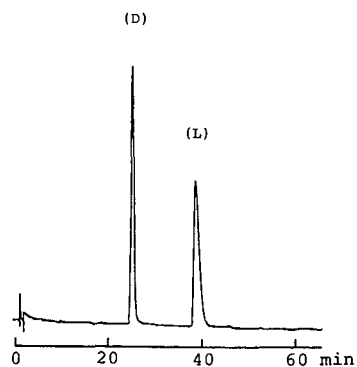


Fig. 5. HPLC separation of racemic lactic acid with phase I. Chromatographic conditions as in Table II.

racemic amino alcohols was effective for the chiral discrimination in these amino compounds.

The separation of amino acid and hydroxy acid enantiomers was not always adequate, but superior separations were obtained with several amino acids and hydroxy acids. Some racemic  $\beta$ -amino acids and  $\beta$ -hydroxy acids were also resolved.

A very interesting result was found in the elution order of amino acid enantiomers. D-Isomers were retained strongly for valine, leucine, isoleucine, etc., and L-isomers for serine, tyrosine, histidine, tryptophan, etc. The interaction between these amino acids and phase I is unclear, but it is noted that amino acids in the latter class contain some polar functional groups other than amino and carboxylic acid groups attached to the asymmetric carbon atom. We consider that such polar groups may produce a difference in the interaction to form the complex with I, and the inversion of the elution order of enantiomers may depend on the nature of the polar groups.

It should be noted that the durability of the column was influenced by the mobile phase. The compositions of the mobile phases were as given in Table II. The column conditioning by passing a 1 mM aqueous solution of copper(II) acetate after daily use was effective in preventing changes in the retention parameters, enantioselectivity or efficiency of the column.

The use of the copper(II) complex 2 as a chiral stationary phase in gas chromatography was reported previously [25–27]. It is expected that the use

TABLE II

## ENANTIOMER SEPARATIONS BY HPLC WITH PHASE I

Mobile phase: (A) 1 mM copper(II) sulphate in water; (B) 2 mM copper(II) sulphate in water–acetonitrile (85:15); (C) 2 mM copper(II) sulphate in water–acetonitrile (80:20). A flow-rate of 1 ml/min was typically used for the 150 × 4.6 mm I.D. column at room temperature. An injection volume of 5  $\mu$ l (2 mg/ml) was typically used.  $k'_1$ ,  $k'_2$  = Capacity factors of first- and second-eluted isomers, respectively;  $\alpha$  = separation factor ( $k'_2/k'_1$ ).

Compound	$k'_1$	$k'_2$	$\alpha$	Mobile phase
<i>Amino alcohols</i>				
Norphenylephrine	2.90	3.57	1.23	A
Normetanephrine	6.25	7.19	1.15	A
Norephedrine	3.85	4.27	1.11	A
<i>p</i> -Hydroxynorephedrine	1.56	1.76	1.13	A
Atenolol	5.98	6.40	1.07	A
Propranolol	9.85	10.44	1.06	B
Phenylalaninol	5.43	11.07	2.04	A
<i>Amines</i>				
1-Phenyl-2-( <i>p</i> -tolyl)ethylamine	17.60	28.51	1.62	C
$\alpha$ -Amino- $\epsilon$ -caprolactam	0.70	1.34	1.91	A
Homocysteine thiolactone	6.03	7.19	1.19	A
Ketamine	1.47	1.85	1.26	B
<i>Amino acids</i>				
Serine	0.21 (D)	0.25 (L)	1.19	A
Allothreonine	0.32 (D)	0.55 (L)	1.72	A
Proline	0.69 (L)	0.84 (D)	1.22	A
Valine	1.40 (L)	1.81 (D)	1.29	A
Methionine	3.04 (D)	3.95 (L)	1.30	A
Allo-isoleucine	3.19 (L)	3.82 (D)	1.20	A
Histidine	3.82 (D)	4.51 (L)	1.18	A
<i>tert</i> -Leucine	5.45 (L)	7.30 (D)	1.34	A
Leucine	5.66 (L)	6.17 (D)	1.09	A
Aspartic acid	5.87 (L)	6.52 (D)	1.11	A
Isoleucine	6.39 (L)	7.34 (D)	1.15	A
Phenylalanine	2.18 (D)	3.79 (L)	1.74	B
Tryptophan	3.21 (D)	6.58 (L)	2.05	B
3-Aminobutyric acid	1.91	2.29	1.20	A
3-Amino-2-methylpropionic acid	2.87	3.09	1.08	A
<i>Hydroxy acids</i>				
Lactic acid	17.36	27.06	1.56	B
Glyceric acid	13.61	15.40	1.13	B
2-Hydroxybutyric acid <sup>a</sup>	41.86	91.59	2.19	B
3-Hydroxybutyric acid <sup>b</sup>	53.53	62.07	1.16	B

<sup>a</sup> Column: 10 mm × 4 mm I.D.

<sup>b</sup> Column: 50 mm × 4.6 mm I.D.

of both HPLC and GC with copper(II) complexes of Schiff bases of chiral amino alcohols may extend the scope of enantiomer separations to a wide range of racemic compounds.

## CONCLUSIONS

The copper(II) complexes of Schiff bases of chiral amino alcohols **1** and **2** are very promising as coat-

ing agents on reversed-phase material for the direct enantiomer separation of racemic amino alcohols, amines, amino acids and hydroxy acids by ligand-exchange HPLC. It is suggested that amino or hydroxyl groups attached to the asymmetric carbon atom and other polar functional groups may play an important cooperative role in the complexation with phase **1** or **2** for chiral discrimination.

#### ACKNOWLEDGEMENTS

The authors thank Dr. T. Aratani and Sumitomo Chemical for the gift of the copper(II) complexes **1** and **2** and other chemicals used in this work.

#### REFERENCES

- 1 V. A. Davankov, *Adv. Chromatogr.*, 18 (1980) 139.
- 2 V. A. Davankov, A. A. Kurganov and A. S. Bochkov, *Adv. Chromatogr.*, 22 (1983) 71.
- 3 V. A. Davankov, in A. M. Krstulovic (Editor), *Chiral Separations by HPLC*, Ellis Horwood, Chichester, 1989, p. 446.
- 4 V. A. Davankov and S. V. Rogozhin, *J. Chromatogr.*, 60 (1971) 280.
- 5 E. Gil-Av, A. Tishbee and P. E. Hare, *J. Am. Chem. Soc.*, 102 (1980) 5115.
- 6 V. A. Davankov, A. S. Bochkov and A. A. Kurganov, *Chromatographia*, 13 (1980) 677.
- 7 V. A. Davankov, A. S. Bochkov and Yu. P. Belov, *J. Chromatogr.*, 218 (1981) 547.
- 8 G. Gübitz, F. Juffmann and W. Jellenz, *Chromatographia*, 16 (1982) 103.
- 9 N. Nimura, A. Toyama, Y. Kasahara and T. Kinoshita, *J. Chromatogr.*, 239 (1982) 671.
- 10 G. Gübitz, *J. Liq. Chromatogr.*, 9 (1986) 519.
- 11 H. Kuniwa, Y. Baba, T. Ishida and H. Katoh, *J. Chromatogr.*, 461 (1989) 397.
- 12 N. Ôi, H. Kitahara and R. Kira, *J. Chromatogr.*, 592 (1992) 291.
- 13 J. N. LePage, W. Lindner, G. Davies, D. E. Setiz and B. L. Karger, *Anal. Chem.*, 51 (1979) 433.
- 14 A. A. Kurganov and V. A. Davankov, *J. Chromatogr.*, 218 (1981) 559.
- 15 C. Corradini, F. Fedeci and M. Sinibaldi, *Chromatographia*, 23 (1987) 118.
- 16 Y. Yuki, K. Saigo, H. Kimoto, K. Tachibana and M. Hasegawa, *J. Chromatogr.*, 400 (1987) 65.
- 17 H. G. Kicinski and A. Kettrup, *Fresenius' Z. Anal. Chem.*, 320 (1985) 51.
- 18 W. F. Lindner and I. Hirschböck, *J. Liq. Chromatogr.*, 9 (1986) 551.
- 19 H. G. Kicinski and A. A. Kettrup, *React. Polym.*, 6 (1987) 229.
- 20 L. R. Gelber, B. L. Karger, J. L. Neumeyer and B. Feibush, *J. Am. Chem. Soc.*, 106 (1984) 7729.
- 21 C. H. Shieh, B. L. Karger, L. R. Gelber and B. Feibush, *J. Chromatogr.*, 406 (1987) 343.
- 22 N. Ôi, H. Kitahara, R. Kira and F. Aoki, *Anal. Sci.*, 7, Suppl. (1991) 151.
- 23 T. Aratani, Y. Yoneyoshi and T. Nagase, *Tetrahedron Lett.*, 1707 (1975).
- 24 T. Aratani, *Pure Appl. Chem.*, 57 (1985) 1839.
- 25 N. Ôi, M. Horiba, H. Kitahara, T. Doi and T. Tani, *Bunseki Kagaku*, 29 (1980) 156.
- 26 N. Ôi, M. Horiba, H. Kitahara, T. Doi, T. Tani and T. Sakakibara, *J. Chromatogr.*, 202 (1980) 305.
- 27 N. Ôi, K. Shiba, T. Tani, H. Kitahara and T. Doi, *J. Chromatogr.*, 211 (1981) 274.

# Retention and enantioselective properties of racemic compounds on modified ovomucoid columns

## II. Reaction with glyceraldehyde, formaldehyde and glutaric anhydride

Jun Haginaka, Tokiko Murashima and Chikako Seyama

*Faculty of Pharmaceutical Sciences, Mukogawa Women's University, 11-68, Koshien, Kyuban-cho, Nishinomiya, Hyogo 663 (Japan)*

Hiroya Fujima and Hiroo Wada

*Shinwa Chemical Industries, 50 Kagekatsu-cho, Fushimi-ku, Kyoto 612 (Japan)*

---

### ABSTRACT

Modified ovomucoid (OVM) columns were prepared by reaction with glyceraldehyde, formaldehyde and glutaric anhydride. The retention and enantioselective properties of racemic compounds on these modified OVM columns were compared with those on an unmodified OVM column. The retentions of racemic compounds on the modified OVM columns were lower than or approximately equal to those on the unmodified OVM column (except for basic compounds on the OVM column reacted with glutaric anhydride). The modified OVM columns gave lower or approximately equal enantioselectivities than the unmodified OVM column for acidic and uncharged compounds, whereas the modified OVM columns gave higher enantioselectivity for basic compounds. These differences may be mainly attributed to changes in protein conformation, especially changes in chiral recognition site(s) as a result of modification. The results reveal that modification of OVM proteins may be effective for the chiral separation of basic compounds on an OVM column.

---

### INTRODUCTION

An ovomucoid (OVM) column was prepared for chiral separations of racemic compounds by Miwa *et al.* [1]. Recently, OVM columns have been utilized for the chiral resolution of acidic, basic and uncharged compounds owing to the wider chiral recognition properties [2–8] compared with other protein columns such as  $\alpha_1$ -acid glycoprotein, bovine serum albumin and human serum albumin. Also, it has been reported that OVM columns have

greater flexibility of operating parameters and superior long-term stability [5].

In a previous paper [7], we compared the retention and enantioselective properties of racemic compounds on two modified OVM columns, one cross-linked with glutaraldehyde and the other further reduced with sodium tetrahydroborate, with those on an unmodified OVM column. The OVM column cross-linked with glutaraldehyde had much better stability against repetitive injections of samples and/or changes in eluent composition (eluent pH, type and content of organic modifier) than the unmodified OVM column. This paper deals with the retention and enantioselective properties of racemic compounds on OVM columns modified

---

*Correspondence to:* Dr. J. Haginaka, Faculty of Pharmaceutical Sciences, Mukogawa Women's University, 11-68, Koshien, Kyuban-cho, Nishinomiya, Hyogo 663, Japan.

with glyceraldehyde, formaldehyde and glutaric anhydride.

## EXPERIMENTAL

### Reagents and materials

Ibuprofen, ketoprofen, chlorpheniramine maleate and hexobarbital were kindly donated by Kaken Pharmaceutical (Tokyo, Japan), Chugai Pharmaceutical (Tokyo, Japan), Essex Nippon (Osaka, Japan) and Teikoku Chemicals (Osaka, Japan). Alprenolol, pindolol, tolperisone hydrochloride and benzoin were purchased from Sigma (St. Louis, MO, USA). The structures of the racemic compounds used in this study are shown in Fig. 1. OVM proteins from egg white were purchased from Eisai (Tokyo, Japan). 2-Propanol, ethanol, methanol and acetonitrile of HPLC grade were obtained from Wako (Osaka, Japan). Formaldehyde, DL-glyceraldehyde, glutaric anhydride, sodium cyanoborohy-

dride and zinc sulphate 7-hydrate were obtained from Nacalai Tesque (Kyoto, Japan) and used without further purification.

Water purified with a Nanopure II unit (Barnstead, Boston, MA, USA) was used for the preparation of the eluent and sample solutions.

### Preparation of OVM, OVM-DIOL, OVM-ME and OVM-GLA materials

OVM was bonded to an aminopropylsilica gel (Ultron-NH<sub>2</sub>, 5 μm, 120 Å; Shinwa Chemical Industries, Kyoto, Japan) via the N,N-disuccinimidyl carbonate reaction as reported previously [7].

Six grams of OVM material were added to 100 ml of 20 mM phosphate buffer (pH 7.5), then 600 mg of sodium cyanoborohydride, 560 mg of zinc sulphate and 1.16 g of glyceraldehyde were added. After adjusting the pH to 7.5, the mixture was slowly rotated at 30°C for 15 h. The mixture was then filtered and washed with water and methanol. The

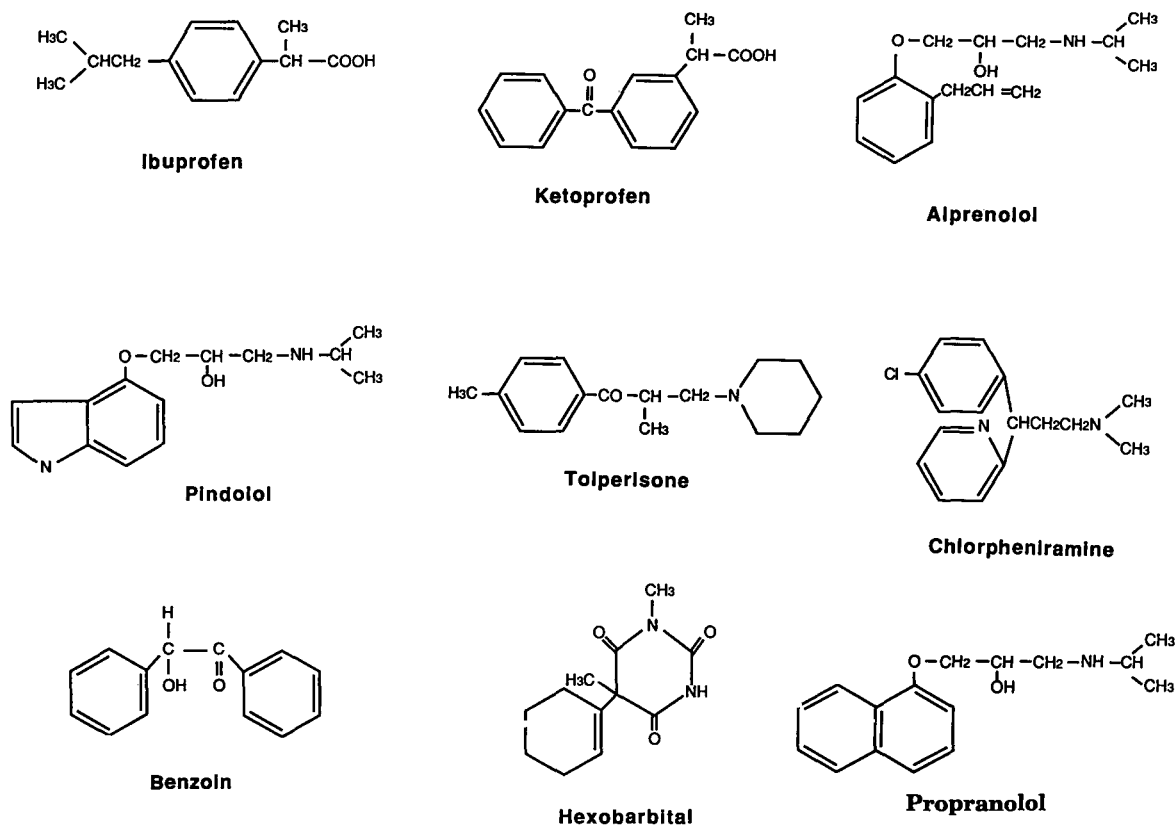


Fig. 1. Structures of the racemic compounds used.

isolated material (OVM-DIOL) was dried *in vacuo* over P<sub>2</sub>O<sub>5</sub> at 40°C for 6 h.

Six grams of the OVM material were added to 100 ml of 20 mM phosphate buffer (pH 7.5), then 600 mg of sodium cyanoborohydride, 560 mg of zinc sulphate and 160 mg of formaldehyde were added. After adjusting the pH to 7.5, the mixture was slowly rotated at 30°C for 15 h. The mixture was then filtered and washed with water and methanol. The isolated material (OVM-ME) was dried *in vacuo* over P<sub>2</sub>O<sub>5</sub> at 40°C for 6 h.

Six grams of the OVM material were added to 100 ml of 100 mM borate buffer (pH 8.5), then 490 mg of glutaric anhydride were added. After adjusting the pH to 8.5, the mixture was slowly rotated at room temperature for 1 h. The mixture was then filtered and washed with water and methanol. The isolated material (OVM-GLA) was dried *in vacuo* over P<sub>2</sub>O<sub>5</sub> at 40°C for 6 h.

These materials were packed into a 100 × 4.6 mm I.D. stainless-steel column by the slurry packing method.

#### Chromatography

The HPLC system used was composed of an LC-9A pump, an SPD-6A spectrophotometer, a SIL-6B autoinjector, a C-R4A integrator and an SCL-6B system controller (all from Shimadzu, Kyoto, Japan). The flow-rate was maintained at 0.8 ml/min. Detection was performed at 220 or 254 nm.

Capacity factors were calculated from the equation  $k' = (t_R - t_0)/t_0$ , where  $t_R$  and  $t_0$  are elution times of retained and unretained solutes, respectively;  $k'_1$  and  $k'_2$  correspond to the capacity factors of the first- and second-eluted peaks, respectively. The retention time of an unretained solute,  $t_0$ , was measured by injecting a solution whose organic modifier content was slightly different from that of the eluent used. The enantioseparation factor was calculated from the equation  $\alpha = k'_2/k'_1$ . Resolution was calculated from the equation  $R_s = 2(t_2 - t_1)/(t_{w1} + t_{w2})$ , where  $t_{w1}$  and  $t_{w2}$  are peak widths of the first- and second eluted peaks, respectively. All separations were carried out at 25°C using a CO-1093C column oven (Uniflows, Tokyo, Japan).

The eluents, which were prepared by using phosphoric acid–sodium dihydrogenphosphate or sodium dihydrogenphosphate–disodium hydrogenphosphate and organic modifier, are specified in the figure and table captions.

#### Sample preparation

A known amount of racemic solute was dissolved in methanol or water and the solution was diluted with the eluent to desired concentration. A 20- $\mu$ l aliquot of the sample solution was loaded on to the column. The amount loaded was below 0.5  $\mu$ g.

## RESULTS

#### *Effect of eluent pH on retention and enantioselectivity of acidic, basic and uncharged compounds*

Tables I–III show the effects of eluent pH on the retention and enantioselectivity of acidic, basic and uncharged compounds on OVM, OVM-DIOL, OVM-ME and OVM-GLA columns, with 20 mM phosphate buffer containing 10% ethanol as the eluent. The capacity factors ( $k'_1$ ) of the first-eluted enantiomers of acidic compounds on the OVM-DIOL and OVM-ME columns were slightly higher than those on the OVM column. The  $k'_1$  of acidic compounds was drastically decreased on the OVM-GLA column, especially when an eluent of pH > 4.0 was used. The enantioselectivity ( $\alpha$ ) of these compounds was slightly lower on the OVM-DIOL and OVM-ME columns and lower on the OVM-GLA column. On the OVM-DIOL and OVM-ME columns, the  $k'_1$  of basic compounds was almost the same as that on the OVM column, whereas the  $k'_1$  on the OVM-GLA column was considerably higher when an eluent of pH > 4.0 was used. The  $\alpha$  values of these compounds were higher or approximately equal on all the modified columns except for separation of chlorpheniramine on the OVM-GLA column. The  $k'_1$  values of uncharged compounds were slightly lower on the OVM-DIOL, OVM-ME and OVM-GLA columns, than on the OVM column. The  $\alpha$  values of uncharged compounds were unchanged on the OVM-DIOL and OVM-ME columns, whereas those of benzoin and hexobarbital on the OVM-GLA column were lower (the latter is not resolved).

#### *Effect of organic modifier on enantioselectivity of acidic, basic and uncharged compounds*

Tables IV–VI show the effects of the organic modifier (ethanol, 2-propanol, methanol and acetonitrile) on the enantioselectivity ( $\alpha$ ) of acidic, basic and uncharged compounds on the OVM, OVM-DIOL, OVM-ME and OVM-GLA columns. For



TABLE I

EFFECT OF pH ON RETENTION AND ENANTIOSELECTIVITY OF ACIDIC COMPOUNDS ON OVM, OVM-DIOL, OVM-ME AND OVM-GLA COLUMNS

Eluent: 20 mM phosphate buffer–ethanol (90:10, v/v).

Column	Compound	pH 3.2 <sup>a</sup>		pH 4.0		pH 5.1		pH 6.0		pH 6.9	
		$k'_1$	$\alpha$	$k'_1$	$\alpha$	$k'_1$	$\alpha$	$k'_1$	$\alpha$	$k'_1$	$\alpha$
OVM	Ibuprofen	4.79	1.29	7.35	1.29	4.62	1.15	1.48	1.06	0.39	1.00
	Ketoprofen	13.6	1.32	20.0	1.20	8.03	1.08	2.32	1.00	0.66	1.00
OVM-DIOL	Ibuprofen	4.82	1.25	7.39	1.22	5.12	1.12	1.53	1.00	0.45	1.00
	Ketoprofen	13.2	1.21	18.0	1.13	8.92	1.06	2.43	1.00	0.67	1.00
OVM-ME	Ibuprofen	5.09	1.24	7.85	1.21	5.30	1.10	1.77	1.00	0.52	1.00
	Ketoprofen	12.7	1.24	17.4	1.15	8.31	1.06	2.61	1.00	0.79	1.00
OVM-GLA	Ibuprofen	4.20	1.15	4.60	1.20	1.43	1.19	0.17	1.00		
	Ketoprofen	8.00	1.14	9.31	1.13	2.28	1.12	0.35	1.00		

<sup>a</sup> Buffer pH.

TABLE II

EFFECT OF pH ON RETENTION AND ENANTIOSELECTIVITY OF BASIC COMPOUNDS ON OVM, OVM-DIOL, OVM-ME AND OVM-GLA COLUMNS

Eluent: 20 mM phosphate buffer–ethanol (90:10, v/v).

Column	Compound	pH 4.0 <sup>a</sup>		pH 5.1		pH 6.0		pH 6.9	
		$k'_1$	$\alpha$	$k'_1$	$\alpha$	$k'_1$	$\alpha$	$k'_1$	$\alpha$
OVM	Alprenolol	0.18	1.00	2.84	1.00	13.4	1.12	59.4	1.14
	Pindolol			0.29	1.00	1.13	1.22	3.80	1.20
	Tolperisone	0.06	3.29	0.52	1.57	2.28	1.33	9.30	1.24
	Chlorpheniramine	0.22	1.00	1.58	1.54	6.89	1.74	29.3	1.80
OVM-DIOL	Alprenolol	0.13	1.00	2.38	1.00	13.6	1.09	50.9	1.08
	Pindolol	0.01	1.00	0.24	1.36	1.20	1.34	3.83	1.34
	Tolperisone			0.35	2.19	1.87	1.59	7.19	1.44
	Chlorpheniramine	0.41	1.55	1.29	1.63	6.07	1.76	21.8	1.76
OVM-ME	Alprenolol	0.28	1.00	2.35	1.00	12.5	1.10	49.5	1.14
	Pindolol			0.22	1.25	1.07	1.23	3.47	1.20
	Tolperisone			0.35	1.70	1.76	1.41	6.57	1.27
	Chlorpheniramine	0.16	1.69	1.23	1.63	6.52	1.89	21.7	1.97
OVM-GLA	Alprenolol	0.59	1.00	5.53	1.20	27.3	1.17	97.3	1.14
	Pindolol	0.32	1.00	2.39	1.00	6.13	1.11	10.4	1.21
	Tolperisone	0.48	1.53	3.31	1.70	9.37	2.08	18.0	2.01
	Chlorpheniramine	0.98	1.00	6.00	1.16	18.1	1.37	42.8	1.59

<sup>a</sup> Buffer pH.

TABLE III

EFFECT OF pH ON RETENTION AND ENANTIOSELECTIVITY OF UNCHARGED COMPOUNDS ON OVM, OVM-DIOL, OVM-ME AND OVM-GLA COLUMNS

Eluent: 20 mM phosphate buffer–ethanol (90:10, v/v).

Column	Compound	pH 3.2 <sup>a</sup>		pH 4.0		pH 5.1		pH 6.0		pH 6.9	
		$k'_1$	$\alpha$	$k'_1$	$\alpha$	$k'_1$	$\alpha$	$k'_1$	$\alpha$	$k'_1$	$\alpha$
OVM	Benzoin	1.69	1.63	2.29	1.92	2.55	2.40	2.59	2.25	2.95	1.96
	Hexobarbital	0.47	1.00	0.52	1.14	0.62	1.00	0.56	1.22	0.63	1.36
OVM-DIOL	Benzoin	1.51	1.59	2.09	2.12	2.47	2.30	2.59	2.22	2.61	1.93
	Hexobarbital	0.38	1.00	0.47	1.00	0.52	1.15	0.52	1.25	0.53	1.34
OVM-ME	Benzoin	1.58	2.29	2.12	2.16	2.34	2.21	2.42	2.09	2.74	1.86
	Hexobarbital	0.40	1.00	0.49	1.00	0.50	1.12	0.52	1.23	0.58	1.37
OVM-GLA	Benzoin	1.61	1.26	1.93	1.61	2.12	1.78	2.12	1.90	2.22	1.82
	Hexobarbital	0.44	1.00	0.49	1.00	0.51	1.00	0.47	1.00	0.42	1.00

<sup>a</sup> Buffer pH.

acidic compounds, the eluents used were 20 mM phosphate buffer (pH 3.2) containing 10% ethanol, 7% 2-propanol, 15% methanol and 8% acetonitrile, whereas for basic and uncharged compounds, the eluents were 20 mM phosphate buffer (pH 6.0) containing the same percentage of each organic modifier. Almost the same retentions of the solutes tested were observed with use of eluents containing 10% ethanol, 7% 2-propanol, 15% methanol and 8% acetonitrile. In addition, acidic compounds gave better separations with use of acidic eluents, whereas basic and uncharged compounds gave higher enantioselectivities with the use of an eluent of pH 6 or 6.9. Therefore, we checked the enantioselectivity under the conditions as shown in Tables IV–VI. The use of methanol as an organic modifier gave the highest enantioselectivity for ibuprofen, ketoprofen and hexobarbital on the unmodified and modified OVM columns. For the separation of benzoin, 2-propanol gave the highest enantioselectivity on the OVM, OVM-DIOL and OVM-ME columns, whereas methanol gave the highest enantioselectivity on the OVM-GLA column. On the other hand, for the separation of basic compounds, the highest enantioselectivity was obtained with ethanol, 2-propanol or methanol, depending on the solute or column used. However, acetonitrile was not a good organic modifier for the chiral separation of the compounds tested.

#### Separation of racemic propranolol on unmodified and modified OVM columns

Fig. 2A, B, C and D show the separations of racemic propranolol on the OVM, OVM-DIOL, OVM-ME and OVM-GLA columns, respectively, with 20 mM phosphate buffer (pH 5.1)–ethanol (90:1, v/v) as the eluent. The capacity factor of propranolol was lower on the OVM-DIOL and OVM-ME columns than on the unmodified OVM column, whereas on the OVM-GLA column the capacity factor was slightly higher. All the modified columns gave higher enantioselectivity and better resolution than the unmodified OVM column under the conditions employed.

#### DISCUSSION

The OVM-DIOL and OVM-ME columns gave similar retentions and enantioselectivities for acidic, basic and uncharged compounds, whereas the OVM-GLA column gave very different values. By taking into account the  $pK_1$  value of glutaric acid (4.3) and the isoelectric point of ovomucoid ( $pI = 3.8$ – $4.3$ ), the retention properties of acidic and basic compounds on the OVM-GLA column were easily elucidated. With an eluent of  $pH > 4$ – $5$  glutaric acid residues were negatively charged, so the OVM-GLA material was much more negatively charged than the unmodified OVM. Hence the retentions of

TABLE IV

EFFECT OF ETHANOL (EtOH), 2-PROPANOL (2-PrOH), METHANOL (MeOH) AND ACETONITRILE (ACN) ORGANIC MODIFIERS ON ENANTIOSELECTIVITY ( $\alpha$ ) OF ACIDIC COMPOUNDS ON OVM AND MODIFIED OVM COLUMNS

Eluents used were a mixture of 20 mM phosphate buffer (pH 3.2) and 10% EtOH, 7% 2-PrOH, 15% MeOH and 8% ACN.

Column	Compound	EtOH	2-PrOH	MeOH	ACN
OVM	Ibuprofen	1.29	1.17	1.37	1.13
	Ketoprofen	1.32	1.26	1.43	1.23
OVM-DIOL	Ibuprofen	1.25	1.16	1.37	1.16
	Ketoprofen	1.21	1.22	1.36	1.20
OVM-ME	Ibuprofen	1.24	1.15	1.38	1.15
	Ketoprofen	1.24	1.24	1.41	1.22
OVM-GLA	Ibuprofen	1.15	1.09	1.23	1.10
	Ketoprofen	1.14	1.10	1.24	1.11

the positively charged compounds (basic compounds) on the OVM-GLA column were increased and those of the negatively charged compounds (acidic compounds) were decreased. Also, a slight

increase in the retentions of acidic compounds on the OVM-DIOL and OVM-ME columns could be ascribed to hydrophobic interactions caused by suppression of the dissociation of amino groups on

TABLE V

EFFECT OF ETHANOL (EtOH), 2-PROPANOL (2-PrOH), METHANOL (MeOH) AND ACETONITRILE (ACN) ORGANIC MODIFIERS ON ENANTIOSELECTIVITY ( $\alpha$ ) OF BASIC COMPOUNDS ON OVM AND MODIFIED OVM COLUMNS

Eluents used were a mixture of 20 mM phosphate buffer (pH 6.0) and 10% EtOH, 7% 2-PrOH, 15% MeOH and 8% ACN.

Column	Compound	EtOH	2-PrOH	MeOH	ACN
OVM	Alprenolol	1.12	1.10	1.16	1.11
	Pindolol	1.22	1.00	1.24	1.00
	Tolperisone	1.33	1.67	1.33	1.10
	Chlorpheniramine	1.74	2.02	1.87	1.84
OVM-DIOL	Alprenolol	1.09	1.08	1.15	1.00
	Pindolol	1.34	1.13	1.27	1.00
	Tolperisone	1.59	1.47	1.41	1.00
	Chlorpheniramine	1.76	1.60	1.71	1.61
OVM-ME	Alprenolol	1.10	1.08	1.18	1.13
	Pindolol	1.23	1.09	1.21	1.00
	Tolperisone	1.41	1.44	1.37	1.00
	Chlorpheniramine	1.89	1.84	1.95	1.74
OVM-GLA	Alprenolol	1.17	1.04	1.11	1.08
	Pindolol	1.11	1.06	1.15	1.00
	Tolperisone	2.08	1.86	2.58	1.33
	Chlorpheniramine	1.37	1.27	1.51	1.26

TABLE VI

EFFECT OF ETHANOL (EtOH), 2-PROPANOL (2-PrOH), METHANOL (MeOH) AND ACETONITRILE (ACN) ORGANIC MODIFIERS ON ENANTIOSELECTIVITY ( $\alpha$ ) OF UNCHARGED COMPOUNDS ON OVM AND MODIFIED OVM COLUMNS

Eluents used were a mixture of 20 mM phosphate buffer (pH 6.0) and 10% EtOH, 7% 2-PrOH, 15% MeOH and 8% ACN.

Column	Compound	EtOH	2-PrOH	MeOH	ACN
OVM	Benzoin	2.25	2.61	2.15	1.52
	Hexobarbital	1.22	1.26	1.37	1.14
OVM-DIOL	Benzoin	2.22	2.30	2.20	1.46
	Hexobarbital	1.25	1.21	1.31	1.00
OVM-ME	Benzoin	2.09	2.36	2.20	1.43
	Ketoprofen	1.23	1.18	1.31	1.00
OVM-GLA	Benzoin	1.90	1.91	2.08	1.40
	Hexobarbital	1.00	1.00	1.17	1.00

OVM proteins as a result of the modification. We previously reported [7] that hydrophobic and electrostatic interactions play an important role in the retention of these compounds on both cross-linked and unmodified OVM columns. This is true with

the OVM columns modified with glyceraldehyde, formaldehyde and glutaric anhydride.

With respect to enantioselectivity, it is interesting that the OVM column gave the highest enantioselectivity against the acidic and uncharged com-

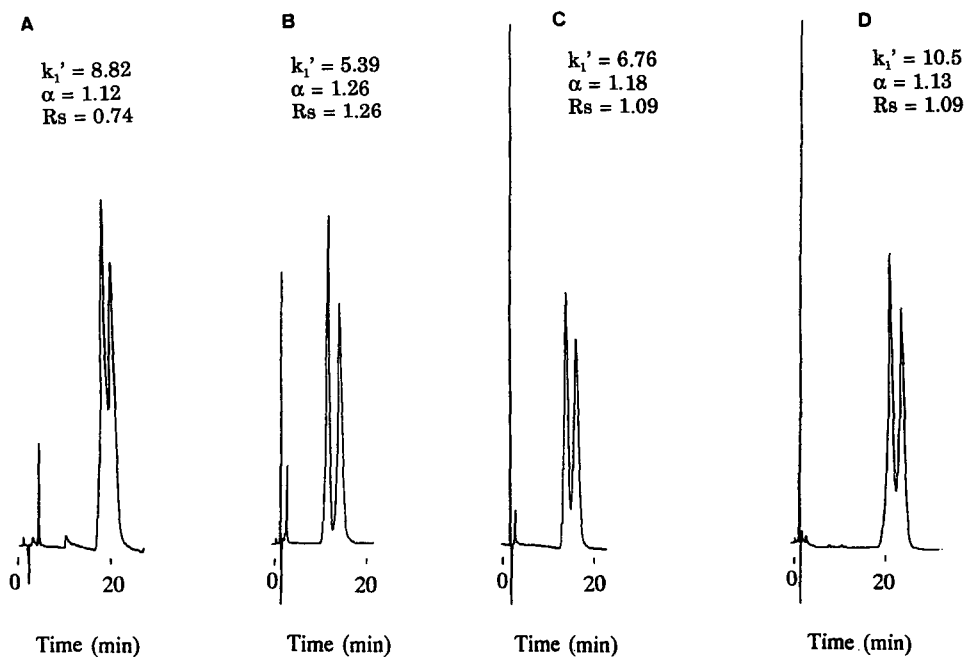


Fig. 2. Separation of racemic propranolol on (A) OVM, (B) OVM-DIOL, (C) OVM-ME and (D) OVM-GLA columns. Eluent, 20 mM phosphate buffer (pH 5.1) containing 10% ethanol; injection volume, 20  $\mu$ l (concentration, 10  $\mu$ g/ml); detection, 220 nm.  $k_1'$ ,  $\alpha$  and  $R_s$  are the capacity factor of the first-eluted enantiomer, enantioselectivity factor and resolution, respectively.

pounds tested, whereas the modified columns gave better separations against the basic compounds. Also; chiral recognition of basic compounds on the unmodified and modified OVM columns was affected by the organic modifier used. As reported by Iredale *et al.* [4], these results suggest that competition between the organic modifier and the solutes for the chiral binding site(s) might occur. Hence, it is important to select the most suitable organic modifier and eluent pH for the chiral separation of a compound of interest.

Although the blocking of amino groups of ovomucoid proteins with methyl or glyceryl group(s) (*i.e.*, OVM-ME or OVM-DIOL column) did not affect the retentions of acidic, basic and uncharged compounds so much, the OVM-DIOL and OVM-ME columns gave higher or almost equal enantioselectivities for  $\beta$ -blockers (alprenolol, pindolol and propranolol) compared with the unmodified OVM column. The OVM-GLA column gave much longer retentions for basic compounds, whereas it gave a much higher enantioselectivity for tolperisone and a lower enantioselectivity for chlorpheniramine. These results may be mainly attributed to changes

in protein conformation, especially changes in chiral recognition site(s) as a result of modification. Also, the carboxylate ion of glutaric acid residue might contribute to the chiral recognition of basic compounds. These results indicate that modification of OVM proteins may be effective for chiral separations of basic compounds.

#### REFERENCES

- 1 T. Miwa, M. Ichikawa, M. Tsuno, T. Hattori, T. Miyakawa, M. Kayano and Y. Miyake, *Chem. Pharm. Bull.*, 35 (1987) 682.
- 2 T. Miwa, H. Kuroda, S. Sakashita, N. Asakawa and Y. Miyake, *J. Chromatogr.*, 511 (1990) 89.
- 3 M. Okamoto and H. Nakazawa, *J. Chromatogr.*, 504 (1990) 445.
- 4 J. Iredale, A.-F. Aubry and I. W. Wainer, *Chromatographia*, 31 (1991) 329.
- 5 K. M. Kirkland, K. L. Nelson and D. A. McCombs, *J. Chromatogr.*, 545 (1991) 43.
- 6 K. M. Kirkland, K. L. Neilson, D. A. McCombs and J. J. DeStefano, *LC · GC*, 10 (1992) 322.
- 7 J. Haginaka, Ch. Seyama, H. Yasuda, H. Fujima, H. Wada, *J. Chromatogr.*, 592 (1992) 301.
- 8 J. Haginaka, Ch. Seyama, H. Yasuda and K. Takahashi, *J. Chromatogr.*, 598 (1992) 67.

# Direct chiral separation of almokalant on Chiralcel OD and Chiralpak AD for liquid chromatographic assay of biological samples

Karin Balmér, Per-Olof Lagerström, Sam Larsson and Bengt-Arne Persson

Bioanalytical Chemistry and Analytical Chemistry, Astra Hässle AB, S-431 83 Mölndal (Sweden)

## ABSTRACT

The four isomers of almokalant, a new antiarrhythmic substance under investigation, were separated by liquid chromatography on a Chiralcel OD and a Chiralpak AD column containing cellulose and amylose tris(3,5-dimethylphenylcarbamate), respectively. Both chiral stationary phases separate almokalant into the four isomers, but the retention orders are different if the carbamate is derivatized on cellulose or amylose. The Chiralcel OD column was used for the separation and determination of the isomers in urine at levels down to 100 nmol/l for the first three eluted and 200 nmol/l for the last with a relative standard deviation of less than 15%. The fluorescence response was increased by post-column ionization after stereoselective separation on the Chiralpak AD column. The isomers of almokalant could be determined at levels down to 10 nmol/l in plasma with a relative standard deviation of less than 15%.

## INTRODUCTION

Almokalant, 4-(3-{ethyl[3-(propylsulphinyl)propyl]amino}-2-hydroxypropoxy)benzonitrile (Fig. 1), is an antiarrhythmic drug substance under investigation in the early clinical phase. The compound contains one chiral carbon atom and one sulphoxide group in the molecule and is given as a stereoisomeric mixture of the four isomers. For pharmacokinetic purposes it is of interest to develop a liquid chromatographic method for the chiral separation of the four stereoisomers in biological samples. Almokalant contains an amino alcohol function and compounds of this kind have previously been separated on protein-based chiral columns, e.g., Chiral-AGP, with good selectivity in many instances [1,2]. Recently the chiral stationary phases Chiralcel OD and Chiralpak AD, containing cellulose tris(3,5-dimethylphenylcarbamate) and amylose tris(3,5-dimethylphenylcarbamate), respective-

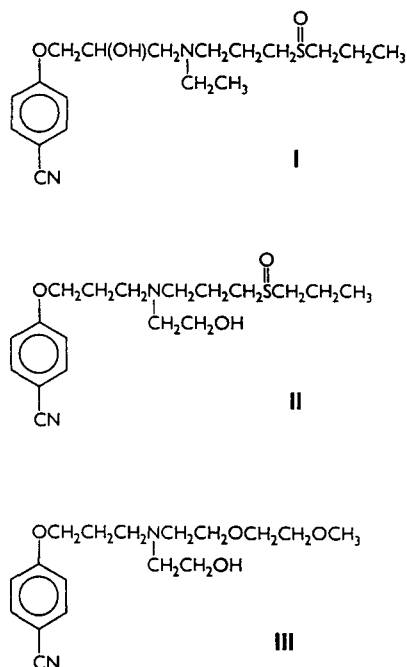


Fig. 1. Structures of almokalant (I) and the internal standards H 222/98 (II) and H 222/82 (III).

Correspondence to: K. Balmér, Bioanalytical Chemistry, Astra Hässle AB, S-431 83 Mölndal, Sweden.

ly, as a selector coated on to a macroporous silica gel have been used for the direct chiral resolution and assay of amino alcohol derivatives with  $\beta$ -adrenergic blocking activity [3,4]. The chromatographic conditions, such as type of alcohol and water content in the hexane mobile phase, influence the stereoselective properties of Chiralcel OD for amino alcohols [5,6]. Substances with a chiral sulphoxide group as in almokalant have been separated on Chiralcel (OB, OC, and OD) columns, as reported in the Application Guide from Daicel [7] and by Gaffney *et al.* [8]. The interactions of the polar carbamate group on the solute are different if the carbamate is derivatized on cellulose or amylose [9].

This paper reports the effects of the composition of the mobile organic phase on the stereoselectivity of Chiralcel OD and Chiralpak AD for the four isomers of almokalant. For assay in biological samples such as plasma a simple post-column reaction method was introduced to increase the detectability of the substance at least fivefold.

## EXPERIMENTAL

### Chemicals

Almokalant as racemate, the pure stereoisomers (*R*)-(–)H 262/15, (*R*)-(+)H 262/18, (*S*)-(–)H 262/20, and (*S*)-(+)H 262/21 and H 222/82 and H 222/98 (internal standards) in citrate buffer solutions (pH 5) were obtained from Medicinal Chemistry, Astra Hässle. The absolute configuration of the four isomers of almokalant is not yet known. The *R* and *S* refer to the carbon with the alcohol substituent (Fig. 1) and (+) and (–) to the optical activity of the sulphoxide group.

Hexane, 1-propanol, 2-propanol, acetonitrile and dichloromethane (HPLC grade) were from Rathburn (Walkerburn, UK) and diethylamine and trifluoroacetic acid from Fluka (Buchs, Switzerland). A Milli-Q system (Millipore, Molsheim, France) was used to supply deionized water. All buffer substances were of analytical-reagent grade (Merck, Darmstadt, Germany).

### Instrumentation

The liquid chromatographic system consisted of two LKB (Bromma, Sweden) pumps, a Kontron 460 autosampler (Tegimenta, Rotkreuz, Switzerland) and a Shimadzu (Kyoto, Japan) RF-551 fluo-

rescence detector operated at 248 nm (excitation) and 306 nm (emission), cell volume 12  $\mu$ l. A thermostatted bath (Lauda RMS, Königshofen, Germany) controlled the water temperature in the column jacket. The chromatograms were processed by a Multichrom version 1-8.2 chromatography data system from Fisons (Manchester, UK) or an SP 4400 integrator (Spectra-Physics, San Jose, CA, USA). A Metrohm (Herisau, Switzerland) 684 KF coulometer was used to measure the water content of the mobile phase. The analytical columns (250  $\times$  4.6 mm I.D.), Chiralcel OD and Chiralpak AD from Daicel Chemical Industries (Tokyo, Japan), were used with flow-rates of 0.5 ml/min at a temperature of 35°C, unless stated otherwise. The mobile phase contained hexane with addition of 1-propanol, 2-propanol, acetonitrile and water, the composition being given in each experiment. All the mobile phases contained 0.1% diethylamine. Before use the Chiralpak AD column had to be conditioned for more than 24 h by passing mobile phase through it in order to remove fluorescent impurities that caused a high detector background.

For the analyses of biological samples a CN guard column (15  $\times$  3.2 mm I.D., 7  $\mu$ m) from Brownlee Labs. (Santa Clara, CA, USA) was used. A corresponding guard column with silica was tested as a mixing chamber for the post-column reaction. A Shodex DP-1 pulse damper was used between the pump and the T-tube to generate a back-pressure. The T-tube was made in-house.

### Test solutions

Standard solutions of the substances were prepared in citrate buffer solutions (pH 5, *I* = 0.1). Test solutions in the organic mobile phase were prepared from alkalized standard solutions by extraction with hexane–dichloromethane (1:1). After phase separation (freezing of the aqueous phase) and evaporation of the organic phase under nitrogen, the amines were dissolved in the mobile phase.

### Analytical procedure

Biological samples, 1.0 ml of urine or plasma, were alkalized with 100  $\mu$ l of 1 *M* NaOH, 100  $\mu$ l of internal standard solution H 222/82 or H 222/98 (Fig. 1) were added and the mixture was extracted with 5.0 ml of hexane–dichloromethane (1:1) by shaking for 20 min. After centrifugation and freez-

ing of the aqueous phase, the organic phase was transferred into a test-tube and evaporated under a stream of nitrogen. The residue was reconstituted in 250  $\mu$ l of the organic mobile phase by vigorous mixing and 100  $\mu$ l of the solution were injected on to the column.

#### Recovery and precision

The absolute recovery of almokalant was deter-

mined by adding known amounts to blank plasma and processing the samples according to the analytical procedure. The chromatographic peaks were then measured and compared with those from injection of known solutions in the mobile phase.

The repeatability at different concentration levels was determined by assaying replicate samples ( $n = 8$ ) with added almokalant.

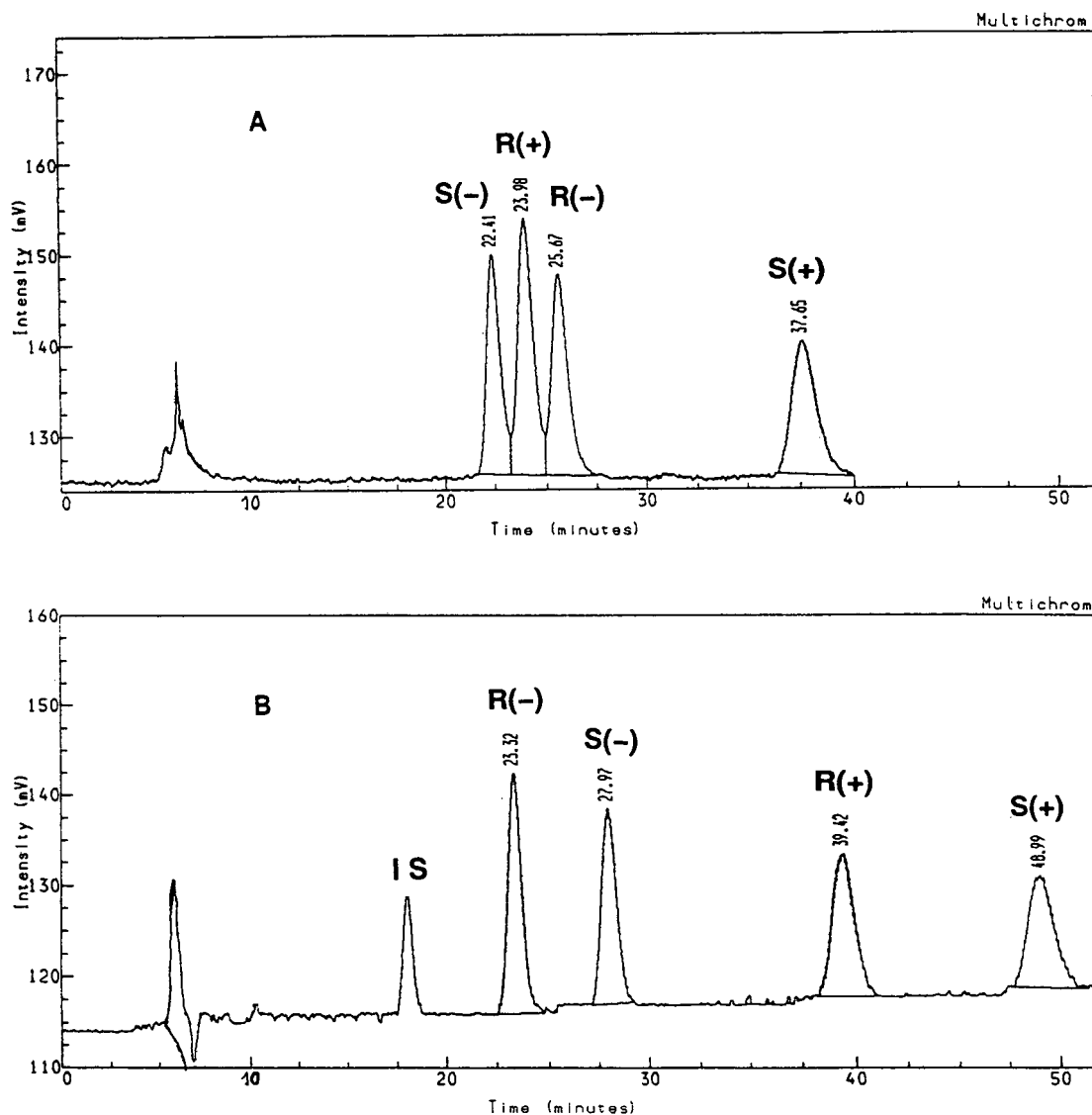


Fig. 2. Chromatograms for the separation of almokalant. Temperature, 30°C; flow-rate, 0.5 ml/min. (A) Chiralcel OD with a mobile phase of 15% 1-propanol–0.1% diethylamine–0.4 g/l water in hexane. (B) Chiralpak AD with a mobile phase of 14% 1-propanol–6% acetonitrile–0.1% diethylamine in hexane. IS = internal standard (H222/98).



## RESULTS AND DISCUSSION

*Chiral separation*

We investigated different chromatographic systems for the resolution of the stereoisomers of almokalant. Previously Chiral-AGP with  $\alpha_1$ -acid glycoprotein as chiral selector was successfully used for the separation of the enantiomers of metoprolol [2]. Almokalant is also an aryloxyalkanolamine and is structurally related to a  $\beta$ -adrenoceptor blocking drug such as metoprolol, although it is more hydrophilic. On Chiral-AGP almokalant was incompletely resolved into two peaks at pH 6.5–7.5 (phosphate buffer) and it was not retained as much as desired. Other systems were also tested without success but on Chiralcel OD, cellulose tris(3,5-dimethylphenylcarbamate) on silica, also previously used for metoprolol [6], almokalant as base could be resolved into its four isomers. The elution order was (S)(-), (R)(+), (R)(-) and (S)(+) and the  $\alpha$ -values for adjacent peaks were 1.1, 1.1 and 2.6 (Fig. 2A). As for metoprolol and  $\alpha$ -hydroxymetoprolol [6], the water content of the mobile organic phase influences the stereoselectivity. The presence of a moderate amount of water in the mobile phase of 1-propanol and diethylamine in hexane decreased the retention of the (R)(+) isomer, thus permitting separation. The addition of an excess of an aliphatic amine, diethylamine, is needed for peak symmetry, and an elevated temperature (35°C) and 1–2% of acetonitrile improve the column efficiency. This Chiralcel OD system was employed for stereoselective assay in urine (Fig. 3).

Chiralpak AD, amylose tris(3,5-dimethylphenylcarbamate), also separated the four stereoisomers but with a different retention order, (R)(-), (S)(-), (R)(+) and (S)(+), with  $\alpha$ -values for the adjacent peaks 1.3, 1.5 and 1.3 (Fig. 2B). The  $\alpha$ -value for the sulphoxide group, (R)(+)/(R)(-) and (S)(+)/(S)(-), is about 2.0 and for the chiral carbon, (S)(+)/(R)(+) and (S)(-)/(R)(-), about 1.3. The content of water in the organic mobile phase is not critical here but too large an amount of water will decrease  $k'$  for the (R)(+) isomer and also its separation from the (S)(-) isomer. The Chiralpak AD column was used for the measurement of the almokalant isomers in blood plasma.

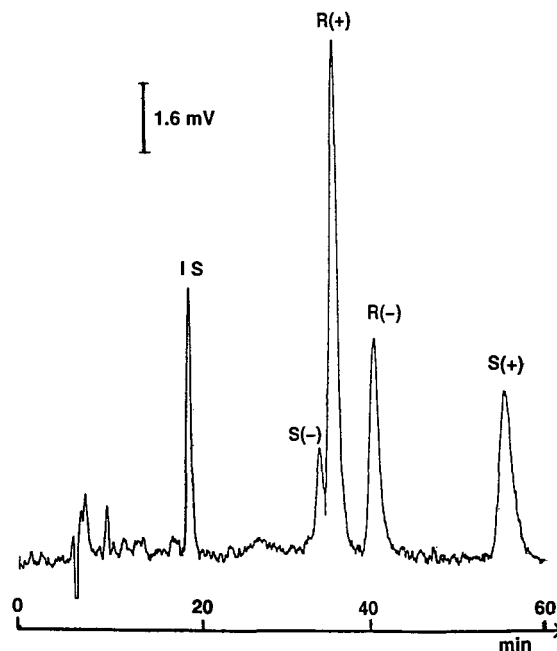


Fig. 3. Chromatogram from an authentic human urine sample on Chiralcel OD. Mobile phase, 7% 1-propanol–6% 2-propanol–1% acetonitrile–0.1% diethylamine–0.4 g/l water in hexane; temperature, 30°C; flow-rate, 0.5 ml/min. The concentrations of the isomers were 0.49  $\mu\text{mol/l}$  (S)(-), 1.26  $\mu\text{mol/l}$  (S)(+), 2.42  $\mu\text{mol/l}$  (R)(+) and 1.28  $\mu\text{mol/l}$  (R)(-). IS = internal standard (H 222/82).

*Separation from urine samples on Chiralcel OD*

When applying the separation system, demonstrated in Fig. 2A, on an extract from a rat perfusate sample it was found that a metabolite of almokalant, the corresponding sulphone, interfered with the last-eluted (S)(+) isomer on the Chiralcel OD column. By replacing some of the 1-propanol in the mobile phase with 2-propanol the (S)(+) form was more retained and separated from this sulphone. A chromatogram of an authentic urine sample prepared according to the analytical procedure is shown in Fig. 3. The limit of quantitation for the three first eluted isomers was calculated to be 100 nmol/l and for the last isomer 200 nmol/l.

The selectivity of this method was checked by analysing a series of samples by an achiral reversed-phase method. The eluate fraction containing almokalant was collected and, after an additional extraction procedure, injected on to the Chiralcel OD col-

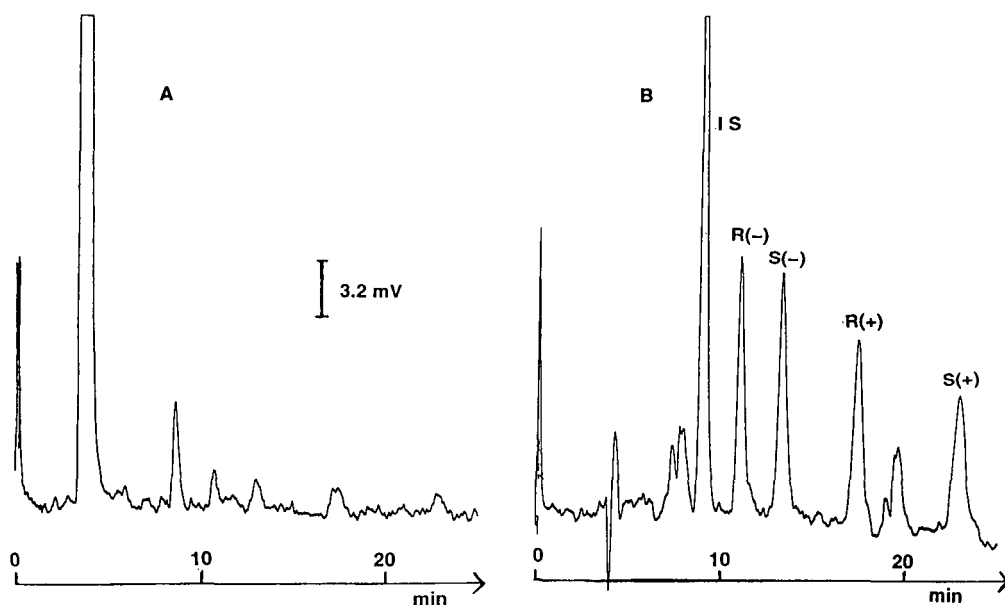


Fig. 4. Chromatograms from an authentic plasma sample containing 420 nmol/l almokalant on Chiralpak AD. Temperature, 35°C; flow-rate, 0.75 ml/min; mobile phase, 14% 1-propanol–6% acetonitrile–0.1% diethylamine in hexane, no extra water added. IS = internal standard (first-eluted isomers of H 222/98). (A) Mobile phase alone; (B) after postcolumn reaction with 0.3 mol/l TFA in hexane–ethanol (4:1) (0.15 ml/min).

umn. The results obtained confirmed those from the analytical procedure, without excessive sample work-up, as regards both the ratio between the different isomers and their individual concentrations. Studies on the stereoselective excretion of almokalant are in progress.

#### Fluorescence amplification after separation on Chiralpak AD

The fluorescence intensity of almokalant is much lower for the base form than for the protonated form, as was observed in the development of an achiral LC assay. The stereoselective separation of almokalant on Chiralcel OD or Chiralpak AD has to be performed under basic conditions, in the presence of an excess of diethylamine. However, the detector response was too low for the stereoselective assay of therapeutic concentrations in blood plasma samples. The more spacious separation pattern with the Chiralpak AD column enabled us to apply a post-column procedure to convert the resolved isomers into ionic form. The mobile phase flow of 0.75 ml/min from the analytical column was combined through a T-connection with a flow of

0.15 ml/min of trifluoroacetic acid (TFA) in hexane–ethanol (4:1). A Brownlee guard column with silica particles was inserted as a mixing chamber just before the inlet to the fluorescence detector, but it was later found to be unnecessary. By this procedure the fluorescence response of the four peaks of the almokalant isomers increased about eight-fold and the signal-to-noise ratio more than five-fold. There was a decrease in column efficiency of 10–20% but still satisfactory resolution. Chromatograms from an authentic plasma sample without and with TFA addition are shown in Fig. 4A and B, respectively. The separation on Chiralpak AD may also be used for the stereoselective assay of almokalant in urine samples. This has so far not been investigated as detection enhancement was not needed.

#### Analytical validation

In urine the isomers of almokalant could be measured at levels down to 100 nmol/l for the first three eluted peaks and 200 nmol/l for the last with a relative standard deviation of less than 15%. The calibration graph was linear between 100 nmol/l and 10

$\mu\text{mol/l}$ . The repeatability (within-day) for the four isomers was about 1.6–3.5% at a level of 1.8  $\mu\text{mol/l}$  and the reproducibility (between-day) was 3.5–5.0% at 2  $\mu\text{mol/l}$ .

In plasma, concentrations down to 10 nmol/l could be measured with a relative standard deviation of less than 15%. The calibration graph was linear between 10 and 1000 nmol/l, which covers the expected therapeutic range. The repeatability for plasma samples was 5.4–17.8% at the 15 nmol/l level and 0.7–1.5% at 300 nmol/l of each stereoisomer. The reproducibility (between-day) was 2.1–4.3% at 100 nmol/l. The absolute recovery of almokalant from the biological samples was 100.5%.

The durability of the Chiralcel OD columns was found to be excellent and the same column could be used for more than 1 year, as reported earlier [6]. For Chiralpak AD one of the columns has been in use for more than 6 months with consistent performance. It has been possible to reproduce chiral separations from one column to the other provided that the temperature and water content of the mobile phase are controlled.

#### NOTE ADDED IN PROOF

The absolute configuration of the four isomers of almokalant have recently been established: H 262/15 2*R*,3*R*; H 262/18 2*R*,3*S*; H 262/20 2*S*,3*R*; H 262/21 2*S*,3*S*.

#### REFERENCES

- 1 G. Schill, I. W. Wainer and S. A. Barkan, *J. Liq. Chromatogr.*, 9 (1986) 641.
- 2 B.-A. Persson, K. Balmér, P.-O. Lagerström and G. Schill, *J. Chromatogr.*, 500 (1990) 629.
- 3 Y. Okamoto, M. Kawashima, R. Aburatani, K. Hatada, T. Nishiyama and M. Masuda, *Chem. Lett.*, (1986) 1237.
- 4 D. R. Rutledge and C. Garrick, *J. Chromatogr.*, 497 (1989) 181.
- 5 I. W. Wainer, R. M. Stiffin and T. Shibata, *J. Chromatogr.*, 411 (1987) 139.
- 6 K. Balmér, A. Persson, P.-O. Lagerström, B.-A. Persson and G. Schill, *J. Chromatogr.*, 553 (1991) 391.
- 7 *Applications Guide for Chiral Column*, Diacel, Tokyo, 1989.
- 8 M. H. Gaffney, R. M. Stiffin and I. W. Wainer, *Chromatographia*, 27 (1989) 15.
- 9 Y. Okamoto, R. Aburatani, Y. Kaida, K. Hatada, N. Inotsume and M. Nakano, *Chirality*, 1 (1989) 239.

## Rapid direct resolution of the stereoisomers of all-*trans* astaxanthin on a Pirkle covalent L-leucine column

Saleh A. Turujman

US Food and Drug Administration, Center for Food Safety and Applied Nutrition, 200 C Street SW, HFF-445, Washington, DC 20204 (USA)

---

### ABSTRACT

Astaxanthin, 3,3'-dihydroxy- $\beta,\beta$ -carotene-4,4'-dione, gives salmon flesh its distinctive color. Synthetic all-*trans* astaxanthin consists of a racemic mixture of two enantiomers (3*R*,3'*R* and 3*S*,3'*S*) and a meso form (3*R*,3'*S*). The stereoisomeric composition of endogenous astaxanthin in wild salmon differs from that of synthetic astaxanthin added to the fish feed of pond-bred salmon. In order to determine the origin of astaxanthin in salmon flesh, a method is needed that can distinguish the various isomeric forms. HPLC conditions are described for the rapid direct resolution of the three stereoisomers of all-*trans* astaxanthin on a Pirkle covalent L-leucine column. This method also partially resolves the stereoisomeric forms of the major *cis* isomer.

---

### INTRODUCTION

The endogenous color of the flesh of Salmonid fish may be duplicated by the addition of oxycarotenoid color additives to the fish feed. However, to meet FDA requirements, color additives must be specifically listed for this use in the Code of Federal Regulations (CFR).

Two oxycarotenoids are believed to be widely used as color additives in fish feed to enhance the color of pond-bred salmonids—canthaxanthin and astaxanthin (Fig. 1). Canthaxanthin can be easily distinguished from astaxanthin by TLC [1] and HPLC [2]. Astaxanthin, but not canthaxanthin, is normally found in wild salmonids (*Salmo salar* and *Oncorhynchus*). The distribution of astaxanthin stereoisomers found in wild salmonids (endogenous astaxanthin) differs from that in synthetic astaxanthin added to fish feed. Endogenous astaxanthin is reported to consist of 78–85% of the (3*S*,3'*S*)

enantiomer, 12–17% of the (3*R*,3'*R*) enantiomer and 2–6% of the meso form [3]. In contrast, synthetic astaxanthin consists of 25% of each enantiomer and 50% of the meso form. This difference in stereoisomer distribution can be used to differentiate synthetic and endogenous astaxanthin in commercial fish.

Maoka *et al.* [4] resolved all-*trans* astaxanthin on a Pirkle covalent D-phenylglycine type column manufactured in Japan; however, the analysis time was 70 min.

Mobile phases of similar polarity have been found that allow the stereoisomers of all-*trans* astaxanthin to be directly resolved on a Pirkle covalent L-leucine column in 10–15 min. With this modified method, it should be possible to distinguish between synthetic astaxanthin extracted from the flesh of pond-bred salmon and endogenous astaxanthin, by comparison of their chromatographic profiles.

The 13-*cis* isomer of astaxanthin is more strongly retained and better resolved than the all-*trans* isomer under the same chromatographic conditions. To resolve a mixture of the two isomers, a 20-min analysis time is required.

---

Correspondence to: S. A. Turujman, US Food and Drug Administration, Center for Food Safety and Applied Nutrition, 200 C Street SW, HFF-445, Washington, DC 20204, USA.

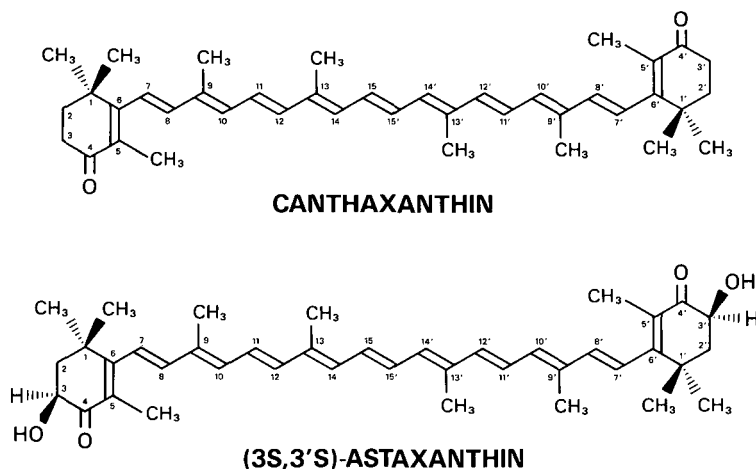


Fig. 1. Structures of astaxanthin and canthaxanthin.

## EXPERIMENTAL

### Materials

Synthetic astaxanthin was obtained from Hoffmann-La Roche, Nutley, NJ, USA. Hexane (Baxter), tetrahydrofuran (THF) (Baxter), acetonitrile (Baxter), methanol (Baker), ethanol (EM Science), 2-propanol (Baxter), 1-butanol (Fisher), *tert.*-butanol (EM Science), triethylamine (Fluka) and diethylamine (Fluka) were HPLC grade. Trioctylamine (Aldrich) was ACS reagent grade.

### Apparatus

The analysis was performed on a computer-controlled Hewlett-Packard 1090 Series II/M liquid chromatograph, equipped with an auto-injector and autosampler, a diode array detector, and ternary solvent delivery system, with low-volume metering for each of the three solvent channels, and low-pressure mixing of the metered solvent.

### HPLC conditions

A Pirkle covalent L-leucine column (5  $\mu\text{m}$ ), 250  $\times$  4.6 mm I.D. (Regis Chemical Company, Morton Grove, IL, USA), was used under isocratic conditions. The flow-rate was 1.5 ml/min and the monitoring wavelength was 470 nm. Solvents were filtered, and sparged with He as recommended by the instrument manufacturer. All mobile phases contained 77% hexane and 15–22% THF, with the bal-

ance supplied by other modifiers as listed. The modifiers were chosen so that the polarity of the mobile phase remained unchanged. Other modifiers that were used, either separately or together, included acetonitrile (ACN) and various alcohols and amines, each ranging in concentration from 0.1 to 6%. Alcohols that were used are methanol, ethanol, isopropanol (IPA), *tert.*-butanol and 1-butanol. Amines that were used are diethyl-, triethyl- ( $\text{Et}_3\text{N}$ ) and tri-*n*-octyl amine.

## RESULTS AND DISCUSSION

Resolution of the three stereoisomers of all-*trans* astaxanthin was obtained with the following mobile phases:

- hexane–THF– $\text{Et}_3\text{N}$  (77:19:2),  $\alpha_{RR/SS} = 1.29$ ;
- hexane–THF– $\text{Et}_3\text{N}$ –ACN (77:17:2:2),  $\alpha_{RR/SS} = 1.34$  (see Fig. 2);
- hexane–THF–IPA–ACN (77:17:2:2),  $\alpha_{RR/SS} = 1.2$ ; and
- hexane–THF– $\text{Et}_3\text{N}$ –ACN–methanol (77:20.5:1:1:0.5),  $\alpha_{RR/SS} = 1.23$ .

Like other carotenoids, all-*trans* astaxanthin undergoes *trans/cis* isomerization when exposed to light or heat [5]. To avoid isomerization, the astaxanthin solution should be placed in an amber vial and analysed soon after dissolution.

When a solution of all-*trans* astaxanthin in a sealed vial was exposed to available light (daylight

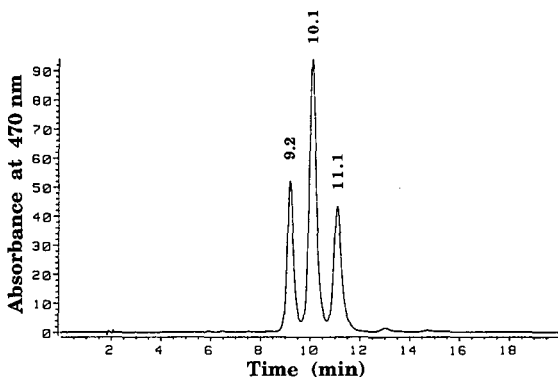


Fig. 2. Elution profile of all-*trans* astaxanthin on a Pirkle covalent L-leucine column ( $5\ \mu\text{m}$ ),  $250 \times 4.6\ \text{mm}$  I.D. Mobile phase: hexane-THF- $\text{Et}_3\text{N}$ -ACN (77:19:2:2);  $\alpha_{\text{RR/SS}} = 1.34$ .

and fluorescent) in the laboratory, 13-*cis* and 15-*cis* astaxanthin peaks appeared in the chromatograms, overlapping the peaks of the all-*trans* components in mobile phases (a) to (d) above. The mobile phases were therefore further modified in order to resolve the nine stereoisomers of all-*trans*, 13-*cis*, and 15-*cis* astaxanthin. The three all-*trans* isomers were resolved from the *cis* isomers, and the *cis* stereoisomers were resolved from each other. However, the 15-*cis* stereoisomer peaks appeared as shoulders on the 13-*cis* isomer peaks [6] (Fig. 3).

Representative mobile phases are as follows:

(e) hexane-THF-IPA- $\text{Et}_3\text{N}$  (77:20:1.5:1.5),

$\alpha_{(\text{trans})\text{RR/SS}} = 1.26$ ,  $\alpha_{(\text{cis})\text{RR/SS}} = 1.32$  (see Fig. 3);

(f) hexane-THF-IPA- $\text{Et}_3\text{N}$ -methanol-1-butanol (77:19:0.8:1.6:0.8:0.8),  $\alpha_{(\text{trans})\text{RR/SS}} = 1.2$ ,

$\alpha_{(\text{cis})\text{RR/SS}} = 1.25$ .

This method can therefore be used to quickly detect *trans/cis* isomerization of all-*trans* astaxanthin.

For the determination of the stereoisomer ratio of all-*trans* astaxanthin, mobile phase (b) may be used. However, if *trans/cis* isomerization occurs, then mobile phase (e) is recommended.

Preliminary results indicate that by using this method, synthetic astaxanthin extracted from the flesh of pond-bred salmon can be quickly distin-

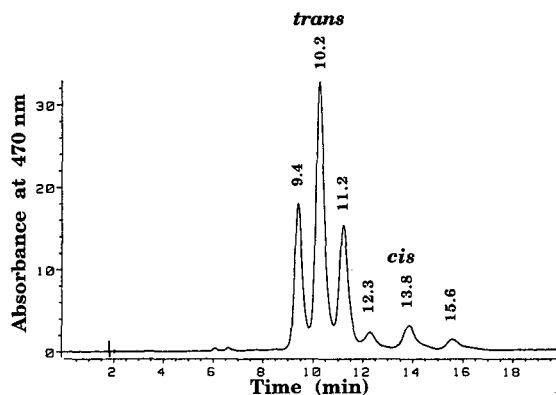


Fig. 3. Elution profile of all-*trans* astaxanthin with a minor amount of the 13-*cis* isomer, on a Pirkle covalent L-leucine column ( $5\ \mu\text{m}$ ),  $250 \times 4.6\ \text{mm}$  I.D. Mobile phase: hexane-THF-IPA- $\text{Et}_3\text{N}$  (77:20:1.5:1.5);  $\alpha_{(\text{trans})\text{RR/SS}} = 1.26$ ,  $\alpha_{(\text{cis})\text{RR/SS}} = 1.32$ .

guished from endogenous astaxanthin by comparison of their chromatographic profiles [7]. Being less polar than astaxanthin, other associated carotenoids found in small amounts in the skin of salmon, such as the mono- and diesters of astaxanthin, elute in the first 5 min and therefore do not interfere with the resolution of astaxanthin. A statistical study is under way to validate the distribution of the stereoisomers of endogenous all-*trans* astaxanthin extracted from the flesh of six subspecies of authenticated wild salmon.

## REFERENCES

- 1 S. Scalia, M. Isakson and G.W. Francis, *Archiv. Lebensmittelhyg.*, 40 (1989) 121.
- 2 T. S. Piwowar, *Laboratory Information Bulletin*, US Food and Drug Administration, Rockville, MD, 1987, p. 3155.
- 3 K. Schiedt, F.J. Leuenberger and M. Vecchi, *Helv. Chim. Acta*, 64 (1981) 449.
- 4 T. Maoka, T. Komori and T. Matsuno, *J. Chromatogr.*, 318 (1985) 122.
- 5 L. Zechmeister, *Cis-trans Isomeric Carotenoids Vitamins A and Arylpolyenes*, Springer, Vienna, 1962.
- 6 G. Englert and M. Vecchi, *Helv. Chim. Acta*, 63 (1980) 1711.
- 7 S. Turujman, poster presented at the 106th Annual AOAC International Meeting, Cincinnati, OH, August 31–September 3, 1992.



# Determination of ephedrines in urine by high-performance liquid chromatography

C. Imaz, D. Carreras, R. Navajas, C. Rodriguez, A. F. Rodriguez, J. Maynar and R. Cortes

*Laboratorio de Control del Dopaje, ICEF y D, Consejo Superior de Deportes, Greco s/n, 28040 Madrid (Spain)*

---

## ABSTRACT

An improved high-performance liquid chromatographic method with ultraviolet detection for the simultaneous determination of norephedrine, norpseudoephedrine, ephedrine, pseudoephedrine, methylephedrine and ethylephedrine in urine is described. The six substances were separated on a reversed-phase column with phosphate buffer–triethylamine (pH 5.5) as the mobile phase. The linearity and reproducibility were satisfactory for the levels usually found in urine (1–30 µg/ml).

---

## INTRODUCTION

Ephedrine (EPH)–pseudoephedrine (PEPH) and norephedrine (NEPH)–norpseudoephedrine (NPEPH) are pairs of diastereoisomeric compounds [1] which are included in the doping list of pharmacological forbidden substances indicated by the Medical Commission of the International Olympics Committee (IOC) [2]. As they are widely available in asthma, ophthalmic, cold and allergy products [3] and as they are found in more than 100 pharmaceutical formulations, the Commission has defined concentrations above which they are considered positive. For this reason the determination of such pairs of diastereoisomeric compounds is necessary.

The most commonly used technique for such determinations is gas chromatography coupled with mass spectrometry [4]. In this event a previous selective derivatization [5] is needed (O-trimethylsilyl, N-trifluoroacetic acid), but the reproducibility obtained is not always sufficient because more than one derivative may be obtained for the same com-

pound. Several HPLC methods have been reported for the determination of pseudoephedrine [6,7] and also for the pair pseudoephedrine–norpseudoephedrine [8] in pharmaceutical preparations and biological fluids. In this work, attempts were made to develop a simple, rapid, selective and accurate HPLC method without any previous derivatization process for the determination of the two pairs of diastereoisomers and also methylephedrine (MEPH) and ethylephedrine (ETEPH) (Fig. 1).

Positive urine samples taken from athletes were also analysed and very good results were obtained.

## EXPERIMENTAL

### *Reagents*

NEPH, NPEPH, EPH, PEPH, MEPH, ETEPH were obtained from Sigma (St. Louis, MO, USA). Diethyl ether was purchased from Carlo Erba (Milan, Italy) and phenylpropylamine [internal standard (I.S.)],  $\text{KH}_2\text{PO}_4$ ,  $\text{H}_3\text{PO}_4$  and triethylamine (TEA) from Merck (Darmstadt, Germany). Water was doubly distilled, deionized and purified with a Milli-Q system (Millipore, Milford, MA, USA). All other reagents and solvents were of analytical-reagent grade.

---

*Correspondence to:* C. Imaz, Laboratorio de Control del Dopaje ICEF y D, Consejo Superior de Deportes, Greco s/n, 28040 Madrid, Spain.



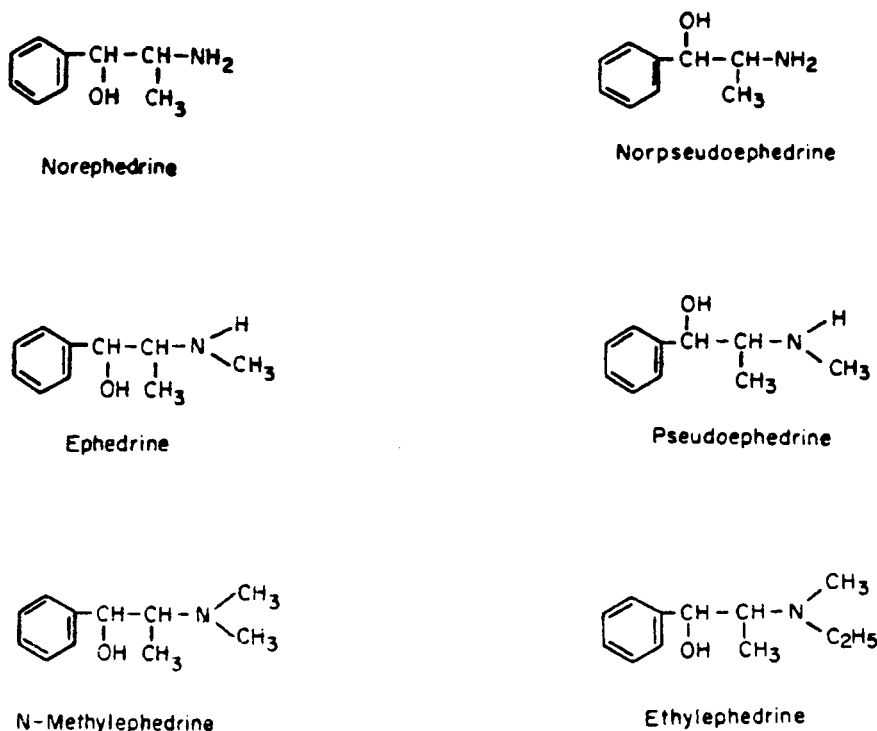


Fig. 1. Structures of ephedrines.

#### Standard solutions and calibration standards

Stock solutions of EPH, PEPH, NEPH, NPEPH, MEPH, ETEPH and the I.S. were prepared in the mobile phase described below at a concentration of 1000  $\mu\text{g/ml}$ . These stock solutions were then diluted further to yield appropriate working solutions for the preparation of the calibration standards. The solutions were sealed and refrigerated at 4°C until used.

#### Preparation of mobile phase

The mobile phase was 200 mM phosphate buffer with TEA added to a final concentration of 150 mM. The pH was adjusted to 5.5. Before analysis, this mobile phase was filtered through a 0.22- $\mu\text{m}$  filter and pumped through the column for 30 min. At the end of each chromatographic session, the column was washed for 15 min with deionized water and then with methanol.

#### Analytical procedure

To 5 ml of urine in a 15-ml glass tube were added

25  $\mu\text{l}$  of I.S. solution (1000  $\mu\text{g/ml}$ ), 100  $\mu\text{l}$  of 10 M NaOH and 2 ml of diethyl ether, then the urine was saturated with 3 g of sodium sulphate and shaken for 20 min. The tubes were centrifuged at 1200 g for 5 min and the organic layer was removed and evaporated to dryness. The residue was dissolved in 100  $\mu\text{l}$  of the mobile phase and 20  $\mu\text{l}$  of the solution was injected into the liquid chromatograph.

#### Chromatographic conditions

The chromatographic system consisted of a Hewlett-Packard (Palo Alto, CA, USA) HP 1090 Series A liquid chromatograph equipped with an auto-sampler/autoinjector and an HP 1040 A diode-array UV detector. Chromatography was performed at 40°C on a Hewlett-Packard reversed-phase analytical column (LiChrospher 60 RP Select B, 5  $\mu\text{m}$ ) (125 mm  $\times$  4 mm I.D.). The mobile phase was 200 mM phosphate buffer–150 mM TEA (pH 5.5) at a flow-rate of 1.3 ml/min. The injection volume was 20  $\mu\text{l}$  and the column effluent was monitored at 215 nm (band width 4 nm), where the ephedrine exhibit

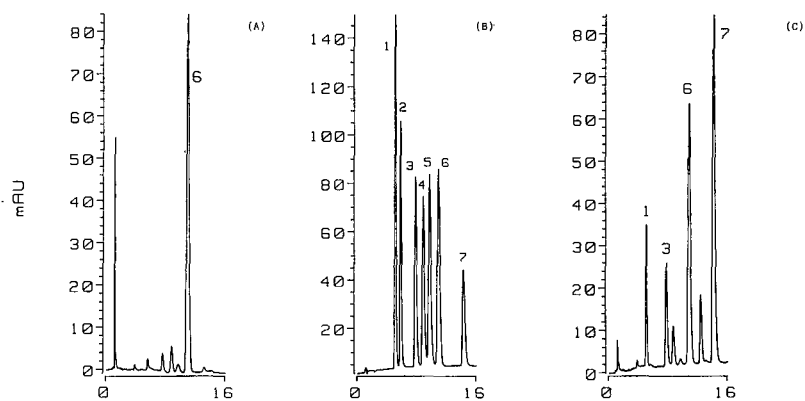


Fig. 2. Chromatograms obtained after analysis of (A) blank urine to which internal standard at a concentration of 5  $\mu\text{g}/\text{ml}$  (peak 6) was added; (B) urine standard spiked with (1) NEPH, (2) NPEPH, (3) EPH, (4) PEPH, (5) MEPH, (7) ETEPH and (6) I.S., each at a concentration of 5  $\mu\text{g}/\text{ml}$ ; (C) urine sample from an athlete who had taken ETEPH, where levels close to 10  $\mu\text{g}/\text{ml}$  for ETEPH and 1  $\mu\text{g}/\text{ml}$  for its metabolites (NEPH and EPH) were found.

maximum absorption. For data evaluation and HP 79994 A Chemstation was used, which consisted of an HP 900 Series 300 computer, a 10 Mbyte Winchester disk drive and a Thinkjet printer.

## RESULTS

Representative chromatograms for urine analyses are shown in Fig. 2. The peaks of interest were well separated from potential interferences. Preliminary experiments indicated that the separation depends significantly on the column used. The best results were obtained when a Select B column was used.

The composition of the mobile phase was selected in such a way that all the ephedrines were resolved in the shortest analysis time possible. As it is

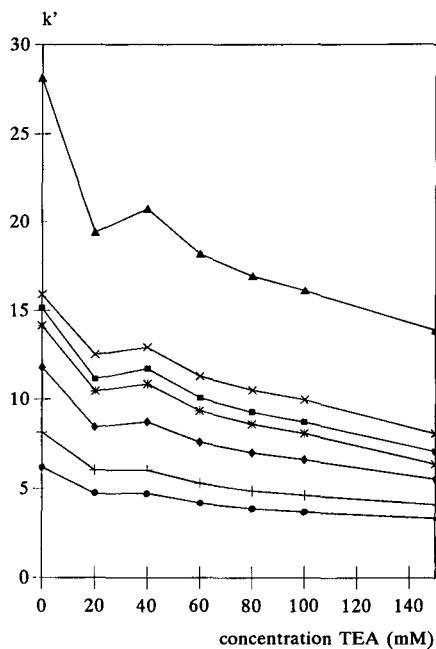


Fig. 3. Effect of the concentration of TEA in the column on  $k'$  values of ephedrines. Mobile phase, 200 mM phosphate (pH 4); column, LiChrospher 60 RP Select B, 5  $\mu\text{m}$  (125 mm  $\times$  4 mm I.D.). ● = NEPH; + = NPEPH; \* = PEPH; ■ = MEPH; x = I.S.; ◆ = EPH; ▲ = ETEPH.

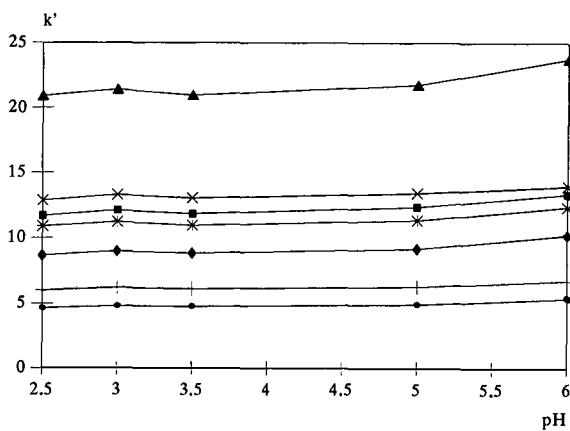


Fig. 4. Effect of pH on  $k'$  values. Concentration of TEA in the mobile phase, 150 mM; other conditions and compounds as in Fig. 3.

TABLE I  
BETWEEN-DAY ACCURACY AND REPRODUCIBILITY OF THE DETERMINATION OF EPHEDRINES IN HUMAN URINE OVER A PERIOD OF 2 WEEKS ( $n = 6$ )

Concentration added ( $\mu\text{g/ml}$ )	NEPH		NPEPH	
	Mean $\pm$ S.D. ( $\mu\text{g/ml}$ )	R.S.D. (%)	Mean $\pm$ S.D. ( $\mu\text{g/ml}$ )	R.S.D. (%)
2	1.98 $\pm$ 0.07	3.5	2.05 $\pm$ 0.03	1.3
8	8.04 $\pm$ 0.05	5.3	8.22 $\pm$ 0.06	0.7
24	25.93 $\pm$ 0.26	0.9	24.34 $\pm$ 0.28	1.1
	EPH		PEPH	
	Mean $\pm$ S.D. ( $\mu\text{g/ml}$ )	R.S.D. (%)	Mean $\pm$ S.D. ( $\mu\text{g/ml}$ )	R.S.D. (%)
2	1.96 $\pm$ 0.09	2.2	1.92 $\pm$ 0.02	1.0
8	8.27 $\pm$ 0.04	0.4	8.07 $\pm$ 0.06	0.7
24	26.00 $\pm$ 1.17	4.5	25.59 $\pm$ 0.23	0.9
	MEPH		ETEPH	
	Mean $\pm$ S.D. ( $\mu\text{g/ml}$ )	R.S.D. (%)	Mean $\pm$ S.D. ( $\mu\text{g/ml}$ )	R.S.D. (%)
2	1.97 $\pm$ 0.05	2.69	1.87 $\pm$ 0.12	3.1
8	7.95 $\pm$ 0.04	0.56	7.23 $\pm$ 0.21	4.4
24	22.47 $\pm$ 0.28	1.26	25.14 $\pm$ 1.49	6.4

shown in Fig. 1, ephedrine has a hydroxyl group on the  $\beta$ -carbon and hence they can interact with free silanol groups. With TEA in the mobile phase these interactions decrease because such silanol groups are masked [9]. When the concentration of TEA in the mobile phase is increased, the  $k'$  values decreased (Fig. 3).

The pH of the mobile phase also influences the determination of the six ephedrine (Fig. 4). The  $k'$  values increased with increase in the pH of the mobile phase, but a better resolution was achieved, especially for the pseudoephedrine-methylephedrine pair, where resolution was complete at pH 5.5 ( $R_s = 1.25$ ).

The precision and accuracy were measured using urine samples spiked at concentrations of 2, 8 and 24  $\mu\text{g/ml}$ . The samples were extracted and subjected to HPLC. Each concentration was calculated on the basis of the peak-height ratio with respect to the I.S. The results are given in Table I. The linearity was

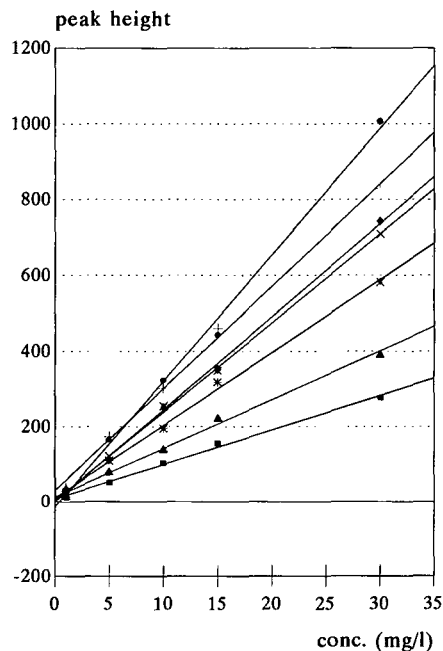


Fig. 5. Linear calibration graphs for the ephedrines specified in Fig. 3.

evaluated over the range of concentrations 1–30  $\mu\text{g/ml}$  using duplicate samples spiked at levels of 1, 5, 10, 15 and 30  $\mu\text{g/ml}$ . The calibration graphs obtained and the equations of the mean plots are shown in Fig. 5 and Table II, respectively.

The limit of detection was defined as the lowest concentration of each ephedrine resulting in a signal-to-noise ratio of 3. For NEPH, NPEPH and EPH the limit of detection was 0.2  $\mu\text{g/ml}$  and for

TABLE II  
EQUATIONS OF LINEAR CALIBRATION GRAPHS

Compound	Equation <sup>a</sup>	$r^2$
NEPH	$y = 33.38x - 13.63$	0.9978
NPEPH	$y = 27.02x + 30.64$	0.9983
EPH	$y = 24.58x - 0.92$	0.9991
PEPH	$y = 19.27x + 10.82$	0.9987
MEPH	$y = 9.12x + 8.78$	0.9975
I.S.	$y = 23.55x + 3.66$	0.9993
ETEPH	$y = 12.93x + 13.08$	0.9971

<sup>a</sup>  $y$  = Peak height (arbitrary units);  $x$  = concentration (mg/l)

PEPH, MEPH and ETEPH it was 0.5  $\mu\text{g}/\text{ml}$ . The limit of detection in urine is dependent on the amount of interferences present, but in all instances it was less than the stated limits.

Other pharmacological substances examined in order to establish possible interferences were amfepramone, amphetamine, caffeine, chlorphentermine, cocaine, codeine, cropropamide, crotethamide, dimethylamphetamine, etamivan, fencamfamine, heptaminol, leptazol, lidocaine, methoxamine, methylamphetamine, methylphenidate, nicotine, niketamine, pethidine, phendimetrazine, phenmetrazine, pipradol, procaine, prolintane and strychnine. None of these interfered with the determination of the ephedrines.

#### CONCLUSION

The elution and separation of ephedrines were clearly affected by the column used, the concentration of TEA and the pH of the mobile phase. As the use of a modifier was not necessary, endogenous compounds were eluted at very long times, resulting in very clear chromatograms where no interferences

from such endogenous compounds were observed. This method has been applied since January 1992 to urine samples taken from athletes. Over this period, we have analysed more than 20 physiological samples with different levels of ephedrines.

#### REFERENCES

- 1 I. W. Wainer and A. L. Marcotte, in I. W. Wainer and D. E. Drayer (Editors), *Drug Stereochemistry, Analytical Methods and Pharmacology*, Marcel Dekker, New York, 1988, pp. 31–41.
- 2 *List of Doping Classes and Methods*, International Olympic Committee, Lausanne, 1991.
- 3 J. E. F. Reynolds (Editor), *Martindale. The Extra Pharmacopoeia*, Pharmaceutical Press, London, 28th ed., 1982.
- 4 M. Donike, presented at the 9th Workshop on Dope Analysis, Cologne, March 17–22, 1991.
- 5 M. Donike and J. Derenbach, *Fresenius' Z. Anal. Chem.*, 279 (1976) 128.
- 6 I. L. Honigberg, J. T. Stewart, and A. P. Smith, *J. Pharm. Sci.*, 63 (1974) 766.
- 7 A. Yacobi, Z. M. Look and C. M. Lai, *J. Pharm. Sci.*, 67 (1978) 1668.
- 8 C. M. Lai, R. G. Stoll, Z. M. Look and A. Yacobi, *J. Pharm. Sci.*, 68 (1979) 1243.
- 9 Z. Varga-Puchony and Gy. Vigh, *J. Chromatogr.*, 257 (1983) 380.



# Porous graphitized carbon and octadecylsilica columns in the separation of some monoamine oxidase inhibitory drugs

Esther Forgács, Klára Valkó and Tibor Cserhádi

*Central Research Institute for Chemistry, Hungarian Academy of Sciences, P.O. Box 17, H-1525 Budapest (Hungary)*

Kálmán Magyar

*Department of Pharmacology, Semmelweis University of Medicine, Budapest (Hungary)*

---

## ABSTRACT

The retentions of seventeen monoamine oxidase inhibitory drugs (propargylamine derivatives) were determined on a porous graphitized carbon (PGC) column using unbuffered methanol–water and acetonitrile–water eluents and on an octadecylsilica column with methanol–water eluents using constant and varying buffer concentrations. Principal component analysis showed that the retention characteristics of the PGC and octadecylsilica columns differ considerably. A marked deviation between the selectivities of methanol and acetonitrile organic modifiers was observed on PGC. The buffer concentration has a significant impact on the retention of drugs on the octadecylsilica column. The type of substitution (heterocyclic, condensed ring, substituted benzene) accounts for the retention differences irrespective of the type of column, eluent and buffer concentration.

---

## INTRODUCTION

Porous graphitic carbon (PGC) columns have been developed in the last decade [1,2]. The development of this highly pH-stable type of column was motivated by the fact that the application of silica or silica-based supports in high-performance liquid chromatography (HPLC) is limited by the low stability of silica at high pH values [3] and by the undesirable electrostatic interactions between the polar substructures of solutes and the free silanol groups not covered by the hydrophobic ligand [4]. PGC columns have been used for the separation of diastereoisomers [5], geometric isomers [6] and various alkaline compounds [7] such as tioconazole deriv-

atives. The effect of various physico-chemical parameters of solutes on their retention behaviour on PGC columns has been studied in detail and the importance of electronic interactions between solutes and the stationary phase has been emphasized [8].

Reversed-phase HPLC (RP-HPLC) has been extensively used to determine the hydrophobicity (lipophilicity) of various compounds [9,10]. To increase the accuracy of the lipophilicity determination, linear correlations were calculated between the  $\log k'$  value and the concentration of organic modifier in the eluent. The intercept of the correlation was considered as a good estimate of lipophilicity [11] and the slope was considered to be related to the specific hydrophobic surface area [12]. The good correlation between the intercept and slope values indicates the structural homogeneity of solutes [13]. When the compound contains one or more dissociable polar substituents, the pH values of the

---

*Correspondence to:* Esther Forgács, Central Research Institute for Chemistry, Hungarian Academy of Sciences, P.O. Box 17, H-1525 Budapest, Hungary.

eluent [14,15] and the ionic strength [16] modify the retention. The buffers used to control the pH value of the eluent can modify the chromatographic system in two different manners: they change the pH value and at the same time they increase the ionic strength of the eluent. As each buffer contains more or less dissociable salts the two effects cannot be separated experimentally in common chromatographic practice. To our knowledge, their relative impact on the retention behaviour of polar solutes has never been studied in detail.

Various substituted propargylamine derivatives are promising therapeutic compounds as monoamine oxidase inhibitory drugs [17,18], but their exact mode of action has not been elucidated in detail [19].

Principal component analysis (PCA) [20] have frequently been used to extract maximum information from retention data matrices of considerable dimensions [21,22]. The advantages of the application of PCA in chromatography is that it allows a reduction in the number of variables whilst maintaining most of information content. PCA is suitable not only for calculations of two–two variables relationships, but also for the simultaneous study of all-variables relationships.

The objectives of our investigation were to determine the retentions of seventeen monoamine oxidase inhibitory drugs on PGC and on octadecylsilica columns with various eluent systems, to evaluate the retention data with multivariate mathematical statistical methods and to find the relationship between the retention characteristics of the columns.

## EXPERIMENTAL

The PGC column (Shandon Hypercarb,  $100 \times 4.7$  mm I.D., particle diameter  $7 \mu\text{m}$ ) was purchased from Shandon Scientific (Runcorn, UK). The HPLC system consisted of a Liqueopump Model 312 pump (LaborMIM, Budapest, Hungary), a Cecil CE-212 variable-wavelength UV detector (Cecil Instruments, Cambridge, UK), a Valco (Houston, TX, USA) injector with a  $20\text{-}\mu\text{l}$  sample loop and a Waters Model 740 integrator (Waters–Millipore, Milford, MA, USA). The flow-rate was  $1\text{ml}/\text{min}$  and the detection wavelength was  $254\text{ nm}$ . Methanol–water and acetonitrile–water mixtures were used as eluents with methanol and acetonitrile con-

centrations ranging from 95 to 77 and from 97 to 64% (v/v), respectively. Buffers were not used as it was previously established that the inert surface of PGC makes the application of buffers unnecessary. The measurements were also carried out on an octadecylsilica column (LiChrospher  $\text{C}_{18}$ ,  $150 \times 4$  mm I.D.; ChromLab, Budapest, Hungary), using methanol– $10\text{ mM}$   $\text{K}_2\text{HPO}_4$  mixtures containing 60–90% (v/v) of methanol.

To study the effect of buffer concentrations, the same eluents were applied, always containing a  $10\text{ mM}$   $\text{K}_2\text{HPO}_4$  end concentration. The application of constant and changing buffer concentrations was motivated by the supposition that the buffer concentration may also influence the retention of the polar drugs. The other chromatographic conditions were as before.

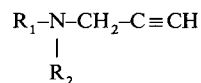
The structures of the monoamine oxidase inhibitory drugs are shown in Table I. The drugs were dissolved in methanol or acetonitrile at a concentration of  $0.05\text{ mg}/\text{ml}$ . The retention time of each compound was determined in each eluent with three consecutive determinations. As the correlation between the  $\log k'$  value and the organic phase concentration is generally linear in HPLC, we also applied linear equations to describe the dependence of  $\log k'$  on the organic mobile phase concentration:

$$\log k' = \log k'_0 + bC \quad (1)$$

where  $k'$  = capacity factor,  $k'_0$  = capacity factor extrapolated to zero organic modifier content in the mobile phase (intercept, related to molecular lipophilicity),  $b$  change in  $\log k'$  value caused by unit change (1% v/v) of organic mobile phase concentration (slope, related to the specific hydrophobic surface areas) and  $C$  = organic mobile phase concentration (% v/v).

To find the similarities and dissimilarities between the retention behaviour of columns and drugs, PCA was applied. The parameters of eqn. 1 were the eight variables (slope and intercept values for PGC column with methanol–water and acetonitrile–water eluents, slope and intercept values for an octadecylsilica column with constant and changing buffer concentration) and the seventeen drugs were the observations. For the easier visualization of the results the two dimensional non-linear map [23] of PC loadings and PC variables was also calculated.

TABLE I  
CHEMICAL STRUCTURE OF MONOAMINE OXIDASE INHIBITORS



No. of compound	R <sub>1</sub>	R <sub>2</sub>	No. of compound	R <sub>1</sub>	R <sub>2</sub>
1 (+)		CH <sub>3</sub>	10		CH <sub>3</sub>
2 (-)		CH <sub>3</sub>			
3		CH <sub>3</sub>	11		H
4		H	12		CH <sub>3</sub>
5		CH <sub>3</sub>	13		CH <sub>3</sub>
6		CH <sub>3</sub>	14		CH <sub>3</sub>
7		CH <sub>3</sub>	15		CH <sub>3</sub>
8		CH <sub>3</sub>	16		CH <sub>3</sub>
9		C <sub>4</sub> H <sub>7</sub>	17		CH <sub>3</sub>

## RESULTS AND DISCUSSION

Each drug showed narrow and symmetrical peaks in each eluent system (Figs. 1 and 2), that is, the carbon column can be successfully used for the

separation of this class of monoamine oxidase inhibitory drugs. The parameters of eqn. 1 are compiled in Tables II–V. The relationship between the logarithm of the capacity factor and the concentration of organic phase in the eluent was significantly



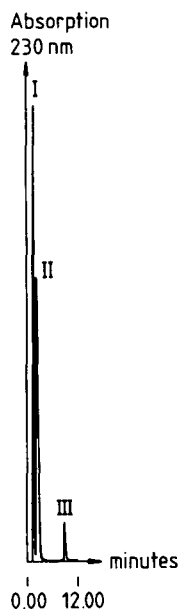


Fig. 1. Separation of monoamine oxidase drugs on the porous graphitized carbon column. Eluent, methanol–water (82:18, v/v); flow-rate, 1 ml/min; detection, 230 nm. I = dead volume; II and III refer to drugs 5 and 17 in Table I, respectively.

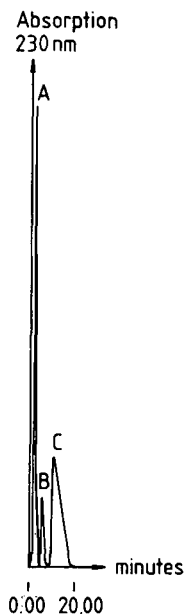


Fig. 2. Separation of monoamine oxidase drugs on the porous graphitized carbon column. Eluent, acetonitrile–water (92:8, v/v); flow-rate, 1 ml/min; detection, 230 nm. A = dead volume; B and C refer to drugs 8 and 12 in Table I, respectively.

linear in each instance that is, the retention of propargylamine derivatives decreases linearly with increasing concentration of the organic component in the eluent. This finding further indicates that the propargylamine derivatives follow the general rule also on the PGC column (Tables II and III); no anomalous retention behaviour was observed. The slope and intercept values differ from each other, which means that these drugs can be easily separated on the PGC column using either acetonitrile–water or methanol–water eluents. The result that the slope and intercept values of a solute are different in eluents containing methanol or acetonitrile proves the different selectivity of the organic modifiers.

The parameters compiled in Tables II–V make possible the calculation of retention time differences for each pair of propargylamine derivatives at each eluent composition:

$$t_1 - t_2 = t_0(10^{a_1+b_1C} - 10^{a_2+b_2C}) \quad (2)$$

where  $a$  and  $b$  are the intercept and slope values for compounds 1 and 2 at an organic phase concentration  $C$ .

TABLE II

PARAMETERS OF THE LINEAR CORRELATIONS BETWEEN THE LOG  $k'$  VALUE OF MONOAMINE OXIDASE INHIBITORY DRUGS AND THE METHANOL CONCENTRATION ( $C\%$ , v/v) IN THE ELUENT

Porous graphitized carbon column. Numbers refer to drugs in Table I.  $\text{Log } k' = k'_0 + bC$

No. of drug	Log $k'_0$	$-b \times 10^{-2}$	$s_b \times 10^{-3}$	$r$
1	1.01	4.47	4.13	0.9721
2	1.01	4.47	4.13	0.9721
3	1.06	6.69	3.89	0.9902
4	1.87	52.20	9.81	0.9817
5	1.04	5.99	3.47	0.9875
6	0.94	1.73	3.94	0.9425
7	0.99	2.56	4.56	0.9986
8	1.06	5.40	3.92	0.9848
9	0.97	2.03	2.08	0.9621
10	1.00	4.03	5.40	0.9351
11	1.39	26.96	37.31	0.9311
12	0.97	1.48	1.26	0.9773
13	0.97	1.74	1.69	0.9768
14	1.04	2.44	1.19	0.9909
15	1.00	2.59	1.50	0.9899
16	1.10	1.07	16.35	0.9181
17	1.14	3.73	7.27	0.9329

TABLE III

PARAMETERS OF THE LINEAR CORRELATIONS BETWEEN THE LOG  $k'$  VALUE OF MONOAMINE OXIDASE INHIBITORY DRUGS AND THE ACETONITRILE CONCENTRATION (C%, v/v) IN THE ELUENT

Porous graphitized carbon column. Number refer to drugs in Table I.  $\text{Log } k' = \text{log } k'_0 + bC$

No. of drug	$\text{Log } k'_0$	$-b \times 10^{-2}$	$s_b \times 10^{-3}$	$r$
1	0.94	4.28	9.90	0.9371
2	0.94	4.28	9.90	0.9371
3	1.14	13.19	15.73	0.9361
4	1.10	10.51	3.24	0.9955
5	1.27	17.43	15.32	0.9569
6	0.97	2.83	2.57	0.9707
7	1.07	6.98	3.15	0.9922
8	1.06	5.65	4.06	0.9823
9	1.03	4.73	3.39	0.9849
10	0.98	5.71	8.07	0.9138
11	0.99	2.24	1.46	0.9807
12	1.03	3.45	3.12	0.9651
13	1.00	4.07	5.21	0.9548
14	1.02	4.50	1.63	0.9927
15	1.01	3.84	4.89	0.9265
16	1.06	4.86	5.24	0.9671
17	1.11	6.26	3.47	0.9913

The slope and intercept values differ considerably in eluents with constant and changing buffer concentration (Tables IV and V). This indicates that with polar compounds the lipophilicity value determined in a buffered eluent may depend on the concentration of the buffer, and therefore its application in quantitative structure–activity relationship studies is questionable. We strongly advocate the application of various buffer and organic modifier concentrations that are not intercorrelated and the extrapolation of the  $\text{log } k'_0$  values to zero organic modifier and zero buffer concentrations.

The parameters of the PCA describing the relationship between the retention characteristics of drugs on various columns are compiled in Table VI. Three principal components explained most (95.09%) of the total variance. This means that the eight variables can be substituted by three background (abstract) variables without a substantial loss of information. Unfortunately, PCA does not define these three background variables, it only indicates their mathematical possibility.

Each chromatographic parameter determined on

TABLE IV

PARAMETERS OF THE LINEAR CORRELATIONS BETWEEN THE LOG  $k'$  VALUE OF MONOAMINE OXIDASE INHIBITORY DRUGS AND THE METHANOL CONCENTRATION (C%, v/v) IN THE ELUENT

Changing buffer concentration. Octadecylsilica column. Numbers refer to drugs in Table I.  $\text{Log } k' = \text{log } k'_0 + bC$

No. of drug	$\text{Log } k'_0$	$-b \times 10^{-2}$	$s_b \times 10^{-3}$	$r$
1	3.13	3.89	1.34	0.9981
2	3.13	3.89	0.96	0.9991
3	3.32	4.04	0.65	0.9996
4	2.18	3.28	1.72	0.9958
5	2.68	3.61	2.53	0.9926
6	3.91	4.33	1.72	0.9975
7	3.88	4.28	1.19	0.9988
8	3.76	4.39	1.72	0.9984
9	5.31	5.50	1.12	0.9939
10	3.00	3.76	1.18	0.9984
11	2.99	3.85	0.81	0.9929
12	4.34	5.05	1.02	0.9959
13	3.43	3.86	1.49	0.9977
14	2.17	3.13	1.71	0.9974
15	3.62	4.06	0.46	0.9998
16	2.91	3.53	1.59	0.9969
17	3.23	3.67	0.99	0.9989

TABLE V

PARAMETERS OF THE LINEAR CORRELATIONS BETWEEN THE LOG  $k'$  VALUE OF MONOAMINE OXIDASE INHIBITORY DRUGS AND THE METHANOL CONCENTRATION (C%, v/v) IN THE ELUENT

Constant (10 mM) buffer concentration. Octadecylsilica column. Numbers refer to drugs in Table I.  $\text{Log } k' = \text{log } k'_0 + bC$

No. of drug	$\text{Log } k'_0$	$-b \times 10^{-2}$	$s_b \times 10^{-3}$	$r$
1	-1.86	2.95	2.31	0.9939
2	-1.86	2.95	2.31	0.9939
3	3.27	3.94	1.98	0.9962
4	1.99	2.95	2.41	0.9901
5	2.59	3.45	1.10	0.9984
6	3.90	4.36	5.12	0.9800
7	4.23	4.83	3.64	0.9915
8	3.64	4.18	1.83	0.9971
9	6.54	7.03	4.68	0.9977
10	2.82	3.46	1.31	0.9978
11	2.94	3.71	2.01	0.9955
12	4.23	4.89	3.12	0.9938
13	4.12	4.76	4.88	0.9895
14	1.88	2.70	1.83	0.9931
15	4.18	4.79	6.68	0.9810
16	3.75	4.60	6.92	0.9781
17	3.96	4.60	6.63	0.9798

TABLE VI

RELATIONSHIP BETWEEN THE RETENTION PARAMETERS OF SOME MONOAMINE OXIDASE INHIBITORY DRUGS

Results of principal component analysis.

No. of PC component	Eigenvalues	Variance explained (%)	Total variance explained (%)
1	4.57	57.07	57.05
2	1.72	21.45	78.52
3	1.33	16.57	95.09
4	0.31	3.85	98.94

Parameter <sup>a</sup>	Principal component loadings		
	1	2	3
A, intercept (MET)	-0.70	0.00	0.71
A, slope (MET)	-0.66	-0.01	0.74
A, intercept (ACN)	-0.34	0.92	-0.08
A, slope (ACN)	-0.45	0.85	-0.13
B, intercept (VAR)	0.95	0.16	0.18
B, slope (VAR)	0.88	0.16	0.28
B, intercept (CONST)	0.92	0.20	0.25
B, slope (CONST)	0.88	0.25	0.29

<sup>a</sup> A = Porous graphitized carbon column; MET = methanol-water eluents; ACN = acetonitrile-water eluents; B = octadecylsilica column; VAR = varying buffer concentration; CONST = constant buffer concentration.

the octadecylsilica column has a high loading in the first principal component, that is, the first PC can be related to the reversed-phase separation mechanism irrespective of constant or varying buffer concentrations. The retention parameters of the PGC column are distributed according to the type of organic modifier; the acetonitrile-water and methanol-water eluents have high loadings in the second and third PCs, respectively. This indicates that methanol and acetonitrile have different selectivities and the type of organic modifier has a considerable effect on the separation of the monoamine oxidase inhibitory drugs.

The conclusions drawn from the two dimensional non-linear map of PC loadings (Fig. 3) entirely support our previous conclusions. The retention characteristics of PGC (cluster A) and octadecylsilica (cluster B) columns form two widely separated clusters, which means that the retention characteristics of the columns are markedly different. The four

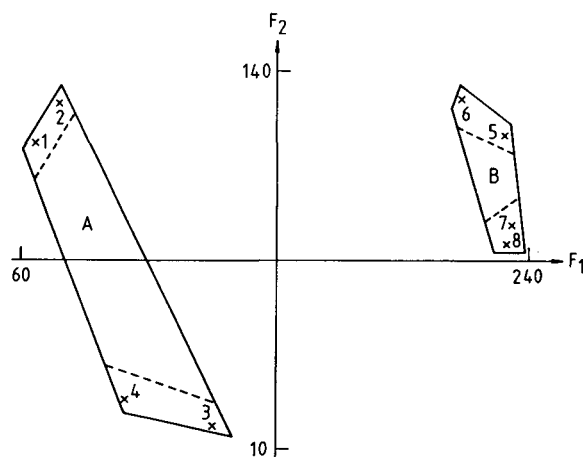


Fig. 3. Two dimensional non-linear map of principal component loadings. No. of iterations, 36; maximum error,  $4.58 \cdot 10^{-3}$ ; 1 and 2 = intercept and slope values, PGC column, methanol organic modifier; 3 and 4 = intercept and slope values, PGC column, acetonitrile organic modifier; 5 and 6 = intercept and slope values, octadecylsilica column, varying buffer concentration; 7 and 8 = intercept and slope values, octadecylsilica column, constant buffer concentration.

eluent systems are also separated, but, the differences between the organic modifiers are higher than the differences between the effect of constant or varying buffer concentrations.

The monoamine oxidase inhibitory drugs form distinct clusters according to the type of substituents (Fig. 4). This result suggests that heterocyclic, condensed ring or substituted benzene substructures account for the retention behaviour irre-

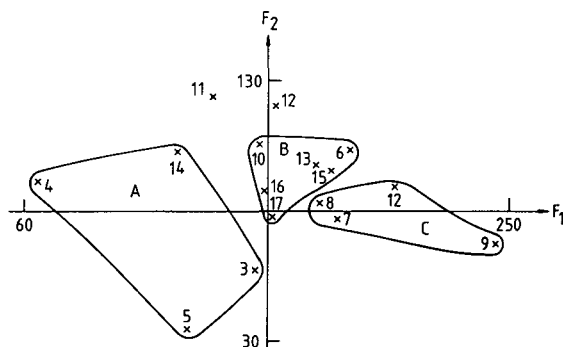


Fig. 4. Two-dimensional non-linear map of principal component variables. No. of iterations, 130; maximum error,  $1.55 \cdot 10^{-2}$ ; A = heterocyclic substituents; B = substituents with condensed ring; C = substituents with benzene derivatives.

spective of the type of column and eluent composition. The position of compounds 11 and 12 indicates that the increased polarity and the number of chlorine atoms also influence the retention.

#### ACKNOWLEDGEMENT

This work was supported by grant OTKA 2670 of the Hungarian Academy of Sciences.

#### REFERENCES

- 1 M. T. Gilbert, J. H. Knox and B. Kaur, *Chromatographia*, 16 (1982) 138.
- 2 J. H. Knox, B. Kaur and G. R. Millward, *J. Chromatogr.*, 352 (1986) 3.
- 3 A. Berthod, *J. Chromatogr.*, 549 (1991) 1.
- 4 H. Tayar, H. Waterbend and B. Testa, *J. Chromatogr.*, 305 (1985) 320.
- 5 B. Kaur, *LC · GC*, 3 (1990) 41.
- 6 D. Berek and J. Novak, *Chromatographia*, 30 (1990) 582.
- 7 J. C. Berridge, *J. Chromatogr.*, 449 (1988) 317.
- 8 R. Kaliszán and K. Osmialowski, *J. Chromatogr.*, 333 (1990) 499.
- 9 W. J. Haggerty and E. A. Murrill, *Res. Dev.*, 25 (1974) 30.
- 10 J. M. McCall, *J. Med. Chem.*, 18 (1975) 549.
- 11 K. Valkó, S. Olajos and T. Cserhádi, *J. Chromatogr.*, 499 (1990) 361.
- 12 C. Horvath, W. Melander and I. Molnar, *J. Chromatogr.*, 125 (1976) 129.
- 13 K. Valkó, *J. Liq. Chromatogr.*, 7 (1984) 1405.
- 14 B. Rittich, M. Polster and O. Kralik, *J. Chromatogr.*, 197 (1980) 43.
- 15 G. Vigh, J. Varga-Puhony, J. Hlavay and E. Pap, *J. Chromatogr.*, 236 (1982) 51.
- 16 E. Pap and G. Vigh, *J. Chromatogr.*, 259 (183) 49.
- 17 J. Knoll, E. S. Vizi and G. Somogyi, *Arzneim.-Forsch.*, 18 (1968) 109.
- 18 J. Knoll and K. Magyar, *Adv. Biochem. Psychopharmacol.*, 5 (1972) 393.
- 19 J. Knoll, Z. Ecsery, K. Magyar and É. Satory, *Biochem. Pharmacol.*, 27 (1978) 1739.
- 20 K. V. Mardia, J. T. Kent, J. M. Bibby, *Multivariate Analysis*, Academic Press, London and New York, 1979.
- 21 T. Cserhádi and Z. Illés, *Chromatographia*, 31 (1991) 152.
- 22 T. Cserhádi, *J. Chromatogr.*, 543 (1991) 425.
- 23 J. W. Sammon, Jr., *IEEE Trans. Comput.*, C18 (1969) 401.



# Liquid chromatography–mass spectrometry for the determination of medetomidine and other anaesthetics in plasma

Hideko Kanazawa, Yoshiko Nagata and Yoshikazu Matsushima

*Kyoritsu College of Pharmacy, Shibakoen 1-5-30, Minato-ku, Tokyo 105 (Japan)*

Nobuharu Takai and Hidefumi Uchiyama

*Institute of Industrial Science, University of Tokyo, Roppongi 7-22-1, Minato-ku, Tokyo 106 (Japan)*

Ryohei Nishimura and Akira Takeuchi

*Faculty of Agriculture, University of Tokyo, Yayoi 1-1-1, Bunkyo-ku, Tokyo 113 (Japan)*

---

## ABSTRACT

A liquid chromatographic–atmospheric pressure chemical ionization mass spectrometric method is presented for the simultaneous determination of medetomidine and other anaesthetic drugs in solutions and dog plasma. The drugs examined were flumazenil, butorphanol, atropine, ketamine, xylazine, medetomidine, atipamezole and midazolam. The separation was carried out on a reversed-phase column using methanol–0.1 M ammonium acetate (3:2) as eluent.

---

## INTRODUCTION

Medetomidine, 4-[1-(2,3-dimethylphenyl)ethyl]-1*H*-imidazole hydrochloride, is used as an analgesic sedative for animals. It is a full agonist at both pre- and postsynaptic  $\alpha_2$ -adrenoreceptors. Human use for premedication is under investigation. Medetomidine has no significant absorption at wavelengths longer than 220 nm and lacks native fluorescence, which make it difficult to develop a chromatographic assay method for the drug and its metabolites. Vuorilehto *et al.* [1] reported its gas chromatographic–mass spectrometric assay in serum. Although the method is very sensitive, the need for

derivatization with pentafluorobenzoyl chloride makes it tedious.

Medetomidine and related sedatives and anaesthetics used in human and animals are shown in Fig. 1. Atipamezole, 4-(2-ethyl-2,3-dihydro-1*H*-inden-2-yl)-1*H*-imidazole, is an  $\alpha_2$ -adrenoreceptor antagonist, while xylazine, 2-(2,6-dimethylphenylamino)-4*H*-5,6-dihydro-1,3-thiazine, is an agonist as well as medetomidine. Butorphanol tartrate, 17-(cyclobutylmethyl)morphinan-3,14-diol tartrate, is a narcotic agonist–antagonist analgesic, and is available for use in humans and animals. Ketamine, 2-(*o*-chlorophenyl)-2-(methylamino)cyclohexanone hydrochloride, is an anaesthetic. Midazolam, 8-chloro-6(*o*-fluorophenyl)-1-methyl-4*H*-imidazol-[1,5-*a*] [1,4]benzodiazepine, is a benzodiazepine agonist and flumazenil, ethyl 8-fluoro-5,6-dihydro-5-methyl-6-oxo-4*H*-imidazol[1,5-*a*] [1,4]benzodi-

---

*Correspondence to:* Y. Matsushima, Kyoritsu College of Pharmacy, Shibakoen 1-5-30, Minato-ku, Tokyo 105, Japan.

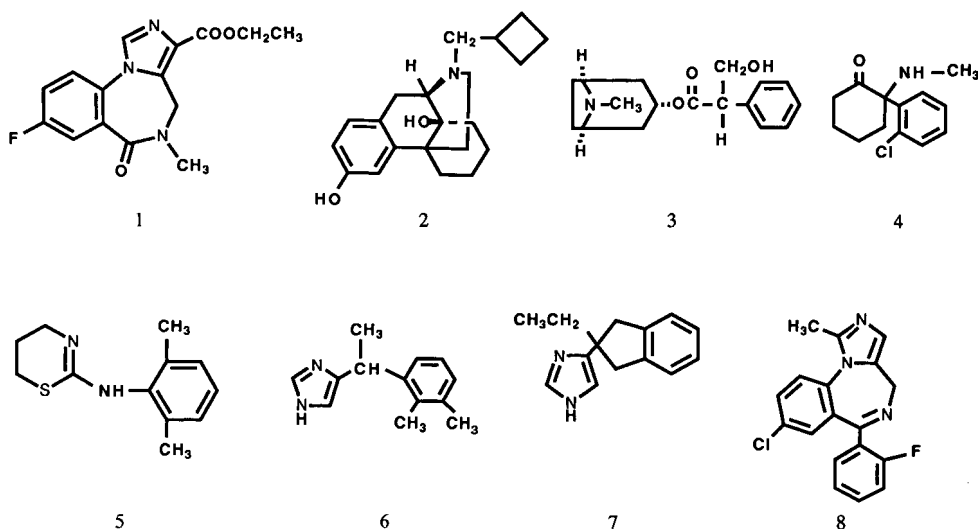


Fig. 1. Structures of the anaesthetic drugs studied. 1 = Flumazenil; 2 = butorphanol; 3 = atropine; 4 = ketamine; 5 = xylazine; 6 = medetomidine; 7 = atipamezole; 8 = midazolam.

azepine-3-carboxylate, a benzodiazepine antagonist. Atropine is a common anticholinergic drug.

These drugs have recently been used in combination with medetomidine or used for premedication for balanced anaesthesia and sedation in veterinary science. Assay methods by means of gas chromatography (GC) or high-performance liquid chromatography (HPLC) have been reported for xylazine [2], ketamine [3,4], midazolam [5], atipamezole [6] and butorphanol [7]. A suitable simultaneous method for the determination of the drugs in biological samples is required.

HPLC is one of the most widely used methods for the determination of drugs in biological samples. Among the various HPLC techniques, liquid chromatography–atmospheric pressure chemical ionization mass spectrometry (LC–APCI–MS) shows promise in various field [8]. This paper describes an LC–APCI–MS assay for the simultaneous determination of the drugs in solution and dog plasma.

## EXPERIMENTAL

### Instrumentation

The apparatus used was a Hitachi L-6200 HPLC instrument with a Rheodyne Model 7125 valve, connected to a Hitachi M1000 mass spectrometer–computer system through the APCI interface. The

nebulizer and vaporizer temperatures were 260 and 399°C, respectively. The chromatographic separation was carried out on a column of octadecylsilylsilica (Hitachi gel 3056, 150 mm × 4.6 mm I.D.) using methanol–0.1 M ammonium acetate (3:2) as the eluent at room temperature.

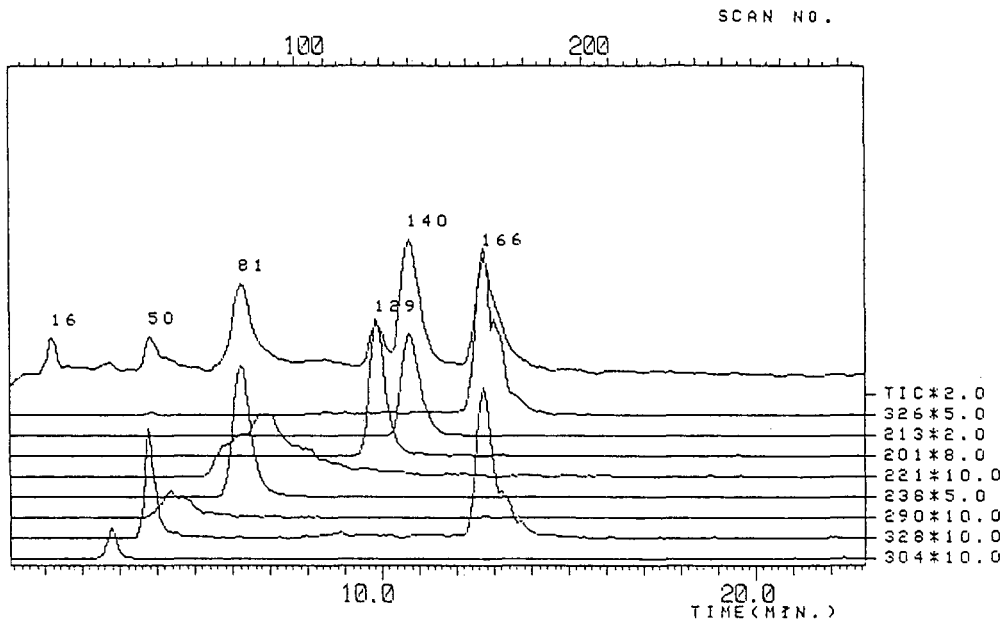
### Reagents

The drugs used were obtained from commercial sources as follows: medetomidine hydrochloride (Domitor; Famos Group, Turku, Finland); butorphanol tartrate (Stadol; Bristol–Myers Squibb, Tokyo, Japan); midazolam (Dormicum; Yamanouchi Pharmaceutical, Tokyo, Japan); xylazine hydrochloride (Celactal; Bayer, Tokyo, Japan); atipamezole hydrochloride (Antisedan; Famos Group); atropine sulphate (Tanabe, Osaka, Japan); ketamine hydrochloride (Ketalar; Sankyo, Tokyo, Japan); flumazenil (Hoffman–La Roche, Nutley, NJ, USA).

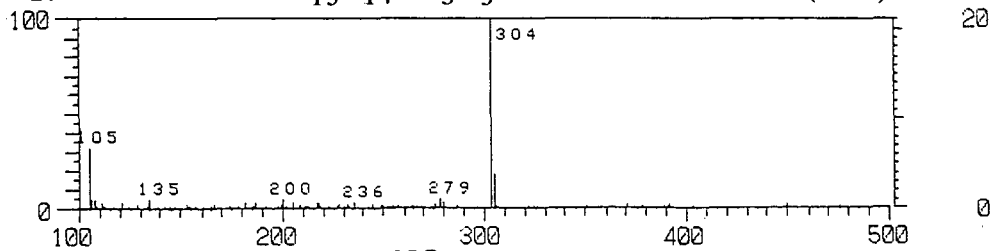
Water was distilled and passed through a Milli-Q purification system (Millipore, Bedford, MA, USA). All other chemicals were of analytical-reagent grade.

### Sample preparation

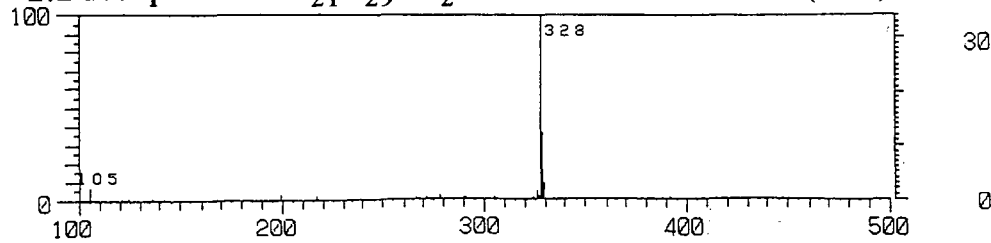
A standard solution was prepared so as to contain 0.1, 1.0, 0.5, 0.5, 2.0, 1.0, 5.0 and 0.5 mg/ml of



1. Flumazenil  $C_{15}H_{14}FN_3O_3$  M.W.303.3 TIME(MIN): 2.7



2. Butorphanol  $C_{21}H_{29}NO_2$  M.W.327.5 TIME(MIN): 3.8



3. Atropine  $C_{17}H_{23}NO_3$  M.W.289.3 TIME(MIN): 4.3

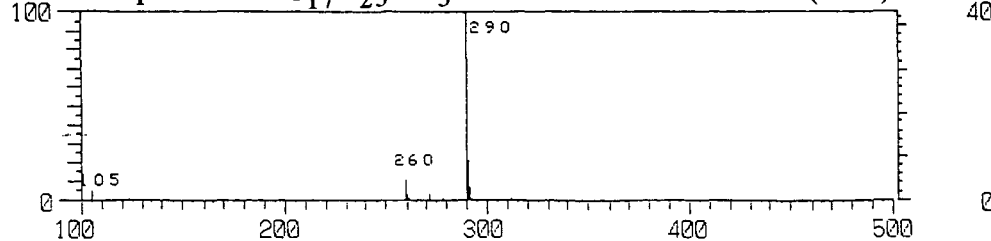


Fig. 2.

(Continued on p. 218)



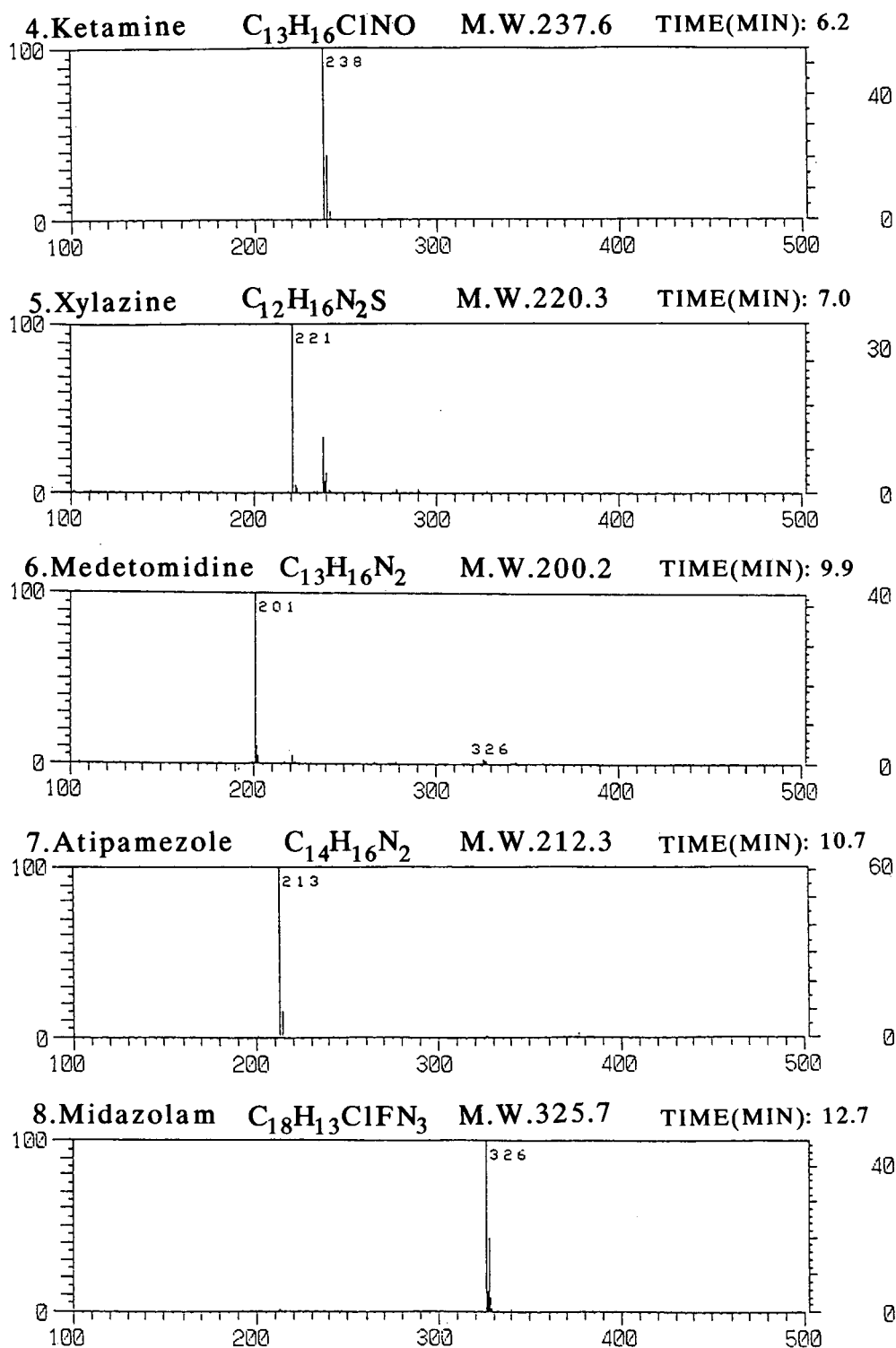


Fig. 2. Mass chromatograms of a mixture of the drugs and mass spectra scanned at the peak tops of the mass chromatograms. The HPLC conditions are described in the text. The mass spectrometer was scanned from  $m/z$  100 to 500 at 4 s per scan. M.W. = Molecular mass. Numbers at right-hand side axis of mass chromatogram indicate  $m/z$  multiplied by a factor. TIC = total ion chromatogram.

flumazenil, butorphanol, atropine, ketamine, xylazine, medetomidine, atipamezole and midazolam, respectively. A 20- $\mu$ l volume of the solution was injected into the HPLC system.

A 200- $\mu$ l volume of dog plasma spiked with 20  $\mu$ l of the standard solution was applied to a Sep-Pak C<sub>18</sub> cartridge pretreated with water, methanol and 0.1 M ammonium acetate. After washing the column with 0.1 M ammonium acetate, the sample was eluted with methanol–0.1 M ammonium acetate (3:1) and the eluate was evaporated to dryness under reduced pressure. The residue was dissolved in 200  $\mu$ l of the eluent and 20  $\mu$ l of the solution were injected into the HPLC system.

## RESULTS AND DISCUSSION

Mass chromatograms and mass spectra of a standard solution of the eight drugs obtained using the LC–APCI–MS system are shown in Fig. 2. The well resolved chromatograms were obtained with methanol–0.1 M ammonium acetate (3:2) as the eluent at a flow-rate of 1 ml/min in 15 min. Although the

peak shapes of **3** and **5** were poor, the mass spectra showed that they were well separated. In the LC–APCI–MS system, quasi-molecular ions  $[M + H]^+$  of these drugs were observed as base peaks.

Solutions containing 0–500 ng of the drugs were injected and the corresponding peak areas were integrated. The limits of the detection were 10–50 pg per injection (signal-to-noise ratio = 3). The calibration graphs were linear and reproducible. The relationship calculated between the peak area ( $y$ ) and the concentration of the drugs ( $x$ ) and the correlation coefficients ( $r$ ) were as follows: **1**,  $y = 2.59x + 0.36$  ( $r = 0.9999$ ); **2**,  $y = 1.84x - 0.11$  ( $r = 0.9995$ ); **3**,  $y = 1.38x + 0.26$  ( $r = 0.9999$ ); **4**,  $y = 2.21x + 0.29$  ( $r = 0.9995$ ); **5**,  $y = 2.09x + 0.54$  ( $r = 0.9999$ ); **6**,  $y = 3.17x + 0.86$  ( $r = 0.9999$ ); **7**,  $y = 1.65x - 0.43$  ( $r = 0.9998$ ); and **8**,  $y = 5.39x - 0.37$  ( $r = 0.9994$ ).

Mass chromatograms of an extract of dog plasma spiked with the drugs are shown in Fig. 3. The peaks were separated satisfactorily to allow the determination of each component. The recoveries of the drugs from plasma were 84.5, 73.1, 106.7, 84.0,

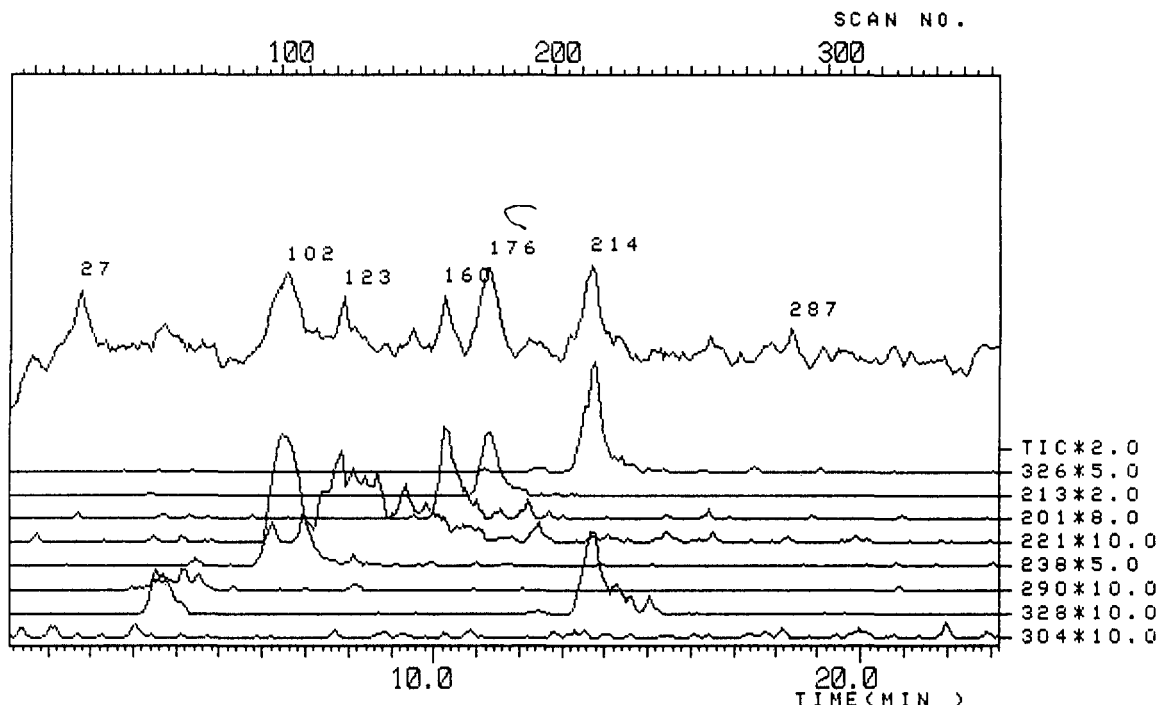


Fig. 3. Mass chromatograms of dog plasma spiked with the eight drugs. Numbers at right indicate  $m/z$  multiplied by a factor. TIC = total ion chromatogram.

101.9, 97.4, 95.4 and 96.1% ( $n = 3$ ) for **1**, **2**, **3**, **4**, **5**, **6**, **7** and **8**, respectively.

The method can be also used for the identification and determination of metabolites of medetomidine and the other drugs in plasma. Work on this aspect is in progress.

#### ACKNOWLEDGEMENT

This work was supported in part by the Science Research Promotion Fund of the Japan Private School Promotion Foundation.

#### REFERENCES

- 1 L. Vuorilehto, J. S. Salonen and M. Anttila, *J. Chromatogr.*, 497 (1989) 282.
- 2 M. Alvinerie and P. L. Toutain, *J. Chromatogr.*, 222 (1981) 308.
- 3 L. L. Needham and M. M. Kochhar, *J. Chromatogr.*, 114 (1975) 220.
- 4 R. M. Hanna, R. E. Borchard and S. L. Schmidt, *J. Vet. Pharmacol. Ther.*, 11 (1988) 84.
- 5 J. Vasiliades and T. H. Sahawneh, *J. Chromatogr.*, 225 (1981) 266.
- 6 S. Karhuvaara, A. Kallio, M. Scheinin, M. Anttila, J. S. Salonen and H. Scheinin, *Br. J. Clin. Pharmacol.*, 30 (1990) 97.
- 7 M. Pfeffer, R. D. Smyth, K. A. Pittman and P. A. Nardella, *J. Pharm. Sci.*, 69 (1980) 801.
- 8 E. C. Horning, D. I. Carroll, I. Dzidic, K. D. Haegele, M. G. Horning and R. N. Stillwell, *J. Chromatogr.*, 99 (1974) 13.

# Reversed-phase high-performance liquid chromatography of the cardiac glycoside LNF-209 with refractive index detection

Paul H. Zoutendam, David L. Berry and Douglas W. Carkuff

*Procter and Gamble Pharmaceuticals, P.O. Box 191, Norwich, NY 13815 (USA)*

---

## ABSTRACT

LNF-209 is a glycoside, similar to digoxin, which has potential for use in the treatment of congestive heart failure. However, unlike digoxin it exhibits virtually no useful UV absorption spectra, making detection difficult. One means of detection is the refractive index detector, but like most bulk property detectors it has certain limitations. Its sensitivity is limited and it is sensitive to small changes in a number of parameters, such as temperature, mobile phase composition, and flow-rate. These parameters must be closely controlled to obtain a stable baseline. This paper describes the steps taken to control the system and the development and validation of an assay for LNF-209 in dosing solutions. The method developed is capable of quantitating LNF-209 in solutions of sterile water and 5% dextrose at concentrations ranging from 8 to 6000  $\mu\text{g/ml}$ . The method is linear over this range and quantitative recovery is obtained. The overall average relative standard deviation for replicate analysis of several samples at various concentrations assayed over two days was 2.3%.

---

## INTRODUCTION

LNF-209 is a cardiac glycoside similar to digoxin which has potential for use in the treatment of congestive heart failure [1,2]. A method was needed to determine levels of this aminosteroid in dosing solutions in sterile water and 5% dextrose (D5W). These dosing solutions would be used in animal toxicology studies. Concentrations used would span a very broad concentration range (10–5000  $\mu\text{g/ml}$ ). An assay with sufficient sensitivity to accurately quantitate LNF-209 at 10  $\mu\text{g/ml}$  was needed. The most widely used and accepted method of determining digoxin is reversed-phase HPLC with UV detection at 220 nm [3–7]. A simple unbuffered acetonitrile–water mobile phase and a ODS column are most often used [3]. This compound, unlike digoxin, exhibits virtually no useful UV absorption spectra. This makes detection of LNF-209 difficult. A variety of means of detecting LNF-209 have been eval-

uated. One possibility of doing so, is to use refractive index detection. Refractive index detection, like most bulk property detectors, has certain advantages and disadvantages [8–10]. The advantages of RI detection are that it is a universal method of detection and that it gives similar responses for similar compounds. The disadvantages of RI detection are that it has poor sensitivity and that it is a universal method of detection.

One of the major advantages and disadvantages of RI detection is the fact that it is a universal method of detection. All kinds of solutes can be detected, however, small changes in the temperature, pressure, flow-rate, or mobile phase composition will also be detected, often as noise and/or drift. To accurately quantitate LNF-209 at the low end of the desired concentration range, the refractive index detector is operated on a setting that corresponds to  $2.0 \cdot 10^{-7}$  refractive index units (RIU) full scale. For methanol, a change in temperature of 0.005°C or a change in pressure of 0.68 p.s.i. corresponds to a change of  $2 \cdot 10^{-6}$  in refractive index [8]. For a methanol–water mixture, a change of 0.04% in the meth-

---

*Correspondence to:* P. H. Zoutendam, Procter and Gamble Pharmaceuticals, P.O. Box 191, Norwich, NY 13815, USA.

anol–water ratio corresponds to a change of  $2.0 \cdot 10^{-6}$  in refractive index. Hence, to achieve detection at useful levels of sensitivity these variables must be closely controlled, *i.e.* maintained constant. A variety of methods of controlling these variables have been discussed in the literature [8–11]. In order to reduce the noise and drift to acceptable levels for this application, it was necessary to utilize almost all of the recommended procedures. The steps that were taken are summarized below.

Control the temperature of the column. (Use a column heater.)

Control the temperature of the detector cell. (Use a detector with a thermostated cell.)

Continuously stir the mobile phase.

Use a properly operating low pulsation pump. Using an extra pulse dampener is often helpful.

Control the gas content of the mobile phase. Either use helium sparging or use air-saturated mobile phase. (In our hands, helium sparging give slightly superior results.)

Autozero the detector at the start of each injection.

## EXPERIMENTAL

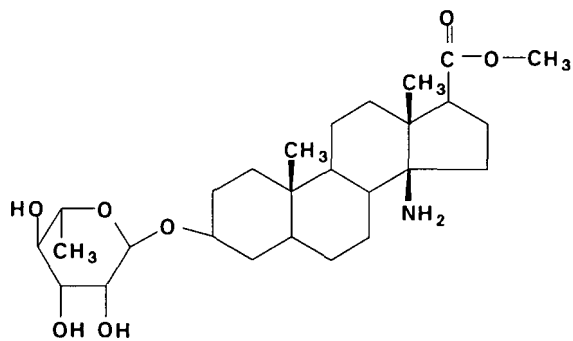
The HPLC system consisted of a Waters 510 pump or a Beckman 100A pump, a Perkin-Elmer ISS-100 autosampler or a Waters WISP 712 autosampler, a Waters Model 410 Differential Refractometer with a column heater, and a Linear Model 1201 recorder. Data was collected and integrated on a Hewlett-Packard LDS data system. An Orion Model 520 pH meter with glass combination electrodes was used to adjust the pH. All reagents and buffers were reagent or HPLC grade. Solvents were HPLC or Spectro grade. Water purified via a Millipore Milli-Q system was used in all cases.

The column was a Spherisorb C<sub>8</sub> column (250 × 4.6 mm, I.D., 5 μm). The mobile phase consisted of 560 ml purified water, 440 ml methanol, 3.4 ml phosphoric acid, and 8.0 g ammonium nitrate. The apparent pH of the mobile phase was adjusted to  $3.0 \pm 0.1$  with ammonium hydroxide. The flow-rate was 1.0 ml/min. The detector and column heater were maintained at 35°C. The detector sensitivity was set to 256 and the scale factor was 10. An injection volume of 100 μl was used. The salt-enriched mobile phase was prepared by adding five times as much phosphoric acid and ammonium nitrate as was in the mobile phase to a 56:44 mixture of water and methanol. The pH was adjusted to  $3.0 \pm 0.1$  with ammonium hydroxide.

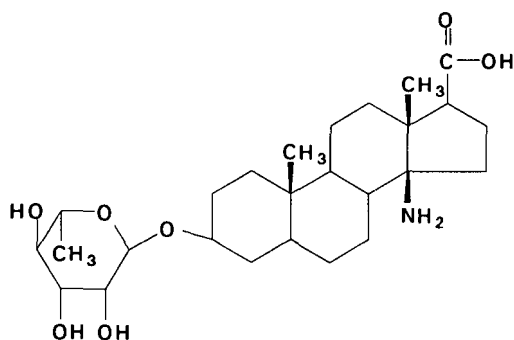
The hydrochloride salt form of LNF-209 is hygroscopic, while the free base form is not. Standards were prepared using the free base form. Samples were quantitated *versus* a standard curve. Standards were prepared in mobile phase at concentrations of 6, 12, 25, 40 and 60 μg/ml. Samples with concentrations above the range of the standard curve were simply diluted with mobile phase until they were within the range of the standard curve. Low-concentration samples (<60 μg/ml) were mixed 4:1 with salt-enriched mobile phase. The use of the salt-enriched solution was found necessary to obtain quantitative recovery.

## RESULTS AND DISCUSSION

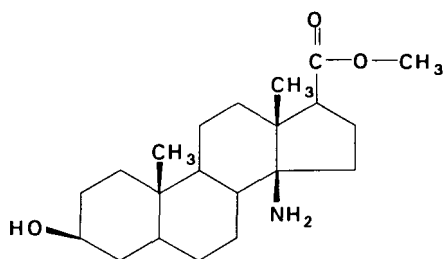
On a typical reversed-phase HPLC system, this aminosteroid gives rather broad, tailing peaks. This is due to the presence of an amine group. See Fig. 1 for the structures of LNF-209 and its potential degradation products. Amine groups are known to cause tailing via interaction with the surface silanols. A large number of mobile phase additives, solvents, columns, etc. were investigated concerning their effect on the chromatographic behavior of these compounds. It was found that the peak shape could be improved by adding a high concentration of cations to the mobile phase. This is illustrated in Fig. 2, which shows the effect of adding ammonium nitrate on the number of theoretical plates, *N*, and the tailing factor [USP Tailing Factor, 12] of LNF-209. Adding 100 mM ammonium nitrate to the mobile phase is effective at improving the peak shape. Methanol was selected for use as the organic solvent in the mobile phase, because better peak shape was obtained with its use as compared to using acetonitrile. It is of note that the chromatographic behavior of this compound is significantly different when acetonitrile is used in the mobile phase. On a C<sub>8</sub> column with a mobile phase consisting of methanol–water (45:55), LNF-209 eluted with a capacity factor of about 5. If acetonitrile is substituted for methanol in the mobile phase in the same proportion, no peak is observed. The compound is completely retained on the column. If the percentage of acetonitrile is reduced to 25% and triethylamine (7 ml/l) is added to the mobile phase, LNF-209 elutes, but it is barely retained and is not completely resolved from the void volume disturb-



LNF-209



Free acid



aglycone

Fig. 1. Structure of LNF-209 and related compounds.

ance. In a typical reversed-phase application, methanol and acetonitrile normally give nearly equivalent results. This is not the case here. The reason for this unusual behavior is that LNF-209 is highly soluble in methanol, but has very limited solubility in acetonitrile.

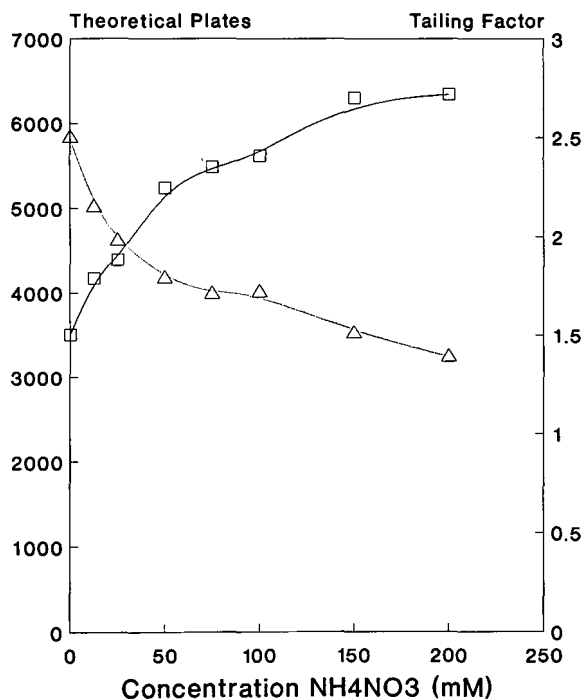


Fig. 2. Effect of adding ammonium nitrate to mobile phase on (□) the number of theoretical plates and (△) the tailing factor,

The HPLC system developed separates LNF-209 from its potential degradation products, the free acid and the aglycone. A chromatogram illustrating this is shown in Fig. 3. The pH of the mobile phase

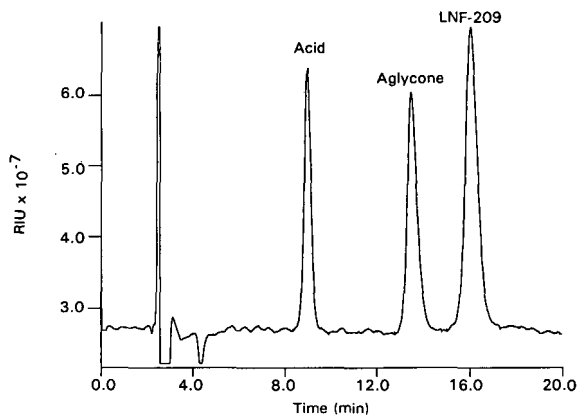


Fig. 3. Chromatogram of LNF-209 spiked with the free acid and the aglycone. Column: Spherisorb C<sub>8</sub> (250 × 4.6 mm I.D., 5 μm); flow-rate: 1.0 ml/min; mobile phase: 560 ml water, 440 ml methanol, 3.4 ml phosphate acid, 8 g ammonium nitrate, pH adjusted to 3.0 with ammonium hydroxide. See Experimental section for additional conditions.

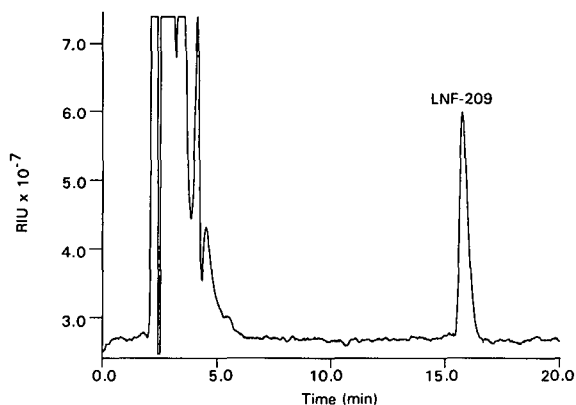


Fig. 4. Chromatogram of a sample preparation of a 36  $\mu\text{g}/\text{ml}$  solution of LNF-209 in 5% dextrose. The conditions were identical to those described in Fig. 3.

must be adjusted to 3.0 to insure that the free acid is protonated and retained. At higher pH it elutes in the void volume. A chromatogram of a typical sample preparation for a solution of LNF-209 in 5% dextrose (D5W) is shown in Fig. 4. Dextrose elutes just after the void volume. It produces a large peak, but it is well separated from the drug peak and does not interfere with the analysis.

The linearity of the system was examined by preparing a series of solutions of LNF-209 in mobile phase and injecting them. The solutions were prepared via serial dilution and ranged in concentration from 2–500  $\mu\text{g}/\text{ml}$ . Concentration *versus* peak area is linear over the entire range studied (slope = 38961, intercept = -38905, correlation coefficient = 0.9998). Concentration *versus* peak height is not linear over the entire range. At higher concentrations, the line falls off. Over the range from 2–100  $\mu\text{g}/\text{ml}$ , concentration *versus* height is linear. The reduction in peak height response at high concentrations is due to increasing peak tailing. Peak tailing increases as more compound is loaded on the column. An injection volume of 100  $\mu\text{l}$  was used for this study, therefore the concentrations injected correspond to 0.2 to 50  $\mu\text{g}$  injected on column. Peak tailing continuously increases as more material is injected on column, however the increase is very gradual from 0.2 to 5.0  $\mu\text{g}$ . Tailing increases more rapidly as the amount injected in column increases from 10 to 50  $\mu\text{g}$  and the plot of concentration *versus* peak height begins to fall off in this range. Even

though, the working concentration for this assay was selected to be in the range where the system is linear by both peak areas and peak heights, peak areas were used for all investigations. The limit of detection of the method was also investigated. The limit of detection for LNF-209, where this is defined as a peak corresponding to three times the noise level, was estimated to be 1  $\mu\text{g}/\text{ml}$  (or 0.1  $\mu\text{g}$  injected on column).

When solutions of LNF-209 in water or D5W at very low concentrations (8–30  $\mu\text{g}/\text{ml}$ ) were injected directly into the HPLC, complete recovery was not obtained. Quantitative recovery was obtained for samples containing more than 30  $\mu\text{g}/\text{ml}$ . Very high concentration (> 60  $\mu\text{g}/\text{ml}$ ) samples which were diluted 5:1 or greater with mobile phase also gave quantitative recoveries. Simply diluting the low concentration samples with mobile phase was not an option as this would result in final sample concentrations that were below the level where the RI detector could accurately quantitate this material. Several sample preparation methods designed to provide quantitative recovery at low concentrations were evaluated. It was found that adding 2.0 ml of a salt-enriched mobile phase to 8.0 ml of sample resulted in quantitative recoveries. The salt-enriched mobile phase contained five times the concentration of phosphoric acid and ammonium nitrate that was in the mobile phase and its pH was adjusted to 3.0 with ammonium hydroxide. Hence, when this was added to an aqueous solution, the resultant solution had the same buffer and salt concentration as the mobile phase. This procedure results in a minimal dilution of the sample. This procedure was used for samples in the lowest concentration range. Samples with higher concentrations were simply diluted with mobile phase and injected.

The precision of this method was estimated by preparing a series of solutions in either water or D5W and assaying each solution in triplicate. The concentrations of the solutions spanned the entire concentration range of this assay. The experiment was repeated on a second day by a different analyst. The average result and the relative standard deviation for the three determinations of each solution for samples prepared in water and 5% dextrose are listed in Tables I and II, respectively. The average R.S.D. values in water for days 1 and 2 were 2.53% and 2.10%, respectively. The average R.S.D. values

TABLE I

## TRIPPLICATE ASSAYS OF LNF-209 IN DOSING SOLUTIONS IN WATER

Based on peak area measurements.

Day 1		Day 2	
Average ( $\mu\text{g/ml}$ )	R.S.D. (%)	Average ( $\mu\text{g/ml}$ )	R.S.D. (%)
9.0	3.33	8.5	5.02
16.4	2.18	15.9	2.3
35.0	1.98	34.5	0.66
57.3	2.54	59.2	0.22
89.5	2.22	87.1	0.55
292	0.98	312	0.95
359	1.81	357	0.58
588	2.53	586	6.90
740	2.51	752	2.01
1439	3.07	1445	2.70
1929	4.65	1895	3.00
5752	2.52	6000	0.26
Average	2.53	Average	2.10

TABLE II

## TRIPPLICATE ASSAYS OF LNF-209 DOSING SOLUTIONS IN 5% DEXTROSE

Based on peak area measurements.

Day 1		Day 2	
Average ( $\mu\text{g/ml}$ )	R.S.D. (%)	Average ( $\mu\text{g/ml}$ )	R.S.D. (%)
7.9	2.37	9.1	5.73
15.6	1.48	16.0	1.26
34.7	3.48	33.8	2.26
60.2	2.29	34.3	3.45
89.8	1.72	91.6	4.26
304	2.53	295	1.72
352	4.95	358	0.54
590	2.13	609	1.79
733	2.63	748	1.18
1547	3.82	1484	1.83
1975	0.71	1998	0.25
6043	2.56	6014	0.53
Average	2.56	Average	2.07

in D5W for days 1 and 2 were 2.56% and 2.07%, respectively.

A spiked recovery study was performed to assess the accuracy and linearity of this method. Solutions containing known concentrations of LNF-209 in water and D5W were prepared. The concentrations of the solutions spanned the entire concentration range of this assay. The samples were assayed and

the amount recovered was determined. The experiment was repeated a second time at each concentration by a different analyst. Results for samples in water and D5W are summarized in Tables III and IV, respectively. The overall average recoveries were 100.1% and 99.1% for samples in water and D5W, respectively. Linear regressions were performed on the amount added *versus* the amount

TABLE III

## LINEARITY AND RECOVERY OF LNF-209 IN WATER

Based on peak area measurements.

	Day 1	Day 2	Day 3
Range ( $\mu\text{g/ml}$ )	8–6076	8–300	298–5830
<i>n</i>	16	9	9
Average recovery (%)	100.5	101.3	98.0
R.S.D. (%)	2.39	1.82	1.22
<i>Results of linear regression for plots of amount added vs. amount found</i>			
Slope	1.0045	1.0261	0.9789
Standard error slope	0.0036	0.0053	0.0024
Intercept	5.0616	–0.5369	–2.1255
Standard error intercept	6.3699	0.7699	0.0024
Correlation coefficient	0.99991	0.99990	0.99998



TABLE IV  
LINEARITY AND RECOVERY OF LNF-209 IN 5% DEXTROSE

Based on peak area measurements.

	Day 1	Day 2	Day 3
Range ( $\mu\text{g/ml}$ )	8–6180	8–294	280–5950
<i>n</i>	24	10	9
Average recovery (%)	98.9	99.6	99.2
R.S.D. (%)	3.17	1.26	2.24
<i>Results of linear regression for plots of amount added vs. amount found</i>			
Slope	1.0408	0.9966	1.0006
Standard error slope	0.0031	0.0019	0.0090
Intercept	–10.7775	–0.0213	–4.7151
Standard error intercept	4.6411	0.2798	21.326
Correlation coefficient	0.99990	0.99985	0.99971

found. The results of the regression analysis are summarized in Tables III and IV. The results indicate that this assay is linear in nature.

#### CONCLUSIONS

Refractive index detection has been found to be a reliable means of quantitating LNF-209, an aminosteroid with little to no UV absorption. By controlling the temperature of the system and the composition of the mobile phase, adequate sensitivity for detecting LNF-209 at the levels required for this application was achieved. The assay developed is capable of accurately quantitating this material in dosing solutions in water and 5% dextrose over a broad concentration range. The HPLC system developed gives well shaped peaks and is capable of separating the major component from its potential degradation products, the acid and the aglycone. The addition of a high concentration of cations to the mobile phase was found to be effective at improving the peak shape and reducing peak tailing.

#### REFERENCES

- 1 L. Brown, *Clin. Exp. Pharmacol. Physiol.*, 17 (1990) 589.
- 2 D. Rocher and P. Lechat, *J. Mol. Cell Cardiol.*, 23 (1991) Supplement IV, S52, no. 156.
- 3 *USP XXII-NSF XVII*, US Pharmacopeial Convention, Rockville, MD, 1990, p. 438.
- 4 F. Erni and R. W. Frei, *J. Chromatogr.*, 130 (1977) 169.
- 5 Y. Fujii, Y. Ikeda and M. Yamazaki, *J. Chromatogr. Sci.*, 28 (1980) 288.
- 6 B. Desta and K. M. McErlane, *J. Pharm. Sci.*, 71 (1982) 1018.
- 7 Y. Fujii, Y. Ikeda and M. Yamazaki, *J. Chromatogr.*, 448 (1988) 157.
- 8 M. N. Munk, in T. M. Vickrey (Editor), *Liquid Chromatography Detectors*, Marcel Dekker, New York, 1983, Ch. 6, p. 165.
- 9 R. P. W. Scott, *Liquid Chromatography Detectors*, Elsevier, Amsterdam, 2nd ed., 1986, Ch. 3, p. 49.
- 10 E. S. Yeung, *Detectors for Liquid Chromatography*, Wiley, New York, 1986, Ch. 1, p. 1.
- 11 W. A. Dark, *J. Chromatogr. Sci.*, 24 (1986) 495.
- 12 *USP XXII-NF XVII*, US Pharmacopeial Convention, Rockville, MD, 1990, p. 1567.

# Determination of oxiracetam in human plasma by reversed-phase high-performance liquid chromatography with fluorimetric detection

Richard C. Simpson, Venkata K. Boppana, Bruce Y.-H. Hwang and Gerald R. Rhodes

*Department of Drug Metabolism and Pharmacokinetics, SmithKline Beecham Pharmaceuticals, P.O. Box 1539, King of Prussia, PA 19406 (USA)*

---

## ABSTRACT

Reversed-phase HPLC methodology utilizing pre-column derivatization and post-column reaction fluorimetric detection has been developed and applied to the determination of oxiracetam in human plasma. The method involves preliminary isolation of oxiracetam and internal standard from plasma by solid-phase extraction prior to the formation of their *n*-propyl carbamate derivatives. The carbamate derivatives were subsequently isolated by solid-phase extraction and subjected to a gradient liquid chromatographic separation on an octadecylsilica column prior to on-line post-column alkaline hydrolysis to produce the corresponding primary amine, which was in turn derivatized with *o*-phthalaldehyde and 3-mercaptopropionic acid to yield a fluorescent isoindole. The isoindole was then quantified using a fluorescence detector. The method provided an on-column detection limit of 0.5 ng of oxiracetam and was sufficiently sensitive, accurate, and precise to support pre-clinical or clinical pharmacokinetic studies.

---

## INTRODUCTION

Oxiracetam (4-hydroxy-2-oxo-1-pyrrolidine acetamide) is a highly polar achromophoric monohydroxy investigational nootropic agent, which has shown potential for the treatment of various cognitive disorders [1–3]. Oxiracetam has also been shown to improve both learning and memory processes [4,5]. In order to support pharmacokinetic characterization of the drug, a sensitive and specific assay was required for the determination of oxiracetam in human plasma. Previous analytical methods for the determination of oxiracetam in physiological matrices have utilized normal-phase HPLC [6–10], many of which employed column-switching techniques [7–10]. Due to a lack of native fluorophoric or suitable chromophoric properties, detection of oxiracetam was typically performed at low

wavelength in the UV region. Major limitations of these methods include lack of sensitivity and/or specificity encountered with low-wavelength UV detection and long run times required by the column-switching techniques. The goal of our study was to develop a sensitive and specific assay for oxiracetam in human plasma which would eliminate or minimize such limitations. We recently reported an approach for the pre-column derivatization and post-column reaction detection of monohydroxy compounds [11]. The technique involved the pre-column conversion of the monohydroxy compound to an *n*-alkyl carbamate, which was then subjected to reversed-phase HPLC separation, followed by post-column alkaline hydrolysis to the corresponding free primary amine. The primary amine was subsequently derivatized with *o*-phthalaldehyde (OPA) and 3-mercaptopropionic acid (3-MPA) to yield a fluorescent isoindole which was quantified by fluorescence detection. The current paper describes the utilization of this methodology to develop a sensitive and specific assay for oxiracetam in

---

*Correspondence to:* R. C. Simpson, Department of Drug Metabolism and Pharmacokinetics, SmithKline Beecham Pharmaceuticals, P.O. Box 1539, King of Prussia, PA 19406, USA.

human plasma in order to permit pharmacokinetic evaluation of the drug. Although oxiracetam was used as its racemate, the assay described here is not enantio-specific. Thus no differentiation between the two enantiomeric forms of oxiracetam was achieved.

## EXPERIMENTAL

### Materials

Materials and reagents were obtained from the sources previously described [11].

### *o*-Phthalaldehyde reagent solution

The post-column OPA reagent solution was prepared as previously described [11].

### Standards solutions

Working aqueous standard solutions of oxiracetam at concentrations of 40, 4, and 0.4  $\mu\text{g}/\text{ml}$  were prepared by appropriate dilutions of a 500  $\mu\text{g}/\text{ml}$  aqueous stock solution. These solutions were stable for 5 weeks when stored at 5°C. Similarly, a working aqueous solution of internal standard at a concentration of 25  $\mu\text{g}/\text{ml}$  was prepared by appropriate dilution of a 1000  $\mu\text{g}/\text{ml}$  aqueous stock solution. The working internal standard solution was stable at ambient temperatures for 2 weeks.

### Sample preparation

*Solid-phase extraction from plasma.* A 200- $\mu\text{l}$  aliquot of human plasma, 50  $\mu\text{l}$  of water (or aqueous standard solutions when preparing calibration standards), and 50  $\mu\text{l}$  of working internal standard solution were mixed in a 1.5-ml polypropylene microcentrifuge tube. Plasma proteins were precipitated by the addition of 500  $\mu\text{l}$  of acetonitrile. Following vortex-mixing and centrifugation for 10 min at 8800 g, the resulting supernatant was transferred to a borosilicate tube containing 500  $\mu\text{l}$  of 0.1 M potassium phosphate buffer (pH 8.5). After brief vortex-mixing, the sample was applied to a phenylboronic acid solid-phase extraction cartridge which had been conditioned with one column volume of 0.1 M potassium phosphate buffer (pH 8.5). Using vacuum, the sample was slowly passed through the cartridge and collected in a 75  $\times$  12 mm polypropylene tube. The sample was evaporated to dryness at 50°C under a nitrogen flow. The resulting residue was re-

constituted with 1 ml of methanol, followed by brief sonication to break up phosphate salt residue and vortex-mixing to aid the dissolution of the drug and internal standard. The tube was centrifuged for 5 min at 1500 g. The resulting supernatant, free of insoluble potassium phosphate, was transferred to a borosilicate tube and evaporated to dryness at 50°C under a nitrogen flow.

*Pre-column formation and extraction of carbamate derivatives.* To the dry residue from the previous step, 200  $\mu\text{l}$  of anhydrous pyridine and 100  $\mu\text{l}$  of *n*-propyl isocyanate were added followed by vortex-mixing. The tube was sealed with Parafilm and immersed in a water bath at 50°C for 1 h to achieve formation of the *n*-propyl carbamate derivatives of the drug and internal standard. After the reaction period, the crude derivatization solution was evaporated to dryness under a nitrogen flow. The dry residue was dissolved in two 0.5-ml aliquots of acetonitrile and the resulting solutions were applied to a silica solid-phase extraction cartridge which had been conditioned with one column volume of acetonitrile. The sample was passed through the cartridge and discarded. The cartridge was washed with 1 ml of acetonitrile, followed by elution of the carbamate derivatives with 1 ml of 50% (v/v) methanol in acetonitrile. The eluate was collected in a 75  $\times$  10 mm borosilicate tube and evaporated to dryness at 50°C under a nitrogen flow. The residue was reconstituted with 200  $\mu\text{l}$  of HPLC-grade water and transferred to an autosampler via. Volumes of 10–25  $\mu\text{l}$  were injected for HPLC analysis. The *n*-propyl carbamate derivatives were stable in aqueous solution for a period of 4 days at ambient temperatures.

### High-performance liquid chromatography

The HPLC system used has been described elsewhere [11]. In addition, a 500-p.s.i. pump pre-load cartridge (Upchurch Scientific, Oak Harbor, WA, USA) and a pulse damper (Scientific Systems, State College, PA, USA) were used in conjunction with the post-column reagent pump in order to provide a more stable baseline.

### Standard curves

Using the oxiracetam and internal standard working solutions described above, a series of 200- $\mu\text{l}$  plasma samples were prepared at drug concentrations of 40, 60, 100, 200, 600, 1000, 2000,

6000 and 10 000 ng/ml. These samples were subjected to the solid-phase extractions and derivatization procedure described above to generate a nine-point standard curve. The peak-height ratios of drug to internal standard were obtained, weighted by a factor of  $1/y$  (based on analysis of residuals) and plotted *versus* plasma drug concentrations. Linear regression analysis gave a calibration curve that was used to calculate plasma oxiracetam concentrations.

## RESULTS AND DISCUSSION

### Derivatization

The general reactions involved in the derivatization and detection scheme have previously been described [11]. The scheme essentially consists of two steps. The first step is the pre-column derivatization of oxiracetam (and internal standard) with *n*-propyl isocyanate to form the corresponding *n*-propyl carbamate derivative. A study to determine the optimal reaction conditions indicated a 1-h reaction time at 50°C maximized the formation of the *n*-propyl carbamate derivative of oxiracetam.

In addition to *n*-propyl isocyanate, the use of phenyl isocyanate was also investigated. Although formation of the phenyl carbamate derivative would permit the use of UV detection, phenyl isocyanate does not possess the high volatility of propyl isocyanate, which prohibited a simple evaporation of excess reagent. Consequently it was difficult to completely remove excess phenyl isocyanate and a large reagent peak was encountered which interfered in the HPLC resolution of the drug and internal standard carbamate derivatives. Therefore, propyl isocyanate was the reagent of choice.

The second step in the derivatization scheme is the on-line alkaline hydrolysis of the carbamate de-

rivative to the corresponding primary amine and subsequent derivatization of the primary amine (*n*-propylamine) with OPA and 3-MPA to yield the isoindole fluorophore, which is the species fluorimetrically monitored and quantified.

The effects of several variables on the post-column reaction were examined. Variation of sodium hydroxide concentration in the post-column reagent from 0.01 to 0.3 *M* indicated a concentration of 0.05 *M* provided optimal response. Similarly, varying the reaction coil temperature from 40 to 110°C showed a temperature of 90°C to provide maximal fluorimetric response. Additionally, use of a 0.5-ml reaction coil (providing a reaction time of approximately 1 min) yielded optimal detector response. Use of larger-volume reaction coils to increase the reaction time did not result in increased detector response, but did begin to introduce significant extra-column band broadening.

### Recovery

Known amounts of oxiracetam (80, 800, and 8000 ng/ml) and internal standard (6250 ng/ml) were dissolved in drug-free human plasma and processed according to the described method. Recovery was determined as a percentage relative to the results obtained for aqueous reference standards at the same concentrations. The results of the recovery study are summarized in Table I. The recovery of oxiracetam and the internal standard were high and consistent at the concentrations examined.

### Sensitivity, linearity, and selectivity

Typical chromatograms of extracts of drug-free human plasma and plasma spiked with both oxiracetam (800 ng/ml) and internal standard are shown in Fig. 1. Retention times for the *n*-propyl

TABLE I  
RECOVERY OF OXIRACETAM AND INTERNAL STANDARD FROM HUMAN PLASMA

Compound	Concentration (ng/ml)	Recovery (mean ± S.D.) (%)	R.S.D. (%)	<i>n</i>
Oxiracetam	80	91.19 ± 7.95	8.72	6
Oxiracetam	800	113.21 ± 10.26	9.06	4
Oxiracetam	8000	99.35 ± 2.90	2.92	5
Internal standard	6250	81.06 ± 6.72	8.30	15

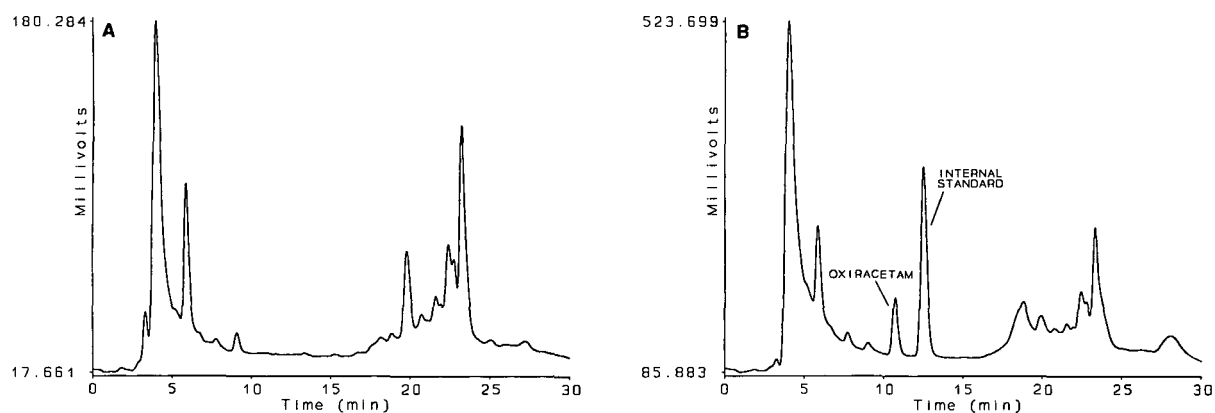


Fig. 1. Chromatograms of extracts of (A) drug-free plasma and (B) plasma spiked with both oxiracetam (800 ng/ml) and internal standard. See text for chromatographic conditions.

TABLE II  
SUMMARY OF ACCURACY AND PRECISION STUDY

	Plasma concentration of oxiracetam (ng/ml) ( $n = 6$ )		
	80	800	8000
<i>Day 1 statistics</i>			
Mean found concentration (ng/ml)	80.83	825.50	8217.21
S.D. (ng/ml)	7.54	34.61	392.20
R.S.D. (%)	9.33	4.19	4.77
Mean accuracy (%)	101.04	103.19	102.72
<i>Day 2 statistics</i>			
Mean found concentration (ng/ml)	94.21	804.53	8004.15
S.D. (ng/ml)	5.16	42.46	171.92
R.S.D. (%)	5.47	5.28	2.15
Mean accuracy (%)	117.76	100.57	100.05
<i>Day 3 statistics</i>			
Mean found concentration (ng/ml)	78.40	739.96	8638.86
S.D. (ng/ml)	6.86	52.12	88.34
R.S.D. (%)	8.75	7.04	1.02
Mean accuracy (%)	98.00	92.49	107.99
Within-day R.S.D. (%) <sup>a</sup>	7.85	5.50	2.65
<i>Between-day statistics (all three days)</i>			
Mean found concentration (ng/ml) <sup>b</sup>	84.48	789.99	8286.74
S.D. (ng/ml) <sup>c</sup>	6.95	36.40	263.74
R.S.D. (%) <sup>d</sup>	8.23	4.61	3.18
Mean accuracy (%) <sup>e</sup>	105.60	98.75	103.58

<sup>a</sup> Mean of daily R.S.D.s.

<sup>b</sup> Mean of daily means.

<sup>c</sup> S.D. of daily means.

<sup>d</sup> R.S.D. of daily means.

<sup>e</sup> Mean of daily accuracies.

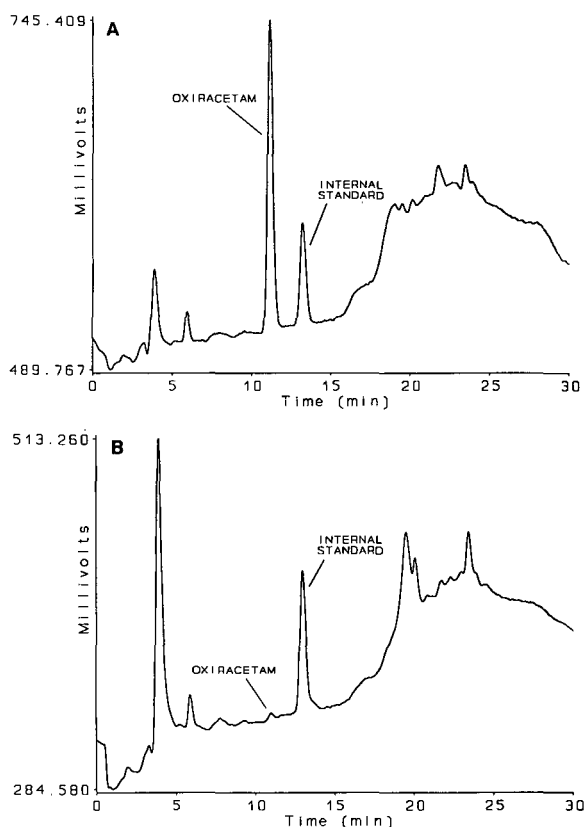


Fig. 2. Chromatograms of authentic human plasma samples obtained (A) 2.5 h (8658 ng/ml) and (B) 97.3 h (136 ng/ml) after an 800-mg oral dose of oxiracetam. See text for chromatographic conditions.

carbamate derivatives of oxiracetam and the internal standard were 10.9 and 12.9 min, respectively. As can be observed, endogenous plasma components did not interfere with the measurement of oxiracetam or internal standard over the concentration range described here.

Utilizing a 2.1 mm I.D. HPLC column and optimizing the derivatization conditions, the on-column limit of detection (at a signal-to-noise ratio of 3) for oxiracetam was 0.5 ng (3.2 pmol). Based on a 200- $\mu$ l plasma sample volume, linear detector response for the peak-height ratio of drug to the internal standard was observed for plasma oxiracetam concentrations ranging from 40 to 10 000 ng/ml. Correlation coefficients obtained using weighted ( $1/y$ ) linear regression analysis data were typically 0.996 or better.

#### Accuracy and precision

Accuracy and precision results obtained in a three-day validation study are presented in Table II. Replicate plasma samples ( $n = 6$ ) at oxiracetam concentrations of 80, 800, and 8000 ng/ml were assayed each day by the described method. The between-day mean accuracy of the assay ranged from 98.8 to 105.6%. The within-day precision of the method, indicated by the mean of the daily relative standard deviation (R.S.D.) at each concentration, ranged from 2.6 to 7.8%. The between-day precision, calculated as the R.S.D. of the daily means at each concentration, ranged from 3.2 to 8.2%.

#### Authentic plasma samples

The method has also been applied to human plasma samples obtained following oral administration of oxiracetam. Fig. 2 presents the chromatograms for human plasma samples obtained 2.5 and 97.3 h following an 800-mg oral dose of oxiracetam. These chromatograms illustrate the utility of the assay to determine plasma oxiracetam concentrations over a wide concentration range, for use in pharmacokinetic evaluation in clinical studies.

#### CONCLUSIONS

This paper described a sensitive and selective HPLC assay for oxiracetam in human plasma. The method involves pre-column derivatization prior to post-column reaction fluorimetric detection. The assay is sensitive, with an on-column detection limit of 0.5 ng for oxiracetam, and provides a linear detector response range of 40–10 000 ng/ml based on a 200- $\mu$ l plasma sample volume. Employing manual sample preparation procedures and an autoinjector, a reasonable estimate of sample throughput is in the range of 60–70 per day. The method has successfully been applied to human plasma samples for orally dosed patients and provides sufficient sensitivity, accuracy, and precision to support clinical pharmacokinetic studies.

#### REFERENCES

- 1 G. Pifferi and M. Pinza, *Farmaco, Ed. Sci.*, 32 (1977) 602.
- 2 T. M. Itil, C. Soldatos, M. Bozak, E. Ramadanoglu, G. Dayican, V. Morgan and G. N. Menon, *Curr. Ther. Res.*, 26 (1979) 525.
- 3 B. Saletu, L. Linzmayer, J. Grünberger and H. Pietschmann, *Neuropsychobiology*, 13 (1985) 44.

- 4 S. Benfi, L. Dorigotti, M. P. Abbracchio, W. Bolduini, E. Coen, C. Ragusa and F. Cottabeni, *Pharma. Res. Commun.*, 16 (1984) 69.
- 5 G. Spignoli and G. Pepeu, *Eur. J. Pharm.*, 126 (1986) 253.
- 6 E. Perucca, A. Albrici, G. Gatti, R. Spalluto, M. Visconti and A. Crema, *Eur. J. Drug Metab. Pharmacokin.*, 3 (1984) 267.
- 7 J. B. Lecaillon, N. Febvre and C. Souppart, *J. Chromatogr.*, 317 (1984) 493.
- 8 M. Visconti, R. Spalluto, T. Crolla, G. Pifferi and M. Pinza, *J. Chromatogr.*, 416 (1987) 433.
- 9 J. B. Lecaillon, C. Souppart, J. P. Dubois and A. Delacroix, *Methodol. Surv. Biochem. Anal.*, 18 (1988) 225.
- 10 J. B. Lecaillon, C. Souppart, F. LeDuigou and J. P. Dubois, *J. Chromatogr.*, 497 (1989) 223.
- 11 V. K. Boppana, R. C. Simpson, K. Anderson, C. Miller-Stein, T. J. A. Blake, B. Y.-H. Hwang and G. R. Rhodes, *J. Chromatogr.*, 593 (1992) 29.

# Column-switching high-performance liquid chromatographic method for the determination of SK&F 106203 in human plasma after fluorescence derivatization with 9-anthryldiazomethane

Cynthia Miller-Stein, Bruce Y.-H. Hwang, Gerald R. Rhodes and Venkata K. Boppana

Department of Drug Metabolism and Pharmacokinetics, SmithKline Beecham Pharmaceuticals, P.O. Box 1539, Mail Code UW2711, King of Prussia, PA 19406-0939 (USA)

## ABSTRACT

A sensitive and selective high-performance liquid chromatographic method was developed for the determination of SK&F 106203 3-(2-carboxyethylthio)-3-[2-(8-phenyloctyl)phenyl]propanoic acid, a potent peptidoleukotriene end organ receptor antagonist, in human plasma. The method involves isolation of SK&F 106203 and the internal standard (SK&F 104736) from plasma samples by liquid-liquid extraction prior to derivatization with 9-anthryldiazomethane. The derivatized samples were first subjected to a solid-phase extraction procedure prior to injection onto a short silica column, which is part of a chromatographic system equipped with an automated column-switching device. Column switching was used to heart-cut the chromatographic zone containing the peaks of interest from this first column and transfer it to an analytical silica column for further chromatographic separation. The peaks were quantified with an in-line fluorometer by measuring the fluorescence emission intensity at 415 nm after excitation at 365 nm. An on-column detection limit of 0.625 ng was achieved for SK&F 106203 by optimizing the derivatization and chromatography conditions. The limit of quantification for SK&F 106203, using 250  $\mu$ l of plasma, was 20 ng/ml. Linear response in SK&F 106203/internal standard peak-height ratios was observed for SK&F 106203 concentrations ranging from 10 to 5000 ng/ml of plasma. Precision and accuracy were within 5% across the calibration range. The assay was sufficiently sensitive, accurate, and precise to support pharmacokinetic studies in humans.

## INTRODUCTION

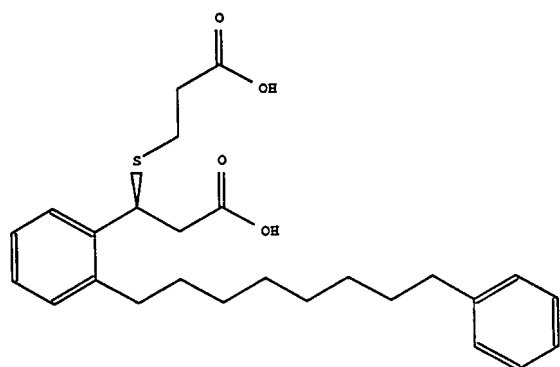
SK&F 106203, 3-(2-carboxyethylthio)-3-[2-(8-phenyloctyl)phenyl]propanoic acid (S, Fig. 1), is a novel peptidoleukotriene end organ receptor antagonist indicated for the treatment of asthma and other pulmonary diseases. The compound has a high affinity for the leukotriene D<sub>4</sub> receptor on lung membranes. This binding prevents and reverses leukotriene-dependent airway contraction and inhibits the leukotriene component of antigen-induced air-

way contraction [1]. In order to support pharmacokinetic studies, a sensitive method for quantification of S was required. Development of a sensitive high-performance liquid chromatographic (HPLC) method was complicated by the lack of a chromophoric or fluorophoric group in the molecule. Derivatization of the carboxyl groups of S with a suitable fluorophore was considered necessary in order to enhance the detectability of the compound.

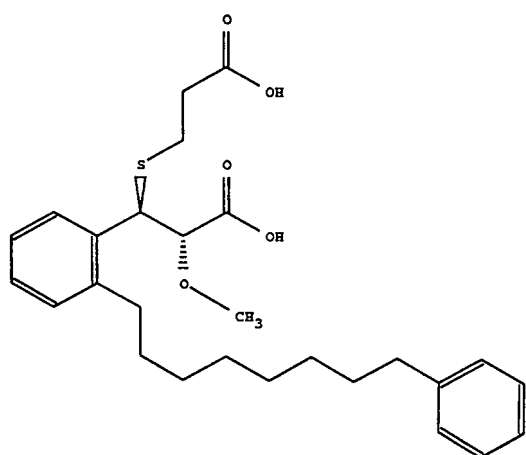
Previous reports concerning HPLC analysis of fatty acids and prostaglandins via pre-column fluorescence derivatization with 9-anthryldiazomethane (ADAM) [2–8] have suffered from a lack of routine applicability in measuring these compounds at very low concentrations. These limitations were mainly associated with the relative instability of commer-

Correspondence to: C. Miller-Stein, Department of Drug Metabolism and Pharmacokinetics, SmithKline Beecham Pharmaceuticals, P.O. Box 1539, Mail Code UW2711, King of Prussia, PA 19406-0939, USA.





S



IS

Fig. 1. Structures of SK&F 106203 (S) and the internal standard, SK&F 104736 (IS).

cially purchased ADAM, interferences arising from this reagent, and from degradation and by-products formed during the reaction of ADAM with plasma extracts. In the present report, these difficulties were overcome by generating ADAM just prior to use, partially purifying the reaction mixture, and employing automated column switching in order to eliminate various chromatographic interferences.

The method reported here involves isolation of S and the internal standard (SK&F 104736, I.S.) from plasma samples by liquid-liquid extraction prior to derivatization with ADAM prepared *in situ* just pri-

or to use. The derivatized products were then subjected to a solid-phase extraction before injection onto a short silica column, which was part of a chromatographic system equipped with an automated column-switching device. Column switching was used to heart-cut the chromatographic zone containing the peaks of interest from this first column and transfer it to a second analytical column for further chromatographic separation and fluorescence detection.

## EXPERIMENTAL

### Materials

SK&F 106203 (S) and SK&F 104736 (I.S.) were supplied by Drug Substances and Products, Smith-Kline Beecham Pharmaceuticals (Swedeland, PA, USA). 9-Anthraldehyde, 80% hydrazine hydrate, anhydrous ethyl acetate and quinuclidine were obtained from Aldrich (Milwaukee, WI, USA). N-Chlorosuccinimide was obtained from Fluka (Ronkonkoma, NY, USA). Chloroform was purchased from Polysciences (Warrington, PA, USA). Monobasic and dibasic potassium phosphate, HPLC-grade methanol, hexane, acetonitrile and ethyl acetate were purchased from J. T. Baker (Phillipsburg, NJ, USA). Glacial acetic acid was obtained from Mallinckrodt (Paris, KY, USA). C<sub>18</sub> solid-phase extraction cartridges (1 ml) and the Vac-Elut SPS 24 manifold were purchased from Analytichem International (Harbor City, CA, USA).

### 9-Anthraldehyde hydrazone

9-Anthraldehyde hydrazone was synthesized according to a method described previously [9]. An ethanolic solution of 9-anthraldehyde (10 g in 150 ml) was stirred with 80% hydrazine hydrate (10 g) for 3 h at room temperature. The yellow-orange crystals obtained were filtered and dried under vacuum. The compound was stable for three months when stored at  $-80^{\circ}\text{C}$  in amber vials.

### 9-Anthryldiazomethane

ADAM was generated just prior to use by reacting 9-anthraldehyde hydrazone, N-chlorosuccinimide and quinuclidine in ethyl acetate, using a modified method based upon that described by Yoshida *et al.* [3]. To 1 ml of a 13.8 mM solution of 9-anthraldehyde hydrazone (3.05 mg/ml of anhydrous

ethyl acetate), 1 ml of 138 mM quinuclidine (15.3 mg/ml of anhydrous ethyl acetate) and 1 ml of 13.8 mM N-chlorosuccinimide (1.84 mg/ml of anhydrous ethyl acetate) were added and allowed to react for 30 min at room temperature in the dark. The resulting solution was used immediately for derivatization of S and I.S.

#### *Standard solutions and reagents*

The stock standard solutions of S and I.S. were prepared by separately dissolving appropriate amounts of each compound in methanol to give a concentration of 1 mg/ml. The stock solution of I.S. was diluted 1:250 with 50% aqueous methanol to give a working standard concentration of 4 µg/ml. Appropriate dilutions of the stock solution of S were made with 50% aqueous methanol to generate a series of working standard solutions (100, 10, 1 and 0.1 µg/ml) which were used in the generation of calibration lines. All stock and working standard solutions were stable for two months when stored at 4°C.

#### *Extraction of SK&F 106203 from plasma*

An aliquot of plasma (0.25 ml) containing 75 µl of 50% aqueous methanol (contains standards when preparing calibration curve) and 50 µl of I.S. (4 µg/ml) was mixed with hexane (5 ml) in a 16 × 100 mm screw-cap borosilicate tube. The tube was capped and placed on a linear shaker operating at low speed for 5 min. The tube was then centrifuged for 5 min at 1500 g and the hexane layer was aspirated to waste. To the aqueous phase, 5 ml of ethyl acetate – hexane (20:80, v/v) and 0.5 ml of 1 M acetic acid were added. The tube was shaken at low speed for 30 min and then centrifuged at 1500 g for 5 min. The organic phase was transferred to a clean silanized 16 × 100 mm borosilicate tube and the solvent was evaporated under nitrogen at 40°C. The sample was reconstituted with 100 µl of anhydrous ethyl acetate.

#### *Derivatization with ADAM*

To the reconstituted sample from the previous step, 200 µl of freshly prepared ADAM solution were added and allowed to react for 1 h at room temperature in the dark. The reaction mixture was evaporated to dryness under nitrogen at room temperature. The residue was reconstituted with 100 µl of acetonitrile.

#### *Solid-phase extraction of ADAM derivative of SK&F 106203*

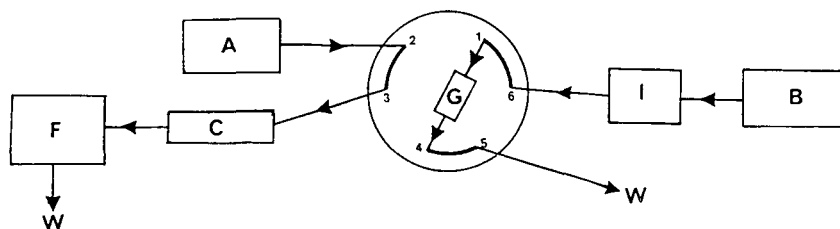
A C<sub>18</sub> solid-phase extraction cartridge (100 mg/1 ml) was conditioned with 1 ml of methanol and 1 ml of water. The acetonitrile solution, containing the ADAM derivatives of S and I.S., was applied onto the conditioned column and vacuum applied slowly. The column was successively washed with 1 ml of phosphate buffer (0.1 M, pH 8.0), 1 ml of water and 3 ml of 85% aqueous acetonitrile. S and I.S. were eluted from the column with 2 ml of acetonitrile. The eluent was evaporated under nitrogen at 40°C. The sample was redissolved first in 10 µl of ethyl acetate and then diluted with 90 µl of hexane. The extract was transferred to a WISP vial and 10–50 µl were injected onto the HPLC system. This partially purified sample was stable for at least 48 h prior to chromatographic analysis.

#### *High-performance liquid chromatography*

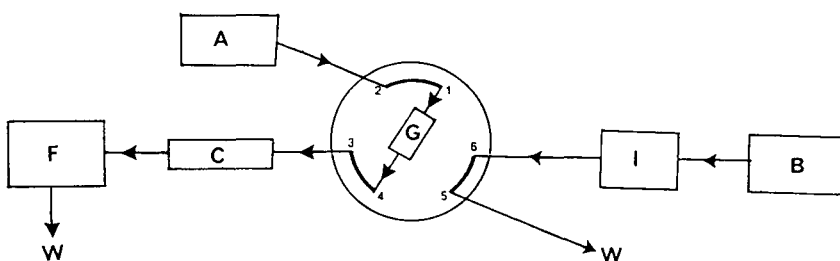
The HPLC system consisted of a column-switching device (Millipore, Milford, MA, USA), two Model 116 isocratic pumps (Beckman, Palo Alto, CA, USA), a Model 710B WISP autosampler (Millipore), and a Model F-1000 fluorescence detector (Hitachi, Danbury, CT, USA). Two columns, a 30 mm × 4.6 mm I.D., 5 µm particle size Spheri-5 silica guard column (Brownlee, San Jose, CA, USA) and a 250 mm × 4.6 mm I.D., 5 µm particle size, Ultrasphere silica analytical column (Beckman) were connected through a column-switching valve as shown in Fig. 2. The analytical column was maintained at 35°C with a temperature controller (Sys-Tec, Minneapolis, MN, USA). The mobile phase consisted of chloroform–ethyl acetate–hexane–glacial acetic acid (2:4:93.8:0.2, v/v) and the flow-rates for the guard and analytical columns were 1 and 1.1 ml/min, respectively. Mobile phase eluents were filtered through a GVWP 0.22 µm filter (Millipore). Detection was accomplished utilizing excitation at 365 nm while monitoring the fluorescence emission at 415 nm. The chromatographic data were collected and analyzed with an automated laboratory system (PE/Nelson Access\*Chrom, V 1.6, Cupertino, CA, USA).

#### *Column-switching procedure*

The injector (I), two HPLC pumps (A and B), a guard column (G), an analytical column (C), and a



Switch Setting 1 (Off)



Switch Setting 2 (On)

Fig. 2. HPLC system used in this study, showing positions 1 (switch setting off) and 2 (switch setting on). I = Injector; A and B = HPLC pumps; G = guard column; C = analytical column; F = fluorescence detector; W = waste.

fluorescence detector (F) were connected through a column-switching device as shown in Fig. 2. The position of the column-switching device alternated between positions 1 and 2 and was controlled through the timed events option present in the HPLC pump controller. When the column-switching valve was set at position 1 (off position), the solvent from pump B flowed to waste (W) via the injector and guard column, whereas the solvent from pump A flowed through the analytical column and fluorometer to waste. When the valve was switched to position 2 (on position), the solvent from pump B flowed to waste via the injector only and the solvent from pump A flowed through the guard column, analytical column, and fluorimeter. In a typical chromatographic run, the column-

switching valve was initially set to position 1 (off) and the sample was injected onto the guard column. The column-switching valve remained in this position for 2.3 min and components which were not retained on the guard column were directed to waste. At the end of this period, the column-switching valve changed to position 2 (on) and remained at this position for 2 min, routing the effluent fraction containing the derivatized products of S and I.S. from the guard column to the analytical column for further chromatographic separation. At the end of the 2-min period (4.3 min post-injection), the column-switching valve was reset to position 1 and remained at this position until the next injection. During this time all the late-eluting components from the guard column were vented to waste. A typical chromatographic run was 40 min in duration.

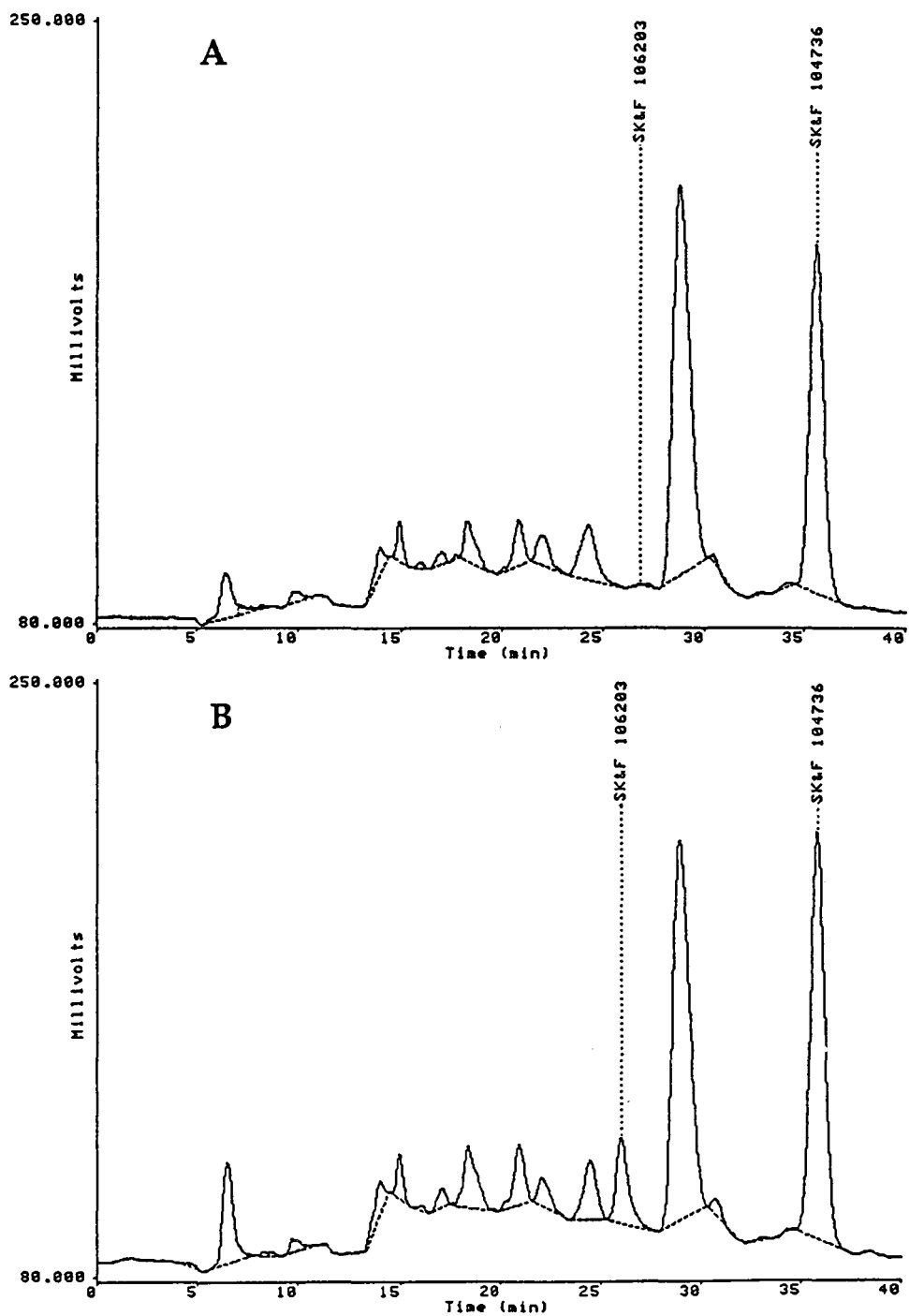


Fig. 3. Chromatograms of (A) drug-free human plasma and (B) plasma to which 100 ng/ml S was added.

TABLE I  
ACCURACY AND PRECISION DATA FOR SK&F 106203 IN HUMAN PLASMA

Sample (n = 5)	Day 1	Day 2	Day 3	Intra-day precision <sup>a</sup>	Inter-day precision <sup>b</sup>	Mean accuracy <sup>c</sup>
<i>20 ng/ml</i>				4.44	3.52	103.6
Mean	20.58 <sup>d</sup>	20.06	21.50			
S.D.	0.79	0.87	1.11			
C.V. (%)	3.84	4.33	5.16			
Accuracy (%)	102.9	100.3	107.5			
<i>200 ng/ml</i>				2.91	2.25	99.3
Mean	196.97	195.06	203.58			
S.D.	5.92	9.00	2.25			
C.V. (%)	3.01	4.61	1.11			
Accuracy (%)	98.5	97.5	101.8			
<i>2000 ng/ml</i>				1.84	3.18	97.1
Mean	2010.71	1921.98	1892.13			
S.D.	12.00	48.80	45.08			
C.V. (%)	0.60	2.54	2.38			
Accuracy (%)	100.5	96.1	94.6			

<sup>a</sup> Mean of the daily coefficients of variation.

<sup>b</sup> Coefficient of variation of the daily means.

<sup>c</sup> Mean of the daily accuracy calculations.

<sup>d</sup>  $n = 3$ .

#### Validation procedure

Three pools of plasma precision samples containing 20, 200, and 2000 ng/ml SK&F 106203 were prepared by adding appropriate volumes of standard solutions to drug-free plasma. Five replicate samples from each pool were extracted and ana-

lyzed on three separate days. Concentrations were determined by comparison with a calibration curve prepared on the day of analysis. From the data obtained, intra-day and inter-day precision and mean accuracy were calculated.

TABLE II  
BACK-CALCULATED STANDARD CURVE CONCENTRATIONS FOR SK&F 106203

Standard concentration (ng/ml)	Concentration (ng/ml)					C.V. (%)	Accuracy (%)
	Day 1	Day 2	Day 3	Mean ±	S.D.		
10	8.71	7.72	7.10	7.84	0.81	10.4	78.4
20	20.05	21.67	17.41	19.71	2.15	10.9	98.6
30	30.48	33.58	27.56	30.54	3.01	9.9	101.8
50	47.97	50.02	48.90	48.96	1.03	2.1	97.9
100	106.93	114.65	103.60	108.39	5.67	5.2	108.4
200	220.59	210.22	219.13	216.65	5.61	2.6	108.3
500	546.88	497.73	418.27	487.63	64.90	13.3	97.5
1000	1024.36	992.79	974.62	997.26	25.17	2.5	99.7
2000	2025.82	2096.63	2246.72	2123.06	112.80	5.3	106.2
5000	4888.54	4895.57	4894.86	4892.99	3.87	0.1	97.9

## RESULTS AND DISCUSSION

Several features of this method were designed to overcome problems encountered with the use of ADAM as a fluorimetric derivatizing agent for carboxylic acids. The instability and decomposition of ADAM during storage, which lead to potential interferences, were circumvented by generating ADAM from the corresponding hydrazone just prior to derivatization. The hydrazone intermediate was stable to storage and was conveniently converted to ADAM via a one-step reaction. Immediate preparation of ADAM not only eliminated the need to store ADAM but also produced reproducible yields of the ester product with fewer interfering degradation products. The reproducibility of the reaction was determined by derivatizing six replicate plasma extracts containing 200 ng/ml each of S and I.S. and measuring the peak heights of the corresponding diester derivatives. The reaction displayed excellent reproducibility, yielding coefficients of variation (C.V.) of 9.0 and 8.6% for S and I.S., respectively. Use of an automated column-switching device also helped to eliminate interfering peaks from the chromatograms, which were related to both reagent impurities and interferences resulting from derivatized endogenous components. Consequently, the overall sensitivity of the method was improved.

Since S was a dicarboxylic acid, reaction with ADAM could possibly yield three fluorescent products, two mono-derivatives and one di-derivative. Chromatographic analysis of the crude reaction mixture, resulting from the reaction of radiolabelled S with ADAM, showed one major fluorescence peak and two very minor peaks related to the drug. Mass spectral analysis of the major fluorescent component indicated that this product corresponded to the di-derivative of S. S was quantified following derivatization with ADAM and chromatographic analysis by monitoring the fluorescent signal resulting from this di-derivative.

The fluorescence HPLC assay described here for the analysis of S involved hexane–ethyl acetate extraction of drug and the I.S. from acidified plasma prior to derivatization with ADAM. Preliminary extraction of plasma with hexane before acidification and final extraction of drug with hexane–ethyl acetate were necessary to remove several neutral

lipids that affected both derivatization and chromatography. Solid-phase extraction of S from plasma was also investigated, however, higher recovery of S and I.S. with fewer endogenous peaks was observed with the liquid–liquid extraction method. Direct analysis of plasma extracts, after reaction with ADAM, precluded quantitation of S below 1  $\mu\text{g}/\text{ml}$  of plasma due to impurities present in the reagent and interferences resulting from the reaction of ADAM with endogenous components. Solid-phase extraction of the reaction mixture prior to chromatographic analysis eliminated most of the interfering peaks from the chromatogram, but failed to completely eliminate many other minor interfering components. In order to facilitate quantification of S at low nanogram levels, a column-switching system was incorporated. The partially purified derivatized plasma extract was first injected onto a short silica column, which was connected to an analytical column through the column-switching device. After sending the early-eluting interferences to waste, the short column was connected in-line with the analytical column, and derivatized S and I.S. were transferred to the analytical column, for further chromatographic separation.

*Sensitivity, linearity, and selectivity*

Typical chromatograms of plasma extracts obtained from drug-free human plasma and plasma to which S was added at a concentration of 100 ng/ml are shown in Fig. 3. Endogenous plasma components did not interfere with the quantification of the drug or the I.S. over the concentration range described here. The limit of quantification for S in human plasma was 20 ng/ml, using a 0.25-ml plasma sample. Linear response in the peak-height ratio of S to the I.S. was observed with concentrations of analyte ranging from 10 to 5000 ng/ml. Weighted (1/y) linear regression analysis of calibration lines provided the equation  $y = 0.001983x + 0.010401$  and a correlation coefficient greater than 0.998.

*Accuracy and precision*

Results of a three-day validation study are displayed in Table I. At plasma concentrations of S of 20, 200, and 2000 ng/ml, the intra-day precision of the method, as indicated by the mean of the daily C.V.s, was found to be 4.44, 2.91 and 1.84%, respectively. The inter-day precision, as indicated by

the C.V. of the daily means, was 3.52, 2.25, and 3.18% at concentrations of 20, 200, and 2000 ng/ml, respectively. The accuracy of the method, determined from the percent ratio of actual to predicted concentrations, was found to be 103.6, 99.3, and 97.1% at concentrations of S of 20, 200, and 2000 ng/ml, respectively. The precision of the assay was further assessed through back-calculation of the standard curve concentrations. The results are shown in Table II.

#### *Recovery and stability*

The recovery of S from plasma was determined using radiolabelled compound, during the initial isolation of drug from plasma by liquid–liquid extraction. The recovery, based on the amount of radioactivity recovered in the organic phase following liquid–liquid extraction, was 84%. The recovery of S and I.S. in the final extract could not be determined due to a lack of authentic standards of the diester derivatives of S and I.S. Plasma samples were stable for at least four months at  $-80^{\circ}\text{C}$ . The derivatized extracts were stable for at least 48 h at room temperature.

The quantitative HPLC methodology described here provided for the sensitive and selective determination of S in human plasma, utilizing pre-column derivatization with ADAM and automated column switching. The limit of quantitation using

0.25 ml of plasma was 20 ng/ml. The HPLC method described here has comparable sensitivity to the gas chromatographic–mass spectrometric assay [10], which has been routinely used to quantitate S in various clinical samples, and can be used as an alternative to the instrumentally complex mass spectrometric method.

#### REFERENCES

- 1 D. W. P. Hay, R. M. Muccitelli, L. M. Vickery-Clark, L. S. Novak, R. R. Osborn, J. G. Gleason, L.-A. P. Yodis, C. M. Saverino, R. D. Eckardt, H. M. Sarau, M. A. Wasserman, T. J. Torphy and J. F. Newton, *Pulm. Pharm.*, 4 (1991) 177.
- 2 S. A. Barker, J. A. Monti, S. T. Christian, F. Benington and R. D. Morin, *Anal. Biochem.*, 107 (1980) 116–123.
- 3 T. Yoshida, A. Uetake, H. Yamaguchi, N. Nimura and T. Kinoshita, *Anal. Biochem.*, 173 (1988) 70–74.
- 4 N. Ichinose, K. Nakamura, C. Shimizu, H. Kurokura and K. Okamoto, *J. Chromatogr.*, 295 (1984) 463–469.
- 5 Y. Yamauchi, T. Tomita, M. Senda, A. Hirai, T. Terano, Y. Tamura and S. Yoshida, *J. Chromatogr.*, 357 (1986) 199–205.
- 6 G. M. Ghiggeri, G. Candiano, G. Delfino, C. Queirolo, F. Ginevri, F. Perfumo and R. Gusmano, *J. Chromatogr.*, 381 (1986) 411–418.
- 7 K. Wessel, V. Kaever and K. Resch, *J. Liq. Chromatogr.*, 11 (1988) 1273–1292.
- 8 G. Kargas, T. Rudy, T. Spennetta, K. Takayama, N. Querishi and E. Shrago, *J. Chromatogr.*, 526 (1990) 331–340.
- 9 T. Nakaya, T. Tomomoto and M. Imoto, *Bull. Chem. Soc. Jpn.*, 40 (1967) 691–692.
- 10 N. Moore, S. Yachetti, G. R. Rhodes and S. Yevlet, unpublished results, 1990.

# Determination of baicalin and puerarin in traditional Chinese medicinal preparations by high-performance liquid chromatography

Kuo-Ching Wen, Cheng-Yu Huang and Fen-Ling Lu

National Laboratories of Foods and Drugs, Department of Health, Executive Yuan, 161-2 Kuen-Yang Street, Nankang, Taipei (Taiwan)

---

## ABSTRACT

HPLC methods for the determination of baicalin in *Scutellariae Radix* and puerarin in *Puerariae Radix* were established for the quality control of Chinese medicinal preparations containing these drugs. Ethyl paraben and methyl paraben were used as the internal standards for baicalin and puerarin, respectively. The samples were separated on a Cosmosil 5C<sub>18</sub> column with 0.03% phosphoric acid–acetonitrile (79:21), 0.03% phosphoric acid–acetonitrile (87:13) and 2% acetic acid–methanol (79:21) as mobile phases at flow-rates of 1.0 ml/min. Very satisfactory and reproducible results were obtained within 25 min for baicalin and 50 min for puerarin. These methods were also applicable to other prescriptions containing *Scutellariae Radix* and *Puerariae Radix* such as Chair-Ger-Jie-Ji-Tang, Dang-Guei-Nian-Tong-Tang and San-Jong-Kuey-Jian-Tang.

---

## INTRODUCTION

Traditional Chinese medicines were used for thousands of years in China because of the advantages of low toxicity and rare complications. Nowadays, the concentrated herbal preparations are very popular in Taiwan for their convenience of use, but whether there is the same efficacy between the traditional preparation and the concentrated type is still very difficult to establish. There are many variants among Chinese herbs. Therefore, it is very important to establish simple, convenient and efficient methods for the qualification of Chinese herbs and quality control of concentrated herbal preparations.

In Japan, since 1985 the Ministry of Health and Welfare has required that all concentrated herbal preparations submitted for inspection and registration should include a content analysis with at least

two chemical components as markers [1]. In this study, we selected the preparations Chair-Ger-Jie-Ji-Tang, Dang-Guei-Nian-Tong-Tang and San-Jong-Kuey-Jian-Tang, which all contain *Scutellariae Radix* and *Puerariae Radix* in their prescriptions, and searched for the optimum conditions for the determination of baicalin (present in *Scutellariae Radix*) and puerarin (present in *Puerariae Radix*) in both standard decoction and commercially available concentrated herbal preparations. *Scutellariae Radix* is the root of *Scutellaria baicalensis* Georgi (Labiatae) and *Puerariae Radix* is the root of *Pueraria pseudohirsuta* Tang, et Wang. (Leguminosae). The structures of the two flavonoids are shown in Fig. 1.

Although a number of high-performance liquid chromatographic (HPLC) methods for the determination of *Scutellariae Radix* [2–7] and *Puerariae Radix* [8–11] have been reported, only two reports concerning the determination of baicalin or puerarin in preparations have been published [12–13]. In this study, we have developed rapid and simple HPLC methods for the determination of baicalin

---

Correspondence to: K.-C. Wen, National Laboratories of Foods and Drugs, Department of Health, Executive Yuan, 161-2 Kuen-Yang Street, Nankang, Taipei, Taiwan.



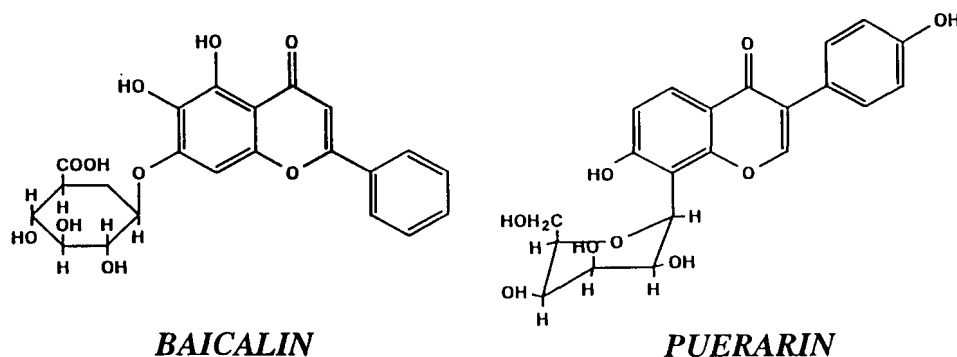


Fig. 1. Structures of the two marker components.

and puerarin that should be suitable for the routine quantitative analysis of concentrated herbal preparations and might also be applicable to some other preparations containing *Scutellariae Radix* and *Puerariae Radix*.

#### EXPERIMENTAL

##### Materials

According to the literature [14], the following materials listed are used to prepare each prescription: Chair-Ger-Jie-Ji-Tang: *Bupleuri Radix* 4.0 g, *Puerariae Radix* 4.0 g, *Notopterygii Rhizoma* 2.0 g, *Angelicae Radix* 2.0 g, *Scutellariae Radix* 3.0 g, *Paeoniae Radix* 3.0 g, *Platycodi Radix* 2.0 g, *Gypsum Fibrosum* 5.0 g, *Glycyrrhizae Radix* 2.0 g and *Zingiberis Rhizoma* 1.0 g; Dang-Guei-Nian-Tong-Tang: *Angelicae Sinensis Radix* 2.5 g, *Anemarrhena Rhizoma* 2.5 g, *Notopterygii Rhizoma* 2.5 g, *Artemisiae Capillaris Herba* 2.5 g, *Scutellariae Radix* 2.5 g, *Atractylodis Macrocephalae Rhizoma* 2.5 g, *Polyporus* 2.5 g, *Alismatis Rhizoma* 2.5 g, *Atractylodis Rhizoma* 2.0 g, *Ledebouriellae Radix* 2.0 g, *Puerariae Radix* 2.0 g, *Ginseng Radix* 2.0 g, *Sophorae Radix* 1.0 g, *Cimicifugae Rhizoma* 1.0 g and *Glycyrrhizae Radix* 1.0 g; and San-Jong-Kuey-Jian-Tang: *Angelicae Sinensis Radix* 1.5 g, *Paeoniae Radix* 1.5 g, *Bupleuri Radix* 1.5 g, *Scutellariae Radix* 1.5 g, *Coptidis Rhizoma* 1.5, *Forsythiae Fructus* 1.5 g, *Cortex Phellodendri* 1.5 g, *Anemarrhena Rhizoma* 1.5 g, *Trichosanthis Radix* 1.5 g, *Platycodi Radix* 1.5 g, *Gentianae Radix* 1.5 g, *Puerariae Radix* 1.5 g, *Scirpi Rhizoma* 1.5 g, *Zedoariae*

*Rhizoma* 1.5 g, *Laminariae Thallus* 1.5 g, *Sargassi Thallus* 1.5 g, *Cimicifugae Rhizoma* 1.5 g, *Zingiberis Rhizoma* 1.5 g and *Glycyrrhizae Radix* 1.5 g.

For the concentrated herbal preparations, samples were obtained from three different manufacturers.

##### Chemicals and reagents

Reference standards of baicalin and puerarin were purchased from Nacalai Tesque (Kyoto, Japan). The internal standards ethyl paraben and methylparaben were obtained from Sigma (St. Louis, MO, USA).

All solvents used were of HPLC grade.

##### Liquid chromatography

The HPLC system was equipped with a Holo-chrome variable-wavelength UV detector (Gilson). Peak areas were calculated with a Shiunn Haw computing integrator. A stainless-steel column (150 mm × 4 mm I.D.) packed with ODS chemically bonded silica gel (Cosmosil 5C<sub>18</sub>, 5 μm), (Nacalai Tesque) was used. The solvent systems were as follows: 0.03% phosphoric acid–acetonitrile (79:21) for baicalin in the three preparations; 0.03% phosphoric acid–acetonitrile (87:13) for puerarin in Chair-Ger-Jie-Ji-Tang and Dang-Guei-Nian-Tong-Tang and 2% acetic acid–methanol (79:21) for puerarin in San-Jong-Kuey-Jian-Tang. The analyses were carried out at a flow-rate of 1.0 ml/min, with UV detection at 270 nm for baicalin and 250 nm for puerarin. Pretreatment of the solvent with a solvent filter kit for degassing was carried out.

### Sample preparation for HPLC

**Calibration graphs.** Baicalin and puerarin were accurately weighed and dissolved in 70% methanol to give various concentrations within the ranges 0.0625–0.1000 and 0.00625–0.05000 mg/ml, respectively. An appropriate amount of internal standard was added to each solution to give concentrations of 1.0 mg/ml of ethyl paraben or 0.1 mg/ml of methyl paraben. Calibration graphs were plotted based on linear regression analysis of the peak-area ratios with concentration.

**Standard decoction.** Amounts of crude drug equivalent to a daily dose of each preparation were weighed and pulverized, a twentyfold mass of water was added and the mixture was boiled for more than 30 min to halve the original volume. After filtration, the filtrate was diluted with methanol to give a 70% methanol solution and a suitable amount of internal standard was then added to the solution to give concentrations of 1.0 mg/ml of ethyl paraben or 0.1 mg/ml of methyl paraben.

**Concentrated herbal preparations.** Samples of about 1.0 g of each concentrated herbal preparation obtained from three different factories were weighed accurately and extracted with 70% methanol (25 ml) for 30 min by using an ultrasonic bath. After extraction, the samples were filtered and diluted to 25 ml with the addition of internal standard to give concentrations of 1.0 mg/ml of ethyl paraben or 0.1 mg/ml of methyl paraben.

## RESULTS AND DISCUSSION

### HPLC conditions

Baicalin and puerarin are bioactive components and have been determined previously using reversed-phase systems [2–10, 12–13], so we chose an ODS column with 0.03% phosphoric acid–acetonitrile (79:21), 0.03% phosphoric acid–acetonitrile (87:13) or 2% acetic acid–methanol (79–21) as mobile phases for baicalin or puerarin in three preparations.

The peak purities of these two components were tested at two or three wavelengths. Baicalin was detected at 254, 270 and 280 nm and puerarin at 242 nm and 250 nm; no interferences were found.

For the selection of internal standards, we tried many compounds with structures similar to that of the marker, but many overlapped with other com-

ponents in the preparations or the retention times were too long. Finally, methyl paraben was used as the internal standard for puerarin and ethyl paraben for baicalin, because these two compounds could be well resolved from other components in the complex preparations and their retention times are reasonable for routine analysis.

Calibration graphs for baicalin and puerarin were obtained for the ranges of 0.0625–0.1000 and 0.00625–0.05000 mg/ml, respectively. The regression equations were  $y = 1.234 - 0.161 x$  ( $r = 0.9994$ ) for baicalin,  $y = 0.336 - 0.0046 x$  ( $r = 0.9998$ ) for puerarin in Chair-Ger-Jie-Ji-Tang and Dang-Guei-Nian-Tong-Tang and  $y = 0.443 - 0.00025 x$  ( $r = 0.9997$ ) for puerarin in San-Jong-Kuey-Jian-Tang, where  $y$  is the peak-area ratio of the marker to the internal standard and  $x$  is the concentration of the marker.

### Sample preparation

Traditional Chinese medicines are usually prepared by boiling with water. However, extraction of concentrated preparations with water may lead to difficult filtration, so 70% methanol was employed as the extraction solvent for concentrated herbal preparations in routine work.

The components of Chinese herbal preparation are very complex. In this study, blank solutions without *Scutellariae Radix* or *Puerariae Radix* were prepared and analysed, to monitor the absence of interference of other crude drugs with the marker component. The comparison of the chromatograms of baicalin and its blank solutions of three preparations (Figs. 2–4) shows that satisfactory separations were obtained. Figs. 5–7 show the analysis of puerarin and its blank solutions of three preparations. Two different mobile phase systems were used for the determination of puerarin; indeed, these preparations cannot be measured with the same mobile phase because some interferences in three blank solutions at the retention time of puerarin were detected.

### Determination of baicalin and puerarin

The markers used for the quality control of concentrated herbal preparations from crude drugs to the concentrated type should satisfy some characteristics: (1) soluble in water; (2) stable; (3) not destroyed by boiling; and (4) non-volatile. In this

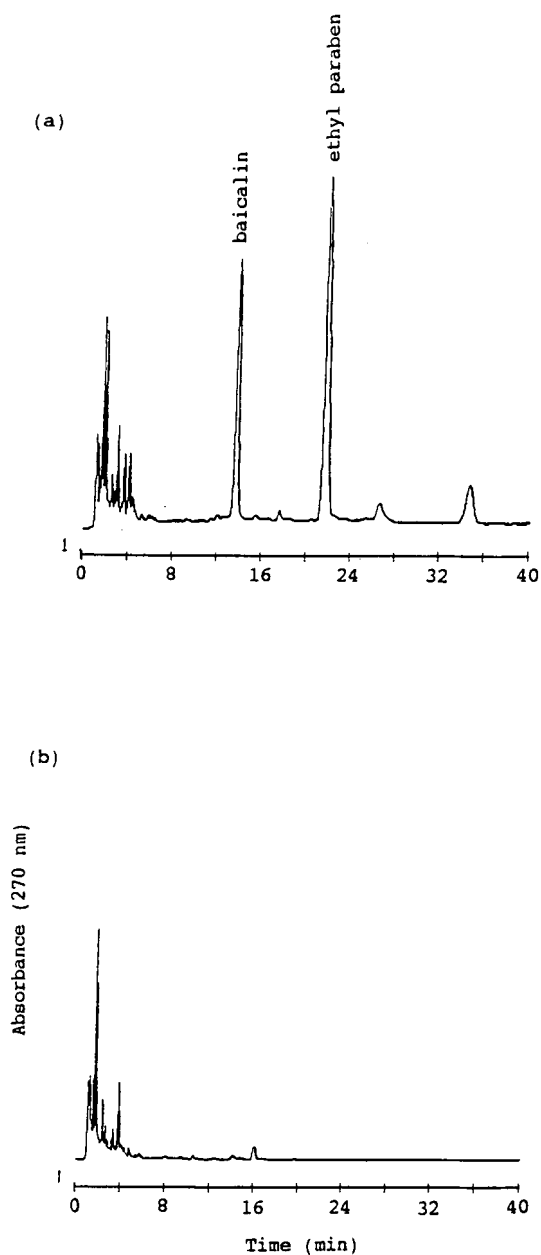


Fig. 2. Chromatogram of baicalin in Chair-Ger-Jie-Ji-Tang and its blank solution. Column, Cosmosil 5C<sub>18</sub> (5  $\mu$ m) (150  $\times$  4 mm I.D.); mobile phase, 0.03% phosphoric acid-acetonitrile (79:21); flow-rate, 1.0 ml/min. (a) Standard decoction; (b) standard decoction without Scutellariae Radix.

work we chose baicalin and puerarin as markers they both satisfy these characteristics and both have been used previously as marker components [1,15].

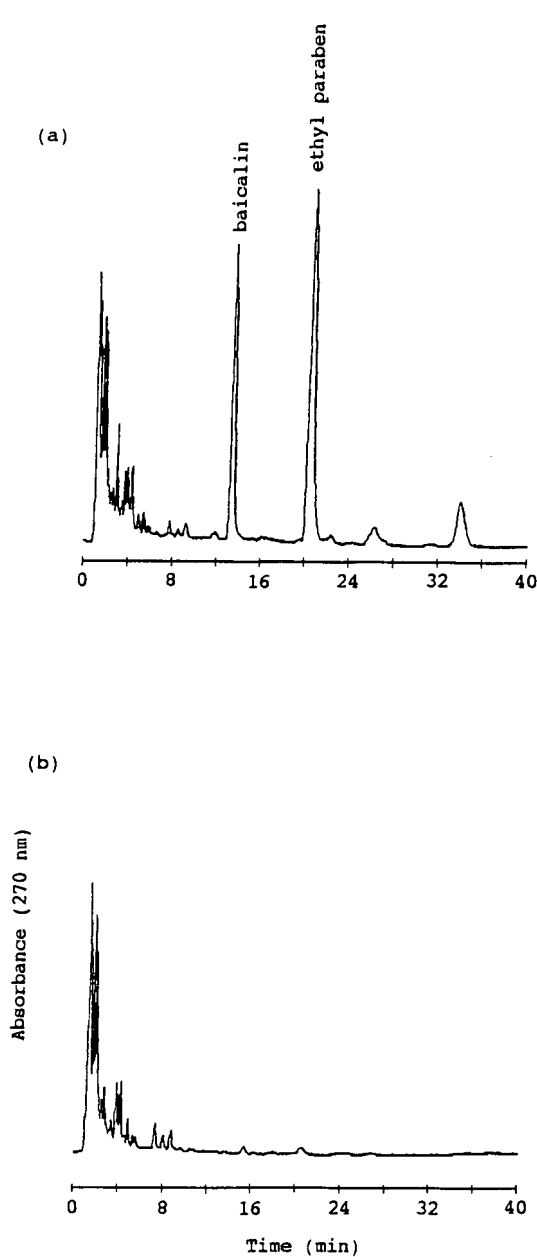


Fig. 3. Chromatogram of baicalin in Dang-Guei-Nian-Tong-Tang and its blank solution. Conditions as in Fig. 2. (a) Standard decoction; (b) standard decoction without Scutellariae Radix.

The quantitative results for the standard decoctions prepared in our laboratory and the purchased concentrated herbal preparations are given in Ta-

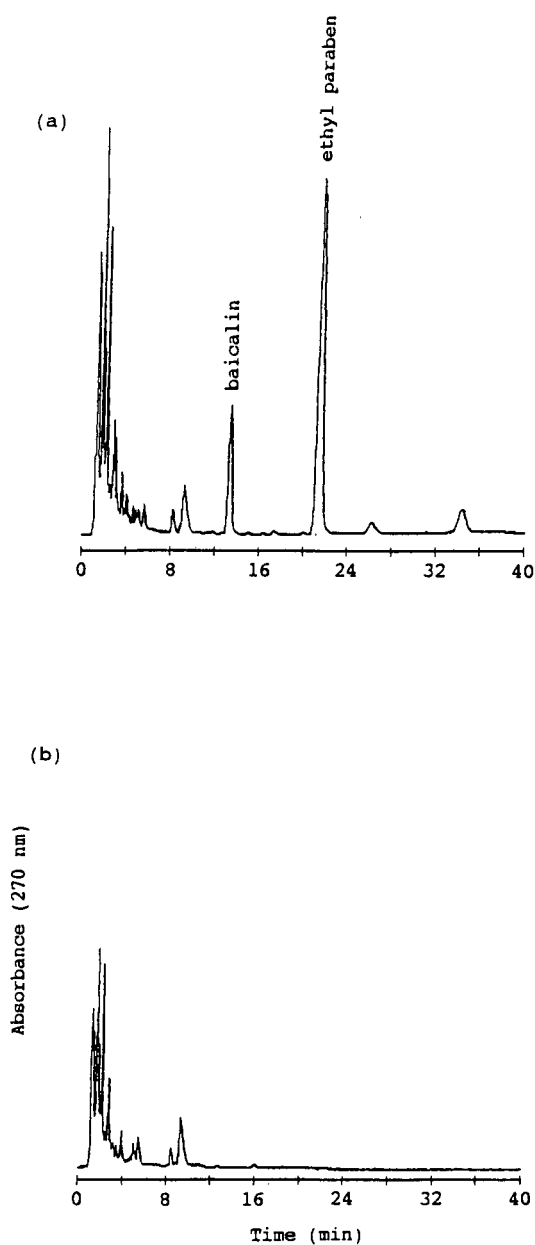


Fig. 4. Chromatogram of baicalin in San-Jong-Kuey-Jian-Tang and its blank solution. Conditions as in Fig. 2. (a) Standard decoction; (b) standard decoction without *Scutellariae Radix*.

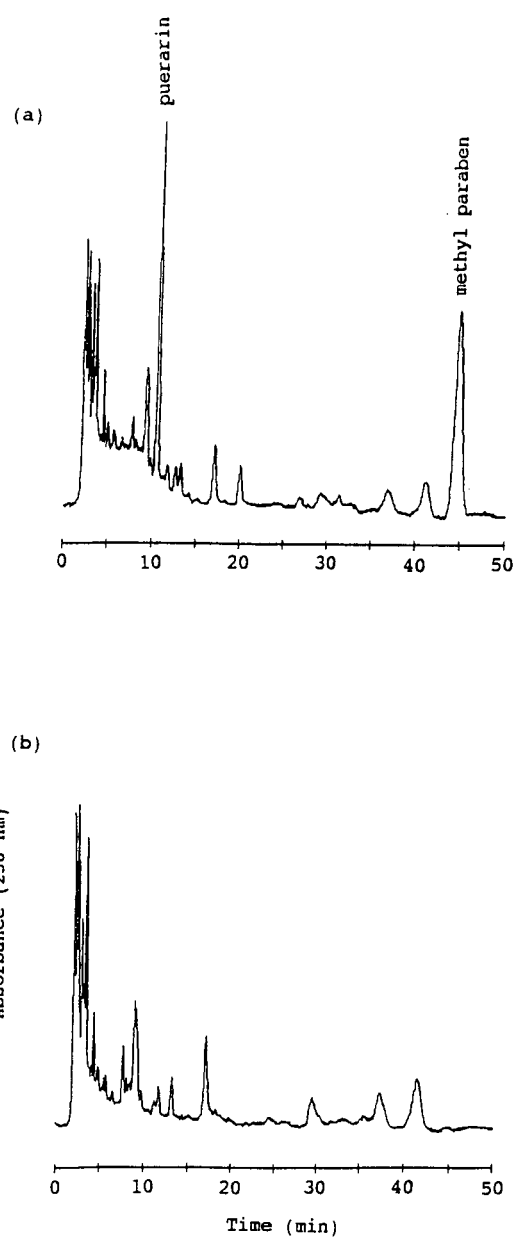


Fig. 5. Chromatogram of puerarin in Chair-Ger-Jic-Ji-Tang and its blank solution. Mobile phase, 0.03% phosphoric acid–acetonitrile (87:13); other conditions as in Fig. 2. (a) Standard decoction; (b) standard decoction without *Puerariae Radix*.

bles I–III. The daily dose was used for calculating the contents of the marker components in order to compare the products from different manufacturers.

The contents of the marker components in the standard decoctions were found to be much higher than those in concentrated herbal preparations, and there were differences among the products from dif-

CONTENTS OF MARKER COMPONENTS IN STANDARD DECOCTION AND CONCENTRATED HERBAL PREPARATIONS OF CHAIR-GER-JIE-JI-TANG

Sample <sup>a</sup>	Crude drug	Content of crude drug in a daily dose in preparation (g/g)	Marker component	Content of marker component		Marker component in crude drug (mg/g)
				in prescription mg/g	mg/day	
Standard decoction	Scutellariae Radix	3.0/30	Baicalin	3.21	96.24	30.08
	Puerariae Radix	4.0/30	Puerarin	0.18	5.32	1.33
Concentrated herbal preparation A	Scutellariae Radix	2.4/6	Baicalin	3.02	18.11	7.55
	Puerariae Radix	2.4/6	Puerarin	1.20	7.22	0.46
Concentrated herbal preparation B	Scutellariae Radix	2.5/6	Baicalin	5.14	30.81	12.32
	Puerariae Radix	2.0/6	Puerarin	0.31	1.84	0.77
Concentrated herbal preparation C	Scutellariae Radix	2.0/6	Baicalin	2.13	12.79	6.39
	Puerariae Radix	2.0/6	Puerarin	0.09	0.54	0.27

<sup>a</sup> A, B, C = concentrated herbal preparations from three different manufactures.

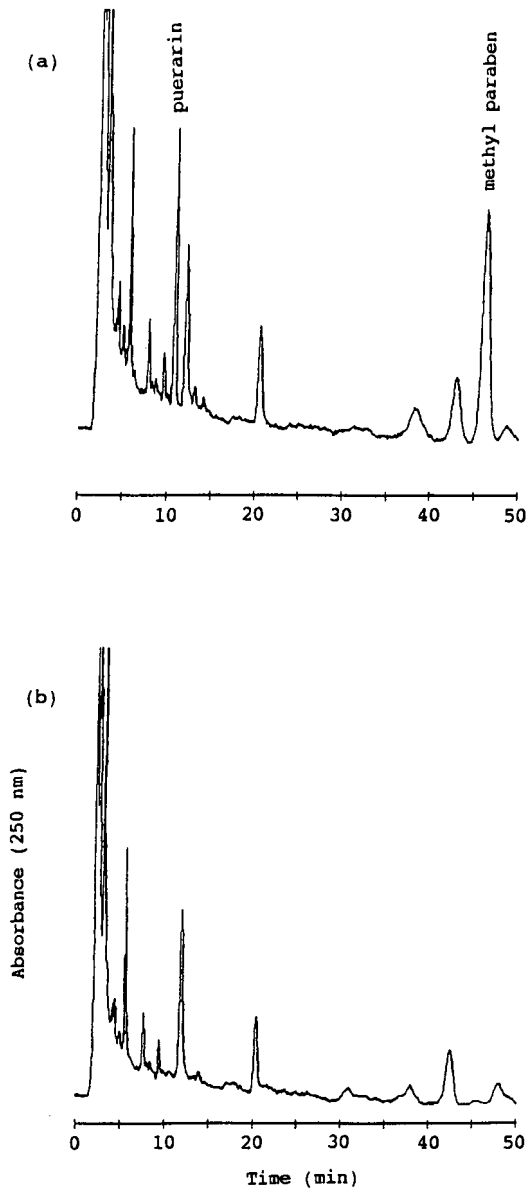


Fig. 6. Chromatogram of puerarin in Dang-Guei-Nian-Tong-Tang and its blank solution. Conditions as in Fig. 5. (a) Standard decoction; (b) standard decoction without Puerariae Radix.

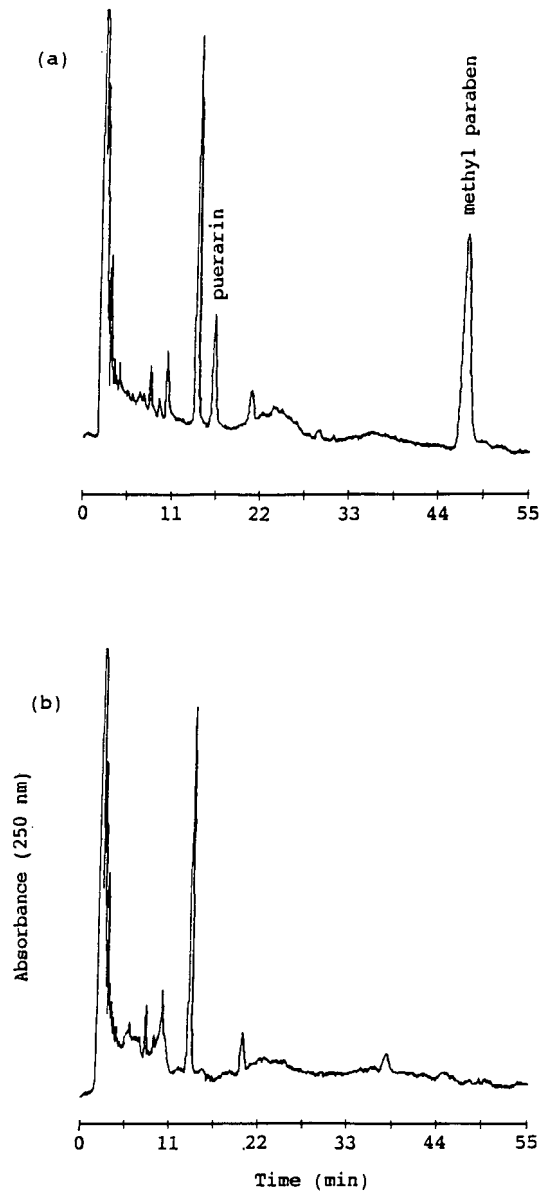


Fig. 7. Chromatogram of puerarin in San-Jong-Kuey-Jian-Tang and its blank solution. Mobile phase, 2% acetic acid-methanol (79:21); other conditions as in Fig. 1. (a) Standard decoction; (b) standard decoction without Puerariae Radix.

ferent companies. The standard decoctions were prepared by boiling with water and then filtering; the concentrated herbal preparations, in addition to boiling with water and filtering, were further con-

centrated and dried. Whether these latter processes affected the constitution of the products needs further investigation.

TABLE II  
 CONTENTS OF MARKER COMPONENTS IN STANDARD DECOCTION AND CONCENTRATED HERBAL PREPARATIONS OF DANG-GUEI-NIAN-TONG-TANG

Sample <sup>a</sup>	Crude drug	Content of crude drug in a daily dose in preparation (g/g)	Marker component	Content of marker component		Marker component in crude drug (mg/g)
				in prescription	mg/day	
Standard decoction	Scutellariae Radix	2.5/31	Baicalin	2.10	65.13	26.05
	Puerariae Radix	2.0/31	Puerarin	0.10	3.02	1.51
Concentrated herbal preparation A	Scutellariae Radix	1.0/6	Baicalin	0.23	1.37	1.37
	Puerariae Radix	0.5/6	Puerarin	0.08	0.49	0.97
Concentrated herbal preparation B	Scutellariae Radix	1.25/6	Baicalin	4.76	28.55	22.84
	Puerariae Radix	0.75/6	Puerarin	0.19	1.16	1.55
Concentrated herbal preparation C	Scutellariae Radix	2.5/6	Baicalin	3.86	23.15	9.26
	Puerariae Radix	1.0/6	Puerarin	0.07	0.39	0.39

<sup>a</sup> A, B, C = concentrated herbal preparations from three different manufacturers.

TABLE III  
 CONTENTS OF MARKER COMPONENTS IN STANDARD DECOCTION AND CONCENTRATED HERBAL PREPARATIONS OF SAN-JONG-KUEY-JIAN-TANG

Sample <sup>a</sup>	Crude drug	Content of crude drug in a daily dose in preparation (g/g)	Marker component	Content of marker component in prescription		Marker component in crude drug (mg/g)
				mg/g	mg/day	
Standard decoction	Scutellariae Radix	1.5/28.5	Baicalin	1.39	39.56	26.37
	Puerariae Radix	1.5/28.5	Puerarin	0.09	2.49	1.66
Concentrated herbal preparation A	Scutellariae Radix	1.5/6	Baicalin	0.92	5.53	3.68
	Puerariae Radix	0.5/6	Puerarin	0.11	0.66	1.32
Concentrated herbal preparation B	Scutellariae Radix	1.5/6	Baicalin	0.85	5.11	3.40
	Puerariae Radix	1.5/6	Puerarin	0.09	0.51	0.34
Concentrated herbal preparation C	Scutellariae Radix	2.4/6	Baicalin	0.56	3.34	1.39
	Puerariae Radix	0.6/6	Puerarin	0.03	0.20	0.33

<sup>a</sup> A, B, C = concentrated herbal preparations from three different manufacturers.



## CONCLUSIONS

The proposed HPLC method is applicable to the quality control of concentrated herbal preparations containing *Scutellariae Radix* and *Puerariae Radix*. The advantages of the systems developed in this study are following: (1) the mobile phases are easy to prepare; (2) the isocratic elution requires simple equipment; (3) no pretreatment is required; and (4) quantification is effected with an internal standard. Therefore, these methods are simple, rapid and expedient for the routine quality control of Chinese herbal preparations.

## REFERENCES

- 1 M. Harada, Y. Ogihara, Y. Kano, A. Akahori, Y. Ichio, O. Hiura and H. Suzuki, *Iyakuhin Kenkyu*, 19 (1988) 852.
- 2 T. Tani, T. Katsushiro, M. Higashino, M. Kubo and S. Arich, *10th Symposium on Analysis of Crude Drugs, Kobe, Japan, July 13, 1981*, Abstracts, p. 1.
- 3 Y. Saito, M. Shiragami and E. Yumioka, *11th Symposium on Analysis of Crude Drugs, Kobe, Japan, August 6, 1982*, Abstracts, p. 42.
- 4 T. Tomimori, H. Jin, Y. Miyaichi, S. Toyofuku and T. Namba, *Yakugaku Zasshi*, 105 (1985) 148.
- 5 K. Sagara, Y. Ito, T. Oshima, T. Misaki and H. Murayama, *J. Chromatogr.*, 328 (1985) 289.
- 6 T. Tomimori, Y. Miyaichi, H. Jin, S. Toyofuku and M. Yamamoto, *Shoyakugaku Zasshi*, 40 (1986) 381.
- 7 Y. Takino, T. Miyahara, E. Arichi, S. Arichi, T. Hayashi and M. Karikura, *Chem. Pharm. Bull.*, 35 (1987) 3494.
- 8 Y. Akada, S. Kawano and M. Yamagishi, *Yakugaku Zasshi*, 100 (1980) 1057.
- 9 H. Kaizuka and K. Takahashi, *J. Chromatogr.*, 258 (1983) 135.
- 10 Y. Kitada, M. Mizobuchi and Y. Ueda, *J. Chromatogr.*, 347 (1985) 438.
- 11 Y. Ohshima, T. Okuyama, K. Takahashi, T. Takizawa and S. Shibata, *Planta Med.*, 54 (1988) 250.
- 12 K. Sagara, Y. Ito, T. Oshima, H. Murayama and H. Itokawa, *Shoyakugaku Zasshi*, 40 (1986) 84.
- 13 J. Hayakawa, N. Noda, S. Yamada and K. Uno, *Yakugaku Zasshi*, 104 (1984) 50.
- 14 H. Y. Hsu and C. S. Hsu, *Commonly Used Chinese Herb Formulas with Illustrations*, Oriental Healing Arts Institute, Taiwan, 1980.
- 15 M. Harada, Y. Ogihara, Y. Kano, A. Akahori, Y. Ichio, O. Miura, K. Yamamoto and H. Suzuki, *Iyakuhin Kenkyu*, 20 (1989) 1300.

# Normal-phase high-performance liquid chromatographic determination of epristeride, a prostatic steroid $5\alpha$ -reductase enzyme inhibitor, in human plasma

Venkata K. Boppana, Cynthia Miller-Stein and Gerald R. Rhodes

Department of Drug Metabolism and Pharmacokinetics, SmithKline Beecham Pharmaceuticals, P.O. Box 1539, Mail Code L-712, King of Prussia, PA 19406 (USA)

## ABSTRACT

An highly sensitive and selective high-performance liquid chromatographic method was developed for the determination of epristeride [17  $\beta$ -(*N*-*tert*-butyl carboxamido)-androst-3,5-diene-3-carboxylic acid, SK&F 105657], a potent inhibitor of the prostatic steroid  $5\alpha$ -reductase enzyme, in human plasma samples. Epristeride is currently in development for the treatment of benign prostatic hyperplasia. The analytical method involves isolation of epristeride and the internal standard [17  $\beta$ -(*N*,*N*-diisopropyl carboxamido) estra-1,3,5(10)-triene-3-carboxylic acid, SK&F 105419] from plasma by solid-phase extraction prior to chromatographic separation on an aminopropyl silica column, using hexane–methylene chloride–2-propanol–acetic acid as the mobile phase, with subsequent ultraviolet absorption detection. The absolute recovery of epristeride from plasma was  $90.2 \pm 2.96$ . The limit of quantification for epristeride was 2.5 ng/ml. Linear response was observed for concentrations of epristeride ranging from 1 to 500 ng/ml plasma. The assay was sufficiently sensitive, accurate and precise to support pharmacokinetic studies in human subjects.

## INTRODUCTION

Epristeride (17  $\beta$ -(*N*-*tert*-butylcarboxamido)-androst-3,5-diene-3-carboxylic acid, SK&F 105657, Fig. 1) is a potent and selective inhibitor of the prostatic steroid  $5\alpha$ -reductase enzyme, which converts testosterone to dihydrotestosterone (DHT) [1–3]. This steroid analogue is currently under development for the treatment of benign prostatic hyperplasia (BPH).

This report describes a sensitive and specific HPLC method for the determination of epristeride in human plasma samples. The approach involves isolation of the steroid analogue from plasma by solid-phase extraction followed by quantitative normal-phase chromatographic analysis with ultraviolet absorbance (UV) detection.

Correspondence to: V. K. Boppana, Department of Drug Metabolism and Pharmacokinetics, SmithKline Beecham Pharmaceuticals, P.O. Box 1539, Mail Code L-712 King of Prussia, PA 19406, USA.

## MATERIALS AND METHODS

### Chemicals

Epristeride (free acid, SK&F 105657, Fig. 1) and the internal standard (17  $\beta$ -(*N*,*N*-diisopropyl carboxamido) estra-1,3,5(10)-triene-3-carboxylic acid, SK&F 105419, free acid, I.S.), were supplied by Drug Substances and Products, SmithKline Beecham Pharmaceuticals (Swedeland, PA, USA). Glacial acetic acid was obtained from Mallinckrodt (Paris, KY, USA). Monobasic potassium phosphate, dibasic potassium phosphate, HPLC-grade methanol, hexane, 2-propanol and methylene chloride were obtained from J. T. Baker (Phillipsburg, NJ, USA). Octadecylsilica ( $C_{18}$ ) solid-phase extraction cartridges (100 mg, 1 ml) and the Vac-Elut manifold were purchased from Analytichem International (Harbor City, CA, USA).

### Standard solutions and reagents

The stock standard solutions of epristeride and

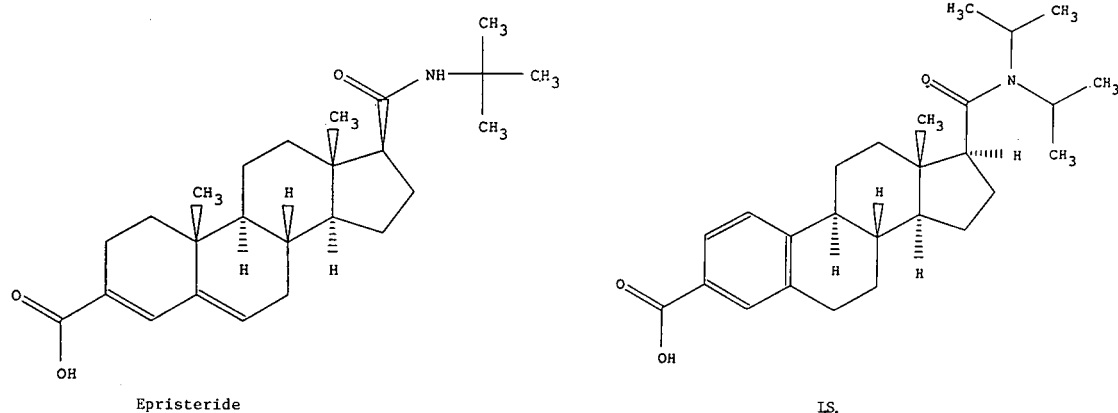


Fig. 1. Structures of epristeride and I.S.

the internal standard were prepared by dissolving 10 mg of the free acid in methanol in a 10-ml volumetric flask to give a final solution concentration of 1 mg/ml. Appropriate dilutions of the stock solution of epristeride were made with 50% aqueous methanol to generate a series of working standard solutions (100, 10, 1 and 0.1  $\mu\text{g/ml}$ ). All stock and working standard solutions were stable for 4 months when stored at 4°C. The stock solution of I.S. was diluted 1:50 with 50% aqueous methanol solution to give a solution concentration of 20  $\mu\text{g/ml}$ . The solution was stable for 2 months when stored at 4°C.

#### Calibration

A set of plasma calibration standards (concentrations of epristeride; 0, 1, 2, 5, 10, 20, 50, 100, 200, 500 ng/ml) was analyzed with every determination of epristeride in plasma samples of unknown concentration, by adding appropriate volumes of the working standards of epristeride to 1.0 ml of heparinized plasma. The standard curve was established by weighted linear least-squares regression [weighting factor =  $1/y$ ; due to the large difference between low and high concentrations of the analyte, the peak-height ratios ( $y$ ) were weighted in order to get better estimates of analyte ( $x$ ) concentrations] of the measured peak-height ratios of epristeride to internal standard *versus* the concentration of epristeride added to the plasma. Epristeride concentrations in unknown plasma samples were calculated from the following regression equation:

$$\text{Concentration of epristeride } (x) = (y - a)/b$$

where,  $b$  = slope of the regression line,  $a$  =  $y$ -intercept of regression line and  $y$  = peak-height ratio of epristeride to internal standard. The linear regression analysis was performed with a FIT FUNCTION program of RS/1 software (version 4.3.1, BBN Research Systems, Cambridge, MA, USA). In FIT FUNCTION, the fitting is done in a series of iterations, in which the parameters are systematically adjusted by the Marquardt–Levenberg method until a least-squares solution is reached. The FIT FUNCTION program, besides generating The Equation Of The Best Fit, also compute Goodness-Of-Fit Statistics and generate ANOVA table calculating correlation coefficient ( $r^2$ ) and standard deviation of the regression and also calculates the 95% confidence intervals for the standard curve.

#### Mobile phase

Hexane–methylene chloride–2-propanol–glacial acetic acid (410:50:40:1, v/v) is used as mobile phase.

#### Extraction of epristeride from plasma

The  $C_{18}$  extraction column was conditioned by successive washings with 1 ml of methanol and 1 ml of water. An aliquot of plasma (1 ml) containing 50  $\mu\text{l}$  of 50% aqueous methanol (contains standards when preparing standard curve), 50  $\mu\text{l}$  of internal standard solution (20  $\mu\text{g/ml}$ , I.S.) and 500  $\mu\text{l}$  of 0.5 M phosphate buffer, pH 8.0, were mixed in a 75  $\times$

12 mm borosilicate tube. The sample was then poured onto the C<sub>18</sub> column and vacuum was applied. The column was washed successively with 3 ml water, 1 ml of 20% (v/v) aqueous methanol and 1 ml of hexane. The column was then eluted with 1 ml of mobile phase eluent and the eluate was collected into a 75 × 12 mm borosilicate tube. The eluate was evaporated under a gentle stream of nitrogen at 40°C and the residue was reconstituted in 200 µl of mobile phase and transferred to an autosampler vial. 10–75 µl were injected into the HPLC system for analysis.

#### *High-performance liquid chromatography*

The isocratic HPLC system consisted of a Beckman pump (Model 116, Beckman, Palo Alto, CA, USA) and an ultraviolet absorbance detector (Model 783, ABI, Ramsey, NJ, USA). Chromatographic separations were carried out on a 22 cm × 2.1 mm I.D. amino-propyl silica column (Pierce, Rockford, IL, USA) connected in-line to a 3 cm × 2.1 mm I.D. amino-propyl silica guard column. The column was maintained at room temperature and the mobile phase eluent, hexane–methylene chloride–2-propanol–glacial acetic acid (409:50:40:1, v/v), was pumped at a flow-rate of 300 µl/min. The mobile phase was filtered through a 0.2-µm nylon-66 filter and degassed before use. UV detection was accomplished at 274 nm. Samples were injected using an HPLC autosampler (WISP model 710B, Waters, Milford, MA, USA). The chromatographic data were collected with an automated laboratory system (Nelson, Cupertino, CA, USA).

#### *Validation procedures*

Four pools of plasma precision samples containing 2.5, 25, 250 and 450 ng/ml of epristeride were prepared by adding appropriate volumes of standard solutions to drug-free heparinized plasma. These plasma samples were stored at –20°C until analysis was performed. Five replicate samples from each pool were extracted and analyzed on three separate days. Concentrations were determined by comparison with a calibration curve prepared on the day of analysis. From the data obtained, intra-day precision (determined as the mean of the daily relative standard derivations, R.S.D.s), inter-day precision (determined as the R.S.D. of the daily means) and mean accuracy were calculated.

## RESULTS AND DISCUSSION

The assay described here for the analysis of epristeride involves solid-phase extraction of the steroid from plasma as a preliminary isolation step, followed by quantitative HPLC analysis with subsequent UV absorbance detection. The high extinction coefficient of the molecule (exceeding 20 000 at 274 nm) and the use of HPLC columns of reduced internal diameter (2 mm) provided enhanced sensitivity for epristeride in developing highly sensitive analytical methodology for this molecule. The specificity of the method was also attributable to reversed-phase solid-phase extraction of the steroid from plasma samples followed by normal-phase chromatographic analysis of the plasma extract on a amino-propyl silica column, using hexane–methylene chloride–2-propanol–acetic acid as the mobile phase. Use of four component mobile phase is necessary to resolve the analyte and internal standard peaks from the endogenous plasma peaks and to obtain sharper peaks.

#### *Recovery and stability*

The recovery of epristeride and the internal standard from plasma was estimated with five determinations by comparing the peak height obtained with processed samples to that obtained by direct injection of an amount of standard equivalent to 100% recovery. At 25 ng/ml, a mean plasma recovery of  $90.2 \pm 2.96\%$  was obtained for epristeride. In addition, epristeride and internal standard were found to be stable in the final extract at room temperature for at least 48 h.

#### *Sensitivity, selectivity and linearity*

By utilizing a 2.1 mm I.D. HPLC column, the on-column limit of detection of epristeride (signal-to-noise ratio 3) was 100 pg. Under the conditions used in this assay, the lowest concentration of epristeride that could be determined quantitatively in 1 ml of plasma samples was 2.5 ng. Calibration curves obtained were linear over the range of 1–500 ng/ml of epristeride. In this range, no interference either from endogenous substances or from the known metabolites of epristeride were observed. Weighted ( $1/y$ ) linear regression analysis of calibration curves provided the equation  $y = 0.03635x - 0.000307$  and a correlation coefficient greater than

TABLE I  
ACCURACY AND PRECISION DATA FOR EPRISTERIDE IN HUMAN PLASMA

Parameter	Concentrations in plasma (ng/ml)			
	2.5	25	250	450
R.S.D. (%)				
Day 1	6.0	1.8	1.7	3.3
Day 2	4.8	6.3	3.4	5.3
Day 3	8.2	1.0	1.1	3.9
Error (%) <sup>a</sup>				
Day 1	-14.0	-8.1	-0.2	-3.0
Day 2	-18.8	-7.5	-2.4	-1.9
Day 3	-11.2	-14.9	-6.0	-5.8
Inter-day R.S.D. <sup>b</sup>	4.5	4.4	3.0	2.1
Intra-day R.S.D. <sup>c</sup>	6.3	3.0	2.0	4.2
Mean accuracy (%)	85.3	89.5	97.2	96.4

<sup>a</sup> (Calculated concentration - actual concentration)/actual concentration × 100.

<sup>b</sup> Coefficients of variation of daily means.

<sup>c</sup> Mean of the daily R.S.D.s.

0.999. The calibration curves were highly reproducible and the precision, as measured by the R.S.D.s at each of the spiked concentrations, was within 17% across the calibration range. The accuracy, evaluated by the average concentration back-calculated from the composite standard curve, was within 10% of the seeded value at each concentration.

#### Accuracy and precision

Table I summarizes the results obtained from a three-day validation study in which five replicate-seeded standards at four concentrations, 2.5, 25, 250 and 450 ng/ml, were analyzed each day by this methodology. The mean accuracy of the assay at these concentrations ranged from 85.3 to 97.2%, whereas the intra-day precision, indicated by the mean of the daily R.S.D.s, varied from 2.0 to 6.3%. The reproducibility of the assay was high with inter-day precision, indicated by the R.S.D.s of the daily means, ranging from 2.1 to 4.4%. Similar accuracy and precision results were obtained when the assay

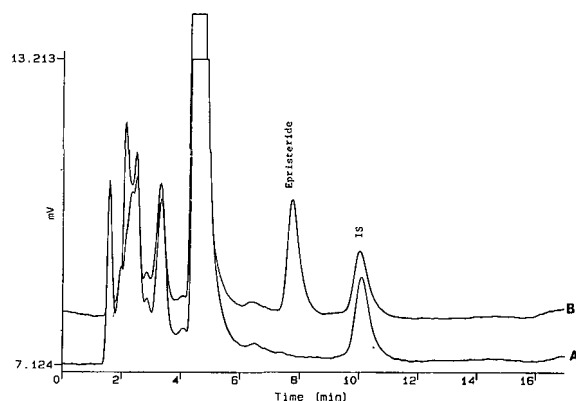


Fig. 2. Chromatograms of plasma extracts from blank human plasma with (A) I.S. and (B) plasma sample spiked with 20 ng/ml of epristeride.

was revalidated with smaller volume of plasma (200  $\mu$ l), but with a proportional drop in sensitivity.

#### Application of the procedure to plasma samples

The quantitative HPLC methodology described here provided for selective and sensitive detection of epristeride in human plasma samples. A typical chromatogram of a plasma extract obtained from drug-free plasma and a plasma sample spiked with 20 ng/ml of epristeride is shown in Fig. 2. The chromatography was highly reproducible and provided a retention time for epristeride and the internal standard of 7.9 and 10.2 min, respectively. To date the method has been used successfully in the analysis of biological samples from clinical studies. This method was also adopted for monkey, dog, rat and mouse plasma samples utilizing smaller volumes (100  $\mu$ l) of plasma for quantification of epristeride in various pre-clinical pharmacokinetic studies.

#### REFERENCES

- 1 M. A. Levy, M. Brandt, D. A. Holt and B. W. Metcalf, *J. Steroid Biochem.*, 34 (1989) 571.
- 2 M. A. Levy, M. Brandt, J. R. Heys, D. A. Holt and B. W. Metcalf, *Biochemistry*, 29 (1990) 2815.
- 3 J. C. Lamb, H. English, P. L. Levandoski, G. R. Rhodes, R. K. Johnson and J. T. Isaacs, *Endocrinology*, 130 (1992) 685.

# Rapid, sensitive high-performance liquid chromatographic method for the quantification of promethazine in human serum with electrochemical detection

Arlene R. Fox and Debra A. McLoughlin

*PharmaKinetics Laboratories, Inc., 302 W. Fayette, Baltimore, MD 21201 (USA)*

---

## ABSTRACT

A method of analysis has been developed to quantify promethazine in human serum with a sensitivity that was suitable for bioavailability studies following a 50.0-mg rectal dose. The limit of quantification from 1.0 ml of serum for promethazine using electrochemical detection was 0.200 ng/ml. At this concentration, the total coefficient of variation obtained from seven replicates over the course of three days of validation was 7.53%. The amount of serum required, the ease of sample preparation and the precision of the method at the limit of quantification demonstrated an improvement over previous assays. A validation study was completed that included an evaluation of recovery, ruggedness, linearity of response, accuracy, precision, sensitivity, stability and selectivity. The method was then used to determine promethazine serum levels in a 36-subject bioavailability study following a 50.0-mg suppository dose.

---

## INTRODUCTION

The objective of this work was to develop and validate an HPLC procedure for the determination of promethazine in human serum for use in the bioavailability testing of formulations of promethazine. Due to the anticipated levels and limited sample volume, it was important to improve the precision at the limit of quantification of the assay. A 1-ml volume of serum was required in order to achieve a limit of quantification of 0.200 ng/ml.

The amount of serum required, the ease of sample preparation and the precision of the method at the limit of quantification demonstrated an improvement over previous assays [1,2].

A three-day validation included an evaluation of recovery, ruggedness, linearity of response, accuracy, precision, sensitivity, stability and selectivity. The validated method was subsequently used for the determination of promethazine in human serum

following a 50.0-mg suppository dose. The precision of the method following the analysis of 36 subjects was 6.98% at 0.200 ng/ml.

## EXPERIMENTAL

### *Instrumentation and reagents*

All reagents were analytical grade. The following reagents were used during the validation and the analysis of the subject samples: ethyl acetate, pentane, methanol, acetonitrile, isopropanol, water, glacial acetic acid, ammonium hydroxide and sodium carbonate. Human serum was obtained from Biological Specialities (Landsdale, PA, USA). Reference standards for promethazine and chlorpromazine hydrochloride (internal standard) were obtained from the USP.

The instrumentation used in this study included a Spectroflow 400 isocratic pump (ABI Analytical), a Model ISS-100 autosampler (Perkin Elmer), a Model 5100A Coulochem detector (ESA) and a Model 5011 analytical cell (ESA). Analog signals from the detector were converted to a digital output and stored in a VAX computer. Subsequently, these

---

*Correspondence to:* A. R. Fox, PharmaKinetics Laboratories, Inc., 302 W. Fayette, Baltimore, MD 21201, USA.

signals were integrated using Waters 860 (Version 2.2) software.

#### Chromatographic conditions

A Burdick & Jackson 15 cm  $\times$  4.6 mm I.D., 5  $\mu$ m CN column was used for the analysis. The mobile phase consisted of acetonitrile–methanol–isopropanol–HPLC-grade water–1.0 M ammonium acetate, pH 7.2 (83:5:5:6.65:0.35) at a flow-rate of 1.5 ml/min. The potential for detector 1 was +0.50 V and the potential for detector 2 was +0.70 V. The gain on detector 2 was set at  $10 \times 4$ .

#### Sample preparation

A 1-ml sample was pipetted into a 125 mm  $\times$  16 mm culture tube. A 100- $\mu$ l volume of chlorpromazine hydrochloride (100 ng base per ml) was added to each sample. The samples were then vortexed for 10 s at low speed. A 1-ml volume of 0.65 M sodium carbonate solution was added to each sample followed by vortex-mixing. A 7-ml volume of the extraction solvent (pentane–ethyl acetate, 50:50) was added to each sample. The tubes were capped with polyethylene stoppers and shaken vigorously for 15 min. The samples were then centrifuged for 10 min at 1110 g. The organic layer was transferred to a 100 mm  $\times$  16 mm culture tube and evaporated to dryness at 65°C in a dry heating block with a nitrogen purge. The samples were then reconstituted in 300  $\mu$ l of a solution containing acetonitrile–methanol–isopropanol–HPLC-grade water–1.0 M ammonium acetate, pH 5.0 (83:5:5:6.65:0.35), sonicated for 5 min, vortexed for 30 s, and 100- $\mu$ l samples were injected. The run time was 15 min. The retention time for promethazine was between 7.0 and 8.5 min and between 9.5 and 11.0 min for chlorpromazine hydrochloride (internal standard).

#### RESULTS AND DISCUSSION

The combination of the extraction technique and chromatography provided an assay which was free from interfering endogenous serum peaks. Typical chromatograms for spiked human serum standards and a 7-h post-dose subject sample are shown in Fig. 1. The calibration standard line obtained for promethazine added to serum in amounts ranging from 0.200 to 15.0 ng/ml had a coefficient of determination of greater than 0.99. Best-fit calibration

lines of chromatographic response *versus* concentration were determined by weighted least-squares regression analysis with a weighting factor of  $1/\text{concentration}$ .

The intra-day precision at the limit of quantifica-

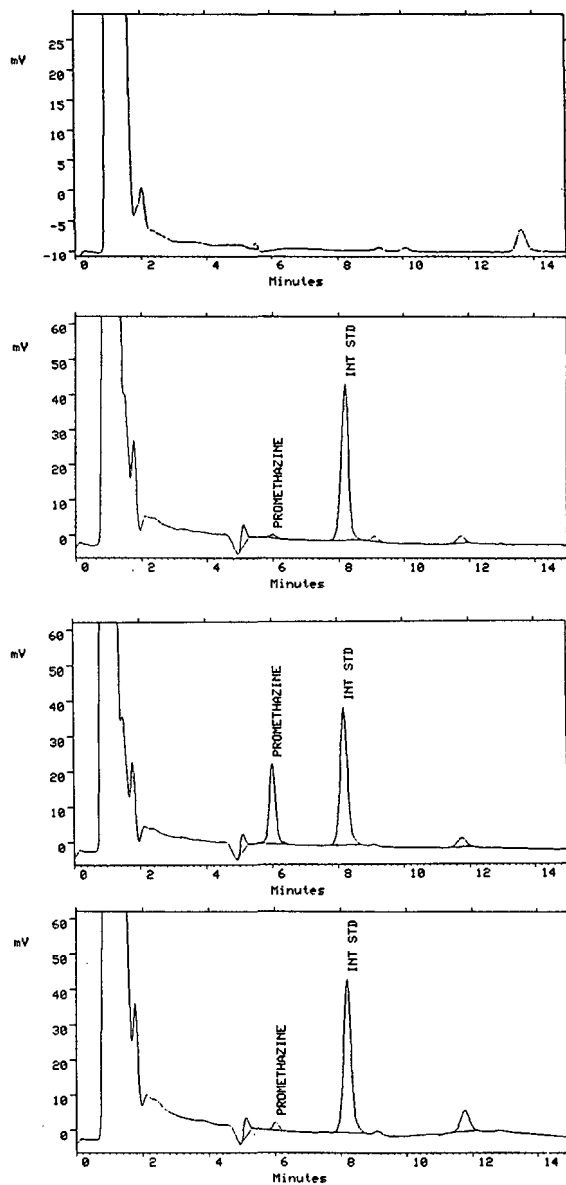


Fig. 1. Representative chromatograms of promethazine in human serum containing 0 (no internal standard), 0.500 and 10.0 ng/ml, respectively. The final chromatogram is a 7-hour post-dose subject sample.

TABLE I

INTER-DAY PRECISION AND ACCURACY DATA FOR A THREE-DAY VALIDATION FOR PROMETHAZINE IN HUMAN SERUM BY HPLC

Theoretical concentration (ng/ml)	Concentration measured (mean $\pm$ S.D.) (ng/ml)	Precision R.S.D. (%)	Accuracy (%)	<i>n</i>
0.200	0.220 $\pm$ 0.02	7.53	110	27
0.500	0.493 $\pm$ 0.04	9.04	98.6	8
1.00	0.982 $\pm$ 0.09	9.35	98.2	9
2.00	1.91 $\pm$ 0.11	5.88	95.5	29
5.00	4.73 $\pm$ 0.31	6.57	94.6	9
10.0	10.1 $\pm$ 0.38	3.78	101	30
15.0	15.5 $\pm$ 0.78	5.02	103	9

tion ranged from 3.98 to 5.95% R.S.D. during a three-day validation. Inter-day precision was 7.53% R.S.D. During analysis of a 36-subject study, the precision for the 0.200 ng/ml standard was 6.98% R.S.D. This sensitivity was achieved through the use of a mobile phase composition that maintained a low background for electrochemical detection. This low background resulted in an acceptable signal-to-noise ratio (6:1). It was important to achieve a sensitivity of 0.200 ng/ml in human serum because of limited sample volume available.

The inter-day precision of the method for pro-

methazine ranged from 3.78 to 9.35%. The inter-day accuracy of the method ranged from 94.6 to 110% (see Table I).

The percentage recovery was determined by measuring the absolute peak heights of promethazine and chlorpromazine (the internal standard), respectively, from prepared serum validation samples at concentrations of 10.0, 2.00 and 0.200 ng/ml. The peak heights of the serum validation sample were compared to the absolute peak heights obtained by direct injection of aqueous standards in the reconstituting solution the same concentrations of promethazine and internal standard. The recovery for promethazine was 104%. The recovery for chlorpromazine (internal standard) was 74.3% (see Table II).

The issue of stability during storage and sample handling was addressed by several experiments. Stability was determined by measuring the concentration after two freeze-thaw cycles and after 24 h at room temperature (see Tables III and IV). During the course of the study, stability samples were analyzed. After two months at  $-20^{\circ}\text{C}$ , 90.5% of the drug was remaining in the serum. The solution used to reconstitute the sample had a pH of 5.0 to ensure maximum autosampler stability. During the study, duplicate quality control samples containing 10.0, 2.00 and 0.500 ng/ml promethazine were determined after approximately 50 and 100% of the unknown samples. This sequence of sample analysis was used to monitor and confirm the stability of the analytes under actual conditions of the assay. There was no noticeable degradation of any of the ana-

TABLE II

RECOVERY OF PROMETHAZINE AND CHLORPROMAZINE (INTERNAL STANDARD) FROM HUMAN SERUM

Values in parentheses are R.S.D.s (%).

Concentration (ng/ml)	Mean recovery (%)	
	Promethazine ( <i>n</i> = 7)	Chlorpromazine ( <i>n</i> = 21)
10.0	102 (5.50)	N.A. <sup>a</sup>
2.00	98.6 (6.30)	N.A. <sup>a</sup>
0.200	112 (6.3)	N.A. <sup>a</sup>
33.3	N.A. <sup>a</sup>	74.3 (6.70)

<sup>a</sup> N.A. = not applicable.



TABLE III  
STABILITY DATA FOR PROMETHAZINE IN HUMAN  
SERUM FOLLOWING A FREEZE-THAW CYCLE

Replicate No.	Promethazine concentration (ng/ml)	
	9.99 ng/ml <sup>a</sup>	0.458 ng/ml <sup>a</sup>
1	9.26	0.465
2	9.41	0.514
3	9.51	0.532
Mean	9.39	0.504
Precision (% R.S.D.)	1.34	6.88
Stability (%)	94.0	110
<i>n</i>	3	3

<sup>a</sup> Concentration at 0 h.

lytes during the performance of the analytical procedure as demonstrated by the control values. The mean value for control samples ranged in accuracy from 104 to 109% with a precision ranging from 7.68 to 11.3%.

Ruggedness was evaluated by validating the method on two different columns. There was column-to-column variation in the tailing factor for both promethazine and chlorpromazine. This factor became the critical system suitability check for the assay. During the validation, the tailing factor ranged from 1.05 to 1.35 for promethazine and from 1.16 to 1.20 for chlorpromazine.

TABLE IV  
STABILITY DATA FOR PROMETHAZINE IN HUMAN  
SERUM FOLLOWING 24 h AT ROOM TEMPERATURE

Replicate No.	Promethazine concentration (ng/ml)	
	9.99 ng/ml <sup>a</sup>	0.458 ng/ml <sup>a</sup>
1	11.5	0.540
2	9.80	0.486
3	10.0	0.526
Mean	10.4	0.517
Precision (% R.S.D.)	8.93	5.42
Stability (%)	104	113
<i>n</i>	3	3

<sup>a</sup> Concentration at 0 h.

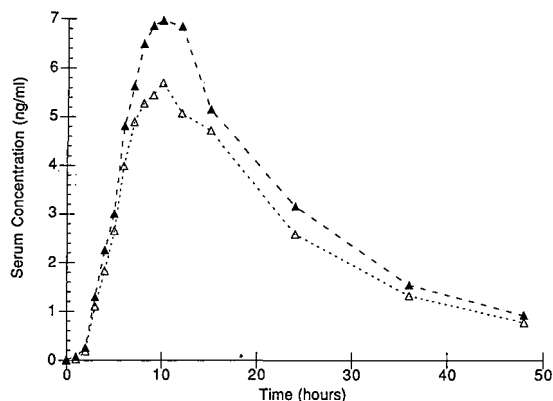


Fig. 2. Mean concentrations of promethazine measured in serum after administration of 50-mg suppositories from two different lots to 24 volunteers.  $\blacktriangle$  = Lot 1;  $\triangle$  = lot 2.

To ensure ruggedness of the extraction procedure, three lots of serum were tested. The mean values of the duplicate analysis of three spiked (10 ng/ml) lots of serum had an R.S.D. of 4.59%.

TABLE V  
CONCENTRATIONS OF PROMETHAZINE MEASURED  
IN SERUM AFTER ADMINISTRATION OF 50-mg SUP-  
POSITORIES FROM TWO DIFFERENT LOTS TO 24 VOL-  
UNTEERS

Time (h)	Concentration (mean $\pm$ S.D.) (ng/ml)	
	Lot 1	Lot 2
0	0.020 $\pm$ 0.097	0.000 $\pm$ 0.000
1	0.076 $\pm$ 0.165	0.024 $\pm$ 0.081
2	0.254 $\pm$ 0.308	0.193 $\pm$ 0.254
3	1.29 $\pm$ 1.57	1.10 $\pm$ 0.855
4	2.25 $\pm$ 2.45	1.83 $\pm$ 1.21
5	3.00 $\pm$ 3.40	2.66 $\pm$ 1.70
6	4.81 $\pm$ 5.53	3.99 $\pm$ 2.34
7	5.63 $\pm$ 5.83	4.90 $\pm$ 3.05
8	6.49 $\pm$ 7.02	5.28 $\pm$ 2.91
9	6.86 $\pm$ 7.46	5.45 $\pm$ 3.44
10	6.96 $\pm$ 7.58	5.70 $\pm$ 4.02
12	6.84 $\pm$ 7.71	5.07 $\pm$ 3.96
15	5.15 $\pm$ 6.25	4.71 $\pm$ 3.75
24	3.16 $\pm$ 3.24	2.59 $\pm$ 2.44
36	1.54 $\pm$ 1.55	1.32 $\pm$ 1.18
48	0.921 $\pm$ 0.903	0.772 $\pm$ 0.723

## CONCLUSION

This assay method for promethazine in plasma is rapid, sensitive and precise. The sensitivity has been improved at the limit of quantification so that 0.200 ng/ml can be quantified from 1 ml of serum with good precision and accuracy. This method was successfully used to determine concentrations of promethazine in subjects samples following a 50-mg suppository dose (see Fig. 2). Fig. 2. is a graph of the 24 subjects that did not have a bowel movement within 4 h of dosing. Table V provides the mean serum concentrations with the standard deviation for these subjects.

## ACKNOWLEDGEMENTS

The authors would like to thank Drs. Elizabeth A. Lane and Lawrence J. Lesko for their assistance in this study.

## REFERENCES

- 1 J. E. Wallace, E. L. Shimek, S. Stavchansky and S. C. Harris, *Anal. Chem.*, 53 (1981) 960–962.
- 2 D. E. Leelavathi, D. E. Dressler, E. F. Soffer, S. D. Yachetti and J. A. Knowles, *J. Chromatogr.*, 339 (1985) 105–115.



# High-performance liquid chromatography of human glycoprotein hormones

Michael A. Chlenov, Ephym I. Kandyba, Larisa V. Nagornaya, Irina L. Orlova and Yury V. Volgin

*NPO "Biotechnologia", 8 Nauchny pr., 117246 Moscow (Russian Federation)*

---

## ABSTRACT

The chromatographic behaviour of the glycoprotein hormones from human pituitary glands and of placental origin [thyroid-stimulating hormone, luteinizing hormone and chorionic gonadotropin (CG)] was studied. It was shown that hydrophobic interaction chromatography on a microparticulate packing and anion-exchange HPLC can be applied for the purification of these hormones. Reversed-phase HPLC on wide-pore C<sub>4</sub>-bonded silica at neutral pH can be applied for the determination of the above hormones and for the isolation of pure CG and its subunits.

---

## INTRODUCTION

The protein hormones from human pituitary glands and of placental origin include those of glycoprotein nature such as thyroid-stimulating hormone (TSH), luteinizing hormone (LH) and chorionic gonadotropin (CG), consisting of two non-covalently associated dissimilar subunits and containing up to 30% of carbohydrates with total relative molecular mass ( $M_r$ ) *ca.* 30 000. The  $\alpha$ -subunit is identical for all three hormones whereas the  $\beta$ -subunits differ and confer distinct biological properties on each molecule [1].

There are a number of lengthy procedures for the purification of these glycoprotein hormones, involving extraction from the corresponding sources followed by sequential chromatographic purification using supports with low efficiency [2].

It has been shown that the human glycoprotein hormones and their subunits can be purified using reversed-phase (RP) HPLC [3,4]. However, the data

were considered to be controversial, especially for the retention of the biological activity [5]. Recent publications [6,7] demonstrated the real applicability of RP-HPLC and hydrophobic interaction chromatography (HIC) to the isolation of pure biologically active human TSH, LH and follicle-stimulating hormone (FSH).

The human glycoprotein hormones are of great practical value because they are used as medical preparations, components of diagnostic kits and the substances for immunization in antibody production [8]. The development of reliable procedures for the preparation of highly purified glycoprotein hormones demands the choice of the optimum method for the determination of the content of these hormones in the fractions at various stages in their isolation and the application of the best chromatographic method for their final purification with high recovery and retention of immuno and biological activities. These aspects were the subject of this work, dealing with comparisons of the application of RP-HPLC, ion-exchange (IE) HPLC and HIC for the isolation and characterization of human TSH, CG and LH.

---

*Correspondence to:* M. A. Chlenov, NPO "Biotechnologia", 8 Nauchny pr., 117246 Moscow, Russian Federation.

## EXPERIMENTAL

*Materials*

A CG preparation with a biological potency (b.p.) of 3500 I.U./mg and an LH sample with an immunopotency (i.p.) of 7800 I.U./mg by radioimmunoassay were purchased from Sigma (St. Louis, MO, USA). The purified TSH and LH samples were obtained from acetone-dried human pituitaries by extraction with 70% aqueous ethanol with 10% (w/v) ammonium acetate (the dry mass of the crude extract from 100 pituitaries was 65 mg with TSH i.p. = 0.9 I.U./mg), followed by chromatographic purification. The first step was purification on Sephacryl S-200 (Pharmacia, Uppsala, Sweden) with 4 mM ammonium acetate (pH 4.0) as eluent followed by separation on CM-Cellulose (Whatman, Maidstone, UK) with 1 M ammonium acetate (pH 4.0) as eluent, then Sephadex G-25 (Pharmacia) with 5 mM sodium glycinate buffer (pH 9.5) and finally DEAE-Sephacryl (Pharmacia) with 0.2 M sodium glycinate–0.1 M NaCl to give the TSH-containing fraction. This TSH sample (6.3 mg, yield 43%) had an i.p. of 4.0 I.U./mg. The LH sample (1.5 mg, i.p. = 6300 I.U./mg) was isolated in the final stage of TSH purification as a fraction from DEAE-Sephacryl, eluting before TSH with 0.2 M sodium glycinate buffer. The CG preparations (b.p. = 500–2500 I.U./mg) were obtained from urine from pregnant women by a modified procedure from various stages of purification [9].

The dissociation of a given hormone into subunits was carried out by treatment of its solution with 6 M guanidine hydrochloride (GH) or 10% trifluoroacetic acid (TFA) at 37°C for 1 h.

HPLC-grade acetonitrile (MeCN) was purchased from Merck (Darmstadt, Germany). All other reagents were of analytical-reagent grade. Distilled water was further purified with a Milli-Q System (Millipore, Bedford, MA, USA).

*HPLC*

Analytical HPLC was carried out with a Millipore–Waters liquid chromatograph consisting of two M-501 pumps, an M-680 gradient controller, a Rheodyne Model 7125 injector, an M-441 spectrophotometer set at 280 nm and an M-750 computing integrator. The volume of the hormone solutions (1 mg/ml) injected was 20–50  $\mu$ l. The chromatographic conditions are given in the figure captions.

Preparative HPLC was carried out using a Gilson Auto-Prep system equipped with a Waters (Milford, MA, USA) Lambda-Max M-481 UV detector operated at 220 and 280 nm.

A Pharmacia fast protein liquid chromatography (FPLC) system was used for IE-HPLC and HIC and consisted of two P-500 syringe pumps, an MV-7 injector and a 280-nm fixed-wavelength single-path UV monitor, coupled to a two-channel REC 482 pen recorder. Gradient elution was controlled with an LCC-500 programmer.

The following prepacked columns were applied for HPLC: Vydac 214 TP, 10  $\mu$ m (Separations Group, Hesperia, CA, USA) (250  $\times$  4.6 mm I.D.), Mono Q HR 5/5, 10  $\mu$ m (Pharmacia) (50  $\times$  5 mm I.D.) and Separon HEMA BIO 1000 Phenyl, 10  $\mu$ m (Tessek, Prague, Czechoslovakia) (80  $\times$  8 mm I.D.). Packing materials such as anion exchangers, Accell QMA, 37–55  $\mu$ m (Waters), and HB-IV, 10  $\mu$ m (Vagos, Tallin, Estonia) (a macroporous polymer-based support with secondary and tertiary amino groups), and reversed-phase support, laboratory-made C<sub>4</sub>-modified and end-capped LiChrospher Si 500, 10  $\mu$ m (Merck) (LC-4) [10], were slurry packed according to the standard procedure.

*Hormone bioassay*

The immunopotencies of human LH and FSH were determined using Bio-Rad (Richmond, CA, USA) Novo Path, that of TSH with Bio Merieux (Marcy l'Etoile, France) and Boehringer (Mannheim, Germany) and that of CG with Roche (Basle, Switzerland) enzyme immunoassay kits. The biological potencies of CG samples were estimated on the basis of the increase in mass of male rat testicular glands [11].

Sodium dodecyl sulphate–polyacrylamide gel electrophoresis (SDS-PAGE) of some hormones was performed according to the standard Laemmli procedure [12].

## RESULTS AND DISCUSSION

*Reversed-phase HPLC at low pH*

Gradient elution with a mixture of MeCN with 0.1% TFA is widely used for the RP-HPLC of protein hormones [13]. Various silica-based packings with different porosity and modified with hydrocarbon groups with various chain lengths have been applied for their separation. These sorbents are also

varied with the degree of surface modification and in the use of the end-capping process. We previously compared [14] a number of commercial packings differing in the above respects and also a domestic-made LC-4 support in order to find those most suitable for peptide and glycoprotein hormones. It was found that the end-capped packings with bonded  $C_4$  groups and a pore size of more than 300 Å are the optimum for the analytical RP-HPLC of relatively large hormones ( $M_r > 20\,000$ ), including glycoproteins, whereas bare silica is more suitable for the separation of relatively small hormones.

It was subsequently shown [15] that highly pure porcine calcitonin could be isolated from a crude extract of porcine thyroid glands using sequential preparative HPLC separation on RP and bare silica supports with a mixture of acetic acid and ethanol as the eluent.

Information available on the separation of mixtures containing glycoprotein hormones and their subunits using RP-HPLC at low pH even with macroporous  $C_4$  packings was contradictory. For example, Bristow *et al.* [16] reported a better separation of TSH subunits at acidic pH, whereas Parsons

*et al.* [17] demonstrated good resolution of human CG, TSH and LH subunits at neutral pH. Wilks and Butler [5] compared various mobile phases and packing materials and demonstrated that CG retained only 10–60% of its biological activity following RP-HPLC.

In previous work [14,15] we demonstrated that RP-HPLC of glycoprotein hormones under standard acidic conditions (MeCN–0.1% TFA gradient) results in good separations and peak shapes. A serious decrease in the biological activity of the preparations obtained after purification under such conditions was observed with porcine FSH and CG. Similar results were demonstrated by other workers [5,17].

Thus RP-HPLC in acidic media, in spite of the convenience of using volatile buffers, fails to give reliable data for the isolation of pure biologically active glycoprotein hormones. Such difficulties in the isolation of active hormones at low pH may result from dissociation of the hormone subunits and probably partial elimination of terminal carbohydrate moieties.

RP-HPLC at low pH is still used for the analysis of complex mixtures containing glycoprotein hormones due to the high selectivity of separation. An example of such a separation is presented in Fig. 1 for a partially purified CG sample (Sigma). The separation profile is different from that obtained for the same sample with the same column but at neutral pH (Fig. 2a). These data demonstrate the effect of pH on the character of separation.

#### Reversed-phase HPLC at neutral pH

In spite of the rare application of neutral eluents for the RP-HPLC of proteins, these conditions were shown to be suitable for the analytical and preparative HPLC of human glycoprotein hormone subunits [17]. Hiyama and co-workers [6,7] clearly demonstrated that RP-HPLC on a  $C_4$  column at neutral pH using a gradient of MeCN in 0.1 M triethylamine phosphate buffer (pH 6.5) is efficient for the separation of a mixture of human FSH, TSH and LH and for their final purification.

We applied the chromatographic conditions given by Parsons *et al.* [17] using  $C_4$  rather than  $C_{18}$ -modified macroporous silica and successfully controlled different stages of the isolation of human glycoprotein hormones such as TSH, CG and LH

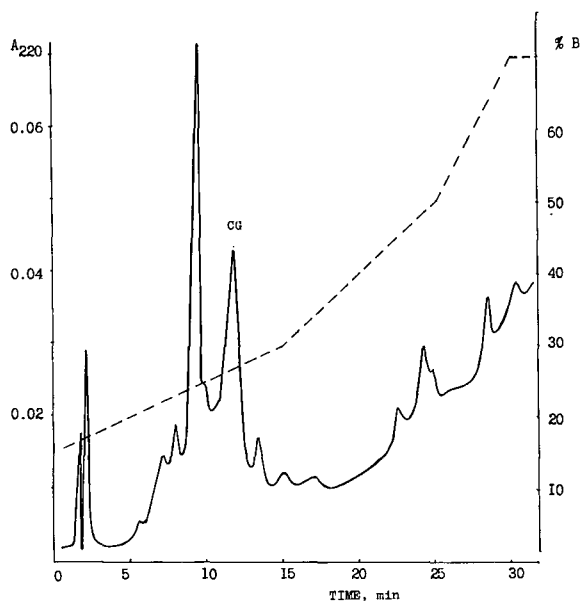


Fig. 1. Chromatography of CG (Sigma) on Vydac 214TP (250 × 4.6 mm I.D.). Mobile phase A, 10% MeCN plus 0.1% TFA; mobile phase B, 90% MeCN plus 0.1% TFA; sample loaded, 20  $\mu$ l; flow-rate, 1 ml/min. The linear gradient for mobile phase B is indicated by the broken line.

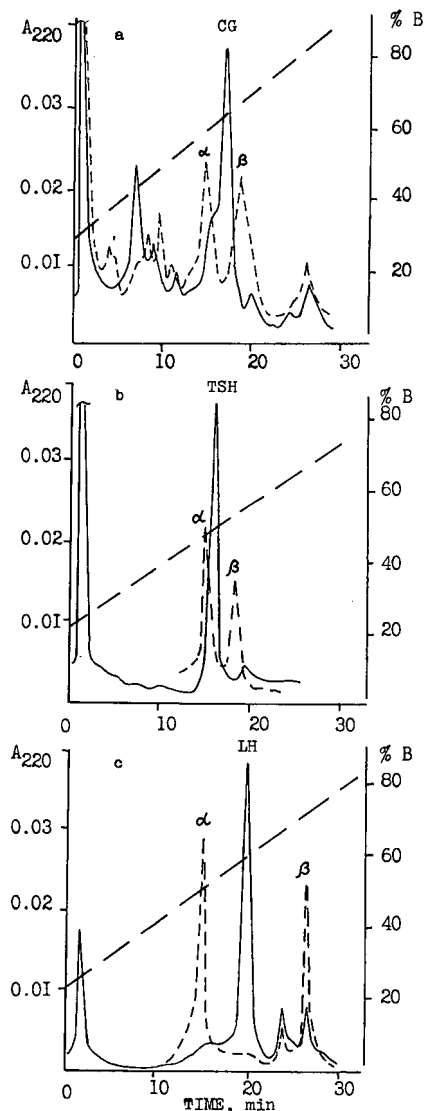


Fig. 2. Chromatography of (a) CG (Sigma), (b) TSH (i.p. = 6.2 I.U./mg) and (c) LH (i.p. = 6300 I.U./mg) on Vydac 214TP. Mobile phase A, 0.1 M sodium phosphate (pH 6.8); mobile phase B, 50% MeCN plus 50% mobile phase A; sample loaded, 20  $\mu$ l; flow-rate, 2 ml/min. Linear gradient from 25 to 100% B in 40 min. The solid lines are intact hormone and the dashed lines are the same sample after incubation with 6 M GH.

and achieved the preparation of purified CG and its subunits.

The chromatographic profiles of partially purified CG and relatively pure TSH and LH are presented in Fig. 2. The peaks of the corresponding

hormones are separated from the other admixtures. This facilitates the collection of the related fractions of the purified hormones. For example, we isolated relatively pure CG from the partially purified preparation (22 mg, b.p. = 2400 I.U./mg) after HPLC under the above conditions, desalting and lyophilization. The purified sample obtained (3.4 mg) had a high specific immunoactivity and its b.p. was about 11 000 I.U./mg (yield 71%). It can be also seen (Fig. 2b and c) that TSH and LH samples purified by HIC and IE chromatography, respectively, are fairly homogeneous, as also demonstrated by SDS-PAGE.

After incubation with 6 M GH, resulting in dissociation of the hormones into subunits, we obtained the chromatographic profiles shown as dashed lines in Fig. 2. It can be seen that the intact hormones dissociate into subunits. The positions of the LH subunits were identified by comparison with those of the Sigma LH sample. The elution volumes of TSH and LH subunits correspond to those observed by Hiyama and Renwick [6] in a similar neutral eluent. CG subunits were identified after their isolation by RP-HPLC with specific antibodies immobilized on the polymer support. We obtained 2.0

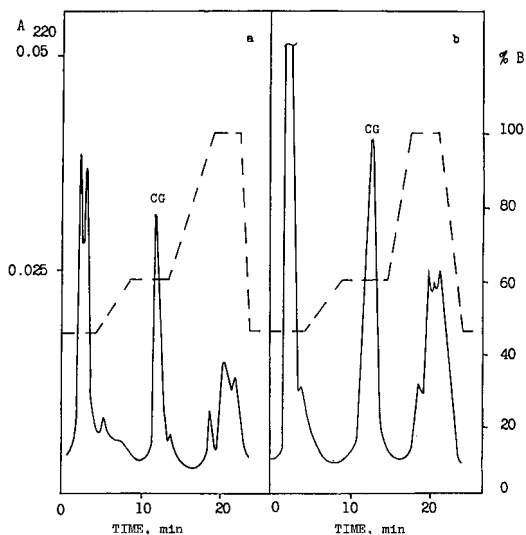


Fig. 3. Chromatography of CG preparation (a) from Sigma and (b) analysed sample on Vydac 214TP with specific gradient profile. Mobile phases and flow-rate as in Fig. 2. Sample loaded, (a) 20  $\mu$ l and (b) 60  $\mu$ l. The gradient for mobile phase B is indicated by the broken line.

mg of  $\alpha$ - and 2.8 mg of  $\beta$ -subunit from 8 mg of intact hormone (yield 60%). The latter data demonstrate the possibility of isolating fairly pure subunits of the above hormones with a reasonable yield after HPLC.

The elution volumes ( $V_e$ ) of human CG, TSH and LH subunits correlate with their structures each containing identical  $\alpha$ -subunits ( $V_e = 29$  ml) and  $\beta$ -subunits specific for each hormone ( $V_e = 39$ , 37 and 53 ml for CG, TSH and LH, respectively). The presence of two peaks instead of one in the chromatogram after incubation of the hormone preparation with GH may also be an indirect identification of the elution volume of the intact hormone if the corresponding standard is absent.

We also obtained the specific gradient profile for the HPLC of CG-containing samples (see Fig. 3). Such conditions allow the main peak to be separated from all admixtures and thus to the peak area of the intact hormone be determined and then normalized to a given amount of CG (611 arbitrary units per 20  $\mu$ g in Fig. 3b). This permits an approximate determination of the biological potency of the sample to be obtained by comparison of the CG peak area with that of the sample (e.g., Sigma) with known b.p. = 3500 I.U./mg (peak area = 1070 AU in Fig. 3a). Hence the found b.p. of the unknown sample was about 2000 I.U./mg. Biological analysis of the above sample gave 2200 I.U./mg. We performed such determinations on ten samples with a relative error of about 20%. This determination, although approximate, makes the HPLC control of the CG isolation process easier and facilitates the realization of the biological analysis where the linearity range is limited and dependent on the selected dose [11].

Similar results for the isolation and determination of CG were obtained on application of domestic LC-4 supports under similar chromatographic conditions.

#### Anion-exchange HPLC

Ion-exchange chromatography is a traditional method for the separation and purification of protein hormones [1,8]. With regard to human glycoprotein hormones, IE-HPLC has been successfully applied to the investigation and isolation of CG, TSH and FSH [15,18,19]. It has been demonstrated that HPLC on silica-based IE packings did not al-

ways give reproducible results, probably owing to the presence of residual silanol groups [18]. In fact, a high recovery on isolation with retention of biological potency and reliable analytical data on IE-HPLC of glycoprotein hormones were obtained using mainly either a polymer-based anion exchanger, Mono Q [19], a cation exchanger, Protein Pak SP 5PW (Waters) [18], or macroporous silica covered with a polymer layer with bonded ionogenic groups, Accell QMA [15]. In the last study we demonstrated that bovine FSH with the required biological potency and high recovery can be obtained from a crude extract from bovine pituitary glands with a high throughput (load up to 80 mg of extract per gram of sorbent).

Good separations of the components of a crude precipitate containing CG (b.p. = 400 I.U./mg) and a crude extract containing TSH (i.p. = 0.9 I.U./mg) were obtained using the macroporous anion exchanger HB-IV and Mono Q, respectively. The chromatographic profiles obtained are presented in Figs. 4 and 5. Good selectivity can be seen and the fractions containing the purified hormones (hatched zones) after desalting and lyophilization exhibit a ninefold increase in b.p. for CG (1.3 mg,

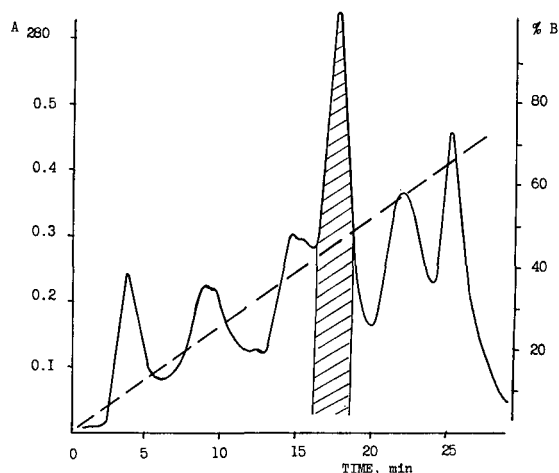


Fig. 4. Chromatography of CG samples (b.p. = 400 I.U./mg) on HB-IV anion-exchange column (140  $\times$  4.6 mm I.D.). Mobile phase A, 0.01 M ammonium hydrogencarbonate buffer (pH 8.75); mobile phase B, 0.2 M ammonium hydrogencarbonate buffer (pH 8.75). The linear gradient of from 0 to 100% B in 40 min is indicated by the broken line. Sample loaded, 16 mg in 1 ml.



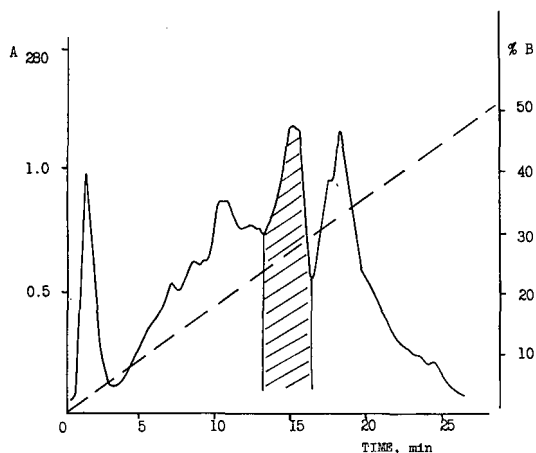


Fig. 5. Chromatography of TSH sample (i.p. = 0.9 I.U./mg) on a Mono-Q column. Mobile phase A, 20 mM Tris-HCl (pH 8.1); mobile phase B, 20 mM Tris-HCl (pH 8.1)-1 M NaCl. Linear gradient from 0 to 60% B in 35 min. Sample loaded, 15 mg in 1 ml. Flow-rate, 1 ml/min.

yield 55%) and a fourfold increase in i.p. for TSH (2.6 mg, yield 70%). Both supports have five times lower loading capacities than Accell QMA but allow fairly pure hormones to be obtained especially after rechromatography. The efficiency of separation of CG and TSH samples with Accell QMA was markedly lower, mainly owing to the larger particle size of the packing. The purification steps were controlled by RP-HPLC at neutral pH and by immunoenzyme analysis.

Hence anion-exchange HPLC on polymer-based macroporous supports, in spite of its lower efficiency in comparison with RP-HPLC, is a more promising method for primary purification of the crude extracts and for the isolation of those glycoprotein hormones which are required in relatively large amounts, owing to the much lower cost of the eluents and the higher loading capacity.

#### Hydrophobic interaction chromatography

HIC is now widely used for the purification of various proteins, including glycoproteins [20]. Its popularity resulted from the low price of the eluents and the suitability of the salt solutions for the preservation of biological activity of labile proteins. HIC was first applied to the separation of TSH subunits using low-efficiency pentyl-Sepharose 4B [21].

Recently, Hiyama *et al.* [7] demonstrated that HIC on a similar support, phenyl-Sepharose CL-4B, can be successfully employed to prepare highly purified biologically active human LH and TSH. These hormones were obtained with good yields although the separation procedure was long (more than 4 h).

We developed a procedure for the purification of CG and TSH using a column packed with the microparticulate packing Separon HEMA BIO 1000 Phenyl (10  $\mu$ m) and a descending gradient of ammonium sulphate. The chromatographic conditions used for the HIC of partially purified CG and of TSH purified according to the traditional scheme (see Experimental) are presented in Fig. 6. As these hormones behave like hydrophobic compounds we add 10% ethanol to buffer B. It is interesting that the glycoprotein hormones studied are distinctly

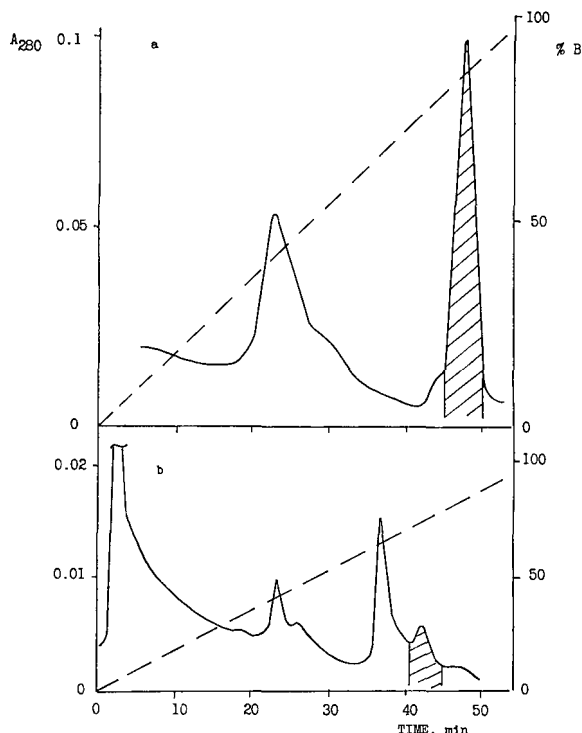


Fig. 6. Chromatograms of (a) TSH (i.p. = 4 I.U./mg) and (b) CG (b.p. = 1800 I.U./mg) samples on a Separon HEMA BIO 1000 phenyl column. Mobile phase A, 0.1 M ammonium acetate (pH 6.8)-2 M ammonium sulphate; mobile phase B, 0.1 M ammonium acetate-10% ethanol. Linear gradient from 0 to 100% B in 60 min. Sample loaded, (a) 15 mg and (b) 5 mg, both in 1 ml. Flow-rate, 1 ml/min.

separated from most of the admixtures and eluted similarly at the end of the gradient. The fractions containing the purified hormones (Fig. 6, hatched zones) were analysed by RP-HPLC at neutral pH using a C<sub>4</sub> column and by immunoenzyme assay. The i.p. of the TSH sample obtained (4.5 mg, yield 48%) was 6.3 I.U./mg and the contamination of this sample with FSH and LH was less than 0.05% and 2.3%, respectively. The b.p. of the CG sample (0.9 mg, yield 54%) was 5500 I.U./mg.

It seems possible to use HIC for the purification of mixtures containing small amounts of the glycoprotein hormones in question and for their final purification. The loading capacity of this column (80 × 8 mm I.D.) was shown to be high, e.g., about 100 mg of partially purified CG per column. Thus the application of HIC may provide new possibilities for the creation of an inexpensive and efficient scheme for the isolation of human glycoprotein hormones, e.g., like that proposed by Hiyama *et al.* [7].

#### CONCLUSIONS

The results obtained from these comparative studies of the application of various modes of HPLC to the human glycoprotein hormones CG, TSH and LH demonstrated that RP-HPLC at neutral pH, in contrast to that under acidic conditions, can be used for the isolation and characterization of human glycoprotein hormones and their subunits.

For the preparative isolation of the glycoprotein hormones from partially purified mixtures, IE-HPLC on macroporous polymer-based anion exchangers and HIC on phenyl-modified polymeric microparticulate supports can be applied.

#### ACKNOWLEDGEMENTS

We express our appreciation to Dr. G. I. Kovalevkaya and L. K. Korjazova for immunoenzyme analyses.

#### REFERENCES

- 1 M. R. Sairam, in C. H. Li (Editor), *Gonadotropic Hormones (Hormonal Proteins and Peptides, Vol. 11)*, Academic Press, New York, 1983, Ch. 1, p. 2.
- 2 B. B. Saxena and P. Rathnam, in K. W. McKerns (Editor), *Structure and Function of Gonadotropins*, Plenum Press, New York, 1978, p. 183.
- 3 C. J. Putterman, M. B. Spear, K. S. Meade-Cobun, M. W. W. Hixson, *J. Liq. Chromatogr.*, 5 (1982) 715.
- 4 N. R. Moudgal and C. H. Li, *Proc. Natl. Acad. Sci. U.S.A.*, 79 (1982) 500.
- 5 J. W. Wilks and S. R. Butler, *J. Chromatogr.*, 298 (1984) 123.
- 6 J. Hiyama and A. G. C. Renwick, *J. Chromatogr.*, 529 (1990) 33.
- 7 J. Hiyama, A. Surus and A. G. C. Renwick, *J. Endocrinol.*, 125 (1990) 493.
- 8 J. G. Pierce and T. F. Parsons, *Annu. Rev. Biochem.*, 50 (1981) 465.
- 9 A. Albert, S. Kelli and L. Silver, *J. Clin. Endocrinol.*, 18 (1958) 600.
- 10 S. M. Staroverov, M. A. Chlenov, E. V. Titova and L. I. Kudrjashov, in *Proceedings of the 3rd Symposium on Molecular Liquid Chromatography, Riga, October 1984*, Nauka, Moscow, 1984, p. 125.
- 11 E. Disfaluzi, *Acta Endocrinol.*, 17 (1954) 58.
- 12 U. K. Laemmli, *Nature*, 227 (1970) 680.
- 13 M. T. Hearn, in C. Horvath (Editor), *HPLC. Advances and Perspectives, Vol. 3*, Academic Press, New York, 1983, p. 87.
- 14 M. A. Chlenov and Yu. V. Volgin, in H. Kalasz (Editor), *Chromatography 87*, Akadémiai Kiadó, Budapest, 1988, p. 111.
- 15 M. A. Chlenov, E. I. Kandyba, Yu. V. Volgin and I. L. Orlova, in *Proceedings of the 9th International Symposium on Preparative and Industrial Chromatography, Nancy, April 1992*, INPL, Nancy, 1992, p. 347.
- 16 A. F. Bristow, C. Wilson and N. Sutcliffe, *J. Chromatogr.*, 270 (1983) 285.
- 17 T. F. Parsons, T. W. Strickland and J. G. Pierce, *Endocrinology*, 114 (1984) 2223.
- 18 P. Hallin and S. A. Khan, *J. Liq. Chromatogr.*, 9 (1986) 2855.
- 19 R. C. Johnston, P. G. Stanton, D. M. Robertson and M. T. Hearn, *J. Chromatogr.*, 397 (1987) 389.
- 20 A. J. Alpert, *J. Chromatogr.*, 444 (1988) 269.
- 21 G. Jacobson, P. Roos and L. Wide, *Biochim. Biophys. Acta*, 536 (1978) 363.



# Immunoaffinity chromatography of recombinant *Amb a I* in the presence of a denaturing agent

K. M. Keating, B. L. Rogers, L. Weber, J. P. Morgenstern, D. G. Klapper and M. Kuo

*ImmuLogic Pharmaceutical Corporation, Cambridge, MA (USA) and Department of Microbiology and Immunology, University of North Carolina, Chapel Hill, NC (USA)*

---

## ABSTRACT

Recombinant proteins expressed in *E. coli* are often sequestered into inclusion bodies and require the use of denaturing agents in order to solubilize them. The recombinant form of *Amb a I*, the major allergen from short ragweed pollen, is one such protein. In some cases solubility can be maintained after the removal of the denaturing agent, particularly if the protein can be folded into its native conformation. However, not all proteins refold readily and after the removal of the denaturing agent the proteins will reaggregate and/or precipitate. In the case of *Amb a I*, the recombinant protein stays in solution at low concentrations but aggregates with itself and other proteins. The recombinant *Amb a I* is not expressed at high levels and may be toxic to *E. coli*. Therefore, isolation from a complex mixture of *E. coli* proteins was necessary. Monoclonal antibodies which recognize the denatured form of *Amb a I* were available, allowing for immunoaffinity purification. However, because the protein was not monomeric, this chromatographic technique did not provide an improvement in the purity level when run in normal buffer solutions. Analysis of one monoclonal antibody's stability to urea indicated it could tolerate the presence of 2 M urea and recover full activity. Use of this antibody as an immunoaffinity reagent in a column run in 2 M urea, which minimized aggregation of the *E. coli* produced proteins, gave a high degree of purification of recombinant *Amb a I* in one step. This illustrates the potential for the use of denaturing and other solubilizing agents in immunoaffinity chromatography of recombinant proteins.

---

## INTRODUCTION

Short ragweed pollen is a major cause of hayfever in North America. The major allergen in this pollen was identified as an  $M_r$  38 000 amino-terminally blocked protein and termed antigen E in 1964 [1] and later renamed *Amb a I* according to standardized nomenclature [2]. Recently, the cDNAs encoding *Amb a I* were cloned and the protein shown to be composed of a mixture derived from a homologous multigene family [3]. The relative level of expression of the different gene products in ragweed pollen is unknown, however, the predominant protein sequence derived from biochemically purified *Amb a I* corresponds to the cDNA designated *Amb*

*a I.1* [3]. However, when three different cDNAs, *Amb a I.1*, *I.2*, and *I.3*, were expressed as recombinant proteins in *E. coli* lysates, they all bound human IgE and stimulated the proliferation of T cells from ragweed allergic patients in *in vitro* cultures [4]. In T cell assays, the antigen is taken up by presenting cells, processed to peptide fragments, and recognized by T cells as linear epitopes when bound to surface expressed major histocompatibility complexes [5,6]. Therefore, it is not always necessary to refold the recombinant protein for use in such a system.

Purification of these recombinant proteins was required in order to further study their relative importance as allergens. Recombinant *Amb a I*s were produced at relatively low levels in *E. coli*. The proteins formed inclusion bodies which required the use of denaturants in order to solubilize them. When the denaturants were removed the proteins

---

Correspondence to: M. Kuo, ImmuLogic Pharmaceutical Corp., One Kendall Square, Bldg. 600, Cambridge, MA 02139, USA.

tended to aggregate and at high concentrations they precipitated, as is often observed with recombinant proteins.

Immunoaffinity chromatography is a very selective protein purification technique due to the specificity of the interaction between monoclonal antibodies and their cognate antigens. Therefore, it is particularly useful for purifying low-abundance proteins, such as recombinant *Amb a I* proteins, from complex mixtures such as *E. coli* lysates. Elution of an antigen from an immunoaffinity column often requires harsh conditions which can denature the antibody and render the column inactive. Therefore, the running and elution conditions should be optimized for each immunoaffinity column in order for it to be reusable [7]. Monoclonal antibodies which bind to denatured, pollen-derived *Amb a I* had been previously produced and characterized [8]. Here we describe the use of the monoclonal antibody, JB4E3-3, as an immunoaffinity reagent in low denaturant concentrations under which the antibody is stable and the recombinant protein is less aggregated.

## MATERIALS AND METHODS

### *Recombinant Amb a I protein expression*

*Amb a I.1* cDNA [3] was cloned into the vector pTrc99A [9] and recombinant *Amb a I.1* (*rAmb a I.1*) expression was induced by the addition of isopropyl- $\beta$ -D-thiogalactopyranoside (IPTG) in the JM109 strain of *E. coli*. The protein formed inclusion bodies which were pelleted after cell lysis and solubilized with 8 M urea as has been described previously [4].

### *Sodium dodecyl sulfate–polyacrylamide gel electrophoresis (SDS-PAGE) and Western blot analyses*

The SDS-PAGE and transfer procedures were performed as described elsewhere [10]. Gel electrophoresis was performed on 12% acrylamide gels under reducing conditions. For Western blot analysis proteins were transferred from the gels to nitrocellulose (0.1  $\mu$ m, Schleicher & Schuell, Keene, NH, USA) in a Hoefer apparatus (San Francisco, CA, USA). The nitrocellulose blots were blocked with 1% defatted milk, stained with India ink and probed with JB4E3-3 at 1 ng/ml. The JB4E3-3 was detected with biotinylated rat anti-mouse antibody

(Kirkegaard and Perry, Gaithersburg, MD, USA) and  $^{125}$ I-streptavidin. Films were developed by autoradiography at  $-80^{\circ}\text{C}$  with an intensifying screen.

### *Enzyme-linked immunosorbent assay (ELISA) detection of recombinant Amb a I.1*

A qualitative ELISA assay for the detection of the protein in fractions from chromatographic separations was developed. Immulon II 96-well plates (Dynatech, Chantilly, VA, USA) were coated with JB4E3-3 (0.1  $\mu$ g/well) overnight at  $4^{\circ}\text{C}$ . Plates were washed between steps with phosphate-buffered saline (PBS). Blocking was done with 0.5% gelatin. Blocking and subsequent steps were performed for 1 h at room temperature. Aliquots of chromatographic fractions were incubated in the wells to allow capture of the antigen. Plates were incubated with rabbit anti-denatured *Amb a I* antisera at a 1:500 dilution. The polyclonal antisera was used in this assay to give a greater probability that proteolytic fragments, as well as intact *rAmb a I.1*, would be detected. Rabbit antibodies were detected with biotinylated goat anti-rabbit antibody (1:5000 dilution, Southern Biotechnology, Birmingham, AL, USA). Plates were incubated with streptavidin-conjugated horseradish peroxidase. Color was developed with the addition of 3,3',5,5'-tetramethylbenzidine (TMB) peroxidase substrate (Kirkegaard and Perry) and the development stopped with the addition of 1 M phosphoric acid. Positive fractions were identified by absorbance at 450 nm read on a Bio-Tek Model 310 plate reader (Winooski, VT, USA).

### *Gel filtration chromatography*

Chromatograms were run on an FPLC system (Pharmacia, Piscataway, NJ, USA) with a Superose 12 (HR 10/30, 30  $\times$  1 cm) column in 200 mM sodium phosphate (pH 7) at 0.5 ml/min. The detectors were set at 0.5 and 0.05 AUFS for 214 and 280 nm, respectively. Urea-solubilized cell pellets were either dialyzed against PBS or used directly. Samples were filtered and 100  $\mu$ l was injected onto the column. Fractions of 0.5 ml were collected and analyzed by ELISA.

### *ELISA analysis of JB4E3-3 stability*

A direct ELISA was used to optimize the conditions for the use of JB4E3-3 as an immunoaffinity

reagent. Short ragweed (*Ambrosia artemisiifolia*) pollen (Greer Labs, Lenoir, NC, USA) was extracted with PBS at 10 g/l overnight at 4°C. The extract was clarified by centrifugation and filtering and denatured by boiling. This was used to coat the wells of Immulon II 96-well plates (Dynatech, Chantilly, VA, USA) at 1 ng *Amb a I*/well overnight at 4°C. Plates were washed between steps with PBS. Subsequent steps were performed at room temperature for 1 h each. Plates were blocked with 1% bovine serum albumin in PBS. JB4E3-3 was added at 0.1 µg/well with pretreatment or treatment on the plate with various reagents described in the text. The JB4E3-3 was detected with biotinylated rat anti-mouse antibody (Kirkegaard and Perry). The plates were developed as described above.

#### Immunoaffinity chromatography

The immunoaffinity agent, murine monoclonal antibody JB4E3-3, was raised against denatured *Amb a I* derived from ragweed pollen [8]. The antibody was produced in ascites and purified by precipitation with ammonium sulfate at 45% of saturation. The antibody was coupled to cyanogen bromide-activated Sepharose (Pharmacia, Piscataway, NJ, USA) at 5 mg/ml according to the manufacturer's protocol and a 7-ml open column was prepared. The column was equilibrated with PBS containing 2 M urea by gravity flow. The *E. coli* cell pellet was obtained and solubilized with 8 M urea as previously described [4]. The solubilized pellet was diluted 1:4 with PBS, filtered, and loaded onto the column. The column was washed with approximately 50 ml of PBS containing 1 M NaCl and 2 M urea. The column was then eluted with 10 mM cyclohexylaminopropanesulfonic acid (CAPS) containing 2 M urea (pH 10.5). Fractions of 100 drops were collected and analyzed by absorbance at 280 nm and by SDS-PAGE.

#### RESULTS AND DISCUSSION

*Amb a I* can be purified from ragweed pollen by a series of biochemical purification steps including two batch ion-exchange steps, three ammonium sulfate precipitations, gel filtration chromatography and finally an ion-exchange chromatographic step [11]. Due to the proteolytic sensitivity of the protein, it is degraded during this procedure and in our

laboratory approximately 5 mg of intact pure protein is recovered from 100 g of pollen. The cDNAs encoding several related *Amb a I* proteins have been expressed in *E. coli* in order to provide large quantities of unambiguous gene products [3]. However, the *rAmb a I* proteins are not expressed at high levels, producing only 0.5–3 mg per liter of culture grown in shaker flasks. This represented approximately 1–4% of the cellular protein. Efforts aimed at increasing expression levels by modifying or changing the expression vector or *E. coli* strain used have yielded increased levels of mRNA but not of protein.

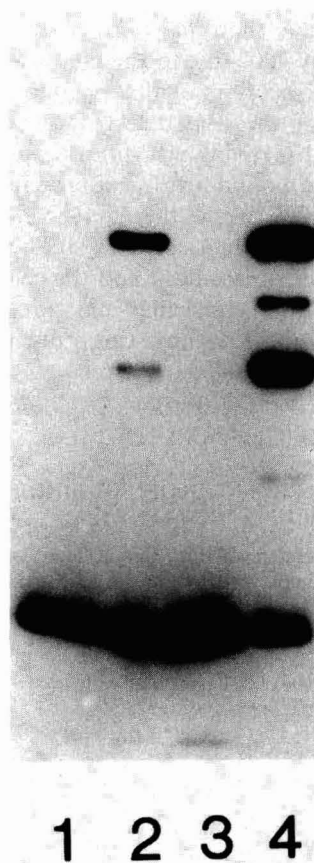


Fig. 1. JB4E3-3-probed Western blot of *rAmb a I.1* expressed in *E. coli*. An SDS-PAGE immunoblot was generated with the following samples: lane 1, JM109 negative control *E. coli* lysate; lane 2, *E. coli* lysate containing expressed *rAmb a I.1*; lane 3, supernatant after centrifugation of *E. coli* lysate containing expressed *rAmb a I.1*; lane 4, urea-solubilized pellet after centrifugation of *E. coli* lysate containing expressed *rAmb a I.1*.

In order to purify a low-abundance protein it is preferable to use a high-resolution chromatographic technique such as affinity chromatography. A panel of monoclonal antibodies which recognize denatured *Amb a I* derived from pollen had been raised [8]. Some of these monoclonal antibodies were available for use as potential immunoaffinity reagents. Here we describe the characterization of the monoclonal antibody JB4E3-3. This antibody was tested by Western blot analysis to determine if it recognized r*Amb a I*. As shown in Fig. 1, the antibody specifically recognized the expressed r*Amb a I* at an apparent molecular mass close to the predicted molecular mass of 42 000, as well as three proteolysis products. The molecular mass of the recombinant protein is higher than that of the native protein by approximately 4000 due to the presence of a leader sequence. Proteolysis of this recombinant protein had been previously detected on a Western blot probed with a rabbit anti-*Amb a I* antiserum [4]. JB4E3-3 also bound an *E. coli* protein of  $M_r$  approximately 14 000 seen in the *E. coli* control cell lysate in Fig. 1, lane 1. As seen in lanes 3 and 4, containing the cell supernatant and the cell pellet, respectively, this lower-molecular-mass protein is soluble. It was possible to remove this protein

by washing the cell pellet (see Fig. 4, panel B, lanes 1 and 2).

A direct-binding ELISA assay was developed to determine the optimal elution conditions for use of JB4E3-3 as an immunoaffinity reagent (Table I). A number of potential solutions for elution of the column were tested in this assay including low-pH and high-pH buffers, as well as high-salt, and chaotropic solutions. In the pretreated samples, the antibody solution was diluted 1:100 with the test solution, then dialyzed against PBS. It was then used in the binding assay and detected with biotinylated rat anti-mouse antibody in order to determine if the JB4E3-3 had been permanently inactivated. The activity of the antibody was decreased by pretreatment with a buffer at pH 12.5 and by solutions containing very high salt. In addition, the ability of the different solutions to dissociate the antibody-antigen (Ab-Ag) complex was assayed by incubating the antibody (diluted 1:100 with PBS) in the coated wells, washing, adding the test solutions for a brief period of time, removing the solution, and continuing the assay to detect the amount of JB4E3-3 still bound to the *Amb a I* on the plate. Phosphate buffer at pH 11.0 proved to be the most effective dissociating reagent of those that did not denature the anti-

TABLE I

ABSORBANCE READINGS FROM THE DIRECT BINDING ELISA TO DETERMINE THE OPTIMAL ELUTION CONDITIONS FOR AFFINITY CHROMATOGRAPHY

Pretreated Ab, JB4E3-3, was diluted with the solutions indicated, dialyzed, and used in the binding assay. Complexes of JB4E3-3 and denatured *Amb a I* (Ab-Ag complex) were formed on the plate and then treated with the solutions indicated.

Treatment	Absorbance at 450 nm of the Ab-Ag complex treated	Absorbance at 450 nm of the pretreated Ab
0.1 M Glycine (pH 2.5)	0.934	1.037
0.1 M Glycine and 0.5 M NaCl	1.065	1.062
0.1 M Phosphate (pH 10.0)	1.021	1.175
0.1 M Phosphate (pH 11.0)	0.171	1.124
0.1 M Phosphate (pH 12.5)	0.133	0.283
3 M MgCl <sub>2</sub>	1.059	0.992
5 M MgCl <sub>2</sub>	0.317	0.491
5 M LiCl	1.134	1.069
10 M LiCl	0.180	0.271
1 M NH <sub>4</sub> SCN	1.118	1.198
2 M NH <sub>4</sub> SCN	1.030	1.182
3 M NH <sub>4</sub> SCN	1.000	0.491
10 mM CAPS and 2 M Urea	0.013	0.861

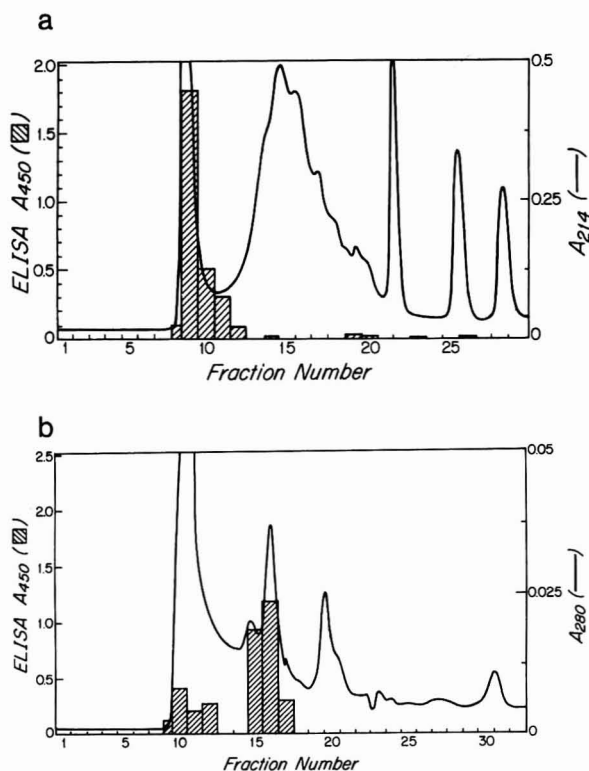


Fig. 2. Gel filtration chromatography of urea-solubilized pellet from *E. coli* lysate containing expressed *rAmb a* I.1 (a) after dialysis into PBS and (b) without dialysis. The capture ELISA data detecting *rAmb a* I.1, shown in shaded areas, is overlaid on the chromatograms.

body. In a later assay a CAPS buffer at pH 10.5 was also shown to be an effective eluting agent (Table I) and that buffer was preferred for use in the purification protocol because the lower pH would provide a less hostile environment for the antibody.

A JB4E3-3 Sepharose column was prepared for purification of *rAmb a* I.1 and run essentially as described in Materials and Methods except that the elution buffer was a pH 11 phosphate buffer and urea was not included. The protein which was eluted from the column showed a large number of bands and an insignificant increase in the level of purity of *rAmb a* I.1 when analyzed by SDS-PAGE (data not shown). In order to understand this result, gel filtration chromatograms were run on the urea-solubilized cell pellet both with and without prior removal of urea by dialysis. The *rAmb a* I.1 was detected by the capture ELISA described in Materi-

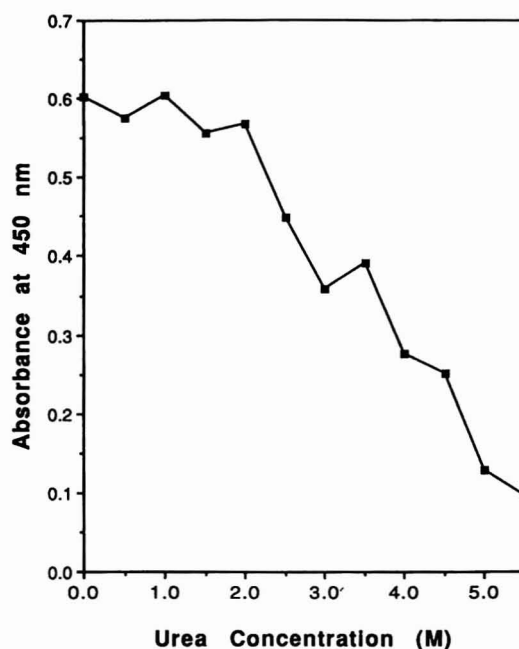


Fig. 3. Direct binding ELISA to determine the effect of urea on JB4E3-3 binding to *Amb a* I in denatured pollen extract. Absorbances are plotted as a function of the urea concentration.

als and Methods. Fig. 2a shows that dialysis of the solubilized pellet caused the protein to aggregate to a high-molecular-mass form with essentially all of the *rAmb a* I.1 activity eluting at the column void (> 300 000 dalton). In contrast, the undialyzed recombinant protein, shown in Fig. 2b, eluted predominantly at the approximate molecular mass of a monomer, although some higher-molecular-mass aggregates were detected probably due to the fact that the mobile phase in the column did not contain urea. These results suggest that when the dialyzed *rAmb a* I.1 was loaded onto the immunoaffinity column it was aggregated with other proteins as well as with itself and therefore its relative abundance was not increased significantly by the chromatography. Previously, ion-exchange chromatography and hydrophobic interaction chromatography had been used in an attempt to purify the protein but no activity was recovered from those columns. Aggregation of the proteins could have contributed to those results in addition to the hydrophobic nature of the unfolded protein.

To prevent protein aggregation, detergents are



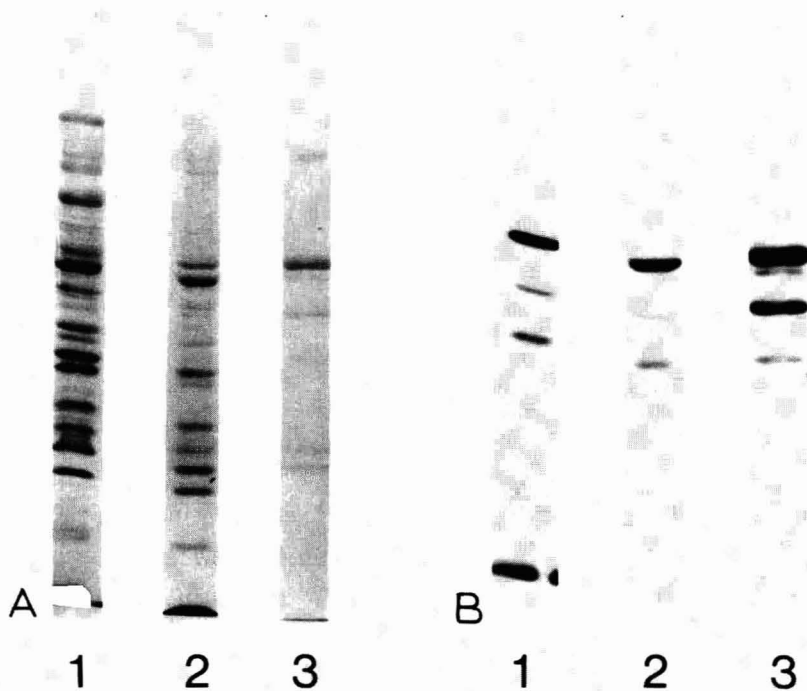


Fig. 4. SDS-PAGE and Western blot analysis of *rAmb a I.1* purified in the presence of 2 *M* urea. (A) Coomassie blue-stained gel analysis; (B) analogous lanes from a duplicate gel which was blotted and probed with JB4E3-3. Lanes: 1 = whole cell lysate of *E. coli* expressing *rAmb a I.1*; 2 = urea-solubilized washed cell pellet of these cells; 3 = JB4E3-3 Sepharose-purified *rAmb a I.1*.

often used. However, the *rAmb a I.1* was to be used in cellular assays where detergents could potentially adversely affect cell viability. Another approach to preventing reaggregation of solubilized inclusion body proteins is to refold the proteins to their native conformation [12]. Determining the conditions for refolding of a protein often requires testing a number of variables and is generally monitored by an activity assay. In the case of *rAmb a I.1*, its only known biological activity is as an allergen and in the denatured form it is capable of stimulating T cells from allergic individuals and binding IgE, although IgE binding is reduced [4,13]. Consequently, development of an assay for refolding would be very difficult. Therefore, we considered diluting the urea and the protein and loading immediately onto the immunoaffinity column with the expectation that the kinetics of protein aggregation would be slow in low denaturant concentrations. In order for this approach to be effective, the antibody must tolerate exposure to some level of urea. Urea is sometimes

used as an elution reagent in immunoaffinity chromatography at either 2 or 8 *M*, and columns can sometimes be regenerated after treatment with 2 *M* urea [7]. Therefore, it is not unreasonable to expect that a monoclonal antibody could tolerate low denaturant concentrations. The stability of JB4E3-3 in the presence of urea was assayed in a direct binding ELISA, the results of which are shown in Fig. 3. The antibody showed no decrease in binding activity at concentrations of urea up to 2 *M*. An additional direct ELISA was performed which demonstrated that JB4E3-3 was not irreversibly denatured by the combination of high pH (10.5) and 2 *M* urea to be used during elution (Table I).

Immunoaffinity purification of *rAmb a I.1* was done with 2 *M* urea present throughout the procedure. Fig. 4 shows the result of this purification step analyzed on duplicate 12% acrylamide SDS-PAGE gels, one Coomassie Blue stained (panel A) and the other analyzed by a Western blot probed with JB4E3-3 (panel B). Approximately a twenty-fold in-

crease in purity of the recombinant protein as compared to the whole cell lysate was achieved as determined by densitometric analysis of the Coomassie Blue stained gel shown (panel A, lanes 1 and 3). The intact *Amb a* I.1 and its proteolytic fragments, identified by Western blot analysis (panel B, lane 3), made up approximately 80% of the protein recovered from the column (panel A, lane 3). The JB4E3-3 Sepharose column was run four times in 2 *M* urea with no detectable loss of activity. Changes in the column capacity were not assessed.

We have demonstrated that it is possible to use an antibody as an immunoaffinity reagent in the presence of a denaturing agent. Although it is preferable to run immunoaffinity columns under the mildest possible conditions in order to maximize their lifespan, the use of harsh reagents may be necessary in order to solve particularly difficult purification problems. Protein aggregation is a problem often encountered with recombinant proteins solubilized from inclusion bodies. However, if an antibody can be chosen as an immunoaffinity reagent based on its stability in the presence of harsh reagents such as denaturants or detergents, protocols can be designed which allow purification of the protein of interest and preserve the activity of the immunoaffinity column.

## REFERENCES

- 1 T. P. King, P. S. Norman and J. T. Connel, *Biochemistry*, 3 (1964) 458.
- 2 D. G. Marsh, L. Goodfriend, T. P. King, H. Lowenstein and T. A. E. Platts-Mills, *Bull. WHO*, 64 (1986) 767.
- 3 T. Rafnar, I. G. Griffith, M. C. Kuo, J. F. Bond, B. L. Rogers and D. G. Klapper, *J. Biol. Chem.*, 266 (1991) 1229.
- 4 J. F. Bond, R. D. Garman, K. M. Keating, T. J. Briner, T. Rafnar, D. G. Klapper and B. L. Rogers, *J. Immunol.*, 146 (1991) 3380.
- 5 B. Babbitt, P. Allen, G. Matsueda, E. Haber and E. Unanue, *Nature (London)*, 317 (1985) 361.
- 6 S. Buus, A. Sette, S. Colon, C. Miles and H. M. Grey, *Science, (Washington, D.C.)*, 235 (1987) 1358.
- 7 E. Harlow and D. Lane (Editors), *Antibodies: A Laboratory Manual*, Cold Spring Harbor Laboratories, New York, 1988, Ch. 13, pp. 547–552.
- 8 J. J. Smith, J. R. Olson and D. G. Klapper, *Mol. Immunol.*, 25 (1988) 355.
- 9 E. Amann, B. Ochs and K.-J. Abel, *Gene*, 69 (1988) 301.
- 10 H. Towbin, T. Staehlin and J. Gorgon, *Proc. Natl. Acad. Sci. U.S.A.*, 76 (1979) 4350.
- 11 T. P. King, A. Alagon, L. Kochoumian, J. Kuan, A. K. Sobotka and L. M. Lichtenstein, *Arch. Biochem. Biophys.*, 212 (1981) 127.
- 12 F. A. Marston and D. L. Hartley, *Methods Enzymol.*, 182 (1990) 264.
- 13 T. P. King, P. S. Norman and N. Tao, *Immunochemistry*, 11 (1974) 83.



## Separation of interleukins by a preparative chromatofocusing-like method

Seth P. Monkarsh, Emil A. Russoman and Swapan K. Roy

Department of Protein Biochemistry, Roche Research Center, Hoffmann–La Roche Inc., Nutley, NJ 07110 (USA)

---

### ABSTRACT

A chromatofocusing-like method used in the large-scale separation of deamidated from amidated recombinant human interleukin-1 $\alpha$  (amino acids 117–271), derived from *Escherichia coli*, is described. Two major protein species having isoelectric points (pI) of approximately 5.3 and 5.1 were separated by high-performance liquid chromatography using a sulfopropyl strong cation-exchange column. Unlike standard chromatofocusing technique, this method does not use carrier ampholytes during gradient separation of proteins, nor does it employ increased ionic strength for protein elution, the usual method for performing standard ion-exchange chromatography. N-Terminal sequence analysis of the protein with a pI of 5.3 revealed an Asn residue at position 32 as predicted by the cDNA sequence. The pI 5.1 species showed an Asp residue at the same position as a result of deamidation of Asn. This method was also used in the large-scale separation of N-Met from des-Met recombinant human interleukin-1 $\beta$ .

---

### INTRODUCTION

The separation of proteins using chromatofocusing technique is a widely accepted method because of its excellent resolving power. This technique has been predominantly used on an analytical basis in the conventional mode on glass columns [1–4], but can also be adapted to the high-performance liquid chromatographic (HPLC) mode and subsequently modified to preparative scale.

The isolation and characterization of recombinant human interleukin-1 $\alpha$  (rhIL-1 $\alpha$ ) from *Escherichia coli* cells was previously described [5]. Recently, two major isoelectric species of purified rhIL-1 $\alpha$  were detected on an analytical isoelectric focusing (IEF) gel following the previous observation of a single protein band in sodium dodecyl sulfate–polyacrylamide electrophoresis (SDS-PAGE) [6]. A scaleable, “chromatofocusing-like” technique was developed in an attempt to separate and isolate these species for further characterization. The term

“chromatofocusing-like” is suggested to describe a distinct branch of ion-exchange chromatography. Unlike standard chromatofocusing technique, this method does not use carrier ampholytes during gradient separation of proteins, nor does it employ high concentrations of counter-ions for protein elution, the usual method for performing standard ion-exchange chromatography. The basis for this powerful separation technique is in the titration of chemical functional groups attached to an ion-exchange column, in this case the sulfopropyl (SP) functionality of a strong cation-exchange HPLC column, with low-buffering-capacity buffers.

We have also applied our method to resolve two forms of recombinant human interleukin-1 $\beta$  (rhIL-1 $\beta$ ) in a manner similar to the rhIL-1 $\alpha$  separation.

### EXPERIMENTAL

#### Apparatus

The chromatographic system consisted of the following from Waters Chromatography Division (Millipore, Milford, MA, USA): Delta Prep 3000 HPLC system, Lamda-Max Model 480 variable-

---

Correspondence to: S. P. Monkarsh, Department of Protein Biochemistry, Roche Research Center, Hoffmann–La Roche Inc., Nutley, NJ 07110, USA

wavelength detector, Model 740 data module. The preparative fraction collector used was a Model PF-30 unit (Pharmacia, Piscataway, NJ, USA). The peak detector (Hoffmann–La Roche Instrument Support Section, Nutley, NJ, USA) activated a collection valve (Valcor Engineering, Springfield, NJ, USA) for automated peak collection.

#### Columns

The stainless-steel HPLC columns were all silica-based SP-strong cation-exchange columns (Separation Industries, Metuchen, NJ, USA; NuGel P-SP).

#### Buffers

Buffers for rhIL-1 $\alpha$  separation consisted of the following: buffer A was 3.7 mM acetic acid, adjusted to pH 4.8, with sodium hydroxide; buffer B was 10 mM potassium phosphate, dibasic, adjusted to pH 6.8, with hydrochloric acid.

Buffers for rhIL-1 $\beta$  separation consisted of the following: buffer A was 20 mM acetic acid, adjusted to pH 5.0 with sodium hydroxide; buffer B was the same as that for the rhIL-1 $\alpha$  separation, except adjusted to pH 7.1 with hydrochloric acid.

Filtration of buffers and samples was done using a combination 0.8–0.2  $\mu$ m filter (Sartorius Filters, Hayward, CA, USA).

All buffers were sparged continuously with ultra-high-purity helium (Linde Specialty Gases, Danbury, CT, USA).

#### Separation of isoelectric species of rhIL-1 $\alpha$

Initially, an eight-fold dilution of purified rhIL-1 $\alpha$ , amino acids 117–271 (0.8 mg protein per ml of 0.1 M sodium chloride), with buffer A for rhIL-1 $\alpha$  separation was made, the pH adjusted to 4.8 and the sample filtered.

After thorough column equilibration with buffer A, the diluted sample was applied to the column. A steady baseline was established by equilibration with buffer A washing off any unabsorbed contaminants. A linear, ascending pH gradient (4.8–6.8) was performed from 0 to 80% buffer B in 120 min, and monitored at 280 nm absorbance.

#### Separation of two forms of rhIL-1 $\beta$

Twenty-fold dilution of purified rhIL-1 $\beta$  (4 mg protein per ml of 0.1 M sodium chloride) was made with buffer A for rhIL-1 $\beta$  separation, the pH ad-

justed to 5.0 and the sample filtered. Column equilibration with buffer A for rhIL-1 $\alpha$  separation was established. A linear, ascending pH gradient (5.0–7.1) was performed from 0 to 100% buffer B in 100 min, and monitored at 280 nm absorbance.

#### Analytical evaluation of purity

IEF of rhIL-1 $\alpha$  was performed on a LKB Model 2117 Multiphor horizontal unit using pH 4.0–6.5 and rhIL-1 $\beta$  using pH 5.5–8.5 gradient polyacrylamide gels as described by the manufacturer (Ampholine PAGplates, pH 4–6.5, Part No. 80-1124-81 and pH 5.5–8.5, Part No. 80-1124-82; Pharmacia). Proteins on the gel were fixed in a fresh solution containing 5% (w/v) sulfosalicylic acid and 10% (w/v) trichloroacetic acid for 30 min at room temperature. Gels were stained in 0.025% Coomassie blue R-250 (BioRad Labs., Richmond, CA, USA; Cat. No. 161-0500) in destain solution (acetic acid–ethanol–water; 9.5:30:60.5, v/v/v) for 40 min and destained overnight with several additional changes. Calibration standards for IEF (Sigma, St. Louis, MO, USA) were run simultaneously with samples and *pI* values calculated by plotting the standard *pI* values versus the distance from the cathode (–) in mm. The unknown *pI* values were then measured in millimeters from the cathode and extrapolated from the standard curve to determine their approximate *pI*.

Total rhIL-1 $\alpha$  concentration was obtained by performing the automated immunoaffinity chromatographic assay [7]. Each of the species reacts equally with antibody. Protein concentration was monitored using the BCA protein assay (Pierce, Rockford, IL, USA).

#### RESULTS AND DISCUSSION

Two major isoelectric species were observed in the purified rhIL-1 $\alpha$  preparation by analytical IEF (Fig. 1, lane 2), one having a *pI* of 5.1 and the other a *pI* of 5.3. These species were indistinguishable from each other and appeared as a homogeneous band on SDS-PAGE. Two proteins were separated on the SP-strong cation-exchange HPLC column (Fig. 1, peaks 1 and 2) and reanalyzed for purity by analytical IEF (Fig. 1, lanes 3 and 4). An Asp residue at position 32 in the IL-1 $\alpha$  with a *pI* of 5.1 (Fig. 1, lane 3, peak 1) and Asn residue at the identical posi-

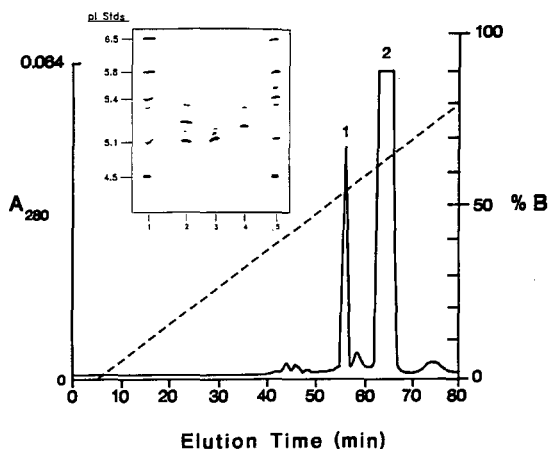


Fig. 1. Separation of deamidated (peak 1,  $pI$  5.1) from amidated (peak 2,  $pI$  5.3) rhIL-1 $\alpha$  (amino acids 117–271) performed on SP-strong cation-exchange HPLC. Separation conditions were as follows: column size, 250 mm  $\times$  50 mm I.D.; particle size, 15–20  $\mu$ m; pore size, 300  $\text{\AA}$ ; sample load, 250 mg; flow-rate, 75 ml/min; gradient, 0–80% B in 120 min, buffer A (3.7 mM acetic acid, pH 4.8), buffer B (10 mM potassium phosphate, dibasic, pH 6.8). Inset: analytical isoelectric focusing of rhIL-1 $\alpha$  (amino acids 117–271) performed on pH 4.0–6.5 IEF gel. Samples derived from SP-HPLC separations. Lanes: 1, 5 = standard proteins,  $pI$  values indicated; 2 = SP-HPLC sample load, 3 = peak 1, deamidated species ( $pI$  5.1); 4 = peak 2, amidated species ( $pI$  5.3).

tion in the species with a  $pI$  of 5.3 (Fig. 1, lane 4, peak 2) was determined by N-terminal protein sequence analysis of up to the first 74 residues for each of the proteins. These determinations were confirmed by comparison of each sequence to the predicted cDNA precursor gene sequence [8]. Results indicated that the Asn–Asp difference at residue 32 is due to the conversion of the amide side-chain of the Asn ( $pI$  5.3) to a carboxyl group in Asp ( $pI$  5.1), also known as deamidation, as previously reported [9–11].

A rhIL-1 $\alpha$  sample (250 mg total protein) loaded on the 250 mm  $\times$  50 mm I.D. SP-HPLC column typically yielded recoveries of 85% amidated species ( $pI$  5.3), 10% deamidated species ( $pI$  5.1) and 5% consisting of other minor contaminants.

Similar deamidated and amidated species of rhIL-1 $\alpha$  from *E. coli* were previously isolated by chromatofocusing by other investigators [12].

Two forms of the rhIL-1 $\beta$  were observed during its large-scale purification by analytical IEF (Fig. 2,

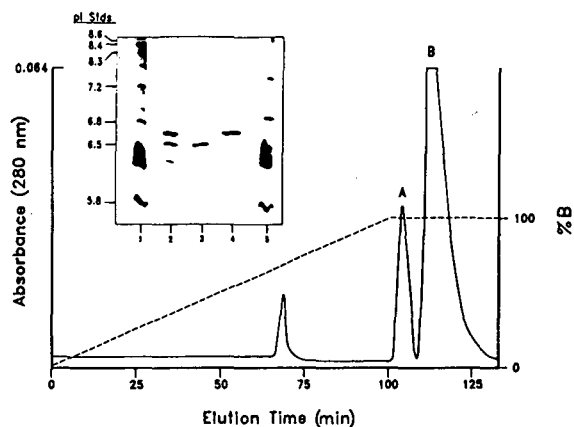


Fig. 2. Separation of N-Met (peak A,  $pI$  6.5) from des-Met (peak B,  $pI$  6.7) rhIL-1 $\beta$  performed on SP-strong cation-exchange HPLC. Separation conditions were as follows: column size 250 mm  $\times$  25 mm I.D., particle size, 15–20  $\mu$ m; pore size, 300  $\text{\AA}$ ; sample load, 125 mg; flow-rate 20 ml/min; gradient, 0–100% B in 100 min, buffer A (3.7 mM acetic acid, pH 4.8), buffer B (10 mM potassium phosphate, dibasic, pH 7.1). Inset: analytical isoelectric focusing of rhIL-1 $\beta$  performed on pH 5.5–8.5 IEF gel. Samples derived from SP-HPLC separations. Lanes: 1, 5 = standard proteins,  $pI$  values indicated; 2 = SP-HPLC sample load; 3 = peak A, N-Met form ( $pI$  6.5); 4 = peak B, des-Met form ( $pI$  = 6.7).

lane 2), the des-Met form having a  $pI$  of 6.7 and the N-Met form having a  $pI$  of 6.5. These appeared as a single band on SDS-PAGE. Separation was made possible by our HPLC method (Fig. 2, peaks A and B) and subsequent analysis by analytical IEF (Fig. 2, lanes 3 and 4). The presence of an incompletely processed N-terminal methionine (N-Met) in the earlier-eluting HPLC peak A and that of a correctly processed physiological N-terminal alanine (des-Met) form, the later-eluting peak B on HPLC, was established by comparison of each sequence to the predicted cDNA precursor gene sequence [8].

Mixtures of similar forms were previously isolated from recombinant-derived interleukin-1 $\beta$  by chromatofocusing and characterized by others on an analytical scale [13].

There are several advantages to using our method for the separation of closely related isoelectric species. First, expensive ampholytes are not needed which are impractical for scale-up. Also, because ampholytes are not used, their somewhat difficult removal from protein samples is not an issue. The

presence of sodium chloride in the elution buffers for both rhIL-1 $\alpha$  and rhIL-1 $\beta$  in the separations we performed resulted in an extreme loss in resolution, or even co-elution of species or forms. For other proteins which may be highly charged, salt may be required in the elution buffer to resolve species of interest. In any case, salts should be used sparingly to avoid interference in protein charge differences which normally enhance resolution between peaks.

#### ACKNOWLEDGEMENTS

We thank Leo Bowski (Bioprocess Development) for providing *E. coli* cells. We are grateful to Jeff Hulmes and May Meidel for performing amino acid and N-terminal sequence analyses, and to Yu-Ching Pan for helpful discussions and manuscript review. We would also like to thank Dennis Tighe for art work and Lisa Nieves for manuscript preparation.

#### REFERENCES

- 1 L. A. E. Sluyterman and J. Wijdenes, in B. J. Radola and D. Graesslin (Editors), *Proceedings of the International Symposium on Electrofocusing and Isotachopheresis*, Walter de Gruyter, Berlin, 1977, p. 463.
- 2 L. A. E. Sluyterman and O. Elgersma, *J. Chromatogr.*, 150 (1978) 17.
- 3 L. A. E. Sluyterman and J. Wijdenes, *J. Chromatogr.*, 150 (1978) 31.
- 4 *Chromatofocusing with Polybuffer and PBE*, Pharmacia Fine Chemicals, Uppsala, 1980.
- 5 U. Gubler, A. O. Chua, A. S. Stern, C. P. Hellmann, M. P. Vitek, T. M. Dechiara, W. R. Benjamin, K. J. Collier, M. Dukovich, P. C. Familletti, C. Fiedler-Nagy, J. Jenson, K. Kafka, P. L. Kilian, D. Stremlo, B. H. Wittreich, D. Woehle, S. B. Mizel and P. T. Lomedico, *J. Immunol.*, 136 (1986) 2492.
- 6 U. K. Laemmli, *Nature*, 227 (1970) 680.
- 7 S. K. Roy, W. C. McGregor and S. T. Orichowsky, *J. Chromatogr.*, 327 (1985) 189.
- 8 C. J. March, B. Mosley, A. Larsen, D. P. Cerretti, G. Braedt, V. Price, S. Gillis, C. S. Henney, S. R. Kronheim, K. Grabstein, P. J. Conlon, T. P. Hopp and D. Cosman, *Nature*, 315 (1985) 641.
- 9 A. B. Robinson and C. J. Rudd, in B. J. Horecker and E. R. Stadtman (Editors), *Curr. Top. Cell Regul.*, Vol. 8, Academic Press, New York, 1973, p. 247.
- 10 A. A. Kossiakoff, *Science*, 240 (1988) 191.
- 11 T. Geiger and S. Clarke, *J. Biol. Chem.*, 262 (1987) 785.
- 12 P. T. Wingfield, R. J. Mattaliano, H. R. MacDonald, S. Craig, G. M. Clore, A. M. Gronenborn and U. Schmeissner, *Protein Eng.*, 1 (1987) 413.
- 13 P. T. Wingfield, P. Graber, K. Rose, M. G. Simona and G. J. Hughes, *J. Chromatogr.*, 387 (1987) 291.

# Kinetic analysis of biotinylation of specific residues of peptides by high-performance liquid chromatography

Alexander Kurosky

*Department of Human Biological Chemistry and Genetics, University of Texas Medical Branch, Galveston, TX 77555-0645 (USA)*

Brian T. Miller

*Department of Anatomy and Neurosciences, University of Texas Medical Branch, Galveston, TX 77555-0843 (USA)*

Susan L. Knock

*Marine Biomedical Institute, University of Texas Medical Branch, Galveston, TX 77555-0843 (USA)*

---

## ABSTRACT

A procedure employing  $C_{18}$  reversed-phase high-performance liquid chromatography (HPLC) is described for evaluating the kinetics of biotinylation of specific residues of peptides after reaction with N-hydroxysuccinimide esters of biotin. Utilizing this HPLC method, we determined the observed pseudo-first-order reaction rate constant ( $k'_1$ ) of biotinylation of lysyl residues in two model peptides, [biotinyl-Ser<sup>108</sup>]ProA-egg laying hormone (108–121) and pGlu-Lys-Trp-Ala-Pro, to be  $1.22 \cdot 10^{-2} \text{ s}^{-1}$  and  $1.08 \cdot 10^{-2} \text{ s}^{-1}$ , respectively, in 0.05 M sodium phosphate buffer, pH 8.2, at 25°C. The respective reaction half-lives of the two peptides were 57 s and 64 s. In addition, HPLC analytical methods were established for determining the time-course of hydrolysis of biotinylating reagents at acidic and alkaline pH and for evaluating biotin reagent homogeneity.

---

## INTRODUCTION

Since the earliest days of biochemical research, chemical modification studies have proven to be invaluable for investigating the structure and function relationships of biologically important molecules. One particularly versatile technology, based on the covalent attachment of the vitamin biotin to peptides, proteins, and nucleic acids, has emerged during the last two decades [1]. This technology exploits the strong affinity ( $K_a \approx 10^{15} \text{ M}^{-1}$ ) that is characteristic of the interaction between biotin and the tetrameric egg-white protein avidin. Bioactive compounds which are linked to the valeric acid side

chain of biotin typically retain their biological properties. These modified molecules are able to bind to their specific biological targets (*e.g.*, receptors) allowing the biotinyl group to be available for interaction with avidin. Since a variety of reporter groups can be conjugated to avidin, the avidin–biotin system can be utilized in a host of applications involving the localization, visualization, or isolation of specific biomolecules.

An important aspect of the application of the avidin–biotin system is the synthesis of a specific, bioactive, biotinylated protein or peptide. There are a variety of reagents that can biotinylate different functional groups on proteins and peptides. The N-hydroxysuccinimide esters of biotin (NHS-biotin) are a widely used class of biotinylating reagent which are reported to react with primary amino groups to form N-acylated derivatives [1]. Typical

---

*Correspondence to:* Dr. Alex Kurosky, Department of Human Biological Chemistry and Genetics, The University of Texas Medical Branch, Galveston, TX 77555-0645, USA.



ly, these reagents are either simple NHS-biotin esters or related compounds which contain a spacer of 6-aminohexanoic acid between the biotin and NHS moieties. These compounds can also be sulfonated on the NHS moiety to increase their solubility characteristics in aqueous solutions. Although the biotin reagents are widely employed for labeling peptides and proteins they have not been evaluated in depth as chemical modification reagents. Little information is available regarding the kinetics of their reactivity with specific reactive groups of proteins.

In a series of experiments with several different bioactive peptides, we have reported that the NHS-biotin esters can be used to identify differences in the intrinsic reactivity of amino groups [2–5]. Furthermore, we have found that unexpected modifications of seryl and tyrosyl residues can occasionally occur [2]. These experiments have underscored the need to more fully investigate the chemical modification of bioactive peptides and proteins with NHS-biotin esters by conducting a careful analysis of the reaction kinetics of biotinylation with these esters. To this end, we have developed HPLC methods employing a  $C_{18}$  reversed-phase column to determine the relative reactivity of NHS-biotin esters during reactions with different model peptides. In this report, we describe these HPLC methods in detail and demonstrate how they may be applied to kinetic analysis of the biotinylation of specific peptide residues. In addition, we have also established HPLC methods to investigate biotinylating reagent homogeneity and the extent of their hydrolysis under described reaction conditions.

## EXPERIMENTAL

### Materials

Trifluoroacetic acid (HPLC grade), N,N-dimethylformamide, dimethylsulfoxide, sulfosuccinimidyl-6-(biotinamido) hexanoate (sulfo-NHS- $\epsilon$ Ahx-biotin), succinimidyl-6-(biotinamido) hexanoate (NHS- $\epsilon$ Ahx-biotin), sulfosuccinimidyl D-biotin (sulfo-NHS-biotin), and succinimidyl D-biotin (NHS-biotin) were obtained from Pierce. NHS- $\epsilon$ Ahx-biotin was also purchased from Sigma and Molecular Probes. NHS was from Sigma and  $\epsilon$ Ahx-biotin was obtained from Molecular Probes. Acetonitrile (HPLC grade) was obtained from Mal-

linckrodt. Sodium acetate, sodium phosphate and urea were obtained from Fisher Scientific. Glycine was purchased from Calbiochem. Reagents for amino acid compositional analysis were from Applied Biosystems. Synthetic egg-laying hormone (ELH) [6] and ProA-ELH(108–121) (Ser–Leu–Glu–Ser–Gly–Ile–Ser–Lys–Arg–Ile–Ser–Ile–Asn–Gln–NH<sub>2</sub>) [7] were prepared in the Biosynthesis Laboratory of the University of Texas Medical Branch by solid-phase synthesis [8] using a fully automated synthesizer (Biosearch Model 9600). Synthetic peptide, <EKWAP (pGlu–Lys–Trp–Ala–Pro), was obtained from Bachem Bioscience. Vydac  $C_{18}$  (5  $\mu$ m particle size; 300 Å pore diameter) reversed-phase columns (25 cm  $\times$  1.0 cm; phase 218TP) and direct connect guard columns containing Vydac  $C_{18}$  (5  $\mu$ m particle size) cartridges were purchased from Alltech Applied Science Labs. An Asahipak ODP-50  $C_{18}$  (5  $\mu$ m particle size) reversed-phase column (15 cm  $\times$  0.6 cm) was purchased from Keystone Scientific, Bellefonte, PA, USA.

### Biotinylation reactions

For the preparation of monobiotinyl- $\alpha$ NH<sub>2</sub>-ProA-ELH(108–121), sulfo-NHS- $\epsilon$ Ahx-biotin was weighed and the peptide, dissolved in 0.05 M sodium phosphate buffer, pH 8.2, was added to the dry powder. The molar ratio of reagent:peptide was 2.5:1. The biotinylated peptide derivatives were subsequently separated by HPLC on a Vydac semi-preparative  $C_{18}$  column (results not shown) and chemically characterized by amino acid compositional analysis and automated peptide sequence analysis. The HPLC fractions containing monobiotinyl- $\alpha$ NH<sub>2</sub>-ProA-ELH(108–121) were pooled and lyophilized.

For reagent hydrolysis and kinetic analysis of peptide biotinylation, NHS- $\epsilon$ Ahx-biotin was dissolved in 25  $\mu$ l N,N-dimethylformamide just prior to reaction. Tight sealing Whatman 1.5-ml conical screw cap microtubes containing 0.25 mg or 0.5 mg of reagent were prepared by aliquoting reagent (50  $\mu$ l) dissolved in N,N-dimethylformamide and immediately drying by vacuum centrifugation. The biotinylating reagent stored in these tubes was stable for at least 2–3 weeks at 4°C. For kinetic studies, peptides <EKWAP and monobiotinyl- $\alpha$ NH<sub>2</sub>-ProA-ELH(108–121) dissolved in 200  $\mu$ l of 0.05 M phosphate buffer, pH 8.2, were added to the biotin

reagent in 25  $\mu$ l N,N-dimethylformamide and reacted for the times indicated. Reactions were stopped by the addition of 125  $\mu$ l of 1 M glycine-HCl, pH 3.0. The reaction mixtures were injected immediately onto the C<sub>18</sub> HPLC column. The molar ratio of reagent:peptide was 25:1 for the biotinylation of <EKWAP and 57:1 for the biotinylation of mono-biotinyl- $\alpha$ NH<sub>2</sub>-ProA-ELH(108–121). For all biotinylation reactions described the NHS- $\epsilon$ Ahx-biotin used was that obtained from Molecular Probes; however, the NHS- $\epsilon$ Ahx-biotin obtained from Sigma was also found to be homogenous by HPLC. The stability of NHS- $\epsilon$ Ahx-biotin in aqueous solution over 90 min was tested at pH 8.2 (sodium phosphate buffer), pH 6.5 (sodium phosphate-trifluoroacetic acid buffer) and pH 4.0 (sodium acetate buffer). The biotinylating reagent (0.25 mg) was dissolved in 25  $\mu$ l of N,N-dimethylformamide and 200  $\mu$ l of buffer was added. At designated times 0.5 ml of 0.1% trifluoroacetic acid was added and the mixture was immediately injected onto the HPLC column. All above reactions were conducted at 25°C.

#### High-performance liquid chromatography

A Beckman Model 332 gradient liquid chromatograph with an on-line Hitachi Model 100-40 variable-wavelength spectrophotometer was used for most of the studies. A second Model 332, which was on-line with a Beckman Model 160 fixed-wavelength absorbance detector, was also employed.

Reaction mixtures containing biotinylating reagents or biotinylated peptides were applied to a Vydac C<sub>18</sub> reversed-phase HPLC column and eluted with a linear gradient of solvent A (0.1% trifluoroacetic acid) and solvent B (100% acetonitrile containing 0.1% trifluoroacetic acid) at a flow-rate of 1.75 ml/min. The column eluate was monitored at 215 nm and 1.0-min fractions were collected. Fractions were pooled based on absorbance and were subjected to amino acid compositional analysis. All fractions were dried by vacuum centrifugation and stored at 4°C.

The linear gradient employed to fractionate biotinylating reagents and biotinylated peptides is shown in the top figure panel for each experiment. Three gradient programs were used for these studies. The gradient program for evaluating reagent homogeneity and hydrolysis was simply 5% acetonitrile to 50% acetonitrile over 60 min. To fraction-

ate the biotinylation reaction products of [biotinyl-Ser<sup>108</sup>]ProA-ELH(108–121) the HPLC program was 16% isocratic acetonitrile for 10 min whereupon the gradient was increased from 16% acetonitrile to 50% over 110 min. To separate the biotinylation reaction mixtures of the <EKWAP peptide the gradient conditions were 10% acetonitrile to 55% over 60 min.

#### Amino acid analysis

The amount of biotin was determined by amino acid analysis of 6-aminohexanoic acid as we previously described [3]. Samples of those NHS-biotin esters containing a 6-aminohexanoic acid spacer arm were applied directly to an Applied Biosystems 420H (derivatizer/hydrolyzer) amino acid analyzer with on-line acid hydrolysis and pre-column phenylthiocarbonyl derivatization.

#### RESULTS AND DISCUSSION

We have previously reported that biotinylated peptide derivatives were readily separated by C<sub>18</sub> reversed-phase HPLC [2,4]. In fact, we have found that the resolution of various biotinylated peptide derivatives was consistently remarkable for a number of peptides investigated. For example, the monobiotinylated derivatives of the three amino groups ( $\alpha$ NH<sub>2</sub>-Ile<sup>1</sup>;  $\epsilon$ NH<sub>2</sub>-Lys<sup>8</sup> and  $\epsilon$ NH<sub>2</sub>-Lys<sup>36</sup>) of ELH of *Aplysia* can be well separated on a Vydac 300 Å C<sub>18</sub> column (Fig. 1A) [4]. To inquire whether this resolution was unique to the Vydac column, a comparative elution profile of the biotinylation reaction products of ELH was made using an Asahipak ODP-50 column packed with a C<sub>18</sub> modified polymer gel (Fig. 1B). The elution profile from the Asahipak column was essentially comparable to that of the Vydac column except that the elution of fractions 4 and 5 from the Asahipak column was reversed (Fig. 1A and B). The observed high degree of resolution of biotinylated peptides was therefore not likely due to interactions with the base material support since the Vydac column contained a silica gel base and the Asahipak column contained a polymer base support. We have consistently observed that the elution pattern of peptides after biotinylation typically demonstrated increased bandwidths, similar to that observed during isocratic elution conditions, suggesting a relatively strong in-

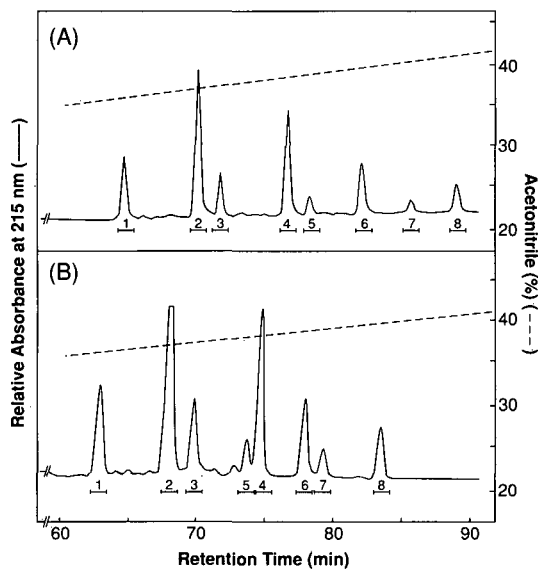


Fig. 1. Comparative  $C_{18}$  reversed-phase HPLC separation of a reaction mixture of NHS- $\epsilon$ Ahx-biotin with *Aplysia* egg-laying hormone. Biotinylating reagent was dissolved in 25  $\mu$ l N,N-dimethylformamide and 225  $\mu$ l of 0.05 M  $\text{NaHCO}_3$ , pH 8.2, containing 15 nmol (66  $\mu$ g) of ELH, was added. The molar ratio of reagent to peptide was 8:1. After 30 min of reaction at 25°C the pH was lowered to 6.0 by addition of 1 ml of 20% acetonitrile in 0.1% trifluoroacetic acid and the reaction mixture was immediately injected onto the HPLC column. (A) Vydac semipreparative column, flow-rate 1.75 ml/min; (B) Asahipak ODP-50 column, flow-rate 1.0 ml/min. Gradient conditions (identical for both columns) and the chemical characterization of each fraction were as we previously reported [4].

teraction between the biotinylated solute and the  $C_{18}$  bonded phase. The covalent addition of a single biotin group usually significantly increased the retention time of the peptide [2,4]. Furthermore, even with proteins, we have observed that small differences in the number of biotinyl groups can be reflected in significant retention time differences [3].

Prior to conducting kinetic studies of biotinylation of peptides we evaluated the homogeneity of a number of available NHS-biotin esters including the sulfonated derivatives. These initial studies were important since we had previously observed some variation of peptide biotinylation that we had attributed to the quality of the biotinylation reagents [2]. Evaluation of biotinylation reagent homogeneity is shown in Figs. 2 and 3. Fig. 2 compares the  $C_{18}$  HPLC elution profile of NHS- $\epsilon$ Ahx-biotin obtained from three vendors. All reagents were analyzed

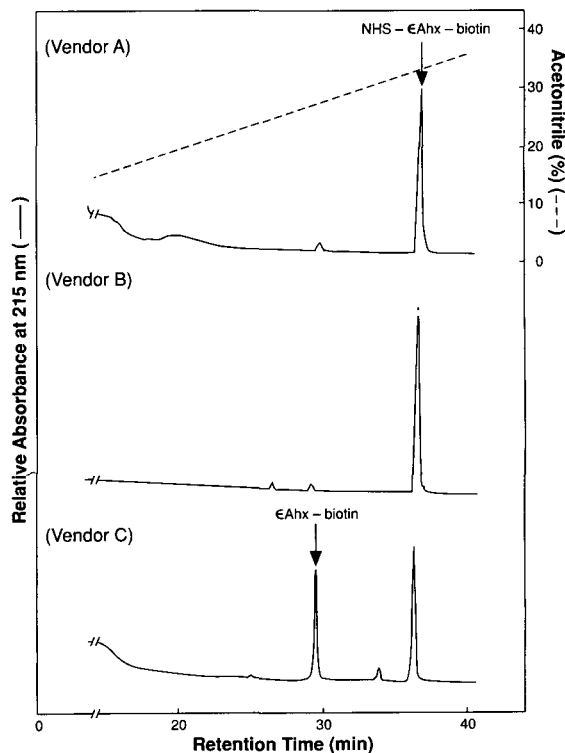


Fig. 2.  $C_{18}$  reversed-phase HPLC isolation of NHS- $\epsilon$ Ahx-biotin obtained from three vendors on a Vydac semipreparative column. Flow-rate was 1.75 ml/min. Biotinylating reagent (0.25 mg) was dissolved in 25  $\mu$ l N,N-dimethylformamide, followed by 0.5 ml 0.1% trifluoroacetic acid and injected immediately onto the HPLC column: Reagent obtained from vendor C was considerably hydrolyzed as evidenced by the  $\epsilon$ Ahx-biotin peak.

within 2 weeks of their receipt from vendors and were stored desiccated at 4°C. As indicated in Fig. 2, the product obtained from vendor C contained substantial amounts of  $\epsilon$ Ahx-biotin, presumably as a result of hydrolysis during manufacture or subsequent storage. Various lots of reagents purchased from vendor C at different times, no more than one year prior to these studies, varied 40–60% in the amount of  $\epsilon$ Ahx-biotin present. The quantitation of NHS- $\epsilon$ Ahx-biotin and  $\epsilon$ Ahx-biotin was achieved by amino acid analysis of the 6-aminohexanoic acid spacer arm as we previously described [3]. The observed  $A_{215\text{nm}}$  molar absorptivity was higher for NHS- $\epsilon$ Ahx-biotin than  $\epsilon$ Ahx-biotin by a factor of 1.34:1.

In a separate series of analyses, using HPLC con-

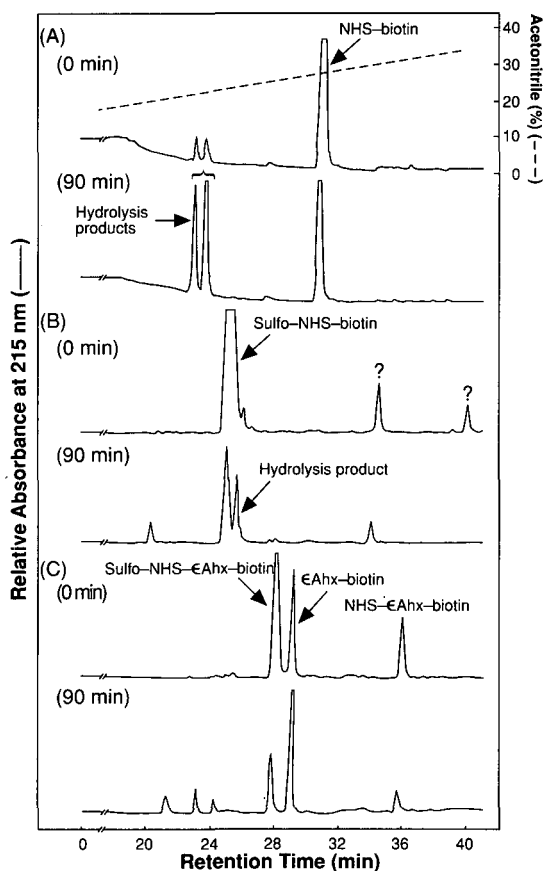


Fig. 3. Evaluation of other biotinylating reagents and 90-min hydrolysis products by  $C_{18}$  reversed-phase HPLC on a Vydac semipreparative column. Flow-rate was 1.75 ml/min. Non-sulfonated biotinylating reagents (0.5 mg) were dissolved in 25  $\mu$ l  $N,N$ -dimethylformamide followed by addition of 200  $\mu$ l 0.05  $M$  sodium phosphate buffer, pH 8.2. For sulfonated reagents, phosphate buffer was added to 0.5 mg dry reagent. For 0 time of reaction, 0.5 ml of 0.1% trifluoroacetic acid was added prior to the buffer; for the 90-min reaction time the acid was added at 90 min.

ditions identical to those described for the separation of NHS- $\epsilon$ Ahx-biotin, we also evaluated the homogeneity and hydrolysis products of other NHS-biotin esters (Fig. 3). Fig. 3A shows the elution of NHS-biotin at time 0 and after 90 min of hydrolysis. The two hydrolysis products indicated by arrows were not identified. Fig. 3B illustrates a similar analysis of sulfo-NHS-biotin. The only obvious hydrolysis product evident in this reaction was a peak which eluted immediately after the reagent. The ab-

sorbance of this hydrolysis product, however, was considerably lower than expected when compared to comparable products from other esters.

Analysis of sulfo-NHS- $\epsilon$ Ahx-biotin (Fig. 3C) indicated that this reagent contained  $\epsilon$ Ahx-biotin and surprisingly some NHS- $\epsilon$ Ahx-biotin. In these analyses special attention was paid to preventing carry-over and reagent contamination. A blank run conducted immediately prior to analysis indicated no evidence of NHS- $\epsilon$ Ahx-biotin. Also, the injection port was well rinsed before analysis. Confirmation that the contaminant peak was in fact NHS- $\epsilon$ Ahx-biotin was supported by three observations: (1) the retention time was identical to authentic NHS- $\epsilon$ Ahx-biotin; (2) amino acid analysis confirmed the presence of 6-aminohexanoic acid; and (3) the peak diminished after 90 min of hydrolysis at pH 8.2. Taken together these results established the utility of  $C_{18}$  reversed-phase HPLC for evaluating the homogeneity of commercial or otherwise obtained NHS-biotin esters. Clearly, the quality of some of the commercially available NHS-biotin esters was variable. Furthermore, in view of the fact that these esters can hydrolyze during storage, this HPLC procedure also offers a convenient method of measuring the extent of spontaneous reagent hydrolysis. It is also of value to point out that HPLC analysis of authentic NHS indicated that it eluted with the salt front early in the gradient elution program.

In order to establish the kinetics of biotinylation of our model peptides it was necessary to ensure that our reaction conditions were pseudo-first-order and that we were sufficiently in excess in regard to concentration of the selected biotinylating reagent, NHS- $\epsilon$ Ahx-biotin. Since the hydrolysis of NHS- $\epsilon$ Ahx-biotin was an important factor, we investigated the extent of hydrolysis of the reagent under our described reaction conditions using HPLC. Fig. 4 shows the time-course of hydrolysis of NHS- $\epsilon$ Ahx-biotin at pH 8.2, 6.5 and 4.0. As indicated, the rate of hydrolysis was significantly slower at acid pH. Importantly, these results indicated that over the time-course of our peptide kinetic studies the extent of reagent hydrolysis was not sufficiently large to influence our reaction kinetics and that we could readily maintain reagent excess. Fig. 5A shows three representative chromatograms of HPLC analysis of selected reaction times of spontaneous reagent hydrolysis at pH 8.2.

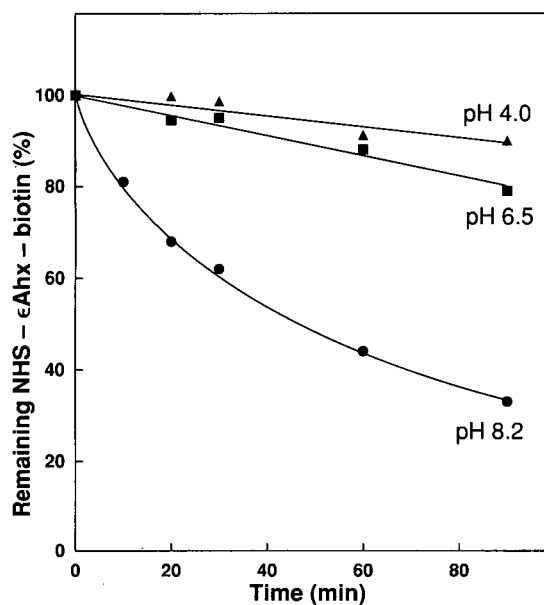


Fig. 4. Time-course of hydrolysis at 25°C of NHS- $\epsilon$ Ahx-biotin at pH 4.0 ( $\blacktriangle$ ), 6.5 ( $\blacksquare$ ), and 8.2 ( $\bullet$ ). Conditions were as described under Experimental.

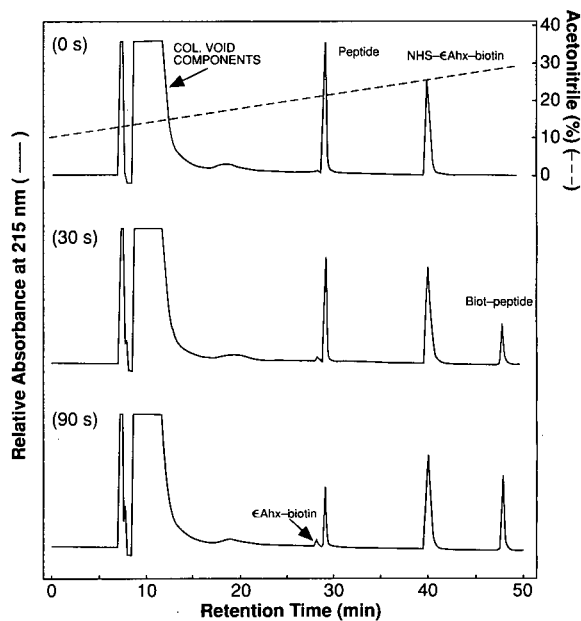


Fig. 6. Representative chromatograms from Vydac  $C_{18}$  reversed-phase HPLC analysis of the time-course of biotinylation of 21.8 nmol (13.3  $\mu$ g) of the peptide <EKWAP by NHS- $\epsilon$ Ahx-biotin at 25°C for times shown. "Biotin-peptide" (30 s and 90 s panels) was monobiotinylated on Lys<sup>2</sup>.

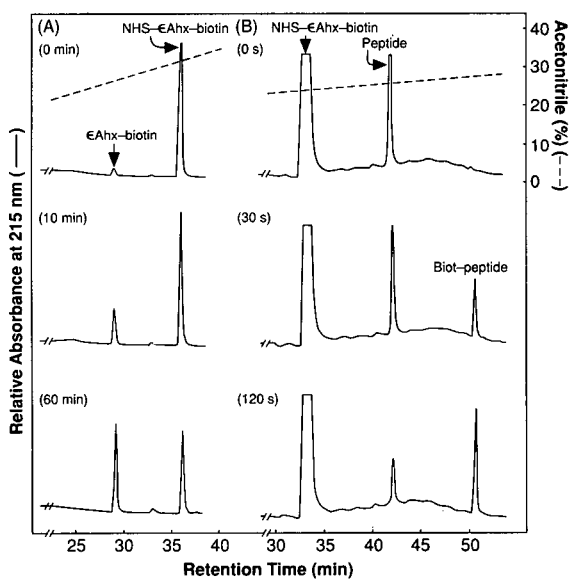


Fig. 5. Representative chromatograms from Vydac  $C_{18}$  reversed-phase HPLC analysis of (A) the time-course of hydrolysis of 550 nmol (0.25 mg) of NHS- $\epsilon$ Ahx-biotin at reaction times indicated and (B) the time-course of biotinylation of 9.7 nmol (18.1  $\mu$ g) of monobiotinyl- $\alpha$ NH<sub>2</sub>-A-ELH(108–121) by NHS- $\epsilon$ Ahx-biotin at 25°C for times indicated.

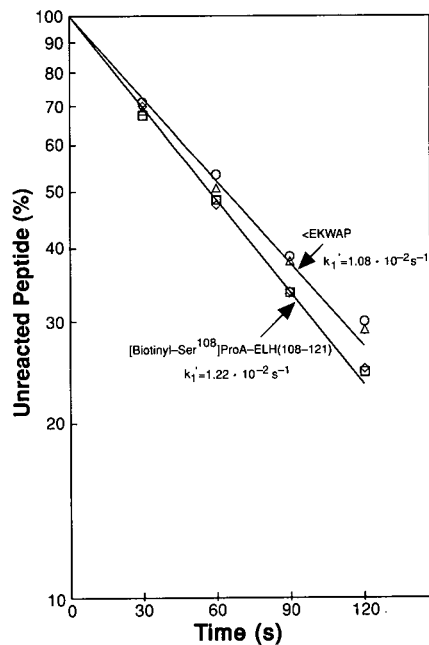


Fig. 7. Observed pseudo-first-order reaction kinetics of the two peptides shown with NHS- $\epsilon$ Ahx-biotin at 25°C. Duplicate reaction times are indicated for each curve:  $\square$ ,  $\diamond$  = [biotinyl-Ser<sup>108</sup>]ProA-ELH(108–121);  $\circ$ ,  $\triangle$  = <EKWAP.

The kinetics of biotinylation of two different lysyl residues in two model peptides are described in Figs. 5B, 6 and 7. HPLC chromatograms of representative time-course biotinylation reactions of [biotinyl-Ser<sup>108</sup>]ProA-ELH(108–121) are presented in Fig. 5B. Similarly, representative chromatograms of biotinylation of the peptide pGlu–Lys–Trp–Ala–Pro are given in Fig. 6. For a representative comparison the results given in Fig. 6 show the entire chromatograms, whereas, for convenience, the early elution regions of all previous chromatograms were abbreviated. Fig. 7 gives the observed pseudo-first-order log plots of biotinylation of the lysyl  $\epsilon$ NH<sub>2</sub> groups of the two model peptides shown. The observed  $k'_1$  values for [biotinyl-Ser<sup>108</sup>]ProA-ELH(108–121) and <EKWAP were  $1.22 \cdot 10^{-2} \text{ s}^{-1}$  and  $1.08 \cdot 10^{-2} \text{ s}^{-1}$ , respectively. The  $k'_1$  values obtained for the two peptides were similar and likely represented the reactivity of a fully exposed  $\epsilon$ NH<sub>2</sub>-group since the reactivity of <EKWAP was identical in 8 M urea (results not shown). The reaction half-life for [biotinyl-Ser<sup>108</sup>]ProA-ELH(108–121) was 57 s and for <EKWAP was 64 s. The observed reactivities of the  $\epsilon$ NH<sub>2</sub>-groups of these two peptides was somewhat faster than that observed for the reaction of 2,4,6-trinitrobenzenesulfonate with the  $\epsilon$ NH<sub>2</sub>-groups of glycyllsine in 0.05 M sodium borate buffer, pH 9.5. The half-life for the two peptide reactions with NHS- $\epsilon$ Ahx-biotin averaged to be *ca.* 61 s (pH 8.2) whereas that reported for the reaction of glycyllsine with 2,4,6-trinitrobenzenesulfonate was 105 s (pH 9.5) [9].

The above described HPLC method for determining reaction rates of amino acid residues of peptides with the NHS-biotin esters clearly offers a number of advantages. These include (1) evaluation of biotinylating reagent quality, (2) determination of the extent of spontaneous reagent hydrolysis, (3) simultaneous measurement of the amounts of all reaction components including reagent, reagent hydrolysis products, unmodified peptide and biotinylated peptide, (4) reasonably high sensitivity using low nmol amounts of peptide and (5) potential for

comparative kinetic analyses. An additional advantage of using the NHS- $\epsilon$ Ahx-biotin reagent is that it allows for accurate measurement of all reaction components by quantitation of the amount of 6-aminohexanoic acid spacer arm by amino acid analysis [3]. Peptides that contain mixtures of reactive groups can be initially reacted under more limiting reagent conditions to obtain suitable biotinylated peptides with only a single reactive group [2,4].

In summary, we have established HPLC methods for characterizing the kinetics of biotinylation of peptides using NHS-biotin esters. Also included in these studies are chromatographic procedures for evaluating reagent homogeneity and determining the extent of biotinylating reagent hydrolysis.

#### ACKNOWLEDGEMENTS

This work was supported by National Institutes of Health Grants NS 29261 (A.K.) and NS 07185 (W.D. Willis, Jr.), by Grant H-1190 from the Robert A. Welch Foundation (A.K.), and a grant from the Pearl and Aaron Forman Research Foundation (B.T.M.). We thank Ms. Angelina Mouton for preparation of the manuscript and Mr. J. Steve Smith and Ms. Anna Garcia for expert technical assistance.

#### REFERENCES

- 1 M. Wilchek and E. A. Bayer, *Methods Enzymol.*, 184 (1990) 5.
- 2 B. T. Miller, T. J. Collins, G. T. Nagle and A. Kurosky, *J. Biol. Chem.*, 267 (1992) 5060.
- 3 J. S. Smith, B. T. Miller, S. L. Knock and A. Kurosky, *Anal. Biochem.*, 197 (1991) 247.
- 4 S. L. Knock, B. T. Miller, J. E. Blankenship, G. T. Nagle, J. S. Smith and A. Kurosky, *J. Biol. Chem.*, 266 (1991) 24413.
- 5 J. S. Smith, B. T. Miller and A. Kurosky, *Anal. Biochem.*, 197 (1991) 254.
- 6 G. T. Nagle, S. D. Painter, J. E. Blankenship, J. D. Dixon and A. Kurosky, *J. Biol. Chem.*, 261 (1986) 7853.
- 7 G. T. Nagle, S. D. Painter, J. E. Blankenship and A. Kurosky, *J. Biol. Chem.*, 263 (1988) 9223.
- 8 R. B. Merrifield, *J. Am. Chem. Soc.*, 85 (1963) 2149.
- 9 R. Fields, *Methods Enzymol.*, 25 (1972) 464.



## PUBLICATION SCHEDULE FOR THE 1993 SUBSCRIPTION

*Journal of Chromatography and Journal of Chromatography, Biomedical Applications*

MONTH	O 1992	N 1992	D 1992	J	F	
Journal of Chromatography	623/1 623/2 624/1 + 2	625/1 625/2	626/1 626/2 627/1 + 2	628/1 628/2 629/1 629/2	630/1 + 2 631/1 + 2 632/1 + 2 633/1 + 2	The publication schedule for further issues will be published later
Cumulative Indexes, Vols. 601-650						
Bibliography Section						
Biomedical Applications				612/1	612/2	

### INFORMATION FOR AUTHORS

(Detailed *Instructions to Authors* were published in Vol. 609, pp. 439-445. A free reprint can be obtained by application to the publisher, Elsevier Science Publishers B.V., P.O. Box 330, 1000 AH Amsterdam, The Netherlands.)

**Types of Contributions.** The following types of papers are published in the *Journal of Chromatography* and the section on *Biomedical Applications*: Regular research papers (Full-length papers), Review articles, Short Communications and Discussions. Short Communications are usually descriptions of short investigations, or they can report minor technical improvements of previously published procedures; they reflect the same quality of research as Full-length papers, but should preferably not exceed five printed pages. Discussions (one or two pages) should explain, amplify, correct or otherwise comment substantively upon an article recently published in the journal. For Review articles, see inside front cover under Submission of Papers.

**Submission.** Every paper must be accompanied by a letter from the senior author, stating that he/she is submitting the paper for publication in the *Journal of Chromatography*.

**Manuscripts.** Manuscripts should be typed in **double spacing** on consecutively numbered pages of uniform size. The manuscript should be preceded by a sheet of manuscript paper carrying the title of the paper and the name and full postal address of the person to whom the proofs are to be sent. As a rule, papers should be divided into sections, headed by a caption (*e.g.*, Abstract, Introduction, Experimental, Results, Discussion, etc.). All illustrations, photographs, tables, etc., should be on separate sheets.

**Abstract.** All articles should have an abstract of 50-100 words which clearly and briefly indicates what is new, different and significant. No references should be given.

**Introduction.** Every paper must have a concise introduction mentioning what has been done before on the topic described, and stating clearly what is new in the paper now submitted.

**Illustrations.** The figures should be submitted in a form suitable for reproduction, drawn in Indian ink on drawing or tracing paper. Each illustration should have a legend, all the *legends* being typed (with double spacing) together on a *separate sheet*. If structures are given in the text, the original drawings should be supplied. Coloured illustrations are reproduced at the author's expense, the cost being determined by the number of pages and by the number of colours needed. The written permission of the author and publisher must be obtained for the use of any figure already published. Its source must be indicated in the legend.

**References.** References should be numbered in the order in which they are cited in the text, and listed in numerical sequence on a separate sheet at the end of the article. Please check a recent issue for the layout of the reference list. Abbreviations for the titles of journals should follow the system used by *Chemical Abstracts*. Articles not yet published should be given as "in press" (journal should be specified), "submitted for publication" (journal should be specified), "in preparation" or "personal communication".

**Dispatch.** Before sending the manuscript to the Editor please check that the envelope contains four copies of the paper complete with references, legends and figures. One of the sets of figures must be the originals suitable for direct reproduction. Please also ensure that permission to publish has been obtained from your institute.

**Proofs.** One set of proofs will be sent to the author to be carefully checked for printer's errors. Corrections must be restricted to instances in which the proof is at variance with the manuscript. "Extra corrections" will be inserted at the author's expense.

**Reprints.** Fifty reprints will be supplied free of charge. Additional reprints can be ordered by the authors. An order form containing price quotations will be sent to the authors together with the proofs of their article.

**Advertisements.** The Editors of the journal accept no responsibility for the contents of the advertisements. Advertisement rates are available on request. Advertising orders and enquiries can be sent to the Advertising Manager, Elsevier Science Publishers B.V., Advertising Department, P.O. Box 211, 1000 AE Amsterdam, Netherlands; courier shipments to: Van de Sande Bakhuizenstraat 4, 1061 AG Amsterdam, Netherlands; Tel. (+31-20) 515 3220/515 3222, Telefax (+31-20) 6833 041, Telex 16479 els vi nl. UK: T. G. Scott & Son Ltd., Tim Blake, Portland House, 21 Narborough Road, Cosby, Leics. LE9 5TA, UK; Tel. (+44-533) 753 333, Telefax (+44-533) 750 522. USA and Canada: Weston Media Associates, Daniel S. Lipner, P.O. Box 1110, Greens Farms, CT 06436-1110, USA; Tel. (+1-203) 261 2500, Telefax (+1-203) 261 0101.

20.10.91 (20 Oct 1991)



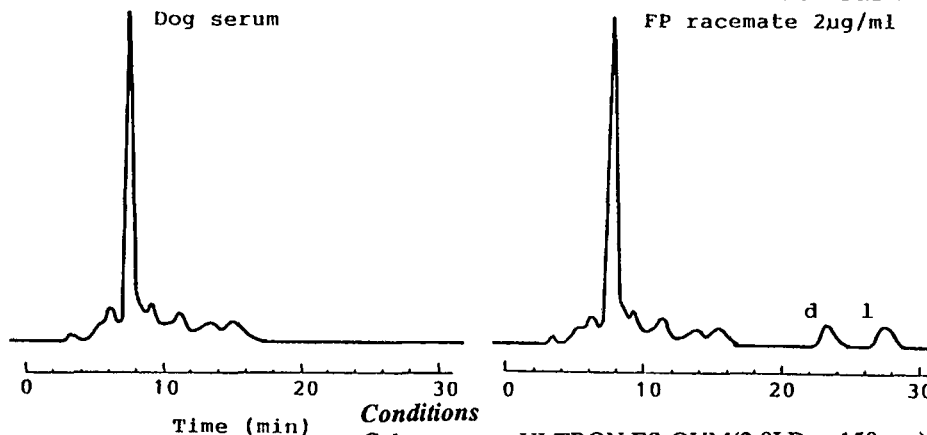
# Ovomucoid Bonded Column for Direct Chiral Separation

## ULTRON ES-OVM

Narrow-Bore Column ( 2.0 I.D. x 150 mm ) for Trace Analyses  
Analytical Column ( 4.6 I.D. , 6.0 I.D. x 150 mm ) for Regular Analyses  
Semi-Preparative Column ( 20.0 I.D. x 250 mm ) for Preparative Separation

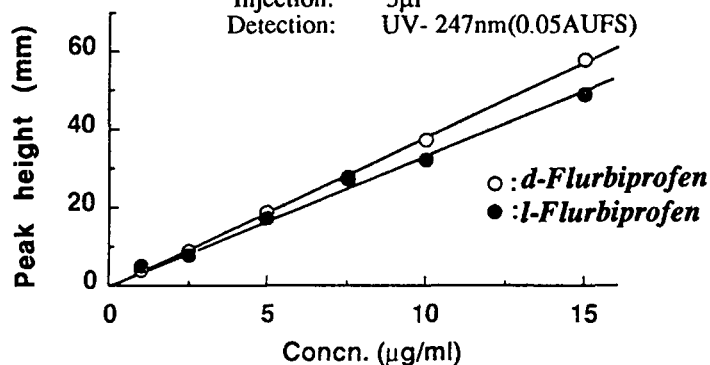
### Analysis of Trace FLURBIPROFEN in Metabolite

with NARROW-BORE COLUMN



#### Conditions

Column: ULTRON ES-OVM(2.0I.D. x 150mm)  
Mobile Phase: 20mMPhosphate Buffer(pH=3.0)/CH<sub>3</sub>CN  
=100/15  
Flow Rate: 0.1ml/min  
Temperature: 25°C  
Injection: 5µl  
Detection: UV- 247nm(0.05AUFS)



Calibration Curve for Each Enantiomer of Flurbiprofen

## SHINWA CHEMICAL INDUSTRIES, LTD.

50 Kagekatsu-cho, Fushimi-ku, Kyoto 612, JAPAN  
Phone:+81-75-621-2360 Fax:+81-75-602-2660

In the United States and Europe, please contact:

### Rockland Technologies, Inc.

538 First State Boulevard, Newport, DE 19804, U.S.A.

Phone: 302-633-5880 Fax: 302-633-5893

This product is licenced by Eisai Co., Ltd.